Arthritis & Rheumatology

An Official Journal of the American College of Rheumatology
www.arthritisrheum.org and wileyonlinelibrary.com

Cover design: Todd Machen

♾This journal is printed on acid-free paper.

Arthritis & Rheumatology

An Official Journal of the American College of Rheumatology
www.arthritisrheum.org and wileyonlinelibrary.com

VOLUME 78 • February 2026 • NO. 2

Cover image: The image on the cover (Lakin et al; pages 418–427) shows imaging mass cytometry of diffuse cutaneous systemic sclerosis skin revealing distinct fibroblast microenvironments. In a patient with disease duration of six months who clinically improved at 52 weeks, CD34+ fibroblasts localize to superficial dermal layers with lower collagen density, whereas α-SMA+ fibroblasts predominate in deeper dermal layers with higher collagen density.

In this Issue

Highlights from this issue of *A&R* | By Lara C. Pullen, PhD

Cellular Mechanisms Underlying Transition from Psoriasis to Psoriatic Arthritis

Multiple lines of evidence indicate that T cells are key drivers of immunopathology in psoriasis and psoriatic arthritis. **In this issue, Graßhoff et al. (p. 332)** p. 332 report the results of the first cross-sectional study to investigate the immunological characteristics of 116 patients across the spectrum of psoriatic disease. The investigators found that the transition from psoriasis to psoriatic arthritis is associated with distinct alterations in the peripheral blood T cell compartment, with T cytotoxic 17 (Tc17) cells being most predictive of the transition.

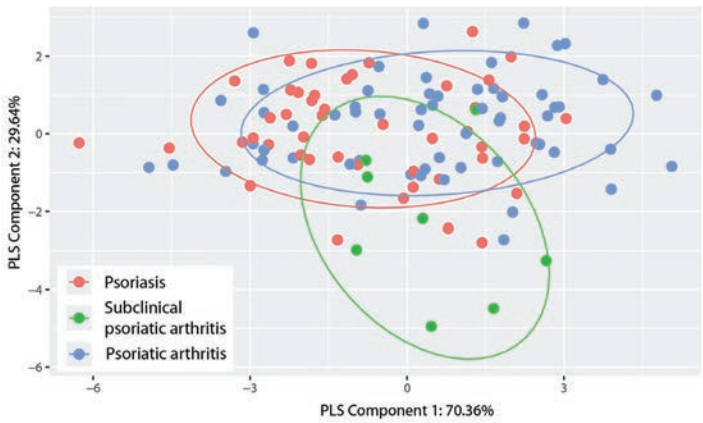

Figure 1. Patients with psoriasis (red), subclinical psoriatic arthritis (green), and psoriatic arthritis (blue) display overlapping T cell subset endotypes with remarkable divergence in subclinical psoriatic arthritis, as shown by a partial least squares–discriminant analysis (PLS-DA). The results are illustrated as a PLS score plot with confidence ellipses set at 80%.

Analysis of the frequencies of effector memory CD4$^+$ T (TEM) cells, T helper 17 (Th17), and Tc17 cells revealed overlapping T cell endotypes among patient subgroups with psoriasis, subclinical psoriatic arthritis, and psoriatic arthritis. In the study cohort, approximately one-third of patients with subclinical psoriatic arthritis and half of those with rheumatologist-diagnosed psoriatic arthritis had enthesitis. Machine learning–assisted, unsupervised clustering analysis identified changes in Tc17 cell frequencies associated with transition to psoriatic arthritis and the presence of enthesitis. The investigators found higher Tc17 frequencies in patients with subclinical psoriatic arthritis compared with psoriasis and definitive psoriatic arthritis, as well as in patients with enthesitis compared with those without enthesitis.

The authors write that the findings provide insight into immunopathologic mechanisms that drive disease progression from psoriasis to psoriatic arthritis and suggest that CD4$^+$ TEM, Th17, and, in particular, Tc17 cells may migrate to joints and entheses during this transition. If true, Tc17 cells may be a novel potential therapeutic target for preventing transition.

Skin Biopsies Can Enhance Prediction of SSc Outcomes

Although systemic sclerosis (SSc) clinical trials frequently obtain skin biopsies to evaluate treatment effects at the tissue level, such biopsies are used less often in clinical care. **In this issue, Lakin et al. (p. 418)** p. 418 report that skin biopsy assessments provide insight into the heterogeneity of diffuse cutaneous SSc (dcSSc). Specifically, fibroblast immunophenotype varied with baseline duration of disease and improved performance of a logistic regression model to identify patients who responded to mycophenolate mofetil (MMF).

The investigators evaluated an international cohort of 105 patients with dcSSc enrolled in clinical interventional trials. Patients underwent baseline biopsies and had 52-week, high-quality, trial-level clinical data with minimal missing values. The authors note that a majority (70%) of patients receiving MMF in the trials had clinical improvement, underscoring the utility of MMF as treatment for dcSSc as well as the challenges clinical trials face when incorporating MMF as background therapy.

Baseline fibroblast immunophenotype, but not the modified Rodnan skin score (mRSS), varied with disease duration. Moreover, the α-smooth muscle actin and CD34 fibroblast markers coexisted in a substantial number of patients, and imaging mass cytometry revealed regional variation of fibroblast subtypes within samples. The researchers' final model did not identify RNA polymerase III antibody status or baseline mRSS as independent predictors of clinical improvement on MMF but relied instead on patients' fibroblast profile. The prognostic impact of the fibroblast profile varied by disease duration at the time of biopsy, and the authors concluded that skin biopsies may help refine dcSSc prognosis and guide patient management decisions.

Telomere Length Predicts SSc-ILD Disease Outcomes

Telomere dysfunction is associated with several age-related diseases, as well as all-cause mortality. Previous studies have found shortened peripheral blood leukocyte telomere length (PBL-TL) across several forms of interstitial lung disease (ILD) and systemic sclerosis (SSc). These findings have led researchers to hypothesize that aberrant aging and telomere dysfunction may directly contribute to the onset and progression of SSc lung disease. **In this issue, Yang et al. (p. 428)** report study results showing that short PBL-TL is associated with pulmonary disease severity and predicts worse SSc outcomes.

p. 428

The investigators compared PBL-TL measurements from a large, well-characterized longitudinal cohort of SSc patients against those from age-matched healthy controls. PBL-TL was significantly shorter in patients with SSc than in healthy controls, with the shortest PBL-TL in individuals with concurrent ILD and pulmonary hypertension. PBL-TL was not associated with skin disease or peripheral vascular disease. Moreover, TL was shorter in lung epithelial cells from SSc-ILD patients compared with those from healthy controls, although no TL difference was found in skin epithelial cells of the two groups.

Regardless of baseline length, PBL-TL shortened more rapidly in SSc patients than in the general healthy population and faster in patients with early SSc compared to those with longer disease duration. The degree of telomere shortening was associated with worse clinical outcomes, including increased hospitalizations for respiratory failure and poorer event-free survival. The authors suggest these findings could be used to stratify SSc patients at risk of more severe or progressive disease, particularly more severe pulmonary involvement, and conclude by calling for further investigation into the role of telomere dysfunction in SSc pathogenesis and for validation of TL as a prognostic biomarker in SSc.

Journal Club

A monthly feature designed to facilitate discussion on research methods in rheumatology.

Gut Microbiota Community Types and Response to Fecal Microbiota Transplantation in Patients With PsA

Qin et al. *Arthritis Rheumatol.* 2026;78:320–331.

Psoriatic arthritis (PsA) is a systemic inflammatory disease increasingly linked to changes in the gut microbiota. This randomized, controlled study examined whether gut microbiota composition before treatment might predict how well patients would respond to fecal microbiota transplantation (FMT)—a procedure that transfers gut microbes from a healthy donor to a patient to restore microbial balance. Patients with a *Bacteroides*-dominated community structure at baseline were more likely to experience lasting clinical benefit after just one FMT.

Although only a few FMT studies have investigated the impact of microbiota community types (or "enterotypes"), research in obesity and inflammatory bowel disease has shown that people with different enterotypes can display distinct immune and metabolic profiles. When we observed two clearly separated community types among PsA patients, we wondered whether this underlying microbial community could influence FMT outcomes. The results supported this idea and suggested that community structure may be a key factor shaping the therapeutic response to microbiota-based interventions.

We used shotgun metagenomic sequencing to characterize the gut microbiota, which provided deeper insight into microbial dynamics. This approach provides higher taxonomic and functional resolution than traditional 16S rRNA amplicon sequencing and allowed us to track donor and recipient strains after transplantation. By capturing these strain-level changes, we began to link microbial engraftment patterns with clinical response. Overall, the findings add a new perspective on the role of gut microbiota in PsA and raise the possibility that baseline microbial features could help guide future FMT strategies.

Questions

1. **What are the strengths and limitations of shotgun metagenomic sequencing compared with 16S rRNA sequencing for characterizing gut microbiota in FMT studies and beyond?**
2. **How were community types defined in this study, and what statistical or bioinformatic methods can best capture such clustering in microbiome data?**
3. **What factors might explain the greater donor strain persistence observed in long-term responders?**
4. **Could repeated or personalized FMTs improve outcomes in patients with non-*Bacteroides*-dominated microbiota?**
5. **Could gut microbiota community typing also be relevant for predicting response to conventional therapies in PsA and other autoimmune or inflammatory rheumatic diseases?**

Clinical Connections

Performance of an Idiopathic Pulmonary Fibrosis–Derived Multibiomarker Panel for RA-ILD

Luedders et al. *Arthritis Rheumatol.* 2026;78:302–310.

CORRESPONDENCE
Bryant England, MD, PhD: Bryant.england@unmc.edu

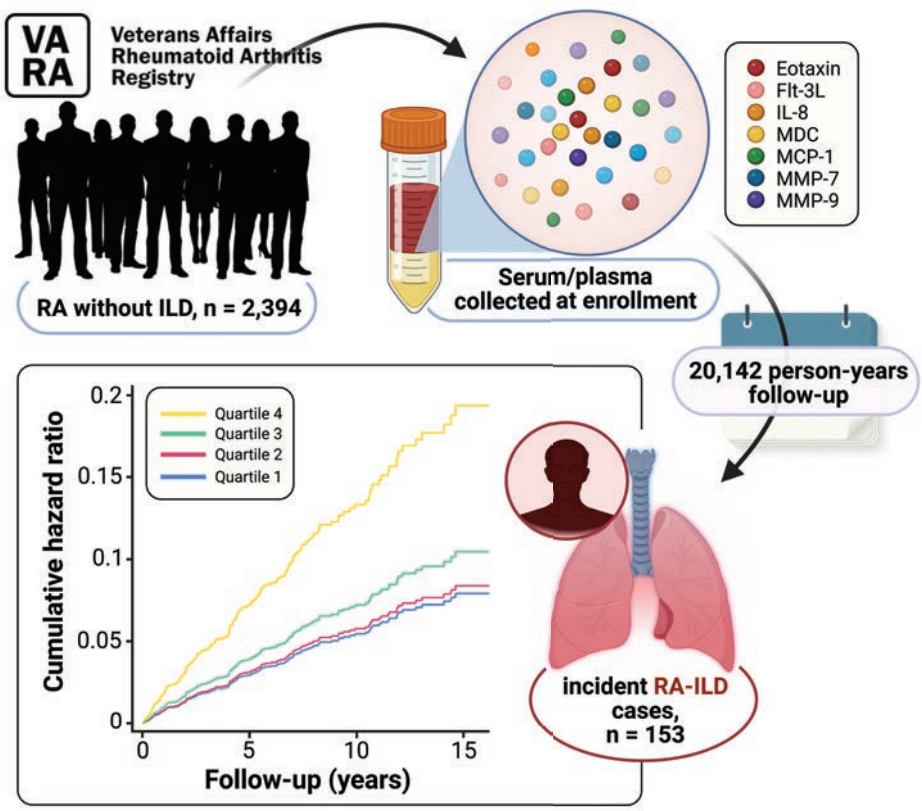

KEY POINTS

- Overlapping peripheral biomarker associations of IPF and RA-ILD suggest shared pathways in disease pathogenesis.
- Over 15 years of longitudinal follow-up, RA patients with the highest multibiomarker scores had a cumulative hazard for ILD approaching 20%, whereas for all other quartiles this risk was less than 10%.
- Future studies are needed to identify clinically relevant risk scores for RA-ILD incorporating peripheral biomarkers in combination with other clinical and genetic risk factors.

SUMMARY

Rheumatoid arthritis–associated interstitial lung disease (RA-ILD) is an extra-articular manifestation of RA associated with increased morbidity and mortality. While ACR/CHEST guidelines recommend screening at-risk RA patients for ILD, selecting which patients are most likely to benefit from screening remains a challenge in the clinical setting.

In this study by Luedders et al., a multibiomarker score incorporating peripheral blood biomarkers associated with idiopathic pulmonary fibrosis (IPF) was derived in independent development cohorts and subsequently validated within the Veterans Affairs Rheumatoid Arthritis (VARA) registry. Individuals with the highest quartile multibiomarker scores were over two times as likely to have RA-ILD at baseline and to develop new RA-ILD during follow-up. These findings suggest a potential role for IPF-associated peripheral blood biomarkers in RA-ILD risk stratification that may also clarify the overlap in pathogenesis with IPF.

Prognostic Value of Lupus Anticoagulant and Anti-β2GPI Antibody in Adverse Pregnancy Outcomes

Nonobe et al. *Arthritis Rheumatol*. 2026;78:371–384.

CORRESPONDENCE
Mayumi Sugiura-Ogasawara MD, PhD: og.mym@med.nagoya-cu.ac.jp

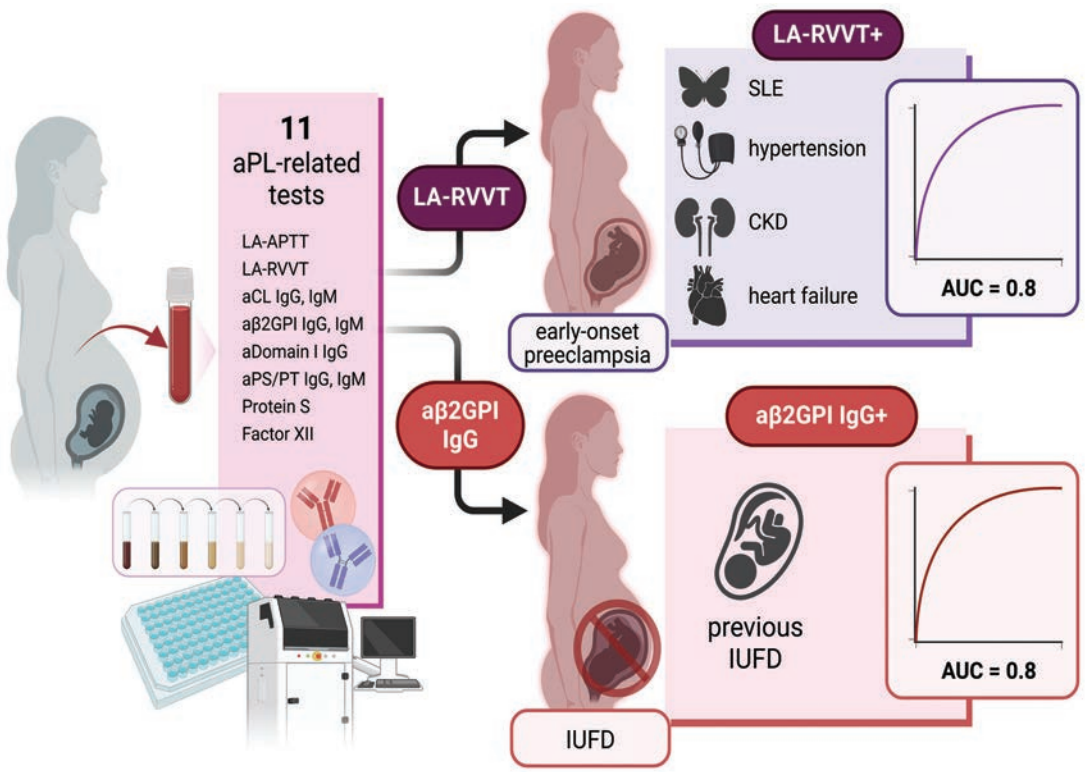

KEY POINTS

- LA-RVVT and anti-β2GPI IgG demonstrated predictive value for early-onset preeclampsia and IUFD, respectively, in pregnant women.
- Measuring LA-RVVT and anti-β2GPI IgG may be essential to the diagnosis of obstetric APS.
- Important complications associated with obstetric APS include SLE, hypertension, chronic kidney disease, heart failure, and a history of IUFD.

SUMMARY

Obstetric antiphospholipid syndrome (APS) is considered one of the most treatable causes of recurrent pregnancy loss. To confirm a diagnosis of APS, international criteria require presence of antiphospholipid antibodies (aPLs), including lupus anticoagulant (LA), anticardiolipin (aCL) IgG and IgM, and anti-β2-glycoprotein I (β2GPI) IgG and IgM. Although the efficacy of these aPL assays has been demonstrated in studies of thrombotic APS, their utility in obstetric APS has not yet been established. Nonobe et al. examined whether the presence of criteria and non-criteria aPLs could predict adverse pregnancy outcomes in pregnant women.

Blood samples from more than 1,200 pregnant women living in Japan were tested using a variety of aPL-related assays. Pregnancy outcomes were followed, and receiver operating characteristic curves and area under the curve (AUC) were calculated to assess diagnostic performance. LA-RVVT and anti-β2GPI IgG were each found to be predictors of early-onset preeclampsia and intrauterine fetal death (IUFD), respectively. The AUC for early-onset preeclampsia increased to ~0.8 when combined with complications of systemic lupus erythematous (SLE), hypertension, chronic kidney disease (CKD) and heart failure. The AUC for IUFD increased to ~0.8 when combined with a history of IUFD.

Telomere Length Predicts SSc-ILD Disease Outcomes

Telomere dysfunction is associated with several age-related diseases, as well as all-cause mortality. Previous studies have found shortened peripheral blood leukocyte telomere length (PBL-TL) across several forms of interstitial lung disease (ILD) and systemic sclerosis (SSc). These findings have led researchers to hypothesize that aberrant aging and telomere dysfunction may directly contribute to the onset and progression of SSc lung disease. **In this issue, Yang et al. (p. 428)** report study results showing that short PBL-TL is associated with pulmonary disease severity and predicts worse SSc outcomes.

p. 428

The investigators compared PBL-TL measurements from a large, well-characterized longitudinal cohort of SSc patients against those from age-matched healthy controls. PBL-TL was significantly shorter in patients with SSc than in healthy controls, with the shortest PBL-TL in individuals with concurrent ILD and pulmonary hypertension. PBL-TL was not associated with skin disease or peripheral vascular disease. Moreover, TL was shorter in lung epithelial cells from SSc-ILD patients compared with those from healthy controls, although no TL difference was found in skin epithelial cells of the two groups.

Regardless of baseline length, PBL-TL shortened more rapidly in SSc patients than in the general healthy population and faster in patients with early SSc compared to those with longer disease duration. The degree of telomere shortening was associated with worse clinical outcomes, including increased hospitalizations for respiratory failure and poorer event-free survival. The authors suggest these findings could be used to stratify SSc patients at risk of more severe or progressive disease, particularly more severe pulmonary involvement, and conclude by calling for further investigation into the role of telomere dysfunction in SSc pathogenesis and for validation of TL as a prognostic biomarker in SSc.

Journal Club

A monthly feature designed to facilitate discussion on research methods in rheumatology.

Gut Microbiota Community Types and Response to Fecal Microbiota Transplantation in Patients With PsA

Qin et al. *Arthritis Rheumatol.* 2026;78:320–331.

Psoriatic arthritis (PsA) is a systemic inflammatory disease increasingly linked to changes in the gut microbiota. This randomized, controlled study examined whether gut microbiota composition before treatment might predict how well patients would respond to fecal microbiota transplantation (FMT)—a procedure that transfers gut microbes from a healthy donor to a patient to restore microbial balance. Patients with a *Bacteroides*-dominated community structure at baseline were more likely to experience lasting clinical benefit after just one FMT.

Although only a few FMT studies have investigated the impact of microbiota community types (or "enterotypes"), research in obesity and inflammatory bowel disease has shown that people with different enterotypes can display distinct immune and metabolic profiles. When we observed two clearly separated community types among PsA patients, we wondered whether this underlying microbial community could influence FMT outcomes. The results supported this idea and suggested that community structure may be a key factor shaping the therapeutic response to microbiota-based interventions.

We used shotgun metagenomic sequencing to characterize the gut microbiota, which provided deeper insight into microbial dynamics. This approach provides higher taxonomic and functional resolution than traditional 16S rRNA amplicon sequencing and allowed us to track donor and recipient strains after transplantation. By capturing these strain-level changes, we began to link microbial engraftment patterns with clinical response. Overall, the findings add a new perspective on the role of gut microbiota in PsA and raise the possibility that baseline microbial features could help guide future FMT strategies.

Questions

1. **What are the strengths and limitations of shotgun metagenomic sequencing compared with 16S rRNA sequencing for characterizing gut microbiota in FMT studies and beyond?**
2. **How were community types defined in this study, and what statistical or bioinformatic methods can best capture such clustering in microbiome data?**
3. **What factors might explain the greater donor strain persistence observed in long-term responders?**
4. **Could repeated or personalized FMTs improve outcomes in patients with non-*Bacteroides*-dominated microbiota?**
5. **Could gut microbiota community typing also be relevant for predicting response to conventional therapies in PsA and other autoimmune or inflammatory rheumatic diseases?**

Arthritis & Rheumatology
Vol. 78, No. 2, February 2026, pp 277–279
DOI 10.1002/art.43450

American College of Rheumatology
Empowering Rheumatology Professionals

EDITORIAL

Your FLORA Matters: Microbiome Modulation in Psoriatic Arthritis

Emilie Dumas and Dirk Elewaut

The last decade witnessed a paradigm shift in our understanding of immune-mediated inflammatory diseases (IMIDs), with an emerging role of the microbiome in disease pathogenesis and progression. Barrier sites, such as the gut, skin, and lung, are not merely anatomic structures but active interfaces between host and the environment, mediating complex host–microbe interplay.[1,2] Disruption of these interfaces—referred to as "barrier dysfunction"—is now a hallmark feature across multiple IMIDs, including spondyloarthritides, inflammatory bowel disease (IBD), psoriasis, psoriatic arthritis (PsA), and even rheumatoid arthritis.[2–4]

Among these, PsA stands out as a particularly compelling disease model. PsA is uniquely characterized by its multitissue involvement—skin, joints, entheses, and gut—several of which constitute critical barrier sites. A growing body of literature pinpoints intestinal dysbiosis in PsA pathogenesis, and recent studies suggest dysbiosis of the skin microbiome as well.[5,6] These findings raise a tantalizing question of whether targeted modulation of the microbiome may improve outcomes in PsA.

In this issue of *Arthritis & Rheumatology*, Qin and colleagues report a novel investigation into this question through the FLORA trial, a randomized study evaluating the impact of fecal microbiota transplantation (FMT) in patients with PsA receiving methotrexate.[7] The authors applied high-resolution shotgun metagenomic sequencing to samples from both donors and recipients, aiming to identify microbiome profiles associated with treatment response. Although FMT has been trialed in other IMIDs with mixed results, FLORA represents the first and only controlled study of FMT in a spondyloarthritis population, making this work both timely and novel.

Setting the stage: dysbiosis and immune modulation

The rationale for using FMT in PsA stems from compelling, if still evolving, evidence that the gut microbiota modulates systemic immunity. PsA shares genetic and immunopathologic features with IBD, particularly Crohn disease, in which gut dysbiosis is well characterized. Animal models have demonstrated that alterations in gut microbial composition can drive Th17-mediated inflammation at distal sites, including joints and skin. Clinical studies in PsA have identified reduced microbial diversity and altered abundance of key taxa, including *Prevotella*, *Bacteroides*, and *Faecalibacterium*.

FMT, the transfer of fecal material from a healthy donor to a recipient, has been most extensively studied in *Clostridioides difficile* infection, in which it has demonstrated high efficacy. Its application to chronic inflammatory conditions, however, remains experimental. Small trials in ulcerative colitis have shown promise, with steroid-free remission achieved in a subset of patients. In contrast, results in systemic lupus erythematosus and multiple sclerosis have been variable. Thus, the field has been eagerly awaiting controlled trials exploring the role of FMT in arthritides.

Key findings from FLORA

Qin et al randomized patients with active PsA (on stable methotrexate therapy) to receive FMT from four different healthy donors or a sham procedure consisting of colored saline. Although the original trial's primary endpoint was negative, with FMT achieving lower treatment success (40%) compared to sham (81%),[8] the present microbiome-focused analysis provides rich insights into microbial community dynamics and potential predictive biomarkers of response.

The most notable finding was the identification of two distinct baseline gut microbiota profiles among patients with PsA: a P-type, dominated by *Prevotella* species, and a B-type, which is dominated by *Bacteroides* species and associated with greater microbial richness. Patients with B-type profiles appeared more likely to benefit clinically from FMT. This stratification introduces the possibility that microbial community type could serve as a predictive biomarker for response to microbiome-based

Dr Elewaut's work was supported by grants from VLAIO and FWO-Flanders and by the Research Council of Ghent University.

VIB Center for Inflammation Research, Ghent University and Department of Rheumatology, Ghent University Hospital, Ghent, Belgium.

Author disclosures are available at https://onlinelibrary.wiley.com/doi/10.1002/art.43450.

Address correspondence via email to Dirk Elewaut, MD, PhD, at dirk.elewaut@ugent.be.

Submitted for publication August 22, 2025; accepted August 27, 2025.

interventions—an idea that warrants urgent validation. However, these results should be confirmed as microbiome trajectories varied among clinical responders: three remained B-type, two transitioned from B- to P-type, and one shifted from P- to B-type. These transitions suggest that donor–recipient compatibility may be critical and that pretreatment microbial profiling could inform personalized donor selection strategies in future FMT trials.

Limitations and unresolved questions

Although these findings are compelling, several limitations still need further consideration. First, the clinical endpoints employed—treatment failure and the Health Assessment Questionnaire Disability Index—are not standard metrics in PsA trials. More widely accepted and broadly validated composite indices, such as the Disease Activity index for Psoriatic Arthritis or the Minimal Disease Activity criteria, would provide greater granularity and enhance interpretability. Without these, it remains difficult to align microbial changes with meaningful improvements in disease activity.

Second, although the microbiome analysis is sophisticated, it excludes data from sham-treated patients, limiting the ability to discern natural variability and placebo-associated shifts. This is particularly important given the unexpectedly high placebo response (81%) in the original trial. Including all arms in future analyses will be essential for robust interpretation.

Third, although the study includes multiple timepoints (baseline, week 4, week 12, week 26), there is a missed opportunity for integrated longitudinal analysis. Understanding the temporal dynamics of microbial communities—how they shift, stabilize, or regress—could shed light on whether FMT induces lasting ecological reprogramming or only transient perturbations.

Finally, the functional implications of these microbial shifts remain largely unexplored. Although taxonomic changes are informative, they do not necessarily reflect alterations in microbial function or metabolite production. The integration of metabolomics, transcriptomics, and immunophenotyping will be critical in future studies to link microbial composition with downstream effects on host immunity.

Moving toward precision microbiome therapy

Clearly, the field of rheumatology is entering an exciting era when microbiome-based stratification may augment our therapeutic toolbox. The findings by Qin et al support a conceptual model in which baseline microbiota composition influences response to FMT and in which microbial richness and community type could inform patient selection. This raises several testable hypotheses for next-generation trials:

1. Donor–recipient matching may be critical to enhance FMT efficacy. In this context, could microbial similarity or diversity metrics guide optimal donor selection?
2. Sequential FMT or combination therapy: Would repeated FMTs or adjunctive use with probiotics, prebiotics, or dietary interventions improve microbiome engraftment and durability?
3. Microbiome engineering: Rather than whole-stool transplantation, could defined microbial consortia or synthetic ecology approaches yield more targeted and reproducible outcomes?
4. Mechanistic correlates: What are the immune signatures associated with microbial shifts? Can we identify microbial-derived metabolites that mediate inflammation?

Conclusions

Qin and colleagues should be commended for pioneering the first FMT trial in PsA and for advancing our understanding of microbiome–host interactions in this complex disease. Despite the negative primary outcome, their post hoc analysis reveals important microbial features that could inform future therapeutic strategies. The identification of P- and B-type microbial profiles, with differing associations to treatment response, provides a foundation for precision microbiome interventions in PsA.

To translate these insights into clinical practice, future trials must incorporate validated disease activity metrics, sham-controlled microbiome analyses, and integrated multi-omics profiling. Only through such rigor can we unravel the complex interplay between gut ecology and systemic inflammation and harness the microbiome as a true therapeutic frontier in rheumatology.

AUTHOR CONTRIBUTIONS

Both authors contributed to at least one of the following manuscript preparation roles: conceptualization AND/OR methodology, software, investigation, formal analysis, data curation, visualization, and validation AND drafting or reviewing/editing the final draft. As corresponding author, Dr Elewaut confirms that the authors have provided the final approval of the version to be published and takes responsibility for the affirmations regarding article submission (eg, not under consideration by another journal), the integrity of the data presented, and the statements regarding compliance with institutional review board/Declaration of Helsinki requirements.

REFERENCES

1. Scher JU, Nayak R, Clemente JC. Microbiome research in autoimmune and immune-mediated inflammatory diseases: lessons, advances and unmet needs. Ann Rheum Dis 2025;84(1):9–13.

2. Gracey E, Vereecke L, McGovern D, et al. Revisiting the gut-joint axis: links between gut inflammation and spondyloarthritis. Nat Rev Rheumatol 2020;16(8):415–433.
3. Schatteman L, Mielants H, Veys EM, et al. Gut inflammation in psoriatic arthritis: a prospective ileocolonoscopic study. J Rheumatol 1995;22(4):680–683.
4. Mielants H, Veys EM, Cuvelier C, et al. The evolution of spondyloarthropathies in relation to gut histology. III. Relation between gut and joint. J Rheumatol 1995;22(12):2279–2284.
5. Scher JU, Ubeda C, Artacho A, et al. Decreased bacterial diversity characterizes the altered gut microbiota in patients with psoriatic arthritis, resembling dysbiosis in inflammatory bowel disease. Arthritis Rheumatol 2015;67(1):128–139.
6. Boix-Amorós A, Badri MH, Manasson J, et al. Alterations in the cutaneous microbiome of patients with psoriasis and psoriatic arthritis reveal similarities between non-lesional and lesional skin. Ann Rheum Dis 2023;82(4):507–514.
7. Qin P, Kragsnaes MS, Holm DK, et al. Clinical significance of gut microbiota community types for long-term response to fecal microbiota transplantation in patients with psoriatic arthritis. Arthritis Rheumatol 2026;78(2):320–331.
8. Kragsnaes MS, Kjeldsen J, Horn HC, et al. Safety and efficacy of faecal microbiota transplantation for active peripheral psoriatic arthritis: an exploratory randomised placebo-controlled trial. Ann Rheum Dis 2021;80(9):1158–1167.

American College of Rheumatology
Empowering Rheumatology Professionals

Arthritis & Rheumatology
Vol. 78, No. 2, February 2026, pp 280–284
DOI 10.1002/art.43405

EDITORIAL

A Polyamine Takes the Fast Track to Attack Crystal-Induced Inflammation

Monica Guma and Robert Terkeltaub

Recent gout flare, diagnosis of gout, and initiation of urate-lowering therapy (ULT) for gout are associated with increased risk of cardiovascular events including myocardial infarction, stroke, and deep venous thrombosis.[1–3] Acute calcium pyrophosphate (CPP) crystal arthritis also has been linked to increased short- and long-term risk of a major adverse cardiovascular event.[4] In addition, there is evidence of decreased cardiovascular event risk in patients with gout prescribed daily low-dose colchicine prophylaxis when initiating pharmacologic ULT. These two observations have galvanized interest in means to prevent and treat both articular and systemic inflammation in crystal arthropathy. In 2023, the US Food and Drug Administration (FDA) approved a sustained, daily low-dose colchicine prophylaxis regimen for secondary prevention of cardiovascular events and death in adults with multiple risk factors for, or with established, atherosclerotic cardiovascular disease. However, clinical trials of colchicine prophylaxis specifically to prevent assorted cardiovascular events have provided variable results. In addition, colchicine and other anti-inflammatory drugs commonly used for crystal arthritis flares (nonsteroidal anti-inflammatory drugs, glucocorticoids, biologic interleukin 1 [IL-1] inhibitor drugs) can trigger adverse effects, have limits in the extent of quick pain relief, and do not always completely resolve inflammation. Thus, there are compelling reasons to exploit natural mechanisms that limit and spontaneously resolve crystal-induced arthritis flares.

Caloric restriction and inflammation interdiction

Several preclinical and clinical studies of nonpharmacologic approaches to limit crystal-induced inflammation have focused on high-intensity exercise[5] and on dietary measures and related changes in mediators such as the ketone body β-hydroxybutyrate (BHB).[6–8] BHB is produced not only in the liver but also by myeloid cells.[7] BHB limits monosodium urate (MSU) crystal-induced inflammation largely by inhibiting NLRP3 inflammasome activation.[6–8] Systemic BHB levels markedly increase with caloric restriction, low-carbohydrate ketogenic diet, and short-term high-intensity exercise.[6–8] In this issue of *Arthritis and Rheumatology*, Pham et al demonstrated that a murine fasting regimen (two nonconsecutive fasting days in one week) reproduced a pronounced induction of BHB.[8] Fasting also elevated hepatic and systemic levels of many other anti-inflammatory metabolites such as corticosterone, oleic acid, and the omega-3 fatty acid eicosapentaenoic acid (EPA) and many other anti-inflammatory lipids. In addition, fasting led to downregulation of multiple proinflammatory mediators and pathways.[8] The fasting regimen sharply limited acute MSU and CPP deposition (CPPD) crystal-induced inflammation in the synovitis-like murine subcutaneous air pouch model[8] (Figure 1).

Caloric restriction cannot be realistically sustained in most patients with gout or CPPD. Also, fasting can lead to hyperinflammatory rebound upon refeeding.[10,11] Specifically, prolonged fasting (defined as ≥24 hours) acts partly by stimulating a temporary monocyte mass migration into the bone marrow mechanistically dependent on glucocorticoids and the glucocorticoid-inducible chemokine receptor CXCR4, thereby promoting monocytopenia.[10,11] Refeeding stimulates a monocyte proinflammatory burst powered by relatively long-lived monocytes with a distinct transcriptional program.[10,11] Potential clinical significance of this event cascade in crystal arthropathy merits further investigation.

The focus of Pham et al was unbiased searching for individual fasting-induced metabolites and associated gene program changes sufficient to inhibit monocyte/macrophage lineage cell and air pouch inflammatory responses to MSU and CPPD crystals.[8] They analyzed data from metabolomics of the mouse liver, serum, and air pouch membrane, and transcriptomics of mouse liver and transformed human THP-1 macrophage lineage cells. The results uncovered increased amino acid catabolism linked

Dr Guma's work was supported by the NIH (grant AR-083584).
[1]Department of Medicine, Division of Rheumatology, Autoimmunity and Inflammation, University of California San Diego, La Jolla, California.
Author disclosures are available at https://onlinelibrary.wiley.com/doi/10.1002/art.43405.

Address correspondence via email to Robert Terkeltaub, MD, at rterkeltaub@health.ucsd.edu.
Submitted for publication September 2, 2025; accepted in revised form September 15, 2025.

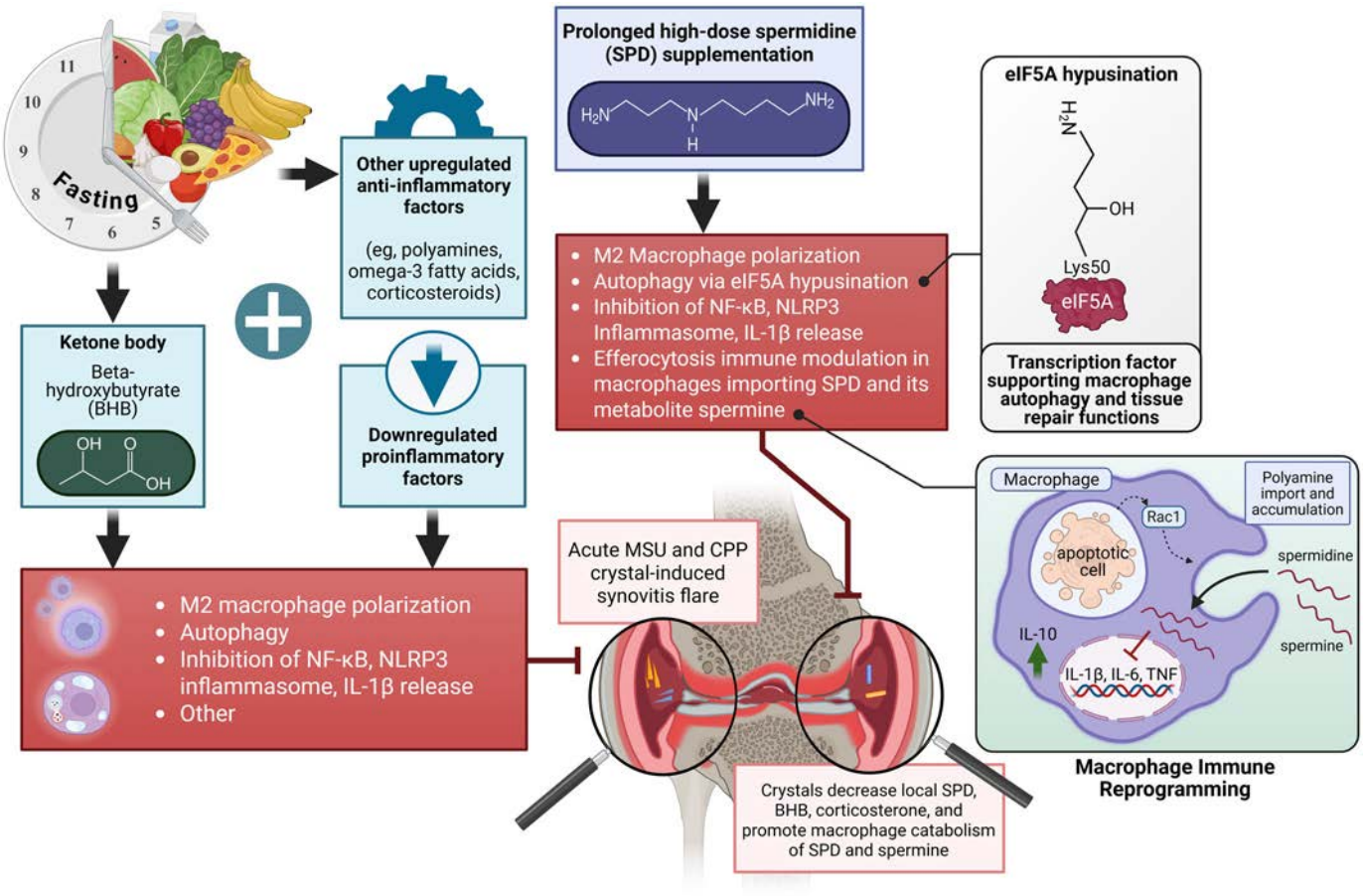

Figure 1. Model of how SPD supplementation suppresses experimental crystal arthritis flare employing some mechanisms similar to those induced by fasting. The schematic diagram compares several putative mechanisms for suppression of murine experimental crystal-induced synovitis flare by fasting (left panels) and prolonged SPD supplementation (right panels). The SPD supplementation model assumes promotion by SPD of autophagy and tissue repair programming, mediated via posttranslational modification of the transcription factor eIF5A, via binding at eIF5A lysine 50 of the unique amino acid hypusine, a catabolic product of SPD. The model also assumes promotion by SPD of efferocytosis with associated macrophage immune reprogramming, driven by import of SPD and its polyamine metabolite spermine. BHB, β-hydroxybutyrate; CPP, calcium pyrophosphate; eIF5A, eukaryotic translation initiation factor 5A; IL, interleukin; MSU, monosodium urate; TNF, tumor necrosis factor. Adapted from Yurdagul A Jr et al, 2021.[9]

with polyamine generation, a novel potential target for therapeutic intervention.[8]

Polyamines: seemingly everywhere, in everything, all at once

Polyamines are ubiquitous organic molecules containing two or more amino (NH_2) groups, which allow interaction with and modulation of negatively charged molecules.[12] In humans and mice, polyamines circulate at micromolar concentrations that are regulated by diet and decline with age. Generation of the naturally occurring human polyamines putrescine, spermine, and spermidine (SPD) begins via catabolism of arginine, specifically by arginase, followed by downstream metabolism of methionine and the nonproteinogenic amino acid ornithine, supplemented by the putrescine precursor agmatine from the diet and gut microbial arginine metabolism.[12,13] Polyamines influence the function of ion channels, affect DNA and RNA stability and function, regulate the growth of normal and tumor cells, modulate cell differentiation, limit oxidative stress and inflammation, promote longevity, and modulate multiple critical functions (eg, protein translation, apoptosis and other cell death programs, insulin secretion, and immune and inflammatory responses).[14–17]

Observations supporting the relevance of polyamine biology to rheumatic diseases include marked elevation of polyamine concentrations in rheumatoid arthritis (RA) joint tissue and peripheral and circulating mononuclear cells, the ability of methotrexate to increase polyamines in immune cells, and the capacity of SPD to suppress IL-2 production.[16] SPD also inhibits activation of both NF-κB and the NLRP3 inflammasome, validated by Pham et al specifically for MSU and CPP crystal-induced macrophage activation.[8] Moreover, several beneficial biologic effects of caloric restriction are mediated by SPD and replicated by SPD supplementation alone. These include the capacity of SPD to promote

longevity and autophagy by inhibiting the mammalian target of rapamycin (mTOR) and, in young K/BxN mice, to flatten peak arthritis activity in the serum transfer model.[13] On the other hand, Th17 cell pathogenicity has been linked with the metabolism of arginine and downstream polyamines.[13] Also, polyamine effects on collagen-induced arthritis are unclear.[18,19] Hence, the effects of polyamines on inflammatory synovitis may depend on the pathogenic trigger. Given the expanding universe of polyamine-related therapeutic opportunities,[8,12–19] we need to connect the dots to build the big picture of polyamine biology for rheumatic diseases.

The work of Pham et al now places SPD as an endogenous and exogenous regulator of acute flare in crystal arthropathy[8] (Figure 1). First, fasting increased the relative abundance of circulating SPD by an undetermined mechanism. Second, MSU and CPP crystal injection markedly decreased relative abundance of SPD, BHB, and certain other anti-inflammatory metabolites and inflammation-controlling pathways in the air pouch membrane. Third, sustained SPD supplementation in drinking water >21 days, combined with a single injection of SPD into the air pouch on the fasting day immediately before crystal injection, robustly suppressed the pouch inflammatory response and associated induction of IL-1β and the chemokine CXCL1.[8]

Injection of SPD into the air pouch 1 day before crystal injection was not sufficient to blunt the tissue inflammatory response.[8] Also, MSU and CPP crystal-*induced modifications in cultured* macrophage lineage cell *polyamine metabolism and catabolism gene programs* included *marked increase in messenger RNA (mRNA) of SPD/spermine acetyltransferase 1 (SAT1*), the rate-limiting enzyme in polyamine catabolism. Conversely, *SAT1* mRNA knockdown reduced crystal-induced IL-1β in vitro in cultured macrophage lineage cells. These findings set the stage for work to determine the overall impact of this putative SAT1 and polyamine inflammation regulatory circuit[8] in vivo in MSU and CPP crystal-induced synovitis.

Figure 1 compares a few of the broad anti-inflammatory effects of fasting to the most likely actions of SPD supplementation that modulate responses to MSU and CPPD crystals.[8] SPD appears unlikely to be the predominant factor blunting the crystal-induced inflammatory response by fasting.[8] Metabolomics analyses did not calculate absolute SPD serum and tissue concentrations during the fasting protocol. Moreover, SPD and other polyamines were immersed in a sizable pool of BHB, corticosterone, EPA, and other up-regulated anti-inflammatory metabolites, with many down-regulated proinflammatory mediators.[8] As such, increased endogenous SPD, which is sufficient to promote autophagy upon caloric restriction,[13] can be insufficient to blunt the vicious acute tissue inflammatory response to MSU and CPP crystals. Notably, inhibition of polyamine production via sustained oral administration of difluoromethylornithine (DFMO),[13] an irreversible inhibitor of ornithine decarboxylase (ODC; the rate-limiting putrescine-generating enzyme in polyamine biosynthesis), did not reverse the suppressive effects of fasting on crystal-induced air pouch inflammation.[8] Dose-response experiments and alternative approaches, such as studies of available ODC or SAT1 knockout mice models, should be more definitive.

Potential fit of SPD in the crystal arthropathy therapy pipeline

Therapeutic potential of SPD supplementation for crystal-induced inflammatory disease is bolstered by a web of biologic mechanisms limiting, spontaneously resolving, and repairing tissue injury. Clearly, caloric restriction taps into this network and so does SPD. For example, in the macrophage efferocytosis process, the import of SPD (and its active metabolite spermine) is triggered by uptake of apoptotic neutrophils and other cell types in macrophages; this activates a tissue repair program and immune reprogramming.[9,20–22] IL-1β, IL-6, and tumor necrosis factor are suppressed, whereas IL-10 and other inflammation resolving mediators are up-regulated.[9,20–22]

SPD supports posttranslational modification of the transcription factor eukaryotic initiation factor 5A (eIF5A),[8] thereby promoting tissue repair functions as well as macrophage autophagy, which proteolytically degrades multiple proinflammatory mediators.[13,23] The mechanism involves binding at eIF5A lysine 50 of the unique, natural amino acid hypusine, a catabolic product of SPD. Also, SPD promotes not only epigenetic anti-inflammatory effects via certain histone posttranslational modifications but also anti-inflammatory M2 macrophage polarization.[8] M2 macrophage expression of arginase-1 launches arginine use specifically for polyamine generation rather than proinflammatory arginine metabolism predominant in M1 macrophages. The latter metabolic pathway, which is up-regulated in RA synovium, produces nitric oxide and citrulline.

Beneficial effects of SPD supplementation in animal models include increases in microbial diversity, enrichment in short-chain fatty acid–producing bacteria, and reduction of proinflammatory taxa while strengthening the anti-inflammatory functions of intestinal barrier integrity. However, potential off-target SPD effects cannot be ignored in the clinical development of SPD and SPD analogs. As a prime example, SPD metabolism has been implicated in carcinogenesis, and SPD-induced autophagy can promote the survival of certain cancer cell types. Thus, DFMO is being widely studied as a tumor growth inhibitor, cancer stem cell–targeting agent, and adjuvant immunotherapy in cancer treatment. DFMO is already FDA-approved as maintenance therapy following conventional treatment of neuroblastoma at high risk of relapse.[24] Conversely, SPD analogs also are in clinical development to suppress the growth of various tumors, target cancer stem cells, and slow diseases of aging.[12]

SPD diet supplements (many using wheat germ to deliver SPD) are abundant in the nonpharmacologic marketplace. However, results have been inconsistent for numerous SPD clinical studies and trials across the spectrum of disease.[12] The source

and formulation of SPD in in vivo studies should be high-purity, pharmaceutical grade (eg, SPD trihydrochloride from non–wheat germ sources). Further considerations include that dietary SPD can be converted to spermine before systemic absorption.[25] SPD supplement dosing appears to require ≥15 mg/day to exert substantial short-term biologic effects.[25] Also, direct and indirect biologic effects of the entire polyamine pathway beyond SPD are considerable.

Conclusions

In conclusion, the work of Pham et al[8] poses provocative new questions regarding polyamines in epidemiology, pathogenesis, and unmet therapy needs in crystal arthropathy. The case for therapeutic opportunities of SPD and SPD analogs in gout and CPPD flare prophylaxis[8] may be particularly cogent in older adults and patients with advanced chronic kidney disease, conditions commonly associated with systemic decrease in polyamines.[12,13] Evidence suggests that arthritis flare prophylaxis,[8] in the months following the initiation of ULT, is a fitting clinical scenario for assessing sustained SPD/SPD analog treatment. Susceptibility to gout flares is sharply increased in this timeframe.[3] Moreover, we reported that circulating SPD and spermine levels substantially decreased (by ∼25% and 50%, respectively, in a mechanistically undefined manner), in the first 6 months of combined xanthine oxidase inhibitor and low-dose colchicine flare prophylaxis therapy.[26]

On-demand oral or intra-articular SPD therapy for acute gout and CPP crystal arthritis flare could face a challenging road to the clinic, because MSU and CPP crystals induced SAT1 in air pouch membrane cells.[8] A synthetic SPD analog specifically designed for resistance to acetylation by SAT1 would be a logical candidate for further study. Nevertheless, the characteristically severe pain in gout and CPPD flares raises a cautionary signal regarding therapeutic boosting of intra-articular polyamines, because polyamines can increase the acute inflammatory pain response and allodynia via effects on selective ion channels.[14,15,27]

AUTHOR CONTRIBUTIONS

All authors contributed to at least one of the following manuscript preparation roles: conceptualization AND/OR methodology, software, investigation, formal analysis, data curation, visualization, and validation AND drafting or reviewing/editing the final draft. As corresponding author, Dr Terkeltaub confirms that all authors have provided the final approval of the version to be published and takes responsibility for the affirmations regarding article submission (eg, not under consideration by another journal), the integrity of the data presented, and the statements regarding compliance with institutional review board/Declaration of Helsinki requirements.

REFERENCES

1. Cipolletta E, Tata LJ, Nakafero G, et al. Association between gout flare and subsequent cardiovascular events among patients with gout. JAMA 2022;328(5):440–450.
2. Cipolletta E, Nakafero G, Richette P, et al. Short-term risk of cardiovascular events in people newly diagnosed with gout. Arthritis Rheumatol 2025;77(2):202–211.
3. Cipolletta E, Nakafero G, McCormick N, et al. Cardiovascular events in patients with gout initiating urate-lowering therapy with or without colchicine for flare prophylaxis: a retrospective new-user cohort study using linked primary care, hospitalisation, and mortality data. Lancet Rheumatol 2025;7(3):e197–e207.
4. Tedeschi SK, Huang W, Yoshida K, et al. Risk of cardiovascular events in patients having had acute calcium pyrophosphate crystal arthritis. Ann Rheum Dis 2022;81(9):1323–1329.
5. Jablonski K, Young NA, Henry C, et al. Physical activity prevents acute inflammation in a gout model by downregulation of TLR2 on circulating neutrophils as well as inhibition of serum CXCL1 and is associated with decreased pain and inflammation in gout patients. PLoS One 2020;15(10):e0237520.
6. Youm YH, Nguyen KY, Grant RW, et al. The ketone metabolite β-hydroxybutyrate blocks NLRP3 inflammasome-mediated inflammatory disease. Nat Med 2015;21(3):263–269.
7. Goldberg EL, Asher JL, Molony RD, et al. β-hydroxybutyrate deactivates neutrophil NLRP3 inflammasome to relieve gout flares. Cell Rep 2017;18(9):2077–2087.
8. Pham CN, Castelli F, Finet F, et al. Spermidine reproduces the anti-inflammatory effects of intermittent fasting and prevents urate and calcium pyrophosphate crystal-induced inflammation. Arthritis Rheumatol 2026;78(2):449–462.
9. Yurdagul A Jr, Kong N, Gerlach BD, et al. ODC (ornithine decarboxylase)-dependent putrescine synthesis maintains MerTK (MER tyrosine-protein kinase) expression to drive resolution. Arterioscler Thromb Vasc Biol 2021;41(3):e144–e159.
10. Yuan H, Wu SX, Zhou YF, et al. Spermidine inhibits joints inflammation and macrophage activation in mice with collagen-induced arthritis. J Inflamm Res 2021;14:2713–2721.
11. Janssen H, Kahles F, Liu D, et al. Monocytes re-enter the bone marrow during fasting and alter the host response to infection. Immunity 2023;56(4):783–796.e7.
12. O'Brien CJO, Domingos AI. Old and "hangry" monocytes turn from friend to foe under assault. Immunity 2023;56(4):747–749.
13. Arthur R, Jamwal S, Kumar P. A review on polyamines as promising next-generation neuroprotective and anti-aging therapy. Eur J Pharmacol 2024;978:176804.
14. Hofer SJ, Daskalaki I, Bergmann M, et al. Spermidine is essential for fasting-mediated autophagy and longevity. Nat Cell Biol 2024;26(9):1571–1584.
15. Gewehr C, da Silva MA, dos Santos GT, et al. Contribution of peripheral vanilloid receptor to the nociception induced by injection of spermine in mice. Pharmacol Biochem Behav 2011;99(4):775–781.
16. Middleton SJ, Markússon S, Åkerlund M, et al. SLC45A4 is a pain gene encoding a neuronal polyamine transporter. Nature 2025;646(8084):404–412.
17. Flescher E, Bowlin TL, Ballester A, et al. Increased polyamines may downregulate interleukin 2 production in rheumatoid arthritis. J Clin Invest 1989;83(4):1356–1362.
18. Wagner A, Wang C, Fessler J, et al. Metabolic modeling of single Th17 cells reveals regulators of autoimmunity. Cell 2021;184(16):4168–4185.e21.
19. Geng Z, Ming B, Hu S, et al. α-Difluoromethylornithine suppresses inflammatory arthritis by impairing myeloid-derived suppressor cells. Int Immunopharmacol 2019;71:251–258.
20. Rose DM, Sydlaske AD, Agha-Babakhani A, et al. Transglutaminase 2 limits murine peritoneal acute gout-like inflammation by regulating macrophage clearance of apoptotic neutrophils. Arthritis Rheum 2006;54(10):3363–3371.

21. Tang X, Peng Y, Jiang Z, et al. Efferocytosis and its role in rheumatic diseases. Arthritis Rheumatol 2025;77(12):1635–1650.
22. McCubbrey AL, McManus SA, McClendon JD, et al. Polyamine import and accumulation causes immunomodulation in macrophages engulfing apoptotic cells. Cell Rep 2022;38(2):110222.
23. Vazirpanah N, Ottria A, van der Linden M, et al. mTOR inhibition by metformin impacts monosodium urate crystal-induced inflammation and cell death in gout: a prelude to a new add-on therapy? Ann Rheum Dis 2019;78(5):663–671.
24. Schramm J, Sholler C, Menachery L, et al. Polyamine inhibition with DFMO: shifting the paradigm in neuroblastoma therapy. J Clin Med 2025;14(4):1068.
25. Senekowitsch S, Wietkamp E, Grimm M, et al. High-dose spermidine supplementation does not increase spermidine levels in blood plasma and saliva of healthy adults: a randomized placebo-controlled pharmacokinetic and metabolomic study. Nutrients 2023;15(8):1852.
26. Guma M, Dadpey B, Coras R, et al. Xanthine oxidase inhibitor urate-lowering therapy titration to target decreases serum free fatty acids in gout and suppresses lipolysis by adipocytes. Arthritis Res Ther 2022;24(1):175.
27. Silva MA, Klafke JZ, Rossato MF, et al. Role of peripheral polyamines in the development of inflammatory pain. Biochem Pharmacol 2011; 82(3):269–277.

Arthritis & Rheumatology
Vol. 78, No. 2, February 2026, pp 285–286
DOI 10.1002/art.43402

American College of Rheumatology
Empowering Rheumatology Professionals

EDITORIAL

Old Techniques Still Have Relevance in Personalized Predictive Medicine

Kristina E. N. Clark[1] and Christopher P. Denton[2]

As we advance toward personalized and precision medicine, it is essential that new tools are developed to predict outcome or response to treatment. This fuels interest in prognostic and predictive biomarkers. The hope of finding a robust and practical predictor of treatment response has long been the holy grail in many difficult-to-treat conditions, of which systemic sclerosis (SSc) is included. Lakin et al present here a potential immunohistochemical predictor of clinical trajectory and response to mycophenolate mofetil (MMF) in their paper published in this issue of *Arthritis & Rheumatology*.[1]

Although skin involvement is the hallmark of diffuse cutaneous SSc (dcSSc) and represents a major cause of morbidity and an unmet need,[2] to date, very few clinical studies have shown significantly greater improvement over placebo in skin disease in SSc, as measured by the modified Rodnan skin thickness score (MRSS). As a clinical tool, the MRSS itself carries drawbacks, given the high documented variability among different assessors, leading to an ongoing emphasis to find improved means of measuring disease response going forward. With the natural tendency of improvement in skin disease over time in both the placebo and treatment arm, this has resulted in many clinical trials failing to reach the required efficacy standard.[3–5] This is likely to be more of an issue in the future as background therapy with MMF, which appears to substantially enhance MRSS improvement, becomes permitted in clinical trials that reflect the current standard of care.[6] However, subgroup analyses have suggested specific patient groups who would have had a significant benefit had the trial correctly been enriched, be it with autoantibody subgroups, skin severity, or disease duration.[2]

With advancements in molecular and cellular research, newer insights into patient subgroups and cellular basis for disease are being uncovered. Milano et al[7] used bulk RNA sequencing of skin biopsies to subgroup patients with SSc into their molecular intrinsic subsets, namely fibroproliferative, inflammatory, limited, or normal like. Early-phase clinical trials have suggested that, for example, fibroproliferative groups were more likely to respond to dasatinib,[8] whereas the inflammatory subset showed greater response to MMF compared to the fibroproliferative group.[9] Single-cell analysis, especially by RNA sequencing platforms, has also provided insight into fibroblast subsets in SSc, not only by how the subsets differ by stage and autoantibody subset[10] but also highlighting different fibroblast subsets, with differing roles at different stages of disease.[11,12]

Despite these advances in technology, none have proven reliable enough to either enrich clinical trials or be used in clinical practice. Lakin et al highlight that more traditional readily available techniques such as immunohistochemistry do still have a place in SSc and benefit from the unique opportunity of relatively simple sampling of lesional tissue in SSc through forearm punch skin biopsy. Using fibroblast immunophenotyping of α-smooth muscle actin (α-SMA) and CD34, they have devised a score to predict patients more likely to respond to MMF for skin disease management.

α-SMA has itself been used previously to support treatment response to cyclophosphamide. Kissin et al used a semiquantitative scoring (visual ruling) to show that the extent of α-SMA staining was proportional to MRSS, and an improvement in MRSS during the study was reflected in a change in the α-SMA score.[13]

The authors report a disease duration of <18 months, high α-SMA, and high CD34 as being associated with an increased likelihood of improvement in skin fibrosis on MMF, whereas high α-SMA in >18 month disease duration is associated with lower chances of improvement. Although initial transcriptomic studies suggested the intrinsic subsets were stable, Skaug et al confirmed a trend of normalization over time in the intrinsic subsets of patients with early dcSSc.[14] Therefore, it may be that the reduced likelihood of responding to MMF over time reflects the change in the intrinsic subset when whole-tissue gene expression is examined, rather than being able to base it purely on α-SMA staining.

[1]Kennedy Institute of Rheumatology, University of Oxford, Oxford, United Kingdom; [2]Department for Connective Tissue Diseases, University College London, London, United Kingdom.

Author disclosures are available at https://onlinelibrary.wiley.com/doi/10.1002/art.43402.

Address correspondence via email to Kristina E. N. Clark, MRCP, PhD, at Kristina.clark@ndorms.ox.ac.uk.

Submitted for publication August 26, 2025; accepted in revised form August 27, 2025.

However, all the patients included were already taking a stable dose of MMF for at least eight weeks, with some patients not having a clear disease duration available. We, therefore, do not know whether this is also applicable to treatment naïve patients, as it is possible that levels of CD34 or α-SMA had already started changing following MMF initiation. The subgroup of α-SMA low and CD34 low were underrepresented in this study, so therefore, conclusions as how to best serve this subset remain unanswered.

This strategy does result in similar limitations to the MRSS, with the potential for interrater variability for this semiquantitative image analysis by a pathologist. More reliable techniques are still required, which may include percentage saturation to aid with reproducibility.

This study supports a potential accessible and relatively low-cost way to predict patients who are those more likely to respond to MMF. Those patients with minimal response to MMF, a disease duration longer than 18 months, and high α-SMA on skin biopsy can therefore be reassessed earlier and filtered into clinical trials, rather than remaining on a therapy with a potentially lower chance of improvement. The need for improved stratification in trials has never been greater. As Lakin et al highlight, given the 70% response rate to MMF, placebo-controlled trials would be unethical to not include background therapy. Therefore, it is important to enrich a study with those patients that are less likely to improve on MMF to ensure that the true benefit of any test compound is fully assessed.

With an emerging repertoire of second-line therapies for skin disease included in recent consensus treatment guidelines and recommendations[15,16] and further clinical trials on the horizon, this study emphasizes the importance of specialist care early in the disease course of patients with SSc. With an increasing landscape of potential treatment options, identifying tools to help us stratify patients to differing treatments is key, and this study begins to emphasize histologic tools for predicting response to MMF and may prove invaluable for personalized medicine approaches in the future.

AUTHOR CONTRIBUTIONS

All authors contributed to at least one of the following manuscript preparation roles: conceptualization AND/OR methodology, software, investigation, formal analysis, data curation, visualization, and validation AND drafting or reviewing/editing the final draft. As corresponding author, Dr Clark confirms that all authors have provided the final approval of the version to be published, and takes responsibility for the affirmations regarding article submission (eg, not under consideration by another journal), the integrity of the data presented, and the statements regarding compliance with institutional review board/Declaration of Helsinki requirements.

REFERENCES

1. Lakin KS, Spivack J, Gordon JK, et al. Skin biopsies enhance prediction of clinical trajectory in diffuse cutaneous systemic sclerosis. Arthritis Rheumatol 2026;78(2):418–427.
2. Herrick AL, Assassi S, Denton CP. Skin involvement in early diffuse cutaneous systemic sclerosis: an unmet clinical need. Nat Rev Rheumatol 2022;18(5):276–285.
3. Khanna D, Allanore Y, Denton CP, et al. Riociguat in patients with early diffuse cutaneous systemic sclerosis (RISE-SSc): randomised, double-blind, placebo-controlled multicentre trial. Ann Rheum Dis 2020;79(5):618–625.
4. Khanna D, Denton CP, Jahreis A, et al. Safety and efficacy of subcutaneous tocilizumab in adults with systemic sclerosis (faSScinate): a phase 2, randomised, controlled trial. Lancet 2016;387(10038): 2630–2640.
5. Khanna D, Spino C, Johnson S, et al. Abatacept in early diffuse cutaneous systemic sclerosis: results of a phase ii investigator-initiated, multicenter, double-blind, randomized, placebo-controlled trial. Arthritis Rheumatol 2020;72(1):125–136.
6. White B, Furst DE, Frech TM, et al; RESOLVE-1 investigators. Comparative efficacy of immunosuppressive therapies in the treatment of diffuse cutaneous systemic sclerosis. ACR Open Rheumatol 2025; 7(3):e70004.
7. Milano A, Pendergrass SA, Sargent JL, et al. Molecular subsets in the gene expression signatures of scleroderma skin. PLoS One 2008;3 (7):e2696. https://doi.org/10.1371/journal.pone.0002696.
8. Martyanov V, Kim GJ, Hayes W, et al. Novel lung imaging biomarkers and skin gene expression subsetting in dasatinib treatment of systemic sclerosis-associated interstitial lung disease. PLoS One 2017; 12(11):e0187580.
9. Hinchcliff M, Huang CC, Wood TA, et al. Molecular signatures in skin associated with clinical improvement during mycophenolate treatment in systemic sclerosis. J Invest Dermatol 2013;133(8):1979–1989.
10. Clark KEN, Xu S, Attah M, et al. Single-cell analysis reveals key differences between early-stage and late-stage systemic sclerosis skin across autoantibody subgroups. Ann Rheum Dis 2023;82(12):1568–1579.
11. Clark KEN, Xu S, Attar M, et al. Characterization of a pathogenic non-migratory fibroblast population in systemic sclerosis skin. JCI Insight 2025;10(10):e185618.
12. Tabib T, Huang M, Morse N, et al. Myofibroblast transcriptome indicates $SFRP2^{hi}$ fibroblast progenitors in systemic sclerosis skin. Nat Commun 2021;12(1):4384.
13. Kissin EY, Merkel PA, Lafyatis R. Myofibroblasts and hyalinized collagen as markers of skin disease in systemic sclerosis. Arthritis Rheum 2006;54(11):3655–3660.
14. Skaug B, Lyons MA, Swindell WR, et al. Large-scale analysis of longitudinal skin gene expression in systemic sclerosis reveals relationships of immune cell and fibroblast activity with skin thickness and a trend towards normalisation over time. Ann Rheum Dis 2022;81(4):516–523.
15. Denton CP, Lorenzis ED, Roblin E, et al. The 2024 British Society for Rheumatology guideline for management of systemic sclerosis—executive summary. Rheumatology 2024;63(11):2948–2955. https://doi.org/10.1093/rheumatology/keae390.
16. Del Galdo F, Lescoat A, Conaghan PG, et al. EULAR recommendations for the treatment of systemic sclerosis: 2023 update. Ann Rheum Dis 2025;84(1):29–40.

Arthritis & Rheumatology
Vol. 78, No. 2, February 2026, pp 287–297
DOI 10.1002/art.43242

American College of Rheumatology
Empowering Rheumatology Professionals

REVIEW

Mucosal-Associated Invariant T Cells in Rheumatic Diseases

Manon Lesturgie-Talarek,[1] Virginie Gonzalez,[1] Lucie Beaudoin,[1] Noémie Sénot,[1] Corinne Miceli-Richard,[2] Yannick Allanore,[3] Agnès Lehuen,[1] and Jerôme Avouac[3]

Mucosal-associated invariant T (MAIT) cells are innate-like T cells defined by their semi-invariant T cell receptor and restriction by the major histocompatibility complex class I–related molecule (MR1). These cells are primarily activated by microbial-derived metabolites presented by MR1 or by cytokines. Upon activation, MAIT cells rapidly produce pro-inflammatory cytokines, including interferon-γ, tumor necrosis factor α, and interleukin-17, and secrete cytotoxic molecules, such as granzyme B. Because of their ability to interact with microbiota and accumulate in inflamed tissues, MAIT cells have attracted great interest in autoimmune and inflammatory diseases. In this review, we summarize recent findings on MAIT cells in major rheumatic diseases, including rheumatoid arthritis (RA), spondyloarthritis (SpA), psoriatic arthritis (PsA), systemic lupus erythematosus, systemic sclerosis, primary Sjögren disease (pSD), and dermatomyositis. Circulating MAIT cell frequency is reduced in these diseases. Interestingly, the residual MAIT cells exhibit an activated profile and increased cytokine-producing capacity in some conditions. Moreover, an enrichment of MAIT cells in inflamed tissues is described in RA, SpA, PsA, and pSD. This pattern suggests that MAIT cells may migrate from circulation to inflamed tissues, contributing to local immune responses. Furthermore, they have been shown to play a critical role in disease progression in two mouse models. All these findings suggest an involvement of MAIT cells in inflammatory rheumatologic diseases and their potential therapeutic target.

Introduction

Autoimmune and inflammatory rheumatic conditions encompass a broad spectrum of disorders, such as rheumatoid arthritis (RA), spondyloarthritis (SpA), psoriatic arthritis (PsA), systemic lupus erythematosus (SLE), systemic sclerosis (SSc), primary Sjögren disease (pSD) and dermatomyositis (DM). Mucosal-associated invariant T (MAIT) cells, a type of innate-like T cells, are abundant in mucosal tissues. Their ability to interact with gut microbiota[1,2] and accumulate in inflamed tissues[3] suggests that they may play a role in the interplay between microbiota, inflammation, and autoimmune diseases.

Human MAIT cells express a T cell receptor (TCR) α chain, Vα7.2-Jα33, in association with a limited set of β chains,[4–6] mainly Vβ2 and Vβ13. MAIT cells are restricted by the major histocompatibility complex (MHC) class I–related molecule (MR1), which presents riboflavin metabolites derived from bacteria and yeast. Despite their conserved TCR specificity for these ligands, MAIT cells exhibit diverse functional characteristics, including Th1/Th17 cytokine secretion and cytotoxicity.[7–9]

In this review, we will initially outline the development, phenotype, activation, and functions of MAIT cells. Subsequently, we will delve into the current understanding of MAIT cells in rheumatic diseases. To these ends, we searched the following terms on PubMed: "autoimmune diseases OR rheumatic diseases OR arthritis OR rheumatoid arthritis OR spondyloarthritis OR ankylosing spondylitis OR psoriatic arthritis OR Sjogren's syndrome OR systemic lupus erythematosus OR dermatomyositis OR systemic sclerosis AND Mucosal-associated invariant T cells." We found 140 references, and we selected 22 for the purpose of this review after the reading of the abstract and/or the full text.

MAIT cell development. In contrast to conventional T cells, which undergo selection on epithelial cells, MAIT cells undergo selection on $CD4^+$ $CD8^+$ thymocytes that highly express MR1.[10–12] Although they exit the thymus as naive cells, MAIT cells already exhibit a distinct differentiation program in both the

[1]Manon Lesturgie-Talarek, MD, Virginie Gonzalez, BSc, Lucie Beaudoin, MSc, Noémie Sénot, MD, Agnès Lehuen, PhD: Institut Cochin, INSERM U1016, UMR 8104, Paris, France; [2]Corinne Miceli-Richard, MD, PhD: Rheumatology Department, Cochin Hospital, AP-HP, Université Paris Cité, Paris, France; [3]Yannick Allanore, MD, PhD, Jerôme Avouac, MD, PhD: Institut Cochin, INSERM U1016, UMR 8104 and Rheumatology Department, Cochin Hospital, AP-HP, Université Paris Cité, Paris, France.

Author disclosures are available at https://onlinelibrary.wiley.com/doi/10.1002/art.43242.

Address correspondence via email to Jerôme Avouac, MD, PhD, at jerome.avouac@aphp.fr or javouac@me.com.

Submitted for publication December 22, 2024; accepted in revised form May 5, 2025.

thymus and cord blood.[12] This is highlighted by the expression of promyelocytic leukemia zinc finger,[13,14] which imparts innate-like functionality, as well as the expression of the retinoic acid receptor–related orphan nuclear receptor γt (RORγt) transcription factor,[12] along with CD161 and interleukin-18 receptor α (IL-18Rα).[15]

Consequently, upon leaving the thymus, MAIT cells are already programmed in a way that influences their development and function in peripheral tissues. Their expansion in the periphery depends on commensal flora, as germ-free mice harbor only small numbers of mature MAIT cells in the thymus.[4,12] Following development during fetal life and expansion after birth, human MAIT cells acquire a homogenous phenotype by the age of two to four years, before gradually declining in older adults.[16] It is noteworthy that, at the same age, the proportion of circulating MAIT cells is higher in women than men.[16]

MAIT cell phenotype. A distinct developmental pathway in the thymus during fetal life results in the acquisition of unique phenotypic and functional properties of MAIT cells.[17] Until recently, MAIT cells were identified by surface markers CD3, TCR Vα7.2, and CD161.[5] TCR Vα7.2$^+$ CD161$^-$ T cells exhibit a very different gene expression pattern compared to MAIT cells but almost similar to that of TCR Vα7.2$^-$ conventional T cells.[18] In tissues, the accuracy of these cell surface combinations in defining MAIT cells remains uncertain.[5] A significant breakthrough in MAIT cell research has come with the development of MR1 tetramers loaded with 5-OP-RU, which has enabled new investigations and direct evaluation of the efficacy of surrogate phenotypes for analyzing MAIT cells in humans.[7,19]

The majority of circulating MAIT cells are CD8$^+$ (around 70%), whereas a smaller proportion are double negative (CD4$^-$ CD8$^-$), comprising about 10% to 15% of the total population. There are no apparent functional or phenotypic differences between these subsets.[20] A small fraction of MAIT cells are CD4$^+$, although their role remains unclear.[14]

Circulating MAIT cells exhibit a memory phenotype (CD45RO$^+$, CD45RA$^-$, CD27$^+$, IL2Rβ$^+$)[5] but remain noncycling, as indicated by the absence of Ki-67.[21] They also display an effector phenotype (CD95$^+$ CD62L$^-$) and express chemokine receptors (CCR6, CXCR6, CCR5, CCR2) that suggest efficient tissue homing.[5] This aligns with their distribution: 10% to 35% of T cells in the liver, 1.5% to 4% in the intestine, 4% in the lungs, and 0.1% to 10% in the blood.[2,5,22] High expression of these receptors may facilitate their migration to inflamed sites.[3,23]

MAIT cells also show heterogeneous CD56 expression, a marker linked to natural killer cells. CD56$^+$ MAIT cells appear more responsive to innate cytokines, suggesting efficient MR1-independent activation.[24,25] Finally, MAIT cells have a proapoptotic profile (with increased susceptibility to apoptosis in vitro) marked by higher active caspase levels compared to other T cells.[26]

MAIT cell activation and function. The context of stimulation and/or avidity of the TCR influences the acquisition of specific phenotypes and functional features.[15,27] MAIT cells share characteristics of both Th1 and Th17 features[6,21] and exhibit cytotoxic capabilities.[9] They produce high levels of granzyme B and tumor necrosis factor α (TNFα), similarly to CD8 and CD4 memory T cells. They produce lower levels of interferon-γ (IFNγ), IL-2, and IL-17 than CD4 T cells after CD3/CD28 stimulation but similar levels following phorbol myristic acetate (PMA) and ionomycin stimulation.[21]

TCR-dependent activation. Although pathogen-derived peptides are presented by molecules from the MHC to conventional T cells, MR1 presents microbial antigens to MAIT cells.[15] MR1 is mainly intracellular and, similar to MHC molecules, requires ligands as well as β_2-microglobulin for proper refolding. Vitamin B_2–derived metabolites, upon association with glyoxal or methylglyoxal, are the main agonist molecules presented by MR1, whereas vitamin B_9–derived metabolites constitute nonagonist MR1-presented ligands.[8,11,28] There are likely other MR1-binding antigens that could potentially connect MAIT cells to autoimmunity.[3,22] For instance, certain cells such as human B cells express MR1 on their cell surface even without microbial antigens.[5]

TCR stimulation up-regulates CD25/CD69 and induces TNFα, IFNγ, and IL-22 secretion while only low levels of Th2 cytokines are produced.[5,21] Despite IL-23R and RORγt expression, stimulation with infected antigen-presenting cells or CD3/CD28 alone does not results in IL-17 production. This is in contrast to PMA/ionomycin stimulation, indicating that signals other than TCR triggering are necessary for IL-17 production.[21,29] Interestingly, in contrast to memory CD8 T cells, MAIT cells express high levels of IL-18Rα, IL-12β2, IFNγ receptor 1, and IL-7Rα,[22] which may regulate MAIT cell effector activities. Indeed, CD3/CD28 stimulation with IL-7 or IL-1β increases IL-17 production, whereas IL-18 and/or IL-23 are not sufficient.[15] Nevertheless, combined stimulation by CD3/CD28 with IL-7 and/or IL-18 is capable of inducing high levels of IL-17F.[30] MAIT cells also exhibit cytotoxicity, secreting granzyme B after CD3/CD28 stimulation.[21]

TCR-independent activation. MAIT cells can also be activated directly by cytokines.[31] Toll-like receptor ligands induce MAIT cell activation through IL-12 and IL-18 produced by monocytes, leading to increased secretion of IFNγ and granzyme B.[5,31] Cytokine-dependent activation of MAIT cells seems to require a synergistic combination of cytokines rather than the action of a single cytokine.[5]

MAIT cells in rheumatologic diseases

MAIT cells have received significant attention in the context of autoimmune diseases, as many studies indicate their role in the development of immune-related disorders.[3,32] In this review, we focus on MAIT cells in prominent rheumatic diseases. Despite the diverse nature of autoimmune and inflammatory disorders, these diseases commonly involve both innate and adaptive immune systems, with a key role of T cells[33] and IL-17 secreting cells.[34–38] In these autoimmune and inflammatory diseases, dysbiosis contributes to the disruption of immune homeostasis and exacerbation of inflammation.[39,40] Therefore, MAIT cells may contribute to pathogenesis by interacting with the microbiota and producing Th1/Th17 cytokines.

Circulating MAIT cell frequency, phenotype, and function. *Circulating MAIT cell deficiency.* Circulating MAIT cells are decreased in RA,[41–43] axial spondyloarthritis (axSpA),[43–46] PsA,[42,47] SLE,[41,48–51] SSc,[52–54] primary Sjögren disease (pSD),[55–59] and DM[49] (Table 1, Figure 1). In healthy donors, the majority of MAIT cells in the blood consisted of $CD8^+$ and double-negative subsets. In RA[41,43] and SLE,[41] the deficiency of circulating MAIT cells affects these two subsets. In SLE,[49], pSD,[55,57,59] and DM,[49] the predominant residual MAIT cells are mainly of the $CD4^+$ subtype. Because $CD4^+$ MAIT cells express lower levels of IL-12R and IL-18R,[60] the elevated production of IL-12 and IL-18 in DM may preferentially activate $CD8^+$ MAIT cells, leading to activation-induced cell death.[49]

Various studies have reported conflicting findings regarding the frequency of circulating MAIT cells in patients with rheumatic diseases. In axSpA, van der Meer et al[61] found no reduction in the frequency of MAIT cells but only a decrease in the numbers of central memory MAIT cells ($CD45RO^+$ $CCR7^+$). In patients with early untreated RA, Koppejan et al[62] did not observe alteration of MAIT cell frequency when using MR1 tetramer identification, in contrast to previous studies that relied on TCR $V\alpha7.2^+$ and $CD161^{high}$ labeling. However, they observed a shift of $CD8^+$ MAIT cells toward $CD4^+$ MAIT cells.[62]

Circulating MAIT cell phenotype. Activated profile. MAIT cells exhibit an activated profile in SLE,[48,49] SSc,[54] pSD,[59] SpA,[46] and DM,[49] highlighted by their increased expression of $CD69^+$ and/or $CD25^+$ (Table 1, Figure 1). In DM, a negative correlation between MAIT cell frequency and the late activation marker $CD25^+$ has also been described.[49]

Chiba et al[48] suggested two potential mechanisms of MAIT cell activation in SLE: heightened activating capability of monocytes derived from patients with SLE and activation triggered by inflammatory cytokines in the absence of exogenous antigens. Direct contact with monocytes appears to play a role in sustaining chronic activation, whereas during intense inflammation, cytokines such as IL-6, IL-18, and IFNα may contribute to the excessive activation of MAIT cells. This is indicated by the correlation between plasma levels of these cytokines and CD69 expression on MAIT cells.

Exhaustive and apoptotic profile. In patients with SLE and DM, MAIT cells exhibit an exhaustive or even proapoptotic profile. In patients with SLE, an increase expression of PD1, CD39, and CTLA4, as well as apoptosis markers such as caspase 3 and Fas ligand, is observed[48] (Table 1, Figure 1). In DM, an increase of $CD39^+$ and $CTLA4^+$ MAIT cells, along with the $CD45RA^{high}$ $CD28^-$ subtype, associated with cellular senescence has been described.[49] Similarly, in pSD, increased MAIT cell mortality is highlighted by 7-aminoactinomycin D staining.[59] In SSc, transcriptomic data highlight overexpression of inhibitory receptors such as PD1, TIGIT, and LAG3.[53] Interestingly, although MAIT cells exhibit an exhaustive or apoptotic profile in these diseases, an increase in $Ki67^+$ MAIT cells in lupus nephritis may reflect a compensatory mechanism for their deficiency.[50] By contrast, in RA and SpA, MAIT cells show no significant increase in PD1 or apoptosis markers, suggesting other factors contribute to their deficiency.[41,44]

Circulating MAIT cell function. Th17 secretion. Following stimulation (CD3, CD28, recombinant IL-23, PMA/ionomycin), circulating MAIT cells produce significantly more IL-17A in RA and PsA compared to osteoarthritis[42] (Table 1, Figure 1). This increase correlates with IL-23R up-regulation on MAIT cells in RA and PsA, which is functionally active, as evidenced by a strong mitotic effect in the presence of recombinant IL-23.[42] In individuals with lupus nephritis, following stimulation by PMA/ionomycin, circulating MAIT cells produce more IL-17 compared to controls, especially in proliferative lupus nephritis[50] (Table 1, Figure 1).

In axSpA, MAIT cells are the main IL-17A producers after stimulation by PMA/ionomycin, along with increased IL-22 secretion[43–45] (Table 1). Because the increase of IL-17 production by MAIT cells was not MR1 dependent,[43] Gracey et al focused on MAIT cell cytokine priming. IL-17 production is IL-23 independent but is driven by IL-7R up-regulation and IL-7 stimulation.[43] In addition, at the transcriptomic levels, Rosine et al[30] observed an up-regulation of IL-18R1 and IL-18R accessory protein in MAIT cells of patients with axSpA compared to other T cells subtypes. Stimulation with IL-7 and IL-18 induced high transcript levels of IL-17F in MAIT cells in axSpA.[30] The ability to produce IL-17F is particularly interesting because it is targeted by bimekizumab in axSpA.[63] The independence of MAIT cells from IL-23 to secrete IL-17 may explain the limited efficacy of IL-23 blockade in axSpA.[64,65]

In pSD, $CD8^+$ MAIT cells show higher IL-7R expression compared to conventional $CD8^+$ T cells, with this increase correlating to lymphocytic focus scores, the percentage of IgA^+ plasma cells in salivary gland tissue, and serum IgG levels.[57] This suggests that, as in axSpA, IL-7R up-regulation may contribute to MAIT cell activation and potentially promote IL-17 secretion in pSD.

Th1 secretion. As described in other autoimmune diseases,[32] following stimulation with PMA/ionomycin, MAIT cells

Table 1. MAIT cells in rheumatic diseases*

Disease	MAIT cells in peripheral blood	MAIT cells in tissues	Main characteristics related to the disease	Functional studies	Refs
Rheumatoid arthritis	Reduced frequency ($CD8^+$ and DN) Increased migration capacity (↑ CCR6 MFI) ↓ $IFN\gamma^+$ and $TNF\alpha^+$ MAIT cells ↑ $IL\text{-}17A^+$ MAIT cells Up-regulation of IL-23R	Enrichment in synovial fluid compared to blood (matched pairs) and OA Activated profile (↑ $CD69^+$ MAIT cells compared to blood) ↑ $IL\text{-}17A^+$ MAIT cells compared to OA ↑ sLeX MAIT cells compared to blood Up-regulation of IL-23R Detection in synovial biopsy samples (knee)	Absolute number of circulating MAIT cells inversely correlated with Disease Activity Score	Promotion and exacerbation of arthritis in murine models	41–43,62,66,71
Axial spondyloarthritis	Reduced frequency ↑ $IL\text{-}7R^+$ and $IL\text{-}18R^+$ MAIT cells compared to other cells ↑ $IL\text{-}17^+$ and $IL\text{-}22^+$ MAIT cells ↓ $IFN\gamma^+$ MAIT cells IL-17A and IL-17F production on IL-7 and/or IL-18 stimulation	Enrichment in synovial fluid compared to blood Activated profile (↑ $CD69^+$ MAIT cells compared to blood) Decreased migration capacity (↓ $CCR6^+$ MFI compared to blood) ↑ $IL\text{-}17^+$ and GrB^+ MAIT cells compared to blood ↓ $IFN\gamma^+$ and $TNF\alpha^+$ MAIT cells Detection in synovial biopsy samples (knee)	MFI of $CD69^+$ MAIT cells correlated with ASDAS No effect of anti-TNFα or other current therapy	–	30,43–45,61,62
Psoriatic arthritis	Reduced frequency ↑ $IL\text{-}17A^+$ MAIT cells compared to OA Up-regulation of IL-23R Proliferation on IL-23 stimulation	Enrichment in synovial fluid compared to OA (mainly $CD8^+$ MAIT cells) Effector memory phenotype ↑ $IL\text{-}17A^+$ MAIT cells compared to OA Up-regulation of IL-23R Proliferation on IL-23 stimulation	–	–	36
SLE	Reduced frequency ($CD8^+$ and DN) ↑ $CD4^+/CD8^+$ ratio MAIT cells Activated profile (↑$CD69^+$ MAIT cells in active SLE and ↑ $CD25^+$ MAIT cells) Exhaustion profile (↑$PD1^+$, $CD39^+$, and $CTLA4^+$ MAIT cells) ↑ apoptosis (↑ caspase 3^+ and Fas^+ MAIT cells) ↑ $IL\text{-}17^+$ and $IL\text{-}2^+$ MAIT cells ↓ $IFN\gamma^+$ MAIT cells	Detection of MAIT cells in kidneys (lupus nephritis with class III and IV disease)	Absolute number of circulating MAIT cells inversely correlated with SLEDAI % $CD69^+$ MAIT cells correlated with SLEDAI Higher proportion of MAIT cells and decreased proliferation and production of GrB at inclusion in patients with complete remission	Exacerbation of autoantibody production and severity of lupus nephritis in murine models Direct interaction with B cells	41,48,49,67
pSD	Reduced frequency ↑ $CD4^+$ MAIT cells Activated profile (↑$CD69^+$ MAIT cells) ↑ Cell death (staining 7-AAD) Increased migration capacity (↑ $CXCR5^+$ and $CCR9^+$ MAIT cells) ↑ $IL\text{-}7R^+$ MAIT cells compared to $CD8^+$ cells	Enrichment in salivary gland mononuclear cells compared to HD Mainly $CD8^+$, no $CD4^+$ MAIT cells ↑ $IL17^+$ MAIT cells compared to HD ↑ $IL17^+$ MAIT cells on IL-7 and IL-23 stimulation ↑ $RORc^+$ MAIT cells on IL-23 stimulation	–	–	55–59

(Continued)

Table 1. (*Cont'd*)

Disease	MAIT cells in peripheral blood	MAIT cells in tissues	Main characteristics related to the disease	Functional studies	Refs
	↓↑ MAIT TNFα$^+$ and IFNγ$^+$ compared to HD ↑ MAIT GrB$^+$ compared to HD	↑ STAT3$^+$ and HIF1α$^+$ MAIT cells on IL-7 stimulation Detection of salivary gland tissue			
SSc	Reduced frequency Activated profile (↑ CD69$^+$ MAIT cells) Exhaustive profile	–	Blood MAIT cell deficiency even lower in patients with ILD Blood MAIT cells negatively correlated with DLCO and FVC Blood CCR6$^+$ MAIT cells negatively correlated with ILD extension (% ILD) Blood CCR6$^+$ MAIT cells correlated with MAIT cell frequency in SSc-ILD	–	52–54
Dermatomyositis	Reduced frequency ↑ CD4$^+$/CD8$^+$ ratio MAIT cells ↓ CD26$^+$ CD161$^+$ MAIT cells Activated profile (↑ CD25$^+$ MAIT cells) Exhaustion profile (↑ CD39$^+$, CTLA4$^+$, and CD45RA^{high}CD28$^-$ MAIT cells) MAIT cell frequency inversely correlated with CD25 and CTLA4	–	↑ frequency after treatment without return to normal frequency	–	49

* 7-AAD, 7-aminoactinomycin D; ASDAS, Ankylosing Spondylitis Disease Activity Score; DLCO, capacity of carbon monoxide; DN, double negative; FVC, forced vital capacity; GrB, granzyme B; HD, healthy donors; HIF1α, hypoxia-inducible factor 1α; IFNγ, interferon-γ; IL, interleukin; IL-23R, IL-23 receptor; ILD, interstitial lung disease; MAIT, mucosal-associated invariant T; MFI, mean fluorescence intensity; OA, osteoarthritis; pSD, primary Sjögren disease; ROR, retinoic acid receptor–related orphan nuclear receptor; SLE, systemic lupus erythematosus; SLEDAI, Systemic Lupus Erythematosus Disease Activity Index; sLeX, sialyl-Lewis^X; SSc, systemic sclerosis; TNFα, tumor necrosis factor α.

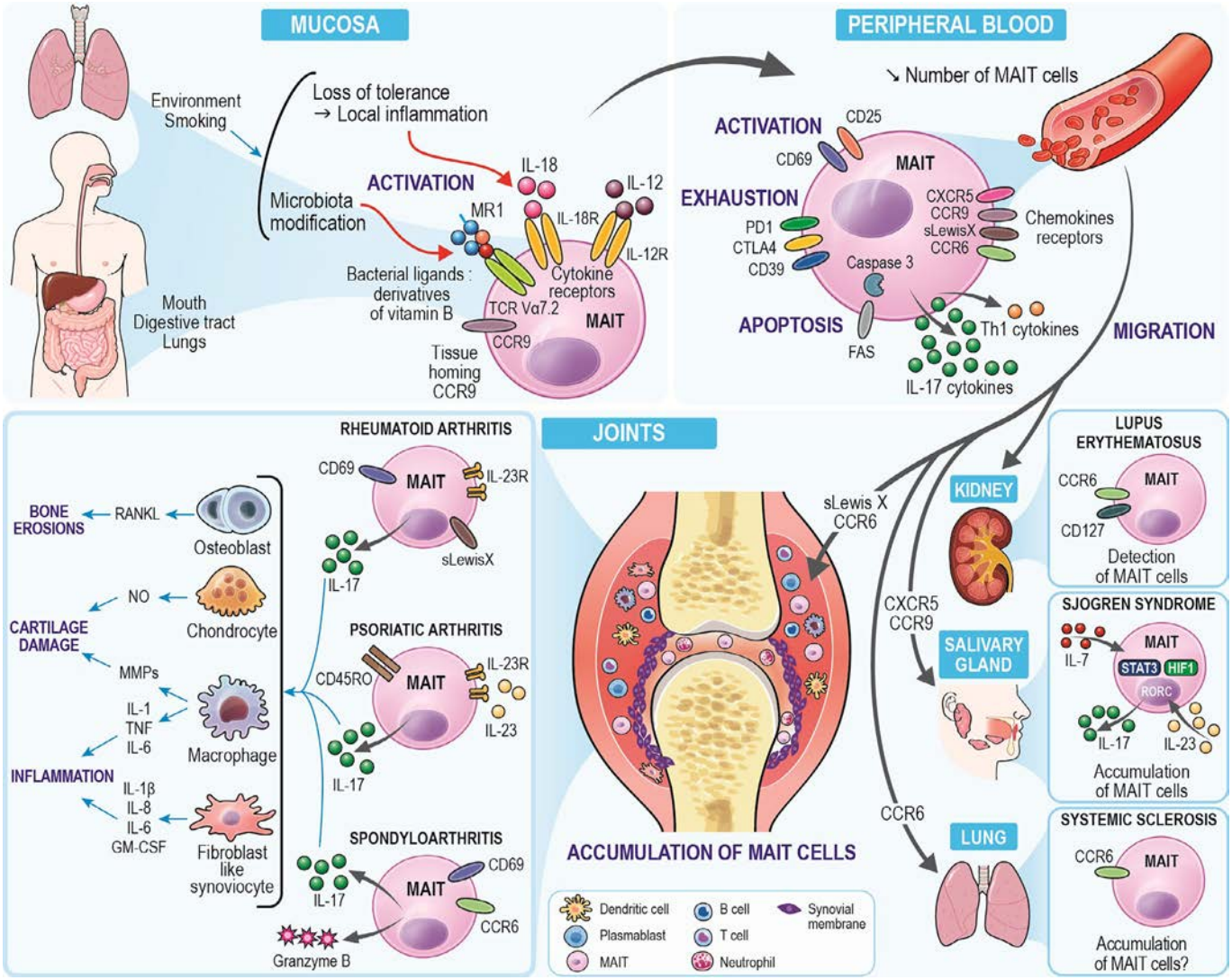

Figure 1. MAIT cells in rheumatologic disorders. MAIT cells are abundant in mucosal tissues, allowing them to interact with the microbiota. They can be activated through various means: either by TCR engagement, in which vitamin B derivatives are presented by MR1, or through cytokines such as IL-12 and IL-18. Changes in the microbiota could alter these bacterial ligands, contributing to the creation of a proinflammatory setting, ultimately triggering MAIT cell activation. The frequency of MAIT cells is decreased in all diseases studied in this review. MAIT cells exhibit an activated profile in SLE (CD69, CD25), SSc (CD69), and DM (CD25) and an exhaustive and/or apoptotic profile in SLE (CD39, CTLA4, PD1, FAS, caspase 3) and DM (CD29, CTL14). They produce higher levels of Th17 cytokines in RA, SpA, and PsA and reduced levels of Th1 cytokines in RA, SpA, SLE, and pSD. One hypothesis is the migration of circulating MAIT cells into inflamed tissues. Circulating MAIT cells in RA, SpA, and PsA could migrate into the joints. In RA, CCR6 and sLewis^X expression may facilitate the migration of these cells into the joint, where they accumulate and secrete IL-17. They also accumulate in SpA and PsA, in which they produce higher levels of IL-17 and/or granzyme B (in SpA). MAIT cells are also detected in the kidneys of patients with lupus nephritis and play a pathogenic role in lupus nephritis in mouse models. In pSD, MAIT cells, which strongly express CXCR5 and CCR9, can migrate into the salivary glands, where they accumulate and produce high levels of IL-17. The presence and function of MAIT cells in the lungs of patients with SSc remain to be elucidated. DM, dermatomyositis; GM-CSF, granulocyte–macrophage colony-stimulating factor; IL, interleukin; MAIT, mucosal-associated invariant T; MMP, matrix metalloproteinase; MR1, major histocompatibility complex class I–related molecule; NO, nitric oxide; PsA, psoriatic arthritis; pSD, primary Sjögren disease; RA, rheumatoid arthritis; SLE, systemic lupus erythematosus; sLewis^X, sialyl-Lewis^X; SpA, spondyloarthritis; SSc, systemic sclerosis; TCR, T cell receptor; TNF, tumor necrosis factor.

produce fewer Th1 cytokines in individuals with RA, SpA, and SLE compared to healthy donors. Specifically, IFNγ and TNFα secretion is reduced in RA,[43] whereas only IFNγ secretion decreases in SLE[41] and SpA[43] (Table 1, Figure 1). In SLE, this reduction in IFNγ levels could be due to intrinsic dysregulation of the NFAT1 transcription factor.[41] Conversely, increased IL-2 production by MAIT cells has been observed in lupus nephritis, particularly in proliferative forms.[50] The Th1 cytokine profile in pSD remains unclear, with some studies reporting decreased levels of IFNγ and TNFα,[55] whereas others have observed increased

expression of these cytokines in patients compared to healthy controls.[59]

Th2 secretion. In patients with lupus nephritis, circulating MAIT cells exhibit an increased production of IL-4 compared to in controls,[50] especially in proliferative nephritis (Table 1).

Cytotoxicity. Data on circulating MAIT cell cytotoxicity are limited. van der Meer et al[61] reported reduced granzyme A production in circulating MAIT cells in individuals with axSpA compared to controls (Table 1, Figure 1). However, this reduction in granzyme A production does not necessarily indicate a reduction in cytotoxicity; it may also reflect cellular maturation or the degree of activation of cytotoxic cells. In individuals with lupus nephritis and pSD, MAIT cells are cytotoxic, as evidenced by increased production of granzyme B, compared to healthy donors.[50,59] Therefore, in the peripheral blood, there is a reduction in MAIT cell frequency, and the residual MAIT cells display an activated and/or exhausted profile. Upon stimulation, they adopt a Th17-like profile and produce lower levels of Th1 cytokines.

Association between circulating MAIT cell phenotype and clinical data. Circulating MAIT cells as a marker of disease activity and severity. Several studies have demonstrated association between circulating MAIT cell counts and clinical characteristics. MAIT cell counts correlate with disease activity in RA (Disease Activity Score in 28 joints) and SLE (Systemic Lupus Erythematosus Disease Activity Index [SLEDAI]),[41] whereas their frequency correlate with the disease activity score in SpA (Ankylosing Spondylitis Disease Activity Score [ASDAS] with C-reactive protein)[46] (Table 1). In SpA[44,46] and SLE,[48,50] higher disease activity scores (ASDAS and SLEDAI, respectively) are associated with an increased proportion of $CD69^+$ MAIT cells. However, although MAIT cells are reduced in patients with lupus nephritis compared to controls, their frequency does not differ between active and nonactive lupus nephritis. In axSpA, adding the frequency of $CD69^+$ MAIT cells to T1 sacroiliac magnetic resonance imaging mapping significantly enhances disease activity assessment,[46] highlighting activated MAIT cells as potential biomarkers. In SSc, MAIT cell frequency is reduced in interstitial lung disease (ILD),[53,54] with a stronger reduction in patients with severe ILD with reduced forced vital capacity or reduced diffusing capacity for carbon monoxide.[54]

Treatment impact on MAIT cell profile. An important question arises regarding whether the previous observations on MAIT cell quantitative and qualitative characteristics (deficiency and altered phenotype of MAIT cells) may be affected upon immunomodulatory therapies. In axSpA, deficiency and altered phenotype of circulating MAIT cells do not appear to be affected by current therapy. Indeed, Hayashi et al[44] did not find any differences in MAIT cell frequency and alteration between patients with and without anti-TNFα therapy. Similarly, in SSc, deficiency of circulating MAIT cells is not influenced by current biologic treatment or conventional synthetic immunosuppression after adjustment for ILD.[54] The impact of treatment in a longitudinal trial has only been studied in DM, in which MAIT cells were reduced in patients with active DM compared to controls. Following DM treatment, MAIT cell levels increased but did not return to normal control frequencies,[49]

In pSD, Hinrichs et al demonstrated, using an ex vivo culture, that IL-7–stimulated MAIT cells exhibit reduced IL-21 production, without affecting IFNγ, when treated with leflunomide and/or hydroxychloroquine. These results suggest that the activity of the remaining MAIT cells could be targeted by disease-modifying antirheumatic drug treatment, such as leflunomide and/or hydroxychloroquine.[57] Further studies are required to evaluate the correlation between the MAIT cell profile and patients' response to treatments. Some alterations in the MAIT cell profile may therefore serve as biomarkers of treatment response.

Beyond their alteration under treatment, another crucial question arises: could MAIT cells serve as predictors of clinical response to immunomodulatory therapies? In SLE, patients achieving complete renal remission after immunosuppressive therapy initially exhibited a higher proportion of MAIT cells with reduced proliferation (Ki67) and cytotoxicity (granzyme B production) at inclusion.[50] Consequently, granzyme B production may serve as a defining factor in a predictive model for complete remission.

MAIT cells in inflamed tissues. Although data on MAIT cells in inflammatory rheumatic diseases remain limited, accumulating evidence suggests their enrichment in inflammatory fluids and their presence in target tissues.

Tissue localization of MAIT cells. Despite the limited number of studies on synovial fluid, evidence suggests an increased frequency of MAIT cells compared to peripheral blood in RA[41,66] and SpA.[43] Additionally, an accumulation of MAIT cells in synovial fluid of patients with RA and PsA has been reported in comparison to osteoarthritis,[42] without association with the patient's disease severity (Table 1, Figure 1). Beyond their enrichment in synovial fluid, MAIT cells have also been identified by immunofluorescence in synovial biopsy samples from patients with RA and SpA, characterized by $CD3^+$, TCR $V\alpha7.2^+$, and $CD161^+$ expression.[62]

In patients with pSD, MAIT cells were enriched among salivary gland mononuclear cells compared to patients with non-pSD sicca and patients with mild sialadenitis[56] or healthy donors.[59] These cells are predominantly $CD8^+$, with a smaller proportion exhibiting a double-negative phenotype, whereas $CD4^+$ MAIT cells are absent.[59] Immunohistochemistry analysis further confirmed the presence of MAIT cells (TCR $V\alpha7.2^+$ cells) in salivary gland tissue, whereas they were not detected in controls[55,59] (Figure 1). In SLE, MAIT cells ($CD3^+$, TCR $V\alpha7.2^+$, $IL18R^+$ cells) have been observed in renal tissue (Figure 1), specifically in glomeruli and the tubulointerstitium of patients with class III and IV lupus nephritis, where they represent a high proportion of $CD3^+$ cells.[67]

Phenotypic characteristics of MAIT cells in inflamed tissues. In PsA, the majority of synovial fluid MAIT cells are $CD8^+$ subtypes and express $CD45RO^+$, suggesting an effector memory phenotype.[42] Synovial fluid MAIT cells also exhibit high levels of CD69, a homing and/or activation marker, compared to MAIT cells in blood in RA[66] and SpA[43] (Table 1, Figure 1). Single-cell profiling of synovial tissues further supports the presence of an activated MAIT cell population in the RA synovium.[68]

Interestingly, synovial fluid MAIT cells express lower levels of $CCR6^+$ compared to MAIT cells in blood in SpA[43] (Table 1, Figure 1), suggesting that high CCR6 expression may facilitate their migration into inflamed tissues. In RA, MAIT cells express higher levels of sialyl-Lewis^X (sLewis^X) in synovial fluid than in blood,[66] which could reflect the residency of MAIT cells highly expressing sLewis^X in the joint.

Functional properties of MAIT cells in inflamed tissues. Following stimulation, synovial fluid MAIT cells produce significantly more IL-17A in PsA compared to osteoarthritis[42] and more IL-17A and granzyme B in SpA compared to MAIT cells in blood.[43] Interestingly, they secrete lower levels of TNFα and IFNγ in SpA compared to MAIT cells in blood, with similar levels observed between SpA and RA[43] (Table 1, Figure 1).

IL-23 appears to be a key driver in MAIT cell activation. Its receptor, IL-23R, is up-regulated in synovial fluid MAIT cells stimulated with CD3/CD28 and IL-23 in PsA and RA compared to osteoarthritis.[42] This stimulation enhances MAIT cell proliferation significantly more than CD3/CD28 alone or PMA/ionomycin, highlighting the mitogenic potential of IL-23 in PsA.[42] Similarly, in pSD, IL-7 and IL-23 drive IL-17 polarization of MAIT cells, as IL-7 up-regulates STAT3/HIF1a, and IL-23 induces RORc expression[54] (Table 1, Figure 1).

Although access to inflamed spinal enthesis in axSpA is challenging, Rosine et al[30] identified MAIT cells in the spinal enthesis of patients with osteoarthritis, where they exhibited a resident memory phenotype and inducible IL-17A production. However, no study has yet investigated MAIT cells in the spinal enthesis of patients with axSpA.

Consequently, MAIT cells are present in target tissues and appear to accumulate at sites of inflammation, where they secrete Th17 cytokines, potentially driving inflammation and tissue damage. Further studies are needed to confirm accumulation in inflamed tissues and to better characterize their profile and role.

MAIT cell migration. The destiny of circulating MAIT cells in these conditions, whether they undergo cell death or migrate to inflamed tissues, remains unclear. In type 1 diabetes, circulating MAIT cells migrate into the pancreas of NOD mice during type 1 diabetes development.[23]

As described previously, chronic inflammatory rheumatologic diseases are characterized by a depletion of circulating MAIT cells alongside their accumulation in inflamed tissues. This preliminary data, based on few studies with a small number of patients, highly suggests that circulating MAIT cells could migrate into inflamed tissues.

MAIT cells express a variety of chemokine receptors, such as CCR6, CXCR6, CCR5, and CCR2, indicating their ability to migrate. In RA, Kim et al[66] investigated the trafficking ability of MAIT cells in the inflamed joint. TNFα and IL-1β in RA synovial fluid up-regulate E-selectin, intercellular adhesion molecule 1, and vascular cell adhesion molecule 1 on endothelial cells, attracting circulating MAIT cells that express high levels of sLewis^X (Figure 1). Additionally, TNFα induces CCL20 expression on endothelial cells, leading to the attraction of $CCR6^+$ MAIT cells. In pSD, circulating MAIT cells overexpress CCR9 and CXCR5,[57] suggesting a potential attraction to the salivary gland (Figure 1). This is supported by the expression of their corresponding ligands in the salivary gland: CCL25,[69] which binds to CCR9, and CXCL13,[70] which binds to CXCR5.

In SSc, the decrease in circulating MAIT cells is more pronounced in patients with SSc-ILD and is correlated with the expression of the tissue-recruitment chemokine CCR6. This suggests that MAIT cells could migrate into lungs.[54] In SLE, the increase in circulating $CCR6^-$ $CD127^-$ MAIT cells could suggest a migration of circulating $CCR6^+$ $CD127^+$ MAIT cells into the kidney.[50] Enhancing our understanding of how MAIT cells are targeted in inflamed tissues and providing evidence of their migration in a mouse model are pivotal research areas.

Functional role of MAIT cells in disease progression. MAIT cells have received limited attention in animal research, with only two studies conducted in mouse models of RA and SLE. In a murine model of RA, MAIT cells were found to promote inflammation and exacerbate disease.[71] Specifically, the severity of collagen-induced arthritis is reduced in $MR1^{-/-}$ mice, which are deficient in MAIT cells. Conversely, the reconstitution of MAIT cells in these mice led to severe arthritis characterized by an inflammatory response rather than a specific type 2 collagen response. This study, albeit conducted in only one RA mouse model, suggests that MAIT cells may contribute to joint inflammation. Further studies with complementary mouse models and other techniques to modulate MAIT cells are necessary to fully elucidate their role in RA.

In a spontaneous animal model of lupus, the $Fc\gamma RIIb^{-/-}$Yaa mice, MAIT cells contributed to lupus pathogenesis by promoting autoantibody production and exacerbating tissue inflammation. Two approaches were used to study the role of MAIT cells: $MR1^{-/-}$ animals, which lack MAIT cells, and treatment with the synthesized inhibitory MR1 ligand isobutyryl 6-formylpterin, which blocks MAIT cell activation. Both genetic deficiency and pharmacologic inhibition improved the lupus course by reducing autoantibody production and mitigating the severity of lupus nephritis. This improvement was evidenced by reduced proteinuria, reduced IgG and C3 deposition, and diminished mononuclear cell infiltration in the kidney.[67]

Conclusions and perspectives

The proportion of circulating MAIT cells is decreased in chronic inflammatory rheumatologic diseases, and those detected in the circulation exhibit an activated profile and/or an increased cytokine-producing capacity. Interestingly, MAIT cells are enriched in the joints of patients with RA, SpA, and PsA, as well as in salivary glands of patients with pSD. The expression of markers implicated in joint homing, such as CCR6, or in the salivary gland, such as CCR9 and CXCR5, coupled with the decrease in circulating MAIT cells, suggests that MAIT cells could migrate from the blood to the inflamed tissues.

This suggests that MAIT cells likely play a pathogenic role in the development of these diseases. However, further studies are needed to precisely elucidate their contribution. Specifically, investigating the interaction between microbiota and alterations of circulating MAIT cells could enhance our understanding of MAIT cell activation (Box 1). Indeed, emerging evidence underscores the pivotal role of microbiomes in the immunopathogenesis of rheumatic diseases.[39] As detailed previously, microbiota-derived metabolites have been demonstrated to impact the selection, expansion, and functional repertoire of MAIT cells. For instance, in alcoholic liver disease, gut dysbiosis contributes to MAIT cell dysfunction.[72] Hence, it becomes imperative to unravel the mechanisms through which microbiota influence MAIT cell phenotypes by examining correlations between intestinal permeability, dysbiosis, and MAIT cell phenotype in rheumatic disorders.

Secondly, further investigations aim to demonstrate the migration of circulating MAIT cells into inflamed tissues (Box 1). Once activated, MAIT cells appear to rapidly migrate from peripheral blood to the inflammation site in inflammatory or autoimmune diseases. The migration causes depletion of MAIT cell frequency in the blood and aggregate at the inflammation site, where they secrete proinflammatory cytokines, leading to inflammation and damage of target organs.

Furthermore, conducting in vitro functional studies is essential to elucidate the precise role of MAIT cells in inflamed tissues (Box 1). These studies could help determine whether MAIT cells exhibit pathogenic or protective functions and whether they interact directly with diseased cells or via other cells or cytokines. Moreover, other murine models would be valuable to further substantiate their involvement in exacerbating these diseases (Box 1).

With a deeper understanding of the underlying mechanisms, MAIT cells may emerge as an attractive therapeutic target (Box 1). In rheumatologic diseases, MAIT cells exhibit reduced production of IFNγ and TNFα, while displaying increased levels of IL-17 and IL-22 in both blood and tissues. Therefore, MAIT cells, as a source of IL-17, a key cytokine in rheumatologic disorders, could be an interesting target. Direct inhibition of MAIT cells can be achieved using MR1-blocking antibodies, which have demonstrated efficacy in reducing tumors by targeting MR1 up-regulation in mouse models.[73] MAIT cell activation can also be inhibited by acetyl-6-formylpterin, a vitamin B_9 metabolite, which is a nonagonist MR1-presented ligand.[67] Another potential approach is to block cytokine secretion by MAIT cells. Selective inhibition of PI3Kδ has been shown to suppress IL-17A and IL-17F production by MAIT cells from healthy donor peripheral blood,[74] which could be effective in IL-17–driven diseases, such as psoriasis and SpA. Finally, strategies aimed at blocking MAIT cell migration into inflamed tissues could offer an innovative approach for therapeutic intervention. Such treatments could be used in early rheumatism (early RA, early SpA, etc) either alone or in combination with targeted therapies to enhance their efficacy.

In addition to evolving into a therapeutic target for enhancing the management of rheumatism, MAIT cells could potentially serve as a biomarker indicating the response to current treatments (Box 1). In SLE, patients in complete renal remission after immunosuppressive therapy exhibited a higher proportion of MAIT cells, which were less proliferative (Ki67) and cytotoxic (granzyme B production) at inclusion.[47] The association of MAIT cell frequency and/or activation profile with disease activity observed in SLE and SpA[41,44,48] strongly suggests their utility as biomarkers. Examining the proportion and characteristics of MAIT cells over time, both before and after treatment, through longitudinal studies could unveil whether a specific MAIT cell phenotype serves as a predictive indicator for a favorable therapeutic response.

Box 1. Research agenda

Research agenda

- How do circulating mucosal-associated invariant T (MAIT) cells become activated? Do they undergo activation in peripheral blood or within mucosal tissues before circulation?
- What are the relationships between intestinal permeability, dysbiosis, and the phenotype of MAIT cells?
- How are MAIT cells recruited and localized within inflamed tissues? Provide evidence of their migration, potentially using mouse models.
- What is the in vitro functional behavior of MAIT cells? Do they exhibit pathogenic or protective effects, and do they directly interact with diseased cells or through intermediary cells and cytokines?
- What is the functional role of MAIT cells in the development of diseases? This includes confirming or establishing their involvement in disease exacerbation.
- Can the proportion and/or profile of MAIT cells serve as biomarkers for treatment response?
- Are MAIT cells promising targets for novel therapeutic interventions?

AUTHOR CONTRIBUTIONS

All authors contributed to at least one of the following manuscript preparation roles: conceptualization AND/OR methodology, software, investigation, formal analysis, data curation, visualization, and validation AND drafting or reviewing/editing the final draft. As corresponding author, Dr Avouac confirms that all authors have provided the final

approval of the version to be published and takes responsibility for the affirmations regarding article submission (eg, not under consideration by another journal), the integrity of the data presented, and the statements regarding compliance with institutional review board/Declaration of Helsinki requirements.

REFERENCES

1. Tastan C, Karhan E, Zhou W, et al. Tuning of human MAIT cell activation by commensal bacteria species and MR1-dependent T-cell presentation. Mucosal Immunol 2018;11(6):1591–1605.
2. Legoux F, Salou M, Lantz O. MAIT cell development and functions: the microbial connection. Immunity 2020;53(4):710–723.
3. Toubal A, Nel I, Lotersztajn S, et al. Mucosal-associated invariant T cells and disease. Nat Rev Immunol 2019;19(10):643–657.
4. Treiner E, Duban L, Bahram S, et al. Selection of evolutionarily conserved mucosal-associated invariant T cells by MR1. Nature 2003; 422(6928):164–169.
5. Godfrey DI, Koay HF, McCluskey J, et al. The biology and functional importance of MAIT cells. Nat Immunol 2019;20(9):1110–1128.
6. Hackstein CP, Klenerman P. MAITs and their mates: "innate-like" behaviors in conventional and unconventional T cells. Clin Exp Immunol 2023;213(1):1–9.
7. Corbett AJ, Eckle SBG, Birkinshaw RW, et al. T-cell activation by transitory neo-antigens derived from distinct microbial pathways. Nature 2014;509(7500):361–365.
8. Kjer-Nielsen L, Patel O, Corbett AJ, et al. MR1 presents microbial vitamin B metabolites to MAIT cells. Nature 2012;491(7426):717–723.
9. Le Bourhis L, Dusseaux M, Bohineust A, et al. MAIT cells detect and efficiently lyse bacterially-infected epithelial cells. PLoS Pathog 2013; 9(10):e1003681.
10. Seach N, Guerri L, Le Bourhis L, et al. Double-positive thymocytes select mucosal-associated invariant T cells. J Immunol 2013; 191(12):6002–6009.
11. McWilliam HEG, Villadangos JA. MR1 antigen presentation to MAIT cells and other MR1-restricted T cells. Nat Rev Immunol 2024;24(3): 178–192.
12. Salou M, Legoux F, Lantz O. MAIT cell development in mice and humans. Mol Immunol 2021;130:31–36.
13. Koay HF, Gherardin NA, Enders A, et al. A three-stage intrathymic development pathway for the mucosal-associated invariant T cell lineage. Nat Immunol 2016;17(11):1300–1311.
14. Martin E, Treiner E, Duban L, et al. Stepwise development of MAIT cells in mouse and human. PLoS Biol 2009;7(3):e54.
15. Franciszkiewicz K, Salou M, Legoux F, et al. MHC class I-related molecule, MR1, and mucosal-associated invariant T cells. Immunol Rev 2016;272(1):120–138.
16. Novak J, Dobrovolny J, Novakova L, et al. The decrease in number and change in phenotype of mucosal-associated invariant T cells in the elderly and differences in men and women of reproductive age. Scand J Immunol 2014;80(4):271–275.
17. Le Bourhis L, Mburu YK, Lantz O. MAIT cells, surveyors of a new class of antigen: development and functions. Curr Opin Immunol 2013; 25(2):174–180.
18. Park D, Kim HG, Kim M, et al. Differences in the molecular signatures of mucosal-associated invariant T cells and conventional T cells. Sci Rep 2019;9(1):7094.
19. Reantragoon R, Corbett AJ, Sakala IG, et al. Antigen-loaded MR1 tetramers define T cell receptor heterogeneity in mucosal-associated invariant T cells. J Exp Med 2013;210(11):2305–2320.
20. Walker LJ, Kang YH, Smith MO, et al. Human MAIT and CD8αα cells develop from a pool of type-17 precommitted CD8+ T cells. Blood 2012;119(2):422–433.
21. Dusseaux M, Martin E, Serriari N, et al. Human MAIT cells are xenobiotic-resistant, tissue-targeted, CD161hi IL-17-secreting T cells. Blood 2011;117(4):1250–1259.
22. Nel I, Bertrand L, Toubal A, et al. MAIT cells, guardians of skin and mucosa? Mucosal Immunol 2021;14(4):803–814.
23. Rouxel O, Da Silva J, Beaudoin L, et al. Cytotoxic and regulatory roles of mucosal-associated invariant T cells in type 1 diabetes. Nat Immunol 2017;18(12):1321–1331.
24. Dias J, Leeansyah E, Sandberg JK. Multiple layers of heterogeneity and subset diversity in human MAIT cell responses to distinct microorganisms and to innate cytokines. Proc Natl Acad Sci USA 2017; 114(27):E5434–E5443.
25. Dias J, Boulouis C, Sobkowiak MJ, et al. Factors influencing functional heterogeneity in human mucosa-associated invariant T cells. Front Immunol 2018;9:1602.
26. Gérart S, Sibéril S, Martin E, et al. Human iNKT and MAIT cells exhibit a PLZF-dependent proapoptotic propensity that is counterbalanced by XIAP. Blood 2013;121(4):614–623.
27. Vorkas CK, Krishna C, Li K, et al. Single-cell transcriptional profiling reveals signatures of helper, effector, and regulatory MAIT cells during homeostasis and activation. J Immunol 2022;208(5):1042–1056.
28. Eckle SBG, Birkinshaw RW, Kostenko L, et al. A molecular basis underpinning the T cell receptor heterogeneity of mucosal-associated invariant T cells. J Exp Med 2014;211(8):1585–1600.
29. Turtle CJ, Delrow J, Joslyn RC, et al. Innate signals overcome acquired TCR signaling pathway regulation and govern the fate of human $CD161^{hi}$ $CD8\alpha^{+}$ semi-invariant T cells. Blood 2011;118(10): 2752–2762.
30. Rosine N, Rowe H, Koturan S, et al. Characterization of blood mucosal-associated invariant T cells in patients with axial spondyloarthritis and of resident mucosal-associated invariant T cells from the axial entheses of non-axial spondyloarthritis control patients. Arthritis Rheumatol 2022;74(11):1786–1795.
31. Ussher JE, Bilton M, Attwod E, et al. $CD161^{++}$ $CD8^{+}$ T cells, including the MAIT cell subset, are specifically activated by IL-12+IL-18 in a TCR-independent manner. Eur J Immunol 2014;44(1):195–203.
32. Chiba A, Murayama G, Miyake S. Mucosal-associated invariant T Cells in autoimmune diseases. Front Immunol 2018;9:1333.
33. Gizinski AM, Fox DA. T cell subsets and their role in the pathogenesis of rheumatic disease. Curr Opin Rheumatol 2014;26(2):204–210.
34. Komatsu N, Takayanagi H. Mechanisms of joint destruction in rheumatoid arthritis - immune cell-fibroblast-bone interactions. Nat Rev Rheumatol 2022;18(7):415–429.
35. Yeremenko N. Out of the shadow of interleukin-17A: the role of interleukin-17F and other interleukin-17 family cytokines in spondyloarthritis. Curr Opin Rheumatol 2021;33(4):333–340.
36. Menon B, Gullick NJ, Walter GJ, et al. Interleukin-17+CD8+ T cells are enriched in the joints of patients with psoriatic arthritis and correlate with disease activity and joint damage progression. Arthritis Rheumatol 2014;66(5):1272–1281.
37. Sippl N, Faustini F, Rönnelid J, et al. Arthritis in systemic lupus erythematosus is characterized by local IL-17A and IL-6 expression in synovial fluid. Clin Exp Immunol 2021;205(1):44–52.
38. Truchetet ME, Brembilla NC, Montanari E, et al. Interleukin-17A+ cell counts are increased in systemic sclerosis skin and their number is inversely correlated with the extent of skin involvement. Arthritis Rheum 2013;65(5):1347–1356.
39. Konig MF. The microbiome in autoimmune rheumatic disease. Best Pract Res Clin Rheumatol 2020;34(1):101473.

40. Zhong D, Wu C, Zeng X, et al. The role of gut microbiota in the pathogenesis of rheumatic diseases. Clin Rheumatol 2018;37(1):25–34.
41. Cho YN, Kee SJ, Kim TJ, et al. Mucosal-associated invariant T cell deficiency in systemic lupus erythematosus. J Immunol 2014;193(8):3891–3901.
42. Raychaudhuri SK, Abria C, Mitra A, et al. Functional significance of MAIT cells in psoriatic arthritis. Cytokine 2020;125:154855.
43. Gracey E, Qaiyum Z, Almaghlouth I, et al. IL-7 primes IL-17 in mucosal-associated invariant T (MAIT) cells, which contribute to the Th17-axis in ankylosing spondylitis. Ann Rheum Dis 2016;75(12):2124–2132.
44. Hayashi E, Chiba A, Tada K, et al. Involvement of mucosal-associated invariant T cells in ankylosing spondylitis. J Rheumatol 2016;43(9):1695–1703.
45. Toussirot É, Laheurte C, Gaugler B, et al. Increased IL-22- and IL-17A-producing mucosal-associated invariant T Cells in the peripheral blood of patients with ankylosing spondylitis. Front Immunol 2018;9:1610.
46. Yang S, Zheng Y, Chen X, et al. Inflammatory activity evaluation in patients with axial spondyloarthritis using MRI relaxometry and mucosal-associated invariant T cells. Front Immunol 2024;15:1391280.
47. Peng L, Chen L, Wan J, et al. Single-cell transcriptomic landscape of immunometabolism reveals intervention candidates of ascorbate and aldarate metabolism, fatty-acid degradation and PUFA metabolism of T-cell subsets in healthy controls, psoriasis and psoriatic arthritis. Front Immunol 2023;14:1179877.
48. Chiba A, Tamura N, Yoshikiyo K, et al. Activation status of mucosal-associated invariant T cells reflects disease activity and pathology of systemic lupus erythematosus. Arthritis Res Ther 2017;19(1):58.
49. Cassius C, Branchtein M, Battistella M, et al. Persistent deficiency of mucosal-associated invariant T cells during dermatomyositis. Rheumatology (Oxford) 2020;59(9):2282–2286.
50. Litvinova E, Bounaix C, Hanouna G, et al. MAIT cells altered phenotype and cytotoxicity in lupus patients are linked to renal disease severity and outcome. Front Immunol 2023;14:1205405.
51. Lien HJT, Pedersen TT, Jakobsen B, et al. Single-cell resolution of longitudinal blood transcriptome profiles in rheumatoid arthritis, systemic lupus erythematosus and healthy control pregnancies. Ann Rheum Dis 2024;83(3):300–311.
52. Mekinian A, Mahevas T, Mohty M, et al. Mucosal-associated invariant cells are deficient in systemic sclerosis. Scand J Immunol 2017;86(4):216–220.
53. Paleja B, Low AHL, Kumar P, et al. Systemic sclerosis perturbs the architecture of the immunome. Front Immunol 2020;11:1602.
54. Lesturgie-Talarek M, Gonzalez V, Beaudoin L, et al. Deficiency and altered phenotype of mucosal-associated invariant T cells in systemic sclerosis. J Scleroderma Relat Disord 2024;9(1):67–78.
55. Wang JJ, Macardle C, Weedon H, et al. Mucosal-associated invariant T cells are reduced and functionally immature in the peripheral blood of primary Sjögren's syndrome patients. Eur J Immunol 2016;46(10):2444–2453.
56. Guggino G, Di Liberto D, Lo Pizzo M, et al. IL-17 polarization of MAIT cells is derived from the activation of two different pathways. Eur J Immunol 2017;47(11):2002–2003.
57. Hinrichs AC, Kruize AA, Leavis HL, et al. In patients with primary Sjögren's syndrome innate-like MAIT cells display upregulated IL-7R, IFN-γ, and IL-21 expression and have increased proportions of CCR9 and CXCR5-expressing cells. Front Immunol 2022;13:1017157.
58. Hou X, Hong X, Ou M, et al. Analysis of gene expression and TCR/B cell receptor profiling of immune cells in primary Sjögren's syndrome by single-cell sequencing. J Immunol 2022;209(2):238–249.
59. Chauffier J, Berger de Gallardo H, Chevalier MF, et al. Role of mucosal-associated invariant T cells dynamics in pathogenesis of Sjögren syndrome. Sci Rep 2024;14(1):17256.
60. Dias J, Boulouis C, Gorin JB, et al. The $CD4^{-}CD8^{-}$ MAIT cell subpopulation is a functionally distinct subset developmentally related to the main $CD8^{+}$ MAIT cell pool. Proc Natl Acad Sci USA 2018;115(49):E11513–E11522.
61. van der Meer RG, Spoorenberg A, Brouwer E, et al. Mucosal-associated invariant T cells in patients with axial spondyloarthritis. Front Immunol 2023;14:1128270.
62. Koppejan H, Jansen DTSL, Hameetman M, et al. Altered composition and phenotype of mucosal-associated invariant T cells in early untreated rheumatoid arthritis. Arthritis Res Ther 2019;21(1):3.
63. van der Heijde D, Gensler LS, Deodhar A, et al. Dual neutralisation of interleukin-17A and interleukin-17F with bimekizumab in patients with active ankylosing spondylitis: results from a 48-week phase IIb, randomised, double-blind, placebo-controlled, dose-ranging study. Ann Rheum Dis 2020;79(5):595–604.
64. Mease P. Ustekinumab fails to show efficacy in a phase III axial spondyloarthritis program: the importance of negative results. Arthritis Rheumatol 2019;71(2):179–181.
65. Baeten D, Østergaard M, Wei JCC, et al. Risankizumab, an IL-23 inhibitor, for ankylosing spondylitis: results of a randomised, double-blind, placebo-controlled, proof-of-concept, dose-finding phase 2 study. Ann Rheum Dis 2018;77(9):1295–1302.
66. Kim M, Yoo SJ, Kang SW, et al. TNFα and IL-1β in the synovial fluid facilitate mucosal-associated invariant T (MAIT) cell migration. Cytokine 2017;99:91–98.
67. Murayama G, Chiba A, Suzuki H, et al. A critical role for mucosal-associated invariant T cells as regulators and therapeutic targets in systemic lupus erythematosus. Front Immunol 2019;10:2681.
68. Dunlap G, Wagner A, Meednu N, et al. Clonal associations of lymphocyte subsets and functional states revealed by single cell antigen receptor profiling of T and B cells in rheumatoid arthritis synovium. bioRxiv Preprint posted online March 21, 2023. https://doi.org/10.1101/2023.03.18.533282
69. Blokland SLM, Hillen MR, Kruize AA, et al. Increased CCL25 and T helper cells expressing CCR9 in the salivary glands of patients with primary Sjögren's syndrome: potential new axis in lymphoid neogenesis. Arthritis Rheumatol 2017;69(10):2038–2051.
70. Barone F, Bombardieri M, Manzo A, et al. Association of CXCL13 and CCL21 expression with the progressive organization of lymphoid-like structures in Sjögren's syndrome. Arthritis Rheum 2005;52(6):1773–1784.
71. Chiba A, Tajima R, Tomi C, et al. Mucosal-associated invariant T cells promote inflammation and exacerbate disease in murine models of arthritis. Arthritis Rheum 2012;64(1):153–161.
72. Riva A, Patel V, Kurioka A, et al. Mucosa-associated invariant T cells link intestinal immunity with antibacterial immune defects in alcoholic liver disease. Gut 2018;67(5):918–930.
73. Yan J, Allen S, McDonald E, et al. MAIT Cells promote tumor initiation, growth, and metastases via tumor MR1. Cancer Discov 2020;10(1):124–141.
74. Chen S, Paveley R, Kraal L, et al. Selective targeting of PI3Kδ suppresses human IL-17-producing T cells and innate-like lymphocytes and may be therapeutic for IL-17-mediated diseases. J Autoimmun 2020;111:102435.

American College of Rheumatology
Empowering Rheumatology Professionals

Arthritis & Rheumatology
Vol. 78, No. 2, February 2026, pp 298–301
DOI 10.1002/art.43275

NOTES FROM THE FIELD

Examples of Treatments That May Be Highly Effective for Osteoarthritis: Do They Provide Insights Into Future Treatment Directions?

David T. Felson[1] and Francis Berenbaum[2]

Introduction

Osteoarthritis (OA), the most common form of arthritis, is a major unconquered chronic disease. On the other hand, great progress has been made in controlling rheumatoid arthritis (RA) and other inflammatory arthritides. Given the lack of success in developing effective nonsurgical treatments for OA, new strategies are needed.

The development of a successful treatment often depends on an understanding of disease pathophysiology, with treatments targeting causes of disease. The last 20 years have seen major advances in our understanding of OA, especially the contribution of inflammation to disease progression and as a cause of pain.[1] OA is often caused by a combination of joint injury and inflammatory response. Animal models simulate OA either by inducing cartilage damage chemically (eg, monoiodoacetate) or by causing physical injury to the joint (eg, destabilization of the medial meniscus). In the latter case, the development of OA is accelerated in an inflammatory environment. Human OA can be triggered entirely by major joint injury, such as a meniscal tear or intra-articular fracture, or by inflammatory damage to joint structures as in OA secondary to longstanding RA.

In this review, we will highlight two nonsurgical treatments that have shown impressive efficacy for OA pain in human trials. These treatments may provide examples of approaches likely to be highly effective in two ways. First, the actual treatments may be highly effective. Second, they may provide examples of general approaches that underlie treatment efficacy, even though actual treatments may be different from those we describe. We will attempt to understand the mechanisms underlying the efficacy of these treatments as models for treatment development. We caution the reader that the two treatments highlighted have each been tested so far in only one large well-done randomized trial, and to better gauge their promise, additional trials are needed for each. We shall focus on knee OA, the best studied site of disease; our observations are likely to be generalizable to OA elsewhere.

Defining "highly effective"

To define "highly effective," we cannot use *P* values because if the trial testing a treatment versus placebo is large, results can show statistically significant efficacy even if the treatment effect is tiny. Because OA trials have generally used continuous outcomes such as pain and quantitative cartilage loss, the most appropriate measure of efficacy is the effect size. In a placebo-controlled trial, the effect size is the mean change in the treated group score minus the mean change in the placebo divided by a pooled SD. For this assessment, we used the pooled baseline SD of active treatment and placebo groups. Because treatment for RA is widely regarded as successful for most patients, we shall use the standard treatment widely regarded as highly effective, methotrexate. A comprehensive meta-analysis of randomized placebo-controlled trials of methotrexate in RA[2] has shown different effect sizes for different outcomes, including an effect size of 0.61 for tender joint counts, the outcome given most weight by rheumatologists when monitoring treatment. Effect sizes greater than 1.00 were seen for both patient and physician global assessments. Averaging effect sizes yields an effect size of 0.75, a number we shall use (0.7–0.8) to characterize a highly effective treatment.

Based on Cochrane meta-analyses of trial data, none of the effect sizes for pain outcomes for guideline-recommended treatments for OA attain the highly effective threshold. As noted in a recent review of OA treartment by Kloppenburg and colleagues,[3]

Supported by the NIH (grant P30-AR-072571). Dr. Felson is a consultant for APOSHealth. Dr. Berenbaum is co-founder and chief marketing officer of 4Moving Biotech, which is developing a GLP-1 analog for treatment of osteoarthritis.

[1]David T. Felson, MD, MPH: Boston University Chobanian and Avedisian School of Medicine, Boston, Massachusetts; [2]Francis Berenbaum, MD: Sorbonne University, INSERM, Department of Rheumatology, AP-HP Saint-Antoine Hospital, Paris, France.

Author disclosures are available at https://onlinelibrary.wiley.com/doi/10.1002/art.43275.

[Correction added on 10 November 2025, after first online publication: article category has been updated in this version.]

Address correspondence via email to David T. Felson, MD, MPH, at dfelson@bu.edu.

Submitted for publication March 13, 2025; accepted in revised form May 28, 2025.

"Evidence of the last years have increased our knowledge of their efficacy, which is unfortunately not high…."

Inflammation as a cause of OA and attempts to abrogate it

A chorus of prominent scientific voices has argued, based on animal models of disease, that inflammation is an essential component to the pathogenesis of OA.[1,4] These models have shown that, in an inflammatory environment, joint destruction and cartilage loss after joint injury are much greater than when inflammation is suppressed. In fact, in one animal model in which inflammatory responses to injury were absent, cartilage loss did not develop after joint trauma.[5]

Human studies suggest also that inflammation increases the risk of disease worsening. For example, synovitis on magnetic resonance imaging (MRI) accelerates cartilage loss and is associated with more severe joint pain. Authors have proposed that suppression of the inflammatory cascade would provide therapeutic opportunities in OA.[4]

The promise of treating OA by abrogating inflammation has led to multiple trials testing different approaches summarized in a recent review.[3] For example, interleukin-1 (IL-1) is a central cytokine activating catabolic processes within cartilage, yet OA trials evaluating IL-1 inhibitors have not shown promise despite a cardiovascular trial of an IL-1 inhibitor showing a reduction in knee replacements over 3.7 years.[6] Other OA trials have tested treatments for RA, including tumor necrosis factor (TNF) inhibitors and an IL-6 inhibitor, and these trials have been negative, with none achieving a highly effective threshold. Hydroxychloroquine has shown no measurable efficacy.[3] Although methotrexate may be modestly effective for hand OA,[3] its efficacy may not extend to knees and, even in hand OA, does not meet a highly effective threshold. Disappointing results from these trials may be due to the heterogeneity of OA, whereby inflammation is critical in only some patients.

Mechanics and OA: An example using knee coronal plane malalignment

Coronal plane malalignment, a chronic mechanical insult, markedly increases risk of OA progression[7] and causes bone marrow lesions on MRI, which represent traumatic lesions to the bone. Given that over 80% of knees with OA in the community-based Multicenter Osteoarthritis Study (MOST) had varus or valgus malalignment and taking into account the increased risk of disease progression in these knees,[7] over half of cases of radiographic disease progression are caused in part by malalignment.

Malalignment can be measured standing using long-limb x-rays or during walking, so-called dynamic malalignment. The knee adduction moment is a measure of dynamic varus malalignment (Figure 1), which, like standing malalignment, has been linked to disease progression and more severe pain. Therapeutic efforts to reduce the adduction moment have involved moving the knee closer to the ground reaction force vector, making the knee less varus. Therapies that attempt knee realignment, such as knee braces and heel wedges and other shoe modifications, yield 4% to 6% reductions in the adduction moment[8] and have not shown great clinical success.[9]

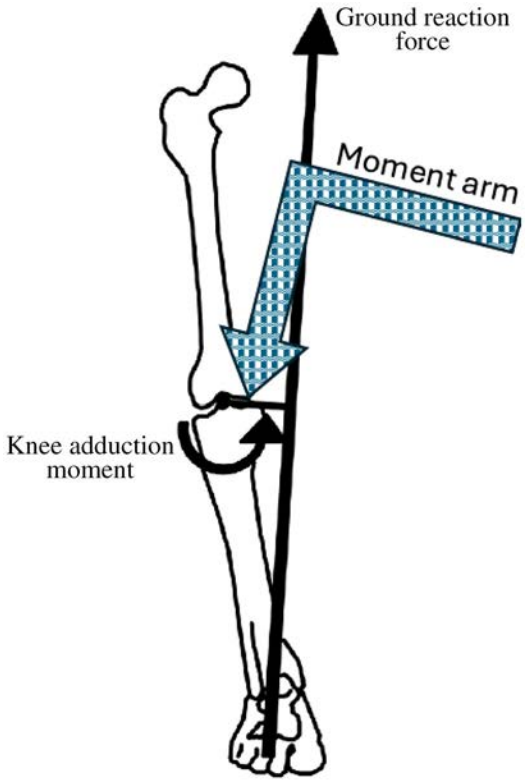

Figure 1. Adduction moment is the product of the length of the moment arm and the ground reaction force. Treatment strategies such as bracing, shoe wedges, and tibial osteotomies all work in part by shortening the moment arm.

One unique approach consists of shoes with hemispheric hard rubber balls screwed into tracks on the bottom of a special shoe. The positions of these balls can be changed depending on the desired gait modification. With ball position adjusted to correct varus malalignment, knee adduction moment drops by 10% to 14%. After months of use, patients walking barefoot have 8% to 13% lower adduction moments than before use of the shoe, suggesting muscle training has occurred.[10] In a randomized controlled trial, this shoe successfully reduced knee pain compared to sham at the preselected time point of six months, with an effect size versus sham of 0.7, suggesting a "highly effective" treatment.[11]

Although not tested in a randomized trial, in joint distraction procedures, a metal frame is inserted into bones above and below the OA joint and pulls apart the joint for six weeks, followed by removal of the frame and normal weight bearing. This

procedure has also shown marked reductions in pain and even improvements in structural disease,[12] confirming the promising therapeutic value of unloading.

Weight loss and OA

Although malalignment increases focal load in the knee, obesity confers an increased load, especially in those compartments bearing most of the load. Persons with obesity have a markedly increased risk of radiographic knee OA but have little increased risk of radiographic hand OA,[13] suggesting that the increased load conferred by obesity amplifies the risk of structural deterioration in the joint. Further, bariatric surgery in persons with obesity reduced pain severity by a mean of 46% in one large study in those with knee OA.[14]

In a randomized placebo-controlled trial, semaglutide, a glucagon-like peptide 1 (GLP-1) agonist,[15] caused 10% greater weight loss in patients with obesity than in controls and produced a marked reduction in knee pain. Reductions in Western Ontario and McMaster Universities Osteoarthritis Index pain scores in active treatment versus placebo translated into an effect size of 0.8, meeting criteria for highly effective therapy. GLP-1 agonists have anti-inflammatory effects, but not all cause this degree of weight loss.

The effects of weight loss on pain reduction are dose related (dependent on the amount of weight loss[16]) and are probably mediated by several independent factors. First, there is the reduction in load sensed by mechanoreceptors in the joint, including in sensory nerves mediated, in part, by the mechanosensitive ion channel Piezo2.[17] Further, weight loss may reduce mechanical instability across the joint, alleviating stress on ligaments and muscles with indirect effects on pain. Also, the reduction in adipose tissue may lessen pain by lowering levels of proinflammatory cytokines (eg, IL-6 and TNF) and adipokines synthesized and released by adipose tissue.[18] The adipokine leptin has been especially implicated as a source of OA pain. Lastly, GLP-1 agonists may have direct anti-inflammatory and analgesic effects on pain independent of weight loss.

Weight loss also has favorable chondroprotective effects, but these are less pronounced than effects on pain and may be mediated differently. Using data from the Osteoarthritis Initiative, Bacon and colleagues[19] showed that those who lost cartilage had almost no change in their knee pain. This idea was corroborated in the sprifermin trial,[20] in which the medication prevented cartilage loss in OA knees but had no effect on pain severity over five years.

Conclusions

In conclusion, two potentially highly effective nonsurgical treatments for OA provide insights into treatment approaches that might be successful in the future. That realignment therapies for osteoarthritic knees can reach the highly effective threshold suggests that ignoring the mechanical contribution to OA may make it nearly impossible to develop successful treatments. Second, the success of GLP-1 agonists and attendant weight loss suggests that either unloading combined with anti-inflammatory treatments may be needed for success or that, to be successful, a treatment may need to home in on multiple targets in the inflammatory cascade.

ACKNOWLEDGMENT

We appreciate valuable discussions with Dr Rick Bucala at Yale University on this article.

AUTHOR CONTRIBUTIONS

Both authors contributed to at least one of the following manuscript preparation roles: conceptualization AND/OR methodology, software, investigation, formal analysis, data curation, visualization, and validation AND drafting or reviewing/editing the final draft. As corresponding author, Dr Felson confirms that all authors have provided the final approval of the version to be published and takes responsibility for the affirmations regarding article submission (eg, not under consideration by another journal), the integrity of the data presented, and the statements regarding compliance with institutional review board/Declaration of Helsinki requirements.

REFERENCES

1. Berenbaum F. Osteoarthritis as an inflammatory disease (osteoarthritis is not osteoarthrosis!). Osteoarthritis Cartilage 2013;21(1):16–21.
2. Lopez-Olivo MA, Siddhanamatha HR, Shea B, et al. Methotrexate for treating rheumatoid arthritis. Cochrane Database Syst Rev 2014;(6):CD000957.
3. Kloppenburg M, Namane M, Cicuttini F. Osteoarthritis. Lancet 2025;405(10472):71–85.
4. Pelletier JP, Martel-Pelletier J, Abramson SB. Osteoarthritis, an inflammatory disease: potential implication for the selection of new therapeutic targets. Arthritis Rheum 2001;44(6):1237–1247.
5. Ward BD, Furman BD, Huebner JL, et al. Absence of posttraumatic arthritis following intraarticular fracture in the MRL/MpJ mouse. Arthritis Rheum 2008;58(3):744–753.
6. Schieker M, Conaghan PG, Mindeholm L, et al. Effects of interleukin-1β inhibition on incident hip and knee replacement: exploratory analyses from a randomized, double-blind, placebo-controlled trial. Ann Intern Med 2020;173(7):509–515.
7. Sharma L, Song J, Dunlop D, et al. Varus and valgus alignment and incident and progressive knee osteoarthritis. Ann Rheum Dis 2010;69(11):1940–1945.
8. Arnold JB, Wong DX, Jones RK, et al. Lateral wedge insoles for reducing biomechanical risk factors for medial knee osteoarthritis progression: a systematic review and meta-analysis. Arthritis Care Res (Hoboken) 2016;68(7):936–951.
9. Parkes MJ, Maricar N, Lunt M, et al. Lateral wedge insoles as a conservative treatment for pain in patients with medial knee osteoarthritis: a meta-analysis. JAMA 2013;310(7):722–730.
10. Haim A, Rubin G, Rozen N, et al. Reduction in knee adduction moment via non-invasive biomechanical training: a longitudinal gait analysis study. J Biomech 2012;45(1):41–45.
11. Reichenbach S, Felson DT, Hincapié CA, et al. Effect of biomechanical footwear on knee pain in people with knee osteoarthritis: the BIOTOK randomized clinical trial. JAMA 2020;323(18):1802–1812.

12. Wiegant K, van Roermund PM, Intema F, et al. Sustained clinical and structural benefit after joint distraction in the treatment of severe knee osteoarthritis. Osteoarthritis Cartilage 2013;21(11):1660–1667.
13. Jiang L, Xie X, Wang Y, et al. Body mass index and hand osteoarthritis susceptibility: an updated meta-analysis. Int J Rheum Dis 2016; 19(12):1244–1254.
14. King WC, Chen JY, Belle SH, et al. Change in pain and physical function following bariatric surgery for severe obesity. JAMA 2016; 315(13):1362–1371.
15. Bliddal H, Bays H, Czernichow S, et al; STEP 9 Study Group. Once-weekly semaglutide in persons with obesity and knee osteoarthritis. N Engl J Med 2024;391(17):1573–1583.
16. Riddle DL, Stratford PW. Body weight changes and corresponding changes in pain and function in persons with symptomatic knee osteoarthritis: a cohort study. Arthritis Care Res (Hoboken) 2013; 65(1):15–22.
17. Obeidat AM, Wood MJ, Adamczyk NS, et al. Piezo2 expressing nociceptors mediate mechanical sensitization in experimental osteoarthritis. Nat Commun 2023;14(1):2479.
18. Binvignat M, Sellam J, Berenbaum F, et al. The role of obesity and adipose tissue dysfunction in osteoarthritis pain. Nat Rev Rheumatol 2024;20(9):565–584.
19. Bacon K, LaValley MP, Jafarzadeh SR, et al. Does cartilage loss cause pain in osteoarthritis and if so, how much? Ann Rheum Dis 2020; 79(8):1105–1110.
20. Hochberg MC, Guermazi A, Guehring H, et al. Effect of intra-articular sprifermin vs placebo on femorotibial joint cartilage thickness in patients with osteoarthritis: the FORWARD randomized clinical trial. JAMA 2019;322(14):1360–1370.

Arthritis & Rheumatology
Vol. 78, No. 2, February 2026, pp 302–310
DOI 10.1002/art.43383

American College of Rheumatology
Empowering Rheumatology Professionals

Performance of an Idiopathic Pulmonary Fibrosis–Derived Multibiomarker Panel for Rheumatoid Arthritis–Associated Interstitial Lung Disease

Brent A. Luedders,[1,2] Daniel Kass,[3] Joshua F. Baker,[4,5] Michael J. Duryee,[1,2] Yangyuna Yang,[2] Punyasha Roul,[2] Halie Frideres,[2] Katherine D. Wysham,[6,7] Paul A. Monach,[8] Andreas Reimold,[9,10] Gail S. Kerr,[11,12,13] Gary Kunkel,[14,15] Grant W. Cannon,[14,15] Scott M. Matson,[16] Jill A. Poole,[2] Geoffrey M. Thiele,[1,2] Ted R. Mikuls,[1,2] Bryant R. England,[1,2] and Dana P. Ascherman[3]

Objective. To assess whether a panel of peripheral blood biomarkers associated with idiopathic pulmonary fibrosis (IPF) is also associated with interstitial lung disease (ILD) in patients with rheumatoid arthritis (RA) using three independent cohorts.

Methods. We first assessed the association of a panel of IPF-associated biomarkers with prevalent ILD among two separate RA cohorts (n = 93 and n = 71). Concentrations of eight IPF-related biomarkers (eotaxin, Flt-3L, interleukin-8, macrophage-derived chemokine, monocyte chemoattractant protein 1, and matrix metalloproteinase 2/7/9 [MMP-2/7/9]) were measured, standardized, and summed to generate a multibiomarker score. We subsequently validated the association of this score (minus MMP-2) with prevalent and incident ILD in an independent multicenter prospective cohort of US veterans with RA (n = 2,507). Multivariable regression models were adjusted for relevant covariates in the validation cohort.

Results. In both development cohorts, participants with RA-ILD had significantly higher IPF multibiomarker scores than those with RA alone. In the independent validation cohort, participants in the highest quartile of multibiomarker scores had a significantly higher likelihood of prevalent ILD (adjusted odds ratio 2.14 [95% confidence interval 1.18–3.87]) and incident ILD (adjusted hazard ratio 2.45 [95% confidence interval 1.55–3.88]) than those in the lowest quartile. The cumulative hazard of incident ILD approached 20% by 15 years for those in the highest quartile, compared to <10% for all other quartiles.

Conclusion. A multibiomarker panel derived from IPF-associated biomarkers was associated with RA-ILD in separate development and validation cohorts. This overlap supports the concept of shared etiopathogenesis of IPF and RA-ILD and illustrates the potential for peripheral blood biomarker panels to stratify ILD risk among patients with RA.

INTRODUCTION

Interstitial lung disease (ILD) is a common extra-articular manifestation of rheumatoid arthritis (RA), with clinically relevant RA-ILD identified in approximately 5% to 15% of people with RA.[1–3] The prognosis after the identification of RA-ILD is poor, with most studies showing a median survival of approximately three to eight years.[4] Given this poor prognosis, strategies to identify RA-ILD at earlier stages are needed. The importance of early identification of ILD is reflected in recent guidelines from the

The views expressed in this article are those of the authors and do not necessarily reflect the position or policy of the Department of Veterans Affairs or the United States government.

Dr Baker's work was supported by VA Rehabilitation Research and Development (I01 RX003644; RX004770). Dr Wysham's work was supported by VA Clinical Science Research and Development (CSR&D) (CX002351). Dr Poole's work is supported by the National Institute of Occupational Safety and Health, NIH (grant R01-OH-01245). Drs Poole and Mikuls's work was supported by the Department of Defense (grant PR200793). Dr Mikuls's work was supported by the NIH (grant 2U54-GM-115458) and the VA Biomedical Laboratory Research and Development (grant BX003635). Dr England's work was supported by the VA CSR&D (grant IK2 CX002203) and the Rheumatology Research Foundation.

[1]VA Nebraska-Western Iowa Health Care System, Omaha; [2]University of Nebraska Medical Center, Omaha; [3]University of Pittsburgh, Pittsburgh, Pennsylvania; [4]Corporal Michael J. Crescenz VA Medical Center, Philadelphia, Pennsylvania; [5]University of Pennsylvania, Philadelphia; [6]VA Puget Sound Health Care System, Seattle, Washington; [7]University of Washington, Seattle; [8]VA Boston Health Care System, Boston, Massachusetts; [9]VA North Texas Health Care System, Dallas; [10]University of Texas Southwestern, Dallas; [11]Washington VA Medical Center, Washington, DC; [12]Howard University, Washington, DC; [13]Georgetown University, Washington, DC; [14]Salt Lake City VA Health Care System, Salt Lake City, Utah; [15]University of Utah, Salt Lake City; [16]University of Kansas, Kansas City.

Drs England and Ascherman are co-senior authors and contributed equally to this work.

American College of Rheumatology (ACR)/American College of Chest Physicians,[5] which recommend screening for ILD in patients with RA at increased risk for ILD. However, guidance is limited on which patients warrant screening and how often screening should be completed. A number of clinical risk factors for RA-ILD have been identified, including cigarette smoking, male sex, older age, and higher articular disease activity,[6] but these clinical risk factors alone are inadequate to accurately identify RA-ILD.[7] Therefore, strategies to more precisely risk-stratify individuals at risk for RA-ILD are needed to help inform individual patient monitoring and treatment, as well as to identify patients at high risk for or with early RA-ILD to include in clinical studies.

Identification of peripheral biomarkers associated with RA-ILD may not only help to inform risk stratification and screening but also further our understanding of the processes leading to the development and/or progression of ILD. Indeed, a number of candidate biomarkers have been evaluated in previous studies.[8] Many of these were initially studied in idiopathic pulmonary fibrosis (IPF), the most common idiopathic interstitial pneumonia and a disease that shares epidemiologic and genetic risk factors as well as histopathologic and radiologic features with RA-ILD.[9] In previous work comparing the levels of 45 protein biomarkers among individuals with RA-ILD or IPF and healthy controls, the levels of eight were significantly higher in individuals with IPF (eotaxin, Flt-3L, interleukin-8 [IL-8], macrophage-derived chemokine [MDC], matrix metalloproteinase 2/7/9 [MMP-2/7/9], and monocyte chemoattractant protein 1 [MCP-1]).[10] Moreover, the levels of six of these (eotaxin, Flt-3L, IL-8, MMP-2/7/9) were also increased in individuals with RA-ILD, demonstrating overlap in peripheral blood biomarker profiles.[10]

The objective of this study was to evaluate the ability of IPF-derived peripheral biomarkers to risk-stratify ILD in independent RA cohorts. Due to the shared histopathologic and radiologic features of RA-ILD and IPF, we hypothesized that a biomarker panel linked to IPF would also be significantly associated with prevalent and incident RA-ILD risk.

PATIENTS AND METHODS

Study design. We initially conducted a cross-sectional study to derive a composite multibiomarker score for RA-ILD using two cohorts of patients with RA with and without ILD. We subsequently validated the score using an independent multicenter prospective RA cohort, the Veterans Affairs Rheumatoid Arthritis (VARA) Registry. Validation was performed with both cross-sectional (prevalent ILD) and cohort (incident ILD) study designs. The study was approved by the participating centers' institutional review boards and by the VARA Scientific Ethics Advisory Committee. All study participants provided informed consent.

Analysis of IPF multibiomarker score. For initial assessment of the IPF multibiomarker score, we used two separate cohorts of patients with RA with and without ILD. Selection of these cohorts has been previously described in detail.[10,11] Briefly, individuals meeting the 1987 ACR RA classification criteria[12] were prospectively enrolled in separate Veterans Affairs (VA) (n = 103) and non-VA (n = 71) cohorts. Participants in the VA cohort were recruited prospectively from three VA facilities (Miami, FL; Washington, DC; and Dallas/North Texas; n = 53) or were enrolled in the VARA Registry (n = 50). Participants from the non-VA cohort were recruited from the University of Pittsburgh and Brigham and Women's Hospital. Individuals were classified as RA without ILD, RA with subclinical ILD, or RA-ILD based on a combination of clinical features, pulmonary function testing, and high-resolution computed tomography (HRCT) findings that included ground glass opacification, septal thickening, subpleural reticulation, honeycombing, and/or traction bronchiectasis. Chest HRCT scans were assessed by radiologists blinded to the clinical data. Those with RA-ILD were further classified as having a usual interstitial pneumonia (UIP) or non-UIP pattern based on the radiologists' determination.

Based on their association with IPF in previous work,[10] we measured concentrations of eotaxin, Flt-3L, IL-8, MDC, MCP-1, and MMP-2/7/9 from serum samples using a Luminex xMAP bead-based multiplex enzyme-linked immunosorbent assay (ELISA) platform (EMD Millipore). Concentrations were standardized based on cohort-specific means and SDs, in which the standardized concentration was equal to the difference between the serum concentration and the cohort mean divided by the SD for each analyte. We then calculated a composite multibiomarker score for each participant by summing the standardized concentrations for individual analytes. MMP-9 was excluded from the biomarker score in the non-VA cohort, as 15 of 71 patients had MMP-9 concentrations above the upper limit of detection, precluding accurate calculation of cohort mean and SD. For each cohort, we performed pairwise comparisons of the multibiomarker score between the RA without ILD, RA with subclinical ILD (imaging evidence of ILD without clinical manifestations of cough or dyspnea), non-UIP RA-ILD, and UIP RA-ILD groups using Mann-Whitney U tests.

Validation in VARA cohort. We externally validated this IPF-derived multibiomarker score in a cohort of US veterans with

Additional supplementary information cited in this article can be found online in the Supporting Information section (https://acrjournals.onlinelibrary.wiley.com/doi/10.1002/art.43383).

Author disclosures are available at https://onlinelibrary.wiley.com/doi/10.1002/art.43383.

Address correspondence via email to Bryant R. England, MD, PhD, at bryant.england@unmc.edu.

Submitted for publication April 9, 2025; accepted in revised form August 18, 2025.

RA enrolled in the VARA Registry, a multicenter prospective cohort of US veterans with RA.[13] All participants in the registry meet 1987 ACR criteria for RA.[12] Clinical data were collected at registry enrollment and longitudinally during clinical follow-up as per standard of care. RA articular disease activity measured by the Disease Activity Score in 28 joints (DAS28) was calculated at registry enrollment. Serum and plasma samples were collected at the time of registry enrollment and stored at −70°C. Anti–cyclic citrullinated peptide (anti-CCP) antibody was measured by ELISA using banked serum samples. Registry enrollment began in 2003, and the current study included data collection through December 4, 2023.

For those patients in the VARA Registry, ILD was identified and validated by systematic medical record review as described previously.[14,15] Registry participants were screened for the presence of RA-ILD by diagnostic codes and were classified as having RA-ILD if they were diagnosed with ILD by their treating provider plus had either chest computed tomography (CT) or lung biopsy features consistent with ILD. ILD pattern was classified as UIP if this was either documented in the clinical radiology read or when honeycombing was present and was classified as non-UIP for all other reads. Prevalent ILD was defined as being present at the time of registry enrollment, and incident ILD defined as developing at any time after registry enrollment during longitudinal follow-up, with censoring for death or the end of the study period.

Using banked samples collected at registry enrollment, plasma/serum analytes included in the multibiomarker score (eotaxin, Flt-3L, IL-8, MDC, MCP-1, and MMP-7/9) were measured using R-PLEX ELISA assays from MesoScale Diagnostics.[15] MMP-2 concentrations were not available in the VARA cohort and therefore were excluded from the score. Concentrations of the biomarkers were log-transformed to normalize their distributions, and the multibiomarker score was calculated as described for the development cohorts using standardized concentrations of the individual analytes. To account for the possibility of nonlinear associations between the multibiomarker score and ILD, we also divided the cohort into quartiles based on the multibiomarker score, with quartile 1 representing the lowest biomarker score values and quartile 4 representing the highest values.

Statistical analysis. The association of the IPF multibiomarker score with prevalent and incident RA-ILD in the VARA cohort was assessed using logistic and Cox regression models, respectively, adjusted for age, sex, race, smoking status, anti-CCP antibody status, and DAS28. For prevalent analyses, participants who developed incident RA-ILD during longitudinal follow-up were excluded, and for incident analyses, participants who had prevalent RA-ILD at baseline were excluded. Discrimination of prevalent RA-ILD was evaluated with receiver operating characteristic (ROC) curves, initially with clinical predictors alone and subsequently with the addition of the multibiomarker score. In exploratory analyses, we evaluated score performance by assessing the sensitivity, specificity, positive predictive value, and negative predictive value at varying cutoff values. The predictive ability of the multibiomarker score for incident RA-ILD compared to clinical predictors alone was assessed with Harrell's C statistic.

Beyond these assessments, we also performed exploratory analyses in which we measured the association of the IPF biomarker score with RA-ILD stratified by radiographic pattern (UIP vs non-UIP). Due to strong associations of both prevalent and incident RA-ILD with MMP-7 concentrations in prior work,[15] we performed sensitivity analyses in which MMP-7 was excluded from the multibiomarker score. Additionally, due to overlap of a small number of participants between the VA development cohort and the VARA validation cohort (n = 50), we performed a sensitivity analysis in which these participants were excluded from the regression models in the VARA validation cohort. Due to the possibility of disease latency, we also performed a sensitivity analysis in which the regression models were performed with prevalent ILD defined as ILD identified before or within the first year after registry enrollment and incident ILD defined as developing one or more years after enrollment.

RESULTS

Patient characteristics in study cohorts. The development cohorts consisted of 103 participants in the VA cohort and 71 participants in the non-VA cohort, characteristics of which have been reported previously.[10] Ten participants were excluded from the original VA cohort due to having incomplete biomarker measurements; therefore, 93 participants from the VA development cohort were included in the current analyses (Supplemental Table 1). In the validation cohort from the VARA Registry, a total of 2,507 participants with complete biomarker measurements were included in analyses. Of these participants, 106 had prevalent ILD and 153 developed incident ILD during 20,142 (mean 8.4 years) patient-years of follow-up (Table 1). Seven participants from the VARA Registry were excluded from analyses because available information was indeterminate for the presence/absence of ILD. Compared to participants without ILD, those with prevalent ILD were older, had a longer duration of RA, and were more likely to be anti-CCP positive and current/former smokers (Table 1).

IPF multibiomarker score in RA development cohorts. For both the VA and non-VA development cohorts, patients with RA with ILD had significantly higher IPF multibiomarker scores than those without ILD (mean biomarker scores: VA 1.1 [non-UIP] and 2.9 [UIP] vs −3.9 [RA alone], $P < 0.0001$; non-VA 0.5 [non-UIP] and 4.0 [UIP] vs −1.8 [RA alone], $P = 0.002$; Figure 1). The multibiomarker score was highest among those with a UIP pattern of ILD compared to those with a non-UIP

Table 1. Baseline characteristics of participants in the Veterans Affairs Rheumatoid Arthritis Registry (validation cohort)*

	RA without ILD	RA-ILD	*P* value
Cross-sectional study of prevalent RA-ILD			
n	2,241	106	–
Age, mean (SD), y	63.8 (11.2)	68.0 (9.4)	<0.001
Male sex, %	88.0	91.5	0.27
White race, %	77.7	77.4	0.94
Body mass index[a]	29.0	29.2	0.67
Smoking status, %[a]			0.015
Never	21.4	9.8	–
Former	53.8	64.7	–
Current	24.7	25.5	–
RA duration, mean (SD), y[a]	11.2 (11.2)	14.3 (13.8)	0.005
Anti-CCP positive, %[a]	76.1	85.8	0.021
DAS28, mean (SD)[a]	3.74 (1.57)	4.03 (1.20)	0.07
Multibiomarker score, mean (SD)	−0.08 (3.78)	1.04 (3.99)	0.003
Eotaxin	0.01 (0.99)	0.09 (1.03)	0.34
Flt-3L	−0.02 (0.97)	0.31 (0.98)	<0.001
IL-8	−0.01 (0.98)	0.04 (1.01)	0.59
MCP-1	0.01 (0.97)	−0.01 (1.17)	0.83
MDC	0.02 (0.96)	−0.08 (1.17)	0.29
MMP-7	−0.04 (0.97)	0.54 (1.27)	<0.001
MMP-9	−0.04 (1.00)	0.15 (0.99)	0.047
Cohort study of incident RA-ILD			
n	2,241	153	–
Age, mean (SD), y	63.8 (11.2)	64.6 (9.1)	0.37
Male sex, %	88.0	92.8	0.07
White race, %	77.7	70.6	0.043
Body mass index[b]	29.0	28.5	0.28
Smoking status, %[b]			0.22
Never	21.4	17.1	–
Former	53.8	52.6	–
Current	24.7	30.3	–
RA duration, mean (SD), y[b]	11.2 (11.2)	10.9 (10.8)	0.78
Anti-CCP positive, %[b]	76.1	83.0	0.052
DAS28, mean (SD)[b]	3.74 (1.57)	4.08 (1.46)	0.010
Multibiomarker score, mean (SD)	−0.08 (3.78)	0.60 (4.08)	0.031
Eotaxin	−0.01 (0.99)	0.06 (1.12)	0.43
Flt-3L	−0.02 (0.97)	−0.06 (1.16)	0.61
IL-8	−0.01 (0.98)	0.15 (1.15)	0.048
MCP-1	0.01 (0.97)	0.04 (1.13)	0.72
MDC	0.02 (0.96)	−0.04 (1.16)	0.45
MMP-7	−0.04 (0.97)	0.26 (0.94)	<0.001
MMP-9	−0.04 (1.00)	0.19 (1.00)	0.005

* CCP, cyclic citrullinated peptide; DAS28, Disease Activity Score in 28 joints; IL, interleukin; ILD, interstitial lung disease; MCP, monocyte chemoattractant protein 1; MDC, macrophage-derived chemokine; MMP, matrix metalloproteinase; RA, rheumatoid arthritis.
[a] Missing data: body mass index (n = 163 RA without ILD, n = 4 RA-ILD), smoking status (n = 59 RA without ILD, n = 4 RA-ILD), RA duration (n = 56 RA without ILD, n = 3 RA-ILD), anti-CCP (n = 1 RA without ILD), DAS28 (n = 162 RA without ILD, n = 6 RA-ILD).
[b] Missing data: body mass index (n = 163 RA without ILD, n = 3 RA-ILD), smoking status (n = 59 RA without ILD, n = 1 RA-ILD), RA duration (n = 56 RA without ILD, n = 3 RA-ILD), anti-CCP (n = 1 RA without ILD), DAS28 (n = 162 RA without ILD, n = 4 RA-ILD).

pattern, though this was only significant in the non-VA cohort. Multibiomarker scores did not significantly differ between those with subclinical ILD and those without ILD.

IPF multibiomarker score in RA validation cohort. In the VARA validation cohort, participants with prevalent ILD had higher IPF multibiomarker scores than those without ILD (mean 1.04 vs −0.08; *P* = 0.003). Among individual analytes in the multibiomarker score, Flt-3L, MMP-7, and MMP-9 concentrations were all significantly higher in participants with prevalent ILD (Table 1). In adjusted analyses, higher multibiomarker scores were associated with greater odds of prevalent ILD (adjusted odds ratio [aOR] 1.07 [95% confidence interval (CI) 1.01–1.14] per one-point increase in multibiomarker score). Those individuals in the highest quartile of IPF multibiomarker scores had greater than two-fold increased odds of prevalent ILD (aOR 2.14 [95% CI 1.18–3.87]; Table 2) compared to those in the lowest quartile.

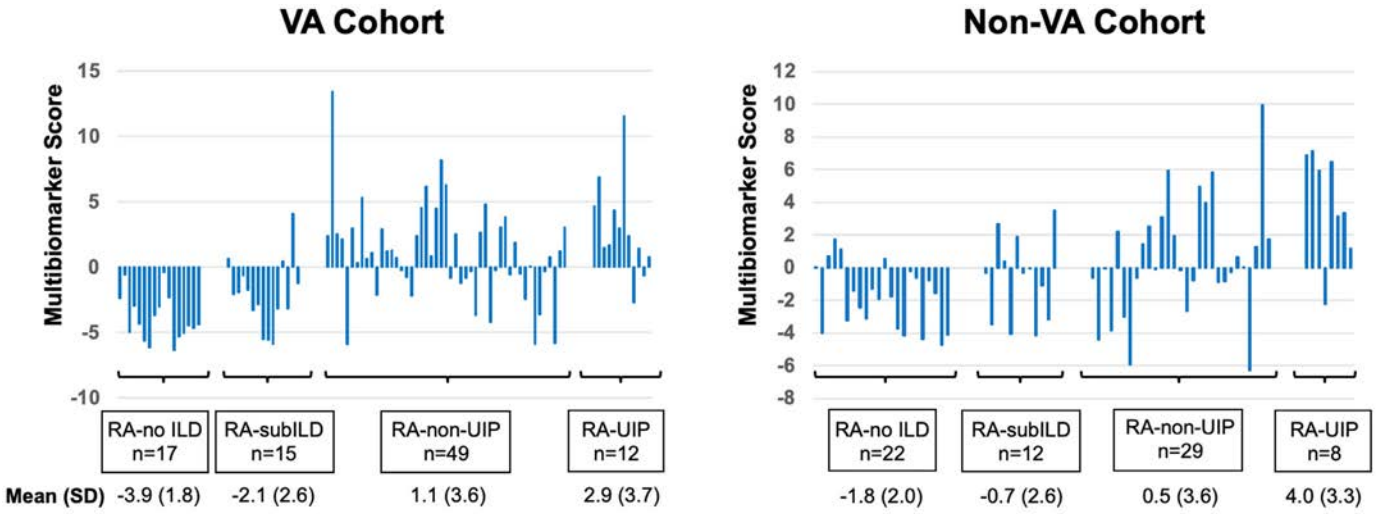

Comparison	p-value
RA-ILD[1] vs. RA-no ILD	<0.0001
RA-subILD vs. RA-no ILD	0.05
RA-non-UIP ILD vs. RA-no ILD	<0.0001
RA-UIP vs. RA-no ILD	<0.0001
RA-UIP vs. RA-non-UIP ILD	0.13
RA-UIP vs. RA-ILD[2]	0.03

[1]includes all subcategories of ILD
[2]includes RA-subILD and RA-non-UIP ILD

Comparison	p-value
RA-ILD[1] vs. RA-no ILD	0.002
RA-subILD vs. RA-no ILD	0.22
RA-non-UIP ILD vs. RA-no ILD	0.006
RA-UIP vs. RA-no ILD	0.0006
RA-UIP vs. RA-non-UIP ILD	0.01
RA-UIP vs. RA-ILD[2]	0.006

[1]includes all subcategories of ILD
[2]includes RA-subILD and RA-non-UIP ILD

Figure 1. IPF multibiomarker score correlates with stage of RA-ILD in independent development cohorts. Bar graphs correspond to composite IPF multibiomarker scores in patients with RA without ILD, with subclinical ILD, or with clinically evident ILD (distinguished by the presence vs absence of UIP-like abnormalities on chest CT). MMP-9 was excluded from the score in the non-VA cohort. Tables list *P* values resulting from subgroup comparisons using Mann-Whitney U tests. CT, computed tomography; ILD, interstitial lung disease; IPF, idiopathic pulmonary fibrosis; MMP, matrix metalloproteinase; RA, rheumatoid arthritis; UIP, usual interstitial pneumonia; VA, Veterans Affairs.

In ROC analyses, the addition of the IPF multibiomarker score to clinical variables alone (age, sex, race, smoking status, anti-CCP antibody positivity, and baseline DAS28) did not significantly improve prevalent RA-ILD discrimination (area under the curve 0.667 vs 0.653, $P = 0.32$; Figure 2). We assessed the sensitivity and specificity, as well as the positive and negative predictive values, of the multibiomarker score at varying cut points (Supplemental Table 2). Although a multibiomarker score greater than −1 had a sensitivity of 80% for RA-ILD, the specificity was only 32%. Scores ≥4 had a specificity of ≥90% but were present in only 11% of the cohort and had a sensitivity of 17%. Overall, positive predictive values were low and negative predictive values were high, reflecting the low prevalence of ILD in the VARA cohort.

Table 2. Associations of the IPF multibiomarker score with prevalent and incident RA-ILD in the VARA validation cohort*

Multibiomarker score quartile	Adjusted odds or hazard ratio (95% CI)[a]	*P* value
Prevalent ILD		
Quartile 1	Ref.	–
Quartile 2	0.74 (0.35–1.55)	0.43
Quartile 3	1.45 (0.78–2.72)	0.24
Quartile 4	2.14 (1.18–3.87)	0.01
P trend	–	0.005
Incident ILD		
Quartile 1	Ref.	–
Quartile 2	1.06 (0.63–1.78)	0.83
Quartile 3	1.32 (0.80–2.19)	0.28
Quartile 4	2.45 (1.55–3.88)	<0.001
P trend	–	<0.001

* CI, confidence interval; ILD, interstitial lung disease; IPF, idiopathic pulmonary fibrosis; RA, rheumatoid arthritis; VARA, Veterans Affairs Rheumatoid Arthritis.
[a] Prevalent ILD estimates are odds ratios, and incident ILD estimates are hazard ratios. Models were adjusted for age, sex, race, smoking status, anti–cyclic citrullinated peptide antibody positivity, and baseline RA disease activity.

Participants who developed incident ILD during longitudinal follow-up had higher IPF multibiomarker scores at registry enrollment than those without ILD (mean 0.60 vs −0.08; $P = 0.031$). Among individual analytes in the score, IL-8, MMP-7, and MMP-9 concentrations were all significantly higher in participants who developed incident ILD (Table 1). In adjusted analyses, higher multibiomarker scores were associated with a greater risk of incident ILD (adjusted hazard ratio [aHR] 1.08 [95% CI 1.03–1.13] per one-point increase). Those in the highest quartile of IPF multibiomarker scores had a greater than two-fold increased risk of incident ILD (aHR 2.44 [95% CI 1.55–3.88]; Table 2). Over 15 years of follow-up, those in the highest quartile of

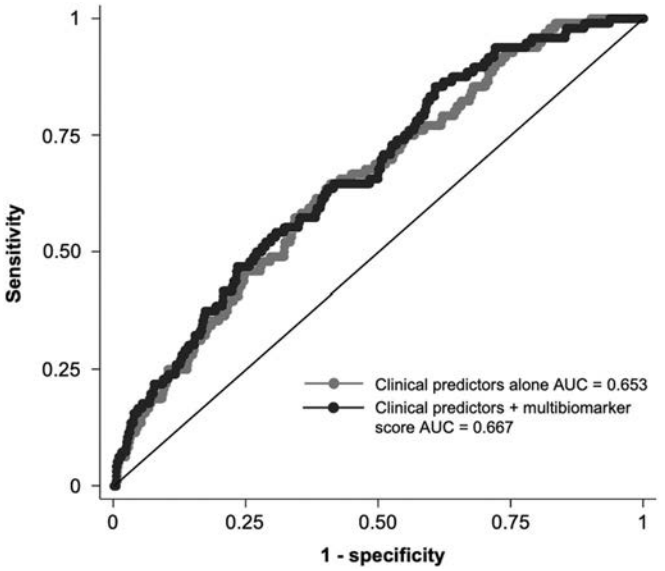

Figure 2. Receiver operating characteristic curves for clinical predictors versus multibiomarker score in cross-sectional analyses of prevalent RA-ILD (validation cohort). Clinical predictors included age, sex, race, smoking status, anti–cyclic citrullinated peptide antibody positivity, and baseline DAS28. The multibiomarker score was measured as a continuous variable. AUC, area under the curve; DAS28, Disease Activity Score in 28 joints; ILD, interstitial lung disease; RA, rheumatoid arthritis.

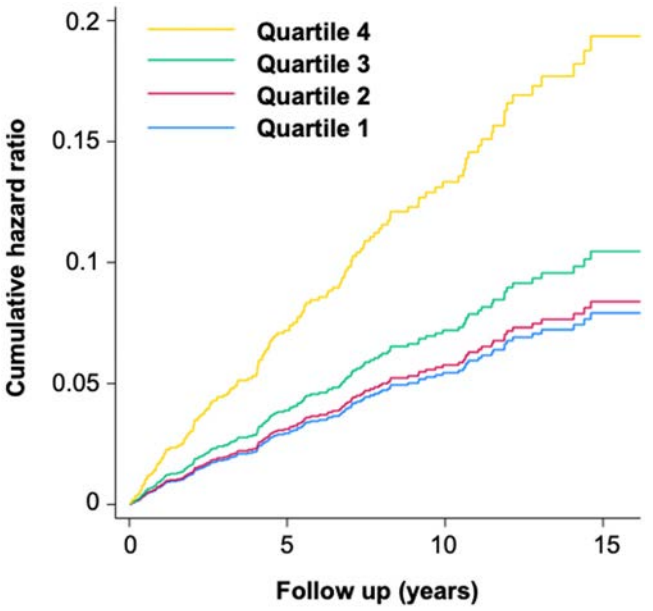

Figure 3. Cumulative hazard of incident RA-ILD by multibiomarker score quartiles (validation cohort). Cumulative hazard plots were constructed using Cox models and adjusted for age, sex, race, smoking, anti–cyclic citrullinated peptide antibody positivity, RA disease activity, and period of enrollment. The x-axis indicates follow-up time (years), and the y-axis indicates the cumulative hazard of incident RA-ILD in adjusted models. ILD, interstitial lung disease; RA, rheumatoid arthritis. Color figure can be viewed in the online issue, which is available at http://onlinelibrary.wiley.com/doi/10.1002/art.43383/abstract.

multibiomarker scores had a cumulative hazard of incident ILD approaching 20%, compared to <10% for quartiles 1, 2, and 3 (Figure 3). Relative to clinical predictors alone, the addition of the multibiomarker score led to a significant but modest improvement in discrimination of incident RA-ILD when divided into quartiles (Harrell's C statistic 0.627 vs 0.666, $P = 0.028$) but not as a continuous measure (Harrell's C statistic 0.627 vs 0.644, $P = 0.29$).

Exploratory analyses in validation cohort. Among VARA participants with prevalent ILD, 55 had ILD patterns classified as UIP and 51 had ILD patterns classified as non-UIP. As a continuous measure, associations of the IPF multibiomarker score with prevalent ILD were similar in non-UIP (aOR 1.10 [95% CI 1.00–1.21] per one-point increase) and UIP (aOR 1.05 [95% CI 0.97–1.14] per one-point increase). Those in the highest quartile of multibiomarker scores had significantly higher odds of prevalent non-UIP (aOR 3.07 [95% CI 1.20–7.83]), whereas odds of UIP did not reach significance for those in the highest quartile of multibiomarker scores (Supplemental Table 3).

Among participants who developed incident ILD, 85 had ILD patterns classified as UIP and 68 had ILD patterns classified as non-UIP. As a continuous measure, the IPF multibiomarker score was similarly associated with incident non-UIP (aHR 1.10 [95% CI 1.02–1.19] per one-point increase) and UIP (aHR 1.06 [95% CI 1.00–1.13] per one-point increase). Those in the highest quartile of multibiomarker scores had a >2.5-fold increased risk of incident ILD, with associations observed for both non-UIP and UIP patterns (Supplemental Table 3).

Sensitivity analyses in validation cohort. When the 50 patients with overlapping data from the validation and development cohorts were excluded from analysis of the VARA cohort, associations of the IPF multibiomarker score (continuous and quartiles) with prevalent and incident ILD were similar in magnitude and significance (Supplemental Table 4) to parallel analyses including these individuals (Table 2). In sensitivity analyses excluding MMP-7 (which has previously been linked to prevalent and incident RA-ILD in this cohort), the IPF multibiomarker score was modestly attenuated and no longer significantly associated with prevalent ILD as a continuous measure (aOR 1.04 [95% CI 0.97–1.11] per one-point increase), and similarly the highest quartile multibiomarker score was no longer significantly associated with prevalent ILD (aOR 1.66 [95% CI 0.92–3.00]). In contrast, although results were attenuated relative to the primary analysis, the IPF multibiomarker score remained significantly associated with incident ILD after excluding MMP-7 (aHR 1.06 [95% CI 1.01–1.11] per one-point increase; aHR 2.00 [95% CI 1.26–3.17] for the highest quartile). Following reclassification of ILD identified within the first year after registry enrollment as prevalent ILD (n = 132) and ILD identified more than one year after registry

enrollment as incident ILD (n = 127), associations of the IPF multibiomarker score with ILD were similar to those observed in the primary analyses, both as a continuous measure (aOR 1.06 [95% CI 1.00–1.12] per one-point increase for prevalent ILD, aHR 1.10 [95% CI 1.04–1.16] per one-point increase for incident ILD) and by quartile (data not shown).

DISCUSSION

In this observational study with independent development and validation cohorts, we found that a panel of IPF-derived peripheral biomarkers was similarly associated with prevalent and incident ILD among participants with RA. These findings were strongest for the development of incident RA-ILD, as those with the highest quartile of multibiomarker scores demonstrated a nearly 20% risk of developing incident RA-ILD over 15 years of longitudinal follow-up. Moreover, these results persisted when analyzing UIP and non-UIP RA-ILD separately. Together, these findings provide further support for a shared etiopathogenesis between RA-ILD and IPF and illustrate the potential value of peripheral blood biomarker panels for RA-ILD risk stratification.

There exists an unmet need to accurately identify patients with RA at an increased risk for the presence or development of ILD, and routinely measured clinical and laboratory data have a limited ability to fill this void.[7] Accurate measures to identify these patients may help to select patients with RA who are more likely to benefit from earlier or more frequent screening for RA-ILD with chest HRCT and pulmonary function tests. The measurement of peripheral blood biomarkers is an attractive, minimally invasive approach with the potential for widespread application to help bridge this gap. In this study, we found that a multibiomarker score of seven IPF-derived peripheral blood biomarkers was associated with both prevalent and incident RA-ILD risk. Even when removing the known RA-ILD–associated biomarker MMP-7 from the panel,[15] the IPF multibiomarker score remained significantly associated with incident, but not prevalent, RA-ILD.

Patients with RA with the highest quartile of IPF multibiomarker scores had a greater than two-fold increased risk of prevalent and incident RA-ILD, although the multibiomarker score did not demonstrate sufficient clinical utility for the identification of prevalent ILD. Model performance metrics (eg, area under the ROC curve) did not show improved discrimination over clinical risk factors alone, and none of the cut points demonstrated sufficient sensitivity and specificity. These results exemplify the challenge of constructing a clinically meaningful biomarker panel that is associated with ILD risk. Further research is needed to identify the clinical, laboratory, and genetic risk factors that can accurately identify patients with RA with or at risk for ILD. An additional unmet need is a strategy to identify patients with RA with subclinical ILD at greater risk to progress to clinically apparent RA-ILD, thus potentially warranting closer monitoring or earlier intervention. In the development cohorts, there was no statistically significant difference in multibiomarker scores between patients with RA without ILD and those with subclinical ILD. However, there was a numerical increase in the mean multibiomarker score across higher stages of disease (no ILD vs subclinical ILD vs clinically apparent ILD). Moreover, the statistically significant association of the IPF multibiomarker panel with the development of incident ILD in the VARA validation cohort suggests that this panel may have clinical utility in identifying at-risk individuals without ILD or with subclinical ILD who would benefit from heightened surveillance for emergence of clinically significant ILD. Based on our findings, future studies with large sample sizes and comprehensive phenotyping of subclinical ILD status are clearly needed to more adequately address this question.

Although this multibiomarker score does not add significantly to established RA-ILD risk factors for the predictive value of RA-ILD, the observed associations with prevalent and incident RA-ILD do lend further support to the existence of common final pathways linking RA-ILD and IPF. RA-ILD shares a number of risk factors, histopathologic and radiologic findings, and clinical features with IPF, suggesting an overlap in the etiopathogenesis of these conditions.[6] Recent genetic studies finding the *MUC5B* promoter variant, the strongest genetic risk factor for IPF, to also be associated with RA-ILD in a UIP pattern further support this connection.[16,17] In this study, we have added to the growing body of literature by observing associations of IPF-derived peripheral blood biomarkers (eotaxin, Flt-3L, IL-8, MDC, MCP-1, and MMP-2/7/9) with prevalent and incident RA-ILD. This observation suggests that similar processes may be occurring on a molecular level in IPF and RA-ILD. Importantly, this potential molecular overlap raises the possibility that treatment responses to pharmacologic therapies could be shared between IPF and some patients with RA-ILD. Indeed, recent studies have suggested that antifibrotic treatments used for IPF may similarly slow the rate of decline in lung function in patients with RA-ILD.[18,19] Given the limited body of evidence for effective immunomodulatory therapy in RA-ILD and the general avoidance of immunomodulatory therapy in IPF,[20,21] it is unknown whether selected molecular "endotypes" may define subsets of RA-ILD and/or IPF with greater response to immunomodulatory therapy.

A recent meta-analysis including studies of RA-ILD reported UIP as the most common pattern of RA-ILD, followed by nonspecific interstitial pneumonia.[22] Consistent with this finding, we observed a slightly higher proportion of UIP-ILD in this study, based on the clinical radiology read. Because UIP is the pattern of IPF, we performed secondary analyses evaluating the performance of the IPF-associated multibiomarker score in patients with UIP versus non-UIP RA-ILD. In incident ILD analyses, the multibiomarker score was associated with both a UIP and a non-UIP RA-ILD pattern. However, in prevalent ILD analyses, associations were stronger for the non-UIP pattern. This finding was unexpected. Given the smaller sample sizes of this secondary analysis and potential misclassification of ILD pattern based on clinical radiology reads, our

findings should be considered hypothesis generating. Of note, previous research in this cohort did show an association of the *MUC5B* rs35705950 promoter variant (an established risk factor for IPF and UIP RA-ILD) with UIP RA-ILD but not non-UIP RA-ILD,[16] suggesting validity of the case definitions for UIP RA-ILD and non-UIP RA-ILD. It is possible non-UIP RA-ILD may later evolve into UIP RA-ILD.[23] In this situation, the molecular pathways leading to UIP could be highly activated in advance of characteristic radiographic abnormalities indicative of UIP. Future studies with longitudinal, comprehensive phenotyping of RA-ILD subtypes are warranted to better understand any potential differences in biomarker profiles that may be present among different clinical, radiographic, and/or histopathologic subtypes.

Although we did not evaluate the progression of radiologic or physiologic ILD parameters in this study, future studies should also evaluate whether levels of these IPF-associated proteins, or other peripheral blood biomarkers, are able to meaningfully predict RA-ILD progression. Not all patients with RA-ILD appear to show substantial progression over time,[24–26] and the identification of patients at the greatest risk for progression may help to identify patients most likely to benefit from immunosuppressive or antifibrotic therapies. Similarly, we were not able to assess whether biomarker measurements differ among patients with early versus established RA-ILD in the validation cohort, which will require studies with longitudinal clinical follow-up and serial biomarkers measurements.

There are limitations to this study. The validation cohort used was a US veteran population with a large proportion of older men who were current or former smokers, which may impact generalizability. However, this is a useful population to study because it represents a high-risk group for the development of RA-ILD, and findings from the non-VA development cohort suggest that similar associations may be seen in other cohorts with more representative clinical/demographic profiles. There were also minor differences in the analytes included in the IPF multibiomarker scores between the development and validation cohorts. Despite these differences, the results consistently showed an association of a composite IPF-derived peripheral biomarker score with RA-ILD. Different methods were used to define the presence of RA-ILD in the development and validation cohorts, but the reproducible results across cohorts emphasize the consistency and generalizability of our findings. Finally, there was partial overlap in participants from the VA development cohort and the VARA validation cohort (n = 50); importantly, however, excluding these participants in a sensitivity analysis did not meaningfully change results.

In conclusion, this study showed that an IPF-derived peripheral blood biomarker panel was associated with RA-ILD in multiple independent cohorts. These findings provide additional evidence supporting a shared etiopathogenesis of RA-ILD and IPF. However, the current multibiomarker score did not demonstrate sufficient performance metrics for clinical utility. Future studies incorporating additional peripheral blood biomarkers, agnostic biomarker analyses, and other clinical measures are needed to develop and validate clinically meaningful tools to stratify ILD risk for patients with RA.

AUTHOR CONTRIBUTIONS

All authors contributed to at least one of the following manuscript preparation roles: conceptualization AND/OR methodology, software, investigation, formal analysis, data curation, visualization, and validation AND drafting or reviewing/editing the final draft. As corresponding author, Dr. England confirms that all authors have provided the final approval of the version to be published and takes responsibility for the affirmations regarding article submission (eg, not under consideration by another journal), the integrity of the data presented, and the statements regarding compliance with institutional review board/Declaration of Helsinki requirements.

REFERENCES

1. Bongartz T, Nannini C, Medina-Velasquez YF, et al. Incidence and mortality of interstitial lung disease in rheumatoid arthritis: a population-based study. Arthritis Rheum 2010;62(6):1583–1591.
2. Duarte AC, Porter JC, Leandro MJ. The lung in a cohort of rheumatoid arthritis patients-an overview of different types of involvement and treatment. Rheumatology (Oxford) 2019;58(11):2031–2038.
3. Samhouri BF, Vassallo R, Achenbach SJ, et al. Incidence, risk factors, and mortality of clinical and subclinical rheumatoid arthritis-associated interstitial lung disease: a population-based cohort. Arthritis Care Res (Hoboken) 2022;74(12):2042–2049.
4. Farquhar HJ, Beckert N, Beckert L, et al. Survival of adults with rheumatoid arthritis associated interstitial lung disease - a systematic review and meta-analysis. Semin Arthritis Rheum 2023;60:152187.
5. Johnson SR, Bernstein EJ, Bolster MB, et al. 2023 American College of Rheumatology (ACR)/American College of Chest Physicians (CHEST) guideline for the screening and monitoring of interstitial lung disease in people with systemic autoimmune rheumatic diseases. Arthritis Care Res (Hoboken) 2024;76(8):1070–1082.
6. Sullivan DI, Ascherman DP. Rheumatoid arthritis-associated interstitial lung disease (RA-ILD): update on prevalence, risk factors, pathogenesis, and therapy. Curr Rheumatol Rep 2024;26(12):431–449.
7. Kronzer VL, Huang W, Dellaripa PF, et al. Lifestyle and clinical risk factors for incident rheumatoid arthritis-associated interstitial lung disease. J Rheumatol 2021;48(5):656–663.
8. Van Kalsbeek D, Brooks R, Shaver D, et al. Peripheral blood biomarkers for rheumatoid arthritis-associated interstitial lung disease: a systematic review. ACR Open Rheumatol 2023;5(4):201–226.
9. Ley B, Collard HR. Epidemiology of idiopathic pulmonary fibrosis. Clin Epidemiol 2013;5:483–492.
10. Kass DJ, Nouraie M, Glassberg MK, et al. Comparative profiling of serum protein biomarkers in rheumatoid arthritis-associated interstitial lung disease and idiopathic pulmonary fibrosis. Arthritis Rheumatol 2020;72(3):409–419.
11. Chen J, Doyle TJ, Liu Y, et al. Biomarkers of rheumatoid arthritis-associated interstitial lung disease. Arthritis Rheumatol 2015;67(1):28–38.
12. Arnett FC, Edworthy SM, Bloch DA, et al. The American Rheumatism Association 1987 revised criteria for the classification of rheumatoid arthritis. Arthritis Rheum 1988;31(3):315–324.
13. Mikuls TR, Reimold A, Kerr GS, et al. Insights and Implications of the VA Rheumatoid Arthritis Registry. Fed Pract 2015;32(5):24–29.
14. Natalini JG, Baker JF, Singh N, et al. Autoantibody seropositivity and risk for interstitial lung disease in a prospective male-predominant

rheumatoid arthritis cohort of U.S. veterans. Ann Am Thorac Soc 2021;18(4):598–605.

15. Luedders BA, Wheeler AM, Ascherman DP, et al. Plasma matrix metalloproteinase concentrations and risk of interstitial lung disease in a prospective rheumatoid arthritis cohort. Arthritis Rheumatol 2024;76(7):1013–1022.
16. Wheeler AM, Baker JF, Poole JA, et al. Genetic, social, and environmental risk factors in rheumatoid arthritis-associated interstitial lung disease. Semin Arthritis Rheum 2022;57:152098.
17. Juge PA, Lee JS, Ebstein E, et al. MUC5B promoter variant and rheumatoid arthritis with interstitial lung disease. N Engl J Med 2018; 379(23):2209–2219.
18. Matteson EL, Aringer M, Burmester GR, et al. Effect of nintedanib in patients with progressive pulmonary fibrosis associated with rheumatoid arthritis: data from the INBUILD trial. Clin Rheumatol 2023;42(9): 2311–2319.
19. Solomon JJ, Danoff SK, Woodhead FA, et al; TRAIL1 Network Investigators. Safety, tolerability, and efficacy of pirfenidone in patients with rheumatoid arthritis-associated interstitial lung disease: a randomised, double-blind, placebo-controlled, phase 2 study. *Lancet* Respir Med 2023;11(1):87–96.
20. Johnson SR, Bernstein EJ, Bolster MB, et al. 2023 American College of Rheumatology (ACR)/American College of Chest Physicians (CHEST) guideline for the treatment of interstitial lung disease in people with systemic autoimmune rheumatic diseases. Arthritis Rheumatol 2024;76(8):1182–1200.
21. Raghu G, Remy-Jardin M, Richeldi L, et al. Idiopathic pulmonary fibrosis (an update) and progressive pulmonary fibrosis in adults: an official ATS/ERS/JRS/ALAT clinical practice guideline. Am J Respir Crit Care Med 2022;205(9):e18–e47.
22. Joy GM, Arbiv OA, Wong CK, et al. Prevalence, imaging patterns and risk factors of interstitial lung disease in connective tissue disease: a systematic review and meta-analysis. Eur Respir Rev 2023;32(167): 220210.
23. Silva CIS, Müller NL, Hansell DM, et al. Nonspecific interstitial pneumonia and idiopathic pulmonary fibrosis: changes in pattern and distribution of disease over time. Radiology 2008;247(1):251–259.
24. Chang SH, Lee JS, Ha YJ, et al. Lung function trajectory of rheumatoid arthritis-associated interstitial lung disease. Rheumatology (Oxford) 2023;62(9):3014–3024.
25. Lee JS, Kim GJ, Ha YJ, et al. The Extent and diverse trajectories of longitudinal changes in rheumatoid arthritis interstitial lung diseases using quantitative HRCT scores. J Clin Med 2021;10(17):3812.
26. Mena-Vázquez N, Rojas-Gimenez M, Romero-Barco CM, et al. Predictors of progression and mortality in patients with prevalent rheumatoid arthritis and interstitial lung disease: a prospective cohort study. J Clin Med 2021;10(4):874.

Arthritis & Rheumatology
Vol. 78, No. 2, February 2026, pp 311–319
DOI 10.1002/art.43337

American College of Rheumatology
Empowering Rheumatology Professionals

Serum Urate Levels Alter the Spatial Distribution of Urate Crystals in Synovium and Correlate With Synovitis and Pain in Non-Gout Female Patients With Anteromedial Knee Osteoarthritis

Hao Xu,[1] Peng Wang,[1] Haiyang Fu,[2] Longxiao Zhang,[2] Fenggang Xiang,[2] and Shuai Xiang[1]

Objective. This study aimed to investigate alterations in the spatial distribution of urate crystals in the osteoarthritic synovium of patients with different levels of serum uric acid (SUA). Additionally, we examined the association between SUA levels and the severity of synovitis and pain in anteromedial osteoarthritis (AMOA) of the knee.

Methods. Patients who underwent knee arthroplasty due to AMOA were prospectively enrolled. Blood, synovial fluid, and synovium samples were collected and UA levels were quantified. The degree of synovitis was evaluated histologically, and the levels of inflammatory cytokines in the synovial fluid were measured. The spatial distribution of urate crystals in the synovium was determined using Gomori methenamine silver staining, and the pain subscale of the Western Ontario McMaster Universities Osteoarthritis Index was used to evaluate knee pain. The relationships among SUA, degree of synovitis, and knee pain were assessed using Spearman rank correlation and multivariable analyses.

Results. The pattern of urate crystal deposition in the osteoarthritic synovium was significantly altered in populations with different SUA levels. The capillary wall, sublining layer, and lining cells were sequentially affected. SUA level was the only risk factor for high-grade synovitis and severe pain in the multivariate analysis. SUA level was also positively correlated with UA level in the synovial fluid and synovium, Krenn histologic score of the synovium, knee pain, and inflammatory cytokine level in the synovial fluid.

Conclusion. Spatial urate crystal distribution in the synovium was altered when SUA levels were elevated. Elevated SUA levels were also associated with aggravated synovitis and pain.

INTRODUCTION

Knee osteoarthritis (OA) is among the most disabling forms of arthritis and is highly prevalent in the older population.[1] OA development and progression are a consequence of a combination of factors rather than a result of a simple wear-and-tear mechanism.[2] Although the level of inflammatory response in OA is relatively low, ample evidence has shown that synovitis, the characteristic inflammation in OA, has an etiopathogenic role.[3] Instead of being considered a consequence of cartilage damage, synovitis is now considered a precursor of OA that contributes to all stages of the disease.[4] Osteoarthritic synovitis is characterized by synovial thickening and synovial fluid effusion and is associated with knee swelling and inflammatory pain due to the secretion of inflammatory mediators, including interleukin (IL)-6 and tumor necrosis factor-α (TNF-α).[3] Increased cartilage damage is also correlated with increased activity of disintegrin and metalloproteinases with thrombospondin motifs and matrix metalloproteinases produced by inflamed fibroblast-like synoviocytes.[3] However, the factors associated with advanced synovitis in OA remain unknown.

Chronic low-grade inflammation has been linked with metabolic disorders and contributes to aggravated symptoms and accelerated progression of knee OA.[5] Therefore, the concept of "metabolic OA" has been widely accepted in recent years.

Supported by the Youth Program of National Natural Science Foundation of China (award 82002349), the Youth Program of Natural Science Foundation of Shandong Province (award ZR2020QH079), and the Postdoctoral Research Science Foundation of China (award 2022M721751).

[1]Hao Xu, MD, Peng Wang, MS, Shuai Xiang, MD: Department of Joint Surgery, the Affiliated Hospital of Qingdao University, Qingdao, Shandong, China; [2]Haiyang Fu, MS, Longxiao Zhang, MS, Fenggang Xiang, MD: Department of Pathology, the Affiliated Hospital of Qingdao University, Qingdao, Shandong, China.

Dr Hao Xu and Mr Peng Wang contributed equally to this work.

Additional supplementary information cited in this article can be found online in the Supporting Information section (https://acrjournals.onlinelibrary.wiley.com/doi/10.1002/art.43337).

Author disclosures are available at https://onlinelibrary.wiley.com/doi/10.1002/art.43337.

Address correspondence via email to Shuai Xiang, MD, at xiangshuai@qdu.edu.cn; or to Fenggang Xiang, MD, at xiangfenggang@163.com.

Submitted for publication October 9, 2024; accepted in revised form July 7, 2025.

Hyperuricemia indicates excessive accumulation of serum uric acid (SUA) due to abnormal purine metabolism and monosodium urate (MSU) crystal deposits in tissues.[6] However, no significant clinical manifestations are found in patients with hyperuricemia before the first gout flare, especially in female patients.[7] Increasing evidence has shown that rather than being asymptomatic, hyperuricemia increases the risk of multiple disorders, particularly cardiovascular and cerebrovascular events.[8] Accumulating evidence has also shown that SUA is associated with an increased prevalence of knee OA, radiologic severity,[9] faster joint space narrowing,[10] and higher effusion-synovitis scores on magnetic resonance imaging (MRI).[2] Another study demonstrated that synovial UA aggravates knee inflammation through inflammasome activation and regarded synovial UA as a danger signal for OA progression.[11]

Clinically assessed OA often coexists with gout in the same joint.[12] Acute gouty arthritis, an inflammatory arthritis with prominent synovitis, often presents with severe joint pain, swelling, and rapid destruction of cartilage and bone. Although limited evidence has shown that SUA level positively correlates with synovial volume determined by contrast-enhanced MRI,[10] the relationship between UA and the histologic features of an osteoarthritic synovium has not been reported, and the spatial distribution of urate crystals in the synovium is also unknown. We hypothesized that SUA levels may be one of the major factors involved in advanced osteoarthritic synovitis in patients with hyperuricemia. This prospective cross-sectional study aimed to investigate the effect of SUA on the distribution of MSU crystals in synovium, intraarticular UA expression, and the relationship among UA level, synovitis, and pain in patients with OA.

PATIENTS AND METHODS

Design population. The severity of osteoarthritic synovitis and pain can be affected by demographic, kinematic, and clinical factors.[13] As a result, patients with anteromedial osteoarthritis (AMOA) were screened because AMOA presents a homogenous pattern characterized by correctable varus deformity, anteromedially centered pain and cartilage damage, and preserved ligament function, which could help minimize bias caused by kinematic factors.[14] Moreover, to minimize the potential bias caused by the different SUA levels for diagnosing hyperuricemia between male (≥420 μmol/L) and female (≥360 μmol/L) patients,[11] only female patients were included. In detail, consecutive female patients who underwent primary unilateral unicompartmental knee arthroplasty or total knee arthroplasty for AMOA at our institution between November 2020 and September 2023 were prospectively enrolled. The inclusion criteria were the following: (1) 50 to 70 years old; (2) restricted pain in the anteromedial knee; (3) radiographic evidence of OA in the medial compartment (Kellgren and Lawrence [KL] grade 3) and lateral and patellofemoral compartments (KL grade ≤1 each) (Supplementary Figure 1); (4) intact function of the anterior cruciate ligament and medial collateral ligament (MCL); (5) range of motion ≥110°; (6) varus deformity ≤10°; (7) flexion deformity ≤10°; and (8) no history of gout flare or the use of uric acid-lowering drugs. Venous blood was collected from each patient preoperatively after fasting for at least eight hours to measure the level of SUA. Hyperuricemia was considered present when the SUA level was ≥360 μmol/L. Patients with traumatic arthritis, previous knee surgery, or inflammatory arthritis were excluded.

Radiographic and symptomatic assessment of knee OA. All patients underwent weight-bearing anteroposterior, lateral, and Merchant radiography of the affected knee. Two experienced radiologists, blinded to patient identification and clinical information, independently evaluated the KL grades of the medial, lateral, and patellofemoral compartments.

Symptomatic assessment was performed preoperatively by a senior orthopedic surgeon who was blinded to patient information. The overall function of the affected knee was evaluated using the Western Ontario McMaster University Osteoarthritis Index (WOMAC). The WOMAC pain subscale was used to evaluate knee pain, with scores ranging from 0 (no pain) to 20 (extreme pain). The cutoff scores for mildly, moderately, and severely symptomatic OA were set at 5 and 14 points, as previously reported.[1] The WOMAC stiffness and physical function subscales were also applied, and the values (0–8 and 0–68, respectively) were recorded.

Synovial tissue and fluid collection. During each surgery, a synovial fluid sample was collected using the superior-lateral suprapatellar approach before incision. The synovium in the medial condyle was collected during total knee arthroplasty and unicompartmental knee arthroplasty and divided into three sections. One section was fixed in 4% paraformaldehyde for histologic analysis, and two sections were fixed in 100% ethanol for Gomori methenamine silver (GMS) staining for urate crystals and UA quantification.

Histologic analysis. The 4% paraformaldehyde samples were embedded in paraffin, cut into 4-μm sections, and stained with hematoxylin and eosin to evaluate synovial activation using Krenn synovitis scores.[15] Three components of synovitis (lining layer hyperplasia, stromal cell activation, and inflammatory infiltrate) were each scored from zero to three and summed to obtain a total score ranging from zero to nine, with scores of zero to four indicating low-grade synovitis and scores of five to nine indicating high-grade synovitis.[16] Two senior pathologists, blinded to patient information, independently evaluated the Krenn synovitis scores. A high correlation was confirmed between the readers (kappa for interrater agreement for scores was 0.81 and for histologic gradings was 0.84).

GMS staining. GMS staining is an accepted approach for the detection of MSU crystals in multiple tissues.[8,17] Paraffin-embedded sections of ethanol-fixed synovial specimens were stained with GMS to detect urate crystals. Slides were deparaffinized in xylene, rinsed three times with absolute alcohol, and incubated for 30 minutes at 60°C with a preheated working solution (methenamine silver). After rinsing with distilled water, the sample was toned with gold chloride for three minutes and rinsed five times with distilled water. We added 3% sodium thiosulfate for five minutes and washed the specimens in tap water for five minutes, followed by rinsing in distilled water. Counterstaining was performed using a light-green working solution for 2 minutes. Finally, the slides were dehydrated through two changes of 95% alcohol followed by two changes of absolute alcohol, cleared in xylene, and mounted with a synthetic mounting medium. All stained sections of the synovial samples were reviewed by two senior pathologists blinded to patient categorization.

Quantification of UA and inflammatory cytokines in the synovium and synovial fluid. Synovial membrane and fluid UA (smUA and sfUA, respectively) were quantified using a UA content assay kit (BC-1365; Solarbio) within 24 hours after sample collection. For the synovium, 0.1 g of tissue was weighed, and 1 mL of an extraction agent was added for homogenization. For the synovial fluid, a 0.5 mL sample was used. Samples were centrifuged at 4°C and 10,000 revolutions per minute for 15 minutes. The supernatant was incubated with reagent A at 37°C for 30 minutes. The absorbance at 505 nm was recorded, and the UA content was calculated and normalized. The levels of smUA and sfUA were reported in μg/g and μg/mL, respectively. The levels of IL-6 and TNF-α in synovial fluid were measured using an enzyme-linked immunosorbent assay according to the manufacturer's instructions (SEKH-0013 and SEKH-0047, Solarbio).

Statistical analyses. All statistical analyses were performed using SPSS (version 26.0; IBM Corp., USA). The Kolmogorov-Smirnov test was used to determine the normality of the distribution of continuous variables in the two groups. The unpaired *t*-test was used to compare two independent groups with a normal distribution, and the statistical distribution is presented as mean ± SD. Variables with an abnormal distribution are presented as median (interquartile range [IQR]) and were compared using the Mann–Whitney test. Fisher's chi-square test was used to compare categorical variables. Spearman rank correlation was used to evaluate the association between SUA level and clinical parameters, as well as histologic scores. Univariate analysis and multivariable logistic regression analysis of SUA levels associated with the severity of synovitis (per 6 μmol/L [0.1 mg/dL] increase) and pain (per 12 μmol/L [0.2 mg/dL] increase) were performed to make the results more clinically interpretable. The variables considered in the multivariable model were demographic factors such as age and body mass index; kinematic factors including the degrees of varus deformity, flexion deformity, and range of motion; and metabolic factors such as the levels of triglyceride, total cholesterol, high-density lipoprotein, low-density lipoprotein, and fasting blood glucose. These covariates have been reported to be associated with the severity of synovitis and osteoarthritic pain.[3,13] The level of significance was set at $P < 0.05$.

RESULTS

Patient characteristics. The clinical data of 219 patients were included in the final analysis, and synovial fluid samples were obtained from 191 patients. Figure 1 shows a flow diagram of the study design and patient recruitment. There were 74 patients in the hyperuricemia group and 145 patients in the non-hyperuricemia group. Higher SUA levels, serum triglyceride levels, total cholesterol, and body mass index were found in the hyperuricemia group. A higher rate of hypertension was also found in this group (Table 1). Compared with those in the non-hyperuricemia group, patients in the hyperuricemia group presented with higher Krenn synovitis scores, WOMAC pain subscale scores, and higher levels of synovial IL-6, TNF-α, sfUA, and smUA (Table 1). The proportions of patients with high-grade synovitis and severely symptomatic OA were also significantly increased (Table 1).

Elevated SUA levels alter the spatial deposition pattern of MSU crystals in the synovium. Representative images of hematoxylin and eosin staining and their corresponding GMS staining are shown in Figure 2. Urate crystal deposition was evaluated in terms of three synovial membrane structures: the capillary wall, the sublining layer, and the lining layer after GMS staining. Overall, MSU was detected in 147 patients (67.12%), and the rate of positive MSU staining in each structure increased with increasing SUA level. Positive staining was found independently in the capillary wall in patients with lower SUA levels, and the sublining layer was then affected. MSU was found in the lining cells of 70 patients (94.59%) with hyperuricemia, whereas it was only found in the lining layer of 11 patients (7.59%) without hyperuricemia. The spatial deposition pattern of MSU crystals in the synovium was significantly different between patients with and without hyperuricemia (Table 2).

Association between UA levels, synovitis, and pain. In total, 81 patients were considered to have high-grade synovitis and 28 were diagnosed with severely symptomatic OA. In the univariate analysis, SUA, total cholesterol, and low-density lipoprotein levels were associated with high-grade synovitis, and only SUA level was associated with severely symptomatic OA. After adjusting for other confounders, SUA level was associated with high-grade synovitis (odds ratio [OR] 1.417; 95% confidence interval [CI] 1.278–1.570; $P = 0.000$) and severe knee pain (OR 1.242; 95% CI 1.154–1.336; $P = 0.000$) in the multivariate analysis (Table 3). A positive correlation was found between SUA

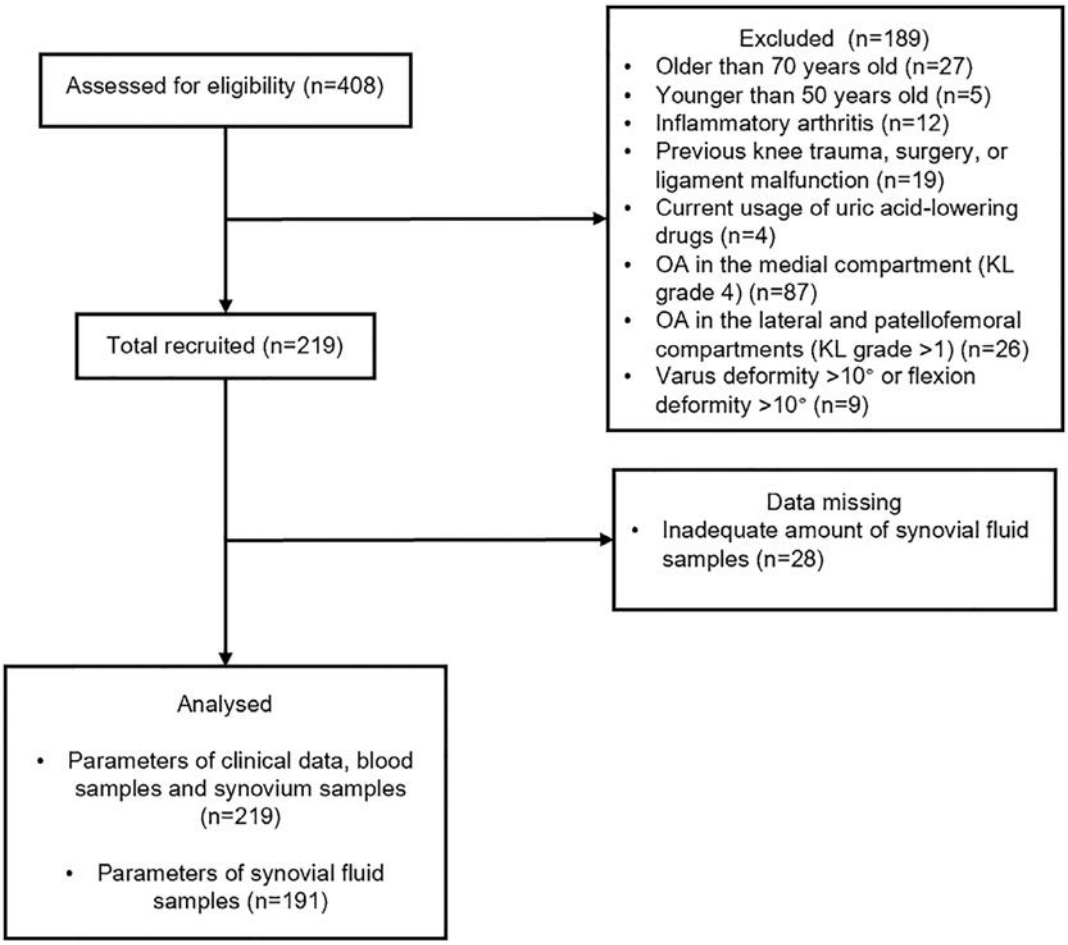

Figure 1. Flowchart of patient deposition. KL, Kellgren and Lawrence; OA, osteoarthritis.

levels and Krenn synovitis scores (r = 0.296; 95% CI 0.166–0.416; P <0.000) and WOMAC pain score (r = 0.335; 95% CI 0.208–0.451; P < 0.000) (Table 4) in the included patients. The levels of IL-6 and TNF-α in the synovial fluid were also found to be correlated with SUA levels (Table 4).

The effect of SUA on intraarticular UA levels was further investigated (Table 4). Elevated SUA levels were associated with increased levels of sfUA (r = 0.505; 95% CI 0.388–0.606; P < 0.000) and smUA (r = 0.639; 95% CI 0.543–0.718; P < 0.000). However, regardless of the levels of SUA, the levels of sfUA of all patients remained below the saturation point of UA. The sfUA and smUA levels were also found to be associated with aggravated intraarticular synovitis, as indicated by their positive correlations with Krenn synovitis scores, synovial fluid levels of IL-6, and TNF-α and WOMAC pain scores (Table 4).

DISCUSSION

This study presents several novel findings. We demonstrated the alteration of the spatial distribution of urate crystals in the synovium of non-gout patients with different SUA levels. Our findings also suggest that SUA level is an independent risk factor for advanced synovitis and severe pain in patients with AMOA of the knee. Moreover, this study suggests that SUA, sfUA, and smUA levels are strongly correlated with each other and are associated with osteoarthritic inflammation. Our results provide a better understanding of urate crystal deposition in the synovium and offer new insights into the implication of hyperuricemia in OA pathogenesis. Our results also emphasize the effects of intraarticular UA on osteoarthritic synovitis and pain, suggesting a potential treatment target for alleviating inflammation in patients with OA and hyperuricemia.

UA is a metabolically active end product of human purine metabolism and is normally soluble in serum.[11] The bidirectional cause-effect relationship between SUA level and OA has attracted much attention in recent years. Krasnokutsky et al found that SUA level could predict joint space narrowing in non-gout patients with medial knee OA during a two-year interval.[10] Colchicine 0.5 mg administered daily has also been reported to significantly decrease the requirement of knee and hip replacements, indicating a possible relationship between SUA level and OA.[18] However, a population-based longitudinal study failed to

Table 1. Demographic, kinematic, metabolic, and clinical data of the included patients*

Parameters	All patients	Hyperuricemia group (n = 74)	Non-hyperuricemia group (n = 145)	*P* value[a]
Demographic data				
Age, mean ± SD, y	65.00 ± 5.00	66.00 ± 5.00	65.00 ± 5.00	0.280
Body mass index, mean ± SD	25.89 ± 5.40	28.18 ± 4.42	26.56 ± 5.78	0.027
Kinematic data				
Varus deformity, mean ± SD, degree	9.90 ± 5.50	9.20 ± 4.98	10.10 ± 5.58	0.236
Flexion deformity, mean ± SD, degree	5.00 ± 5.00	5.00 ± 10.00	5.00 ± 5.00	0.382
Range of motion, mean ± SD, degree	115.00 ± 15.00	115.00 ± 11.30	115.00 ± 15.00	0.421
Metabolic data				
Triglyceride, mean ± SD, mmol/L	1.39 ± 0.88	1.59 ± 1.08	1.24 ± 0.81	<0.000
Total cholesterol, median (IQR), mmol/L	5.32 (1.06)	5.55 (1.16)	5.20 (0.99)	0.021
High-density lipoprotein, median (IQR), mmol/L	1.54 (0.27)	1.51 (0.29)	1.56 (0.26)	0.128
Low-density lipoprotein, median (IQR), mmol/L	3.01 (0.80)	3.07 (0.83)	2.98 (0.79)	0.424
Fasting blood glucose, mean ± SD, mmol/L	5.39 (1.33)	5.46 (1.45)	5.26 (1.09)	0.280
SUA, mean ± SD, μmol/L	323.00 ± 108.00	400.00 ± 85.50	287.00 ± 69.50	<0.000
Comorbidities				
Hypertension, n (%)	156 (71.23)	60 (81.08)	96 (66.20)	0.027
Type 2 diabetes mellitus, n (%)	66 (30.14)	19 (25.68)	47 (32.41)	0.352
Arrhythmia, n (%)	7 (3.20)	4 (5.41)	3 (2.07)	0.230
Coronary heart disease, n (%)	7 (3.20)	3 (4.05)	4 (2.76)	0.691
Hepatitis, n (%)	5 (2.28)	2 (2.70)	3 (2.07)	0.999
Thyroid disorders, n (%)	9 (4.11)	3 (4.05)	6 (4.14)	0.999
Breast disorders, n (%)	18 (8.22)	3 (4.05)	15 (9.93)	0.190
Gastrointestinal tract disorders, n (%)	22 (10.05)	8 (11.11)	14 (9.66)	0.812
Respiratory disorders, n (%)	5 (2.28)	2 (2.70)	3 (2.07)	0.999
Cerebrovascular disorders, n (%)	17 (7.76)	4 (5.41)	13 (8.97)	0.432
Clinical data				
Krenn synovitis score, mean ± SD	4.00 ± 2.00	5.00 ± 2.00	4.00 ± 2.00	0.001
High-grade synovitis, n (%)	81 (36.99)	38 (51.35)	43 (29.66)	0.002
IL-6, mean ± SD, pg/ml[b]	45.65 ± 91.35	69.59 ± 95.13	40.81 ± 81.48	0.007
TNF-α, mean ± SD, pg/ml[b]	28.09 ± 20.52	33.99 ± 30.28	24.47 ± 18.62	0.002
sfUA, mean ± SD, μg/ml[b]	25.41 ± 9.67	30.36 ± 8.76	22.76 ± 7.96	<0.000
smUA, mean ± SD, μg/g	19.10 ± 16.18	37.86 ± 27.76	14.04 ± 12.51	<0.000
WOMAC pain subscale, mean ± SD	8.00 ± 5.00	9.00 ± 4.25	8.00 ± 4.50	0.000
WOMAC stiffness subscale, mean ± SD	4.00 ± 4.00	4.00 ± 3.00	4.00 ± 4.00	0.257
WOMAC physical function subscale, mean ± SD	22.00 ± 10.00	23.00 ± 11.25	21.00 ± 11.00	0.150
WOMAC score, mean ± SD	33.00 ± 14.00	37.00 ± 13.25	33.00 ± 14.00	0.072
Severely symptomatic OA, n (%)	28 (12.79)	16 (21.62)	12 (8.28)	0.009
Moderately symptomatic OA, n (%)	149 (68.04)	52 (70.27)	97 (66.90)	0.649
Mildly symptomatic OA, n (%)	42 (19.18)	6 (8.11)	36 (24.83)	0.003

* IL-6, interleukin-6; IQR, interquartile range; OA, osteoarthritis; sfUA, uric acid in synovial fluid; smUA, uric acid in synovial membrane; SUA, serum uric acid; TNF-α, tumor necrosis factor-α; WOMAC, the Western Ontario McMaster University Osteoarthritis Index.
[a] Compared between OA with hyperuricemia group and OA without hyperuricemia group.
[b] Synovial fluid samples were acquired from 191 patients, among which 64 patients were in hyperuricemia group and 127 were in OA group.

demonstrate SUA as a risk factor for knee OA progression.[19] A recent Mendelian randomization study also found that SUA level was not associated with the risk of knee OA.[20] Most studies have defined OA progression using radiographic evidence of cartilage damage. However, various confounding factors can be implicated in cartilage damage in the long term, and it is difficult to eliminate all confounding factors in any given population. Given that elevated SUA level has been identified as a manifestation of an inflammatory state in patients with or without gout, we hypothesized that the major effect of UA is the aggravation of synovial inflammation. Synovitis could be detected by MRI in patients with normal or minimal cartilage damage, indicating that synovitis influences the early onset of OA and is a precursor in OA pathogenesis[21]; however, the role of osteoarthritic synovitis is underestimated. Although most studies assess synovitis using MRI or ultrasound,[22] biopsy remains the gold standard approach for evaluating the severity of synovitis. Advanced synovitis induces severe pain.[23,24] Osteoarthritic synovitis and pain are determined by complex interactions between multiple factors, including metabolic factors, degree of cartilage damage, and knee instability.[13] To accurately evaluate the relationship between UA levels, degree of synovitis, and knee pain, we included patients who presented with pain, cartilage damage in the anteromedial compartment alone, and ligament stability. A sample of the synovium was also acquired from the medial sulcus, which is adjacent to the site of knee pain. We then included demographic, mechanical, and metabolic variables to comprehensively investigate the risk factors for high-grade synovitis and OA symptoms. Our results showed that SUA level was the only risk factor associated with advanced synovitis

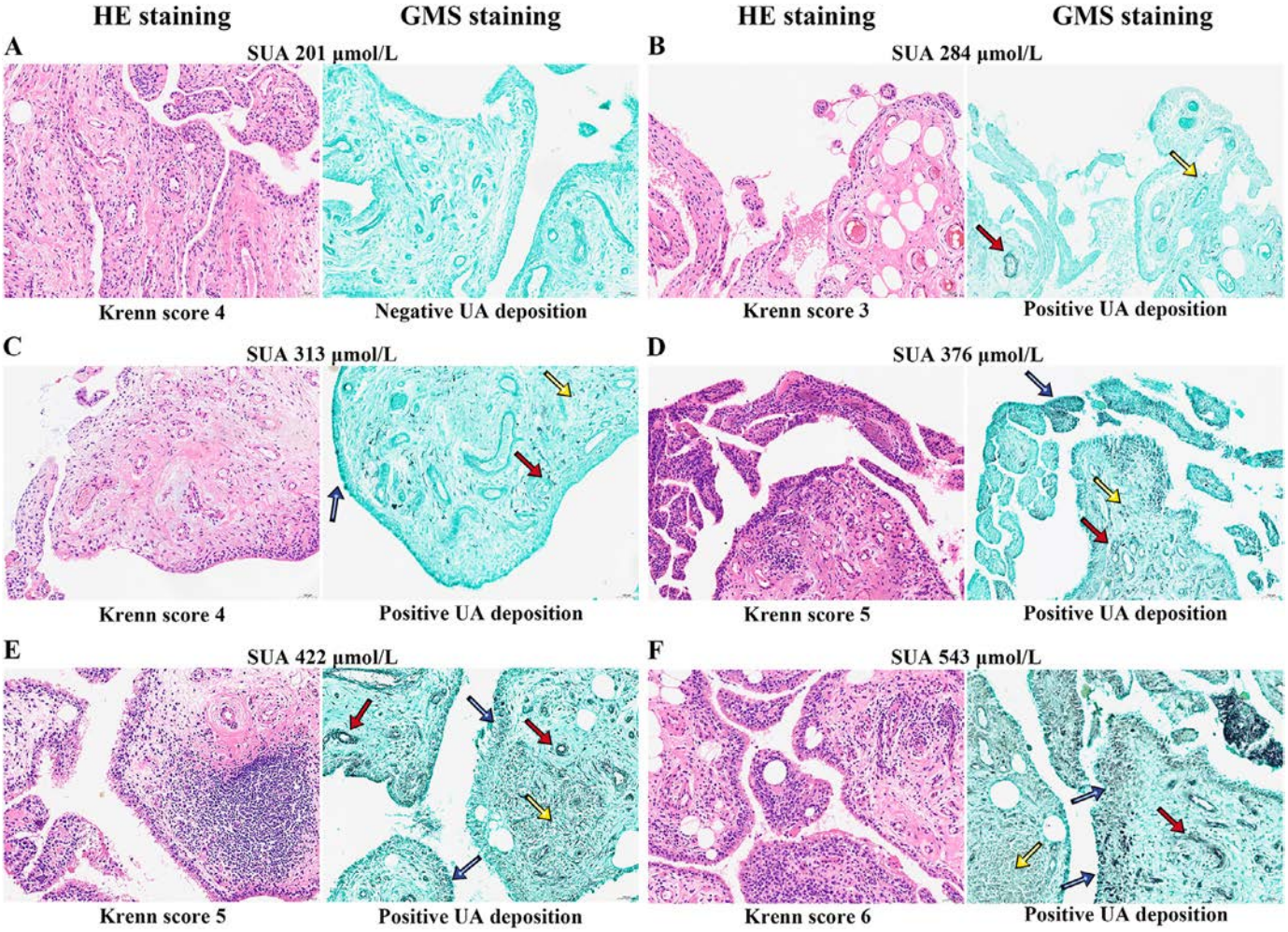

Figure 2. Representative images of hematoxylin and eosin staining and their corresponding GMS staining of patients with different SUA levels (A–F). Positive uric acid crystal deposition in capillary wall, sublining layer, and lining layer are indicated by red arrow, yellow arrow, and blue arrow, respectively. Magnification 10x. GMS, Gomori methenamine silver; HE, hematoxylin and eosin; SUA, serum uric acid.

and severe OA pain after adjustments for other confounders. The SUA level was also found to positively correlate with higher histologic scores for synovitis, higher levels of inflammatory cytokines in the synovial fluid, and knee pain. These results provided histopathological evidence for the previous studies, which reported that elevated SUA level contributed to a higher effusion-synovitis score and quantitative synovial volume determined by contrast-enhanced MRI[2,10] and further suggested the involvement of the SUA in the inflammation and pain in patients with AMOA of the knee.

Not surprisingly, patients with hyperuricemia showed higher levels of intraarticular UA, which was separately defined as sfUA and smUA in this study. The levels of intraarticular UA were correlated with the SUA level, higher pain score, higher Krenn score, and higher levels of inflammatory cytokines in the synovial fluid. These results were similar to what has been previously reported in knee OA that elevated sfUA level is associated with higher SUA level, higher pain scores, and the activation of the intraarticular inflammasome.[11] In the same study, Denoble et al also found a median drop of 1.15 mg/dL of UA from serum to synovial fluid and considered this serum/synovial fluid gradient as precipitated uric acid.[11] However, it is commonly considered that UA precipitates when the SUA level exceeds the limit of urate solubility (408 μmol/L or 6.8 mg/dL). In this study, the sfUA levels of all patients were below the saturation point, indicating a more homeostatic status of sfUA level than SUA level. Therefore, we considered that the serum/synovial fluid difference might represent the MSU crystals precipitated in synovium. Synovium modulates the synovial environment by exchanging components between the systemic circulation and synovial fluid.[25] However, MSU crystal deposition in the synovium has not been emphasized in patients without gout; although it has been noted for decades that MSU crystals are deposited in the synovium long before a gout flare and that they elicit an inflammatory response during acute gouty arthritis. Thus, after quantifying smUA, we investigated the spatial distribution of MSU crystals within the synovium. Our results demonstrated that MSU crystal deposition occurred in nearly 40% of those with an

Table 2. Alteration of the spatial deposition pattern of urate crystals in the synovium*

SUA levels, μmol/L	Capillary wall, n (%)	*P* value[a]	Sublining layer, n (%)	*P* value[a]	Lining layer, n (%)	*P* value[a]
Hyperuricemia group (n = 74)						
>408 (n = 33)	33 (100)	<0.000	33 (100)	<0.000	33 (100)	<0.000
360–408 (n = 41)	41 (100)		41 (100)		37 (90.24)	
Non-hyperuricemia group (n = 145)						
300–360 (n = 60)	32 (53.33)		17 (28.33)		10 (16.67)	
240–300 (n = 59)	22 (37.29)		8 (13.56)		1 (1.69)	
<240 (n = 26)	2 (7.69)		0		0	

* OA, osteoarthritis; SUA, serum uric acid.
[a] Compared between hyperuricemia group and OA group.

SUA level of less than 360 μmol/L. Histologically, advanced synovitis is often characterized by synovial lining hyperplasia and enriched cellularity in the sublining layer, including inflammatory and endothelial cell infiltration of blood vessels.[13] The capillary ensures nutrient and cell transport between the systemic circulation and joints; therefore, the capillary wall seems to be the first structure affected by MSU crystals, followed by the sublining layer. The ability of the cells of the sublining layer to phagocytize and degrade MSU crystals has been demonstrated in a recent synovial organoid study.[25] In patients with higher SUA levels, MSU crystals extensively accumulate in the sublining layer and eventually precipitates within the lining cells. The synovial lining layer controls cellular and molecular transport between the synovium and joint cavity and regulates synovial fluid composition.[26] The production of inflammatory cytokines and their release into the synovial fluid might also be affected by MSU crystals deposition in the synovium,[27] which is indicated by the associations of intraarticular UA levels with the levels of inflammatory cytokines found in this study. Our results preliminarily provide evidence of a mutual interaction among the systemic circulation, synovium, and synovial fluid for UA balancing. However, further studies are still needed to validate the roles of the synovium and the mechanisms to maintain intraarticular UA homeostasis in patients with hyperuricemia.

The major limitation of our study was its cross-sectional design. Although observed extensive MSU crystal staining even in patients with SUA levels <360 μmol/L, the lack of long-term follow-up prevented us from determining whether the SUA level of the patients reached 360 μmol/L or even higher. Longitudinal changes in knee pain and severity of synovitis could not be assessed because of the cross-sectional design. We also could not determine whether MSU crystal deposition in the synovium accelerated cartilage damage in OA, although SUA and sfUA levels have been reported to contribute to increased joint space

Table 3. Univariate analysis and multivariable logistic regression analysis of SUA levels, demographic and clinical factors associated with high-grade synovitis and severely symptomatic OA*

	High-grade synovitis			Severely symptomatic OA		
Variables	OR	95% CI	*P* value	OR	95% CI	*P* value
Univariate analysis						
SUA[a]	1.417	1.278–1.570	0.000	1.242	1.154–1.336	0.000
Total cholesterol, mmol/L	1.455	1.106–1.913	0.007	0.864	0.604–1.236	0.424
Low-density lipoprotein, mmol/L	1.439	1.011–2.048	0.044	1.211	0.757–1.939	0.425
Multivariable model						
Age, years	1.042	0.902–1.205	0.576	0.993	0.877–1.124	0.909
Body mass index	0.970	0.826–1.140	0.712	1.034	0.916–1.167	0.590
Varus deformity, degree	0.944	0.805–1.106	0.474	1.047	0.902–1.214	0.546
Flexion deformity, degree	0.991	0.852–1.152	0.904	0.990	0.867–1.132	0.887
Range of motion, degree	1.053	0.990–1.120	0.101	0.964	0.912–1.018	0.189
Triglyceride, mmol/L	0.748	0.312–1.797	0.517	0.772	0.391–1.525	0.456
Total cholesterol, mmol/L	1.259	0.639–2.479	0.505	0.670	0.376–1.194	0.174
High-density lipoprotein, mmol/L	0.541	0.065–4.517	0.571	1.722	0.291–10.185	0.549
Low-density lipoprotein, mmol/L	1.256	0.511–3.085	0.620	1.530	0.734–3.190	0.257
Fasting blood glucose, mmol/L	1.139	0.782–1.658	0.497	1.105	0.769–1.588	0.590
SUA[a]	1.443	1.290–1.614	0.000	1.273	1.169–1.386	0.000

* Multivariable model adjusted for age, body mass index, varus deformity, flexion deformity, range of motion, triglyceride, total cholesterol, high-density lipoprotein, low-density lipoprotein, and fasting blood glucose. CI, confidence interval; OA, osteoarthritis; SUA, serum uric acid.
[a] The increment of the levels of SUA used to model the association with high-grade synovitis and severely symptomatic OA was per 6 μmol/L (0.1 mg/dL) increase and per 12 μmol/L (0.2 mg/dL) increase, respectively.

Table 4. Associations between uric acid and clinical parameters*

Variables	SUA, umol/L		Uric acid in synovial fluid, μg/mL		Uric acid in synovium, μg/g	
	r (95% CI)	*P* value	*r* (95% CI)	*P* value	*r* (95% CI)	*P* value
Krenn synovitis score	0.296 (0.166–0.416)	<0.000	0.385 (0.253–0.503)	<0.000	0.428 (0.301–0.540)	<0.000
IL-6, pg/mL	0.377 (0.244–0.496)	<0.000	0.335 (0.199–0.459)	<0.000	0.421 (0.293–0.534)	<0.000
TNF-α, pg/mL	0.223 (0.080–0.358)	0.002	0.199 (0.055–0.336)	0.006	0.204 (0.059–0.340)	0.005
WOMAC pain subscale	0.335 (0.208–0.451)	<0.000	0.262 (0.121–0.393)	0.000	0.389 (0.258– 0.507)	<0.000
WOMAC stiffness subscale	−0.104 (−0.237 to 0.033)	0.124	0.062 (−0.085–0.206)	0.397	0.058 (−0.088 to 0.203)	0.420
WOMAC physical function subscale	0.165 (0.029–0.294)	0.015	0.175 (0.029–0.313)	0.016	0.273 (0.133–0.403)	0.000
WOMAC score	0.197 (0.062–0.325)	0.003	0.224 (0.081–0.359)	0.002	0.331 (0.194–0.455)	<0.000
Uric acid in synovial fluid, μg/mL	0.505 (0.388–0.606)	<0.000			0.478 (0.356–0.583)	<0.000
Uric acid in synovium, μg/g	0.639 (0.543–0.718)	<0.000	0.478 (0.356–0.583)	<0.000		

* CI, confidence interval; IL-6, interleukin-6; SUA, serum uric acid; TNF-α, tumor necrosis factor-α; WOMAC, western Ontario McMaster University Osteoarthritis Index.

narrowing.[10,11] The study included only female patients with AMOA to control mechanical variables and unify the diagnostic criteria of hyperuricemia. However, AMOA is only a subtype of OA and often coexists with other lesions that are easily overlooked in diagnosis, and hyperuricemia is increasingly defined using the saturation point (408 μmol/L or 6.8 mg/dL) in the population regardless of sex in recent studies.[28] As a result, the generalizability of the results might be compromised and further investigations are needed. We excluded patients with clinical manifestations of gout in whom the absence of crystals in the synovial fluid was not confirmed using polarizing microscopy; therefore, the diagnostic significance of MSU crystal deposition in synovium remains unclear. Some patients who underwent surgery reported mild pain; however, all patients received proper but ineffective conservative treatment before surgery, and the radiographic severity was confirmed.

In conclusion, the results of this study highlighted the effect of UA on osteoarthritic synovitis and pain and provided new insights into the pattern of UA precipitation in the synovium, suggesting that the lowering the SUA level might have the potential in alleviating synovitis and pain in patients with OA.

ACKNOWLEDGMENTS

We would like to thank Editage (www.editage.cn) for English language editing.

AUTHOR CONTRIBUTIONS

All authors contributed to at least one of the following manuscript preparation roles: conceptualization AND/OR methodology, software, investigation, formal analysis, data curation, visualization, and validation AND drafting or reviewing/editing the final draft. As corresponding author, Drs F Xiang and S Xiang confirm that all authors have provided the final approval of the version to be published and take responsibility for the affirmations regarding article submission (eg, not under consideration by another journal), the integrity of the data presented, and the statements regarding compliance with institutional review board/Declaration of Helsinki requirements.

REFERENCES

1. Cross M, Smith E, Hoy D, et al. The global burden of hip and knee osteoarthritis: estimates from the Global Burden of Disease 2010 Study. Ann Rheum Dis 2014;73(7):1323–1330.
2. Sasaki E, Yamamoto H, Asari T, et al. Metabolomics with severity of radiographic knee osteoarthritis and early phase synovitis in middle-aged women from the Iwaki Health Promotion Project: a cross-sectional study. Arthritis Res Ther 2022;24(1):145.
3. Sellam J, Berenbaum F. The role of synovitis in pathophysiology and clinical symptoms of osteoarthritis. Nat Rev Rheumatol 2010;6(11):625–635.
4. Atukorala I, Kwoh CK, Guermazi A, et al. Synovitis in knee osteoarthritis: a precursor of disease? Ann Rheum Dis 2016;75(2):390–395.
5. Jansen NEJ, Molendijk E, Schiphof D, et al. Metabolic syndrome and the progression of knee osteoarthritis on MRI. Osteoarthritis Cartilage 2023;31(5):647–655.
6. Copur S, Demiray A, Kanbay M. Uric acid in metabolic syndrome: does uric acid have a definitive role? Eur J Intern Med 2022;103:4–12.
7. Dalbeth N, Gosling AL, Gaffo A, et al. Gout. Lancet 2021;397(10287):1843–1855.
8. Nardi V, Franchi F, Prasad M, et al. Uric acid expression in carotid atherosclerotic plaque and serum uric acid are associated with cerebrovascular events. Hypertension 2022;79(8):1814–1823.
9. Howard RG, Samuels J, Gyftopoulos S, et al. Presence of gout is associated with increased prevalence and severity of knee osteoarthritis among older men: results of a pilot study. J Clin Rheumatol 2015;21(2):63–71.
10. Krasnokutsky S, Oshinsky C, Attur M, et al. Serum urate levels predict joint space narrowing in non-gout patients with medial knee osteoarthritis. Arthritis Rheumatol 2017;69(6):1213–1220.
11. Denoble AE, Huffman KM, Stabler TV, et al. Uric acid is a danger signal of increasing risk for osteoarthritis through inflammasome activation. Proc Natl Acad Sci USA 2011;108(5):2088–2093.
12. Roddy E, Zhang W, Doherty M. Are joints affected by gout also affected by osteoarthritis? Ann Rheum Dis 2007;66(10):1374–1377.
13. Sanchez-Lopez E, Coras R, Torres A, et al. Synovial inflammation in osteoarthritis progression. Nat Rev Rheumatol 2022;18(5):258–275.
14. Bunyoz KI, Dixon J, Patel J, et al. Anteromedial knee osteoarthritis (AMOA) evaluated with magnetic resonance imaging (MRI): a cohort study of 100 patients. Arch Orthop Trauma Surg 2024;144(8):3439–3447.
15. Krenn V, Morawietz L, Burmester GR, et al. Synovitis score: discrimination between chronic low-grade and high-grade synovitis. Histopathology 2006;49(4):358–364.

16. Yoshida S, Nishitani K, Yoshitomi H, et al. Knee alignment correction by high tibial osteotomy reduces symptoms and synovial inflammation in knee osteoarthritis accompanied by macrophage phenotypic change from M1 to M2. Arthritis Rheumatol 2023;75(6): 950–960.

17. Wang J, Hao P, Sun X, et al. New animal model of chronic gout reproduces pathological features of the disease in humans. RMD Open 2023;9(4):e003499.

18. Heijman MWJ, Fiolet ATL, Mosterd A, et al. Association of low-dose colchicine with incidence of knee and hip replacements: exploratory analyses from a randomized, controlled, double-blind trial. Ann Intern Med 2023;176(6):737–742.

19. Go DJ, Kim DH, Kim JY, et al. Serum uric acid and knee osteoarthritis in community residents without gout: a longitudinal study. Rheumatology (Oxford) 2021;60(10):4581–4590.

20. Chen D, Xu H, Sun L, Li Y, et al. Assessing causality between osteoarthritis with urate levels and gout: a bidirectional Mendelian randomization study. Osteoarthritis Cartilage 2022;30(4):551–558.

21. Roemer FW, Guermazi A, Felson DT, et al. Presence of MRI-detected joint effusion and synovitis increases the risk of cartilage loss in knees without osteoarthritis at 30-month follow-up: the MOST study. Ann Rheum Dis 2011;70(10):1804–1809.

22. Shakoor D, Demehri S, Roemer FW, et al. Are contrast-enhanced and non-contrast MRI findings reflecting synovial inflammation in knee osteoarthritis: a meta-analysis of observational studies. Osteoarthritis Cartilage 2020;28(2):126–136.

23. Neogi T, Guermazi A, Roemer F, et al. Association of joint inflammation with pain sensitization in knee osteoarthritis: the Multicenter Osteoarthritis Study. Arthritis Rheumatol 2016;68(3):654–661.

24. Kaukinen P, Podlipská J, Guermazi A, et al. Associations between MRI-defined structural pathology and generalized and localized knee pain - the Oulu Knee Osteoarthritis Study. Osteoarthritis Cartilage 2016;24(9):1565–1576.

25. Chen Y, Chen Z, Wang W, et al. Spatiotemporal observation of monosodium urate crystals deposition in synovial organoids using label-free stimulated Raman scattering. Research 2024;7:0373.

26. McInnes IB, Schett G. The pathogenesis of rheumatoid arthritis. N Engl J Med 2011;365(23):2205–2219.

27. Shi Y, Evans JE, Rock KL. Molecular identification of a danger signal that alerts the immune system to dying cells. Nature 2003; 425(6957):516–521.

28. Dalbeth N, House ME, Aati O, et al. Urate crystal deposition in asymptomatic hyperuricaemia and symptomatic gout: a dual energy CT study. Ann Rheum Dis 2015;74(5):908–911.

Arthritis & Rheumatology
Vol. 78, No. 2, February 2026, pp 320–331
DOI 10.1002/art.43359

American College of Rheumatology
Empowering Rheumatology Professionals

Clinical Significance of Gut Microbiota Community Types for Long-Term Response to Fecal Microbiota Transplantation in Patients With Psoriatic Arthritis

Panpan Qin,[1] Maja S. Kragsnaes,[2] Dorte K. Holm,[3] Hans Christian Horn,[4] Anna Christine Nilsson,[3] Jens Kjeldsen,[5] Karsten Kristiansen,[1] and Torkell Ellingsen[2]

Objective. Fecal microbiota transplantation (FMT) holds promises as a beneficial supplement to methotrexate in patients with psoriatic arthritis (PsA). We therefore investigated how gut bacterial signatures in patients and donor strain engraftment were associated with long-term response to FMT.

Methods. This exploratory study is based on the FLORA trial cohort, encompassing 31 patients with moderate-to-high PsA disease activity and four FMT donors. Of the 15 patients receiving one single-donor FMT, 13 were included in the per-protocol (PP) population. Stool samples were collected before and after FMT (week 4, 12, and 26). We performed shotgun metagenomics to characterize gut microbiota features.

Results. At baseline, 17 patients (55%) had a gut microbiota community type dominated by the *Bacteroides* genus (B-type), whereas 14 (45%) had a *Prevotella*-driven community type (P-type). The B- and P-type patients did not differ in disease activity or demographics, but the B-type had a significantly higher species diversity compared to the P-type ($P = 0.005$). In the PP population, five of seven B-type patients versus none of six P-type patients ($P = 0.021$) achieved a long-term clinical beneficial response at week 26. Bacterial strain richness increased significantly from baseline to week 4 and week 26 in B-type ($P = 0.016$), but not in P-type, patients. Eighteen engrafted strains persisted only in B-type recipients by week 26, including a *Bacteroides clarus* strain, which demonstrated a negative effect size regarding arthritis pain and the patients' global assessment of disease.

Conclusion. Recipients with a *Bacteroides*-dominated community structure were more likely to achieve long-term beneficial response following one FMT.

INTRODUCTION

Chronic inflammatory diseases such as psoriatic arthritis (PsA) are associated with disturbances of the human gut microbiota, characterized by a general decrease in anti-inflammatory short-chain fatty acids (SCFA)-producing microbes and an enrichment of potential pro-inflammatory ones.[1] Accumulating evidence suggests that these microbial abnormalities may be important environmental factors contributing to the natural history of disease and may affect drug responses in immune-mediated conditions.[2–4] Because gut microbiota alterations are potentially modifiable, targeting components of the gut microbiota could prove to have complementary beneficial effects to established disease-modifying antirheumatic drugs (DMARDs).[5] Promising

ClinicalTrials.gov identifier: NCT03058900.

Supported by Sygeforsikringen "danmark" (Sundhedsdonationer: 2022-0026), Fabrikant Vilhelm Pedersen Mindelegat (on recommendation by the Novo Nordisk Foundation), Medicine Fund of the Danish Regions (Regionernes Medicin- og behandlingspulje), University of Southern Denmark Research Fund, the Danish Rheumatism Association, the Danish Psoriasis Research Foundation, and Research Fund of Odense University Hospital.

[1]Panpan Qin, MS, Karsten Kristiansen, PhD: Laboratory of Integrative Biomedicine, Department of Biology, University of Copenhagen, Copenhagen, Denmark; [2]Maja S. Kragsnaes, MD, PhD, Torkell Ellingsen, MD, PhD: OUH Frontline Centre for Applied Microbiota and Mucosal Barrier Research (MICARE), Department of Rheumatology, Odense University Hospital and Department of Clinical Research, University of Southern Denmark, Odense, Denmark; [3]Dorte K. Holm, PhD, Anna Christine Nilsson, MD: Department of Clinical Immunology, Odense University Hospital, Odense, Denmark; [4]Hans Christian Horn, MD: Department of Rheumatology, Odense University Hospital, Odense, Denmark; [5]Jens Kjeldsen, MD, PhD: Department of Medical Gastrointestinal Diseases, Odense University Hospital, Odense, Denmark.

Ms Qin and Dr Kragsnaes are co-first authors and contributed equally to this work.

Professors Kristiansen and Ellingsen contributed equally to this work.

Additional supplementary information cited in this article can be found online in the Supporting Information section (https://acrjournals.onlinelibrary.wiley.com/doi/10.1002/art.43359).

Author disclosures are available at https://onlinelibrary.wiley.com/doi/10.1002/art.43359.

Address correspondence via email to Maja S. Kragsnaes, MD, PhD, at maja.kragsnaes@dadlnet.dk.

Submitted for publication January 14, 2025; accepted in revised form July 15, 2025.

therapies targeting the microbial *milieu* of the gastrointestinal system include dietary and lifestyle programs,[6] probiotics,[7] and fecal microbiota transplantation (FMT).[8,9]

FMT products contain minimally manipulated microbial communities donated by healthy, screened individuals.[10,11] In ulcerative colitis, which shares overlapping bacterial abnormalities with PsA,[12] FMT increases the chance for achieving remission when given as a supplement to conventional treatment.[8] Beneficial effects of FMT have also been reported in treatment refractory cases of rheumatoid arthritis,[13] ankylosing spondylitis,[14] and PsA.[15] In a previous trial investigating safety and efficacy of one FMT in methotrexate (MTX)-treated patients with severe PsA (FLORA trial), we observed transitory beneficial clinical effects within weeks of the intervention, although sustained, long-term effects were only observed in 40% treated.[16] This remission rate is comparable with the ones reported for FMT-treated patients with ulcerative colitis.[8] Investigation into biologic mechanisms that can explain the observed differences in treatment outcome following FMT in chronic inflammatory diseases is limited,[17] but a few studies have highlighted specific bacteria and metabolic pathways, including increased production of SCFAs, associated with beneficial disease-modifying, anti-inflammatory effects in ulcerative colitis.[18,19] We have previously shown that FMT led to a marked increase in levels of plasma interferon-γ in patients with PsA,[20] whereas fecal and plasma metabolomic profiles reflected beneficial clinical effects in long-term responders.[21]

FMT recipient factors, donor factors, and donor–recipient complementarity encompassing entire microbial communities to individual strains may be determinants of strain population dynamics,[22] whereas differential strain engraftment likelihoods seem to be associated with microbial taxonomy and phenotypic properties across various diseases.[23] Patients with inflammatory bowel disease have distinct gut microbiota community (GMC) types,[24,25] which have been shown to relate to FMT outcome,[24] but how patients with PsA's GMC types and engraftment of specific strains affect long-term remission of FMT have yet to be investigated. Because bacterial strains within the same species can exhibit different biologic properties,[26] strain-level composition analysis is extremely valuable when exploring engraftment and colonization of donor strains following FMT.

We therefore conducted an exploratory study performing shotgun whole-genome metagenomic sequencing on fecal samples collected before and after FMT to explore how GMC types of donors and recipients and engraftment of donor strains relate to long-term (week 26) beneficial response in patients with active peripheral PsA.

PATIENTS AND METHODS

Study setting and participants. This exploratory study is based on the FLORA trial cohort in which 31 patients with PsA with moderate-to-high peripheral disease activity (3 or more swollen joints) despite ongoing MTX treatment were included in a 26-week, double-blind, parallel-group, 1:1 randomized, sham-controlled trial (FLORA; NCT03058900).[16] Patients fulfilled the Classification Criteria for Psoriatic Arthritis (CASPAR), had no active axial disease, and had received treatment with steady-state dose MTX (monotherapy) administered as subcutaneous injections (n = 25) or oral tablets (n = 6) for at least three months before trial inclusion.[16] They all continued with this MTX treatment throughout the trial. Blood and fecal samples were collected at baseline, week 4, week 12, and week 26.[21] Six fecal samples from four patients (R4, R10, R12, and R5) were missing out of the planned collection of 124 fecal samples. Samples were stored at −80°C until analysis.

Per-protocol population. Patients were randomly allocated to receive either one gastroscopic-guided FMT (n = 15) or a sham transplantation (n = 16). Of the 15 patients who were allocated to FMT (the intention-to-treat [ITT] population), 13 of them strictly followed the study protocol and were included in the per-protocol (PP) population. The reason for excluding two patients from the PP population was to minimize the risk of assessing non-FMT effects that were likely to substantially influence the gut microbiota. This included a major change in living environment (moving to a non-Western country; R4) and not receiving the full dose of the FMT product (R9).

Donors and FMT products. The stool donations came from four healthy and thoroughly screened, HLA-B27 negative, lean individuals who were unrelated to the recipients (two men and two women with an age between 26 and 54 years).[16] Each FMT product was processed from 50-g stool from one of the donors, prepared using standard Danish protocols.[16] Donors donated stool between four and eight times during a donation cycle of 30 days. Both fecal samples and FMT product samples were collected from each donation day. FMT products were stored at −80°C and thawed to 36°C just before the clinical application. Each FMT-treated patient received one FMT product processed from same-day stool collected from one donor. Only one patient (R13) received a mixture of two donations collected from the same donor within a two-day interval.

Primary trial outcome: treatment responder versus failure. If the disease was not well controlled during follow-up based on shared decision-making between the patient and the rheumatologist in accordance with the European PsA recommendations (2019)[27] and/or if the patient was not in clinical remission at week 26, or if the patient needed treatment escalation before week 26 due to insufficient improvement of baseline arthritis symptoms during the closely monitored 26-week follow-up period, he/she was categorized as being treatment failure (primary trial outcome).[16]

Ethics. The study was approved by the Regional Committees on Health Research Ethics for Southern Denmark (DK-S-20150080) and the Danish Data Protection Agency (15/41684). All participants provided written informed consent in accordance with the principles outlined in the Declaration of Helsinki.

Metagenomics DNA extraction, library construction and sequencing. The procedures followed well-established protocols. The detailed description is available in the Supplementary Methods.

Metagenomic data processing, taxonomic profiling, and functional annotation. The procedures followed well-established protocols. The detailed description is available in the Supplementary Methods.

Microbiota community typing. Following the method of Frioux et al,[28] Dirichlet Multinomial Mixtures was used for microbiome community typing. First, the genus-level relative abundance matrixes were multiplied by 10^6 and rounded to the closest integer. Then the Dirichlet Multinomial package (version 1.44.0) in R was used for microbiota community typing. Laplace, Akaike information criterion, and Bayesian information criterion were used to select the optimal number of microbiota communities.

Strain colonization. We analyzed the colonization of engrafted strains at weeks 4, 12, and 26 in the PP population. Based on the strain relative abundance profile, a strain was defined as a week 4 colonized strain if its relative abundance in donors was >0, its relative abundance in recipients at baseline was 0, and its relative abundance in recipients at week 4 was >0. A week 4 colonized strain was further defined as a week 12 colonized strain if its relative abundance in recipients at week 12 remained >0 or as a week 26 colonized strain if its relative abundance in recipients at week 26 remained >0. In addition, a strain was defined as a week 4 disappeared strain if its relative abundance was >0 at baseline in recipients and its relative abundance was 0 at week 4. A week 4 disappeared strain was further defined as a week 12 disappeared strain if its relative abundance in recipients at week 12 remained 0 or as a week 26 disappeared strain if its relative abundance in recipients at week 26 remained 0.

Inflammation-associated plasma proteins. The analysis of inflammation-associated proteins was performed using the Olink inflammation panel encompassing 92 inflammation-associated plasma proteins, as previously described.[20]

Statistical analysis and visualization. Analysis of alpha diversity, nonmetric multidimensional scaling (NMDS), and distance-based redundancy analysis (dbRDA) were implemented using the diversity, metaMDS, and dbRDA functions in the vegan package[29] of R. The distances used in NMDS and dbRDA were measured using Bray-Curtis dissimilarity. An analysis of variance test with 9,999 permutations was used to evaluate the variation in community structure explained by each clinical variable in the dbRDA model. The differences of baseline characteristics, alpha diversity and Shannon index, microbial species relative abundance, and the relative abundance of genes encoding microbial enzymes between time points were tested using the paired Wilcoxon test. *P* values less than 0.05 were considered statistically significant, whereas *P* values between 0.05 and 0.1 were defined as indicating a trend. The effect size of individual strains on the phenotype was measured using the Maaslin2 package[30] in R (Benjamini-Hochberg adjusted *P* values less than 0.1 and effect size greater than 1 were considered statistically significant). Data visualization was performed using R version 4.3.0 (The R Project for Statistical Computing), GraPhlAn[31] version 1.1.3, and an online drawing tool (https://app.diagrams.net/).

Data availability statement. Data are avalible upon reasonal request. Access and subsequent data handling must be in agreement with the European General Data Protection Regulation. Data will be shared after review and approval by the ethical and scientific board of the study. Terms of collaboration will be reached together with a signed data access agreement. The targeted next-generation sequencing reads can be accessed in the Sequence Read Archive database under BioProject accession number PRJNA1160779.

RESULTS

Patient characteristics. The detailed demographics of the 31 patients enrolled in this trial have been published elsewhere.[16]

Two distinct GMC types among patients with PsA at baseline. Based on the 31 patients' relative abundance genus profiles, we identified two GMC types (Figure 1A). The gut microbiota of one type of patient was dominated by the genus *Prevotella* (P-type), whereas the microbiota of the other type of patient were dominated by the two genera *Bacteroides* and *Phocaeicola* (B-type) (Figure 1B and 1C). Subsequently, we assessed whether there were differences between B-type and P-type patients at baseline with respect to demographics, disease characteristics, levels of inflammation-associated plasma proteins, and gut microbiota diversity. We found that neither demographics nor disease characteristics differed significantly between P-type and B-type across all patients (Table 1). This was also the case in the FMT-treated patient population (Supplementary Table S1).

However, plasma levels of chemokine ligand 23 were higher in B-type patients, whereas P-type patients had a higher level of adenosine deaminase (Supplementary Figure S1A). Moreover,

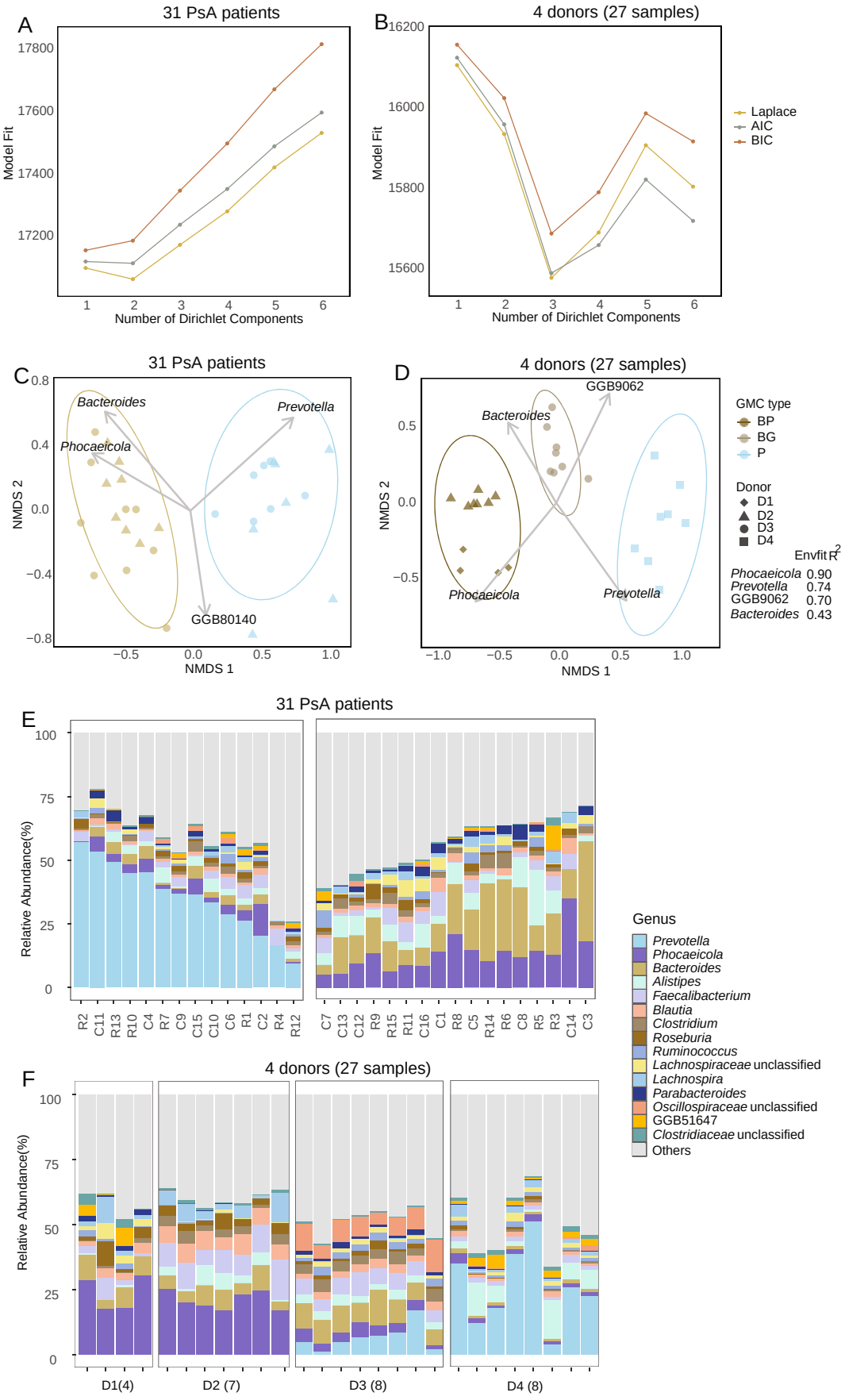

Figure 1. Legend on next page.

the gut microbiota of B-type patients exhibited a significantly higher alpha diversity compared to P-type patients but no significant difference in species richness (Supplementary Figure S1B). From the dbRDA analysis, we further observed that sex (P = 0.019, 3.97% of total variance), Health Assessment Questionnaire Disability Index (P = 0.041, 3.38% of total variance), and fatigue assessed on a visual analog scale (P = 0.018, 3.91% of total variance) could potentially explain a minor proportion of the species-level variance in microbial community structure (Figure 2B and Supplementary Table S2).

Three GMC types among healthy FMT donors. Among the four donors, we identified three GMC types that showed the optimal classification performance (Figure 1D). Samples from donor D4 were dominated by the genus *Prevotella* (P-type), whereas samples from the other three donors were classified under *Bacteroides*. Samples from donor D1 and D2 were also dominated by *Phocaeicola* (BP-type) whereas samples from donor D3 were characterized by GGB9062 (BG-type) (Figure 1E and 1F). However, when combining both patient and donor samples to assess post-FMT changes and the stability of the GMC types over time, only two distinct clusters (the B- and P-types) were identified (Supplementary Figure S2; Figure 2A).

FMT product characteristics. The species richness and alpha diversity (Shannon index) of donor fecal samples did not change significantly after FMT processing (Supplementary Table S3). However, after manufacturing of FMT products, the relative abundance of *Veillonella* species increased. Conversely, *Bifidobacterium* species and butyrate-producing species from the genera *Roseburia*, *Mediterraneibacter*, and *Anaerotruncus* decreased in the final FMT product as compared to the donated stool sample (Supplementary Table S4).

The week 26 response rate was higher in B-type versus P-type patients. Six FMT-treated patients in the ITT population and five in the PP population were responders at week 26 (Figure 2A). In the PP population, the response rate was significantly higher in B-type patients compared to P-type patients (P = 0.021); please see Table 2. Although this difference was not statistically significant in the ITT population, the remission rate in B-type patients was still four times higher compared to P-type patients (Table 2). The responder patients received donations from three donors, each belonging to a different GMC type (Figure 2A).

Changes in bacterial richness and diversity following FMT. Next, we investigated if changes in microbiota diversity following FMT could explain why B-type patients had a higher remission rate than P-type patients. In B-type patients, strain richness significantly increased from baseline to week 4 (P = 0.016) and week 26 (P = 0.016) (Figure 3A). In contrast, alpha diversity only showed an increasing trend (P = 0.062) at week 4 in P-type patients, and this trend was only temporary, as both alpha diversity (P = 0.062) and strain richness (P = 0.062) showed a decreasing trend by week 12 (Figure 3A).

Colonization and decolonization of specific bacterial strains following FMT. We identified 492 specific bacterial strains that colonized or decolonized in the FMT-treated patients from baseline through 4, 12, and 26 weeks (Supplementary Table S5). A total of 291 strains successfully engrafted and colonized in at least one FMT recipient by week 26 (Supplementary Table S5). None of these strains colonized long-term in all of the recipients, but we have provided a list of bacterial strains that engrafted across all recipients of the same donor in the Supplementary Table S6. Only five bacterial strains disappeared long-term through 26 weeks in at least three FMT-treated patients (*Veillonella parvula*, *Veillonella atypica*, *Lacrimispora saccharolytica*, *Haemophilus parainfluenzae*, and *Coprococcus sp. AF21-14LB*), but losing these bacteria did not seem to relate to long-term clinical outcome (P > 0.18; Supplementary Table S7).

Long-term multirecipient colonization strains were associated with clinical improvement. Of the 291 strains that engrafted long-term in at least one recipient, 61 strains (20.96%) colonized in at least three patients. Given the apparently increased likelihood of long-term colonization of these 61 donor-derived strains, we hereinafter refer to them as long-term multirecipient colonization (LMC) strains (Supplementary Figure S3). We next analyzed whether LMC strains could colonize in both B- and P-type recipients. A total of 43 LMC strains (70.49%) colonized in both B-type and P-type patients at week 26, whereas 18 LMC strains (29.50%) only colonized in B-type recipients at week 26. Of these B-type specific LMC strains, five (27.77%) were also detected in week 4 samples (but not in week

Figure 1. GMC types of patients with PsA and healthy donors at baseline. (A) The model fit performance of the 1 to 6 DMM clusters in PsA samples. (B) NMDS of PsA samples based on the genus relative abundance profile. (C) The genus composition of PsA samples. R denotes an FMT recipient and C denotes a control (sham) patient. (D) The model fit performance of the 1 to 6 DMM clusters in donor samples. (E) NMDS of donor based on the genus relative abundance profile. (F) The genus composition of 27 samples collected from the four donors on separate days during a 30-day donation period. B denotes patients with a GMC type dominated by the *Bacteroides* genus (B-type), whereas P denotes patients with a *Prevotella*-driven GMC type (P-type). AIC, Akaike information criterion; BIC, Bayesian information criterion; DMM, Dirichlet Multinomial Mixtures; FMT, fecal microbiota transplantation; GMC, gut microbiota community; NMDS, nonmetric multidimensional scaling; PsA, psoriatic arthritis.

Table 1. Baseline demographics and disease characteristics of B- and P-type patients*

Characteristic	B-type (n = 17)	P-type (n = 14)	Comparison (B vs P) *P* value
Age, y	54.4	45.43	0.07
Female sex, n (%)	12 (70.6)	8 (57.1)	0.69
Body mass index	29.7	33.4	0.14
Time since diagnosis,[a] days	2,447	1,596	0.84
Rheumatoid factor IgM positive, n (%)	0	2 (15.4)	0.35
HLA-B27 positive, n (%)	2 (11.8)	1 (7.14)	1.00
C-reactive protein, mg/L	5.8	4.7	0.37
Fecal calprotectin	39.1	97.14	0.34
HAQ-DI[b]	0.87	0.79	0.58
Swollen joint 66 count	7.00	7.1	0.62
Tender joint 68 count	15.7	16.6	0.81
Tender points	6.82	6.8	1.00
Physician's global assessment of disease activity, VAS	34.9	31.14	0.44
Patient's global assessment of disease activity, VAS	53.4	59.5	0.83
Arthritis pain, VAS	51.5	52.4	1.00
Fatigue, VAS	51.8	63.3	0.23
SPARCC enthesitis index[c]			
Score ≥1, n (%)	16 (94.1)	12 (85.7)	0.86
Score in patients with a score ≥1	7.1	8.3	0.22
Dactylitis			
Affected digit(s) ≥1, n (%)	5 (29.4)	5 (35.7)	1.00
Digits affected in patients with affected digit(s) ≥1	1.4	1.6	0.63
PASI			
Score >0, n (%)	7 (41.2)	7 (50.0)	0.90
Score in patients with a score of >0	2.93	2.6	0.75
Presence of nail disease, n (%)	12 (70.6)	10 (71.43)	1.00
MTX, n (%)			
Oral administration route	4 (23.5)	2 (14.3)	0.85
Subcutaneous administration route	13 (76.5)	12 (85.7)	0.85
Previous use of biologic DMARD, n (%)	4 (23.5)	1 (7.1)	0.46
Previous use of non-MTX conventional synthetic DMARD, n (%)	4 (23.5)	3 (21.4)	1.00
Antibiotics within 1 year of inclusion, n (%)	6 (35.3)	4 (30.8)	1.00
Smoking status, n (%)			0.70
Current	5 (29.4)	5 (35.71)	
Previous	6 (35.3)	6 (42.9)	
Never, value = 2	6 (35.3)	3 (21.4)	

* B denotes patients with a GMC type dominated by the *Bacteroides* genus (B-type) at baseline, whereas P denotes patients with a *Prevotella*-driven GMC type (P-type). Data are presented as mean unless otherwise stated. DMARD, disease-modifying antirheumatic drug; GMC, gut microbiota community; HAQ-DI, Health Assessment Questionnaire Disability Index; MTX, methotrexate; PASI, Psoriasis Area and Severity Index; PsA, psoriatic arthritis; SPARCC, Spondyloarthritis Research Consortium of Canada; VAS, visual analog scale.
[a] Time since diagnosis of PsA is presented as median.
[b] Scores on the HAQ-DI range from 0 to 3, with higher scores indicating greater disability.
[c] The SPARCC Enthesitis Index ranges from 0 to 16, with higher scores indicating more severe disease.

26 samples) of P-type patients, including a *Bacteroides clarus* strain SGB1832 and a *B. cellulosilyticus* strain SGB1844. No LMC strains were found to colonize exclusively in P-type recipients at week 26 (Figure 3B). When counting the total number of LMC strains in each recipient, we observed that week 26 responders tended to engraft more LMC strains than treatment failures ($P = 0.068$; Supplementary Figure S3).

Clinical significance of engraftment and decolonization of specific strains. Some of the LMC strains, which are known as potential SCFA-producing strains, including *B. clarus*, *B. wexlerae*, and *B. cellulosilyticus*, only engrafted and colonized long-term in responders at week 26 (Figure 3B). Notably, a *B. clarus* strain SGB1832 colonized in four responders (80%) at week 26. This bacterium demonstrated a negative effect size regarding arthritis pain and the patients' global assessment of disease (Figure 4). Two other strains (*Clostridiales bacterium* strain SGB15146 and *Eubacterium* strain SGB4961), which also engrafted and colonized long-term in B-type, but not in P-type, patients, showed a similar inverse relations with arthritis pain and the patients' global assessment of disease at week 26 (Figure 4). A complete list of all correlations between LMC strains and clinical variables is presented in the Supplementary Table S8.

Changes in the functional capacity of bacteria in FMT responders. Based on the metagenomics data, we

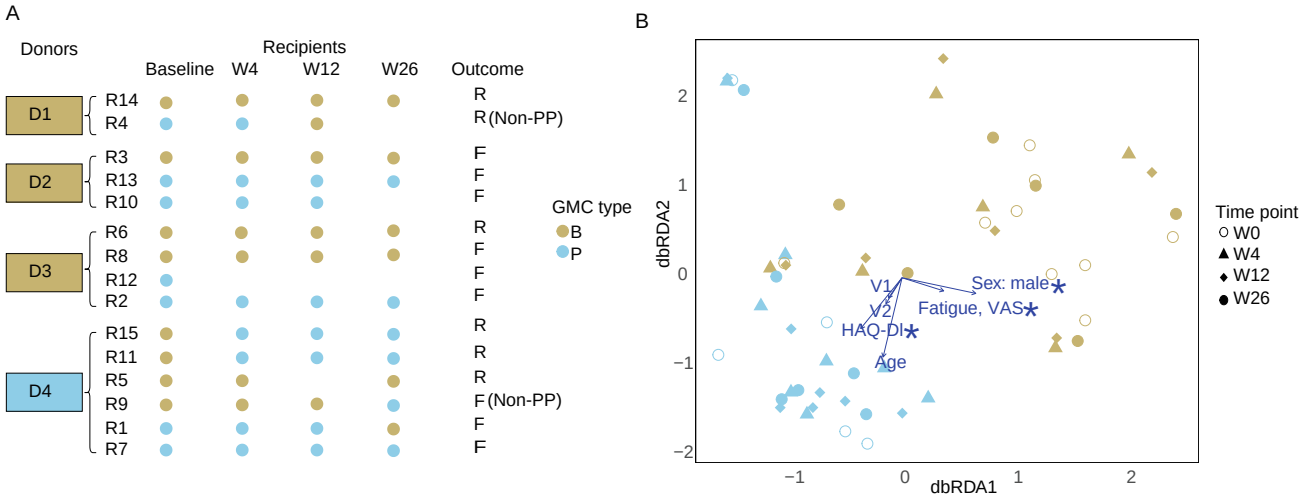

Figure 2. GMC types before/after FMT and long-term clinical outcome. (A) Week 26 outcomes for each patient allocated to FMT, R versus F. Non-PP population denotes patients excluded from the PP population due to major change in living environment (R4) or not receiving the full dose of the FMT product (R9). B denotes patients with a GMC type dominated by the *Bacteroides* genus (B-type) at baseline whereas P denotes patients with a *Prevotella*-driven GMC type (P-type). In donors, the B-type could further be divided into a *Phocaeicola* subtype (BP-type) or a GGB9062 subtype (BG-type). (B) dbRDA of 53 fecal samples from the FMT-treated patients at the species level. The contribution of each clinical variable to the variation in species community is shown in Supplementary Table S2. ANOVA was used to calculate the sum of squares and *P* values for each clinical variable. Variables (HAQ-DI, fatigue VAS, and sex) with $P < 0.05$ are marked with an asterisk (*). V1: Patient's global assessment of disease activity (VAS); V2: Arthritis pain (VAS). ANOVA, analysis of variance; dbRDA, distance-based redundancy analysis; F, failure; FMT, fecal microbiota transplantation; GMC, gut microbiota community; HAQ-DI, Health Assessment Questionnaire Disability Index; PP, per-protocol; R, responder; VAS, visual analog scale. Color figure can be viewed in the online issue, which is available at http://onlinelibrary.wiley.com/doi/10.1002/art.43359/abstract.

observed that the abundance of 14 genes encoding bacterial enzymes changed in long-term FMT responders (Supplementary Table S9), including genes encoding enzymes involved in nucleotide metabolism and bacterial cell wall peptidoglycan production ($P = 0.059$). However, none of these genes showed a significant linear correlation with the clinical variables after adjustment for multiple testing (size effect < 1 and *P* adj > 0.1; Supplementary Table S10).

DISCUSSION

Beneficial effects of microbiota-targeted therapies are believed to be mediated through direct immunomodulatory processes following changes in the gut microbiota and gut barrier physiology and/or indirectly by boosting the efficacy of DMARDs.[32] This study is the first to highlight patient-related gut microbial signatures that are associated with long-term clinical outcome following manipulation of the intestinal *milieu* using one FMT in MTX-treated patients with active PsA. That certain patients may tolerate and benefit more from some therapies than others is a well-known challenge in the management of arthritis and related chronic inflammatory diseases.[33] We here demonstrate that the baseline GMC type of FMT recipients may be an important factor to consider in the context of gut microbiota manipulation in patients with immune-mediated arthritis.

Previous studies have suggested that the gut microbiota of people can be divided into three main compositional categories based on their individual GMC type (also referred to as enterotype), defined by a relatively high abundance of *Bacteroides* spp., *Prevotella* spp., or *Ruminococcus* spp.[34,35] Other groups have proposed a two-cluster or a four-cluster model, which is mainly driven by *Bacteroides* or *Clostridiales* species or by *Prevotella*.[36] In our study, we identified three distinct clusters among the four healthy donors but only two distinct clusters among the 31 patients with PsA. In both cases, the main GMC types were

Table 2. Week 26 response rates of FMT-treated B-type and P-type patients*

Study population	GMC type	Response rates, n (%)	*P* value
ITT population (n = 15)	B-type (n = 8)	5 (62.5)	0.12
	P-type (n = 7)	1 (14.3)	
PP population (n = 13)	B-type (n = 7)	5 (71.4)	0.021
	P-type (n = 6)	0	

* B denotes patients with a GMC type dominated by the *Bacteroides* genus (B-type) at baseline, whereas P denotes patients with a *Prevotella*-driven GMC type (P-type). Reasons for excluding patients from the PP population included major changes in living environment and not receiving the full dose of the FMT product. FMT, fecal microbiota transplantation; GMC, gut microbiota community; ITT, intention to treat; PP, per-protocol.

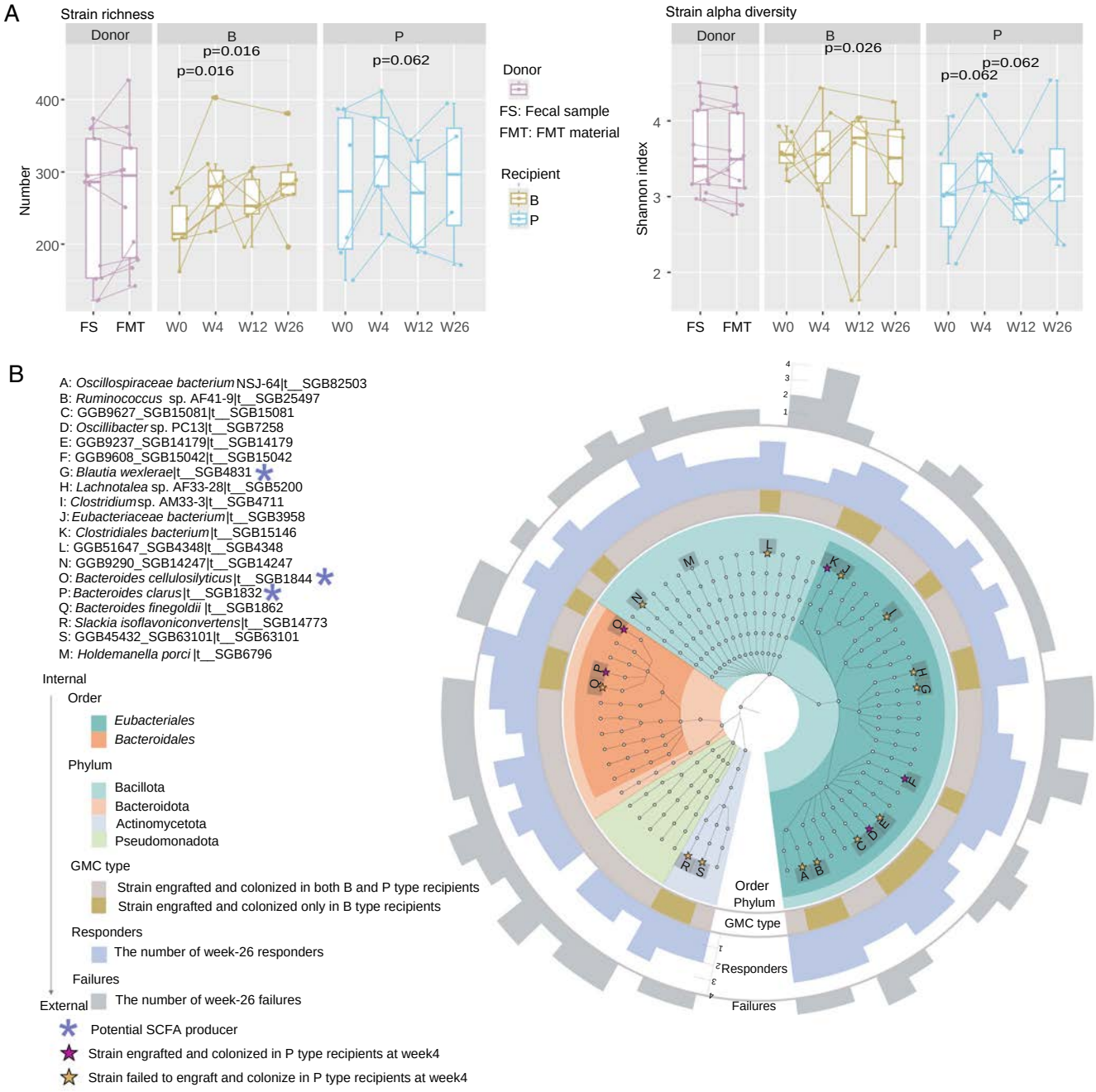

Figure 3. Gut microbiota modifications following one FMT in B- and P-type patients. B denotes patients with a GMC type dominated by the *Bacteroides* genus (B-type) at baseline, whereas P denotes patients with a *Prevotella*-driven GMC (P-type). (A) Changes in strain richness and alpha diversity. *P* values were calculated using a paired Wilcoxon test. (B) LMC strains were defined as strains that engrafted and colonized in at least three patients by week 26. Eighteen LMC strains, which exclusively engrafted in B-type recipients at week 26, are marked with a start and a letter. Star colors differentiate short-term colonization status in P-type recipients at week 4: purple signifies engraftment, whereas yellow signifies lack of engraftment. FMT, fecal microbiota transplantation; FS, fecal sample; GMC, gut microbiota community; LMC, long-term multirecipient colonization; SCFA, short-chain fatty acid. Color figure can be viewed in the online issue, which is available at http://onlinelibrary.wiley.com/doi/10.1002/art.43359/abstract.

dominated by either *Bacteroides* (B-type) or *Prevotella* (P-type). These two genera both belong to the phylum *Bacteroidota* and exhibit an inverse relation in the human gut. The presence of only two GMC types in patients with rheumatoid arthritis was reported by Qiao et al.[3] The robust finding of only two GMC types in patients with PsA may indicate that rheumatoid arthritis and PsA drive the microbiota into a state with only two GMC types, contrasting the situation observed for the healthy donors, or that MTX treatment per se pushes the composition of the gut microbiota into GMC states comprising only the B-type or the P-type.

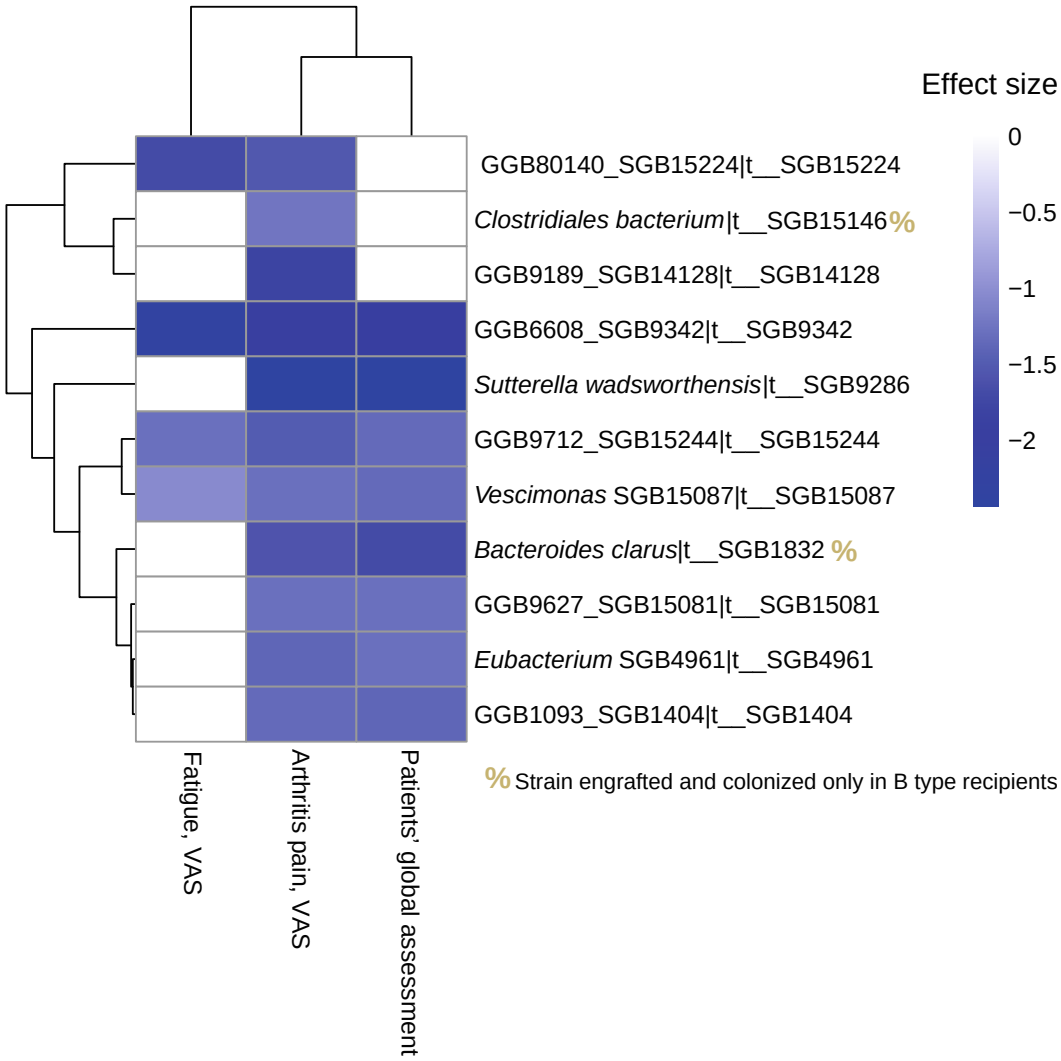

Figure 4. Correlations between strains that engrafted and colonized in week 26 responders and clinical PsA disease scores. PsA, psoriatic arthritis; VAS, visual analog scale. Color figure can be viewed in the online issue, which is available at http://onlinelibrary.wiley.com/doi/10.1002/art.43359/abstract.

Although patients with a P-type microbiota tended to be younger, we did not identify any differences in sex, body mass index, or baseline disease severity, which could explain the significantly higher remission rate among FMT-treated B-type patients compared to P-type patients. Instead, we observed specific microbiota-related differences, which might have contributed to the observed differences in long-term outcome. Firstly, species alpha diversity was significantly higher in B-type than in P-type patients at baseline. Secondly, strain richness significantly increased from baseline to week 4 and week 26 in B-type, but not in P-type, patients, which suggests that the engrafted donor strains did not colonize long-term in P-type patients. This difference in colonization receptivity was further backed by the investigation on the bacterial strain level, in which 18 LMC strains were found exclusively in B-type patients at week 26 whereas none LMC strains were found exclusively in P-type patients.

In line with our findings, Paramsothy et al reported that *Prevotella* was associated with FMT failure in patients with ulcerative colitis whereas *Bacteroides* in donor stool was associated with remission.[18] The predictive value of the recipient's baseline gut microbiota upon treatment with FMT and fiber supplementation has also been shown in individuals with obesity and metabolic syndrome.[37] Previous findings in rheumatoid arthritis further indicate that patients' gut microbiota composition may relate to clinical effects of MTX.[3,38,39] This is an interesting observation that may suggest that patients' gut bacteria can assist in predicting—and potentially modifying—drug responses of established therapies. These previous reports and our current findings in MTX-treated patients with PsA motivate more research into the complementary use of DMARDs and microbiota-targeted therapies in clinical practice.[40]

Because all but two FMT-treated patients received subcutaneous versus orally administered MTX, we do not think that FMT

affected the systemic bioavailability of this drug in the present study. However, the observed changes in abundance of genes encoding enzymes involved in nucleotide metabolism could imply that MTX might have affected the transferred microbiota, as previously described by Nayak and colleagues.[41] Furthermore, ongoing inflammation in treatment-naïve patients with rheumatoid arthritis has also been shown to affect folate metabolism in the gut ecosystem.[42]

One of the observed changes included a decrease in a gene encoding formimidoyltetrahydrofolate cyclodeaminase. This enzyme catalyzes the degradation of histidine, which involves the metabolization of tetrahydrofolate. A decrease in this enzyme may therefore increase the availability of purines and support the intrabacterial production of nucleotides.[43] Simultaneously, the resulting expansion of histidine concentrations could stimulate the histamine synthesis pathway. Interestingly, gut-derived histamine has recently been shown to alleviate arthritis in mice through the gut–CNS–joint axis.[44]

Despite these intriguing theories, the lack of significant correlation between enzyme-related genes and clinical variables implies that the abundance of specific metabolic pathways did not substantially affect individual clinical PsA measures. Instead, bacterial pathogen-associated molecular patterns might directly or indirectly have modulated the immune system, thereby eliciting the beneficial effects of FMT, as indicated by the decrease in genes encoding enzymes involved in bacterial cell wall peptidoglycan production in the FMT responders.

Based on our observations, engraftment of beneficial bacterial strains may be more important than eliminating specific pathogenic ones. Two potential functional catalogs of the identified LMC strains may be involved,[45] including engraftment of potential SCFA producers such as the *B. clarus* strains,[46] which revealed an inverse correlation with patient-reported outcomes such as arthritis pain, global assessment of disease, and fatigue. We further observed a trend toward clustering among certain SCFA-producing strains, in which strains of *B. clarus*, *P. clara*, *D. longicatena*, *E. ventriosum*, and *B. cellulosilyticus* formed one cluster and strains of *B. wexlerae*, *E. ramulus*, and *Butyricicoccus* formed another distinct cluster (Supplementary Figure S3). This suggests the possibility of functional synergy of SCFA-producing strains after FMT. Although data on microbial changes following dietary interventions are very limited in arthritis, studies with beneficial responses show a greater increase in SCFA-producing bacteria as compared to dietary interventions with no clinical disease-modifying effects.[47]

In spite of the high response rate among B-type patients, two failed to achieve long-term clinical remission. Hence, although the GMC type of the recipients and LMC strains seem to play important roles for long-term donor strain colonization, and subsequently FMT efficacy in PsA, these recipient factors may only partially explain the outcome of FMT. Other factors that could be important may be related to donor–patient compatibility and/or the content of the FMT product. In ulcerative colitis, donor microbiota stability, species evenness, and specific microbial species seem to be markers of donor efficacy.[48] Although we observed that FMT products from one donor (D2) with the lowest microbiota richness were unsuccessful in all cases, we found that the characteristics of donor microbiota seemed to be less important for a beneficial outcome compared to the patients' GMC type. Still, we acknowledge that the current study was too small to extensively address this question.

It is well known that the laboratory processing and handling of FMT products, including blending, exposure to oxygen, and freeze–thaw cycles, may affect the composition and viability of transferred donor bacteria. Even though we did not observe any overall changes in alpha diversity or richness of stool donations after FMT processing, we did observe a decrease in the overall abundance of *Bifidobacterium* species and butyrate-producing species from the genera *Roseburia*, *Mediterraneibacter*, and *Anaerotruncus*, all of which have been associated with prohomeostatic and anti-inflammatory, immunomodulatory properties. Therefore, the clinical implication of this inherent variation in the microbial content of FMT products due to differences in FMT manufacturing protocols and/or donor variations still needs to be studied in larger trials.

Both the ability to engraft as well as the disease-modulating properties of the transferred microbiota are important aspects to consider to guide the selection of donors and/or the development of synthetic communities. The list of potential beneficial LMC strains that had the ability to colonize both B- and P-type patients might be relevant targets for future research. Another strategy to overcome resistance toward engraftment of donor strains in P-type patients (and potential also in some B-type patients) could encompass several preplanned weekly FMT administrations to preserve the induction of beneficial changes of the microbial composition and function over time. Similar conclusions have been drawn from previous FMT trials in ulcerative colitis, including the successful application of a "five-day per week" intensive treatment regime and the use of multidonor FMT products.[8,49]

Only one other (cross-sectional) study has characterized the gut bacterial signatures in patients with PsA using shotgun metagenomic sequencing.[50] This study also characterized gut bacterial features, but in contrast to our study, they used metagenome assembly and gene prediction to obtain a gene catalog. Compared to our baseline data, no patients with PsA with a *Prevotella*-dominated GMC type were identified in this other cohort. This discrepancy may be attributed to differences in gut microbiota composition between Western and non-Western populations and/or patients being treatment-naïve versus being on a stable dose of MTX, as well as potential biases resulting from a limited sample size.

In conclusion, we here demonstrate that the *Bacteroides* versus *Prevotella*-dominated GMC type of recipients can modulate long-term clinical outcome of one FMT in active PsA. In

particular, B-type patients have a significantly higher clinical response rates following FMT compared to P-type patients, likely due to a high engraftment potential and long-lasting colonization of donor strains. Given the practical applicability of stratifying individuals according to their GMC type, more research is encouraged to evaluate the clinical value of using GMC typing and other gut microbial features in guiding the selection of therapies and enhancing personalized treatment responses in relation to both the application of microbiota-targeted therapies and the use of established DMARDs.

ACKNOWLEDGMENTS

We thank all patients and donors for their important contribution. We thank L. Albjerg (biomedical laboratory technologist) for the collection of donor fecal samples and fecal microbiota transplantation product samples.

AUTHOR CONTRIBUTIONS

All authors contributed to at least one of the following manuscript preparation roles: conceptualization AND/OR methodology, software, investigation, formal analysis, data curation, visualization, and validation AND drafting or reviewing/editing the final draft. As corresponding author, Dr Kragsnaes confirms that all authors have provided the final approval of the version to be published and takes responsibility for the affirmations regarding article submission (eg, not under consideration by another journal), the integrity of the data presented, and the statements regarding compliance with institutional review board/Declaration of Helsinki requirements.

REFERENCES

1. Wang Y, Wei J, Zhang W, et al. Gut dysbiosis in rheumatic diseases: a systematic review and meta-analysis of 92 observational studies. EBioMedicine 2022;80:104055.
2. Cheng M, Zhao Y, Cui Y, et al. Stage-specific roles of microbial dysbiosis and metabolic disorders in rheumatoid arthritis. Ann Rheum Dis 2022;81(12):1669–1677.
3. Qiao J, Zhang S-X, Chang M-J, et al. Specific enterotype of gut microbiota predicted clinical effect of methotrexate in patients with rheumatoid arthritis. Rheumatology (Oxford) 2023;62(3):1087–1096.
4. Azzouz DF, Chen Z, Izmirly PM, et al. Longitudinal gut microbiome analyses and blooms of pathogenic strains during lupus disease flares. Ann Rheum Dis 2023;82(10):1315–1327.
5. Scher JU, Nayak R, Clemente JC. Microbiome research in autoimmune and immune-mediated inflammatory diseases: lessons, advances and unmet needs. Ann Rheum Dis 2025;84(1):9–13.
6. Wagenaar CA, Walrabenstein W, van der Leeden M, et al. Long-term effectiveness of a lifestyle intervention for rheumatoid arthritis and osteoarthritis: 1-year follow-up of the 'Plants for Joints' randomised clinical trial. RMD Open 2024;10(1):e004025.
7. Sanchez P, Letarouilly JG, Nguyen Y, et al. Efficacy of probiotics in rheumatoid arthritis and spondyloarthritis: a systematic review and meta-analysis of randomized controlled trials. Nutrients 2022; 14(2):354.
8. Imdad A, Pandit NG, Zaman M, et al. Fecal transplantation for treatment of inflammatory bowel disease. Cochrane Database Syst Rev 2023;4(4):CD012774.
9. Huang C, Yi P, Zhu M, et al. Safety and efficacy of fecal microbiota transplantation for treatment of systemic lupus erythematosus: an EXPLORER trial. J Autoimmun 2022;130:102844.
10. Sorbara MT, Pamer EG. Microbiome-based therapeutics. Nat Rev Microbiol 2022;20(6):365–380.
11. Kragsnaes MS, Nilsson AC, Kjeldsen J, et al. How do I establish a stool bank for fecal microbiota transplantation within the blood- and tissue transplant service? Transfusion 2020;60(6):1135–1141.
12. Salem F, Kindt N, Marchesi JR, et al. Gut microbiome in chronic rheumatic and inflammatory bowel diseases: similarities and differences. United European Gastroenterol J 2019;7(8):1008–1032.
13. Zeng J, Peng L, Zheng W, et al. Fecal microbiota transplantation for rheumatoid arthritis: a case report. Clin Case Rep 2020;9(2):906–909.
14. Wang L, Wei Z, Pan F, et al. Case report: fecal microbiota transplantation in refractory ankylosing spondylitis. Front Immunol 2023;14: 1093233.
15. Selvanderan SP, Goldblatt F, Nguyen NQ, et al. Faecal microbiota transplantation for Clostridium difficile infection resulting in a decrease in psoriatic arthritis disease activity. Clin Exp Rheumatol 2019;37(3): 514–515.
16. Kragsnaes MS, Kjeldsen J, Horn HC, et al. Safety and efficacy of faecal microbiota transplantation for active peripheral psoriatic arthritis: an exploratory randomised placebo-controlled trial. Ann Rheum Dis 2021;80(9):1158–1167.
17. Mullish BH, Tohumcu E, Porcari S, et al. The role of faecal microbiota transplantation in chronic noncommunicable disorders. J Autoimmun 2023;141:103034.
18. Paramsothy S, Nielsen S, Kamm MA, et al. Specific bacteria and metabolites associated with response to fecal microbiota transplantation in patients with ulcerative colitis. Gastroenterology 2019;156(5): 1440–1454.e2.
19. Pinto S, Šajbenová D, Benincà E, et al. Dynamics of gut microbiota after fecal microbiota transplantation in ulcerative colitis: success linked to control of prevotellaceae. J Crohns Colitis 2025;19(2): jjae137.
20. Kragsnaes MS, Jensen JRB, Nilsson AC, et al. Dynamics of inflammation-associated plasma proteins following faecal microbiota transplantation in patients with psoriatic arthritis and healthy controls: exploratory findings from the FLORA trial. RMD Open 2024;10(1): e003750.
21. Kragsnaes MS, Miguens Blanco J, Mullish BH, et al. Small intestinal permeability and metabolomic profiles in feces and plasma associate with clinical response in patients with active psoriatic arthritis participating in a fecal microbiota transplantation trial: exploratory findings from the FLORA trial. ACR Open Rheumatol 2023;5(11):583–593.
22. Schmidt TSB, Li SS, Maistrenko OM, et al. Drivers and determinants of strain dynamics following fecal microbiota transplantation. Nat Med 2022;28(9):1902–1912.
23. Ianiro G, Punčochář M, Karcher N, et al. Variability of strain engraftment and predictability of microbiome composition after fecal microbiota transplantation across different diseases. Nat Med 2022;28(9): 1913–1923.
24. He R, Li P, Wang J, et al. The interplay of gut microbiota between donors and recipients determines the efficacy of fecal microbiota transplantation. Gut Microbes 2022;14(1):2100197.
25. He Q, Gao Y, Jie Z, et al. Two distinct metacommunities characterize the gut microbiota in Crohn's disease patients. Gigascience 2017; 6(7):1–11.
26. Schloissnig S, Arumugam M, Sunagawa S, et al. Genomic variation landscape of the human gut microbiome. Nature 2013;493(7430): 45–50.

27. Gossec L, Baraliakos X, Kerschbaumer A, et al. EULAR recommendations for the management of psoriatic arthritis with pharmacological therapies: 2019 update. Ann Rheum Dis 2020;79(6):700–712.
28. Frioux C, Ansorge R, Özkurt E, et al. Enterosignatures define common bacterial guilds in the human gut microbiome. Cell Host Microbe 2023;31(7):1111–1125.e6.
29. *vegan: Community Ecology Package. R package*. Version 2.0-10. The R Project for Statistical Computing. Accessed December 16, 2024. https://CRAN.R-project.org/package=vegan
30. Mallick H, Rahnavard A, McIver LJ, et al. Multivariable association discovery in population-scale meta-omics studies. PLOS Comput Biol 2021;17(11):e1009442.
31. Asnicar F, Weingart G, Tickle TL, et al. Compact graphical representation of phylogenetic data and metadata with GraPhlAn. PeerJ 2015;3:e1029.
32. Nayak RR, Orellana DA. The impact of the human gut microbiome on the treatment of autoimmune disease. Immunol Rev 2024;325(1):107–130.
33. Kerschbaumer A, Smolen JS, Ferreira RJO, et al. Efficacy and safety of pharmacological treatment of psoriatic arthritis: a systematic literature research informing the 2023 update of the EULAR recommendations for the management of psoriatic arthritis. Ann Rheum Dis 2024;83(6):760–774.
34. Arumugam M, Raes J, Pelletier E, et al; MetaHIT Consortium. Enterotypes of the human gut microbiome. Nature 2011;473(7346):174–180.
35. Olsson LM, Boulund F, Nilsson S, et al. Dynamics of the normal gut microbiota: a longitudinal one-year population study in Sweden. Cell Host Microbe 2022;30(5):726–739.e3.
36. Gorvitovskaia A, Holmes SP, Huse SM. Interpreting Prevotella and Bacteroides as biomarkers of diet and lifestyle. Microbiome 2016;4(1):15.
37. Zhang Z, Mocanu V, Deehan EC, et al. Recipient microbiome-related features predicting metabolic improvement following fecal microbiota transplantation in adults with severe obesity and metabolic syndrome: a secondary analysis of a phase 2 clinical trial. Gut Microbes 2024;16(1):2345134.
38. Artacho A, Isaac S, Nayak R, et al. The pretreatment gut microbiome is associated with lack of response to methotrexate in new-onset rheumatoid arthritis. Arthritis Rheumatol 2021;73(6):931–942.
39. Zhang X, Zhang D, Jia H, et al. The oral and gut microbiomes are perturbed in rheumatoid arthritis and partly normalized after treatment. Nat Med 2015;21(8):895–905.
40. Scher JU, Nayak RR, Ubeda C, et al. Pharmacomicrobiomics in inflammatory arthritis: gut microbiome as modulator of therapeutic response. Nat Rev Rheumatol 2020;16(5):282–292.
41. Nayak RR, Alexander M, Deshpande I, et al. Methotrexate impacts conserved pathways in diverse human gut bacteria leading to decreased host immune activation. Cell Host Microbe 2021;29(3):362–377.e11.
42. Thompson KN, Bonham KS, Ilott NE, et al; Inflammatory Arthritis Microbiome Consortium (IAMC) investigators group. Alterations in the gut microbiome implicate key taxa and metabolic pathways across inflammatory arthritis phenotypes. Sci Transl Med 2023;15(706):eabn4722.
43. Kanarek N, Keys HR, Cantor JR, et al. Histidine catabolism is a major determinant of methotrexate sensitivity. Nature 2018;559(7715):632–636.
44. Dürholz K, Ehnes L, Linnerbauer M, et al. Gut-specific histamine 3 receptor signaling orchestrates microglia-dependent resolution of peripheral inflammation. J Clin Invest 2025;135(18):e184697.
45. Wu G, Xu T, Zhao N, et al. A core microbiome signature as an indicator of health. Cell 2024;187(23):6550–6565.e11.
46. Watanabe Y, Nagai F, Morotomi M, et al. Bacteroides clarus sp. nov., Bacteroides fluxus sp. nov. and Bacteroides oleiciplenus sp. nov., isolated from human faeces. Int J Syst Evol Microbiol 2010;60(Pt 8):1864–1869.
47. Wagenaar CA, van de Put M, Bisschops M, et al. The effect of dietary interventions on chronic inflammatory diseases in relation to the microbiome: a systematic review. Nutrients 2021;13(9):3208.
48. Haifer C, Luu LDW, Paramsothy S, et al. Microbial determinants of effective donors in faecal microbiota transplantation for UC. Gut Published July 25, 2022. https://doi.org/10.1136/gutjnl-2022-327742.
49. Paramsothy S, Kamm MA, Kaakoush NO, et al. Multidonor intensive faecal microbiota transplantation for active ulcerative colitis: a randomised placebo-controlled trial. Lancet 2017;389(10075):1218–1228.
50. Liu W, Li C, Xie W, et al. The signature of the gut microbiota associated with psoriatic arthritis revealed by metagenomics. Ther Adv Musculoskelet Dis 2024;16:1759720x241266720.

Arthritis & Rheumatology
Vol. 78, No. 2, February 2026, pp 332–343
DOI 10.1002/art.43396

American College of Rheumatology
Empowering Rheumatology Professionals

Transition From Psoriasis to Psoriatic Arthritis is Characterized by Distinct Alterations in Peripheral Blood Tc17, Th17, and CD4$^+$ Effector Memory Cells

Hanna Graßhoff,[1] Sara Comdühr,[1] Henry Nording,[2,3,4] Jacob von Esebeck,[2] Philine Letz,[1,5,6] Miriam Prohaczka,[1] Handan Gedik,[7] Henner Zirpel,[7] Elisabeth Spallek,[7] Linh Ha-Wissel,[7] El-Baraa Adjailia,[1] Sabrina Arnold,[1] Konstantinos Fourlakis,[1] Sebastian Klapa,[1] Ingo Eitel,[4,8] Oliver J. Müller,[3,4] Jens Y. Humrich,[1] Gabriela Riemekasten,[1] Diamant Thaçi,[7] and Peter Lamprecht[1,7]

Objective. Cellular mechanisms driving transition from psoriasis to psoriatic arthritis have remained largely elusive. Thus, we investigated changes within the peripheral blood T cell compartment associated with the transition phase.

Methods. In an observational study, 116 patients were examined and categorized into subgroups including psoriasis with at least one risk factor for transition to psoriatic arthritis, subclinical psoriatic arthritis according to EULAR taskforce recommendations from 2023, and definitive psoriatic arthritis meeting the Classification Criteria for Psoriatic Arthritis. Demographic and clinical characteristics of patient subgroups were analyzed. Deep T cell phenotyping using multicolor flow cytometry and machine-learning techniques were applied.

Results. Overlapping T cell endotypes were found among patients with subclinical psoriatic arthritis exhibiting the most notable divergence from the others. Frequencies of effector memory CD4$^+$ T cells, Th17, and Tc17 cells differed among patients with psoriasis with at least one risk factor for transition, subclinical psoriatic arthritis, and psoriatic arthritis. Transition-associated changes of Tc17 cell frequencies were confirmed by machine-learning–assisted unsupervised clustering analysis. Moreover, patients with enthesitis could be distinguished from those without, with Tc17 cells being the main distinctive feature.

Conclusion. Transition from psoriasis to psoriatic arthritis was associated with distinct alterations of the peripheral blood T cell compartment, with Tc17 cells exhibiting the greatest discriminatory power. These findings provide insight into pathomechanisms driving disease progression during transition from psoriasis to psoriatic arthritis and identify Tc17 cells as the foremost novel potential therapeutic target for the prevention of transition.

INTRODUCTION

Psoriasis is a chronic systemic immune-mediated disease characterized by T cell–driven epidermal hyperplasia with a prevalence between 0.51% and 11.43% in adults depending on ethnic and geographic variation.[1] In up to 30% of patients, the disease is associated with the development of psoriatic arthritis characterized by synovioentheseal inflammation.[2] Psoriasis precedes psoriatic arthritis in about 70% of the patients by an average of seven to eight years with an annual transition rate of 0.74% and

Supported by the Deutsche Forschungsgemeinschaft (German Research Foundation), grant LA 1339/6-1 to Prof. Dr. Lamprecht and grant EXC2167 (project Clinical Demonstrator 1) to Prof. Dr. Thaçi, and an award from the Deutscher Psoriasis Bund e.V. (German Psoriasis Alliance), to Dr Graßhoff.

[1]Hanna Graßhoff, MD, Sara Comdühr, PhD, Philine Letz, MSc, Miriam Prohaczka, MSc, El-Baraa Adjailia, Sabrina Arnold, MD, Konstantinos Fourlakis, Sebastian Klapa, MD, Jens Y. Humrich, PD, Gabriela Riemekasten, MD, Peter Lamprecht, MD: Department of Rheumatology and Clinical Immunology, University of Lübeck, Lübeck, Germany; [2]Henry Nording, MD, Jacob von Esebeck: Cardioimmunology Group, Medical Clinic II, University Heart Center Lübeck, Lübeck, Germany; [3]Henry Nording, MD, Oliver J. Müller, MD: Department of Internal Medicine V, University of Kiel, Kiel, Germany; [4]Henry Nording, MD, Ingo Eitel, MD, Oliver J. Müller, MD: German Centre for Cardiovascular Research, Partner Site Hamburg/Kiel/Lübeck, Lübeck, Germany; [5]Philine Letz, MSc: Department of Medicine, University Medical Center Hamburg-Eppendorf, Hamburg, Germany; [6]Philine Letz, MSc: Hamburg Center for Translational Immunology, University Medical Center Hamburg-Eppendorf, Hamburg, Germany; [7]Handan Gedik, MD, Henner Zirpel, PhD, Elisabeth Spallek, MD, Linh Ha-Wissel, MD, Diamant Thaçi, MD, Peter Lamprecht, MD: Institute and Comprehensive Center for Inflammation Medicine, University of Lübeck, Lübeck, Germany; [8]Ingo Eitel, MD: University Heart Center Lübeck, Medical Clinic II, University of Lübeck, Lübeck, Germany.

Drs Graßhoff, Comdühr, and Nording are co-first authors and contributed equally to this work. Prof. Dr. Thaçi and Prof. Dr. Lamprecht are co-last authors and contributed equally to this work.

Additional supplementary information cited in this article can be found online in the Supporting Information section (https://acrjournals.onlinelibrary.wiley.com/doi/10.1002/art.43396).

Author disclosures are available at https://onlinelibrary.wiley.com/doi/10.1002/art.43396.

Address correspondence via email to Hanna Graßhoff, at hanna.grasshoff@uksh.de.

Submitted for publication March 9, 2025; accepted in revised form August 26, 2025.

2.7%.[3–5] Risk factors for transition to psoriatic arthritis include younger age at disease onset, psoriasis severity, phenotype (nail, scalp, and inverse psoriasis), comorbidities (obesity), environmental factors (infections, smoking, trauma, emotional stress, medications), and genetic factors.[6–9] Although these risk factors are associated with an increased rate of transition, they do not necessarily indicate an imminent progression to psoriatic arthritis. Instead, they are considered components within a complex, multifactorial landscape that underlies disease progression.

Although T cells are known to be the key drivers of pathophysiology in psoriasis and psoriatic arthritis, current knowledge regarding immunologic processes during disease transition remains scarce. Evidence for $CD8^+$ T cell involvement in the pathogenesis comes from the strong association with major histocompatibility complex (MHC) class I genes, notably *HLA-C*0602*, and single nucleotide polymorphisms of the interleukin (IL)-23 and IL-23 receptor (IL-23R) genes promoting Th17 cell differentiation.[8,9] Increased frequencies of circulating Th1, Th17, and Th22 $CD4^+$ T helper cell subsets have been reported in psoriasis as well as enrichment of Th1, Th9, Th17, and Th22 $CD4^+$ T cells and their $CD8^+$ cytotoxic counterparts (Tc1, Tc17, and Tc22) in psoriatic lesions.[10–16] Unlike psoriasis, immunopathogenic features of T cells are less well characterized in psoriatic arthritis. There is a gap in knowledge of the pathogenic relationship between T cell responses in psoriasis and its link to the development of joint inflammation.[17] It remains unclear which changes in T cell populations occur during transition from psoriasis to psoriatic arthritis and in which way T cells contribute to this transition.

Biologic agents targeting tumor necrosis factor (TNF) α, IL-17, and IL-23 have improved the outcome of psoriatic arthritis, albeit with a rate of 30% to 40% nonresponders or inadequate responders. By contrast, improvement of skin lesions in psoriasis with biologics, particularly those that inhibit the IL-23/IL-17 axis, is far more effective than the joint response to these biologics.[18,19] Notably, unlike Th17 cells, Tc17 cells lack therapeutic responsiveness and are retained in resolved psoriatic skin lesions, thus potentially driving recurrent inflammation and facilitating transition from psoriasis to psoriatic arthritis.[20] A promising strategy to prevent sequelae and improve patient outcomes is therefore the early identification and targeted treatment of individuals at risk of developing psoriatic arthritis.[8] Clinical studies support the concept of a "window of opportunity," during which intervention can alter the progression to psoriatic arthritis, and they indicate that early treatment leads to better long-term outcomes.[8,21] This highlights a significant unmet medical need, namely a deeper understanding of the immunopathological mechanisms underlying the transition phase, and more precise identification of patients with psoriasis at increased risk of developing psoriatic arthritis.[8] To facilitate comparability across studies, an EULAR task force established classification criteria for patients in transitional stages. As an intermediate group bridging psoriasis and early psoriatic arthritis, they identified a category termed "subclinical psoriatic arthritis," characterized by arthralgia and/or imaging evidence of synovioentheseal inflammation.[22,23] According to Zabotti et al, the probability for fulfilling the Classification of Psoriatic Arthritis (CASPAR) criteria among patients with subclinical psoriatic arthritis who report arthralgia is 22.7% after 36 months.[24] This observation emphasizes the importance of recognizing musculoskeletal symptoms for identification of patients undergoing transition early.

In this study, we hypothesized that the transition phase is characterized by changes in the composition of T cell subsets distinct from psoriasis and psoriatic arthritis, assuming that immune dysregulation precedes clinically apparent joint inflammation. To identify changes within the peripheral blood T cell compartment and clinical features associated with the transition from psoriasis to psoriatic arthritis, we studied 116 patients subgrouped into psoriasis with risk factors for psoriatic arthritis, subclinical psoriatic arthritis, and psoriatic arthritis. Demographic and clinical manifestations of psoriasis and psoriatic arthritis were assessed, and deep T cell phenotyping was performed.

MATERIALS AND METHODS

Detailed experimental procedures are provided in the Supplemental Materials. Consecutive patients with psoriasis (n = 46), in the transition phase (n = 8), and with psoriatic arthritis (n = 62) were included. Due to the exploratory nature of the study, no formal sample size calculation was performed, and patient numbers were based on feasibility and the aim to capture relevant clinical diversity. The diagnosis of psoriasis and nail involvement was made clinically by a dermatologist. Inclusion criteria for patients with psoriasis were (i) at least one risk factor for transition to psoriatic arthritis including obesity, severe psoriasis, nail involvement, and a first-degree relative with psoriatic arthritis, and (ii) active disease with an indication for initiation of systemic therapy according to the 2021 S3 guideline for the treatment of psoriasis.[25] The group of patients with psoriasis with at least one risk factor for transition to psoriatic arthritis is termed "psoriasis" in the following. Subclinical psoriatic arthritis was defined as psoriasis with arthralgia and/or imaging evidence of synovial/entheseal inflammation without clinical synovitis, as suggested by an EULAR taskforce in 2023.[23] Psoriatic arthritis was diagnosed by rheumatologists following the CASPAR criteria.[26] Additionally, these patients had an active disease with an indication for initiation of systemic therapy in accordance with current EULAR and Group for Research and Assessment of Psoriasis and Psoriatic Arthritis (GRAPPA) recommendations.[27,28] Individuals who were pregnant or actively lactating were excluded from study participation.

Demographic parameters, clinical data, and laboratory parameters were assessed. Disease activity was scored using Psoriasis Area Severity Index (PASI), Dermatology Life Quality Index (DLQI), itch on a visual analog scale (VAS), tender and swollen joint count according to Disease Activity in Psoriatic Arthritis score, German Psoriasis Arthritis Diagnostic questionnaire, Leeds

Enthesitis Index and the Maastricht Ankylosing Spondylitis Enthesitis as well as Health Assessment Questionnaire (HAQ). Details of the diagnostic pathway to classify study participants are shown in Supplementary Figure 1.

Deep T cell phenotyping was conducted in all patients using multicolor flow cytometry on heparinized blood samples, following standardized staining, lysis, and viability protocols. The samples were acquired using CytoFLEX S spectral analyzer flow cytometer (Beckman Coulter) and CytExpert software (Beckman Coulter). Data analysis was performed using FlowJo version 10 (BD Biosciences). The gating strategy is presented in Supplementary Table 1, Supplementary Figures 2 and 3. Influence of age, sex and BMI of peripheral T cells is shown in Supplementary Figure 4. To assess therapeutic effects on T cell subset frequencies, 114 patients underwent immunophenotyping at therapy initiation and after 2, 4, and 16 weeks.

The statistical analysis to identify T cell subsets important in transition from psoriasis to psoriatic arthritis was performed using the software R version 4.3.3 und GraphPad Prism version 10.0 (GraphPad Software, Inc). These analyses included Partial Least Squares–Discriminant Analysis (PLS-DA), frequency comparison of T cell subsets using Kruskal–Wallis test, and Random Forest analyses. The dataset for Random Forest analyses was prepared by imputing missing values with k-nearest neighbors.

To confirm the importance of identified T cell subsets independent of sex, age, and body mass index (BMI), we performed a machine-learning (ML)-based flow cytometry data processing in R statistical environment (version 4.2). All events from a subcohort matched by age, sex, and BMI were combined into one flow set, gated on live $CD3^+$ lymphocytes. After preprocessing of the data by compensating for spectral overlap, gating for singlets and live cells and applying quality control, the data were transformed and scaled. Thereafter, we performed Gaussian normalization to mitigate batch effects. We then employed the self-organizing map algorithm FlowSOM to perform unsupervised clustering of cells based on the expression states of selected markers. Uniform manifold approximation and projection (UMAP) plots were generated using type markers, with a limit of 20,000 cells per sample. We conducted a differential abundance analysis to compare cluster numbers.

Ethical approval was obtained from local ethics committee (AZ20-170A). The datasets generated and analyzed during the current study are available from the corresponding author on reasonable request. Requests for data access should be directed to Dr Graßhoff at hanna.grasshoff@uksh.de. Patients or the public were not involved in the design, conduct, reporting, or dissemination plans of our research.

RESULTS

Patient demographics and disease subgroups. In this study, 116 consecutive patients were included and observed at the Institute and Comprehensive Center for Inflammation Medicine and Department of Rheumatology and Clinical Immunology at the University of Lübeck. The cohort was composed of patients with psoriasis (n = 46, 39.7%), with subclinical psoriatic arthritis (n = 8, 6.9%), and with psoriatic arthritis (n = 62, 53.4%). Patient demographics and clinical data are summarized in Table 1 and Supplementary Table 2. Patients with psoriatic arthritis tended to be older than patients with psoriasis and subclinical psoriatic arthritis. Sex ratio and BMI were similar among disease groups. Patients with psoriasis showed significantly higher PASI and body surface area scores, indicating more severe skin involvement compared with subclinical psoriatic arthritis and definitive psoriatic arthritis. Moreover, DLQI scoring and mean itch (VAS) were significantly higher in patients with psoriasis, indicating a higher skin disease burden. By contrast, nail psoriasis was more frequent in patients with subclinical psoriatic arthritis and psoriatic arthritis. Pain assessed via VAS and scoring in HAQ—both assessing subjective disease burden mainly caused by musculoskeletal manifestations—was similar in patients with subclinical psoriatic arthritis and those with definitive psoriatic arthritis. In two patients in the subclinical psoriatic arthritis group, a swollen joint was detected caused by trauma and after surgery. Yet, none of the patients in the subclinical psoriatic arthritis group had clinically apparent arthritis, enthesitis, axial disease manifestation, dactylitis, or uveitis. Patients were mainly treated with conventional synthetic disease-modifying antirheumatic drugs (csDMARDs) and biologics.

Patients with psoriasis, subclinical psoriatic arthritis, and psoriatic arthritis display overlapping T cell subset endotypes with remarkable divergence in subclinical psoriatic arthritis. Multicolor flow cytometry was performed in all 116 patients. Total number of lymphocytes as well as frequencies of $CD3^+$ lymphocytes were compared using Kruskal–Wallis test, indicating no statistically significant difference regarding absolute number of lymphocytes among the three patient subgroups [H (2) = 2.05, $P = 0.358$]. There were also no differences in $CD3^+$ T cell frequencies among patient subgroups [H (2) = 4.09, $P = 0.129$, Kruskal–Wallis test].

Figure 1 shows outcomes of the PLS-DA analyzing the T cell composition suggesting the presence of overlapping peripheral blood T cell endotypes among the three patient subgroups. Nevertheless, patients with subclinical psoriatic arthritis displayed the most remarkable divergence from the other two patient subgroups regarding endotypes. Spearman's correlations among T cell subsets were calculated for each group separately and the interrelationships among the T cell subsets within each subgroup illustrated by correlation networks. Patients with subclinical psoriatic arthritis revealed a more intricate and interconnected T cell subset network compared to patients with psoriasis and psoriatic arthritis (Supplementary Figure 5).

Frequencies of Th17, Tc17, and $CD4^+$ effector memory T cells differ among patients with psoriasis, subclinical psoriatic arthritis, and psoriatic arthritis. To investigate the distribution of distinct T cell subsets, a

Table 1. Clinic and demographic characterization of patients with psoriasis, subclinical psoriatic arthritis, and psoriatic arthritis included in the immunophenotyping cohort*

Parameters	Psoriasis (n = 46, 39.7%)	Subclinical psoriatic arthritis (n = 8, 6.9%)	Psoriatic arthritis (n = 62, 53.4%)	Statistical analysis
Demographics and Clinical Data	M (±SD)	M (±SD)	M (±SD)	Kruskal-Wallis statistic: H(2) (P value)
Age, y	43.5 (±14.3)	42.0 (±14.1)	47.9 (±13.3)	4.08 (0.130)
BMI, kg/m^2	32.1 (±7.8)	27.9 (±5.1)	30.5 (±5.5)	3.09 (0.213)
PASI, 0–72	15.3 (±8.9)	2.1 (±3.7)	5.7 (±6.2)	**45.0 (<0.001)**
BSA, %	21.4 (±16.6)	2.5 (±4.0)	6.7 (±7.7)	**43.1 (<0.001)**
DLQI, 0–30	12.8 (±8.4)	5.3 (±6.6)	8.5 (±7.1)	**10.3 (0.006)**
VAS itch mean, 0–10	5.8 (±3.0)	3.8 (±3.7)	4.3 (±3.4)	**0.023 (0.023)**
VAS pain mean, 0–10	3.5 (±3.4)	5.3 (±1.4)	5.9 (±2.7)	**0.001 (0.001)**
	n (%)	n (%)	n (%)	Fisher's exact test: P value
Female	15 (32.6)	5 (62.5)	31 (50.0)	0.106
Nail psoriasis	41 (89.1)	3 (37.5)	48 (77.4)	**0.006**
Therapy	M (±SD)	M (±SD)	M (±SD)	X^2 test: X^2 (P value)
Solely topical therapy	19 (41.3)	5 (62.5)	16 (25.8)	
csDMARD	6 (13.0)	1 (12.5)	20 (32.3)	
Fumarates	8 (17.4)	1 (12.5)	2 (3.3)	
Apremilast	2 (4.4)	1 (12.5)	4 (6.5)	
IL-(12)/23 i	3 (6.5)	0 (0.0)	5 (8.1)	
TNF i	3 (6.5)	0 (0.0)	10[a] (16.1[a])	
IL-17 i	5 (10.9)	0 (0.0)	4[a] (6.5[a])	
JAK i	0 (0.0)	0 (0.0)	1 (1.6)	20.9 (0.104)

* BMI, body mass index; BSA, body surface area; csDMARD, conventional synthetic disease-modifying antirheumatic drug; DLQI, Dermatology Life Quality Index; i, inhibitor; IL, interleukin; PASI, Psoriasis Area Severity Index; TNF, tumor necrosis factor; VAS, visual analog scale.
[a] One of the patients received biologics and methotrexate.

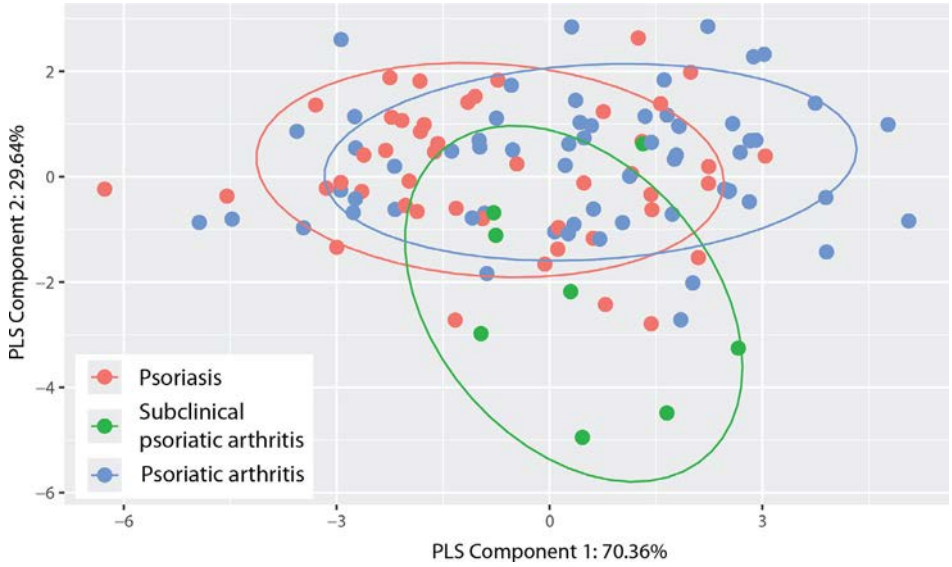

Figure 1. Patients with psoriasis, subclinical psoriatic arthritis, and psoriatic arthritis display overlapping T cell subset endotypes with remarkable divergence in subclinical psoriatic arthritis. Partial Least Squares (PLS)-Discriminant Analysis showed circulating T cell endotypes shared among patients with psoriasis (red), patients with subclinical psoriatic arthritis (green), and patients with psoriatic arthritis (blue). Patients with subclinical psoriatic arthritis displayed the most remarkable divergence from the other two patient subgroups regarding endotypes. The results are illustrated as a PLS score plot with confidence ellipses set at 80%.

comparison of the frequencies of different circulating T cell subsets was performed using Student's *t*-test. The comparison between patients with psoriasis and subclinical psoriatic arthritis revealed a significant difference with a fold change >±1.5 for $CD8^+$ effector memory T cells re-expressing CD45RA (TEMRAs), $CD4^+$ central memory T (TCM) cells, $CD4^+$ effector memory T (TEM) cells, Tc17 cells, $CD103^+$ cutaneous Ly $(CLA)^-$ cells within the $CD4^+$ T cell population, $CD8^+$ TEM cells, $CD4^+$ TEMRAs, and Tc9 cells (Figure 2A). A corresponding comparison of frequencies of T cell subsets between patients with subclinical psoriatic arthritis and psoriatic arthritis showed a significant difference with a fold change >±1.5 for $CD4^+$ TEMRAs, Tc17 cells, $CD103^+CLA^-$ cells within the $CD4^+$ T cell population, $CD4^+$ TEM cells, $CD4^+$ TCM cells, Th17 cells, and Tc22 cells (Figure 2B).

Following identification of differences in T cell subset composition among the patient subgroups, T cell subset frequencies were subsequently compared using Kruskal–Wallis test, followed by Dunn's post hoc analysis to assess pairwise differences. The statistical results, illustrated in Figure 2C, unveiled significant differences in T cell subset frequencies among the patient subgroups. Notably, Th17 cells [H (2) = 8.47, P = 0.0145] were decreased in subclinical psoriatic arthritis compared to psoriatic arthritis. By contrast, Tc17 cells [H (2) = 8.43, P = 0.0148] were increased in subclinical psoriatic arthritis compared with psoriasis and psoriatic arthritis, as were $CD4^+$ TEM cells [H (2) = 10.09, P = 0.0064].

To assess therapeutic effects on T cell subset frequencies, 114 patients underwent immunophenotyping at therapy initiation and after 2, 4, and 16 weeks (Supplementary Figure 6). Significant differences in T cell subset frequencies were observed depending on the therapy and timepoint. Within patients treated with targeted synthetic DMARDs, Th17 cells differed significantly between therapy initiation (week 0) and week 16 as well as weeks 2 and 16, but not between weeks 4 and 16. In patients treated with csDMARDs, Th22 cells differed between therapy initiation and week 16. For IL-(12)/23 inhibitors, significant increases were observed in Th22 and T helper granulocyte–macrophage colony-stimulating factor CD4 T cells, respectively. Additionally, a significant increase in Th22 cell frequencies occurred under IL-17(R) inhibitors between therapy initiation and week 16. However, no consistent shifts across therapies or persistent changes over time were identified.

Distinct T cell phenotype and higher frequencies of Tc17 cells in patients with enthesitis. Having found differences in T cell subset frequencies among patients with psoriasis, subclinical psoriatic arthritis, and definitive psoriatic arthritis, we

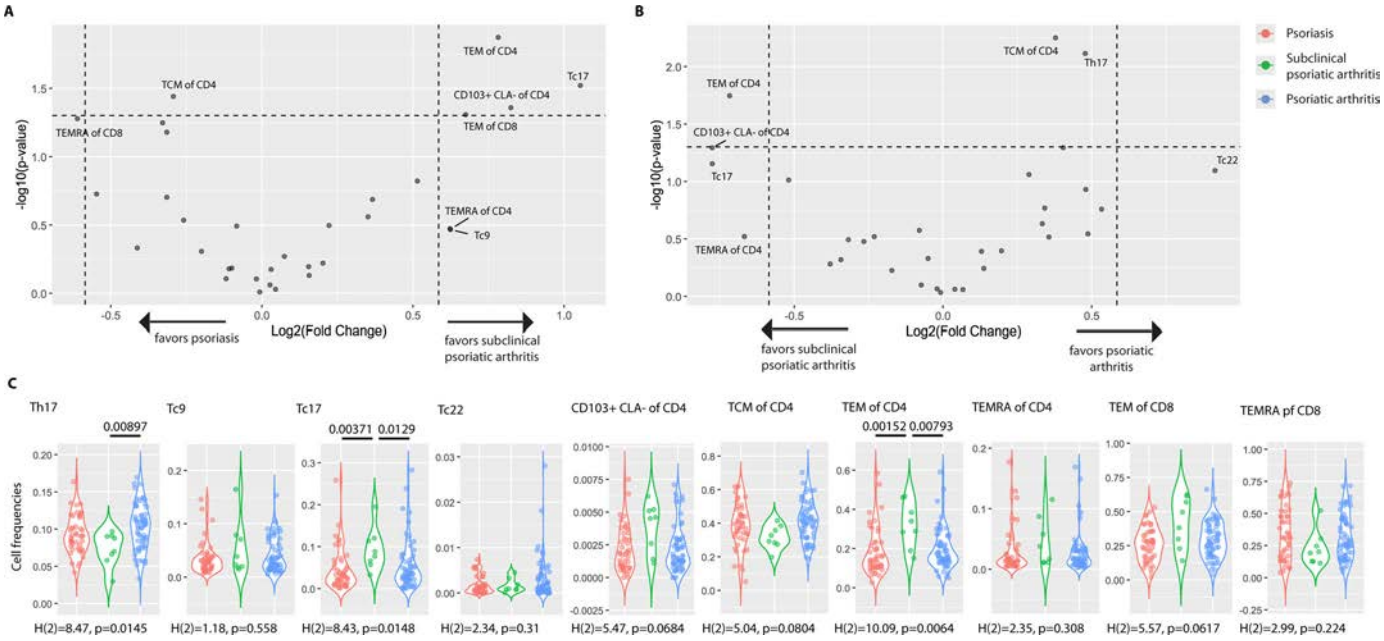

Figure 2. Frequencies of Th17, Tc17, and $CD4^+$ TEM cells differ among patients with psoriasis, subclinical psoriatic arthritis, and psoriatic arthritis. Volcano plots are a visual representation of the results of the Student's *t*-test for different peripheral blood T cell subset frequencies in patients with (A) psoriasis and subclinical psoriatic arthritis and (B) subclinical psoriatic arthritis and psoriatic arthritis. The P values are represented on the y-axis as –log10(P), with a P value of 0.05 indicated by the dotted line. The fold change is illustrated as log2(fold change), and the arrows on the x-axis indicate the direction of change. The dotted line represents a fold change >1.5. T cell subsets with a fold change of 1.5 were labeled. (C) Violin plots representing the distribution of T cell frequencies for the T cell subsets with a fold change >1.5 in patients with psoriasis, subclinical psoriatic arthritis, and psoriatic arthritis. The results of a Kruskal–Wallis analysis and subsequent Dunn's post hoc test are depicted in the respective plots. Significant P values in Dunn's post hoc test are indicated. CLA, cutaneous Ly; TCM, central memory T; TEM, effector memory T; TEMRA; TEM cells re-expressing CD45RA.

reasoned that entheseal inflammation could also be driven by changes in T cell subset composition during transition. Therefore, T cell phenotyping was performed in patients with subclinical and definitive psoriatic arthritis. Within the subgroup of patients with subclinical psoriatic arthritis, four of eight patients (50.00%) showed imaging-confirmed entheseal alterations without clinical signs of enthesitis. Among patients with psoriatic arthritis, 41 of 62 patients (66.13%) were diagnosed with enthesitis. In contrast, none of the patients with psoriasis showed clinical signs of enthesitis. Thus, the subgroup with psoriasis was excluded from analysis. The peripheral blood T cell phenotype and frequencies of individual T cell subsets were assessed and compared between patients with and without enthesitis.

PLS-DA differentiated patient subgroups based on their blood T cell phenotype, achieving an accuracy of 0.7859, as shown in Figure 3A. Receiver operating characteristic (ROC) analysis for predicting enthesitis using T cell subsets yielded an area under the curve (AUC) of 0.8338. The variable importance (VIP) score identified key discriminative T cell subsets including $CD103^{-}CLA^{-}$ cells within the $CD8^{+}$ T cell population, Tc17 cells, and $CD8^{-}CD4^{-}$ double-negative (DN) T cells. Further analysis using the Mann–Whitney *U* test compared the frequencies of these top three T cell subsets between patients with and without enthesitis. A higher frequency of Tc17 cells was found in patients with enthesitis compared to patients without enthesitis (P = 0.0374; Figure 3B). By contrast, no significant differences were found for the frequencies of $CD103^{-}CLA^{-}$ cells within the $CD8^{+}$ T cell population and $CD8^{-}CD4^{-}$ DN T cells between patients with and without enthesitis.

$CCR5^{+}$, $CCR6^{+}$ (Tc17) cells as key cells differentiate among patients with psoriasis, subclinical psoriatic arthritis, and psoriatic arthritis. To confirm our findings suggesting a major role for Tc17 cells in driving transition from psoriasis to psoriatic arthritis, we employed nonsubjective ML-assisted unsupervised clustering as a flow cytometry data readout strategy. The optimal clustering depth identified a total of 15 metaclusters from two panels (Supplementary Figure 7). UMAP parameters were adjusted to optimally display metaclusters, and annotations were performed as described in the Materials and Methods section. The resultant lymphocyte maps of both datasets employed in the study are shown in Supplementary Figure 8A. Further, Supplementary Figure 8B shows the heatmaps of lymphocyte marker expression of all clusters in both datasets as well as their abundance. The estimated spectrum of ML-detectable cell subsets is summarized in Supplementary Table 3. Dataset 1 included $CD4^{+}$ naïve T cells (TN), TCM $CD4^{+}$, TEM $CD4^{+}$, TN $CD8^{+}$, TEM $CD8^{+}$, and DN cells. In panel 2, DN, Tc17, Tc1, Tc2, Th17, and Th2 cells were detected. Subsequently, the abundance of metaclusters in the three groups was assessed. In Supplementary Figure 8C, plots display abundance of metaclusters split by groups. We employed differential abundance analysis of metaclusters as described in the Materials and Methods. Figure 4A shows that $CCR5^{+}$, $CCR6^{+}$ (Tc17) cells were significantly increased in subclinical psoriatic arthritis compared to the two other subgroups (at false discovery rate > 0.05). This was not the case for all other metaclusters. Figure 4B displays UMAP plots split by groups with the significant population of $CCR5^{+}$, $CCR6^{+}$ (Tc17) cells highlighted. Backgating of metacluster $CCR5^{+}$, $CCR6^{+}$ (Tc17) confirmed that patients with subclinical psoriatic arthritis showed increased frequencies of Tc17 cells compared to patients with psoriasis at risk of transition and psoriatic arthritis (Figure 4C).

Random Forest analysis yields high accuracy and robustness in classification of patients. To further assess T cell subset–based stratification of psoriatic disease, we performed Random Forest analyses aimed at distinguishing between psoriasis and subclinical psoriatic arthritis, as well as between subclinical and established psoriatic arthritis. The models incorporated T cell subset frequencies, revealing high accuracy and robustness in classification performance. For comparison of psoriasis versus subclinical psoriatic arthritis, the best-performing model (mtry 6, ntree 200, nodesize 4) achieved an accuracy of 1.000 in the training data, with a balanced accuracy of 69.44% on the test set. VIP analysis indicated that Th9, Tc17, and TEMRAs within the $CD4^{+}$ T cell population were critical for patient classification, underscoring their role during transition. In distinguishing subclinical psoriatic arthritis from established psoriatic arthritis, the optimal model (mtry 7, ntree 40, nodesize 3) also reached 100% accuracy in the training set and 81.48% on the test data. Here, $CCR2^{+}$ $CD8^{+}$ T cells, TEMRAs within the $CD4^{+}$ T cell population, and $CD4^{+}CD8^{+}$ double-positive $CD3^{+}$ T cells emerged as top contributors, reflecting progressive immune activation and tissue involvement. Figure 5A and B presents error rate and VIP plots, revealing T cell subsets driving the classification.

Figure 5C illustrates the ROC analysis for the test dataset based on both Random Forest analyses. For the classification of patients into psoriasis or subclinical psoriatic arthritis, the AUC was 0.79. For distinguishing between patients with subclinical psoriatic arthritis and psoriatic arthritis, the AUC was 0.59 in the test dataset. These findings suggest an adequate discriminative ability for identifying patients with subclinical psoriatic arthritis within the group of patients with psoriasis, at the same time highlighting the challenge in differentiating between patients with subclinical and definitive psoriatic arthritis.

DISCUSSION

Strong MHC class I association, increased frequencies of circulating and tissue-infiltrating cytokine-producing T cell subsets including Th17 cells, and the efficacy of biologic therapies targeting TNFα and the IL-23/IL-17 axis suggest a role of T cells as key drivers of immunopathology in psoriasis and psoriatic arthritis.[8–16,29,30] However, knowledge is lacking with respect to changes of the T cell

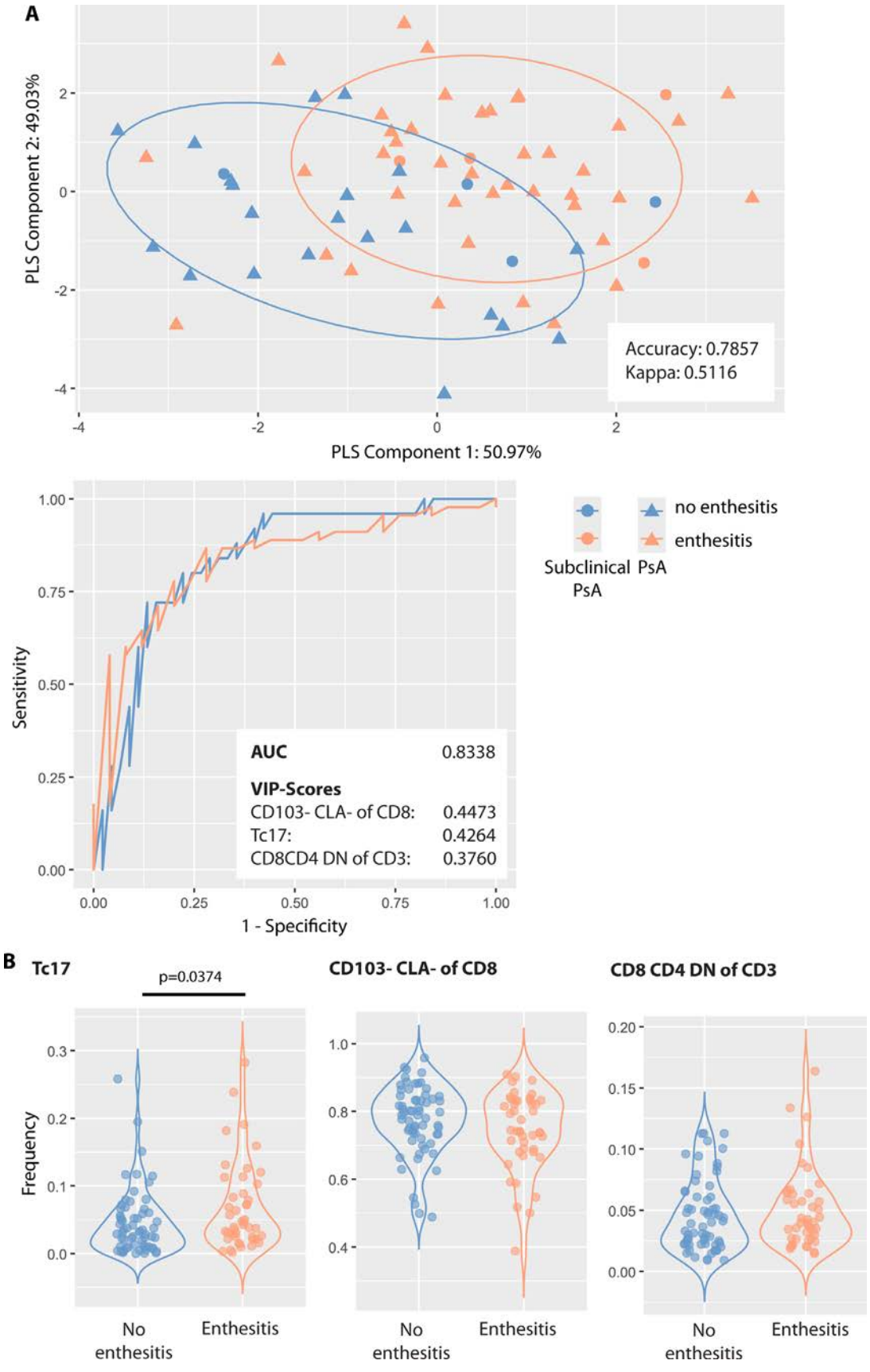

Figure 3. Legend on next page.

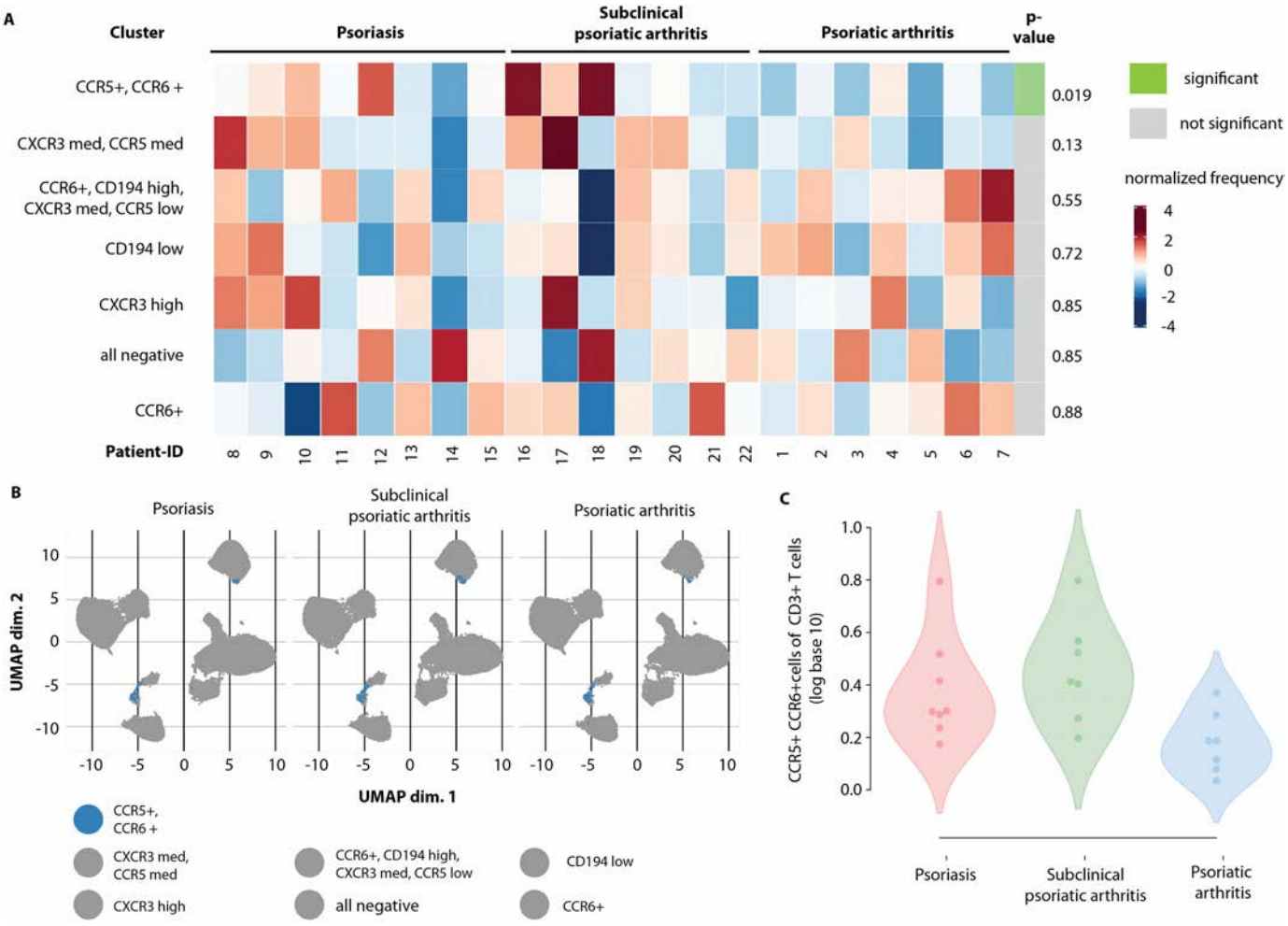

Figure 4. Machine-learning–based analysis reveals CCR5$^+$, CCR6$^+$ (Tc17) cells as key to differentiate among patients with psoriasis, subclinical psoriatic arthritis, and psoriatic arthritis. (A) Diffcyt plot illustrating differential abundance of (CCR5$^+$, CCR6$^+$) Tc17 cells in the prodromal psoriatic arthritis group at false discovery rate >0.05. (B) Significantly altered metacluster highlighted in uniform manifold approximation and projection (UMAP) plot split by condition. (C) Application of gating strategy informed by analysis of metacluster CCR5$^+$, CCR6$^+$ (Tc17). The plot shows results of reanalysis of patients using this gating strategy. Significance was assessed using Kruskal–Wallis test. dim., dimension; med, medium.

compartment driving transition from psoriasis to psoriatic arthritis and providing a link between cutaneous and joint inflammation, which affects about 30% of the patients with psoriatic disease.[17,31] Apart from a study by Gao et al[32] reporting a significantly higher Th1-to-Th2 ratio in patients with psoriatic arthritis compared to those without, studies on changes within the peripheral blood T cell compartment potentially driving transition from psoriasis to psoriatic arthritis are lacking. Therefore, we determined changes within the peripheral blood T cell compartment using deep T cell phenotyping in the transition phase in this study.

Consistent with the role of T cells in psoriatic disease,[8–16,29,30] we found overlapping T cell endotypes among patient subgroups

Figure 3. Patients with enthesitis have a distinct T cell phenotype and display higher levels of Tc17 cells. (A) Partial Least Squares (PLS)-Discriminant Analysis distinguished patients with enthesitis based on their peripheral blood T cell phenotype achieving an accuracy of 0.7859. Patients with enthesitis are depicted in orange, whereas those without enthesitis are shown in blue. Further, patients with subclinical psoriatic arthritis (PsA) are indicated by dots, and those with PsA are represented by triangles. The receiver operating characteristic analysis for predicting enthesitis using T cell subsets yielded an area under the curve (AUC) of 0.8338. Key discriminative T cells identified by the variable importance (VIP) score include CD103$^-$cutaneous Ly (CLA)$^-$ cells within the CD8$^+$ T cell population, Tc17 cells, and CD8$^-$CD4$^-$ double-negative (DN) T cells. (B) Violin plots illustrate the distribution of T cell frequencies for the three most influential subsets as identified by the VIP score in both enthesitis and nonenthesitis groups. The Mann–Whitney *U* test disclosed a statistically significant difference for Tc17 frequencies between the two groups ($P = 0.0374$). However, no significant differences were found in frequencies of CD103$^-$CLA$^-$ cells within the CD8$^+$ T cell population and CD8$^-$CD4$^-$ DN T cells.

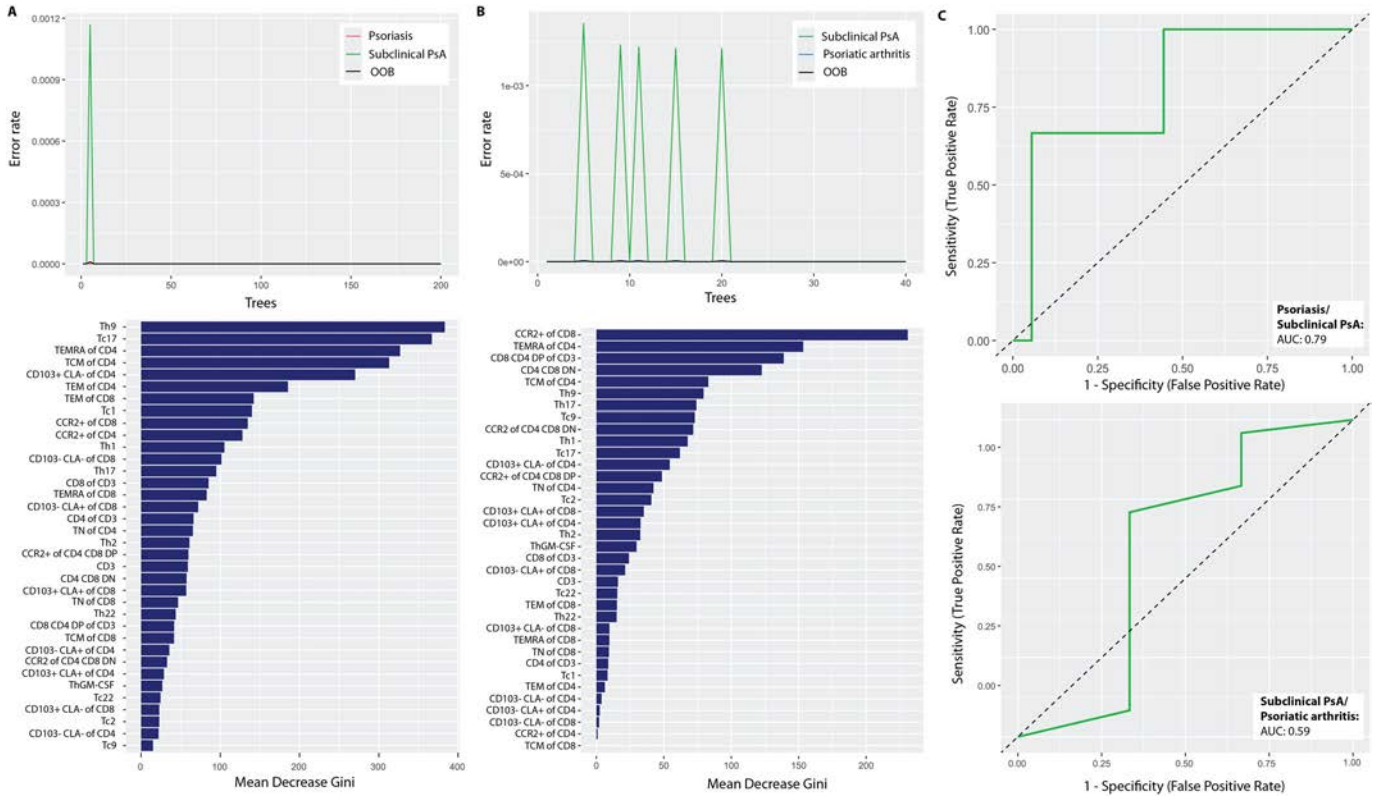

Figure 5. Random Forest analyses reveal a high accuracy and robustness in classification of patients. Results of Random Forest analyses for classification of patients into having (A) psoriasis and subclinical psoriatic arthritis (PsA) or (B) subclinical PsA and PsA are shown as error rate plots visualizing the error rate of the Random Forest model as the number of trees increased with red representing psoriasis, green subclinical PsA, and blue PsA. The out-of-bag error (OOB) is depicted in black. The variable importance plots depict the importance of individual T cell subsets based on the Mean Decrease in Gini, helping to identify which features were most influential in both models. (C) Results of the receiver operating characteristic analysis of the two Random Forest analyses in the test dataset are depicted. Area under the circle (AUC) values are shown in the legends beside the respective model. CLA, cutaneous Ly; DN, double negative; DP, double positive; TCM, central memory T; TEM, effector memory T; TEMRA, TEM cells re-expressing CD45RA; ThGM-CSF, T helper granulocyte–macrophage colony-stimulating factor; TN, naïve T cells.

with psoriasis, subclinical psoriatic arthritis, and psoriatic arthritis, albeit with the transition group (ie, patients with subclinical psoriatic arthritis exhibiting the most notable divergence from the two other subgroups). Earlier studies reported increased frequencies of circulating cytokine-producing Th1, Th17, and Th22 helper cell subsets and enrichment of Th1, Th9, Th17, and Th22 cells and their Tc1, Tc17, and Tc22 cytotoxic T cell counterparts in psoriatic lesions. Moreover, IL-17-producing $CD8^+$ T cells are present in synovial fluid of affected joints in psoriatic arthritis.[10–16,29,30,33,34] Notably, Th17 cells differ from their Tc17 cell counterparts regarding chemokine receptor expression and, thus, responsiveness to chemokine attractants. In contrast to Tc17 cells, Th17 cells express CCR4, a receptor for various chemokines including Cystein-Cystein (CC)-chemokine ligand CCL17 expressed in cutaneous vessels and epidermis.[35] Whereas the above mentioned study by Gao et al included patients with psoriasis and psoriatic arthritis,[32] our study comprised three different subgroups including patients with psoriasis, subclinical psoriatic arthritis according to EULAR definition, and definitive psoriatic arthritis according to CASPAR criteria, thereby representing the whole spectrum ranging from pre- to posttransitional psoriatic disease. In the present study, using deep immunophenotyping, we found significant differences in circulating $CD4^+$ TEM, Th17, and Tc17 cell frequencies among patients with psoriasis, subclinical psoriatic arthritis, and psoriatic arthritis suggestive of IL-17-producing T cells as major drivers of transition from psoriasis to psoriatic arthritis. In particular, a decrease in Tc17 cell frequency in patients with psoriatic arthritis in comparison to patients with subclinical psoriatic arthritis suggests cell migration into joints during transition to arthritis. Notably, migration of TEM cells toward sites of inflammation during active disease resulting in decreased frequency of peripheral blood TEM cells has been shown in various chronic inflammatory diseases.[36,37] $CD4^+$ and $CD8^+$ TEM cells migrate from peripheral blood to peripheral tissues, where they either remain permanently as long-lived tissue-resident memory (TRM) cells or from where they recirculate at a later time point.[38,39] Circulating Tc17 cells infiltrate sites of inflammation and are enriched in psoriatic skin lesions and in synovial fluid in psoriatic arthritis joints.[20,33,40] Moreover, Tc17 cells can convert to long-lived skin-resident TRM cells expressing the

skin-homing sialyl-LewisX glycoprotein CLA and αE integrin-subunit (CD103).[15,16] In contrast to Th17 cells, skin-resident Tc17 cells lack therapeutic responsiveness to narrowband-UV-B and TNFα and IL-23/IL-17 axis–inhibiting biologics. They are retained in resolved lesions, thereby conferring a pathologic site-specific disease memory potentially driving recurrent psoriasis and facilitating transition from psoriasis to psoriatic arthritis.[20] In addition, recirculation of originally skin-resident $CD103^+$ TRM cells may perpetuate inflammation at distant sites.[41] In the present study, however, we found no significant differences in circulating CLA^+CD103^+ TRM cell frequencies among patients with psoriasis, subclinical psoriatic arthritis, and psoriatic arthritis. This does not exclude a role for TRM cell recirculation in transition and disease progression. Similar to the study by Klicznik et al,[41] frequencies of circulating TRM cells were low in all three patient groups of our study and did not allow a conclusion with regard to their potential to reenter the circulation and migrate to other sites.

The potential predominance of IL-17-producing T cells and in particular Tc17 cells in driving transition from psoriasis to psoriatic arthritis is further supported by our finding of higher Tc17 frequencies in those patients displaying imaging-confirmed entheseal alterations without clinical signs of enthesitis in subclinical psoriatic arthritis and enthesitis in definitive psoriatic arthritis. Entheseal inflammation commonly affects patients with subclinical and definitive psoriatic arthritis and is regarded as a prognostic factor of imminent transition from subclinical to clinical manifest psoriatic arthritis.[23] Comparable with other studies,[42,43] one-third of the patients with subclinical psoriatic arthritis and roughly half of the patients with definitive psoriatic arthritis were affected by enthesitis in our study cohort. A spondylarthritis animal model suggests a role of the IL-23/IL-17 axis for synovioentheseal inflammation.[44] Entheseal-resident $CD4^+$ and $CD8^+$ T cells have been reported to produce TNF, but IL-17A production was solely confined to $CD4^+$ T cells.[45] However, Tc17 cells display high plasticity and can switch to Tc1 cells upon recruitment from peripheral blood into tissues.[46]

This study is the first to investigate the immunologic characteristics of patients representing a spectrum of psoriatic disease in transition from psoriasis to psoriatic arthritis in a cross-sectional study. A major strength of the study lies in the precise clinical characterization of the patients.[8,47] Nevertheless, misclassification of individual patients cannot be ruled out because psoriatic disease displays a disease spectrum for which there are currently no clear distinctions between the individual disease phases. Patients presenting with musculoskeletal symptoms and imaging-confirmed enthesopathy lacking overt clinical swelling can be at risk of misclassification because they are in a diagnostic gray area between subclinical and definite psoriatic arthritis. The use of a structured ultrasound scoring system for entheseal assessment could improve diagnosis of enthesitis.[48] There is also a need for further clinical and diagnostic tools as well as biomarkers to accurately stratify patients in the disease stages. Our findings suggest that Th17, Tc17, and $CD4^+$ TEM cells should be investigated for their applicability in diagnostic algorithms for early diagnosis of subclinical psoriatic arthritis. Limitations of our study include its cross-sectional study approach and, thus, lack of individual long-term longitudinal follow-up of changes in T cell composition during transition, potentially biasing the results A further limitation of this study includes the differences in size among the three patient subgroups. However, to compensate for these shortcomings and further validate our findings, we performed ML-assisted readout of flow cytometry data, thereby confirming the main finding of an increased abundance of Tc17 cells in subclinical psoriatic arthritis. As previously shown, ML-assisted flow cytometry readout adds to reproducibility of flow cytometry results.[49] To confirm the results of this study, validation in a larger cohort is required, which may be achieved by a multicenter study design, as well as a longitudinal design, further supported by analysis of tissue samples.

In summary, our findings suggest a role for $CD4^+$ TEM, Th17, and especially Tc17 cells potentially migrating to joints and entheses during transition. Accurately identifying patients at risk of transition from psoriasis to psoriatic arthritis, and understanding T cell compartment changes that drive this process, is crucial to determine the window of opportunity for early and effective therapeutic interventions aimed at preventing disease progression and improving patient outcomes.[8,21] However, lack of therapeutic responsiveness of Tc17 cells[20,33,40] may favor recurrent inflammation and transition from psoriasis to psoriatic arthritis. Potentially, CCR6 expressed by Th17 and Tc17 cells could be an interesting target to reduce migration of these cells to inflamed tissues in psoriasis and psoriatic arthritis. We conclude that future therapeutic approaches to prevent transition from psoriasis to psoriatic arthritis and to provide more effective therapies or even a cure for psoriatic disease must specifically target the IL-23/IL-17 axis and particularly focus on impacting Tc17 cells.

AUTHOR CONTRIBUTIONS

All authors contributed to at least one of the following manuscript preparation roles: conceptualization AND/OR methodology, software, investigation, formal analysis, data curation, visualization, and validation AND drafting or reviewing/editing the final draft. As corresponding author, Dr Graßhoff confirms that all authors have provided the final approval of the version to be published and takes responsibility for the affirmations regarding article submission (eg, not under consideration by another journal), the integrity of the data presented, and the statements regarding compliance with institutional review board/Declaration of Helsinki requirements.

ACKNOWLEDGMENT

We would like to express our deepest gratitude to the patients who participated in this study by sharing time, disease experiences, and medical information. Open Access funding enabled and organized by Projekt DEAL.

REFERENCES

1. Michalek IM, Loring B, John SM. A systematic review of worldwide epidemiology of psoriasis. J Eur Acad Dermatol Venereol 2017;31(2): 205–212.
2. Mease PJ, Gladman DD, Papp KA, et al. Prevalence of rheumatologist-diagnosed psoriatic arthritis in patients with psoriasis in European/North American dermatology clinics. J Am Acad Dermatol 2013;69(5):729–735.
3. Tillett W, Charlton R, Nightingale A, et al. Interval between onset of psoriasis and psoriatic arthritis comparing the UK Clinical Practice Research Datalink with a hospital-based cohort. Rheumatology (Oxford) 2017;56(12):2109–2113.
4. Christophers E, Barker J, Griffiths C, et al. The risk of psoriatic arthritis remains constant following initial diagnosis of psoriasis among patients seen in European dermatology clinics. J Eur Acad Dermatol Venereol 2010;24(5):548–554.
5. Eder L, Haddad A, Rosen CF, et al. The incidence and risk factors for psoriatic arthritis in patients with psoriasis: a prospective cohort study: incidence and risk factors for PsA. Arthritis Rheumatol 2016;68(4): 915–923.
6. Green A, Shaddick G, Charlton R, et al; PROMPT Study Group. Modifiable risk factors and the development of psoriatic arthritis in people with psoriasis. Br J Dermatol 2020;182(3):714–720.
7. Love TJ, Zhu Y, Zhang Y, et al. Obesity and the risk of psoriatic arthritis: a population-based study. Ann Rheum Dis 2012;71(8):1273–1277.
8. Scher JU, Ogdie A, Merola JF, et al. Preventing psoriatic arthritis: focusing on patients with psoriasis at increased risk of transition. Nat Rev Rheumatol 2019;15(3):153–166.
9. Patrick MT, Stuart PE, Raja K, et al. Genetic signature to provide robust risk assessment of psoriatic arthritis development in psoriasis patients. Nat Commun 2018;9(1):4178.
10. Chiricozzi A, Romanelli P, Volpe E, et al. Scanning the immunopathogenesis of psoriasis. Int J Mol Sci 2018;19(1):179.
11. Diani M, Altomare G, Reali E. T helper cell subsets in clinical manifestations of psoriasis. J Immunol Res 2016;2016:7692024.
12. Priyadarssini M, Divya Priya D, Indhumathi S, et al. Immunophenotyping of T cells in the peripheral circulation in psoriasis. Br J Biomed Sci 2016;73(4):174–179.
13. Kagami S, Rizzo HL, Lee JJ, et al. Circulating Th17, Th22, and Th1 cells are increased in psoriasis. J Invest Dermatol 2010;130(5): 1373–1383.
14. Res PCM, Piskin G, De Boer OJ, et al. Overrepresentation of IL-17A and IL-22 producing CD8 T cells in lesional skin suggests their involvement in the pathogenesis of psoriasis. PLoS One 2010;5(11): e14108.
15. Tokura Y, Phadungsaksawasdi P, Kurihara K, et al. Pathophysiology of skin resident memory T cells. Front Immunol 2021;11:618897.
16. Dong C, Lin L, Du J. Characteristics and sources of tissue-resident memory T cells in psoriasis relapse. Curr Res Immunol 2023;4: 100067.
17. Diani M, Altomare G, Reali E. T cell responses in psoriasis and psoriatic arthritis. Autoimmun Rev 2015;14(4):286–292.
18. Boutet MA, Nerviani A, Gallo Afflitto G, et al. Role of the IL-23/IL-17 axis in psoriasis and psoriatic arthritis: the clinical importance of its divergence in skin and joints. Int J Mol Sci 2018;19(2):530.
19. McArdle A, Pennington S, FitzGerald O. Clinical features of psoriatic arthritis: a comprehensive review of unmet clinical needs. Clin Rev Allergy Immunol 2018;55(3):271–294.
20. Cheuk S, Wikén M, Blomqvist L, et al. Epidermal Th22 and Tc17 cells form a localized disease memory in clinically healed psoriasis. J Immunol 2014;192(7):3111–3120.
21. Hackett S, Ogdie A, Coates LC. Psoriatic arthritis: prospects for the future. Ther Adv Musculoskelet Dis 2022;14:1759720X2210867.
22. Zabotti A, De Marco G, Gossec L, et al. EULAR points to consider for the definition of clinical and imaging features suspicious for progression from psoriasis to psoriatic arthritis. Ann Rheum Dis 2023;82(9): 1162–1170.
23. De Marco G, Zabotti A, Baraliakos X, et al. Characterisation of prodromal and very early psoriatic arthritis: a systematic literature review informing a EULAR taskforce. RMD Open 2023;9(2):e003143.
24. Zabotti A, Fagni F, Gossec L, et al. Risk of developing psoriatic arthritis in psoriasis cohorts with arthralgia: exploring the subclinical psoriatic arthritis stage. RMD Open 2024;10(2):e004314.
25. Nast A, Altenburg A, Augustin M, et al. Deutsche S3-leitlinie zur therapie der psoriasis vulgaris, adaptiert von EuroGuiDerm – teil 2: therapiemonitoring, besondere klinische situationen und komorbidität. J Dtsch Dermatol Ges 2021;19(7):1092–1117.
26. Taylor W, Gladman D, Helliwell P, et al; CASPAR Study Group. Classification criteria for psoriatic arthritis: development of new criteria from a large international study. Arthritis Rheum 2006;54(8):2665–2673.
27. Gossec L, Kerschbaumer A, Ferreira RJO, et al. EULAR recommendations for the management of psoriatic arthritis with pharmacological therapies: 2023 update. Ann Rheum Dis 2024;83(6):706–719.
28. Coates LC, Soriano ER, Corp N, et al; GRAPPA Treatment Recommendations domain subcommittees. Group for Research and Assessment of Psoriasis and Psoriatic Arthritis (GRAPPA): updated treatment recommendations for psoriatic arthritis 2021. Nat Rev Rheumatol 2022;18(8):465–479. Erratum in: *Nat Rev Rheumatol* 2022;18:734.
29. Leijten EF, van Kempen TS, Olde Nordkamp MA, et al. Tissue-resident memory CD8+ T cells from skin differentiate psoriatic arthritis from psoriasis. Arthritis Rheumatol 2021;73(7):1220–1232.
30. Povoleri GAM, Durham LE, Gray EH, et al. Psoriatic and rheumatoid arthritis joints differ in the composition of CD8+ tissue-resident memory T cell subsets. Cell Rep 2023;42(5):112514.
31. Mease PJ, Gladman DD, Helliwell P, et al. Comparative performance of psoriatic arthritis screening tools in patients with psoriasis in European/North American dermatology clinics. J Am Acad Dermatol 2014;71(4):649–655.
32. Gao W, Lei Y, Guo X, et al. Comparison and subsets analysis of peripheral CD4+T cells in patients with psoriasis and psoriatic arthritis. Mol Immunol 2023;163:174–180.
33. Menon B, Gullick NJ, Walter GJ, et al. Interleukin-17+CD8+ T cells are enriched in the joints of patients with psoriatic arthritis and correlate with disease activity and joint damage progression. Arthritis Rheumatol 2014;66(5):1272–1281.
34. Steel KJA, Srenathan U, Ridley M, et al. Polyfunctional, proinflammatory, tissue-resident memory phenotype and function of synovial interleukin-17A+ CD8+ T cells in psoriatic arthritis. Arthritis Rheumatol 2020;72(3):435–447.
35. Mousset CM, Hobo W, Woestenenk R, et al. Comprehensive phenotyping of T cells using flow cytometry. Cytometry A 2019;95(6): 647–654.
36. Abdulahad WH, van der Geld YM, Stegeman CA, et al. Persistent expansion of CD4+ effector memory T cells in Wegener's granulomatosis. Kidney Int 2006;70(5):938–947.
37. Dolff S, Abdulahad WH, van Dijk MCRF, et al. Urinary T cells in active lupus nephritis show an effector memory phenotype. Ann Rheum Dis 2010;69(11):2034–2041.
38. Reinhardt RL, Khoruts A, Merica R, et al. Visualizing the generation of memory CD4 T cells in the whole body. Nature 2001;410(6824): 101–105.

39. Masopust D, Vezys V, Marzo AL, et al. Preferential localization of effector memory cells in nonlymphoid tissue. Science 2001; 291(5512):2413–2417.
40. Ortega C, Fernández-A S, Carrillo JM, et al. IL-17-producing CD8+ T lymphocytes from psoriasis skin plaques are cytotoxic effector cells that secrete Th17-related cytokines. J Leuko Biol 2009;86(2): 435–443.
41. Klicznik MM, Morawski PA, Höllbacher B, et al. Human $CD4^{+}CD103^{+}$ cutaneous resident memory T cells are found in the circulation of healthy individuals. Sci Immunol 2019;4(37):eaav8995.
42. Polachek A, Touma Z, Anderson M, et al. Risk of cardiovascular morbidity in patients with psoriatic arthritis: a meta-analysis of observational studies. Arthritis Care Res (Hoboken) 2017;69(1):67–74. Erratum in: Arthritis Care Res (Hoboken) 2019;71:574.
43. Schett G, Lories RJ, D'Agostino MA, et al. Enthesitis: from pathophysiology to treatment. Nat Rev Rheumatol 2017;13(12):731–741.
44. Sherlock JP, Joyce-Shaikh B, Turner SP, et al. IL-23 induces spondyloarthropathy by acting on ROR-γt+ CD3+CD4–CD8– entheseal resident T cells. Nat Med 2012;18(7):1069–1076.
45. Watad A, Rowe H, Russell T, et al. Normal human enthesis harbours conventional CD4+ and CD8+ T cells with regulatory features and inducible IL-17A and TNF expression. Ann Rheum Dis 2020;79(8): 1044–1054.
46. Flores-Santibáñez F, Cuadra B, Fernández D, et al. In vitro-generated Tc17 cells present a memory phenotype and serve as a reservoir of Tc1 cells in vivo. Front Immunol 2018;9:209.
47. Perez-Chada LM, Haberman RH, Chandran V, et al. Consensus terminology for preclinical phases of psoriatic arthritis for use in research studies: results from a Delphi consensus study. Nat Rev Rheumatol 2021;17(4):238–243.
48. Balint PV, Terslev L, Aegerter P, et al; OMERACT Ultrasound Task Force members. Reliability of a consensus-based ultrasound definition and scoring for enthesitis in spondyloarthritis and psoriatic arthritis: an OMERACT US initiative. Ann Rheum Dis 2018;77(12):1730–1735.
49. Kamysheva AL, Fastovets DV, Kruglikov RN, et al. Machine learning (ML)-enabled automation for high-throughput data processing in flow cytometry. Blood 2023;142(Supplement 1):905.

Arthritis & Rheumatology
Vol. 78, No. 2, February 2026, pp 344–356
DOI 10.1002/art.43371

American College of Rheumatology
Empowering Rheumatology Professionals

Reactive Oxygen Species–Induced Modifications of Fibrin Clots as a Link Between Immune Responses and Atherothrombosis in Systemic Lupus Erythematosus

Matteo Becatti,[1] Giacomo Emmi,[2] Alessandra Bettiol,[1] Amanda Mannucci,[1] Flavia Rita Argento,[1] Eleonora Fini,[1] Serena Borghi,[1] Francesca Nencini,[1] Maria Nicastro,[3] Irene Mattioli,[4] Elena Silvestri,[4] Augusto Vaglio,[5] Domenico Prisco,[4] and Claudia Fiorillo[1]

Objective. Cardiovascular events are major determinants of morbidity and mortality in systemic lupus erythematosus (SLE), particularly in patients with renal involvement. Although oxidative stress has been implicated in driving vascular and renal damage in SLE, the specific mechanisms remain unclear. This study investigated the potential role of oxidative stress-induced alterations in fibrinogen structure and function in the pathogenesis of atherothrombosis in SLE.

Methods. In this cross-sectional study, we enrolled 144 adult patients with SLE and 90 matched controls. We measured blood leukocyte reactive oxygen species (ROS) production, systemic redox status, and the structural and functional features of purified fibrinogen. Correlations between these parameters and disease activity were also investigated. In vitro experiments to clarify the causal relationships among ROS levels, protein oxidation, and fibrin abnormalities provided mechanistic insights of the observed alterations.

Results. Patients with SLE showed increased leukocyte ROS production, mainly due to neutrophil NADPH oxidase activation. Interestingly, renal biopsies from patients with SLE with active proliferative lupus nephritis exhibited overexpression of the NADPH oxidase enzyme complex p22phox. This was accompanied by plasma oxidative stress as indicated by elevated plasma lipid peroxidation and reduced antioxidant defenses. Fibrinogen oxidation was associated with structural and functional changes, leading to the formation of denser fibrin networks with lower clot porosity and reduced susceptibility to plasmin-mediated fibrin lysis. Interestingly, these fibrinogen modifications correlated with alterations in redox status and disease activity.

Conclusion. Oxidative stress may drive structural and functional modifications of fibrinogen in SLE, potentially acting as a novel pathogenetic mechanism in atherothrombosis among these patients.

INTRODUCTION

Systemic lupus erythematosus (SLE) is a prototypical autoimmune disease that affects multiple organ systems and often leads to severe complications such as renal failure, neurologic disturbances, cytopenia and a range of systemic symptoms. Compared with the general population, patients with SLE carry a 2- to 10-fold higher risk of cardiovascular events encompassing both arterial and venous complications.[1,2] This heightened risk is attributable not only to traditional cardiovascular risk factors but also to renal disease, which is prevalent in this patient population. Renal impairment in SLE contributes to an increased burden of cardiovascular morbidity, as it is associated with hypertension, dyslipidemia, and systemic inflammation, all of which are critical

[1]Department of Experimental and Clinical Biomedical Sciences "Mario Serio," University of Firenze, Firenze, Italy; [2]Department of Medical, Surgical and Health Sciences, University of Trieste and Clinical Medicine and Rheumatology Unit, Cattinara University Hospital, Trieste, Italy, and Centre for Inflammatory Diseases, Monash University Department of Medicine, Monash Medical Centre, Melbourne, Clayton, Victoria, Australia; [3]Department of Medicine and Surgery, University of Parma and Unit of Occupational Medicine and Industrial Toxicology, University Hospital Parma Medical Center, Parma, Italy; [4]Department of Experimental and Clinical Medicine, Careggi University Hospital, Florence, Italy; [5]Department of Experimental and Clinical Biomedical Sciences "Mario Serio," University of Firenze and Nephrology and Dialysis Unit, Meyer Children's Hospital IRCCS, Firenze, Italy.

Drs Becatti, Emmi, and Bettiol are co-first authors and contributed equally to this work. Drs Prisco and Fiorillo are co-last authors and contributed equally to this work.

Additional supplementary information cited in this article can be found online in the Supporting Information section (https://acrjournals.onlinelibrary.wiley.com/doi/10.1002/art.43371).

Author disclosures are available at https://onlinelibrary.wiley.com/doi/10.1002/art.43371.

Address correspondence via email to Matteo Becatti, PhD, at matteo.becatti@unifi.it.

Submitted for publication April 4, 2025; accepted in revised form August 15, 2025.

contributors to cardiovascular pathology. In addition to renal disease, genetic predisposition,[3] soluble factors (eg, autoantibodies, proinflammatory cytokines) and autoreactive leukocytes[4] contribute to endothelial damage in SLE.

Among nontraditional cardiovascular risk factors, oxidative stress, secondary to increased reactive oxygen species (ROS) production and/or decreased antioxidant defenses, has been suggested as possibly implicated in the pathogenesis of cardiovascular events in SLE[1,2] and positively correlated with SLE clinical activity scores.[5] Accordingly, in patients with SLE, increased amounts of the lipid peroxidation marker malondialdehyde (MDA) were found in plasma[6] and erythrocytes.[7]

Studies from our group recently demonstrated that leukocyte-derived ROS can promote oxidative-mediated alterations in the structure and function of fibrinogen, a key protein bridging inflammation and coagulation, thereby increasing prothrombotic risk in various inflammatory and noninflammatory conditions.[8–13]

In this study, we investigated the primary cellular sources of ROS in a large cohort of patients with SLE and explored the relationship between oxidative stress markers, fibrinogen structural and functional properties, and clinical features. These findings provide a deeper understanding of the pathogenetic mechanisms driving cardiovascular events in this complex disease.

PATIENTS AND METHODS

Population, setting and clinical assessment. The study included 144 adult patients with SLE and 90 controls, comparable in terms of age, sex, and main traditional cardiovascular risk factors (ie, smoking, body mass index [BMI], hypertension, dyslipidemia, diabetes). Patients were recruited between September 2019 and January 2023 at the Lupus Clinic of the Careggi University Hospital, Firenze, Italy. All patients were classified as having SLE according to the 2019 EULAR/American College of Rheumatology Classification Criteria for Systemic Lupus Erythematosus.[14]

Patients with other systemic autoimmune diseases, active infectious, or neoplastic conditions were excluded. Controls were recruited among blood donors. The study protocol was approved by the local Ethics committee (Comitato Etico Regionale per la Sperimentazione Clinica della Regione Toscana, Sezione Area Vasta Centro; approved on November 13, 2018; ref. no. 12804_bio) and written informed consent was obtained from all participants.

At the time of blood sample collection, all patients underwent a review of their medical history, a comprehensive laboratory work-up, and a standardized clinical assessment of potential organ involvement, according to EULAR recommendations.[15] SLE clinical activity at the time of blood sample collection was evaluated using the Systemic Lupus Erythematosus Disease Activity Index (SLEDAI) score, and patients were stratified in three groups: those with a SLEDAI of 0, 1 to 5, and >5.[14] History of cardiovascular events was assessed based on retrospective medical chart review; cardiovascular events were defined based on the same definitions reported in medical records. Also, information on ongoing therapies was retrieved, with reference to the use of moderate/high-dose glucocorticoid treatment (defined as a dose of prednisone or equivalent greater than 7.5 mg/day),[16] immunosuppressants, and hydroxychloroquine. Patients and/or the public were not involved in the design, conduct, reporting, or dissemination plans of this research.

Assessment of systemic redox status and NADPH oxidase activity in peripheral leukocytes. Leukocyte ROS production was measured using H_2DCF-DA (2.5 μM) as previously described.[8] NADPH oxidase activity in leukocyte subsets was assessed by lucigenin-enhanced chemiluminescence and expressed as relative luminescence units/second (RLU/s).[8] In plasma, lipid peroxidation and total antioxidant capacity (TAC) were evaluated by thiobarbituric acid reactive substances (as MDA, nanomoles per milliliter) and oxygen radical absorbance capacity assay (as Trolox equivalents, micromolar), respectively.[8]

Fibrinogen purification, fibrinogen oxidation, structure, and function analysis. Blood samples collected in trisodium citrate or EDTA were used for fibrinogen purification as previously described[8] and determination of its concentration and purity. We observed no differences in fibrinogen concentration and purity between patients and controls.

To evaluate fibrinogen oxidation, dityrosine fluorescence (Excitation: 316 nm; Emission: 367 nm) was assayed and normalized to protein concentration. To assess protein secondary structure, we recorded circular dichroism (CD) spectra of purified fibrinogen (0.5 mg/mL) as previously described.[8] To provide information on three-dimensional (3D) conformational changes of purified fibrinogen, intrinsic fluorescent spectra of the protein were acquired.[8] We finally analyzed fibrin clots by confocal microscopy and by stimulated emission depletion (STED) superresolution, as previously reported.[17]

Fibrinogen functional analysis: thrombin-catalyzed fibrin polymerization and fibrin susceptibility to plasmin-induced lysis. The functional analysis of fibrinogen included assessing the kinetics of thrombin-induced fibrin polymerization and evaluating fibrin's susceptibility to plasmin-mediated lysis. Thrombin-induced fibrin polymerization was initiated and monitored according to previously established methods.[8] Fibrin digestion with plasmin was performed as previously described,[8] and data were expressed as the *ratio* between the densitometric reading of the purified protein at a given digestion time and that of the undigested protein (time 0 of incubation with plasmin).

SLE renal biopsy analysis for NADPH p22phox expression. Kidney biopsies from 10 patients with lupus nephritis were analyzed.[18] Tissue expression of p22phox, a key NADPH oxidase subunit, was evaluated by immunohistochemistry and confocal immunofluorescence. Cell-specific colocalization was assessed using Manders' coefficients.[19] Full experimental details are provided in the Supplementary Materials and Supplementary Table S1.

Investigating oxidative stress-induced thrombus formation: in vitro studies. In another set of experiments, increasing concentrations (0.5–2 mM) of 2,2'–azobis(2–amidinopropane) dihydrochloride (AAPH) were incubated at 37°C for 12 hours with 1 mg of purified human fibrinogen (Sigma) dissolved in 1 mL phosphate buffered saline pH 7.4. To evaluate the potential preventive effect of Trolox on the afore-mentioned AAPH-induced oxidation reaction, 1 mg of purified human fibrinogen (Sigma) dissolved in 1 mL phosphate buffered saline pH 7.4 was incubated with 1 mM AAPH in the presence of 0.1 mM Trolox at 37°C for 12 hours. The obtained samples were used for functional and structural analyses.

Statistical analysis. Continuous variables are presented as mean ± SD or as median and interquartile range (IQR), according to data distribution. Categorical variables are presented as n (%). All experiments were performed in triplicate, and, for each case, the mean of the three experiments ± SD was considered, after having confirmed the low intraexperiment and interexperiment variability and the reproducibility of measures using the analysis of variance (ANOVA) Bonferroni test.

Differences in continuous variables between SLE case and control groups, as well as between patients with SLE with versus those without a history of cardiovascular events, were assessed using the Student *t* or the Mann-Whitney test for two-group comparisons, whereas differences between subgroups of patients with SLE distinguished according to disease activity were assessed using the ANOVA or the Kruskal-Wallis test for comparisons of more than two groups, considering if data distribution respect the normality assumption. Differences in categorical variables were assessed using the Fisher's exact test. Correlations were analyzed using Spearman's test, and ρ correlation coefficient was calculated. For the correlation between continuous and ordinal parameters, Kendall's coefficient of rank correlation was performed, and Kendall's τb was calculated. For all analyses, *P* values <0.05 were considered statistically significant. Statistical analyses were performed using the Graph Pad Prism 5 Software and the software STATA version 14. Data are available upon reasonable request by the corresponding author.

RESULTS

Patient populations and baseline characteristics. The demographic and clinical characteristics of the 144 patients with SLE and 90 controls are reported in Table 1. Most patients were female (126; 87.5%), with a median age at diagnosis of 35.2 years (IQR 26.4–42.8) and a median age at blood sample collection of 42.8 years (IQR 37.0–51.1). The most frequent SLE manifestations included articular (84.7%), cutaneous (57.6%), hematologic (52.8%), and renal involvement (32.6%). Approximately one-third of patients had confirmed antiphospholipid antibodies (aPL) positivity. Of the 47 patients with renal involvement, 40 had a biopsy-proven lupus nephritis and 15 had an associated aPL positivity. The majority of the available kidney biopsies (67%) were categorized as class III to IV (with coexisting class V in 15%) according to the International Society of Nephrology/Renal Pathology Society classification. Regarding traditional cardiovascular risk factors, the median BMI was 24 (IQR 16–42); 41% patients had hypertension, and 28.5% were current or past smokers. Dyslipidemia and diabetes were present in 16% and 6.3% of patients, respectively.

At the time of blood sample collection, most patients were receiving immunosuppressants (alone or in association with prednisone ≤7.5mg/day) (39.6%) or prednisone in monotherapy, at a dosage >7.5mg/day (31.3%). Sixty-six patients were also on hydroxychloroquine (45.8%). Considering SLE disease activity, at the time of blood sample collection, 38 patients (26.4%) were classified as having SLEDAI = 0, 77 (53.5%) as having SLEDAI 1 to 5, and 29 (20.1%) as having SLEDAI >5.

Thirty-three patients (22.9%) had a history of cardiovascular events, including 14 with cases of deep venous thrombosis (DVT; associated with acute lower limb ischemia in two of them), nine cases of stroke or transient ischemic attack, seven of acute myocardial infarction (with subsequent DVT in two of them), one case of pulmonary embolism, one of intracardiac thrombosis, and one of acute lower limb ischemia. Cardiovascular events were significantly more frequent in patients with SLEDAI >5 (51.7%) as compared to those with SLEDAI 1 to 5 (20.8%) or SLEDAI 0 (5.3%) ($P < 0.001$ across the three groups). aPL positivity was found in 21 of the 33 patients with cardiovascular events (63.6%), as compared to 24 of 111 without cardiovascular events (21.6%). aPL positivity was significantly more frequent in patients with SLEDAI >5 (51.7%) as compared to patients with SLEDAI 0 or SLEDAI 1 to 5 (21.1% and 28.6%, respectively, $P = 0.026$). All other demographic and clinical features were comparable between SLE subgroups, stratified according to disease activity (Table 1).

Intracellular ROS assessment and NADPH oxidase activity in peripheral leukocytes. Patients with SLE showed a significant increase in ROS levels in all three leukocyte subpopulations, when compared to controls (values are median [IQR]; for lymphocyte ROS: 871 [719–1,138] vs 689.5 [594–841] relative fluorescence units [RFU] for cases and controls, respectively, $P < 0.001$ [Figure 1A]; for monocyte ROS: 1,709 [1,366–2,186] vs 1,208 [1,066–1,325] RFU, $P < 0.001$ [Figure 1B]; for neutrophil

Table 1. Main demographic and clinical features of the patients in the SLE and control groups included in the study*

	Patients with SLE (n = 144)	Controls (n = 90)	Patients with SLE stratified according to disease activity			*P*-value[a]
			SLEDAI 0 (n = 38)	SLEDAI 1–5 (n = 77)	SLEDAI 6+ (n = 29)	
Demographic data						
Female sex, n (%)	126 (87.5)	79 (87.8)	33 (86.8)	69 (89.6)	24 (82.8)	0.596
Age at diagnosis, median (IQR)	35.2 (26.4–42.8)		32.9 (26.3–42.1)	35.3 (26.0–45.8)	36.9 (28.9–42.9)	0.669
Age at blood sample collection, median (IQR)	42.8 (37.0–51.1)	42.0 (36–52)	44.7 (35.7–54.7)	40.4 (37.0–50.0)	44.2 (38.9–54.5)	0.380
Clinical involvement						
Disease duration, median (IQR), mo	68.9 (9.1–163.0)		100.7 (1.9–190.3)	42.5 (6.0 –155.4)	113.5 (29.0–214.9)	0.194
History of cardiovascular events, n (%)	33 (22.9)		2 (5.3)	16 (20.8)	15 (51.7)	**<0.001**[b]
Articular, n (%)	122 (84.7)		30 (78.9)	68 (88.3)	24 (82.8)	0.400
Cutaneous, n (%)	83 (57.6)		22 (57.9)	42 (54.5)	19 (65.5)	0.594
Hematologic, n (%)	76 (52.8)		19 (50.0)	40 (51.9)	17 (58.6)	0.765
Renal, n (%)	47 (32.6)		11 (29.0)	25 (32.5)	11 (37.9)	0.746
Neuropsychiatric, n (%)	25 (17.4)		6 (15.8)	13 (16.9)	6 (20.7)	0.860
Cardiac, n (%)	9 (6.3)		2 (5.3)	5 (6.5)	2 (6.9)	0.955
Gastrointestinal, n (%)	2 (1.4)		0	1 (1.3)	1 (3.4)	
SLEDAI, median (IQR)	2 (0–4)					
Cardiovascular risk factors						
BMI, median (IQR)	24 (16–42)	24 (16–42)	23 (16–42)	24 (15–42)	24 (16–41)	>0.999
Hypertension, n (%)	59 (41.0)	38 (42.2)	13 (34.2)	35 (45.5)	11 (37.9)	0.480
Smoke, n (%)	41 (28.5)	26 (28.9)	11 (29.0)	22 (28.5)	8 (27.5)	0.992
Dyslipidemia, n (%)	23 (16.0)	14 (15.6)	6 (15.8)	13 (16.9)	4 (13.8)	0.927
Diabetes, n (%)	9 (6.3)	6 (6.7)	2 (5.3)	4 (5.2)	3 (10.3)	0.595
aPL positivity, n (%)	45 (31.3)		8 (21.1)	22 (28.6)	15 (51.7)	**0.026**[a]
Treatments, n (%)						
Prednisone alone (dosage of >7.5mg/d)	45 (31.3)		12 (31.6)	25 (32.5)	8 (27.6)	0.059
Immunosuppressants alone or + prednisone (dosage ≤7.5 mg/d)	57 (39.6)		10 (26.3)	33 (42.9)	14 (48.3)	
Immunosuppressants + prednisone (dosage of >7.5 mg/d)	8 (5.6)		1 (2.6)	7 (9.1)	0 (0)	
Hydroxychloroquine (co)treatment	66 (45.8)		14 (36.8)	36 (46.8)	16 (55.2)	0.317

* aPL, antiphospholipid antibodies; BMI, body mass index; IQR, interquartile range; SLE, systemic lupus erythematosus; SLEDAI, Systemic Lupus Erythematosus Disease Activity Index.
[a] From Kruskal-Wallis or Fischer exact test comparing the three groups of patients with SLE with no, low, and moderate-to-high disease activity.
[b] Statistically significant with $P < 0.05$. Bold values indicate statistically significant differences ($P < 0.05$)

ROS: 2,237 [1961–2,915] vs 1,789 [1,655–1990] RFU, $P < 0.001$ [Figure 1C]).

NADPH oxidase activity resulted significantly increased in neutrophils from patients with SLE compared to those obtained from controls (42,432 ± 18,998 vs 13,234 ± 4,223 RLU/s; $P = 0.001$). Conversely, no significant differences in NADPH oxidase activity were observed in lymphocyte and monocyte from patients with SLE with respect to controls (Supplementary Figure S1).

Lipid peroxidation and total antioxidant capacity estimation. In plasma, we found a significantly increased lipid peroxidation (values are median [IQR]; 1.36 [1.07–1.74] vs 0.39 [0.33–0.45] MDA nmol/mL; $P < 0.0001$) and a reduced total antioxidant capacity (15.71 [13.29–18.45] vs 20.22 [19.23–23.36] Mm Trolox equivalent; $P < 0.0001$) in patients with SLE as compared with controls (Figure 1D and E, respectively).

Fibrinogen oxidation, structure, and function analysis. A significant increase in dityrosine content was evident in fibrinogen from patients with SLE compared to controls (values are median [IQR]; 294 [256–329] vs 163 [121–184] RFU; $P < 0.0001$) (Figure 1F). CD spectroscopy indicated, in fibrinogen purified from controls, a typical α-helix secondary structure with minima at 208 nm and at 222 nm; conversely, a decreased negative peak in the 215- to 225-nm region was observed in SLE fibrinogen, suggesting a reduction in α-helical content (Figure 1G). Intrinsic fluorescence was also significantly reduced in SLE fibrinogen (Figure 1H), indicating altered tertiary structure.[20]

Confocal microscopy analysis revealed marked structural differences between SLE and control fibrin networks, especially in fiber architecture and porosity (Figure 2). In control samples, fibrin gels displayed thick, well-organized fibers forming a loosely arranged meshwork with large, open pores. In contrast, fibrin clots from patients with SLE exhibited a dense, compact network composed of thinner fibers and significantly smaller pores. These structural differences were further highlighted in the pseudocolored images

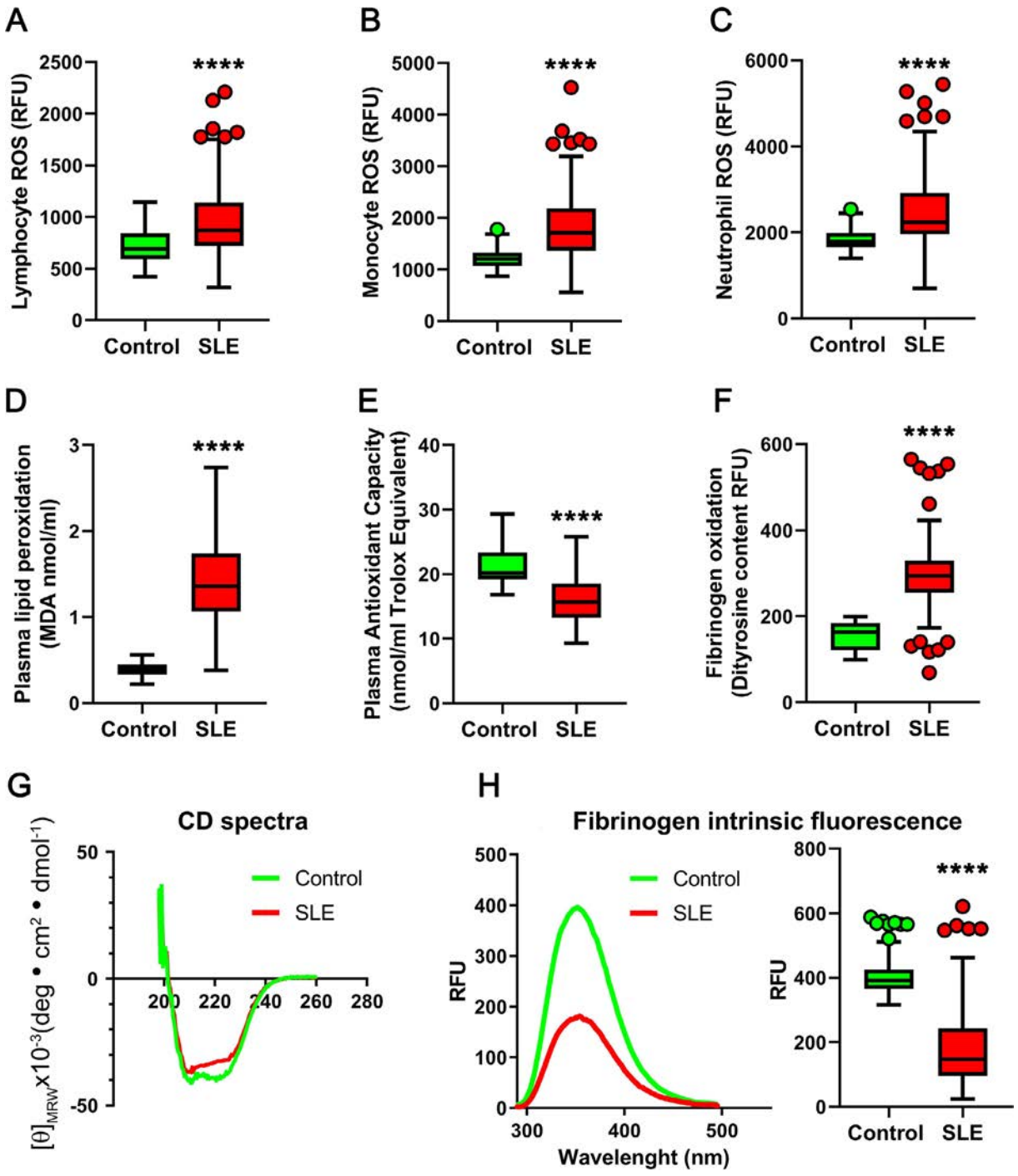

Figure 1. Redox status and fibrinogen structural analyses. (A–C) Lymphocyte, monocyte, and neutrophil ROS production; (D) plasma lipid peroxidation (E) and total antioxidant capacity; (F) dityrosine content; (G) representative CD spectra (H); and intrinsic protein fluorescence spectra of purified fibrinogen from patients with SLE (n = 144) and controls (n = 90). ****Statistical significance is indicated as $P < 0.0001$. CD, circular dichroism; MDA, malondialdehyde; RFU, relative fluorescence units; ROS, reactive oxygen species; SLE, systemic lupus erythematosus.

representing clot porosity, where open spaces (in blue) were prominent in controls but drastically reduced in SLE samples. Surface plot renderings of fluorescence intensity also demonstrated a flatter, more uniform fibrin structure in SLE, consistent with tighter fiber packing and reduced topographical complexity.

To further assess the 3D organization of fibrin gels, we performed 3D confocal volume reconstruction and STED microscopy (Figure 3). STED microscopy is a superresolution imaging technique that surpasses the diffraction limit of conventional confocal microscopy, achieving lateral resolutions down to 20 to 30 nm. Unlike standard confocal microscopy, which is limited to

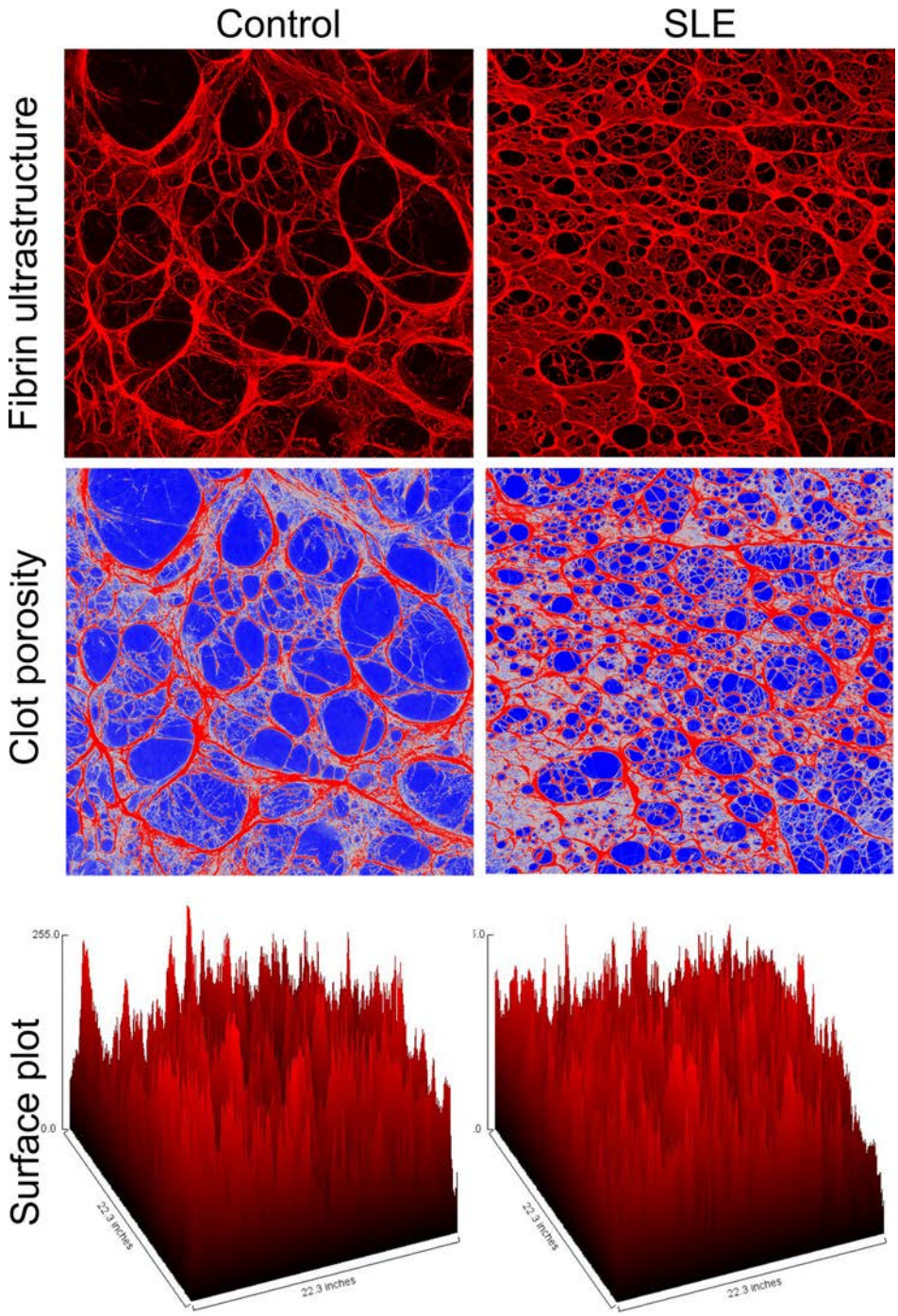

Figure 2. Confocal microscopy analysis of fibrin gel ultrastructure and porosity in fibrinogen samples from controls and patients with SLE. Representative high-magnification confocal images (630×) show distinct structural differences in fibrin networks formed from purified fibrinogen of healthy controls (left column) versus patients with SLE (right column). Top panels (fibrin ultrastructure): In control samples, fibrin fibers appear thick and well-organized and form a loose meshwork with large, well-defined pores. In contrast, SLE-derived fibrin gels are characterized by a denser network composed of thinner, tightly packed fibers with visibly smaller and irregular pores, indicating altered polymerization dynamics. Middle panels (clot porosity): Image processing was applied to highlight pore spaces in blue, overlaid on the red-stained fibrin network. This visualization underscores the stark reduction in clot porosity in SLE samples, reflecting the formation of a more compact and potentially less degradable fibrin matrix. Bottom panels (surface plot): Three-dimensional surface plots generated from fluorescence intensity data of the original confocal images demonstrate topographical differences in clot architecture. The control fibrin gel displays a highly textured surface with pronounced peaks and valleys, corresponding to thick, spaced fibers. In contrast, the SLE fibrin surface is flatter and more uniform, consistent with the presence of tightly packed, fine fibrin strands and reduced spatial variation. SLE, systemic lupus erythematosus. Color figure can be viewed in the online issue, which is available at http://onlinelibrary.wiley.com/doi/10.1002/art.43371/abstract.

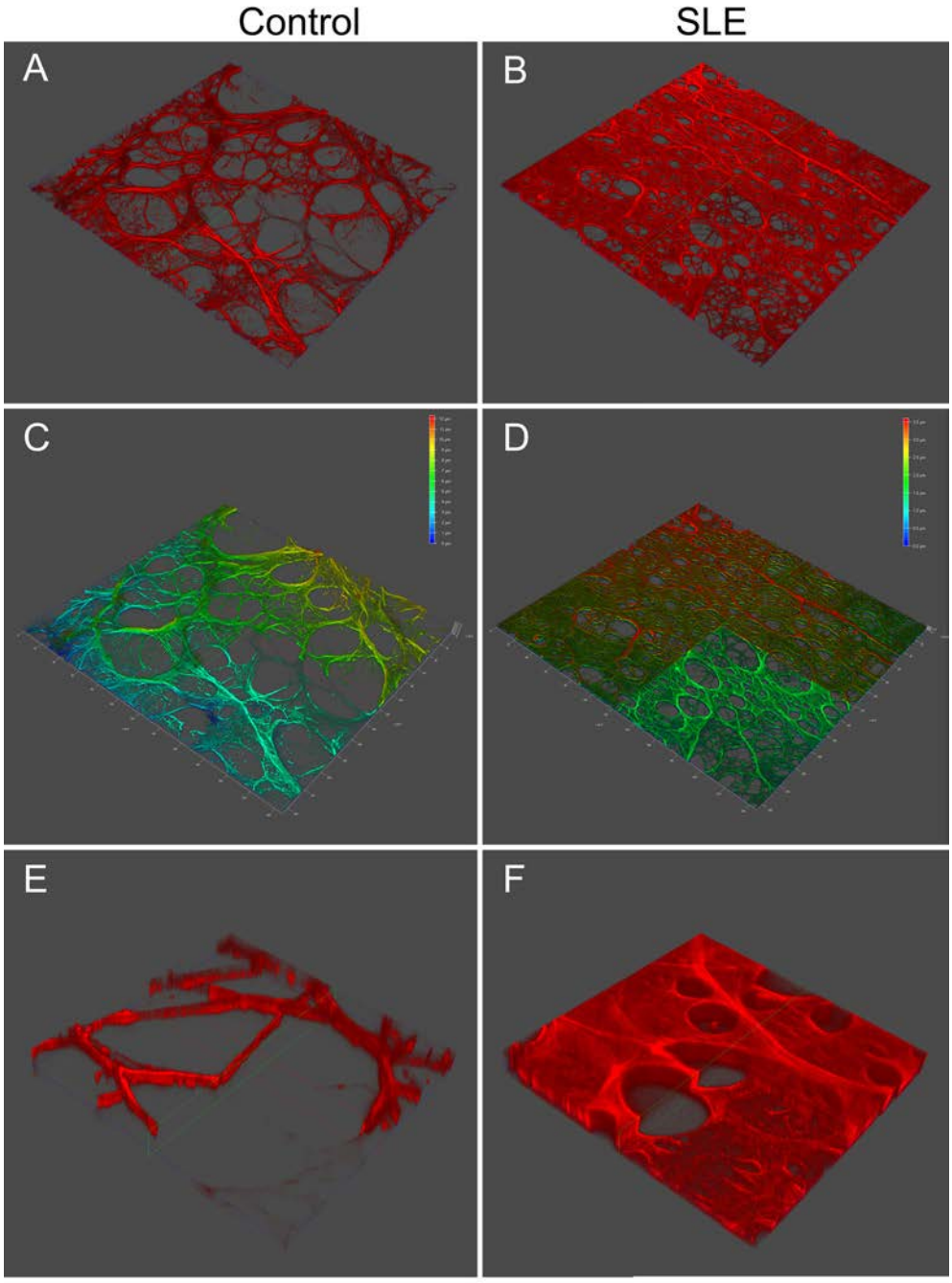

Figure 3. 3D analysis of fibrin gels of fibrinogen purified from patients with SLE and controls. (A, B) 3D confocal microscopy analysis and (C, D) 3D clipping structure of fibrin gels of fibrinogen purified from patients with SLE and controls (630× magnification). SLE fibers were closely packed in the bulk of gel, obscuring the individual fibers and producing thin sheets with small pores. (E, F) 3D STED superresolution microscopy analysis of fibrin gels of fibrinogen purified from patients with SLE and controls (1000× magnification). STED superresolved microscopy revealed a marked increase in fiber density and clot porosity in fibrin from patient with SLE when compared to control. Leica Application Suite X Software analysis demonstrated that fibrin fibers from fibrinogen purified from patients with SLE showed a significant decrease in fiber diameter and clot porosity when compared to controls. 3D, three-dimensional; SLE, systemic lupus erythematosus; STED, stimulated emission depletion. Color figure can be viewed in the online issue, which is available at http://onlinelibrary.wiley.com/doi/10.1002/art.43371/abstract.

a resolution of approximately 200 nm due to the diffraction of light, STED employs a secondary depletion laser that selectively deactivates fluorophores at the periphery of the excitation spot. This process effectively narrows the point of fluorescence emission, allowing for much finer spatial resolution. In our study, STED imaging enabled precise visualization and quantification of individual fibrin fibers, their diameters, and network branching patterns, which would not be resolvable at this level using confocal microscopy alone. This enhanced resolution was critical in revealing the ultrastructural abnormalities here observed, such as thinner, more

tightly packed fibrin fibers in SLE samples compared to controls, which underlie the prothrombotic characteristics of oxidatively modified clots. In Figure 3, panels A and B show 3D volume renderings of control and SLE clots, illustrating the dense and closely packed fiber network in SLE. Clipping analysis with height-based pseudocoloring (panels C and D) confirmed the tighter fibrin mesh in SLE samples, with reduced pore volume and regions displaying a gel-like structure, suggestive of an altered polymerization process and compromised spatial heterogeneity. Whereas Figure 2 provides a high-resolution two-dimensional view of the fibrin ultrastructure, Figure 3 offers complementary and spatially richer 3D data that confirm and extend these findings by revealing differences in internal clot organization, depth, and nanoscale features not visible in traditional confocal projections. Finally, high-resolution 3D STED microscopy (panels E and F) allowed direct visualization of individual fiber diameters and pore morphology. In SLE-derived samples, fibers were notably thinner, and the network appeared uniformly compact with minimal spacing between filaments. These qualitative findings were supported by quantitative analysis, demonstrating a significant reduction in fiber diameter (Figure 4A) and clot porosity (Figure 4B) in SLE.

Fibrinogen functional analysis: thrombin-catalyzed fibrin polymerization and fibrin susceptibility to plasmin-induced lysis. Fibrinogen from patients with SLE showed a reduced ability to polymerize into fibrin as compared with that from controls (Figure 4C). Likewise, we observed significant differences in the main parameters of the fibrin polymerization process (lag phase, maximum velocity [Vmax], and maximum absorbance [Max abs]) between patients with SLE and controls (Figure 4D–F). An impaired fibrin susceptibility to plasmin-induced degradation (Figure 4G), as revealed by the quantification (values are median % [IQR]) of the residual fibrin β chain after six hours of plasmin digestion, indicated the presence of fibrin resistance to plasmin-induced lysis in SLE (densitometric value of 66% [43–80] vs 22% [19–27] at T0 in SLE and control groups, respectively; $P < 0.0001$) (Figure 4H).

Correlation between fibrinogen functional/structural features and redox status. Correlation analyses among redox parameters and fibrinogen structural and functional features are reported in Figure 5. Fibrin resistance to plasmin-induced lysis showed positive correlations with ROS levels in lymphocyte, monocyte, and neutrophil, as well as with fibrinogen oxidation marker (dityrosine content) and functional alterations in fibrin polymerization parameters (lag phase, Vmax, Max Abs). Notably, a strong association with intrinsic fibrinogen fluorescence further indicates that tertiary structural changes play a key role in enhancing clot resistance to degradation. Overall, these findings suggest that oxidative stress promotes the formation of structurally altered, lysis-resistant fibrin clots, contributing to the prothrombotic phenotype observed in SLE. The central role of fibrinogen oxidation in driving structural and functional alterations is underscored by the strong correlations observed between dityrosine content, a marker of fibrinogen oxidation, and both intrinsic fluorescence, which reflects changes in the protein's tertiary structure, and key parameters of fibrin polymerization dynamics (lag phase and Max Abs). These associations highlight that oxidative modifications not only disrupt fibrinogen's conformation but also impair its ability to properly polymerize into fibrin, thereby contributing to the formation of aberrant, prothrombotic clots in SLE (Figure 5).

When stratifying patients with SLE according to disease activity, higher SLEDAI scores were associated with increased levels of intracellular ROS. Conversely, we observed no difference among the three SLE groups in terms of fibrinogen degradation, fibrin polymerization, plasma lipid peroxidation, and plasma total antioxidant capacity (Supplementary Table S2).

These results were confirmed also when assessing the correlation between SLEDAI (as ordinal score) and the considered redox parameters (Supplementary Table S2). To explore the possible impact of treatment on this relationship, we performed stratified analyses according to the treatment category (none or prednisone alone; immunosuppressants with or without prednisone). No statistically significant correlation emerged when assessing the association between SLEDAI and redox parameters according to treatment subgroups, likely due to a low statistical power on smaller sample sizes (data not shown). Also, no statistically significant differences emerged in the levels of ROS and fibrinogen-related parameters in patients with versus without history of cardiovascular events (Supplementary Table S3).

p22phox expression in renal biopsies. p22phox is an essential membrane subunit that plays a central role in NADPH oxidase complex assembly and activation. An intense expression of p22phox was found in all the 10 examined renal biopsies from patients with SLE with active proliferative forms of lupus nephritis, (ie, classified as class III–IV nephritis according to the 2018 International Society of Nephrology/Renal Pathology Society revised classification).[21] Immunohistochemical analysis showed that the tissue expression of p22phox was detectable mainly within the interstitial periglomerular and peritubular inflammatory infiltrates but also in some glomeruli, mainly those showing inflammatory cell infiltration (Supplementary Figure S2).

In agreement with the systemic redox profile observed in patients with SLE, confocal microscopy analysis of renal tissue revealed that $CD15^+$ neutrophils were the predominant cellular source of p22phox expression (Supplementary Figure S3). This NADPH oxidase subunit, critically involved in ROS generation, showed strong colocalization with the neutrophil marker CD15, with a colocalization rate of 76% (Supplementary Table S4).

Investigating oxidative stress-induced thrombus formation: in vitro studies. Quantification of residual β-chain

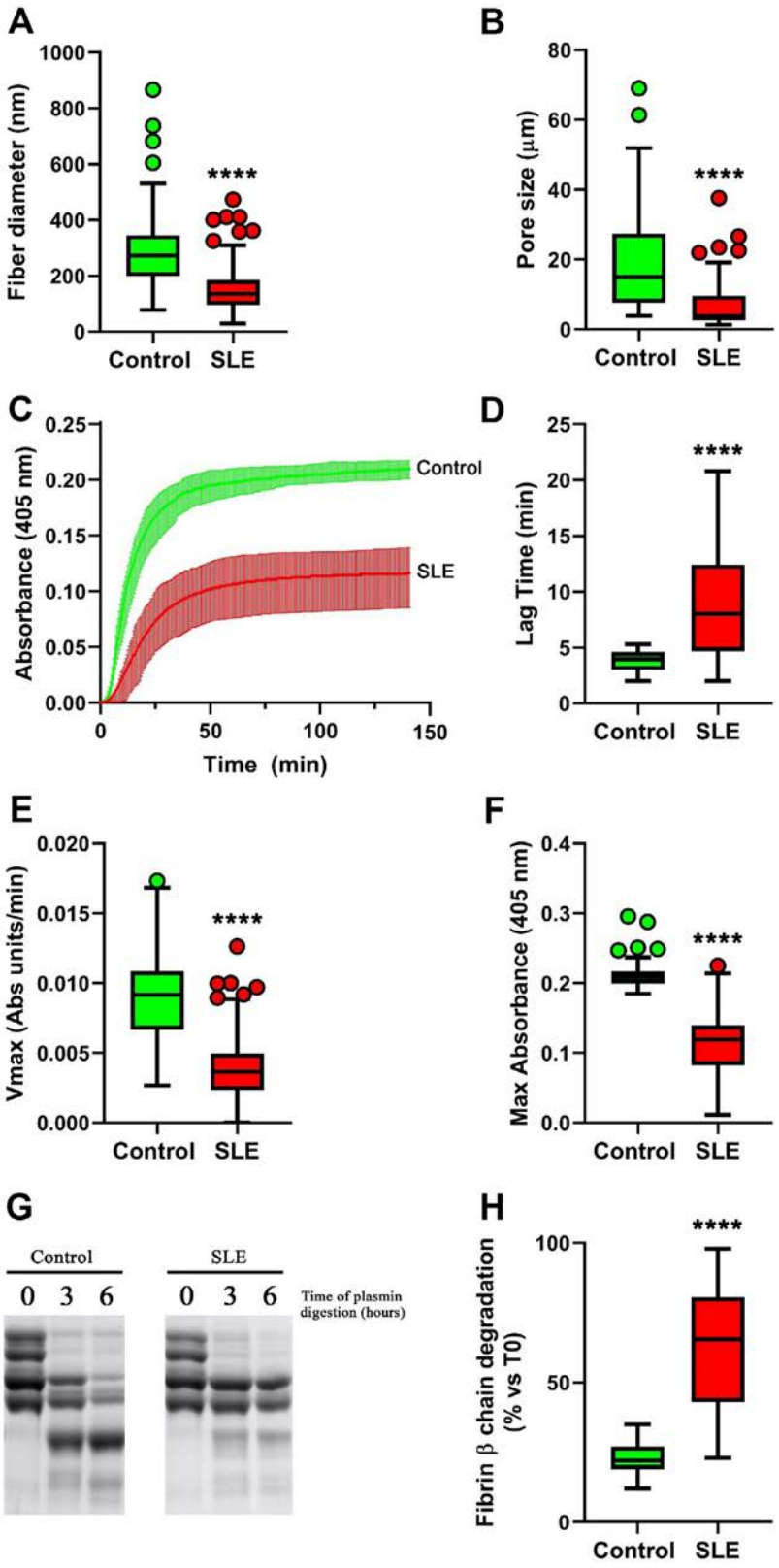

Figure 4. Fibrin structural and functional analyses. (A) Fibrin fiber diameter (B) and pore size of purified fibrinogen from patients with SLE (n = 144) and controls (n = 90). (C) Thrombin-catalyzed fibrin polymerization curves and (D) corresponding lag phase, (E) Vmax, (F) and Max Abs were assessed in the same samples. (G) Representative gel of fibrin lysis after zero to six hours of plasmin incubation (H) and quantification of residual fibrin β chain after six hours of plasmin digestion in both groups. Statistical significance is indicated as ****$P < 0.0001$. Ab, antibody; SLE, systemic lupus erythematosus; Max, maximum; Vmax, maximum velocity. Color figure can be viewed in the online issue, which is available at http://onlinelibrary.wiley.com/doi/10.1002/art.43371/abstract.

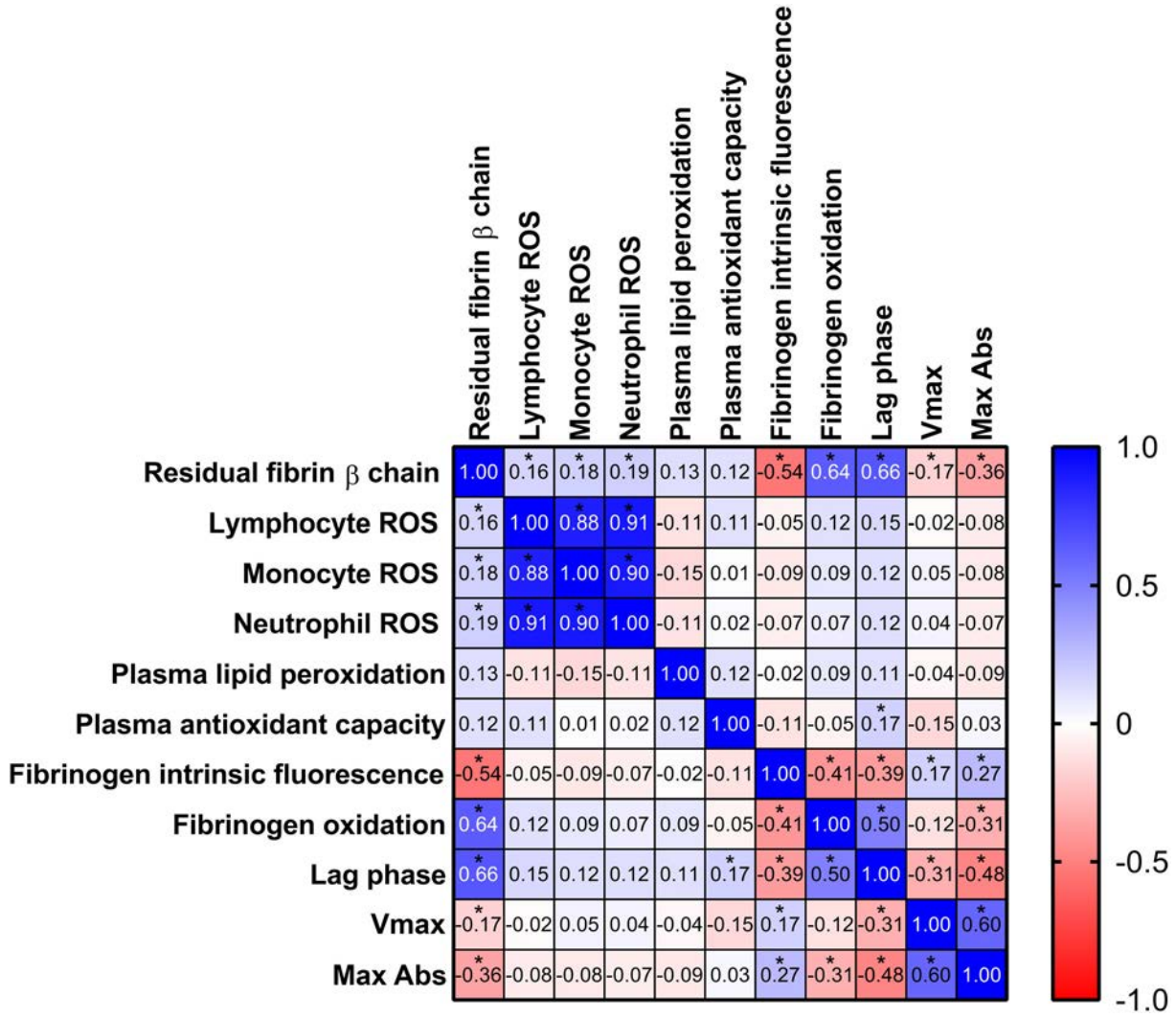

Figure 5. Correlation matrix of the redox status parameters in patients with systemic lupus erythematosus. *Statistically significant for $P < 0.05$. Max Abs, maximum absorbance; ROS, reactive oxygen species; Vmax, maximum velocity. Color figure can be viewed in the online issue, which is available at http://onlinelibrary.wiley.com/doi/10.1002/art.43371/abstract.

intensity after six hours of plasmin digestion of human purified fibrinogen treated with AAPH (a chemical compound with pro-oxidant properties), in the absence or presence of 0.1 mM Trolox, is reported in Supplementary Figure S4A. Fibrin clots incubated with increasing AAPH concentrations showed reduced susceptibility to plasmin-induced lysis at each considered time of plasmin digestion (Supplementary Figure S4B).

As shown in Supplementary Figure S4A, the simultaneous incubation of AAPH and Trolox (a water-soluble derivative of vitamin E with antioxidant properties) was able to prevent the observed changes in fibrin digestion by plasmin. ROS-induced fibrinogen oxidation was assessed by measuring dityrosine content on purified fibrinogen fractions (Supplementary Figure S4C).

In an in vitro fibrinogen polymerization assay, in the presence of increasing AAPH concentrations, lag time increased in a dose-dependent manner (Supplementary Figure S4E), whereas Vmax and Max absorbance progressively and significantly decreased (Supplementary Figure S4F and G). When 0.1 mmol/L Trolox was added to the AAPH incubation reactions and thrombin-catalyzed fibrinogen polymerization was performed, the observed changes were prevented (Supplementary Figure S4D).

When studying fibrinogen structure, in AAPH-treated fibrinogen, a decreased negative peak in the 205- to 225-nm region was observed, suggesting a reduced α-helical content, which was prevented by the simultaneous incubation of AAPH with Trolox (Supplementary Figure S4H). Fibrinogen intrinsic emission fluorescence (tertiary structure) decreased in an oxidation-dependent manner, and Trolox treatment prevented these changes, demonstrating the key role of oxidation in fibrinogen tertiary structure modification (Supplementary Figure S4I).

Confocal microscopy analysis revealed that fibrin gels from oxidized fibrinogen were much denser, with narrow pores and thin fibers when compared to those from controls, which

presented larger pores and thicker fibers (Supplementary Figure S4L). Moreover, AAPH 2-mM–treated fibrinogen showed an unpolymerized fibrin, in accordance with the polymerization assay (Supplementary Figure S4D). Trolox treatment prevented these changes, demonstrating the key role of oxidation in fibrin gel structure modification (Supplementary Figure S4L).

DISCUSSION

Arterial and venous thrombosis are well-established complications of SLE, with a prevalence that can exceed 50% in high-risk patients, representing a major cause of morbidity and mortality, even among young individuals. Beyond traditional cardiovascular risk factors, SLE-specific elements such as disease activity and organ involvement (notably lupus nephritis) have been implicated in the development of atherothrombosis.[22–24]

Although a few studies have reported systemic redox imbalance in active SLE,[25–27] the precise mechanisms linking oxidative stress to vascular and renal damage remain unclear.[28] Increasing evidence supports the role of sustained ROS production in the pathogenesis of autoimmune diseases.[8,29–31] Interestingly, some genetic variants associated with reduced NOX2-derived ROS levels appear to predispose to SLE rather than protect against it.[32]

Here, we provide new insights into the complex role of oxidative stress in SLE, focusing on how ROS-mediated structural and functional alterations of fibrinogen may contribute to thrombotic risk. We confirm a marked redox imbalance in patients with SLE,[33,34] particularly an upregulation of NADPH oxidase activity in circulating neutrophils, a major physiologic sources of ROS. Neutrophils in SLE are known to be hyperactivated, exhibit altered phagocytic function, and spontaneously release neutrophil extracellular traps (NETs), all of which promote a prothrombotic environment.[35]

Oxidation is known to be responsible for protein conformational changes and might lead to (auto)-antigen generation, which in turn drive inflammation, tissue damage, immune profile changes, and autoimmune response.[36,37] Our findings demonstrate that increased oxidative stress is tightly associated with fibrinogen oxidation, resulting in significant structural and functional alterations. These include altered secondary and tertiary structure of SLE fibrinogen, as shown by far-UV CD and intrinsic fluorescence, respectively.

Using STED superresolution microscopy, an advanced technique that enables nanoscale visualization of the fibrin network, we provide the first ultrastructural visualization of SLE fibrin network, revealing thinner fibers, reduced porosity, and a more compact clot architecture, features that are known to confer resistance to plasmin-induced lysis and are frequently observed in other autoimmune and inflammatory conditions.[13,38,39] This can raise the possibility that fibrinogen oxidative modification plays a key role in this process.

We observed that fibrinogen dityrosine content, a marker of fibrinogen oxidation, inversely correlates with thrombin-catalyzed fibrin polymerization rate, suggesting a direct effect of oxidation on fibrin polymerization.[40–43] The presence of oxidation-prone residues such as proline and arginine within the thrombin-cleavage site of fibrinogen may partly explain these alterations observed in patients with SLE.[43] In addition, our results demonstrate that SLE fibrin clots exhibit resistance to plasmin-induced lysis, a feature closely linked to ROS production, fibrinogen oxidation, and structural alterations. Notably, our results indicated that, in patients with SLE, parameters related to fibrinogen structural and functional features were comparable in patients with and without history of cardiovascular events, suggesting the association of SLE per se to an increased thrombotic tendency.

To validate the causal role of oxidative stress in these phenomena, we conducted in vitro experiments exposing purified fibrinogen to the ROS-generating agent AAPH, with or without the antioxidant Trolox. ROS exposure reproduced the structural and functional abnormalities observed in SLE-derived fibrinogen, including impaired polymerization and resistance to plasmin-induced lysis. Co-incubation with the antioxidant Trolox prevented these changes, confirming that ROS are directly responsible for the observed fibrinogen alterations. However, despite this mechanistic clarity, antioxidant therapies have shown some promise in alleviating oxidative stress associated with SLE, but their effectiveness in fully halting or reversing disease progression remains uncertain and is still a matter of ongoing research and debate.[36,44–46]

Importantly, this study uniquely integrates systemic data with kidney biopsies, offering a comprehensive analysis of the potential link among oxidative fibrinogen alternations, SLE renal involvement, and atherothrombotic risk. We confirmed increased p22phox expression (an essential subunit of NADPH oxidase complex) in kidney biopsies from patients with SLE with active lupus nephritis, particularly within $CD15^{+}$ neutrophils infiltrates. These findings expand current understanding on the multifaced role of oxidative stress in SLE, suggesting that neutrophils might represent a key link between fibrinogen modification, lupus nephritis, and atherothrombotic events in SLE.

The association of neutrophil-derived products with lupus nephritis is already described in literature.[47] Namely, decreased NET degradation has been associated with glomerulonephritis, as well as with low complement levels, more severe disease manifestations, and elevated autoantibodies titers in SLE.[48] Also, serum levels of NET remnants (elastase-DNA and HMGB1-DNA complexes) have been associated with worse renal outcomes in patients with active lupus nephritis.[49] Our findings suggest that these neutrophil-derived components may not only drive local tissue damage but also induce systemic prothrombotic changes via fibrinogen alterations. Overall, we could speculate that, in SLE, neutrophils infiltration in the kidney promotes lupus nephritis through the release of

ROS and NETs; concomitantly, neutrophil-derived ROS alter fibrinogen structure and function, contributing to the heightened thrombotic risk.

This study has limitations. First, we did not directly investigate the mechanistic link between fibrinogen alterations and incidence of atherothrombotic events in SLE. Future preclinical studies are needed to further support these findings, providing mechanistic insights through animal models. Additionally, disease activity was assessed at a single timepoint (ie, at time of blood sample collection). Although ROS levels can quickly rise with high disease activity, fibrinogen oxidative modifications may take longer to occur (or to reverse), which makes it more challenging to assess their correlation with point-in-time disease activity scores. Furthermore, a key limitation of our renal analysis is the lack of kidney biopsy samples from healthy individuals, which precluded direct comparison of p22phox expression between SLE-affected and nondiseased renal tissue. Nevertheless, our study offers the first demonstration that ROS-induced fibrinogen modifications profoundly alter clot structure and function, pointing to oxidative stress as a key pathogenetic mechanism in SLE-associated thrombosis and a potential therapeutic target for future interventions.

ACKNOWLEDGMENTS

We sincerely thank Dr Daniele Lana (Department of Health Sciences, Section of Clinical Pharmacology and Oncology, University of Florence, Florence, Italy) for his invaluable contribution to the quantification of colocalization in confocal microscopy images and for his expert support and guidance throughout the imaging analysis process. Open access publishing facilitated by Universita degli Studi di Firenze, as part of the Wiley - CRUI-CARE agreement.

AUTHOR CONTRIBUTIONS

All authors contributed to at least one of the following manuscript preparation roles: conceptualization AND/OR methodology, software, investigation, formal analysis, data curation, visualization, and validation AND drafting or reviewing/editing the final draft. As corresponding author, Dr Becatti confirms that all authors have provided the final approval of the version to be published and takes responsibility for the affirmations regarding article submission (eg, not under consideration by another journal), the integrity of the data presented, and the statements regarding compliance with institutional review board/Declaration of Helsinki requirements.

REFERENCES

1. Papazoglou N, Sfikakis PP, Tektonidou MG. Atherosclerotic plaque progression and incident cardiovascular events in a 10-year prospective study of patients with systemic lupus erythematosus: the impact of persistent cardiovascular risk factor target attainment and sustained DORIS remission. Arthritis Rheumatol 2025;77(6):716–726.
2. Bolla E, Semb AG, Kerola AM, et al; SURF-SLE and APS collaborators. Prevalence and target attainment of traditional cardiovascular risk factors in patients with systemic lupus erythematosus: a cross-sectional study including 3401 individuals from 24 countries. Lancet Rheumatol 2024;6(7):e447–e459.
3. Leonard D, Svenungsson E, Dahlqvist J, et al. Novel gene variants associated with cardiovascular disease in systemic lupus erythematosus and rheumatoid arthritis. Ann Rheum Dis 2018;77(7):1063–1069.
4. Mancardi D, Arrigo E, Cozzi M, et al. Endothelial dysfunction and cardiovascular risk in lupus nephritis: new roles for old players? Eur J Clin Invest 2021;51(2):e13441.
5. Lozovoy MA, Simão AN, Hohmann MS, et al. Inflammatory biomarkers and oxidative stress measurements in patients with systemic lupus erythematosus with or without metabolic syndrome. Lupus 2011;20(13):1356–1364.
6. Bae SC, Kim SJ, Sung MK. Impaired antioxidant status and decreased dietary intake of antioxidants in patients with systemic lupus erythematosus. Rheumatol Int 2002;22(6):238–243.
7. Shah D, Wanchu A, Bhatnagar A. Interaction between oxidative stress and chemokines: possible pathogenic role in systemic lupus erythematosus and rheumatoid arthritis. Immunobiology 2011;216(9):1010–1017.
8. Becatti M, Emmi G, Silvestri E, et al. Neutrophil activation promotes fibrinogen oxidation and thrombus formation in Behçet disease. Circulation 2016;133(3):302–311.
9. Becatti M, Fiorillo C, Gori AM, et al. Platelet and leukocyte ROS production and lipoperoxidation are associated with high platelet reactivity in Non-ST elevation myocardial infarction (NSTEMI) patients on dual antiplatelet treatment. Atherosclerosis 2013;231(2):392–400.
10. Becatti M, Marcucci R, Bruschi G, et al. Oxidative modification of fibrinogen is associated with altered function and structure in the subacute phase of myocardial infarction. Arterioscler Thromb Vasc Biol 2014;34(7):1355–1361.
11. Cellai AP, Lami D, Antonucci E, et al. Fibrinolytic inhibitors and fibrin characteristics determine a hypofibrinolytic state in patients with pulmonary embolism. Thromb Haemost 2013;109(3):565–567.
12. Miniati M, Fiorillo C, Becatti M, et al. Fibrin resistance to lysis in patients with pulmonary hypertension other than thromboembolic. Am J Respir Crit Care Med 2010;181(9):992–996.
13. Becatti M, Emmi G, Bettiol A, et al. Behçet's syndrome as a tool to dissect the mechanisms of thrombo-inflammation: clinical and pathogenetic aspects. Clin Exp Immunol 2019;195(3):322–333.
14. Fanouriakis A, Kostopoulou M, Alunno A, et al. 2019 update of the EULAR recommendations for the management of systemic lupus erythematosus. Ann Rheum Dis 2019;78(6):736–745.
15. Mosca M, Tani C, Aringer M, et al. European League Against Rheumatism recommendations for monitoring patients with systemic lupus erythematosus in clinical practice and in observational studies. Ann Rheum Dis 2010;69(7):1269–1274.
16. Buttgereit F, da Silva JA, Boers M, et al. Standardised nomenclature for glucocorticoid dosages and glucocorticoid treatment regimens: current questions and tentative answers in rheumatology. Ann Rheum Dis 2002;61(8):718–722.
17. Becatti M, Mannucci A, Argento FR, et al. Super-resolution microscopy reveals an altered fibrin network in cirrhosis: the key role of oxidative stress in fibrinogen structural modifications. Antioxidants 2020;9(8):737.
18. Nicastro M, Vescovini R, Maritati F, et al. Fibrocytes in chronic periaortitis: a novel mechanism linking inflammation and fibrosis. Arthritis Rheumatol 2019;71(11):1913–1922.
19. Aditya V, Tambe V, Yue W. Development of a novel automated workflow in Fiji ImageJ for batch analysis of confocal imaging data to quantify protein colocalization using Manders coefficient. Bio Protoc 2025;15(7):e5285.
20. Hellmann N, Schneider D. Hands on: using tryptophan fluorescence spectroscopy to study protein structure. Methods Mol Biol 2019;1958:379–401.

21. Bajema IM, Wilhelmus S, Alpers CE, et al. Revision of the International Society of Nephrology/Renal Pathology Society classification for lupus nephritis: clarification of definitions, and modified National Institutes of Health activity and chronicity indices. Kidney Int 2018;93(4): 789–796.
22. Calvo-Alén J, Toloza SM, Fernández M, et al; LUMINA Study Group. Systemic lupus erythematosus in a multiethnic US cohort (LUMINA). XXV. Smoking, older age, disease activity, lupus anticoagulant, and glucocorticoid dose as risk factors for the occurrence of venous thrombosis in lupus patients. Arthritis Rheum 2005;52(7):2060–2068.
23. Tektonidou MG, Laskari K, Panagiotakos DB, et al. Risk factors for thrombosis and primary thrombosis prevention in patients with systemic lupus erythematosus with or without antiphospholipid antibodies. Arthritis Rheum 2009;61(1):29–36.
24. Watanabe T, Oku K, Amengual O, et al. Effects of statins on thrombosis development in patients with systemic lupus erythematosus and antiphospholipid antibodies. Lupus 2018;27(2):225–234.
25. Kesarwani P, Murali AK, Al-Khami AA, et al. Redox regulation of T-cell function: from molecular mechanisms to significance in human health and disease. Antioxid Redox Signal 2013;18(12):1497–1534.
26. Tse HM, Milton MJ, Schreiner S, et al. Disruption of innate-mediated proinflammatory cytokine and reactive oxygen species third signal leads to antigen-specific hyporesponsiveness. J Immunol 2007; 178(2):908–917.
27. Park JK, Kim JY, Moon JY, et al. Altered lipoproteins in patients with systemic lupus erythematosus are associated with augmented oxidative stress: a potential role in atherosclerosis. Arthritis Res Ther 2016; 18(1):306.
28. Frieri M, Stampfl H. Systemic lupus erythematosus and atherosclerosis: review of the literature. Autoimmun Rev 2016;15(1):16–21.
29. Miglioranza Scavuzzi B, Holoshitz J. Endoplasmic reticulum stress, oxidative stress, and rheumatic diseases. Antioxidants 2022;11(7): 1306.
30. Jing W, Liu C, Su C, et al. Role of reactive oxygen species and mitochondrial damage in rheumatoid arthritis and targeted drugs. Front Immunol 2023;14:1107670.
31. Smallwood MJ, Nissim A, Knight AR, et al. Oxidative stress in autoimmune rheumatic diseases. Free Radic Biol Med 2018;125:3–14.
32. Zhao J, Ma J, Deng Y, et al. A missense variant in NCF1 is associated with susceptibility to multiple autoimmune diseases. Nat Genet 2017; 49(3):433–437.
33. Wang G, Pierangeli SS, Papalardo E, et al. Markers of oxidative and nitrosative stress in systemic lupus erythematosus: correlation with disease activity. Arthritis Rheum 2010;62(7):2064–2072.
34. Morgan PE, Sturgess AD, Davies MJ. Increased levels of serum protein oxidation and correlation with disease activity in systemic lupus erythematosus. Arthritis Rheum 2005;52(7):2069–2079.
35. Wirestam L, Arve S, Linge P, et al. Neutrophils-important communicators in systemic lupus erythematosus and antiphospholipid syndrome. Front Immunol 2019;10:2734.
36. Perl A. Oxidative stress in the pathology and treatment of systemic lupus erythematosus. Nat Rev Rheumatol 2013;9(11):674–686.
37. Scavuzzi BM, Simão ANC, Iriyoda TMV, et al. Increased lipid and protein oxidation and lowered anti-oxidant defenses in systemic lupus erythematosus are associated with severity of illness, autoimmunity, increased adhesion molecules, and Th1 and Th17 immune shift. Immunol Res 2018;66(1):158–171.
38. Fatah K, Silveira A, Tornvall P, et al. Proneness to formation of tight and rigid fibrin gel structures in men with myocardial infarction at a young age. Thromb Haemost 1996;76(4):535–540.
39. Weisel JW, Nagaswami C. Computer modeling of fibrin polymerization kinetics correlated with electron microscope and turbidity observations: clot structure and assembly are kinetically controlled. Biophys J 1992;63(1):111–128.
40. Cai Z, Yan LJ. Protein oxidative modifications: beneficial roles in disease and health. J Biochem Pharmacol Res 2013;1(1):15–26.
41. Azizova OA, Piryazev AP, Aseychev AV, et al. Oxidative modification of fibrinogen inhibits its transformation into fibrin under the effect of thrombin. Bull Exp Biol Med 2009;147(2):201–203.
42. Shacter E, Williams JA, Levine RL. Oxidative modification of fibrinogen inhibits thrombin-catalyzed clot formation. Free Radic Biol Med 1995; 18(4):815–821.
43. Gallwitz M, Enoksson M, Thorpe M, et al. The extended cleavage specificity of human thrombin. PLoS One 2012;7(2):e31756.
44. Yan Z, Chen Q, Xia Y. Oxidative stress contributes to inflammatory and cellular damage in systemic lupus erythematosus: cellular markers and molecular mechanism. J Inflamm Res 2023;16: 453–465.
45. Lupu A, Stoleriu G, Nedelcu AH, et al. Overview of oxidative stress in systemic lupus erythematosus. Antioxidants 2025;14(3):303.
46. Forman HJ, Zhang H. Targeting oxidative stress in disease: promise and limitations of antioxidant therapy. Nat Rev Drug Discov 2021; 20(9):689–709.
47. Carrillo-Vázquez DA, Balderas-Miranda JT, Rivera RIA, et al. Characterization of anti-neutrophil extracellular traps (NET) antibodies according to systemic lupus erythematosus clinical phenotypes. Immunol Res 2025;73(1):79.
48. Leffler J, Gullstrand B, Jönsen A, et al. Degradation of neutrophil extracellular traps co-varies with disease activity in patients with systemic lupus erythematosus. Arthritis Res Ther 2013;15(4):R84.
49. Whittall-Garcia LP, Naderinabi F, Gladman DD, et al. Circulating neutrophil extracellular trap remnants as a biomarker to predict outcomes in lupus nephritis. Lupus Sci Med 2024;11(1):e001038.

Arthritis & Rheumatology
Vol. 78, No. 2, February 2026, pp 357–370
DOI 10.1002/art.43380

American College of Rheumatology
Empowering Rheumatology Professionals

Mesenchymal Stromal Cell Therapy Alleviates Lupus Nephritis Through Inhibiting Caspase-4/5/11–Mediated Noncanonical Pyroptosis in Macrophages

Sha Liu,[1] Zhikang Wang,[1] Yue Zhang,[2] Panpan Zhou,[1] Huimin Zhu,[3] Yang Hang,[3] Xue Xu,[3] Xiaojun Tang,[3] Genhong Yao,[1] Dandan Wang,[3] Linyu Geng,[3] Weiwei Chen,[1] and Lingyun Sun[1,2,3]

Objective. Caspase-4/5/11–mediated noncanonical pyroptosis emerges as a contributing factor in immune responses under pathologic conditions. However, its precise role in the development of lupus nephritis (LN) remains largely unknown. Although mesenchymal stromal cells (MSCs) have demonstrated promising therapeutic effects on LN, whether MSCs influence pyroptosis in macrophages remains unknown. This study aimed to elucidate the role of caspase-4/5/11–mediated noncanonical pyroptosis in macrophages during the pathogenesis of LN and explore the impact of MSCs on macrophages.

Methods. The expression level of noncanonical pyroptosis in macrophages was assessed in patients and mice with LN. Blood samples from 19 patients with refractory systemic lupus erythematosus receiving MSC transplantation (MSCT) were collected. Caspase-11 inhibitor wedelolactone and MSCs were administered to MRL/*lpr* mice to examine the therapeutic efficacy. MSCs were cocultured with macrophages from MRL/*lpr* mice to explore effects and related mechanisms.

Results. Noncanonical pyroptosis signaling was activated in macrophages and kidney tissues from humans and mice with LN. The expression level of caspase-4 was increased and positively correlated with the active index and chronic index in the kidneys of patients with LN. The end products of pyroptosis directly induced cell death and reduced functional markers expression in murine podocytes. The caspase-11 inhibitor effectively alleviated renal damage in lupus mice. MSCT significantly deactivated pyroptosis signaling both in patients and lupus-prone mice. Mechanically, galectin-3 and interleukin-10 (IL-10) are essential for MSCs to inhibit noncanonical pyroptosis of LN macrophages.

Conclusion. Our findings showed that MSCT ameliorates LN by inhibiting the caspase-4/5/11–mediated pyroptosis in macrophages, possibly via secreting galectin-3 and IL-10.

INTRODUCTION

Lupus nephritis (LN), the most important predictor of morbidity and mortality in systemic lupus erythematosus (SLE), affects up to 60% of patients within a decade of diagnosis. Various immune cell types, including B cells, T cells, dendritic cells, and macrophages, are implicated in the pathogenesis of LN. Among these, macrophages are particularly emphasized for their critical role in LN progression.[1] Two major populations of macrophages exist in the kidneys: resident and monocyte-derived macrophages.[1,2] During inflammation, circulating monocytes migrate to injury sites and differentiate into local macrophages. Evidence shows that macrophage infiltration is increased in the LN kidney and associated with poorer renal outcomes,[3] whereas reducing macrophage infiltration exhibits a renal protective effect.[4] Studies have highlighted the

Supported by grants from the National Key R&D Program of China (grant 2020YFA0710800), Key Program of the National Natural Science Foundation of China (grant 82330055), Joint Fund of the National Natural Science Foundation of China (grant U24A20380), Key Projects of the Jiangsu Basic Research Program (grant BK20243061), and Key Project of Nanjing Medical Technology Development Fund (grant ZKX23016).

[1]Department of Rheumatology and Immunology, Nanjing Drum Tower Hospital Clinical College of Nanjing University of Chinese Medicine, Nanjing, China; [2]Department of Rheumatology and Immunology, Nanjing Drum Tower Hospital Clinical College of Jiangsu University, Zhenjiang, China; [3]Department of Rheumatology and Immunology, Nanjing Drum Tower Hospital, The Affiliated Hospital of Nanjing University Medical School, Nanjing, China.

Additional supplementary information cited in this article can be found online in the Supporting Information section (https://acrjournals.onlinelibrary.wiley.com/doi/10.1002/art.43380).

Author disclosures are available at https://onlinelibrary.wiley.com/doi/10.1002/art.43380.

Address correspondence via email to Lingyun Sun, MD, PhD, at lingyunsun@nju.edu.cn; or Weiwei Chen, PhD, at chenweiweinj@163.com.

Submitted for publication March 15, 2025; accepted in revised form August 20, 2025.

proinflammatory effect of intrarenal macrophages.[1,5] Furthermore, macrophages are known to injure podocytes directly,[6] but the exact mechanism is not yet well understood.

Pyroptosis, a gasdermin-mediated programmed necrotic cell death, is characterized by membrane pore formation, cellular swelling, subsequent cell lysis, and the release of abundant intracellular proinflammatory cytokines, mainly mature interleukin-1β (IL-1β).[7] As a key mediator of inflammation,[8] IL-1β orchestrates innate and adaptive immunity, leading to tissue injury.[9] Although a variety of cells in the kidney can produce IL-1β, macrophages are considered the primary cells that produce IL-1β,[8,10] especially in the case of inflammatory lesions.[11] Given that IL-1β is processed and released primarily via pyroptosis, it is reasonable to speculate that macrophage pyroptosis contributes to LN progression.

Pyroptosis occurs mainly through two pathways: canonical and noncanonical. The canonical pathway involves caspase-1 activation via inflammasome complexes, such as NLRP3,[12,13] and subsequent cleavage of gasdermin D (GSDMD), whereas the noncanonical pathway involves two mechanisms: (1) direct cleavage of GSDMD by murine caspase-11 or its human homologs, caspase-4/5; (2) indirect activation of the canonical pathway through NLRP3-mediated caspase-1 induction.[12,13] To date, the functional contribution of noncanonical pyroptosis to macrophage-mediated pathology in LN remains poorly characterized. Notably, type I interferons (IFNs) have been implicated in potentiating noncanonical pyroptosis in macrophages through caspase-11 upregulation.[14,15] Compelling evidence further establishes type I IFNs as central drivers of SLE progression[16] and critical players in the immunopathogenesis of LN.[17] In light of this association, we hypothesize that noncanonical pyroptosis within macrophages may contribute to the pathogenesis of LN.

Over the past two decades, allogeneic mesenchymal stromal cell transplantation (MSCT) has emerged as an effective and safe therapeutic strategy for refractory SLE.[18] Mesenchymal stromal cells (MSCs) mediate immunoregulatory effects primarily through secretion of soluble mediators and interactions with innate and adaptive immune cell populations.[19,20] MSCs can reduce the infiltration of macrophages to the sites of inflammation and promote the conversion of macrophages from the proinflammatory M1 phenotype to the anti-inflammatory M2 phenotype.[21,22] However, their effect on macrophage pyroptosis has yet to be elucidated.

This study shows that the caspase-4/5/11–mediated noncanonical pyroptosis pathway is excessively activated in macrophages from both patients with LN and a murine model. Elevated caspase-4 expression in renal macrophages correlates positively with kidney injury in patients with LN. We also observe that IL-1β induces podocyte injury, whereas inhibiting caspase-11 protects lupus-prone mice against LN progression. Additionally, MSCT alleviates LN by inhibiting macrophage pyroptosis, potentially through the secretion of galectin-3 and IL-10. These findings suggest that noncanonical pyroptosis of LN macrophages contributes to the disease progression and represents a promising therapeutic target.

MATERIALS AND METHODS

Study Population. For isolation of peripheral blood mononuclear cells (PBMCs) and peripheral blood monocytes (PBMs), 47 patients with LN, 30 patients with SLE without LN (SLE without LN was defined as 'SLE-non-LN' in this study), and 30 age- and sex-matched healthy donors were recruited in this study. Among them, 19 patients with refractory SLE receiving umbilical cord MSCT (UC-MSCT) were enrolled. Diagnoses of SLE and LN followed the revised classification criteria of the American College of Rheumatology[23] and the International Society of Nephrology/Renal Pathology Society (2003), respectively.[24] For the human renal biopsy study, 12 patients with LN were enrolled, and 6 normal kidney samples from areas adjacent to renal tumors served as controls. This study was approved by the research ethics board of the Nanjing Drum Tower Hospital. Written informed consent was obtained from all participants or their guardians (Approval No. SC201700201, NCT01741857).

Experimental animals. Female MRL/*lpr* and age-matched MRL/MpJ mice were purchased from SiPeiFu Biotechnology. Female MRL/*lpr* mice served as a spontaneous model for SLE and LN.[25] All mice were housed in a specific pathogen-free environment and kept on a 12:12 hour light/dark cycle with controlled humidity (60–80%) and temperature (22 ± 2°C). All procedures followed guidelines for the care and use of laboratory animals and were approved by the Institutional Animal Care and Use Committee of the Nanjing Drum Tower Hospital (Approval No. 2022AE01030).

Statistical Analysis. Data were analyzed using GraphPad Prism 9.5.0 (GraphPad Software) and expressed as the mean ± SEM. Data with normal distribution were analyzed using the unpaired two-tailed *t*-test for comparisons between two groups and one-way analysis of variance for comparisons among multiple groups. Non-normally distributed data were analyzed by the Mann-Whitney *U* or Kruskal-Wallis tests, as appropriate. For survival analysis, survival curves were compared using the log-rank test. Correlation analysis was performed using the Pearson *r* test. A P value < 0.05 was considered statistically significant.

RESULTS

Noncanonical pyroptosis is activated in PBMCs and PBMs and macrophages in the kidneys of patients with LN. To investigate the role of noncanonical pyroptosis in LN, quantitative polymerase chain reaction (qPCR) analysis of relevant genes—*NLRP3*, *IL-1β*, *CASPASE*-1, *CASPASE*-4, *CASPASE*-5, and *GSDMD*—in human PBMCs was conducted. Figure 1A

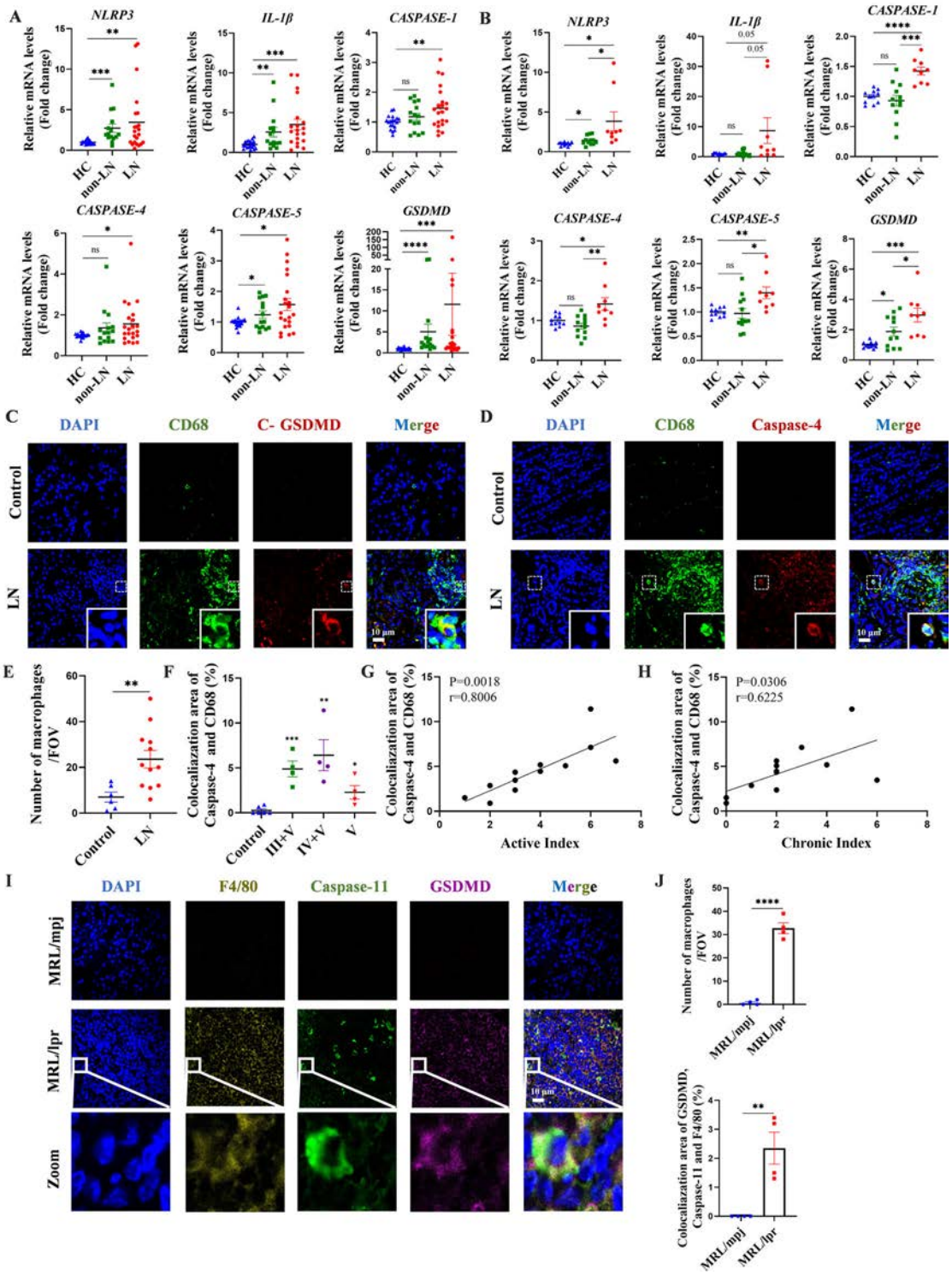

Figure 1. Noncanonical pyroptosis pathway is activated in intrarenal macrophages of LN patients and lupus mice. (A and B) mRNA expression for *NLRP3, IL-1β, CASPASE-1, CASPASE-4, CASPASE-5, and GSDMD* in PBMCs from patients with LN (n = 22), patients with non-LN SLE (n = 15), and healthy controls (n = 19) or in PBMs from patients with LN (n = 9), patients with non-LN SLE (n = 12), and healthy controls (n = 11). (C and D) Immunofluorescence for CD68 and C-GSDMD, CD68, and caspase-4 in renal samples of controls (n = 6) and patients with LN (n = 12). Scale bar is 10 μm. (E and F) Numbers of macrophages or colocalization area of caspase-4 and CD68 per FOV. (G and H) Correlation of colocalization area of caspase-4 and CD68 in kidneys with the active index (n = 12) and chronic index (n = 12). (I) Immunofluorescence staining of F4/80, caspase-11, and GSDMD in kidneys from MRL/MpJ (n = 4) and MRL/*lpr* mice (n = 4). Scale bar is 10 μm. (J) Numbers of macrophages or colocalization area of F4/80, caspase-11, and GSDMD per FOV. *$P < 0.05$; **$P < 0.01$; ***$P < 0.001$; ****$P < 0.0001$. C-GSDMD, cleaved GSDMD; FOV, field of view; GSDMD, gasdermin D; HC, healthy control; IL, interleukin; LN, lupus nephritis; mRNA, messenger RNA; PBM, peripheral blood monocyte; PBMC, peripheral blood mononuclear cell; SLE, systemic lupus erythematosus.

shows that these genes were remarkably up-regulated in PBMCs from patients with SLE compared to those from healthy controls. Additionally, compared to SLE patients without LN, a trend of increased expression of these genes was observed in patients with LN (Figure 1A). During inflammation, monocytes are rapidly recruited to injury sites and differentiate into macrophages.[26] Unlike PBMCs, blood monocytes from patients with LN expressed higher levels of all indicated pathway genes than those from patients without LN (Figure 1B), implying a potentially unique role for the noncanonical pyroptosis pathway in renal injury mediated by the mononuclear phagocyte system in LN.

Having established the upregulation of noncanonical pyroptosis in peripheral circulation, we next investigated its activation in renal macrophages using immunofluorescence (IF) staining on biopsy samples from 12 patients (classes III+V, IV+V, and V). Confocal microscopy revealed significant $CD68^+$ macrophage infiltration in the renal interstitium of LN kidney sections (Figure 1C–F) wherein enhanced expression of cleaved GSDMD, a key executor of pyroptosis, was detected in infiltrated macrophages in the renal interstitium of LN sections compared to controls (Figure 1C). We also examined caspase-4 expression in infiltrated macrophages (Figure 1D). The percentage of caspase-4 and CD68 double-positive area was significantly elevated in renal biopsy sections from patients with LN, especially in class III+V and IV+V (Figure 1F). Furthermore, this double-positive area correlated positively with renal activity and chronicity index scores (Figure 1G and H). Collectively, these results indicated that caspase-4/5–mediated noncanonical pyroptosis in macrophages is involved in human LN.

Noncanonical pyroptosis is triggered in macrophages in the kidneys of MRL/*lpr* mice. Female MRL/*lpr* mice typically develop nephritis-like symptoms,[27] including noticeable renal pathologic changes and elevated urine protein levels. In alignment with human studies, messenger RNA (mRNA) expression of noncanonical pyroptosis-associated genes (*NLRP3*, *IL-1β*, *IL-18*, *Caspase-11*, *Caspase*-1, and *GSDMD*) was significantly increased in the kidneys of 20-week-old MRL/*lpr* mice compared to age-matched MRL/MpJ mice (**Supplemental Figure** 1A). Western blot analysis of caspase-11, caspase-1, and N-terminal GSDMD (GSDMD-N) further confirmed the upregulation of noncanonical pyroptosis (**Supplemental Figure** 1B). IF staining of kidney sections from MRL/*lpr* mice showed diffuse infiltration of F4/80-positive cells and coexpression of caspase-11 and GSDMD in these cells, confirming the activation of caspase-11–mediated pyroptosis (Figure 1I–J). These data highlight the activation of caspase-11–mediated noncanonical pyroptosis in renal macrophages of MRL/*lpr* mice.

IL-1β and IL-18 induce podocyte injury. IL-1β and IL-18 are prominent end products of pyroptosis and widely recognized as proinflammatory factors in autoimmune diseases like LN.[28–30] Podocytes are crucial for preserving the integrity of the glomerular filtration barrier, and their dysfunction is linked to LN.[6] We evaluated the effects of IL-1β and IL-18 on MPC5 cell viability. Calcein-AM/PI staining indicated that both cytokines, alone or in combination, significantly induced cell death in MPC5 cells in vitro (**Supplemental Figure** 2A–B). Consistently, the expression of podocyte markers (synaptopodin, CD2-associated protein [CD2AP], podocalyxin [PODXL], and Wilms' tumor-1 [WT-1]) was also reduced, particularly under the condition of combined treatment (**Supplemental Figure** 2C–D). These results confirmed that the end products of pyroptosis can directly drive podocyte injury in vitro, thereby exacerbating LN.

Inhibition of caspase-11 suppresses the noncanonical pyroptosis pathway in the macrophages of MRL/*lpr* mice. Because pyroptosis could be a potential therapeutic target for LN, a caspase-11 inhibitor, wedelolactone (Wed) was introduced to observe its impact on pyroptosis in lupus macrophages. Peritoneal macrophages (PMs) were isolated from lupus mice for in vitro studies. Morphologically, PMs from lupus mice exhibited typical pyroptotic changes, including swelling and bubbling, which were absent in PMs from MRL/MpJ mice (Figure 2A). qPCR and western blot analyses consistently indicated activation of the noncanonical pyroptosis pathway in lupus PMs (Figure 2B and C), along with increased secretion of IL-1β (Figure 2D). We then treated lupus PMs with Wed and conducted a CCK-8 assay to assess PM viability. Treatment with concentrations of ≤10 μM for 24, 48, or 72 hours did not reduce viability (**Supplemental Figure** 3). Therefore, a concentration of 10 μM and treatment duration of 24 hours were selected for subsequent experiments. At the transcriptional level, Wed suppressed caspase-11 and its downstream genes (Figure 2E). Although pro-caspase-11, pro-caspase-1, and full-length GSDMD (GSDMD-F) levels did not differ significantly between PMs treated with or without Wed at the translational level, the activated forms—cleaved caspase-11, cleaved caspase-1, and GSDMD-N—showed decreased levels or a trend toward reduced expression levels (Figure 2F). Collectively, these findings suggest that inhibiting caspase-11 could suppress the noncanonical pyroptosis pathway in lupus macrophages.

Inhibiting noncanonical pyroptosis of macrophages alleviates LN in MRL/*lpr* mice. Our findings highlighted the significance of the noncanonical pyroptosis pathway in LN. We therefore tested the treatment effect of the caspase-11 inhibitor in the MRL/*lpr* LN model. MRL/*lpr* mice were gavage-fed with Wed or vehicle daily for eight weeks. The survival rates exhibited no significant difference between the two groups (**Supplemental Figure** 4A). The urinary protein-to-creatinine ratios indicated that Wed treatment significantly decreased proteinuria in MRL/*lpr* mice (**Supplemental Figure** 4B). Podocin is a podocyte-specific protein, and alterations in its expression or detection in urine serve

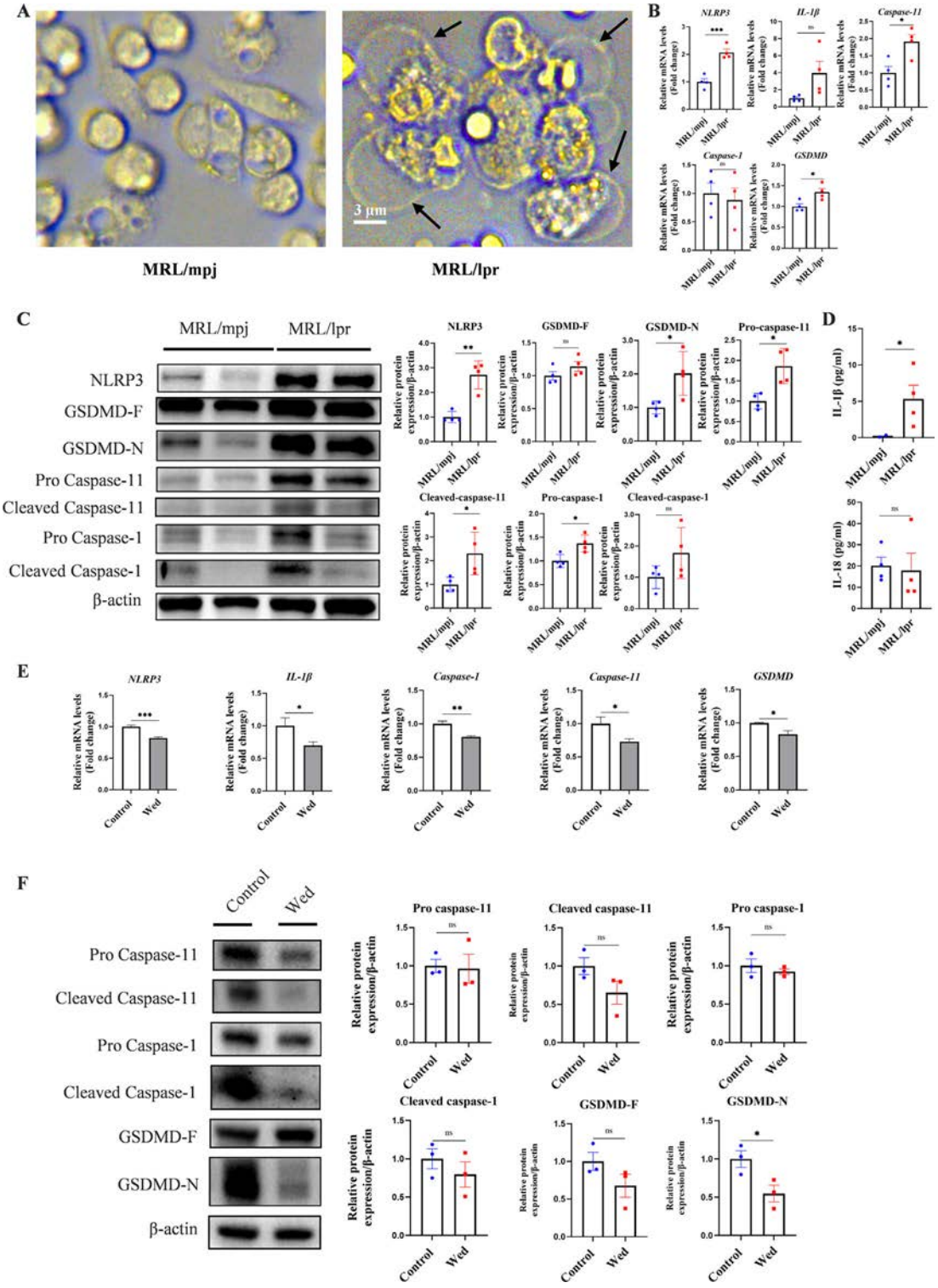

Figure 2. Caspase-11 inhibitor (Wed) suppresses the noncanonical pyroptosis pathway in the macrophages of MRL/*lpr* mice. (A) Representative light microscopy images of PMs from MRL/MpJ control mice and MRL/*lpr* mice. Scale bar is 3 μm. (B) mRNA expression for *NLRP3, IL-1β, Caspase-11, Caspase-1, and GSDMD* in PMs sorted from MRL/MpJ (n = 4) and MRL/*lpr* mice (n = 4). (C) Immunoblotting analysis for NLRP3, GSDMD-F, GSDMD-N, pro caspase-11, cleaved caspase-11, pro caspase-1, and cleaved caspase-1 in PMs sorted from MRL/MpJ (n = 4) and MRL/*lpr* mice (n = 4). (D) Protein levels of IL-1β and IL-18 in the supernatant from the indicated groups. (E) qPCR analysis of *NLRP3, IL-1β, Caspase-1, Caspase-11, and GSDMD* in PMs from MRL/*lpr* mice. Cells were incubated with (n = 3) or without Wed (n = 3). (F) Immunoblot analysis of pro caspase-11, cleaved caspase-11, pro caspase-1, cleaved caspase-1, GSDMD-F, and GSDMD-N expression in PMs from MRL/*lpr* mice. Cells were incubated with (n = 3) or without Wed (n = 3). **P* < 0.05; ***P* < 0.01; ****P* < 0.001. GSDMD-F, full-length gasdermin D; GSDMD-N, N-terminal GSDMD; IL, interleukin; mRNA, messenger RNA; ns, not significant; PM, peritoneal macrophages; qPCR, quantitative polymerase chain reaction; Wed, wedelolactone. Color figure can be viewed in the online issue, which is available at http://onlinelibrary.wiley.com/doi/10.1002/art.43380/abstract.

as a key biomarker for podocyte injury. Enzyme-linked immunosorbent assay results showed that the protein level of urinary podocin was reduced in mice treated with Wed (**Supplemental Figure** 4C). Renal histopathological analyses demonstrated severe glomerular and tubulointerstitial lesions in MRL/*lpr* mice, characterized by glomerular hypercellularity, mesangial matrix deposition, crescent formation, tubular necrosis, and perivascular immune cell accumulation, all of which were attenuated in MRL/*lpr* mice treated with Wed (Figure 3A). Female MRL/lpr mice spontaneously develop dermatitis, which is one of the most common symptoms of SLE. In this study, Wed treatment significantly attenuated the inflammatory skin lesions on the faces of the mice, as evidenced by an improvement in the rash and hair loss (**Supplemental Figure** 4D). IF staining showed a substantial decrease in the number of macrophages and GSDMD-positive macrophages in the kidneys of the Wed-treated group (Figure 3B). Flow cytometry (FCM) showed a trend toward reduced percentages and decreased mean fluorescence intensity of active caspase-1 positive macrophages in the kidneys of Wed group (Figure 3C). Additionally, mRNA expression of *NLRP3*, *Caspase*-11, *Caspase*-1, and *GSDMD* (**Supplemental Figure** 5), as well as protein levels of pro caspase-11, cleaved caspase-11, pro caspase-1, cleaved caspase-1, GSDMD-F, and GSDMD-N, in PMs also decreased greatly (Figure 3D). These results suggest that caspase-11 inhibition can reduce noncanonical pyroptosis of macrophages in LN and ameliorate renal injury.

MSCT suppresses pyroptosis in the macrophages of MRL/*lpr* mice and the PBMCs and PBMs in patients with refractory SLE. We examined the efficacy of MSCT on lupus mice by comparing survival rate and other lupus symptoms in MRL/*lpr* mice treated with MSCs and phosphate-buffered saline (PBS). As shown in **Supplemental Figure** 6A, although statistical significance was not achieved, MSCs treatment demonstrated a favorable survival trend (P = 0.10). The cutaneous lesions in the MSC-treated mice showed notable improvement, with decreased dermatitis clinical scores (**Supplemental Figure** 6D). As for renal outcomes, mice receiving MSCs exhibited significantly reduced proteinuria and urinary podocin levels compared to PBS controls (**Supplemental Figure** 6B–C). Consistently, the renal histopathological scores were improved, indicated by reduced glomerular cell proliferation, mesangial matrix deposition, and perivascular immune cell accumulation (Figure 4A). Meanwhile, IF revealed decreased deposition of IgG and complement component 3 (C3) in the glomeruli of the MSC-treated group (Figure 4B). Furthermore, kidney tissues from MSC-treated mice exhibited lower mRNA levels of proinflammatory cytokines, including *IFNγ*, monocyte chemoattractant protein-1 (*MCP-1*), and inducible nitric oxide synthase (*iNOS*), alongside increased expression of *IL-10* and *Synaptopodin* (**Supplemental Figure** 7). Next, we investigated whether the therapeutic effect of MSCs on LN involves the inhibition of pyroptosis in macrophages. We found a marked reduction in the mRNA levels of pyroptosis-related genes in PMs from the MSC-treated group compared to the PBS-treated group (**Supplemental Figure** 4C). FCM also revealed decreased numbers of total and active caspase-1-positive macrophages in the peripheral blood and kidneys of MSC-treated lupus mice (Figure 4D and E). Next, the mRNA levels of pyroptosis-related key genes, *CASPASE-1*, *CASPASE-5*, and *GSDMD*, were decreased in PBMCs (Figure 5A) and PBMs (Figure 5B) from patients with LN at 12 hours after UC-MSCT compared to their pretreatment levels. Furthermore, we found that the plasma IL-1β and IL-18 levels were significantly decreased after UC-MSCT (Figure 5C). Additionally, FCM showed a reduced percentage of active caspase-1–positive PBMs after UC-MSCT (Figure 5D and E). Collectively, these data suggested that MSCT alleviates LN, with mechanisms involving the suppression of noncanonical pyroptosis in LN macrophages.

MSCs inhibit the noncanonical pyroptosis pathway in lupus macrophages through IL-10 and Galectin-3. Previous studies have shown that MSCs can be remodeled by an inflammatory microenvironment and then secrete soluble factors to regulate the crosstalk between MSCs and immune cells.[31,32] To elucidate the regulatory mechanism of MSCs on macrophage pyroptosis, we first cocultured PMs from MRL/*lpr* mice with MSCs in a transwell system for 48 hours. PMs cocultured with MSCs showed reduced expression of NLRP3, Caspase-11, Caspase-1, and GSDMD at both mRNA (Figure 6A) and protein (Figure 6B) levels. Next, to identify which MSC-secreted factors inhibit macrophage pyroptosis, we tested a range of reported MSC-secreted cytokines. Results showed that MSCs cocultured with PMs had significantly higher levels of *GALECTIN-3* and *TSG-6*, with a trend toward higher *IL-10* expression at mRNA levels (Figure 6C) but no notable increase in levels of other genes (**Supplemental Figure** 8). Subsequently, the increase in galectin-3 expression and a trend toward elevated IL-10 levels were confirmed at the protein level. In contrast, no increase was observed in TSG-6 protein expression. (Figure 6D). Accordingly, we hypothesized that MSCs regulate the noncanonical pyroptosis pathway in LN macrophages via galectin-3 and/or IL-10. To test this, we silenced these genes with small interfering RNA (siRNA) (**Supplemental Figure** 9). Galectin-3– or IL-10–silenced MSCs were cocultured with PMs from MRL/*lpr* mice for 48 hours (Figure 6E). Silencing either gene partially reversed the normal MSC-mediated inhibitory effects on macrophage pyroptosis, evidenced by increased expression of *NLRP3* and *IL-18* in the siGal-3–MSC or siIL-10–MSC groups, as well as a rise in *Caspase-1* expression in the siIL-10–MSC group when compared to the siCtl-MSC group. Changes in *IL-1β*, *Caspase-11*, and *GSDMD* in either group and *Caspase-1* in the siGal-3-MSC group showed no significance (Figure 6E). Considering the temporary silencing effects of siRNAs, we shortened the coculture period to 24 hours to ensure effective knockdown (Figure 6F). An additional group with

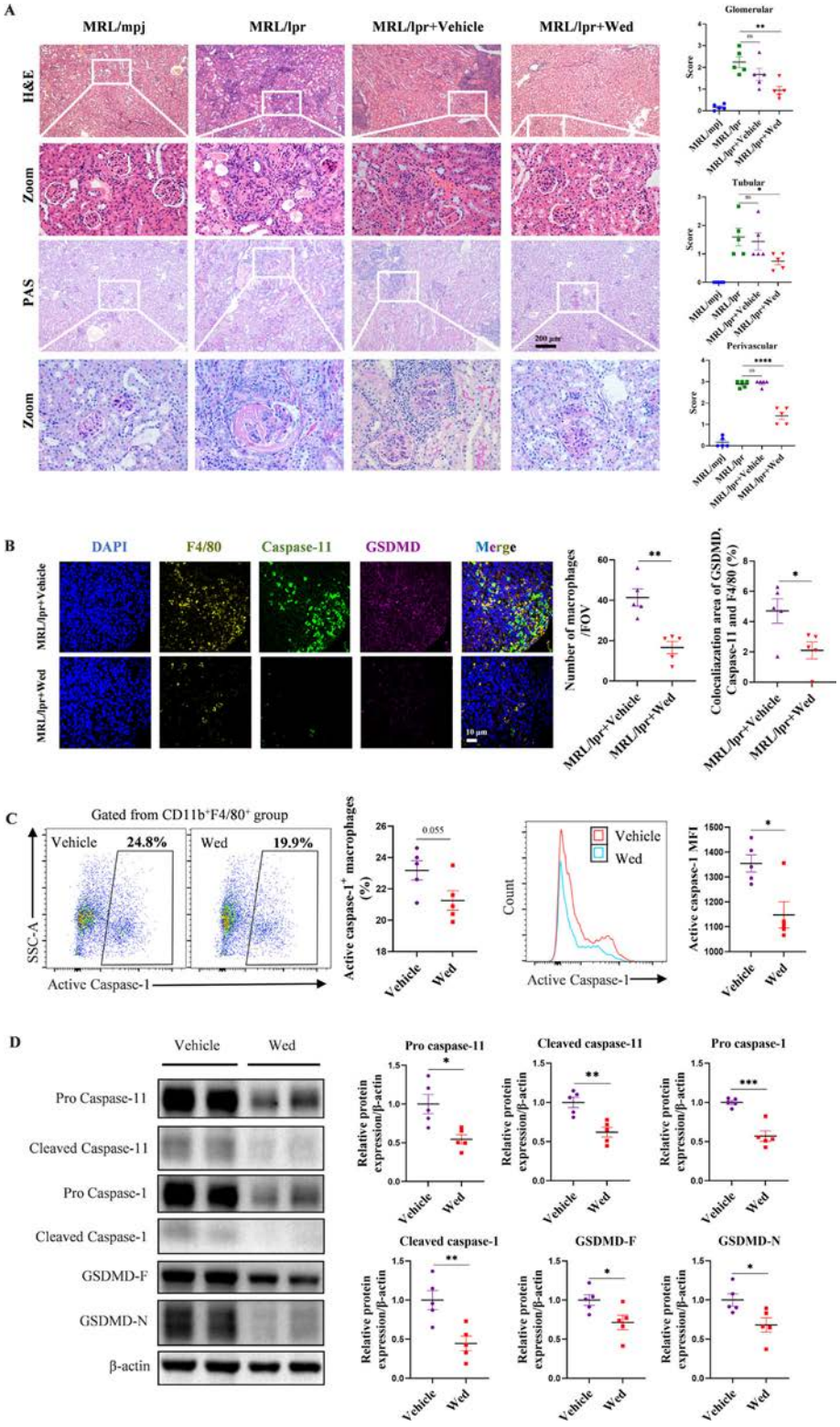

Figure 3. Caspase-11 inhibitor (Wed) ameliorates lupus nephritis of MRL/*lpr* mice by inhibiting noncanonical pyroptosis in macrophages. (A) H&E or PAS staining of kidney sections (n = 5 for each group). Quantitative analysis of glomerular, tubular, and perivascular pathology. Scale bar is 200 μm. (B) Immunofluorescence staining for F4/80, caspase-11, and GSDMD in kidneys from the indicated groups. Scale bar is 10 μm. Quantitative analysis of the numbers of macrophages per FOV or colocalization area of F4/80, caspase-11, and GSDMD per FOV. (C) Flow cytometric analysis of active caspase-1 positive kidney macrophages from mice treated with vehicle or Wed. (D) Immunoblot analysis of pro caspase-11, cleaved caspase-11, pro caspase-1, cleaved caspase-1, GSDMD-F, and GSDMD-N expression in PMs. *$P < 0.05$; **$P < 0.01$; ***$P < 0.001$; ****$P < 0.0001$. FOV, field of view; GSDMD-F, full-length gasdermin D; GSDMD-N, N-terminal GSDMD; H&E, hematoxylin and eosin; ns, not significant; PAS, periodic acid–Schiff; PM, peritoneal macrophage; Wed, wedelolactone.

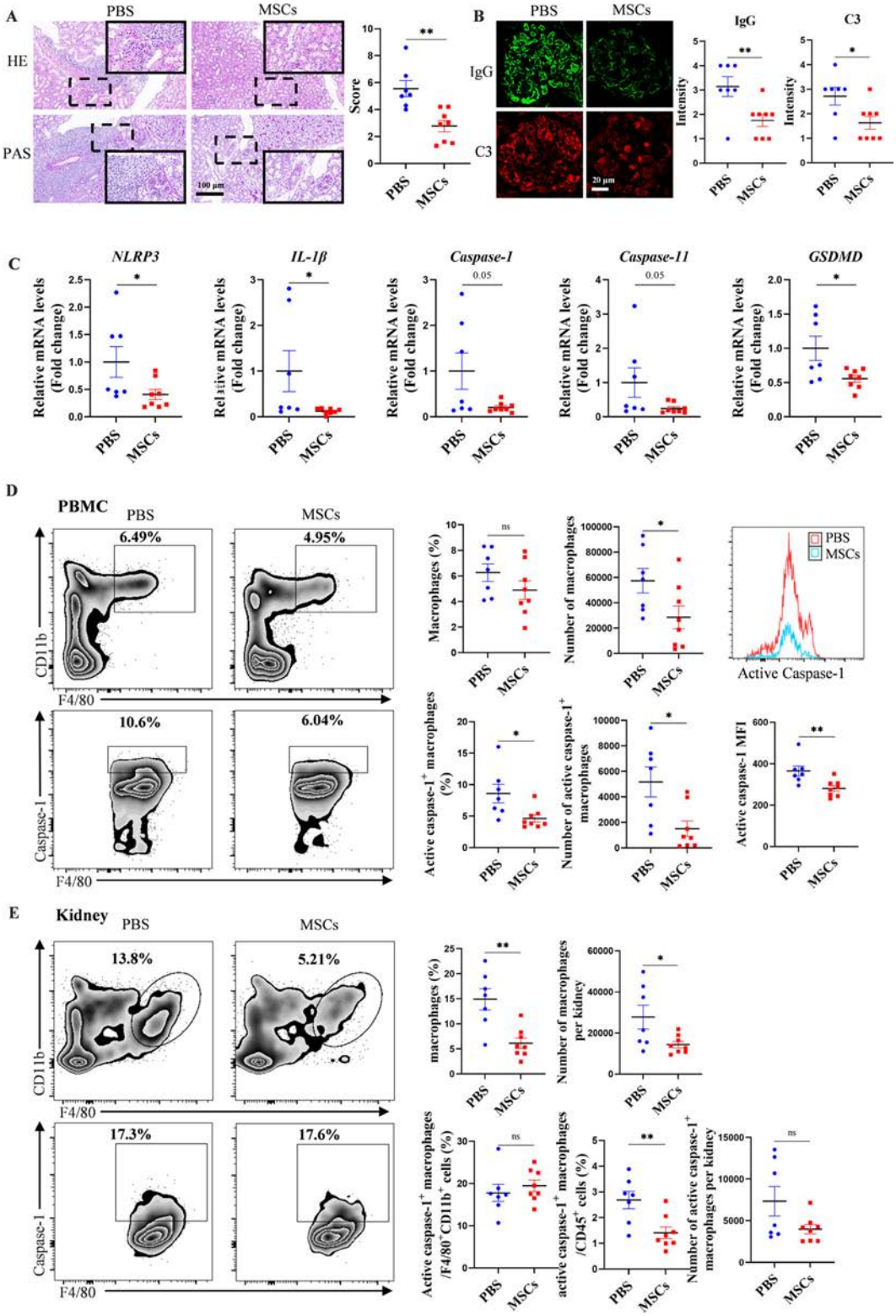

Figure 4. MSCs suppress the pyroptosis pathway in macrophages of MRL/*lpr* mice in vivo. (A) H&E or PAS staining of kidney sections from PBS-treated (n = 7) or UC-MSC–treated (n = 8) mice and scores of renal pathology. Scale bar is 100 μm. (B) Representative images of IgG and C3 deposition in glomeruli and scores for fluorescence intensity. Scale bar is 20 μm. (C) mRNA expression for *NLRP3, IL-1β, Caspase-1, Caspase-11*, and *GSDMD* in PMs. (D) The percentages, numbers, and MFI of total macrophages and active caspase-1 positive macrophages in PBMCs from both groups of mice. (E) The percentages and numbers of total macrophages and active caspase-1 positive macrophages in kidneys from both groups of mice. *$P < 0.05$; **$P < 0.01$. C3, complement component 3; FOV, field of view; H&E, hematoxylin and eosin; MFI, mean fluorescence intensity; IgG, immunoglobulin G; mRNA, messenger RNA; MSC, mesenchymal stromal cell; ns, not significant; PAS, periodic acid–Schiff; PBS, phosphate-buffered saline; PBMC, peripheral blood mononuclear cells; PM, peritoneal macrophage; UC-MSC, umbilical cord MSC.

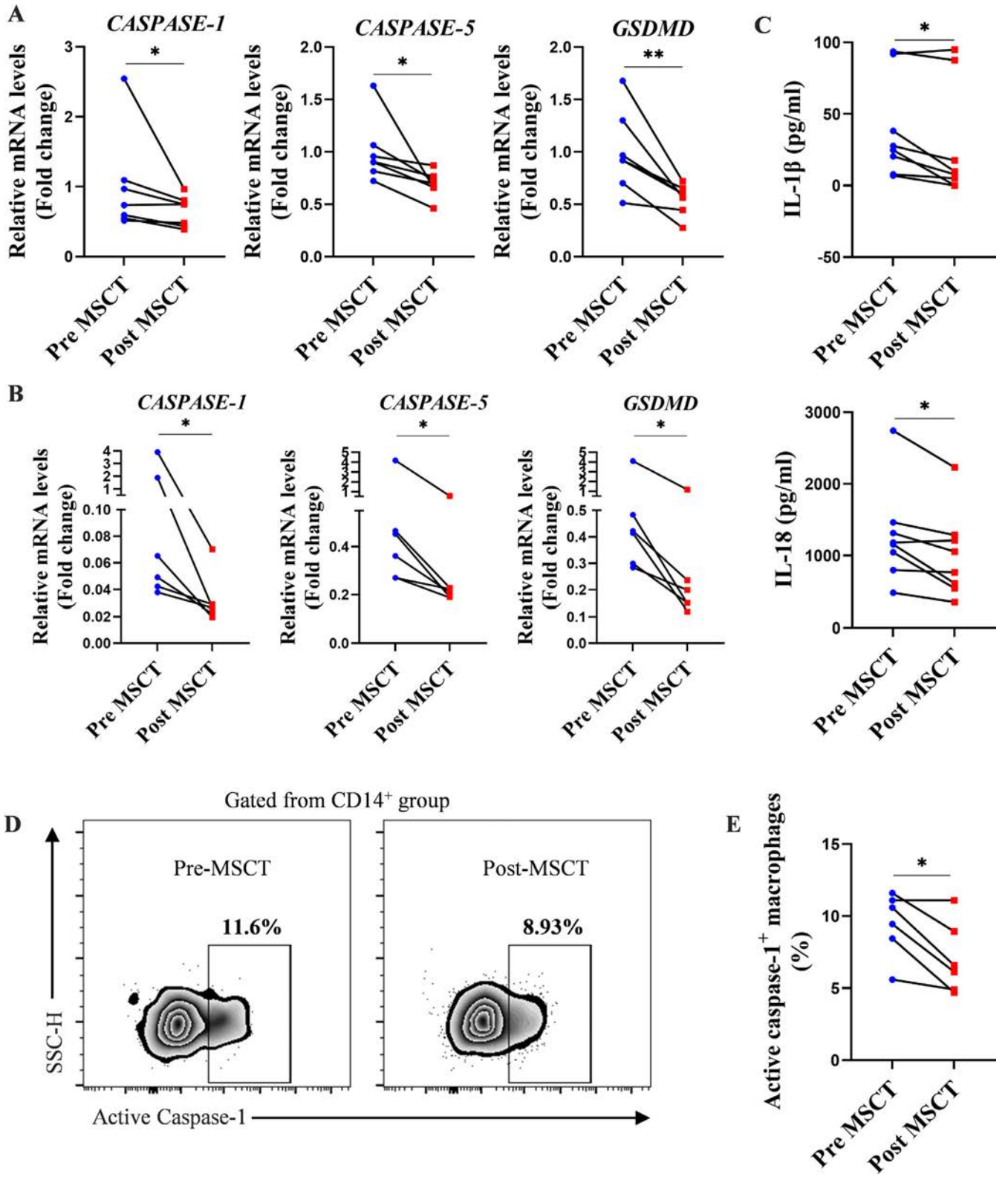

Figure 5. MSCs suppress the pyroptosis pathway in the PBMCs and PBMs in refractory SLE patients. (A) mRNA expression for *CASPASE-1, CASPASE-5, and GSDMD* in PBMCs from patients (n = 7) before and after MSCT. (B) mRNA expression for *CASPASE-1, CASPASE-5, and GSDMD* in PBMs from patients (n = 6) before and after MSCT. (C) Changes in the levels of serum IL-1β and IL-18 detected by enzyme-linked immunosorbent assay in patients (n = 8) before and after MSCT. (D) Flow cytometric analysis of active caspase-1 positive PBMs from patients (n = 6) before and after MSCT. *$P < 0.05$; **$P < 0.01$. IL, interleukin; mRNA, messenger RNA; MSC, mesenchymal stromal cell; MSCT, MSC transplantation; PBM, peripheral blood monocyte; PBMC, peripheral blood mononuclear cell; SLE, systemic lupus erythematosus; SSC-H, side scatter height. Color figure can be viewed in the online issue, which is available at http://onlinelibrary.wiley.com/doi/10.1002/art.43380/abstract.

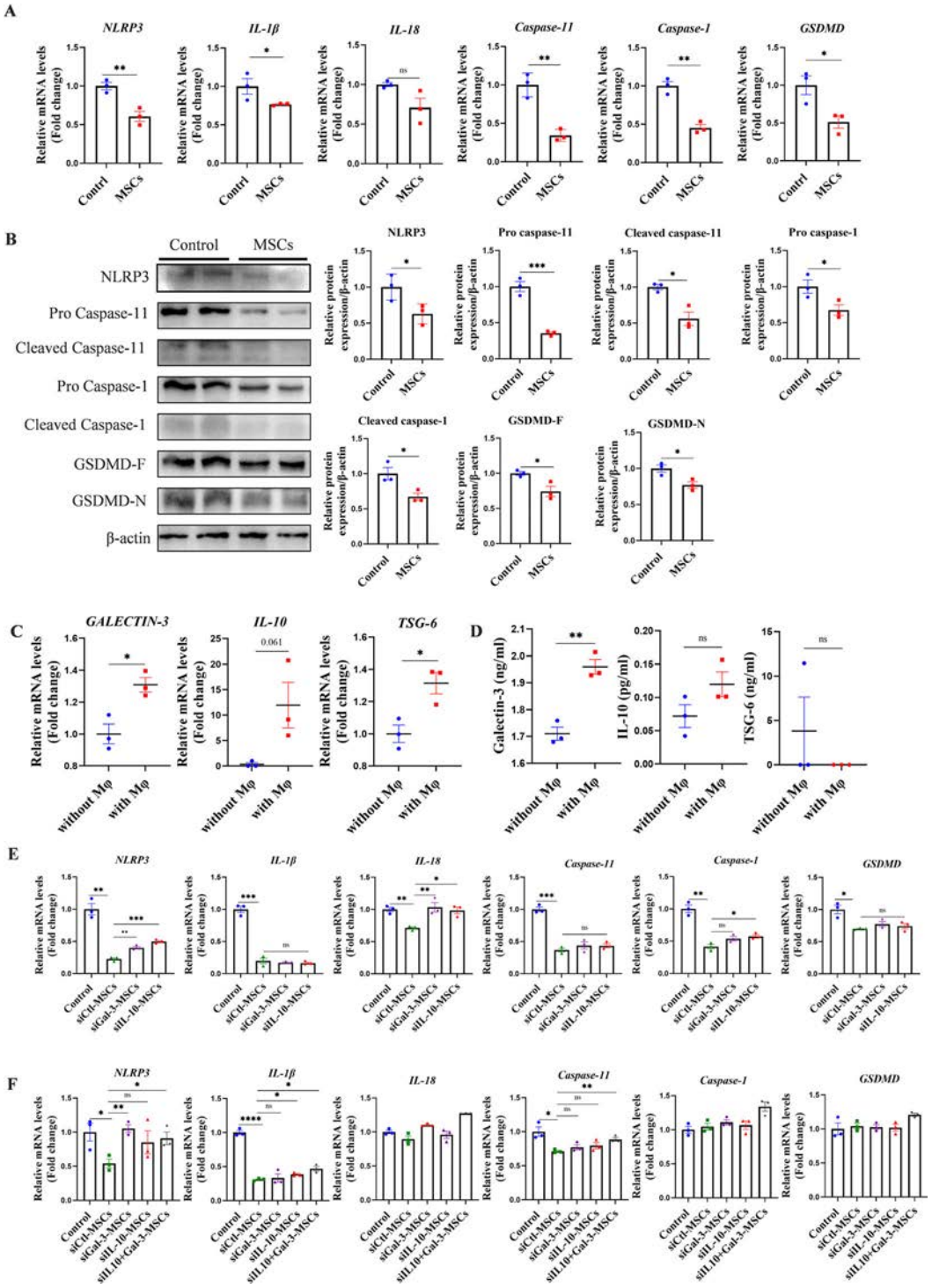

Figure 6. MSCs inhibit the noncanonical pyroptosis pathway through galectin-3 and IL-10. (A) mRNA levels of *NLRP3, IL-1β, IL-18, Caspase-11, Caspase-1*, and *GSDMD* in PMs from MRL/*lpr* mice cocultured with or without MSCs determined by qPCR. (B) Expression levels of NLRP3, pro caspase-11, cleaved caspase-11, pro caspase-1, cleaved caspase-1, GSDMD-F, and GSDMD-N in PMs from MRL/*lpr* mice cocultured with or without MSCs by Western blot analysis. (C) mRNA levels of *GALECTIN-3, IL-10*, and *TSG-6* in MSCs cocultured with or without PMs. (D) Protein levels of galectin-3, IL-10, and TSG-6 in the supernatants of MSCs cocultured with or without PMs detected by enzyme-linked immunosorbent assay. (E) mRNA levels of *NLRP3, IL-1β, IL-18, Caspase-11, Caspase-1, and GSDMD* in PMs cocultured with siCtl-MSCs, siGal-3-MSCs, or siIL-10-MSCs for 48 hours. (F) mRNA levels of *NLRP3, IL-1β, IL-18, Caspase-11, Caspase-1, and GSDMD* in PMs cocultured with siCtl-MSCs, siGal-3-MSCs, siIL-10-MSCs, or siIL-10+Gal-3-MSCs for 24 hours. **P* < 0.05; ***P* < 0.01; ****P* < 0.001; *****P* < 0.0001. GSDMD-F, full-length gasdermin D; GSDMD-N, N-terminal GSDMD; IL, interleukin; MSC, mesenchymal stromal cell; mRNA, messenger RNA; Mφ: macrophages; ns, not significant; PM, peritoneal macrophages; qPCR, quantitative polymerase chain reaction. Color figure can be viewed in the online issue, which is available at http://onlinelibrary.wiley.com/doi/10.1002/art.43380/abstract.

dual silencing of galectin-3 and IL-10 in MSCs was also set (siIL-10+Gal-3-MSC group). Results indicated restored expression of *NLRP3*, *IL-1β*, and *Caspase-11* in the dual silencing group, suggesting enhanced suppression of the caspase-11–mediated pyroptosis pathway. Based on these findings, we concluded that MSCs modulate the pyroptosis phenotype of macrophages via secreting galectin-3 and IL-10.

DISCUSSION

SLE features prominently activated IFNs,[33] especially type I IFNs. Previous studies have demonstrated a positive correlation of type I IFNs with kidney involvement and disease activity in SLE. Type I IFNs levels were higher in patients with LN than in patients without LN.[33] Because type I IFNs play an important role in regulating both the expression and activation of caspase-11,[34] this might explain the findings in our work that the noncanonical pyroptosis pathway was markedly up-regulated in both PBMCs and circulating monocytes in LN but not patients with non-LN SLE.

Here, we confirmed the significant increase of macrophage infiltration in the kidney specimens of patients with class III+V, IV+V, and V of LN and MRL/*lpr* mice. Moreover, these patients showed more intense expression of caspase-4 and cleaved GSDMD, the active form of GSDMD, in CD68-positive cells. Similarly, the number of caspase-11 and GSDMD double-positive macrophages in the kidneys of lupus-prone mice also increased dramatically compared to that of the MRL/MpJ control mice. We further confirmed the localization of caspase-4 and GSDMD in renal macrophages from patients with LN and the colocalization of caspase-11 and GSDMD in murine renal macrophages. The number of caspase-4-positive macrophages was positively correlated with the renal active index and chronic index, predictors indicating rapid, progressive, or permanent, irreversible renal impairment, respectively. These findings provide evidence for the first time that the noncanonical pyroptosis pathway is markedly activated in the macrophages of LN kidneys and participates in the pathogenesis of LN.

It is noteworthy that pyroptotic macrophages were predominantly localized to the renal interstitium but not in the glomeruli. Although not all macrophages undergo pyroptosis, even a limited population of pyroptotic macrophages in the renal interstitium may contribute to LN pathogenesis through several synergistic mechanisms. (1) Amplification of inflammatory signaling: Pyroptotic macrophages release pro-inflammatory mediators such as IL-1β and IL-18, which can activate surrounding immune cells, including T cells, neutrophils, and neighboring macrophages. This local activation can trigger paracrine and autocrine signaling loops, leading to amplification of the inflammatory response and propagation of injury across renal compartments, including glomeruli and tubules.[7,9,35] (2) Systemic pyroptotic activity: Elevated systemic pyroptosis in LN is evidenced by increased expression of pyroptosis-related genes in circulating PBMCs and monocytes (Figure 1A and B), along with higher IL-1β levels (Figure 2D). This systemic inflammatory milieu likely contributes to renal injury beyond the local effects of tissue-resident macrophages. (3) Autoantigen release and immune complex formation: Nuclear components, such as nucleic acids and histones, released during pyroptosis, may serve as autoantigens, thereby promoting autoantibody production and immune complex deposition. These complexes can directly injure glomerular structures and perpetuate autoimmune-mediated damage.

Podocytes are terminally differentiated visceral epithelial cells that line outside the basement membrane of glomeruli. They are the important component of the glomerular filtration barrier that prevents serum proteins from leaking into the urinary space. Podocyte injury and the subsequent detachment is one of the major causes of proteinuria. Potential etiologies include genetic susceptibility, metabolic disturbance, and immunologic processes, among others. Podocytes express IL-1 receptor 1 (IL-1R1), a receptor for IL-1β[36] and IL-18.[37] Herein, we hypothesized that macrophage pyroptosis induces podocyte injury by producing IL-1β and IL-18. IL-1β alters the podocyte structure by inducing rearrangement of the actin cytoskeleton, leading to the loss of slit diaphragms that connect podocytes.[38] IL-1β-treated podocytes are prone to develop lipid accumulation, which adversely affects cellular metabolism and promotes inflammation.[39] Furthermore, lipopolysaccharide-pretreated macrophages induce podocyte apoptosis,[6] which can be rescued by the inactivation of macrophages, underscoring the toxicity of cytokines, primarily IL-1β, on podocytes.[6] To the best of our knowledge, little is known about the influence of IL-18 on podocytes. Our observations demonstrated firstly that IL-1β or IL-18, alone or in combination, reduce podocyte viability and podocyte-specific marker expression in vitro, indicating that macrophage pyroptosis exerts direct cytotoxic effects on podocytes and could be a target for treating LN.

Recent studies have identified that inhibiting caspase-11 shows promise for treating inflammatory diseases like acute lung injury[40] and osteoarthritis.[41] Possible mechanisms involve inhibiting the NK-κB and Nrf2 signaling pathways.[40] Our findings proved that pharmacological inhibition of caspase-11 by Wed can effectively inhibit the overactivation of caspase-11–mediated pyroptosis signaling in macrophages from MRL/*lpr* mice both in vitro and in vivo. Wed treatment led to a significant reduction in proteinuria and urinary podocin levels, as well as improved renal histopathological changes, indicating that inhibition of macrophage pyroptosis mitigates podocyte injury and improves renal outcomes. LN is classically characterized as a form of glomerulonephritis. However, tubulointerstitial injury is also common and strongly correlates with renal dysfunction and poorer prognosis. In our study, Wed treatment significantly reduced not only glomerular pathology but also tubular injury in MRL/*lpr* mice. We propose that this protection may result from two complementary

mechanisms. (1) Reduction of secondary tubular injury: By attenuating glomerular inflammation and proteinuria, Wed likely alleviates downstream stress on the tubules. In LN, excessive protein leakage into the tubular lumen can trigger tubular epithelial injury and inflammation. Thus, mitigating glomerular damage may disrupt this pathogenic cascade. (2) Potential direct effects on the tubulointerstitial compartment: Wed has been shown in previous studies to possess broad anti-inflammatory and tissue-protective properties.[42,43] These systemic effects may also confer direct protection to tubular epithelial cells and the surrounding interstitial microenvironment. Tubular cell-specific responses to Wed would be a potential area for future investigation. Although our findings strongly support a pathogenic role for caspase-4/5/11–mediated pyroptosis in macrophages during LN, quantifying its exact contribution within the complex inflammatory milieu of the disease remains challenging. Further studies are needed to delineate the specific role and relative impact of macrophage pyroptosis in LN pathogenesis.

Evidence indicates that MSCT significantly improves the prognosis of LN, and its underlying mechanisms involve various paracrine actions and cell–cell interplay.[31,32] MSCs orchestrate immune responses in the inflammatory microenvironment. In turn, the inflammatory stimuli at the sites of inflammation influence the immunoregulatory plasticity of MSCs. For instance, IFN-γ, a key factor involved in the pathogenesis of SLE, boosts the production of immunoregulatory factors in MSCs.[31,44] Interestingly, our results showed dramatically decreased IFN-γ expression in the MSC-treated group of lupus kidneys. This phenomenon may be attributed to the suppression of immune cells by MSCs in response to high levels of IFN-γ, representing a negative feedback loop. In addition, the down-regulated gene expression of MCP-1 and iNOS, markers of inflammation for LN,[45] and the elevated level of anti-inflammatory cytokine IL-10 and podocyte marker synaptopodin indicated a favorable intrarenal environment after MSCT.

To date, the relationship between macrophage pyroptosis and MSCs has not yet been reported. Here, we demonstrated for the first time that MSCs inhibited caspase-4/5/11–mediated macrophage pyroptosis, leading to marked improvement in renal pathology and function. Several lines of evidence support this conclusion. First, coculture of MSCs with primary lupus macrophages in vitro led to the downregulation of the caspase-11/GSDMD pathway gene expression. Second, consistent with these in vitro findings, MSC treatment significantly suppressed the caspase-11/GSDMD pathway in both systemic and renal macrophages in lupus-prone MRL/*lpr* mice. Third, MSC-treated mice exhibited reduced renal histopathological injury, decreased glomerular IgG and C3 deposition, and improved renal function, collectively highlighting macrophage pyroptosis as a crucial therapeutic target of MSCs in attenuating LN. Beyond renal protection, both MSCs and Wed treatment also attenuated lupus-associated skin injury, suggesting a potential role for pyroptosis in cutaneous lupus. These findings indicate that targeting pyroptosis may help mitigate dermal manifestations of the disease. Future studies will extend to other organ systems affected by lupus—including the lung, joints, and central nervous system—to further elucidate the systemic contribution of pyroptosis and evaluate the broader therapeutic potential of MSCs and Wed in SLE.

Further mechanistic studies indicated that the inhibitory effect of MSCs on macrophage pyroptosis was potentially mediated through galectin-3 and IL-10. This was demonstrated by the finding that the combined knockdown of these factors in MSCs partially reversed the expression levels of NLRP3, IL-1β, and caspase-11 in macrophages. Galectin-3, a member of the β-galactoside-binding lectin family, has been reported to participate in immune responses and repair processes. Galectin-3 plays an essential role in regulating the proliferation, survival, migration, and immunomodulation of MSCs.[46,47] Of therapeutic relevance, galectin-3 overexpression in MSCs has been shown to attenuate inflammation by driving macrophage polarization toward an immunoregulatory M2 phenotype,[47] a mechanism that aligns with the pyroptosis-suppressive effects of IL-10 observed across multiple disease models.[48,49] Our experimental data demonstrated that the combined genetic silencing of IL-10 and galectin-3 in MSCs led to a significantly enhanced restoration of caspase-11–mediated pyroptosis compared to single-gene knockdown approaches.

In conclusion, our data demonstrate that caspase-4/5/11–mediated pyroptosis is overactivated in LN macrophages and is involved in the pathogenesis of this disease. Inhibition of caspase-11 suppresses pyroptosis, thus attenuating the disease progression. MSCs function by secreting galectin-3 and IL-10 in the presence of macrophages and downregulating the noncanonical pyroptosis pathway. Our findings provide a potential therapeutic target for LN and offer new insights into the mechanisms by which MSCs treatment alleviates LN.

ACKNOWLEDGMENTS

We are grateful to all the faculty of the Department of Rheumatology and Immunology at Nanjing Drum Tower Hospital for their support of this work, and to all the participating patients, donors, and their families for their cooperation. No company had access to the data or participated in the analysis and discussion of results.

AUTHOR CONTRIBUTIONS

All authors contributed to at least one of the following manuscript preparation roles: conceptualization AND/OR methodology, software, investigation, formal analysis, data curation, visualization, and validation AND drafting or reviewing/editing the final draft. As corresponding author, Drs Chen and Sun confirm that all authors have provided the final approval of the version to be published, and takes responsibility for the affirmations regarding article submission (eg, not under consideration by another journal), the integrity of the data presented, and the statements regarding compliance with institutional review board/Declaration of Helsinki requirements.

REFERENCES

1. Jing C, Castro-Dopico T, Richoz N, et al. Macrophage metabolic reprogramming presents a therapeutic target in lupus nephritis. Proc Natl Acad Sci USA 2020;117(26):15160–15171.
2. Maria NI, Davidson A. Renal macrophages and dendritic cells in SLE nephritis. Curr Rheumatol Rep 2017;19(12):81.
3. Dias CB, Malafronte P, Lee J, et al. Role of renal expression of CD68 in the long-term prognosis of proliferative lupus nephritis. J Nephrol 2017;30(1):87–94.
4. Luan J, Fu J, Chen C, et al. LNA-anti-miR-150 ameliorated kidney injury of lupus nephritis by inhibiting renal fibrosis and macrophage infiltration. Arthritis Res Ther 2019;21(1):276.
5. Wada Y, Gonzalez-Sanchez HM, Weinmann-Menke J, et al. IL-34-dependent intrarenal and systemic mechanisms promote lupus nephritis in MRL-*Fas*^{lpr} mice. J Am Soc Nephrol 2019;30(2):244–259.
6. Zhang Z, Niu L, Tang X, et al. Mesenchymal stem cells prevent podocyte injury in lupus-prone B6.MRL-*Fas*^{lpr} mice via polarizing macrophage into an anti-inflammatory phenotype. Nephrol Dial Transplant 2019;34(4):597–605.
7. Broz P, Pelegrín P, Shao F. The gasdermins, a protein family executing cell death and inflammation. Nat Rev Immunol 2020;20(3):143–157.
8. Lopez-Castejon G, Brough D. Understanding the mechanism of IL-1β secretion. Cytokine Growth Factor Rev 2011;22(4):189–195.
9. Anders HJ. Of inflammasomes and alarmins: IL-1β and IL-1α in kidney disease. J Am Soc Nephrol 2016;27(9):25642575.
10. Weber A, Wasiliew P, Kracht M. Interleukin-1 (IL-1) pathway. Sci Signal 2010;3(105):cm1.
11. Dinarello CA. Biologic basis for interleukin-1 in disease. Blood 1996;87(6):2095–2147.
12. Kayagaki N, Stowe IB, Lee BL, et al. Caspase-11 cleaves gasdermin D for non-canonical inflammasome signalling. Nature 2015;526(7575):666–671.
13. Moretti J, Jia B, Hutchins Z, et al. Caspase-11 interaction with NLRP3 potentiates the noncanonical activation of the NLRP3 inflammasome. Nat Immunol 2022;23(5):705–717.
14. Rathinam VA, Vanaja SK, Waggoner L, et al. TRIF licenses caspase-11-dependent NLRP3 inflammasome activation by gram-negative bacteria. Cell 2012;150(3):606–619.
15. Broz P, Ruby T, Belhocine K, et al. Caspase-11 increases susceptibility to Salmonella infection in the absence of caspase-1. Nature 2012;490(7419):288–291.
16. Rönnblom L, Eloranta ML, Alm GV. The type I interferon system in systemic lupus erythematosus. Arthritis Rheum 2006;54(2):408–420.
17. Arazi A, Rao DA, Berthier CC, et al; Accelerating Medicines Partnership in SLE network. The immune cell landscape in kidneys of patients with lupus nephritis. Nat Immunol 2019;20(7):902–914.
18. Wang D, Niu L, Feng X, et al. Long-term safety of umbilical cord mesenchymal stem cells transplantation for systemic lupus erythematosus: a 6-year follow-up study. Clin Exp Med 2017;17(3):333–340.
19. Yuan X, Qin X, Wang D, et al. Mesenchymal stem cell therapy induces FLT3L and CD1c^{+} dendritic cells in systemic lupus erythematosus patients. Nat Commun 2019;10(1):2498.
20. Sun L, Huang J, Wang X, et al. Enucleated bone marrow-derived mesenchymal stromal cells regulate immune microenvironment and promote testosterone production through efferocytosis. Reprod Biol Endocrinol 2025;23(1):21.
21. Zhang QZ, Su WR, Shi SH, et al. Human gingiva-derived mesenchymal stem cells elicit polarization of m2 macrophages and enhance cutaneous wound healing. Stem Cells 2010;28(10):1856–1868.
22. Luz-Crawford P, Djouad F, Toupet K, et al. Mesenchymal stem cell-derived interleukin 1 receptor antagonist promotes macrophage polarization and inhibits B cell differentiation. Stem Cells 2016;34(2):483–492.
23. Hochberg MC. Updating the American College of Rheumatology revised criteria for the classification of systemic lupus erythematosus. Arthritis Rheum 1997;40(9):1725.
24. Weening JJ, D'Agati VD, Schwartz MM, et al; International Society of Nephrology Working Group on the Classification of Lupus Nephritis; Renal Pathology Society Working Group on the Classification of Lupus Nephritis. The classification of glomerulonephritis in systemic lupus erythematosus revisited. Kidney Int 2004;65(2):521–530.
25. Kikawada E, Lenda DM, Kelley VR. IL-12 deficiency in MRL-*Fas*^{lpr}) mice delays nephritis and intrarenal IFN-gamma expression, and diminishes systemic pathology. J Immunol 2003;170(7):3915–3925.
26. Ginhoux F, Jung S. Monocytes and macrophages: developmental pathways and tissue homeostasis. Nat Rev Immunol 2014;14(6):392–404.
27. Chen W, Li W, Zhang Z, et al. Lipocalin-2 exacerbates lupus nephritis by promoting Th1 cell differentiation. J Am Soc Nephrol 2020;31(10):2263–2277.
28. Lamkanfi M, Dixit VM. Mechanisms and functions of inflammasomes. Cell 2014;157(5):1013–1022.
29. Mende R, Vincent FB, Kandane-Rathnayake R, et al. Analysis of serum interleukin (IL)-1β and IL-18 in systemic lupus erythematosus. Front Immunol 2018;9:1250.
30. Jafari-Nakhjavani MR, Abedi-Azar S, Nejati B. Correlation of plasma interleukin-18 concentration and severity of renal involvement and disease activity in systemic lupus erythematosus. J Nephropathol 2016;5(1):28–33.
31. Wang D, Feng X, Lu L, et al. A CD8 T cell/indoleamine 2,3-dioxygenase axis is required for mesenchymal stem cell suppression of human systemic lupus erythematosus. Arthritis Rheumatol 2014;66(8):2234–2245.
32. Chen C, Liang J, Yao G, et al. Mesenchymal stem cells upregulate Treg cells via sHLA-G in SLE patients. Int Immunopharmacol 2017;44:234–241.
33. Baechler EC, Batliwalla FM, Karypis G, et al. Interferon-inducible gene expression signature in peripheral blood cells of patients with severe lupus. Proc Natl Acad Sci USA 2003;100(5):2610–2615.
34. Meunier E, Dick MS, Dreier RF, et al. Caspase-11 activation requires lysis of pathogen-containing vacuoles by IFN-induced GTPases. Nature 2014;509(7500):366–370.
35. Li Y, Jiang Q. Uncoupled pyroptosis and IL-1β secretion downstream of inflammasome signaling. Front Immunol 2023;14:1128358.
36. Angeletti A, Cantarelli C, Petrosyan A, et al. Loss of decay-accelerating factor triggers podocyte injury and glomerulosclerosis. J Exp Med 2020;217(9):e20191699.
37. Yano T, Nozaki Y, Kinoshita K, et al. The pathological role of IL-18Rα in renal ischemia/reperfusion injury. Lab Invest 2015;95(1):78–91.
38. Wright RD, Beresford MW. Podocytes contribute, and respond, to the inflammatory environment in lupus nephritis. Am J Physiol Renal Physiol 2018;315(6):F1683–F1694.
39. Wu M, Yang Z, Zhang C, et al. Inhibition of NLRP3 inflammasome ameliorates podocyte damage by suppressing lipid accumulation in diabetic nephropathy. Metabolism 2021;118:154748.
40. Zhang J, Zhang M, Huo X-K, et al. Macrophage inactivation by small molecule wedelolactone via targeting sEH for the treatment of LPS-induced acute lung injury. ACS Cent Sci. 2023;9(3):440–456.
41. Ebata T, Terkawi MA, Kitahara K, et al. Noncanonical pyroptosis triggered by macrophage-derived extracellular vesicles in chondrocytes leading to cartilage catabolism in osteoarthritis. Arthritis Rheumatol 2023;75(8):1358–1369.

42. Song M, Wang J, Sun Y, et al. Inhibition of gasdermin D-dependent pyroptosis attenuates the progression of silica-induced pulmonary inflammation and fibrosis. Acta Pharm Sin B 2022;12(3):1213–1224.

43. Fan R, Sui J, Dong X, et al. Wedelolactone alleviates acute pancreatitis and associated lung injury via GPX4 mediated suppression of pyroptosis and ferroptosis. Free Radic Biol Med 2021;173:29–40.

44. Ren G, Zhao X, Zhang L, et al. Inflammatory cytokine-induced intercellular adhesion molecule-1 and vascular cell adhesion molecule-1 in mesenchymal stem cells are critical for immunosuppression. J Immunol 2010;184(5):2321–2328.

45. Njoku CJ, Patrick KS, Ruiz P Jr, et al. Inducible nitric oxide synthase inhibitors reduce urinary markers of systemic oxidant stress in murine proliferative lupus nephritis. J Investig Med 2005;53(7):347–352.

46. Souza BSF, da Silva KN, Silva DN, et al. Galectin-3 knockdown impairs survival, migration, and immunomodulatory actions of mesenchymal stromal cells in a mouse model of chagas disease cardiomyopathy. Stem Cells Int 2017;2017:3282656.

47. Jiang Q, Li J, Pan Y, et al. Melatonin-primed MSCs alleviate intrauterine adhesions by affecting MSC-expressed galectin-3 on macrophage polarization. Stem Cells 2022;40(10):919–931.

48. Zhang ZT, Zhang DY, Xie K, et al. Luteolin activates Tregs to promote IL-10 expression and alleviating caspase-11-dependent pyroptosis in sepsis-induced lung injury. Int Immunopharmacol 2021; 99:107914.

49. Wang J, Ren H, Yuan X, et al. Interleukin-10 secreted by mesenchymal stem cells attenuates acute liver failure through inhibiting pyroptosis. Hepatol Res 2018;48(3):E194–E202.

Arthritis & Rheumatology
Vol. 78, No. 2, February 2026, pp 371–384
DOI 10.1002/art.43341

Prognostic Value of Lupus Anticoagulant and Anti–β2 Glycoprotein I Antibody in Adverse Pregnancy Outcomes

Megumi Nonobe,[1] Takahiro Otani,[2] Hiroyuki Yoshihara,[1,3] Shinobu Goto,[1] Tamao Kitaori,[1] Naomi Nishikawa,[4] Yuichiro Fujieda,[5] Tatsuya Atsumi,[5] and Mayumi Sugiura-Ogasawara[1]

Objective. International criteria for antiphospholipid syndrome (APS) include lupus anticoagulant (LA), anticardiolipin (aCL) IgG and IgM, and anti–β2-glycoprotein I (β2GPI) IgG and IgM. However, evidence supporting their prognostic value or treatment efficacy in improving live birth rates is limited. The *Lancet* series on miscarriage recommends testing only for LA and aCL, excluding β2GPI. We aimed to examine whether commercially available antiphospholipid antibody (aPL)-related tests have a prognostic value for obstetric APS.

Methods. This prospective cohort study enrolled 1,237 pregnant women between July 2021 and March 2024. Women using heparin, including those with an obstetric APS diagnosis before pregnancy, were excluded. Pregnancy outcomes were followed until December 2024. The aPL-related tests comprised LA (diluted activated partial prothrombin time and diluted Russell's viper venom time [LA-RVVT]), aCL IgG, IgM, anti-β2GPI IgG, IgM, anti β2GPI domain I IgG, phosphatidylserine-dependent antiprothrombin IgG, IgM, protein S, and coagulation factor XII activity.

Results. The prevalence rates of early-onset preeclampsia, intrauterine fetal death (IUFD), and small for gestational age were 1.4% (17), 0.7% (9), and 0.9% (11), respectively. Logistic regression analysis revealed that LA-RVVT and anti-β2GPI IgG were each predictor of early-onset preeclampsia and IUFD. The area under the curve for these conditions increased to about 0.8 when combined with a history of preeclampsia or IUFD, respectively.

Conclusion. LA-RVVT, anti-β2GPI IgG, complications including hypertension, and a history of IUFD were valuable in identifying obstetric APS. The variation in test results across facilities limits the ability to establish consistent prognostic or treatment value for each aPL.

INTRODUCTION

Obstetric antiphospholipid syndrome (APS) is clinically defined by recurrent early miscarriage; unexplained intrauterine fetal death (IUFD) of a morphologically normal fetus at or beyond 10 weeks' gestation; or one or more preterm births of a morphologically normal neonate before 34 weeks' gestation due to eclampsia, preeclampsia, or placental dysfunction.[1] APS is considered the most important treatable cause of recurrent pregnancy loss (RPL).[2,3] It is hypothesized to be more strongly associated with IUFD than early miscarriage. Noncriteria obstetric complications associated with APS include two consecutive early miscarriages; intrauterine fetal growth restriction (FGR); hemolysis, elevated liver enzymes, and low platelet count syndrome; placental abruption; and oligohydramnios. The overall stillbirth rate is approximately 0.8%, but APS-related IUFD is frequently accompanied by FGR and oligohydramnios, suggesting a pattern of chronic fetoplacental insufficiency.

To confirm a diagnosis of APS, the revised Sydney-Sapporo criteria require the presence of at least one clinical feature and the persistent presence of at least two types of lupus anticoagulant (LA), anticardiolipin (aCL) IgG/IgM, and/or anti–β2-glycoprotein I (β2GPI) IgG/IgM on two or more occasions at least 12 weeks apart.[1] These are referred to as the "criteria antiphospholipid antibody (aPL)."

Supported by the Ministry of Education, Culture, Sports, Science and Technology Promotion of Distinctive Joint Research Center Program (grant JPMXP0621467963).

[1]Department of Obstetrics and Gynecology, Nagoya City University Graduate School of Medical Sciences, Nagoya, Japan; [2]Department of Public Health, Nagoya City University Graduate School of Medical Sciences, Nagoya, Japan; [3]Division of Biomedical Sciences, Clinical Science Research Laboratories, Warwick Medical School, University of Warwick; [4]Department of Obstetrics and Gynecology, Nagoya City University, West Medical Center, Nagoya, Japan; [5]Department of Rheumatology, Endocrinology and Nephrology, Faculty of Medicine and Graduate School of Medicine, Hokkaido University, Sapporo, Japan.

Additional supplementary information cited in this article can be found online in the Supporting Information section (https://acrjournals.onlinelibrary.wiley.com/doi/10.1002/art.43341).

Author disclosures are available at https://onlinelibrary.wiley.com/doi/10.1002/art.43341.

Address correspondence via email to Mayumi Sugiura-Ogasawara, MD, PhD, at og.mym@med.nagoya-cu.ac.jp.

Submitted for publication May 19, 2025; accepted in revised form July 15, 2025.

In 1975, the first case of a woman with three instances of IUFD and LA was reported.[4] In the 1980s, IgG, IgA, and IgM were actively measured against cardiolipin, phosphatidylserine (PS), phosphatidylcholine, phosphatidic acid, phosphatidylinositol, and phosphatidylethanolamine by an enzyme-linked immunosorbent assay (ELISA).[5] In 1990, three independent research groups demonstrated that the true antigen of the aCL antibody was not CL but β2GPI.[6–8] aPL refers to a group of autoantibodies that bind directly to either phospholipids or phospholipid–protein complexes.[9] The primary antigenic targets are β2GPI and prothrombin. Consequently, a wide range of aPL assays are currently available through commercial testing services.

Although the efficacy of these aPLs has been demonstrated in studies of thrombotic APS, their utility in obstetric APS has not yet been established.[10] The *Lancet* reviews recommend the use of LA and aCL, but not anti-β2GPI, due insufficient evidence that test results have prognostic value or that treatment based on test results improves clinical outcomes.[3] In clinical practice in Japan, a wide range of additional aPL tests are randomly used to diagnose APS, and their evaluation varies across facilities. The use of newly available commercial assays has increased, despite the lack of sufficient evidence to support their clinical utility. Furthermore, protein S and coagulation factor XII (FXII) activity have been frequently measured in clinical practice in Japan due to the high prevalence of these deficiencies in the Japanese population, despite the lack of guideline recommendations for routine screening of hereditary thrombophilia.[3,10]

In 2023, the American College of Rheumatology (ACR)/EULAR proposed new APS classification criteria, whereby patients are classified as having APS as they accumulate at least three points each from the clinical and laboratory domains.[11] Under this system, three or more early miscarriages and at least one IUFD are each assigned one point. Consequently, patients with RPL who are positive for aPL may not meet the threshold for classification as obstetric APS. Notably, these criteria do not preclude the measurement of aPL outlined in the original Sapporo classification. Hence, this study aimed to examine whether any of the nine criteria and noncriteria aPL, as well as protein S and FXII activity, could serve as predictors of adverse pregnancy outcomes in pregnant women.

MATERIALS AND METHODS

Study design. The study participants comprised pregnant women who attended prenatal checkups at Nagoya City University Hospital and Nagoya City University West Medical Center from July 2021 to March 2024. Participants (1) whose gestational age at the time of recruitment did not exceed 12 weeks, (2) whose timing of blood test aligned with the routine prenatal health checkup, (3) who were required to be scheduled to give birth at one of the two designated facilities, and (4) who provided written informed were included in the study. Participants with a planned termination of pregnancy were excluded. The following medical data were obtained through interviews conducted by obstetricians: age; body mass index (BMI); marital status; employment status; smoking status; gestational age at sampling; a history of pregnancy, live births, miscarriages, stillbirths, and preeclampsia; a history of diseases; use of in vitro fertilization and embryo transfer; and administration of low-dose aspirin and heparin during pregnancy.

Blood samples were collected at the time of registration. The samples were centrifuged twice to remove platelets and subsequently stored at –80°C until analysis. The parameters measured included LA using diluted activated partial prothrombin time (LA-aPTT) and diluted Russell's viper venom time (LA-RVVT); aCL antibodies IgG and IgM; anti-β2GPI IgG and IgM; anti-β2GPI domain I IgG; PS-dependent antiprothrombin (aPS/PT) antibodies IgG and IgM; protein S; and FXII activity. All parameters were measured at the Werfen company. The aPS/PT IgG and IgM assays were conducted at Hokkaido University to evaluate potential discrepancies in measurement outcomes attributable to different laboratory facilities.

The pregnancy outcomes were prospectively monitored until December 2024. The study was approved by the Research Ethics Committee of Nagoya City University Graduate School of Medical Sciences and Nagoya City University, West Medical Center. Informed consent was obtained from each participant.

Measurement for LA, aCL antibodies, and anti-β2GPI antibodies. LA was measured using aPTT with HemosIL Silica clotting time (SCT) (Werfen Company). Additionally, diluted RVVT (dRVVT) was measured using HemosIL dRVVT screen and confirmatory assays (Werfen Company).[12–14]

LA-aPTT was calculated as follows: SCT normalized ratio = SCT screen patients (seconds)/SCT screen controls (seconds) ÷ SCT confirm patients (seconds)/SCT confirm controls (seconds). LA-RVVT was calculated as follows: dRVVT normalized ratio = dRVVT screen patients (seconds)/dRVVT screen controls (seconds) ÷ dRVVT confirm patients (seconds)/dRVVT confirm controls (seconds). Control plasma was obtained from nonpregnant, healthy women.

The chemiluminescent immunoassay was used for measurement of aCL IgG, aCL IgM, aβ2GPI IgG, and aβ2GPI IgM.[15] The measurement of aCL IgG and IgM was conducted using QUANTA Flash aCL IgG and QUANTA Flash aCL IgM (Werfen Company), respectively. Similarly, the measurement of anti-β2GPI IgG and IgM was performed using QUANTA Flash β2GPI IgG and QUANTA Flash β2GPI IgM (Werfen Company), respectively. Anti–domain I-β2 glycoprotein I IgG was measured with QUANTA Flash β2GPI-Domain 1 Chemiluminescence immunoassay (Werfen Company).[16]

Measurement for aPS/PT IgG and IgM. aPS/PT IgG and IgM antibodies were measured at both Werfen and Hokkaido

University to compare results obtained by different facilities. Werfen used the QUANTA Lite aPS/PT IgG ELISA and QUANTA Lite aPS/PT IgM ELISA kits for these measurements.[17]

At Hokkaido University, an in-house ELISA was employed to detect aPS/PT antibodies.[17] Briefly, nonirradiated microtiter plates (Sumilon type S; Sumitomo Bakelite) were coated with 30 mL of 50 mg/mL PS and dried overnight at 4°C. To prevent nonspecific protein binding, the wells were blocked with 150 mL of Tris-buffered saline (TBS) containing 1% fatty acid–free bovine serum albumin (BSA) (A-6003; Sigma) and 5 mM $CaCl_2$ (BSA-Ca). After three washes with TBS containing 0.05% Tween 20 (Sigma) and 5 mM $CaCl_2$, 50 mL of 10 mg/mL human prothrombin (Diagnostica Stago, Asnieres) in BSA-Ca was added to half the number of the plates, whereas the other half received 50 μL of BSA-Ca alone (sample blank). Following a one-hour incubation at 37°C, the plates were washed, and 50 mL of serum diluted in a 1:100 ratio in BSA-Ca was added in duplicate. The plates were then incubated for one hour at room temperature, followed by the addition of alkaline phosphatase–conjugated goat anti-human IgG and substrate. The optical density in wells containing PS alone was subtracted from that in wells containing the PS/PT complex. The titer of aPS/PT antibodies in each sample was derived from a standard curve generated using serial dilutions of a positive control. A normal range was established based on serum from 36 healthy controls, with cutoff values set at 2.0 units for IgG and 13 units for IgM (representing 5 SDs above the mean of controls). None of the patients showed IgA binding to the PS/PT complex; therefore, an IgA aPS/PT assay was not established.

Measurement of protein S and coagulation FXII activity. Protein S levels were measured using HemosIL protein S activity (Werfen).[18] Additionally, FXII activity was assessed with HemosIL FXII deficient plasma (Werfen).

Outcome measures. The primary outcomes were IUFD of a morphologically normal fetus between 10 and 34 weeks' gestation, early-onset preeclampsia, and placental insufficiency characterized by small for gestational age (SGA) according to the 2023 ACR/EULAR APS classification criteria.[11] The postnatal birth weight was considered indicative of growth restriction if it was below the 10th percentile for gestational age, in the absence of fetal-neonatal syndromes or genetic conditions associated with growth impairment. The evaluation of FGR was conducted using a standardized tool that calculates growth percentiles at birth, developed collaboratively by the Japanese Society for Pediatric Endocrinology, the Japanese Association for Human Auxology, and the Japan Society for Neonatal and Development.[19]

The perinatal outcomes included gestational age at delivery, mode of delivery, placental abruption, thrombosis, and other signs of placental dysfunction occurring before <34 weeks' gestation. Neonatal outcomes comprised body weight, sex, Apgar scores, and the presence of chromosomal and other congenital abnormalities. Relevant data were obtained from the medical records related to pregnancy termination.

Statistical analysis. Spearman's rank correlation coefficients were calculated to assess the relationships among gestational week at sampling, age, BMI, nine aPLs, protein S, and FXII. For variables significantly associated with gestational week,

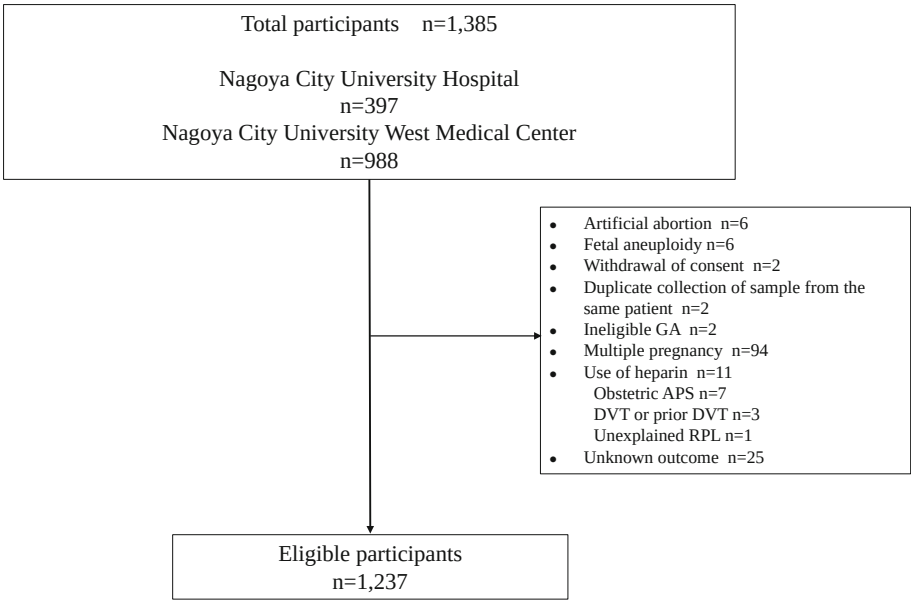

Figure 1. Flow diagram illustrating the participant selection process. APS, antiphospholipid syndrome; DVT, deep vein thrombosis; GA, gestational age; RPL, recurrent pregnancy loss.

adjusted values at seven weeks' gestation were estimated using the residual method based on linear regression models. Specifically, gestational week-adjusted values were obtained by adding the residuals from the regression of each test value on gestational week to the predicted value at seven weeks.

To evaluate whether the nine aPLs, protein S, and FXII could serve as predictors of preeclampsia, IUFD, and SGA, sensitivity and specificity were calculated using the recommended cutoff values for each biomarker. Receiver operating characteristic (ROC) curves were constructed, and the area under the curve (AUC) was calculated to assess their diagnostic performance.

Additionally, logistic regression analyses were performed using several adjustment models: age and BMI (model 1); age, BMI, and complications of systematic lupus erythematosus, hypertension, chronic kidney disease, and heart failure (model 2); age, BMI, complications, and a history of two or more early miscarriages and/or one or more IUFD and/or preeclampsia (model 3); age, BMI, complications, and a history of two or more early miscarriages (model 4); age, BMI, complications, and a history of IUFD (model 5); and age, BMI, complications, and a history of preeclampsia (model 6). To explore the combined diagnostic ability of test items and clinical characteristics, predicted probabilities of outcomes were calculated from each logistic regression model, and ROC curves along with AUC values were derived accordingly.

All statistical analyses were performed using R software (version 4.4.0). A two-sided *P* value of <0.05 was considered significant. Data are not publicly available. However, on reasonable request, data can be obtained from the corresponding author.

RESULTS

Participant characteristics. The total number of participants was 1,385, comprising 397 from Nagoya City University Hospital and 988 from Nagoya City University West Medical Center (Figure 1). Initially, the eligibility criteria were set for pregnancies less than 12 weeks' gestation but were revised in September 2022 to include pregnancies less than 34 weeks' gestation, due to delays in specimen collection. Meanwhile, 6 patients who opted for an artificial abortion after being enrolled, 6 with fetal aneuploidy, 2 who withdrew their consent, 2 whose samples were collected on two separate occasions, 2 beyond the eligible gestational age, 94 with multiple pregnancies, 11 with heparin use, including women with an obstetric APS diagnosis before pregnancy, and 25 with follow-up difficulties due to transfer or relocation were excluded from the study. Following the exclusion of these patients, 1,237 were included in the final analysis.

Table 1 presents the characteristics and previous pregnancy complications of the pregnant women. The median age was 33 years (range: 15–60), and the median BMI was 21.5 (range: 14.8–55.8). Gestational age at the time of sample collection was

Table 1. Maternal characteristics and pregnancy history of the study population (n = 1,237)*

Variables	Values
Age, y	
Median and range	33.0 (15–60)
<20, % (n)	1.0 (12)
20–29, % (n)	23.0 (285)
30–39, % (n)	61.1 (756)
≥40, % (n)	14.9 (184)
Missing, % (n)	0.0 (0)
BMI	
Median (range)	21.5 (14.8–55.8)
<18.5, % (n)	12.0 (149)
18.5–24.9, % (n)	66.7 (825)
≥25.0, % (n)	21.3 (263)
Missing, % (n)	0.0 (0)
Current smoker, % (n)	
Yes	4.4 (54)
No	95.6 (1,183)
Missing	0.0 (0)
Gestational weeks at sampling	
Median and range	11.3 (7.14–33.57)[a]
<10, % (n)	17.5 (216)
10–14, % (n)	61.4 (759)
15–19, % (n)	3.6 (44)
20–24, % (n)	9.0 (111)
25–29, % (n)	3.9 (48)
30–34, % (n)	4.8 (59)
Missing, % (n)	0.0 (0)
Presence of IVF-ET, % (n)	
Presence	28.2 (349)
Absence	71.8 (888)
Missing	0.0 (0)
History of live birth, % (n)	
Presence	50.9 (630)
Absence	49.1 (607)
Missing	0.0 (0)
Number of previous early miscarriages, % (n)	
0	73.1 (904)
1	19.0 (235)
2	5.2 (65)
3 or more	2.7 (33)
Missing	0.0 (0)
Number of previous intrauterine fetal deaths, % (n)	
0	96.0 (1,187)
1	3.8 (47)
2 or more	0.2 (3)
Missing	0.0 (0)
History of preeclampsia, % (n)	
Presence	1.4 (17)
Absence	98.6 (1,220)
Missing	0.0 (0)
Complications, % (n)	
Chronic hypertension	1.5 (19)
Chronic kidney disease[b]	0.3 (4)
Heart failure	0.1 (1)
Systematic lupus erythematosus	0.4 (5)
Missing	0.0 (0)
Low-dose aspirin use, % (n)	
Presence	2.0 (25)
Missing	0.0 (0)

* BMI, body mass index; IVF-ET, in vitro fertilization-embryo transfer.
[a] Equivalent to 7 wk 1 d to 33 wk 4 d.
[b] One woman experienced hypertension and kidney disease.

calculated by dividing the days by 7, with a median value of 11.3 (7 weeks 1 day [7.14] to 33 weeks 4 days [33.57]). Further analysis revealed that 65.5% of the samples were collected during the first trimester. Furthermore, 98 women (7.9%) had a history of two or more early miscarriages confirmed within 12 weeks, 50 women (4%) had a history of one or more IUFD beyond 12 weeks, and 17 (1.4%) participants had a history of preeclampsia.

Results of antiphospholipid antibodies. LA-aPTT demonstrated a significant decrease with advancing gestational week (r = –0.3; Figure 2A). Conversely, LA-RVVT and FXII exhibited a notable increase as gestational weeks progressed (r = 0.2 and 0.36). To account for these variations, the results of these tests were corrected based on gestational age and adjusted to seven weeks' gestation. Scatter plots of all aPL-related tests are provided in Supplementary Figure 1.

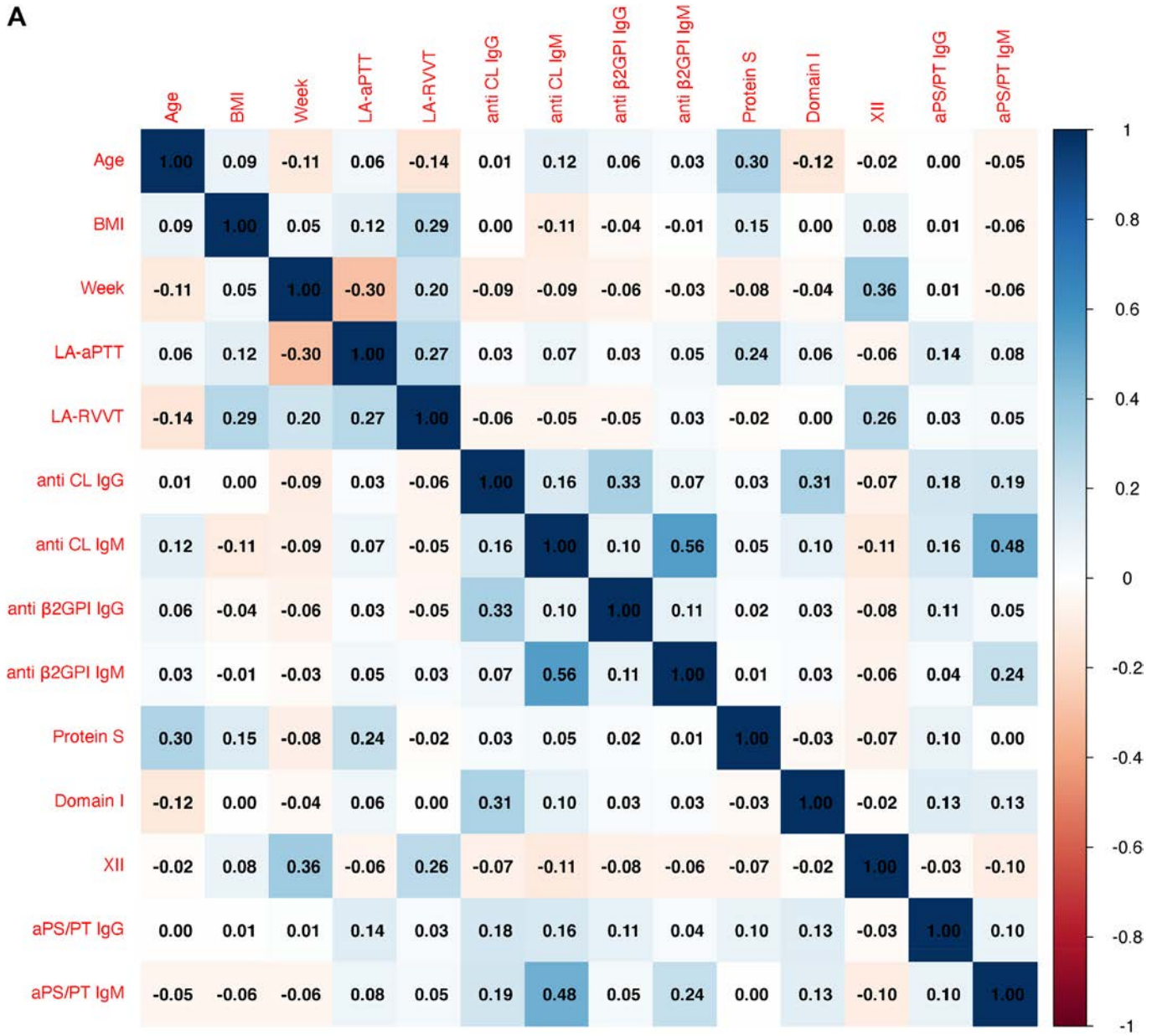

Figure 2. Thefollowing relationships are investigated: those among gestational week at sampling, age, BMI, nine antiphospholipid antibodies, protein S, and FXII. (A) Associations before adjustment. Positive correlation coefficients are indicated in blue, and negative correlation coefficients are indicated in red. (B) Linkage, BMI, gestational age at sampling, and antiphospholipid antibody levels following adjustment for estimated values at seven weeks' gestation. Because LA-aPTT, LA-RVVT, and XII were associated with weeks' gestation, their values were corrected to values at seven weeks' gestation and the correlation was examined. week refers to gestational week. β2GPI, β2-glycoprotein I; aPS/PT, phosphatidylserine-dependent antiprothrombin; BMI, body mass index; CL, cardiolipin; Domain I, anti-Domain I IgG; FXII, factor XII; LA-aPTT, lupus anticoagulant by activated partial prothrombin time; LA-RVVT, lupus anticoagulant by diluted Russell's viper venom time.

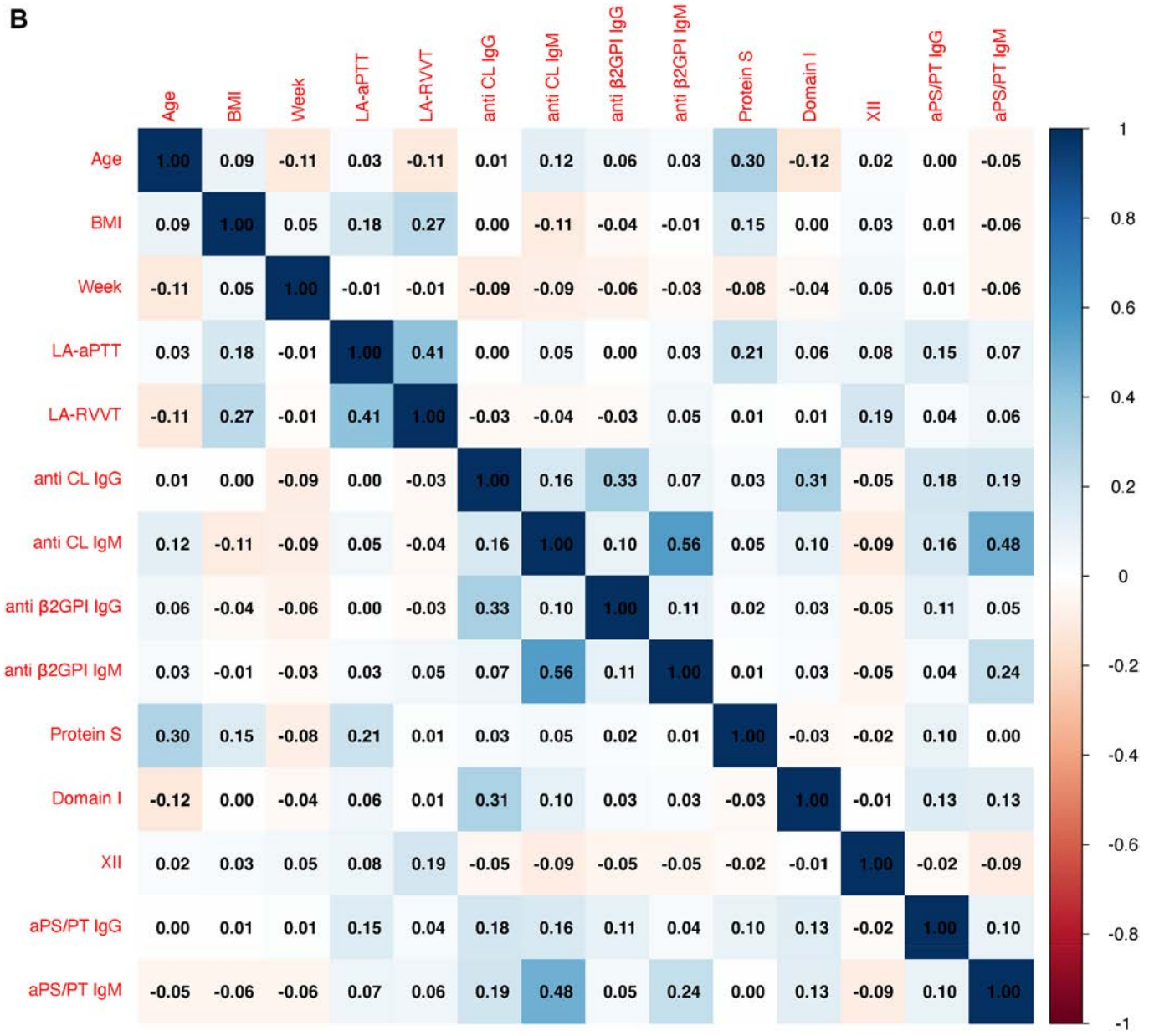

Figure 2. (Continued)

The significant decrease in LA-aPTT was attributed to a reduction in the SCT screen time (seconds) among patients (Supplementary Table 1). The increase in LA-RVVT was due to the shortening of the dRVVT confirmation time (seconds) (Figure 2B). The regression coefficients for week-adjusted analyses were −0.006 (95% confidence interval [CI] −0.007 to −0.005; $P < 0.001$) for LA-aPTT, 0.004 (95% CI 0.003 to 0.005; $P < 0.001$) for LA-RVVT, and 2.124 (95% CI 1.805 to 2.443; $P < 0.001$) for FXII. Positive associations were identified between LA-aPTT and LA-RVVT ($r = 0.41$), aCL IgG and anti-β2GPI IgG ($r = 0.33$), aCL IgM and anti-β2GPI IgM ($r = 0.56$), and aCL IgM and aPS/PT IgM ($r = 0.48$). The correlation coefficients of LA-aPTT ($r = -0.3$) and LA-RVVT ($r = 0.2$) were reduced to −0.01 and 0.01, respectively, after adjustment for gestational weeks.

The measurement of aPS/PT IgG and IgM was conducted by the Werfen company and Hokkaido University. The prevalence rates of aPS/PT IgG and IgM were 0.16% (n = 2) and 5.0% (n = 62), respectively, according to the findings from Werfen. By contrast, Hokkaido University reported prevalence rates of 0.24% (n = 3) and 0%, respectively. Notably, patients with positive aPS/PT IgG test results exhibited significant differences between the two laboratories. Consequently, the results of aPS/PT IgG and IgM were analyzed based on the data obtained from Werfen.

Table 2. Sensitivity and specificity (95% confidence intervals) of commercially performed tests using manufacturer-provided reference values*

Method	Reference value	Interquartile range			Sensitivity			Specificity		
		25th	50th	75th	Early-onset preeclampsia	Intrauterine fetal death	Small for gestational age	Early-onset preeclampsia	Intrauterine fetal death	Small for gestational age
LA-aPTT	Normalized ratio >1.16	0.92	0.99	1.05	0.12 (0.01–0.36)	0.00 (0.00–0.34)	0.05 (0.01–0.10)	0.92 (0.90–0.94)	0.92 (0.90–0.93)	0.92 (0.90–0.93)
LA-RVVT	Normalized ratio >1.2	1.02	1.07	1.13	0.18 (0.04–0.43)	0.11 (0.00–0.48)	0.10 (0.05–0.17)	0.94 (0.92–0.95)	0.94 (0.92–0.95)	0.94 (0.92–0.95)
Anti-CL IgG	20	2.9	4.8	8.1	0.06 (0.00–0.29)	0.00 (0.00–0.34)	0.04 (0.01–0.09)	0.95 (0.94–0.97)	0.95 (0.94–0.97)	0.95 (0.94–0.97)
Anti-CL IgM	20	1.7	2.5	3.7	0.00 (0.00–0.20)	0.00 (0.00–0.34)	0.00 (0.00–0.03)	1.00 (0.99–1.00)	1.00 (0.99–1.00)	1.00 (0.99–1.00)
Anti-β2GPI IgG	20	3.2	3.2	7.6	0.00 (0.00–0.20)	0.11 (0.00–0.48)	0.02 (0.00–0.06)	0.99 (0.98–0.99)	0.99 (0.98–0.99)	0.99 (0.98–0.99)
Anti-β2GPI IgM	20	0.55	0.55	1.4	0.00 (0.00–0.20)	0.00 (0.00–0.34)	0.00 (0.00–0.03)	1.00 (0.99–1.00)	1.00 (0.99–1.00)	1.00 (0.99–1.00)
Protein S	63.5–149	33.65	43.2	55.15	0.94 (0.71–1.00)	0.67 (0.30–0.93)	0.90 (0.83–0.95)	0.16 (0.14–0.18)	0.16 (0.14–0.18)	0.16 (0.14–0.19)
Domain I	20	1.8	1.8	1.8	0.06 (0.00–0.29)	0.11 (0.00–0.48)	0.02 (0.00–0.06)	0.97 (0.96–0.98)	0.97 (0.96–0.98)	0.97 (0.96–0.98)
XII	50–150	85.85	110.3	132.5	0.06 (0.00–0.29)	0.00 (0.00–0.34)	0.04 (0.01–0.09)	0.95 (0.94–0.96)	0.95 (0.94–0.96)	0.95 (0.93–0.96)
aPS/PT IgG	30	4.42	5.42	6.94	0.00 (0.00–0.20)	0.00 (0.00–0.34)	0.00 (0.00–0.03)	1.00 (0.99–1.00)	1.00 (0.99–1.00)	1.00 (0.99–1.00)
aPS/PT IgM	30	8.2	11.92	16.92	0.06 (0.00–0.29)	0.00 (0.00–0.34)	0.03 (0.01–0.08)	0.95 (0.94–0.96)	0.95 (0.94–0.96)	0.95 (0.93–0.96)

* β2GPI, β2-glycoprotein I; aPS/PT, phosphatidylserine-dependent antiprothrombin; CL, cardiolipin; Domain I, anti-domain I IgG; LA-aPTT, lupus anticoagulant by diluted activated partial prothrombin time; LA-RVVT, LA by diluted Russell's viper venom time.

The sensitivity and specificity of each test for early-onset preeclampsia, IUFD, and SGA are presented in Table 2. The majority of the tests exhibited low sensitivity and high specificity, except for protein S. Low protein S activity demonstrated high sensitivity for early-onset preeclampsia (0.94) and SGA (0.90).

Pregnancy outcomes. The prevalence rates observed were 1.4% (17 patients) for early-onset preeclampsia, 0.7% (9 patients) for IUFD, and 0.9% (11 patients) for SGA. Nine women with IUFD between 11 and 30 weeks' gestation exhibited no features of preeclampsia.

Six of the 19 women (31.6%) with chronic hypertension subsequently developed early-onset preeclampsia. Another 6 of the 19 women (31.6%) were positive for LA-RVVT, and 3 of these 6 women developed preeclampsia. The ROC curves for each test related to early-onset preeclampsia, IUFD, and SGA are presented in Figure 3 A–C.

LA-RVVT demonstrated predictive capability for preeclampsia (Table 3). After adjustment across models 1–6, LA-RVVT remained a marginally independent predictor. The AUC for LA-RVVT was consistently approximately 0.8 across all models.

Anti-β2GPI IgG was predictive of IUFD. Its predictive value remained significant after adjustment across all models, as demonstrated using logistic regression analysis. The AUC for anti-β2GPI IgG increased to approximately 0.80 in model 5, which included previous IUFD.

Lower aPS/PT IgM levels were predictive of SGA and served as an independent predictor following adjustment in models 1–5. The AUC of aPS/PT IgM was consistently around 0.6 across all models. The ROC curves for LA-RVVT in predicting early-onset preeclampsia and anti-β2GPI IgG in predicting IUFD, based on logistic regression in model 6 and model 5, are shown in Figure 3D and E.

DISCUSSION

LA-RVVT and anti-β2GPI IgG demonstrated predictive value for early-onset preeclampsia and IUFD, respectively, in 1,237 pregnant women including 165 pregnant women with a history of at least one obstetric APS feature. The AUC for LA-RVVT was approximately 0.8 across all models. By contrast, the AUC for anti-β2GPI IgG increased among women with a history of IUFD.

The Sapporo classification criteria recommend assessing at least two types of LA, aCL IgG and IgM, and anti-β2GPI IgG and IgM, with the 99th percentile established as the cutoff threshold for healthy individuals.[1] The classification criteria recommend following International Society of Thrombosis and Haemostasis guidelines which call for "screening" for LA using two assays.[20] The present study demonstrated that aCL IgG and IgM and anti-β2GPI IgM lack clinical utility in obstetric APS, irrespective of reference values. The 2023 ACR/EULAR APS classification criteria did not oppose the measurement of aPL antibodies recommended in

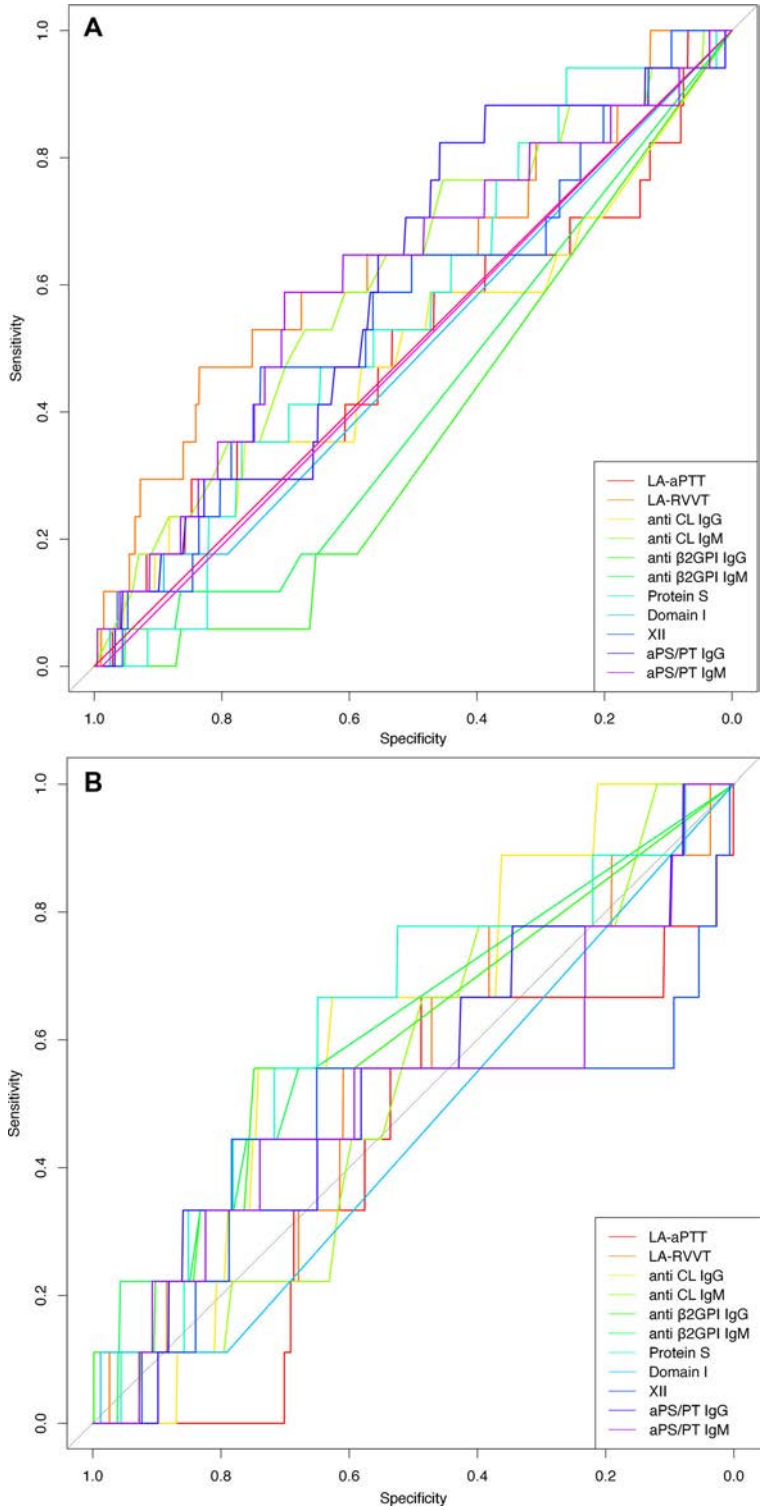

Figure 3. ROC curve for pregnancy outcomes. (A) ROC curve analysis of all antibody tests for early-onset preeclampsia. (B) ROC curve analysis of all antibody tests for IUFD. (C) ROC curve analysis of all antibody tests for SGA neonates. (D) ROC curves comparing LA-RVVT alone; LA-RVVT combined with age and BMI; LA-RVVT combined with age, BMI, and complications; and LA-RVVT combined with age, BMI, complications, and a history of IUFD for predicting early-onset preeclampsia. (E) ROC curves comparing anti-β2GPI IgG alone; anti-β2GPI IgG combined with age and BMI; anti-β2GPI IgG combined with age, BMI, and complications; anti-β2GPI IgG combined with age, BMI, complications, and a history of IUFD. β2GPI, β2-glycoprotein I; aPS/PT, phosphatidylserine-dependent antiprothrombin; BMI, body mass index; CL, cardiolipin; Domain I, anti-Domain I IgG; IUFD, intrauterine fetal death; LA-aPTT, lupus anticoagulant by diluted activated partial prothrombin time; LA-RVVT, LA by diluted Russell's viper venom time; ROC, receiver operating characteristic; SGA, small for gestational age.

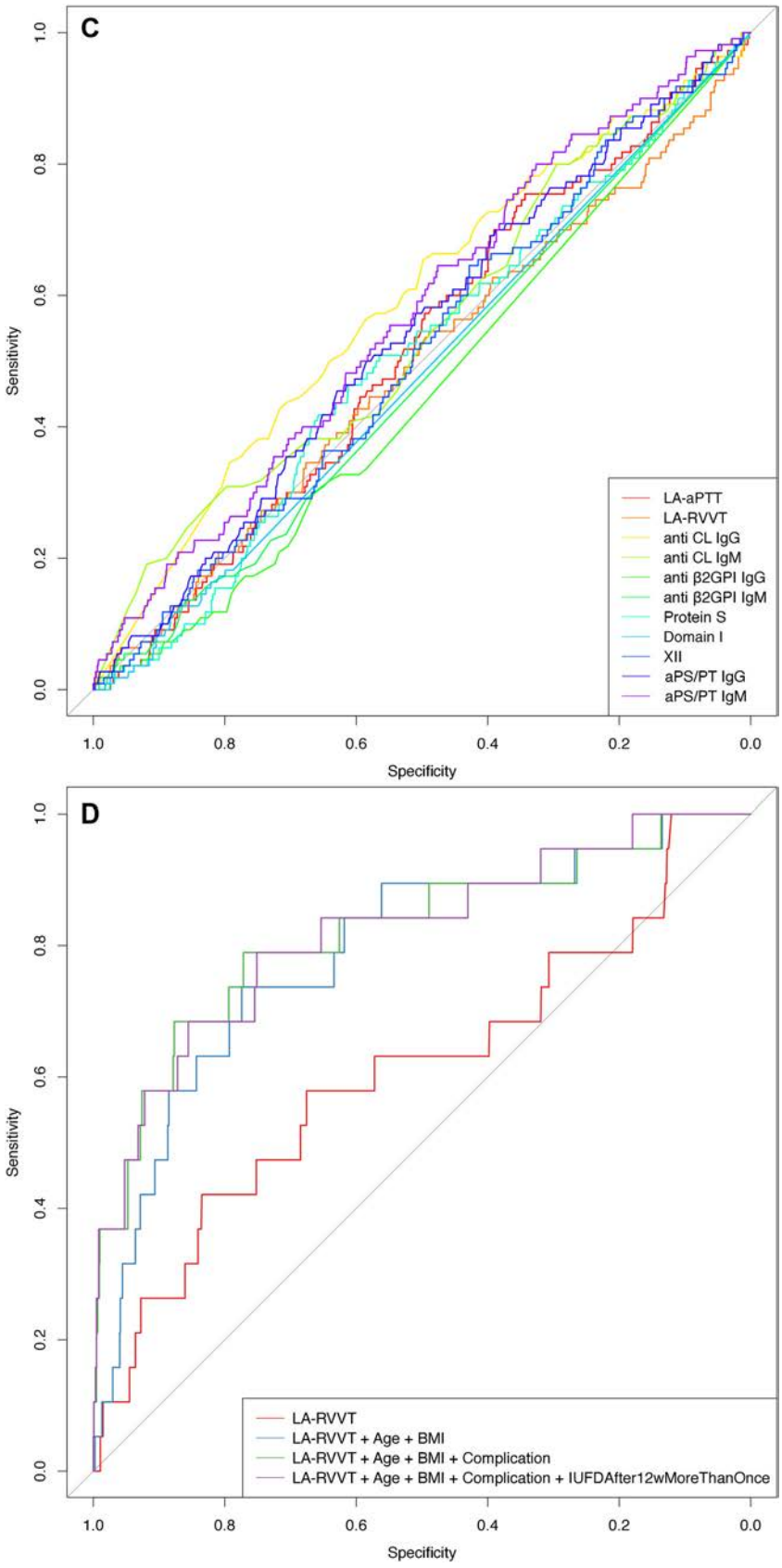

Figure 3. (Continued)

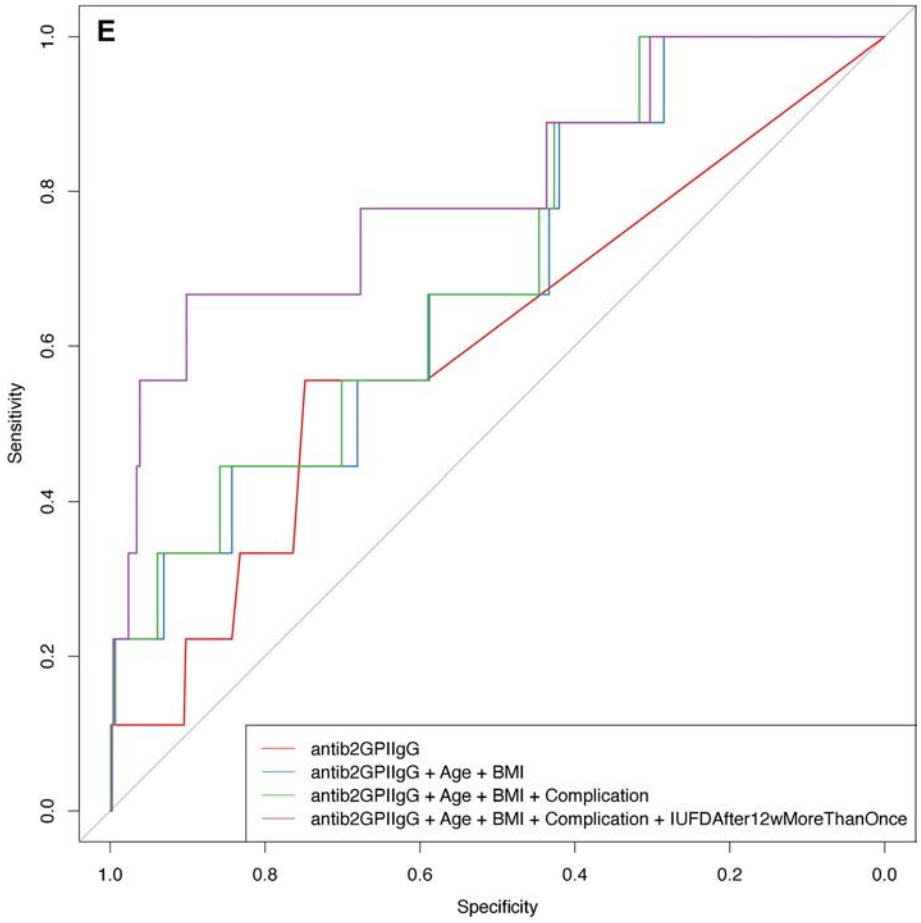

Figure 3. (Continued)

the Sapporo classification criteria.[11] Both the *Lancet* series and the European Society of Human Reproduction and Embryology RPL recommend measuring LA and aCL, but not anti-β2GPI, due to insufficient evidence supporting the prognostic value of anti-β2GPI or the effectiveness of treatment based on its results.[3,10] The prognostic value of anti-β2GPI IgG was established in the present study. The measurement of aPL in obstetric practice serves the goal of improving live birth rates in patients with RPL. Prospective studies remain necessary to determine whether the anticoagulant treatment can improve the live birth rate in patients with positive for anti-β2GPI IgG.

According to the ACR/EULAR APS classification criteria, classification as APS requires the accumulation of at least three points from the clinical and laboratory domains.[11] A history of three or more early miscarriages or one or more IUFDs is each assigned one point. Consequently, aPL-positive patients with RPL may not fulfill the criteria for obstetric APS. Major RPL guidelines recommend the measurement of aPLs, regardless of the antibody type.[3,10] In model 5, which included a history of IUFD, the AUC of anti-β2GPI IgG reached 0.80. A recent systematic review investigating the predictors in systemic lupus erythematosus (SLE) reported that secondary APS was associated with a reduced probability of live birth (0.40, 95% CI 0.27–0.58), an increased risk of pregnancy loss after 20 weeks' gestation (2.77, 95% CI 1.44–5.31), and a higher likelihood of preterm birth (1.65, 95% CI 1.29–2.11).[21] Inclusion of a history of one or more IUFDs should be considered essential in the diagnosis of APS.

As established in previous studies,[22] hypertension also influences preeclampsia in the present study. The prevalence of LA-RVVT was higher among women with chronic hypertension. The findings of this study are limited by modest sample size, necessitating additional research to substantiate these results.

The measurement of LA has been considered important in the evaluation of obstetric APS.[3,23,24] However, the optimal type of LA assay for clinical use has not yet been established. In a previous study, LA-aPTT (StaClot assay) and aPS/PT IgG measured at Hokkaido University, but not aCL IgG measured by Phadia, demonstrated treatment relevance, as anticoagulant therapy improved live birth rates in patients with RPL.[25] In the present study, LA-RVVT, but not LA-aPTT, demonstrated predictive value for features of APS. This finding may be explained by a significant decrease in LA-aPTT results caused by the shortening of the SCT screen phase and a significant increase in LA-RVVT results due to the shortening of the dRVVT confirm phase (Supplementary

Table 3. Logistic regression and area under the curve for pregnancy outcomes*

	Logistic regression odds ratio (95% CI)							Area under curve						
Outcomes	Crude	Model 1: Age and BMI	Model 2: Age, BMI and complications	Model 3: Age, BMI, complications, and 3 pregnancy histories	Model 4: Age, BMI, complications, and a history of 2+ early miscarriages	Model 5: Age, BMI, complications, and a history of 1+ IUFD	Model6: Age, BMI, complications, and a history of preeclampsia	Crude	Model 1: Age and BMI	Model 2: Age, BMI, and complications	Model 3: Age, BMI, complications, and 3 pregnancy histories	Model 4: Age, BMI, complications, and a history of 2+ early miscarriages	Model 5: Age, BMI, complications, and a history of 1+ IUFD	Model 6: Age, BMI, complications, and a history of preeclampsia
Early-onset preeclampsia														
LA-aPTT	1.07 (0.66–1.74), *P* = 0.773	0.97 (0.58–1.63), *P* = 0.916	0.87 (0.53–1.44), *P* = 0.595	0.86 (0.52–1.43), *P* = 0.565	0.85 (0.51–1.42), *P* = 0.533	0.87 (0.53–1.44), *P* = 0.599	0.86 (0.52–1.44), *P* = 0.573	0.51 (0.35–0.51)	0.72 (0.58–0.72)	0.80 (0.67–0.80)	0.81 (0.69–0.81)	0.81 (0.69–0.81)	0.81 (0.69–0.81)	0.80 (0.67–0.80)
LA-RVVT	**1.72 (1.10–2.69), *P* = 0.018**	**1.64 (1.02–2.64), *P* = 0.040**	**1.47 (0.90–2.39), *P* = 0.122**	**1.48 (0.90–2.41), *P* = 0.120**	**1.44 (0.88–2.35), *P* = 0.147**	**1.58 (0.94–2.65), *P* = 0.081**	**1.44 (0.88–2.36), *P* = 0.148**	**0.63 (0.48–0.63)**	**0.77 (0.65–0.77)**	**0.80 (0.67–0.80)**	**0.80 (0.67–0.80)**	**0.81 (0.69–0.81)**	**0.80 (0.68–0.80)**	**0.81 (0.68–0.81)**
Anti-CL IgG	1.02 (0.96–1.08), *P* = 0.505	1.02 (0.96–1.08), *P* = 0.508	1.02 (0.96–1.09), *P* = 0.536	1.02 (0.96–1.09), *P* = 0.548	1.02 (0.96–1.08), *P* = 0.557	1.02 (0.96–1.09), *P* = 0.545	1.02 (0.96–1.09), *P* = 0.503	0.50 (0.34–0.50)	0.73 (0.59–0.73)	0.81 (0.68–0.81)	0.81 (0.68–0.81)	0.82 (0.69–0.82)	0.82 (0.69–0.82)	0.81 (0.68–0.81)
Anti-CL IgM	0.81 (0.58–1.13), *P* = 0.222	0.83 (0.60–1.16), *P* = 0.280	0.87 (0.63–1.20), *P* = 0.391	0.86 (0.62–1.20), *P* = 0.379	0.86 (0.61–1.20), *P* = 0.366	0.87 (0.63–1.20), *P* = 0.402	0.86 (0.62–1.20), *P* = 0.383	0.61 (0.47–0.61)	0.72 (0.58–0.72)	0.80 (0.66–0.80)	0.81 (0.67–0.81)	0.81 (0.68–0.81)	0.81 (0.68–0.81)	0.80 (0.66–0.80)
Anti-β2GPI IgG	0.78 (0.60–1.01), *P* = 0.062	0.77 (0.59–1.00), *P* = 0.052	0.78 (0.59–1.02), *P* = 0.073	0.78 (0.59–1.02), *P* = 0.071	0.78 (0.59–1.02), *P* = 0.072	0.78 (0.59–1.02), *P* = 0.072	0.78 (0.60–1.03), *P* = 0.079	0.63 (0.54–0.63)	0.77 (0.64–0.77)	0.84 (0.73–0.84)	0.84 (0.74–0.84)	0.85 (0.74–0.85)	0.84 (0.74–0.84)	0.84 (0.73–0.84)
Anti-β2GPI IgM	0.76 (0.42–1.36), *P* = 0.350	0.77 (0.43–1.38), *P* = 0.377	0.77 (0.43–1.37), *P* = 0.376	0.77 (0.43–1.37), *P* = 0.369	0.77 (0.43–1.37), *P* = 0.367	0.78 (0.44–1.37), *P* = 0.383	0.77 (0.43–1.37), *P* = 0.378	0.58 (0.49–0.58)	0.72 (0.58–0.72)	0.82 (0.69–0.82)	0.82 (0.70–0.82)	0.83 (0.71–0.83)	0.82 (0.70–0.82)	0.81 (0.69–0.81)
Protein S	1.00 (0.98–1.03), *P* = 0.858	0.99 (0.96–1.01), *P* = 0.315	0.99 (0.96–1.02), *P* = 0.371	0.99 (0.96–1.02), *P* = 0.365	0.99 (0.96–1.02), *P* = 0.348	0.99 (0.96–1.02), *P* = 0.373	0.99 (0.96–1.02), *P* = 0.340	0.55 (0.43–0.55)	0.72 (0.58–0.72)	0.79 (0.66–0.79)	0.79 (0.67–0.79)	0.80 (0.68–0.80)	0.80 (0.67–0.80)	0.79 (0.66–0.79)
Domain I	1.00 (0.96–1.04), *P* = 0.959	1.00 (0.97–1.04), *P* = 0.873	1.00 (0.95–1.05), *P* = 0.924	1.00 (0.95–1.05), *P* = 0.911	1.00 (0.95–1.05), *P* = 0.918	1.00 (0.95–1.05), *P* = 0.904	1.00 (0.95–1.05), *P* = 0.939	0.51 (0.40–0.51)	0.72 (0.59–0.72)	0.80 (0.66–0.80)	0.80 (0.67–0.80)	0.81 (0.68–0.81)	0.81 (0.68–0.81)	0.80 (0.66–0.80)
XII	1.00 (0.99–1.01), *P* = 0.526	1.00 (0.99–1.01), *P* = 0.619	1.00 (0.99–1.02), *P* = 0.883	1.00 (0.99–1.02), *P* = 0.897	1.00 (0.99–1.01), *P* = 0.910	1.00 (0.99–1.02), *P* = 0.869	1.00 (0.99–1.02), *P* = 0.884	0.56 (0.42–0.56)	0.73 (0.60–0.73)	0.80 (0.67–0.80)	0.80 (0.68–0.80)	0.81 (0.69–0.81)	0.81 (0.68–0.81)	0.80 (0.66–0.80)
aPS/PT IgG	0.90 (0.71–1.16), *P* = 0.430	0.89 (0.69–1.16), *P* = 0.400	0.84 (0.64–1.11), *P* = 0.216	0.84 (0.64–1.11), *P* = 0.216	0.84 (0.64–1.10), *P* = 0.207	0.84 (0.64–1.11), *P* = 0.229	0.84 (0.63–1.11), *P* = 0.209	0.60 (0.47–0.60)	0.72 (0.58–0.72)	0.80 (0.66–0.80)	0.80 (0.66–0.80)	0.81 (0.67–0.81)	0.81 (0.68–0.81)	0.80 (0.66–0.80)
aPS/PT IgM	0.96 (0.89–1.03), *P* = 0.275	0.97 (0.90–1.04), *P* = 0.386	0.97 (0.91–1.05), *P* = 0.469	0.97 (0.91–1.05), *P* = 0.467	0.97 (0.91–1.05), *P* = 0.473	0.97 (0.91–1.05), *P* = 0.460	0.97 (0.91–1.05), *P* = 0.472	0.61 (0.46–0.61)	0.72 (0.59–0.72)	0.79 (0.66–0.79)	0.80 (0.68–0.80)	0.81 (0.69–0.81)	0.80 (0.68–0.80)	0.79 (0.66–0.79)
Intrauterine fetal death														
LA-aPTT	0.55 (0.26–1.14), *P* = 0.109	0.51 (0.25–1.06), *P* = 0.070	0.51 (0.25–1.05), *P* = 0.067	0.51 (0.25–1.06), *P* = 0.070	0.51 (0.25–1.05), *P* = 0.067	0.54 (0.27–1.10), *P* = 0.091	0.51 (0.25–1.05), *P* = 0.068	0.42 (0.23–0.42)	0.73 (0.56–0.73)	0.73 (0.57–0.73)	0.80 (0.66–0.80)	0.76 (0.62–0.76)	0.84 (0.70–0.84)	0.74 (0.58–0.74)
LA-RVVT	1.16 (0.57–2.38), *P* = 0.678	1.18 (0.56–2.48), *P* = 0.666	1.19 (0.57–2.50), *P* = 0.647	1.23 (0.58–2.61), *P* = 0.595	1.16 (0.56–2.42), *P* = 0.691	1.29 (0.61–2.72), *P* = 0.505	1.19 (0.57–2.49), *P* = 0.643	0.54 (0.34–0.54)	0.70 (0.53–0.70)	0.71 (0.54–0.71)	0.76 (0.63–0.76)	0.74 (0.58–0.74)	0.81 (0.67–0.81)	0.71 (0.55–0.71)
Anti-CL IgG	1.01 (0.92–1.10), *P* = 0.906	1.01 (0.92–1.10), *P* = 0.887	1.01 (0.92–1.10), *P* = 0.897	1.01 (0.92–1.11), *P* = 0.899	1.01 (0.92–1.10), *P* = 0.909	1.00 (0.91–1.11), *P* = 0.965	1.01 (0.92–1.10), *P* = 0.900	0.62 (0.46–0.62)	0.67 (0.49–0.67)	0.68 (0.51–0.68)	0.75 (0.59–0.75)	0.72 (0.56–0.72)	0.80 (0.63–0.80)	0.69 (0.51–0.69)
Anti-CL IgM	0.97 (0.72–1.30), *P* = 0.818	0.97 (0.72–1.30), *P* = 0.841	0.96 (0.70–1.31), *P* = 0.791	0.96 (0.69–1.32), *P* = 0.786	0.96 (0.71–1.31), *P* = 0.802	0.95 (0.68–1.34), *P* = 0.779	0.96 (0.70–1.31), *P* = 0.791	0.52 (0.35–0.52)	0.68 (0.50–0.68)	0.69 (0.52–0.69)	0.76 (0.60–0.76)	0.73 (0.57–0.73)	0.80 (0.64–0.80)	0.70 (0.53–0.70)
Anti-β2GPI IgG	**1.05 (1.01–1.10), *P* = 0.008**	**1.05 (1.01–1.09), *P* = 0.015**	**1.05 (1.01–1.09), *P* = 0.018**	**1.05 (1.01–1.10), *P* = 0.012**	**1.05 (1.01–1.09), *P* = 0.022**	**1.05 (1.01–1.10), *P* = 0.010**	**1.05 (1.01–1.09), *P* = 0.019**	**0.60 (0.41–0.60)**	**0.69 (0.51–0.69)**	**0.70 (0.52–0.70)**	**0.77 (0.59–0.77)**	**0.73 (0.57–0.73)**	**0.80 (0.63–0.80)**	**0.70 (0.53–0.70)**

(Continued)

Table 3. (*Cont'd*)

	Logistic regression odds ratio (95% CI)							Area under curve						
Outcomes	Crude	Model 1: Age and BMI	Model 2: Age, BMI and complications	Model 3: Age, BMI, complications, and 3 pregnancy histories	Model 4: Age, BMI, complications, and a history of 2+ early miscarriages	Model 5: Age, BMI, complications, and a history of 1+ IUFD	Model6: Age, BMI, complications, and a history of preeclampsia	Crude	Model 1: Age and BMI	Model 2: Age, BMI, and complications	Model 3: Age, BMI, complications, and 3 pregnancy histories	Model 4: Age, BMI, complications, and a history of 2+ early miscarriages	Model 5: Age, BMI, complications, and a history of 1+ IUFD	Model 6: Age, BMI, complications, and a history of preeclampsia
Anti-β2GPI IgM	1.02 (0.91–1.15), *P* = 0.709	1.02 (0.91–1.15), *P* = 0.692	1.02 (0.91–1.15), *P* = 0.710	1.03 (0.91–1.16), *P* = 0.679	1.02 (0.91–1.15), *P* = 0.718	1.03 (0.92–1.16), *P* = 0.625	1.02 (0.91–1.15), *P* = 0.707	0.61 (0.43–0.61)	0.67 (0.48–0.67)	0.68 (0.50–0.68)	0.75 (0.59–0.75)	0.72 (0.56–0.72)	0.80 (0.63–0.80)	0.69 (0.51–0.69)
Protein S	1.02 (0.99–1.05), *P* = 0.319	1.00 (0.97–1.04), *P* = 0.834	1.00 (0.97–1.04), *P* = 0.875	1.00 (0.97–1.04), *P* = 0.929	1.00 (0.97–1.04), *P* = 0.816	1.00 (0.97–1.04), *P* = 0.916	1.00 (0.97–1.04), *P* = 0.876	0.63 (0.43–0.63)	0.67 (0.49–0.67)	0.68 (0.51–0.68)	0.75 (0.60–0.75)	0.72 (0.57–0.72)	0.80 (0.63–0.80)	0.69 (0.51–0.69)
Domain I	1.01 (0.97–1.04), *P* = 0.706	1.01 (0.98–1.04), *P* = 0.557	1.01 (0.98–1.04), *P* = 0.538	1.01 (0.98–1.04), *P* = 0.523	1.01 (0.98–1.04), *P* = 0.531	1.01 (0.98–1.04), *P* = 0.423	1.01 (0.98–1.04), *P* = 0.529	0.46 (0.33–0.46)	0.67 (0.47–0.67)	0.68 (0.49–0.68)	0.75 (0.59–0.75)	0.72 (0.55–0.72)	0.80 (0.63–0.80)	0.69 (0.50–0.69)
XII	0.99 (0.97–1.02), *P* = 0.541	0.99 (0.97–1.01), *P* = 0.486	0.99 (0.97–1.02), *P* = 0.526	0.99 (0.97–1.02), *P* = 0.597	0.99 (0.97–1.01), *P* = 0.483	0.99 (0.97–1.02), *P* = 0.584	0.99 (0.97–1.02), *P* = 0.517	0.46 (0.20–0.46)	0.68 (0.49–0.68)	0.69 (0.51–0.69)	0.76 (0.60–0.76)	0.73 (0.56–0.73)	0.80 (0.64–0.80)	0.69 (0.52–0.69)
aPS/PT IgG	1.00 (0.80–1.25), *P* = 0.995	1.00 (0.79–1.25), *P* = 0.979	1.00 (0.80–1.25), *P* = 0.998	0.99 (0.79–1.25), *P* = 0.957	1.01 (0.81–1.25), *P* = 0.962	0.99 (0.78–1.27), *P* = 0.960	1.00 (0.80–1.25), *P* = 0.993	0.54 (0.33–0.54)	0.67 (0.49–0.67)	0.68 (0.50–0.68)	0.75 (0.59–0.75)	0.72 (0.56–0.72)	0.80 (0.63–0.80)	0.69 (0.51–0.69)
aPS/PT IgM	1.01 (0.94–1.08), *P* = 0.890	1.01 (0.94–1.08), *P* = 0.782	1.01 (0.94–1.08), *P* = 0.810	1.01 (0.94–1.08), *P* = 0.809	1.01 (0.94–1.08), *P* = 0.814	1.02 (0.95–1.09), *P* = 0.665	1.01 (0.94–1.08), *P* = 0.802	0.51 (0.28–0.51)	0.68 (0.49–0.68)	0.69 (0.51–0.69)	0.75 (0.60–0.75)	0.72 (0.56–0.72)	0.80 (0.64–0.80)	0.69 (0.52–0.69)
Small for gestational age														
LA-aPTT	1.00 (0.81–1.22), *P* = 0.977	1.04 (0.85–1.28), *P* = 0.716	1.01 (0.82–1.23), *P* = 0.945	1.01 (0.82–1.23), *P* = 0.944	1.01 (0.82–1.23), *P* = 0.943	1.01 (0.82–1.23), *P* = 0.945	1.00 (0.82–1.23), *P* = 0.965	0.52 (0.46–0.52)	0.57 (0.51–0.57)	0.60 (0.54–0.60)	0.60 (0.54–0.60)	0.60 (0.54–0.60)	0.60 (0.54–0.60)	0.60 (0.55–0.60)
LA-RVVT	1.09 (0.88–1.36), *P* = 0.423	1.21 (0.96–1.53), *P* = 0.112	1.18 (0.93–1.49), *P* = 0.169	1.18 (0.93–1.49), *P* = 0.170	1.17 (0.93–1.48), *P* = 0.185	1.18 (0.93–1.49), *P* = 0.168	1.17 (0.92–1.47), *P* = 0.202	0.49 (0.43–0.49)	0.58 (0.52–0.58)	0.60 (0.55–0.60)	0.60 (0.55–0.60)	0.59 (0.54–0.59)	0.60 (0.55–0.60)	0.60 (0.55–0.60)
Anti-CL IgG	0.97 (0.93–1.01), *P* = 0.101	0.97 (0.93–1.01), *P* = 0.111	0.97 (0.93–1.01), *P* = 0.117	0.97 (0.93–1.01), *P* = 0.117	0.97 (0.93–1.01), *P* = 0.114	0.97 (0.93–1.01), *P* = 0.117	0.97 (0.93–1.01), *P* = 0.121	0.59 (0.53–0.59)	0.58 (0.52–0.58)	0.61 (0.55–0.61)	0.61 (0.55–0.61)	0.60 (0.54–0.60)	0.61 (0.55–0.61)	0.61 (0.55–0.61)
Anti-CL IgM	0.92 (0.83–1.02), *P* = 0.108	0.90 (0.81–1.01), *P* = 0.064	0.91 (0.81–1.01), *P* = 0.073	0.91 (0.81–1.01), *P* = 0.074	0.91 (0.81–1.01), *P* = 0.075	0.91 (0.81–1.01), *P* = 0.073	0.91 (0.81–1.01), *P* = 0.074	0.55 (0.49–0.55)	0.57 (0.52–0.57)	0.60 (0.54–0.60)	0.60 (0.54–0.60)	0.60 (0.54–0.60)	0.60 (0.54–0.60)	0.60 (0.54–0.60)
Anti-β2GPI IgG	0.96 (0.90–1.02), *P* = 0.177	0.96 (0.90–1.02), *P* = 0.153	0.96 (0.90–1.02), *P* = 0.148	0.96 (0.90–1.02), *P* = 0.148	0.96 (0.90–1.02), *P* = 0.148	0.96 (0.90–1.02), *P* = 0.148	0.96 (0.90–1.02), *P* = 0.166	0.54 (0.50–0.54)	0.59 (0.53–0.59)	0.62 (0.56–0.62)	0.62 (0.56–0.62)	0.61 (0.55–0.61)	0.62 (0.56–0.62)	0.62 (0.56–0.62)
Anti-β2GPI IgM	0.94 (0.82–1.07), *P* = 0.333	0.93 (0.81–1.07), *P* = 0.311	0.93 (0.82–1.07), *P* = 0.324	0.93 (0.81–1.07), *P* = 0.322	0.93 (0.81–1.07), *P* = 0.321	0.93 (0.82–1.07), *P* = 0.323	0.93 (0.82–1.07), *P* = 0.330	0.52 (0.48–0.52)	0.57 (0.51–0.57)	0.60 (0.54–0.60)	0.60 (0.54–0.60)	0.59 (0.54–0.59)	0.60 (0.54–0.60)	0.60 (0.54–0.60)
Protein S	1.00 (0.99–1.01), *P* = 0.590	1.00 (0.99–1.01), *P* = 0.729	1.00 (0.99–1.01), *P* = 0.678	1.00 (0.99–1.01), *P* = 0.684	1.00 (0.99–1.01), *P* = 0.710	1.00 (0.99–1.01), *P* = 0.680	1.00 (0.99–1.01), *P* = 0.652	0.51 (0.45–0.51)	0.57 (0.51–0.57)	0.60 (0.54–0.60)	0.60 (0.54–0.60)	0.59 (0.54–0.59)	0.60 (0.54–0.60)	0.60 (0.55–0.60)
Domain I	0.97 (0.93–1.02), *P* = 0.246	0.97 (0.93–1.02), *P* = 0.243	0.97 (0.93–1.02), *P* = 0.204	0.97 (0.93–1.02), *P* = 0.204	0.97 (0.93–1.02), *P* = 0.207	0.97 (0.93–1.02), *P* = 0.204	0.97 (0.93–1.02), *P* = 0.203	0.52 (0.48–0.52)	0.58 (0.52–0.58)	0.61 (0.55–0.61)	0.61 (0.55–0.61)	0.60 (0.55–0.60)	0.61 (0.55–0.61)	0.61 (0.56–0.61)
XII	1.00 (0.99–1.01), *P* = 0.941	1.00 (0.99–1.01), *P* = 0.870	1.00 (0.99–1.01), *P* = 0.901	1.00 (0.99–1.01), *P* = 0.907	1.00 (0.99–1.01), *P* = 0.926	1.00 (0.99–1.01), *P* = 0.902	1.00 (0.99–1.01), *P* = 0.890	0.51 (0.46–0.51)	0.57 (0.51–0.57)	0.60 (0.54–0.60)	0.60 (0.54–0.60)	0.59 (0.54–0.59)	0.60 (0.54–0.60)	0.60 (0.55–0.60)
aPS/PT IgG	0.94 (0.86–1.03), *P* = 0.172	0.94 (0.86–1.03), *P* = 0.169	0.93 (0.85–1.02), *P* = 0.117	0.93 (0.85–1.02), *P* = 0.117	0.93 (0.85–1.02), *P* = 0.120	0.93 (0.85–1.02), *P* = 0.117	0.93 (0.85–1.02), *P* = 0.115	0.54 (0.48–0.54)	0.57 (0.51–0.57)	0.60 (0.54–0.60)	0.60 (0.54–0.60)	0.60 (0.54–0.60)	0.60 (0.54–0.60)	0.60 (0.54–0.60)
aPS/PT IgM	**0.96 (0.94–0.99), *P* = 0.015**	**0.96 (0.93–0.99), *P* = 0.012**	**0.96 (0.93–0.99), *P* = 0.013**	**0.96 (0.93–0.99), *P* = 0.013**	**0.96 (0.93–0.99), *P* = 0.013**	**0.96 (0.93–0.99), *P* = 0.012**	**0.96 (0.93–0.99), *P* = 0.012**	0.57 (0.51–0.57)	0.59 (0.54–0.59)	0.61 (0.56–0.61)	0.61 (0.56–0.61)	0.61 (0.55–0.61)	0.61 (0.56–0.61)	0.61 (0.56–0.61)

* Bold text indicates significance. β2GPI, β2-glycoprotein I; aPS/PT, phosphatidylserine-dependent antiprothrombin; BMI, body mass index; CI, confidence interval; CL, cardiolipin; Domain I, anti-Domain I IgG; IUFD, intrauterine fetal death; LA-aPTT, lupus anticoagulant by diluted activated partial prothrombin time; LA-RVVT, LA by diluted Russell's viper venom time.

Table 1). In LA measurement, a screening test is typically performed using diluted reagents to detect low concentrations of LA, followed by a neutralization test for confirmation.[14,20] In the present study, SCT screening was shortened according to gestational age, likely due to gestational increases in coagulation factors. As a result, LA-aPTT was not detectable during pregnancy. Despite this limitation, the predictive significance of LA-aPTT for obstetric APS remains evident. Although LA is ideally measured outside of pregnancy, the feasibility of conducting cohort studies that involve LA testing in healthy individuals before conception is limited. This challenge represents one of the key limitations of this study.

To the best of our knowledge, only a limited number of studies have demonstrated alterations in aPL measurement according to gestational age in such a large cohort (Supplementary Figure 1). It is imperative to exercise caution when interpreting the results of LA measurements during pregnancy given the potential for LA activity/positivity to diminish in the second and third trimesters. A decline in protein S levels during pregnancy was not observed, as levels had already been significantly reduced in the first trimester. In the present study, a low protein S level was not identified as a predictive factor for both IUFD and preeclampsia, despite previous studies suggesting associations with these outcomes.[26,27] Additionally, low FXII levels did not predict adverse pregnancy outcomes. FXII activity is known to decrease in the presence of LA-aPTT, given that aPTT is used in its measurement.[28] However, FXII activity is also influenced by the C/T genotype. Neither low FXII activity nor genotype demonstrated predictive value for subsequent pregnancy outcomes in this cohort of patients with RPL.

In the present study, women who experienced complications before seven weeks' gestation were excluded, as recruitment occurred after this time point. Thus, the predictive value for early miscarriage could not be examined, representing an additional limitation. Clinical practice generally involves measuring conventional aPL as recommended by guidelines, followed by administration of low-dose aspirin and heparin upon obtaining positive results; withholding treatment in such cases is considered unethical. In a previous study, frozen plasma was analyzed to provide evidence that treatment based on test results improves pregnancy outcomes after completion of pregnancy.[25]

Noncriteria antibodies, including aPS/PT IgG and anti–Domain I IgG, did not predict features of obstetric APS. Furthermore, high levels of aPS/PT IgM were not associated with any adverse pregnancy outcomes. Moyle et al reported that aPS/PT IgG and anti–Domain I IgG served as significant independent predictors of adverse pregnancy outcomes and exhibited strong associations with LA in a high-risk population of pregnant individuals with aPL, with or without SLE.[29] However, patients diagnosed with APS and receiving heparin therapy were excluded from the current study cohort of patients with RPL. These findings suggest that measurement of aPS/PT IgG, IgM, and anti-Domain I IgG may not be necessary in the general RPL population. Limiting testing to a smaller panel of aPL antibodies is advisable to avoid unnecessary financial burden on patients.

Marked discrepancies in aPS/PT IgG positivity were observed between measurements conducted by Werfen and Hokkaido University. In our previous study, significant differences in aCL IgG and IgM positivity were found between assays performed by Phadia and Hokkaido University.[25] Such variability in aPL measurement results between facilities, even when employing the same assay methods, is well recognized. The aPS/PT assay has not undergone international standardization, as it is a noncriteria assay. Our previous international cross-sectional multicenter studies showed moderate agreement between IgG aPS/PT Inova and MBL ELISA kits and revealed that IgG aPS/PT was more prevalent in patients with APS than in those without.[30] The aPL test thus demonstrates a high degree of agreement among medical facilities in identifying high-risk patients, including those diagnosed with APS. Conversely, the performance of the test was less optimal among low-risk populations, specifically those with RPL.

As the present study used measurements provided by the Werfen company, further investigation is required to determine whether LA and anti-β2GPI IgG assays from other testing laboratories demonstrate comparable predictive value for obstetric APS. This variability constitutes an additional limitation of the study.

In conclusion, LA-RVVT and anti-β2GPI IgG were found to possess predictive value for early-onset preeclampsia and IUFD in normal pregnant women, respectively. The AUC of anti-β2GPI IgG increased by 0.8 when combined with a history of IUFD. The measurement of LA-RVVT and anti-β2GPI IgG, along with the complication of chronic hypertension and a history of IUFD, proved essential for the clinical diagnosis of APS. Challenges arise in examining prognostic and treatment evidence for each aPL at different testing facilities due to the variability in measurement results.

ACKNOWLEDGMENTS

We would like to express our deepest gratitude to Professor Yasuhiko Ozaki, from the Graduate School of Nursing at Nagoya City University, for his invaluable support during the initial stages of this study. We would also like to thank Dr Sakura Ogasawara, Ms Fumiko Ozawa and the NCU staff for their help with data acquisition, as well as Dr Eri Nakamoto, Dr Ayana Tokioka, and the WMC members. We would like to thank everyone who contributed to this study.

AUTHOR CONTRIBUTIONS

All authors contributed to at least one of the following manuscript preparation roles: conceptualization AND/OR methodology, software, investigation, formal analysis, data curation, visualization, and validation AND drafting or reviewing/editing the final draft. As corresponding author, Dr Sugiura-Ogasawara confirms that all authors have provided the final approval of the version to be published and takes responsibility for the affirmations regarding article submission (eg, not under

consideration by another journal), the integrity of the data presented, and the statements regarding compliance with institutional review board/Declaration of Helsinki requirements.

REFERENCES

1. Miyakis S, Lockshin MD, Atsumi T, et al. International consensus statement on an update of the classification criteria for definite antiphospholipid syndrome (APS). J Thromb Haemost 2006;4(2):295–306.
2. Quenby S, Gallos ID, Dhillon-Smith RK, et al. Miscarriage matters: the epidemiological, physical, psychological, and economic costs of early pregnancy loss. Lancet 2021;397(10285):1658–1667.
3. Coomarasamy A, Dhillon-Smith RK, Papadopoulou A, et al. Recurrent miscarriage: evidence to accelerate action. Lancet 2021;397(10285):1675–1682.
4. Nilsson IM, Astedt B, Hedner U, et al. Intra-uterine death and circulating anticoagulant. Acta Med Scand 1975;197:153–159.
5. Harris EN, Gharavi AE, Boey ML, et al. Anticardiolipin antibodies: detection by radioimmunoassay and association with thrombosis in systemic lupus erythematosus. Lancet 1983;2(8361):1211–1214.
6. Matsuura E, Igarashi Y, Fujimoto M, et al. Anticardiolipin cofactor(s) and differential diagnosis of autoimmune disease. Lancet 1990;336(8708):177–178.
7. Galli M, Comfurius P, Maassen C, et al. Anticardiolipin antibodies (ACA) directed not to cardiolipin but to a plasma protein cofactor. Lancet 1990;335(8705):1544–1547.
8. McNeil HP, Simpson RJ, Chesterman CN, et al. Anti-phospholipid antibodies are directed against a complex antigen that includes a lipid-binding inhibitor of coagulation: β 2-glycoprotein I (apolipoprotein H). Proc Natl Acad Sci USA 1990;87(11):4120–4124.
9. Bevers EM, Galli M, Barbui T, et al. Lupus anticoagulant IgG's (LA) are not directed to phospholipids only, but to a complex of lipid-bound human prothrombin. Thromb Haemost 1991;66(6):629–632.
10. Bender Atik R, Christiansen OB, Elson J, et al; ESHRE Guideline Group on RPL. ESHRE guideline: recurrent pregnancy loss: an update in 2022. Hum Reprod Open 2023;2023(1):hoad002.
11. Barbhaiya M, Zuily S, Naden R, et al; ACR/EULAR APS Classification Criteria Collaborators. The 2023 ACR/EULAR antiphospholipid syndrome classification criteria. Arthritis Rheumatol 2023;75(10):1687–1702.
12. Chantarangkul V, Tripodi A, Arbini A, et al. Silica clotting time (SCT) as a screening and confirmatory test for detection of the lupus anticoagulants. Thromb Res 1992;67(4):355–365.
13. Thiagarajan P, Pengo V, Shapiro SS. The use of dilute Russell's viper venom time for the diagnosis of lupus anticoagulants. Blood Coagul Fibrinolysis 1990;1:295–296.
14. Pengo V, Tripodi A, Reber G, et al; Subcommittee on Lupus Anticoagulant/Antiphospholipid Antibody of the Scientific and Standardisation Committee of the International Society on Thrombosis and Haemostasis. Update of the guidelines for lupus anticoagulant detection. J Thromb Haemost 2009;7(10):1737–1740.
15. Iwaniec T, Kaczor MP, Celińska-Löwenhoff M, et al. Clinical utility of automated chemiluminescent antiphospholipid antibody assay. Thromb Res 2015;136(5):1033–1039.
16. De Craemer AS, Devreese KM, Devreese KM. Role of anti-domain 1-$ß_2$ glycoprotein I antibodies in the diagnosis and risk stratification of antiphospholipid syndrome: reply. J Thromb Haemost 2016;14(10):2078–2080.
17. Atsumi T, Ieko M, Bertolaccini ML, et al. Association of autoantibodies against the phosphatidylserine-prothrombin complex with manifestations of the antiphospholipid syndrome and with the presence of lupus anticoagulant. Arthritis Rheum 2000;43:1982–1993.
18. Ieko M, Hotta T, Watanabe K, et al. Comparative evaluation of reagents for measuring protein S activity: possibility of harmonization. Int J Hematol 2021;113(4):530–536.
19. The Japanese Society for Pediatric Endocrinology, The Japanese Association for Human Auxology, The Japan Society for Neonatal Health and Development. Standard Birth Size Reference Values (Cross-Sectional Survey, First Report). Accessed April 30, 2025. https://jspe.umin.jp/medical/keisan.html.
20. Devreese KMJ, Bertolaccini ML, Branch DW, et al. An update on laboratory detection and interpretation of antiphospholipid antibodies for diagnosis of antiphospholipid syndrome: guidance from the ISTH-SSC Subcommittee on Lupus Anticoagulant/Antiphospholipid Antibodies. J Thromb Haemost 2025;23(2):731–744.
21. Wind M, Fierro JJ, Bloemenkamp KWM, et al. Pregnancy outcome predictors in systemic lupus erythematosus: a systematic review and meta-analysis. Lancet Rheumatol 2024;6(10):e667–e683.
22. Duckitt K, Harrington D. As established by preceding research, hypertension also exerted an influence on preeclampsia in the present study. The prevalence of LARVVT was found to be higher in women diagnosed with hypertension; however, the findings of this study are limited by the modest sample size, necessitating additional research to substantiate these results. BMJ 2005;330(7491):565.
23. Lockshin MD, Kim M, Laskin CA, et al. Prediction of adverse pregnancy outcome by the presence of lupus anticoagulant, but not anticardiolipin antibody, in patients with antiphospholipid antibodies. Arthritis Rheum 2012;64(7):2311–2318.
24. Clark CA, Davidovits J, Spitzer KA, et al. The lupus anticoagulant: results from 2257 patients attending a high-risk pregnancy clinic. Blood 2013;122(3):341–347.
25. Kitaori T, Sugiura-Ogasawara M, Oku K, et al. Determination of clinically significant tests for antiphospholipid antibodies and cutoff levels for obstetric antiphospholipid syndrome. Lupus 2015;24(14):1505–1519.
26. Ebina Y, Ieko M, Naito S, et al. Low levels of plasma protein S, protein C and coagulation factor XII during early pregnancy and adverse pregnancy outcome. Thromb Haemost 2015;114(1):65–69.
27. Rey E, Kahn SR, David M, et al. Thrombophilic disorders and fetal loss: a meta-analysis. Lancet 2003;361(9361):901–908.
28. Asano E, Ebara T, Yamada-Namikawa C, et al. Genotyping analysis for the 46 C/T polymorphism of coagulation factor XII and the involvement of factor XII activity in patients with recurrent pregnancy loss. PLoS One 2014;9(12):e114452.
29. Moyle KA, Branch DW, Peterson LK, et al. Association between novel antiphospholipid antibodies and adverse pregnancy outcomes. Obstet Gynecol 2025;145(1):55–64.
30. Amengual O, Forastiero R, Sugiura-Ogasawara M, et al. Evaluation of phosphatidylserine-dependent antiprothrombin antibody testing for the diagnosis of antiphospholipid syndrome: results of an international multicentre study. Lupus 2017;26(3):266–276.

Arthritis & Rheumatology
Vol. 78, No. 2, February 2026, pp 385–393
DOI 10.1002/art.43358

American College of Rheumatology
Empowering Rheumatology Professionals

Genome-Wide DNA Methylation Study Reveals Specific Signatures in the Affected Arterial Tissue of Patients With Giant Cell Arteritis

Gonzalo Borrego-Yaniz,[1] Ana Márquez,[1] Elkyn Estupiñán-Moreno,[2] Laura C. Terrón-Camero,[3] Miguel A. González-Gay,[4,5] Santos Castañeda,[6] Giuliana Guggino,[7] David Saadoun,[8] Pietro Lio,[9] Simona Fontana,[10] Martina Bonacini,[11] Alessandro Rossi,[11] Alberto Cavazza,[12] Francesco Muratore,[13,14] Carlo Salvarani,[13,14] Nicolo Pipitone,[14] Javier Martin,[1] Stefania Croci,[11] and Lourdes Ortiz-Fernández[1]

Objective. Giant cell arteritis (GCA) is a large-vessel vasculitis, potentially causing complications such as blindness and strokes. This study aims to gain insights into the pathogenesis of GCA by identifying specific DNA methylation signatures in the arterial tissue of patients with this vasculitis.

Methods. DNA methylation profiling was analyzed in 79 temporal artery biopsy samples (69 patients with GCA and 10 controls) by performing an epigenome-wide association study (EWAS). Differential analysis was performed to identify differentially methylated positions (DMPs) and differentially methylated regions (DMRs). Lastly, we compared our findings with previous transcriptomics and epigenomics studies on GCA-affected arteries.

Results. EWAS identified 3,644 DMPs ($P_{adj} < 0.05$, $|\Delta\beta| > 0.3$), indicating a profound alteration within GCA-affected arterial tissue. These DMPs were annotated to 1,517 potentially dysregulated genes. A total of 282 additional genes were identified by annotation of significant DMRs. Pathway enrichment analysis revealed a significant alteration of inflammatory mechanisms, such as interleukin-2 and interleukin-7, as well as pathways related to vascular remodeling. Omics study comparison revealed 37 genes consistently affected across datasets, many of them linked to immune signaling and T cell regulation. Notably, markers of exhausted T cells, including *SLAMF6* and *HAVCR2*, were present among them.

Conclusion. Our study identified GCA-specific DNA methylation signatures in arterial tissue, revealing disrupted inflammatory and vascular pathways and suggesting the involvement of exhausted T cells in this condition. These findings offer new insights into GCA pathogenesis and provide new potential targets for the treatment of this debilitating disease.

This research is part of the doctoral degree awarded to Gonzalo Borrego-Yaniz, MSc, within the Biomedicine program from the University of Granada.

Supported by a research grant from FOREUM Foundation for Research in Rheumatology. Dr Borrego-Yaniz's contract is part of the grant PREP2022-000712, funded by the MCIN/AEI/10.13039/501100011033 and the ESF+. Dr Ortiz-Fernández's work is supported by a Ramon y Cajal fellowship (RYC2022-036635-I) funded by MICIU/AEI/10.13039/501100011033 and by ESF+.

[1]Gonzalo Borrego-Yaniz, MSc, Ana Márquez, PhD, Javier Martin, MD, PhD, Lourdes Ortiz-Fernández, PhD: Institute of Parasitology and Biomedicine López-Neyra, Consejo Superior de Investigaciones Cientificas (CSIC), Granada, Spain; [2]Elkyn Estupiñán-Moreno, PhD: Josep Carreras Leukaemia Research Institute (IJC), Epigenetics and Immune Disease Group, Badalona, Barcelona, Spain; [3]Laura C. Terrón-Camero, PhD: Bioinformatics Unit, Institute of Parasitology and Biomedicine López-Neyra, Consejo Superior de Investigaciones Científicas (CSIC), Granada, Spain; [4]Miguel A. González-Gay, MD, PhD: Division of Rheumatology, Instituto de Investigación Sanitaria (IIS)-Fundación Jiménez Díaz, Madrid, Spain;[5]Miguel A. González-Gay, MD, PhD: Department of Medicine, University of Cantabria, Santander, Spain; [6]Santos Castañeda, MD, PhD: Division of Rheumatology, Hospital de la Princesa, Instituto de Investigación Sanitaria (IIS)-Princesa, Madrid, Spain; [7]Giuliana Guggino, MD, PhD: PROMISE Department Rheumatology, University of Palermo, Palermo, Italy; [8]David Saadoun, MD, PhD: Hôpital Pitié-Salpêtrière-Charles Foix Hospital, Paris, France; [9]Pietro Lio, PhD: Department of Computer Science and Technology, University of Cambridge, Cambridge, United Kingdom; [10]Simona Fontana, PhD: Dipartimento di Biomedicina, Neuroscienze e Diagnostica Avanzata, University of Palermo, Palermo, Italy; [11]Martina Bonacini, PhD, Alessandro Rossi, MSc, Stefania Croci, PhD: Clinical Immunology, Allergy and Advanced Biotechnologies Unit, Azienda Unità Sanitaria Locale (AUSL)- Istituto di Ricovero e Cura a Carattere Scientifico (IRCCS) di Reggio Emilia, Reggio Emilia, Italy; [12]Alberto Cavazza, MD: Unit of Pathology, Azienda Unità Sanitaria Locale (AUSL)- Istituto di Ricovero e Cura a Carattere Scientifico (IRCCS) di Reggio Emilia, Reggio Emilia, Italy; [13]Francesco Muratore, MD, Carlo Salvarani, MD: University of Modena and Reggio Emilia, Modena, Italy; [14]Francesco Muratore, MD, Carlo Salvarani, MD, Nicolo Pipitone, MD: Unit of Rheumatology, Azienda Unità Sanitaria Locale (AUSL)- Istituto di Ricovero e Cura a Carattere Scientifico (IRCCS)di Reggio Emilia, Reggio Emilia, Italy.

Drs Martin, Croci, and Ortiz-Fernández contributed equally to this work.

Additional supplementary information cited in this article can be found online in the Supporting Information section (http://onlinelibrary.wiley.com/doi/10.1002/art.43358).

Author disclosures are available at https://onlinelibrary.wiley.com/doi/10.1002/art.43358.

Address correspondence via email to Lourdes Ortiz-Fernández, PhD, at lourdes@ipb.csic.es.

Submitted for publication March 10, 2025; accepted in revised form July 30, 2025.

INTRODUCTION

Giant cell arteritis (GCA) is the most common form of vasculitis in individuals aged >50 years old, characterized by chronic inflammation of the aorta and its branches. This condition carries significant morbidity and mortality, with complications such as irreversible vision loss and stroke.[1] Despite its clinical impact, the molecular mechanisms underlying GCA pathogenesis remain insufficiently understood, limiting the development of improved treatments and management strategies.[2,3]

Pathologic hallmarks of GCA are the loss of immune privilege in the arterial tissue, sustained inflammatory damage leading to severe vascular remodeling, and the neovascularization of the extracellular matrix.[4] These processes create a chronic inflammatory microenvironment that sustains the malfunctioning immune response in the vascular tissue. Different studies have shown genetic risk factors and reprogrammed gene regulation associated with this condition,[5–8] showing a complex contribution of genetic and epigenetic drivers to GCA pathogenesis.

Epigenetics is a dynamic mechanism to regulate gene expression, affecting development, tissue differentiation, and cellular responsiveness.[9] DNA methylation is the most studied epigenetic marker, having been associated with pathogenic conditions such as immune-mediated inflammatory diseases (IMIDs).[10] Epigenetic signatures associated with disease progression hold great potential for the discovery of new therapeutic targets because of their reversible nature and potential to address disease mechanisms influenced by genetics, lifestyle, and environmental factors.[11] In GCA, a previous study revealed thousands of methylation changes present in temporal artery biopsies (TABs)[12]; however, because of limited sample size and CpGs coverage, there is an incomplete understanding of the role of this mechanism in GCA pathogenesis.

In this study, we conducted a comprehensive DNA methylation analysis of GCA-affected arteries. By leveraging genome-wide profiling in the largest GCA cohort studied so far, we sought to provide foundational insights into GCA pathogenesis and identify potential therapeutic targets to address the significant clinical burden of this condition.

MATERIALS AND METHODS

Study cohort. TABs from 69 patients with GCA and 10 controls were collected in hospitals from Italy, France, and Spain. All patients with GCA had a positive TAB, with transmural inflammation, and fulfilled the 1990 American College of Rheumatology classification criteria for this disease.[13] Clinical criteria for both inclusion or exclusion from the study is listed in Supplementary Materials section 1. Control samples were obtained from individuals with suspected GCA whose TABs were negative. Moreover, the diagnosis of GCA was discarded based on additional negative large-vessel imaging results (temporal artery color Doppler ultrasonography was performed in 9 of 10 patients, and positron emission tomography and computed tomography was performed in 6 of 10 patients) and a definitive alternative diagnosis deriving from a clinical follow-up of at least one year. The main demographic and clinical characteristics of the study cohort are described in Table 1. All participants signed an informed consent form in accordance with the ethical guidelines of the 1975 Declaration of Helsinki. The protocol adhered to all ethical regulations and obtained approval from the ethics committee Area Vasta Emilia Nord of the principal investigator (protocol 777/2018/OSS/AUSLRE) and from those of the participating institutions involved in this study.

Table 1. Clinical and demographic characteristics of the study cohort

Characteristics	Total	Cases	Controls*
Cohort size, n	79	69	10
Age, mean ± SD	75.54 ± 7.04	74.87 ± 6.72	80.20 ± 7.84
Women, n (%)	62 (70)	58 (84)	6 (60)
GC treatment at TAB, n (%)[a]	43 (53)	41 (61)	2 (20)
Treatment during follow-up period, GC/GC + TCZ	–	64/5	–
Responders to treatment, n (%)[a]	–	32 (48)	–
Any cranial symptoms, n (%)[a,b]	69 (90)	61 (91)	8 (80)
Any visual symptoms, n (%)[a,c]	25 (32)	22 (33)	3 (30)
Any systemic symptoms, n (%)[a,d]	38 (49)	38 (57)	0 (0)
Polymyalgia rheumatica, n (%)[a]	30 (48)	27 (40)	3 (30)

* Control samples were obtained from individuals with suspected giant cell arteritis whose TABs were negative, in addition to further clinical criteria and follow-up of at least one year. The final diagnoses for controls were the following: nonarteritic anterior ischemic optic neuropathy (n = 3), polymyalgia rheumatica (n = 3), Raynaud disease (n = 1), abdominal aortic aneurysm of atherosclerotic genesis (n = 1), temporomandibular joint dysfunction (n = 1), and crowned dens syndrome (n = 1). GC, glucocorticoid; TAB, temporal artery biopsy; TCZ, tocilizumab.
[a] Information about clinical manifestations and response to treatment was not available for two patients with giant cell arteritis.
[b] Any cranial symptoms of the following: headache, scalp dysesthesia, or jaw claudication.
[c] Any systemic symptoms of the following: fever, fatigue, or weight loss ≥4 kg.
[d] Any visual symptoms of the following: permanent visual loss, amaurosis fugax, or diplopia.

DNA methylation profiling. To preserve the in situ cellular and molecular composition, TABs samples were snap frozen in liquid nitrogen and stored at –80°C within 30 minutes of the withdrawal. DNA from TABs was isolated with the DNA/RNA/Protein Purification Plus Kit (Norgen) following the manufacturer's instructions and quantified with Qubit Fluorometric Quantification (Thermo Fisher Scientific). DNA methylation profiling was performed using 500 ng of bisulfite-converted DNA hybridized to the Infinium MethylationEPIC BeadChip array (Illumina) in accordance with the manufacturer's protocol. This array, designed to target 850,000 CpG sites, provides coverage of 99% of annotated RefSeq genes. Probe fluorescence was measured using a BeadArray Reader (Illumina).

Quality controls and normalization. DNA methylation raw data were processed using minfi R package[14] (version 1.55) under R version 4.4. First, we checked for samples showing poor bisulfite conversion (detection $P > 0.05$) and those with discrepancies between recorded sex information and sex inferred from the data. Next, probes showing poor quality (detection $P > 0.01$) were removed. We also filtered out CpGs from chromosomes X and Y as well as those probes containing either a single nucleotide polymorphism at the CpG interrogation site or at the single base extension site. Finally, cross-reactive probes reported in the literature were also removed.[15] Probes were annotated using IlluminaHumanMethylationEPICanno (version 10b5.hg38). Subsequently, we normalized raw methylation values using the stratified quantile normalization method.

Methylation levels were measured as β and M values. β values, representing the fraction of methylated probes on a scale from 0 to 1, were used for visual representation and biologic interpretation. M values (log2-transformed β values) were calculated for statistical purposes, to approximate a normal distribution of methylation values, more adequate for linear modeling. To evaluate potential confounding effects, principal component analysis (PCA) was conducted (Supplementary Materials section 2). In addition, PCA was also used to estimate potential outliers in the cohort. Samples exceeding a threshold of 4 SDs from the cluster centroids were excluded from further analyses.

Genome-wide differential methylation analysis. We compared methylation levels of patients with GCA versus controls of all CpGs that passed quality controls using an empirical Bayes moderated *t*-statistics test from limma R package.[16] For this comparison, we conducted independent sensitivity tests to examine the contribution of all potential confounders (sex, age, treatment at TAB collection, sample plate, slide, and well) to the analysis. Pearson correlation or Wilcoxon signed-rank test was applied depending on whether the variable of interest was continuous or categorical. Variables showing an false discovery rate (FDR) value (P_{adj}) < 0.05 were considered to significantly contribute to DNA methylation profiles (Supplementary Table 1). Accordingly, sample plate and sample slide were included in the final regression model as covariates. To further support that sex was not notably influencing the methylation changes observed in our cohort, we also performed the differential methylation analysis including sex as a covariate in addition to a disease–sex interaction model. These complementary analyses are described in detail in Supplementary Materials sections 3-5. For multiple-testing correction, we applied a FDR of 0.05. To assess the potential influence of unknown confounding factors on our findings, we performed a permutation test in which case and control labels were randomly reassigned within our cohort across 100 iterations, and the resulting differential analyses were compared with those obtained in the original dataset (Supplementary Materials section 6). The differential of β values (Δβ) between the groups considered in each comparison were estimated as the difference in the median values. Those CpG sites with an $P_{adj} < 0.05$ and $|\Delta\beta| > 0.3$ were considered as differentially methylated positions (DMPs). The enrichment of DMPs within genomic locations was analyzed using epigenome-wide association study toolkit.[17] Furthermore, we assessed the presence of differentially methylated regions (DMRs) with DMRcate[18] by using default parameters ($\lambda = 1{,}000$) and considering only DMRs containing at least five significant CpGs.

Pathway enrichment analysis. To explore the potential pathologic relevance of the gene sets identified in our analyses, we conducted pathway enrichment analysis using the EnrichR tool.[19] The analysis was performed by querying two comprehensive databases: Gene Ontology Biological Process[20] and BioPlanet.[21] Pathways needed to be enriched in at least five genes to be considered, and those presenting an $P_{adj} < 0.05$ were considered significant. As methylation changes can either up-regulate or down-regulate genes depending on their genomic context, we included all annotated genes in the pathway enrichment analysis, regardless of whether they contained hypermethylated or hypomethylated CpGs.

Comprehensive overview of GCA-affected genes. To identify genes exhibiting transversal alterations across gene regulation, gene expression, and protein levels, we compared our results on DMPs and DMRs with reported findings from previous bulk omics studies in GCA. Specifically, we evaluated overlaps with (1) DMPs previously reported in temporal arteries,[12] (2) differentially expressed genes identified in temporal arteries,[22] and (3) altered protein levels observed in plasma serum.[23] The characteristics of the experimental design conducted in each of those studies are summarized in Supplementary Table 2. As omics studies reporting a large number of genes were compared, we performed permutation tests to assess whether the observed level of overlap between studies was significantly greater than expected by chance (Supplementary Materials section 7).

Data availability statement. Summary results will be made available upon reasonable request. Individual-level data cannot be shared due to privacy and ethical considerations.

Ethics approval. The study was approved by the ethical committees of all institutions involved in this study. Participants gave informed consent to participate in the study before taking part.

RESULTS

Specific epigenomic signature in GCA-affected arteries. After quality controls, 770,921 CpGs were analyzed, and all samples were included in the analysis. Notably, 89.2% of CpGs showing significantly altered methylation levels in GCA-affected arteries in a previous study[12] were also significant in our results ($P_{adj} < 0.05$) and showed a strong correlation in their $\Delta\beta$ values between studies (Spearman correlation = 0.75; $P < 2.2 \times 10^{-16}$). In addition, all overlapping significant CpGs displayed methylation changes in the same direction (Supplementary Material section 3). Because of the increased statistical power in our experimental design, a total of 228,152 CpG sites presented significant changes in methylation ($P_{adj} < 0.05$), demonstrating an extensive epigenetic alteration present in the GCA-affected artery. Randomized case and control permutations confirmed that the large differences observed between patients with GCA and controls were unlikely to be due to unaccounted confounding factors in our experimental design (Supplementary Material section 6). Across 100 iterations, a maximum of 10 significant CpGs were identified, whereas the majority of permutations (n = 87) yielded no significant CpGs. Because of the large effect of GCA pathogenesis over arterial tissue, we proceeded to focus on those significant CpGs showing major changes in methylation ($|\Delta\beta| > 0.3$; $P_{adj} < 0.05$), comprising 3,644 DMPs, in which 81.1% of them represent novel DMPs for arteries affected by GCA. Among these, 2,680 were hypermethylated, and 964 were hypomethylated (Figure 1; Supplementary Table 3). These DMPs were predominantly located in OpenSea regions and gene bodies (Supplementary Table 4) and were annotated to 1,517 different genes, including relevant genes involved in GCA pathologic mechanisms related to inflammatory response and vascular remodeling, such as *IL6R*, *IL2RA*, *STAT3*, and *JAG1.* Pathway analyses of these DMPs showed 78 significant pathways (Supplementary Tables 5–6), including fundamental immune pathways related to IL-2 and CTLA-4 signaling as well as mechanisms linked to the angiogenic process, such as integrins affecting angiogenesis and CXCR4 signaling (Figure 2).

Epigenetic altered regions and affected pathways in GCA. To determine consistent methylation changes in the epigenome, we conducted a DMR analysis, identifying 12,899 significant regions associated with GCA ($P_{adj} < 0.05$). Among these, 5,393 were hypomethylated and 7,506 hypermethylated, with a mean size of 9.53 CpGs per region. A subset of 918 DMRs showed substantial methylation changes ($|\text{mean } \Delta\beta| > 0.2$) and were annotated to 935 genes (Supplementary Table 7), comprising 282 additional genes from those identified by the annotation of DMPs. This gene set included critical immune and GCA-associated genes, such as *IL17B*, *IL11RA*, *HLA-DPA1*, *TNF*, and *PDGFA*, further supporting a strong alteration of immune activation and tissue remodeling. Pathway enrichment analysis highlighted disruptions in key arterial pathways (155 significant pathways; Supplementary Tables 8–9). Notably, pathways related to arterial remodeling were enriched, including regulation of growth factors VEGF and PDGF. Additionally, signaling pathways relevant for arterial cell migration and immune cell activation were affected, such as leukocyte transendothelial migration, regulation of T cell activation, and natural killer cell–mediated cytotoxicity (Figure 3). These findings emphasize the extensive epigenetic reprogramming that drives the local arterial response in the context of GCA pathogenesis.

Consistently altered genes in GCA omics studies. To contextualize our findings, we evaluated the affected genes identified in this study against previously reported omics datasets on GCA. Notably, we identified 37 genes consistently altered in GCA-affected arteries across three major epigenomics and transcriptomics studies of this tissue, including this current work (Figure 4). This list comprises genes annotated either by DMPs or DMRs from our results, DMPs reported by Coit et al,[12] and genes classified as differentially expressed in Ferrigno et al.[22] For all studies considered, permutation tests demonstrated that the number of overlapping genes was significantly greater than expected by chance, including the overlap of the 37 genes consistently identified in GCA-affected arteries ($P < 0.0001$ for all comparisons; Supplemental Material section 7). These 37 genes carried a robust body of omics evidence supporting their involvement in the pathophysiology of GCA and contain genes related to immune signaling (predominantly related to T cell mechanisms), tyrosine kinases, transcription factors, and integrins as well as other elements. Although the list includes several genes known to be affected in GCA pathogenesis, such as *CD28*, *IL2RA*, and *TNF*, it also highlights many genes whose potential role in the pathogenesis of this disease have not been explored, such as *ICOS*, *GZMA*, *IRF5*, *TLR1*, and *FYN*, among others. *BTLA* and *SLAMF1* were particularly outstanding because they also exhibited significantly altered protein levels in plasma serum from patients with GCA.[23] These findings warrant further investigation given their consistent alterations across independent GCA omics studies.

DISCUSSION

This study represents the largest genome-wide DNA methylation study of GCA-affected arteries conducted to date, providing comprehensive insights into the severe epigenetic dysregulation

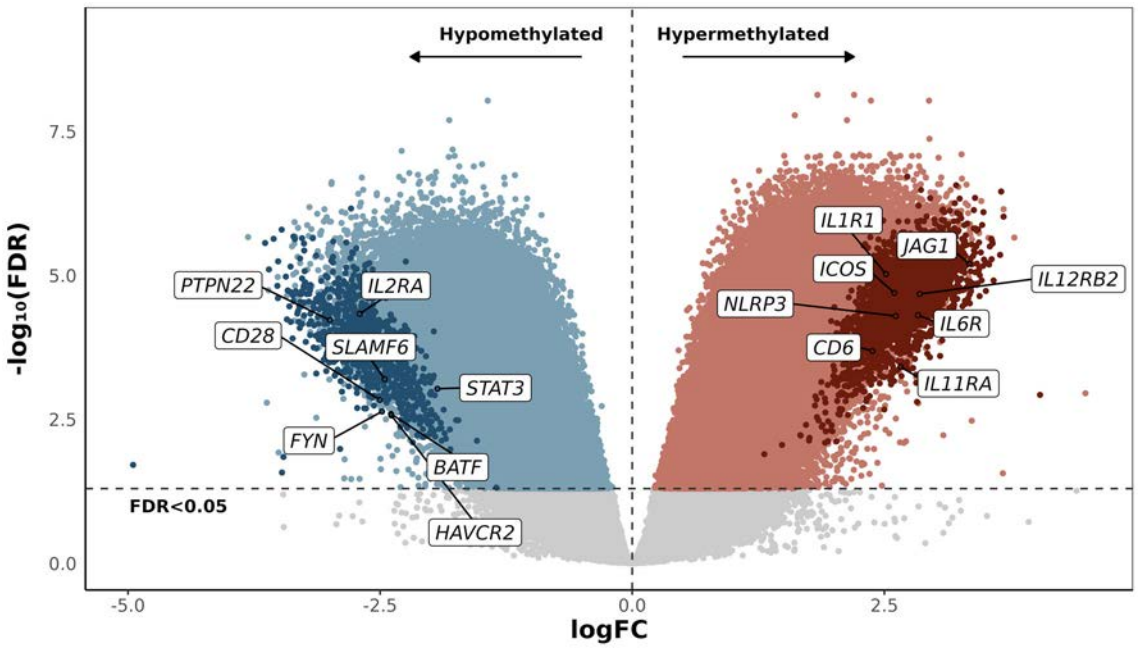

Figure 1. Volcano plot of the epigenome-wide comparison between patients with giant cell arteritis and controls. Gray points represent the non-significant ($P_{adj} > 0.05$) CpGs, and blue and red points represent significant hypomethylated and hypermethylated positions, respectively. Darker-colored points represent differentially methylated positions, significant CpGs showing $|\Delta\beta| > 0.3$.

within arterial tissue underlying this pathology. We analyzed the most notable alterations in the GCA-associated signature, revealing major changes in critical immune and vascular pathways, especially those related to immune activation and vascular remodeling. Furthermore, by leveraging findings from epigenomics and transcriptomics studies, we identified key immune-related genes found consistently altered in GCA-affected arteries, comprising 37 genes that may play a fundamental role in driving this condition.

Interpreting omics data in a complex condition such as GCA is challenging due to the sheer number of genes implicated. To address this, we prioritized genes with strong replicability across

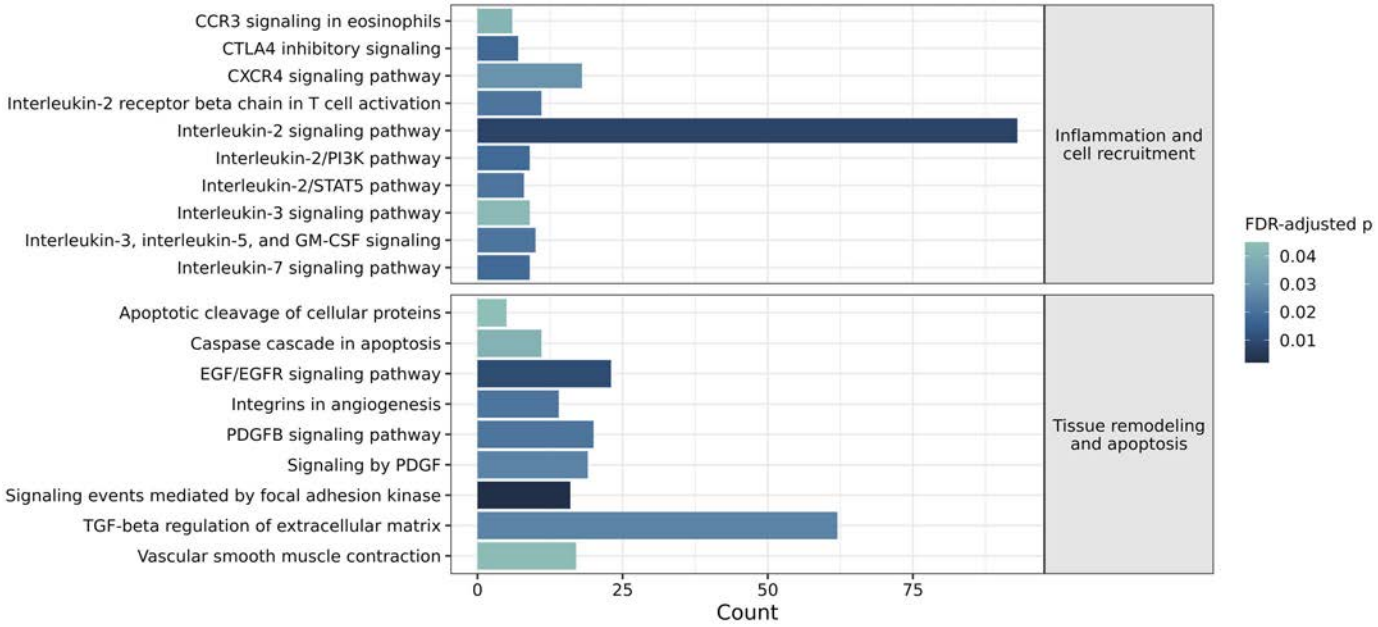

Figure 2. Highlighted significant pathways ($P_{adj} < 0.05$) of the 1,517 genes annotated from differentially methylated positions. FDR, false discovery rate. Color figure can be viewed in the online issue, which is available at http://onlinelibrary.wiley.com/doi/10.1002/art.43358/abstract.

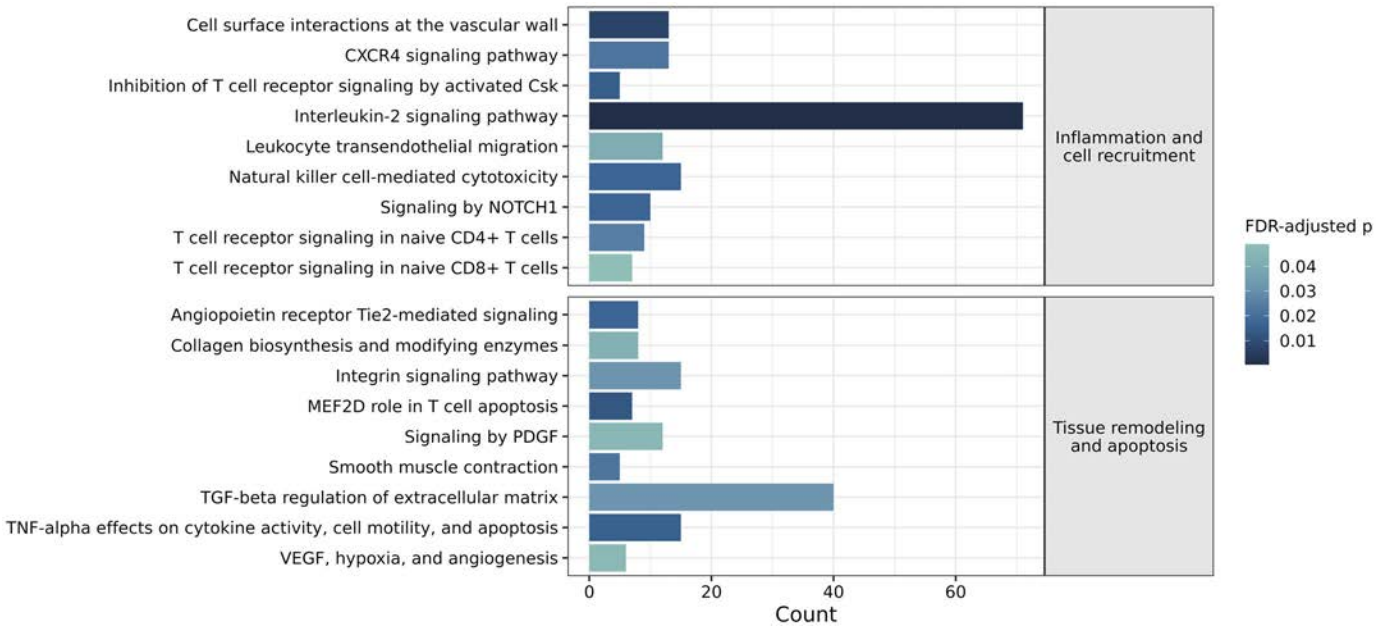

Figure 3. Highlighted significant pathways (FDR-adjusted $P < 0.05$) of the 935 genes annotated from differentially methylated regions. FDR, false discovery rate. Color figure can be viewed in the online issue, which is available at http://onlinelibrary.wiley.com/doi/10.1002/art.43358/abstract.

independent omics studies using TAB samples. Our integrative approach yielded a shortlist of 37 genes exhibiting significant methylation changes (replicated in two independent studies) and altered gene expression levels. This shortlist encompasses a robust set of genes potentially central to GCA, many of them not previously proposed to play a specific role in the pathogenesis of this disease. Among these, we observed a strong representation of costimulatory proteins involved in T cell and antigen-presenting cell interactions, including CD28, CD247, BTLA, ICOS, and SLAM proteins (SLAMF1 and SLAMF6). Additionally, immune-related signaling molecules, such as TNF, FYN, ABL1, PIK3CD, and PIK3CG, as well as transcription factors including RUNX1, RUNX3, and BATF, were prominent. One particularly noteworthy gene in this set is *NLRP3*, which encodes an intracellular pattern recognition receptor that detects pathogens, endogenous damage, and environmental irritants. After activation, it promotes the formation of the NLRP3 inflammasome that leads to proinflammatory signaling and apoptosis. This innate immunity-related pathway plays a central role in cardiovascular diseases[24] and is gaining recognition for its role in autoimmune diseases[25]; therefore, its potential contribution to GCA pathogenesis deserves further study, especially given its established value as a therapeutic target for conditions presenting chronic inflammation.[26]

T cell exhaustion is a process in which T cells, following chronic exposure to antigens and persistent inflammatory signals, progressively lose their effector functions and cytotoxicity while up-regulating inhibitory receptors.[27] Although this phenotype is traditionally linked to chronic infections and cancer, it is now increasingly recognized in autoimmune and inflammatory diseases.[27] Our study, along with other GCA omics studies, identified several markers of exhausted T cells as being altered in GCA-affected arteries at both gene regulation and expression levels. Notable examples include *SLAMF6*, *HAVCR2* (also known as TIM-3), and *CX3CL1* (the ligand for CX3CR1), specific markers of the exhausted T cell phenotype.[28] Additionally, we also observed consistently reported alterations in *BTLA* and *BATF*, regulators of exhausted T cells differentiation.[29] It is also important to note that PD-1 and CTLA4, immune checkpoint molecules implicated in regulating inflammation, are central to the progression of GCA[4,30] and also deeply linked to the development of exhausted T cells.[27] Furthermore, the CXCR4 pathway, significant in our pathway enrichment results, is also related to exhausted T cell differentiation, as it has been reported that CXCR4 can promote T cell exhaustion via JAK2/STAT3.[31] Based on the convergence of GCA-related pathways and T cell differentiation, as well as the replicability of reported alteration of specific markers of exhausted T cells across GCA studies, we hypothesize that the microenvironment of GCA-affected arteries—characterized by persistent inflammation, hypoxia, and extracellular matrix damage—provides favorable conditions for the emergence and maintenance of exhausted T cell phenotypes that would impede the ability of the immune system to regulate the local inflammation occurring in the affected tissue.

Although T cell exhaustion has been primarily described in CD8+ T cells, the role of this T cell subtype in GCA remains poorly understood despite evidence of their presence in inflamed arterial tissue.[32] Emerging evidence suggests that CD4+ T cells can also exhibit an exhausted phenotype,[33] and given the established importance of CD4+ T cells in GCA pathogenesis, it would be particularly relevant to investigate whether exhausted subsets of both

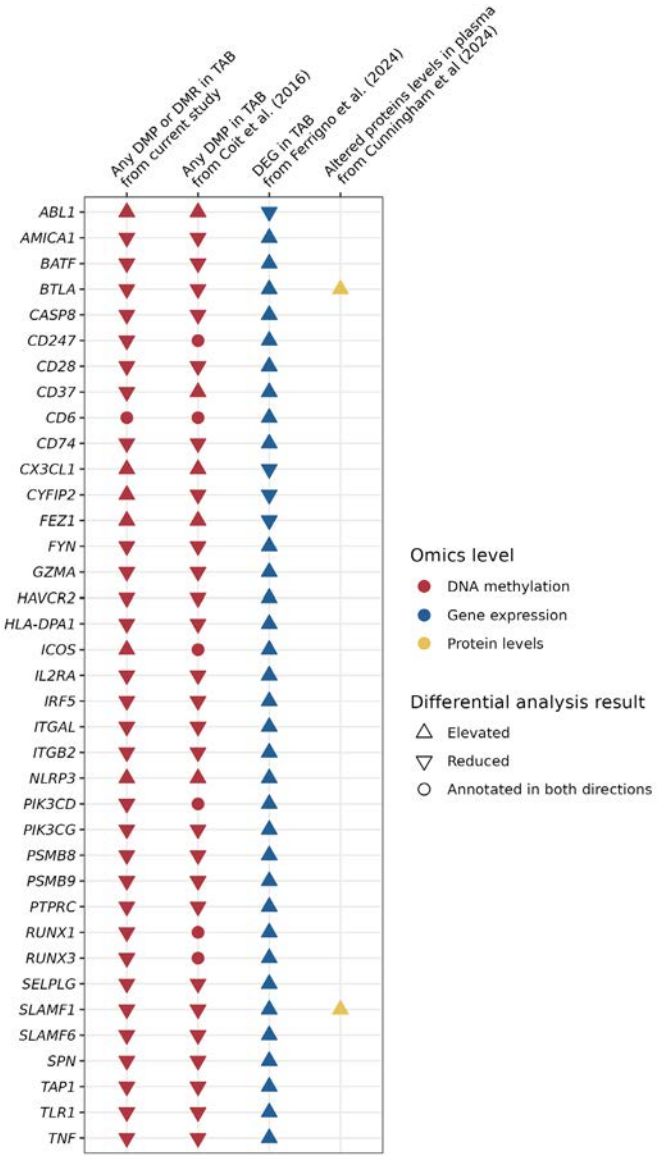

Figure 4. Reported alterations of gene regulation, gene expression, and/or protein abundance levels in independent giant cell arteritis omics studies for the 37 consistently reported genes in giant cell arteritis–affected arteries. DMP, differentially methylated position; DMR, differentially methylated region; TAB, temporal artery biopsy. Color figure can be viewed in the online issue, which is available at http://onlinelibrary.wiley.com/doi/10.1002/art.43358/abstract.

CD8+ and CD4+ T cells contribute to disease progression. Understanding the functional implications of T cell exhaustion in GCA could reveal novel mechanisms of immune dysregulation and provide opportunities for targeted therapeutic interventions aimed at restoring T cell function or mitigating exhaustion pathways, a promising therapeutic strategy currently under active investigation in other conditions.[34,35]

Regarding epigenetic alterations newly identified in this current study, pathway analysis revealed a broad spectrum of disrupted mechanisms in the context of GCA. Among these, the IL-2 signaling pathway emerged prominently, with the highest number of affected genes (n = 93) being annotated to this pathway. This finding emphasizes the contribution of IL-2 signaling in GCA pathophysiology, associated with vascular persistent Th1 cell signature.[36] Notably, low-dose IL-2 therapy has shown significant promise in helping regulate inflammatory responses across a broad range of IMIDs.[37] These results suggest GCA as a compelling candidate for exploring the therapeutic potential of IL-2–based treatments. Similarly, the IL-7 signaling pathway, also related to IL-2, was found to be significantly enriched in our results. Although IL-7 is well documented to play a role in other IMIDs[38] and is known to affect immune cell populations, for example, promoting T cell apoptosis,[39] its involvement in GCA pathogenesis represents a novel finding showing specific therapeutic potential.[40] Furthermore, our study also found a significant change in the regulation of *IL11RA*, which supports the recently proposed contribution of IL-11 in GCA pathogenesis by a multiomics study of blood-derived GCA monocytes.[8] Finally, another notable finding was the novel association of the CXCR4 signaling pathway with this disease, an essential regulator of local inflammation.[41] CXCR4 is instrumental in preserving arterial integrity, regulating vascular inflammation, and promoting angiogenesis and the recruitment of inflammatory cells,[42,43] processes that are central to the pathophysiology of GCA. The implication of CXCR4 in GCA pathogenesis also shows great therapeutic promise, as CXCR4-targeted therapies are under active research.[44] These findings reinforce the relevance of local immune and vascular signaling in GCA and suggest that targeting pathways such as CXCR4 and IL-2 could be pertinent for therapeutic innovation in this disease.

Our study offers valuable insights into the epigenetic changes in GCA-affected arteries, leveraging well-powered genome-wide DNA methylation profiling and multiomics comparison to provide a comprehensive overview of this disease. The use of a notable cohort and robust analytical methods allowed us to identify novel pathways and mechanisms such as T cell exhaustion and CXCR4 signaling. However, several limitations should be acknowledged to fully contextualize these findings. The omics evidence presented here provides statistical evidence but requires further functional studies to clarify how the proposed pathways and genes mechanistically contribute to GCA pathogenesis. It is also important to clarify that because of the lack of reference methods for cell deconvolution in arterial tissue, we were unable to adjust our models for cell composition. Thus, our results represent bulk tissue methylation changes reflecting the combined signal from all cellular components. One important aspect that remains unexplored in our study is how the genetic component of GCA contributes to the extensive epigenomic alterations identified. Achieving this goal will require a comprehensive multiomics approach, including quantitative trait loci analyses. Moreover, the substantial clinical heterogeneity of patients with GCA posed challenges for our analysis. Although we identified a robust epigenetic signature associated with GCA, limitations in the sample size of our cohort prevented the possibility of studying

the effect of particular clinical manifestations in DNA methylation, restricting our ability to detect epigenetic patterns linked to particular phenotypes. It is also noteworthy that, because of the inherent difficulty of obtaining TAB samples from individuals ultimately diagnosed as non-GCA, only 10 control samples were available for analysis, resulting in an imbalanced case–control ratio. These limitations highlight the importance of future research involving larger, clinically well-characterized cohorts and experimental validation to enhance our understanding of the molecular mechanisms driving GCA pathogenesis.

This study represents a methodologically robust analysis into the epigenetic landscape of GCA-affected arteries, leveraging genome-wide DNA methylation profiling and previous omics findings to provide novel insights into the pathogenesis of this disease. Among the key results, the potential involvement of exhausted T cells in GCA pathophysiology represents an intriguing discovery, representing a new potential agent of the immune dysfunction present in GCA-affected arterial tissue. These findings enhance our understanding of GCA pathogenesis and highlight therapeutic targets, paving the way for improved treatment strategies.

ACKNOWLEDGMENTS

We express our gratitude to Sofia Vargas for her exceptional technical support as well as to all the patients and control donors for their indispensable cooperation.

AUTHOR CONTRIBUTIONS

All authors contributed to at least one of the following manuscript preparation roles: conceptualization AND/OR methodology, software, investigation, formal analysis, data curation, visualization, and validation AND drafting or reviewing/editing the final draft. As corresponding author, Dr Ortiz-Fernandez confirms that all authors have provided the final approval of the version to be published and takes responsibility for the affirmations regarding article submission (eg, not under consideration by another journal), the integrity of the data presented, and the statements regarding compliance with institutional review board/Declaration of Helsinki requirements.

REFERENCES

1. Weyand CM, Goronzy JJ. Immune mechanisms in medium and large-vessel vasculitis. Nat Rev Rheumatol 2013;9(12):731–740.
2. Kaymakci MS, Warrington KJ, Kermani TA. New therapeutic approaches to large-vessel vasculitis. Annu Rev Med 2024;75(1):427–442.
3. Pugh D, Karabayas M, Basu N, et al. Large-vessel vasculitis. Nat Rev Dis Primers 2022;7(1):93.
4. Weyand CM, Goronzy JJ. Immunology of giant cell arteritis. Circ Res 2023;132(2):238–250.
5. Borrego-Yaniz G, Ortiz-Fernández L, Madrid-Paredes A, et al; Spanish GCA Group; UK GCA Consortium; Vasculitis Clinical Research Consortium. Risk loci involved in giant cell arteritis susceptibility: a genome-wide association study. Lancet Rheumatol 2024;6(6):e374–e383.
6. González-Gay MÁ, Heras-Recuero E, Blázquez-Sánchez T, et al. Genetics of vasculitis. Best Pract Res Clin Rheumatol 2024;38(4):101969.
7. Estupiñán-Moreno E, Hernández-Rodríguez J, Li T, et al. Decoding $CD4^+$ T cell transcriptome in giant cell arteritis: novel pathways and altered cross-talk with monocytes. J Autoimmun 2024;146:103240.
8. Estupiñán-Moreno E, Ortiz-Fernández L, Li T, et al. Methylome and transcriptome profiling of giant cell arteritis monocytes reveals novel pathways involved in disease pathogenesis and molecular response to glucocorticoids. Ann Rheum Dis 2022;81(9):1290–1300.
9. Feinberg AP. The key role of epigenetics in human disease prevention and mitigation. N Engl J Med 2018;378(14):1323–1334.
10. Mazzone R, Zwergel C, Artico M, et al. The emerging role of epigenetics in human autoimmune disorders. Clin Epigenetics 2019;11(1):34.
11. Berdasco M, Esteller M. Clinical epigenetics: seizing opportunities for translation. Nat Rev Genet 2019;20(2):109–127.
12. Coit P, De Lott LB, Nan B, et al. DNA methylation analysis of the temporal artery microenvironment in giant cell arteritis. Ann Rheum Dis 2016;75(6):1196–1202.
13. Hunder GG, Bloch DA, Michel BA, et al. The American College of Rheumatology 1990 criteria for the classification of giant cell arteritis. Arthritis Rheum 1990;33(8):1122–1128.
14. Aryee MJ, Jaffe AE, Corrada-Bravo H, et al. Minfi: a flexible and comprehensive Bioconductor package for the analysis of Infinium DNA methylation microarrays. Bioinformatics 2014;30(10):1363–1369.
15. Zhou W, Laird PW, Shen H. Comprehensive characterization, annotation and innovative use of Infinium DNA methylation BeadChip probes. Nucleic Acids Res 2017;45(4):e22.
16. Ritchie ME, Phipson B, Wu D, et al. limma powers differential expression analyses for RNA-sequencing and microarray studies. Nucleic Acids Res 2015;43(7):e47.
17. Xiong Z, Yang F, Li M, et al. EWAS Open Platform: integrated data, knowledge and toolkit for epigenome-wide association study. Nucleic Acids Res 2022;50(D1):D1004–D1009.
18. Peters TJ, Buckley MJ, Chen Y, et al. Calling differentially methylated regions from whole genome bisulphite sequencing with DMRcate. Nucleic Acids Res 2021;49(19):e109.
19. Kuleshov MV, Jones MR, Rouillard AD, et al. Enrichr: a comprehensive gene set enrichment analysis web server 2016 update. Nucleic Acids Res 2016;44(W1):W90–W97.
20. Aleksander SA, Balhoff J, Carbon S, et al; Gene Ontology Consortium. The Gene Ontology knowledgebase in 2023. Genetics 2023;224(1):iyad031.
21. Huang R, Grishagin I, Wang Y, et al. The NCATS BioPlanet - an integrated platform for exploring the universe of cellular signaling pathways for toxicology, systems biology, and chemical genomics. Front Pharmacol 2019;10:445.
22. Ferrigno I, Bonacini M, Rossi A, et al. Genes deregulated in giant cell arteritis by Nanostring nCounter gene expression profiling in temporal artery biopsies. RMD Open 2024;10(3):e004600.
23. Cunningham KY, Hur B, Gupta VK, et al. Plasma proteome profiling in giant cell arteritis. Ann Rheum Dis 2024;83(12):1762–1772.
24. Takahashi M. NLRP3 inflammasome as a key driver of vascular disease. Cardiovasc Res 2022;118(2):372–385.
25. Shen H-H, Yang Y-X, Meng X, et al. NLRP3: a promising therapeutic target for autoimmune diseases. Autoimmun Rev 2018;17(7):694–702.
26. Vande Walle L, Lamkanfi M. Drugging the NLRP3 inflammasome: from signalling mechanisms to therapeutic targets. Nat Rev Drug Discov 2024;23(1):43–66.

27. Baessler A, Vignali DAA. T cell exhaustion. Annu Rev Immunol 2024; 42(1):179–206.
28. Belk JA, Daniel B, Satpathy AT. Epigenetic regulation of T cell exhaustion. Nat Immunol 2022;23(6):848–860.
29. Jiang Y, Li Y, Zhu B. T-cell exhaustion in the tumor microenvironment. Cell Death Dis 2015;6(6):e1792.
30. Régnier P, Le Joncour A, Maciejewski-Duval A, et al. CTLA-4 pathway is instrumental in giant cell arteritis. Circ Res 2023;133(4):298–312.
31. Cao C, Xu M, Wei Y, et al. CXCR4 orchestrates the TOX-programmed exhausted phenotype of $CD8^+$ T cells via JAK2/STAT3 pathway. Cell Genom 2024;4(10):100659.
32. Reitsema RD, van der Geest KSM, Sandovici M, et al. Phenotypic, transcriptomic and functional profiling reveal reduced activation thresholds of CD8+ T cells in giant cell arteritis. Rheumatology (Oxford) 2022;62(1):417–427.
33. Saggau C, Bacher P, Esser D, et al. Autoantigen-specific $CD4^+$ T cells acquire an exhausted phenotype and persist in human antigen-specific autoimmune diseases. Immunity 2024;57(10):2416–2432.e8.
34. Pauken KE, Wherry EJ. Overcoming T cell exhaustion in infection and cancer. Trends Immunol 2015;36(4):265–276.
35. Gao Z, Feng Y, Xu J, et al. T-cell exhaustion in immune-mediated inflammatory diseases: new implications for immunotherapy. Front Immunol 2022;13:977394.
36. Koster MJ, Warrington KJ. Giant cell arteritis: pathogenic mechanisms and new potential therapeutic targets. BMC Rheumatol 2017; 1(1):2.
37. Rosenzwajg M, Lorenzon R, Cacoub P, et al. Immunological and clinical effects of low-dose interleukin-2 across 11 autoimmune diseases in a single, open clinical trial. Ann Rheum Dis 2019;78(2):209–217.
38. Meyer A, Parmar PJ, Shahrara S. Significance of IL-7 and IL-7R in RA and autoimmunity. Autoimmun Rev 2022;21(7):103120.
39. Chen D, Tang T-X, Deng H, et al. Interleukin-7 biology and its effects on immune cells: mediator of generation, differentiation, survival, and homeostasis. Front Immunol 2021;12:747324.
40. Mackall CL, Fry TJ, Gress RE. Harnessing the biology of IL-7 for therapeutic application. Nat Rev Immunol 2011;11(5):330–342.
41. Bianchi ME, Mezzapelle R. The chemokine receptor CXCR4 in cell proliferation and tissue regeneration. Front Immunol 2020;11:2109.
42. Döring Y, Noels H, van der Vorst EPC, et al. Vascular CXCR4 limits atherosclerosis by maintaining arterial integrity: evidence from mouse and human studies. Circulation 2017;136(4):388–403.
43. Jin DK, Shido K, Kopp H-G, et al. Cytokine-mediated deployment of SDF-1 induces revascularization through recruitment of CXCR4+ hemangiocytes. Nat Med 2006;12(5):557–567.
44. Saotome K, McGoldrick LL, Ho J-H, et al. Structural insights into CXCR4 modulation and oligomerization. Nat Struct Mol Biol 2025; 32:315–325.

American College of Rheumatology
Empowering Rheumatology Professionals

Arthritis & Rheumatology
Vol. 78, No. 2, February 2026, pp 394–402
DOI 10.1002/art.43354

BRIEF REPORT

Longitudinal Autoantibody and Proteomic Signatures of Disease Progression in Systemic Sclerosis

Muyao Guo,[1] Sijia Liu,[1] Jing Huang,[1] Ying Long,[1] Yu Wei,[1] Quanzhen Li,[2] Hui Luo,[1] and Honglin Zhu[1]

Objective. To evaluate dynamic changes in autoantibody and proteomic profiles in treatment-naïve patients with systemic sclerosis (SSc) and to identify biomarkers and mechanisms associated with disease progression.

Methods. Serum samples from 30 baseline and 49 follow-up patients with SSc, along with 38 controls, were analyzed. Autoantibody profiles were assessed using an autoantigen microarray targeting 120 autoantibodies, whereas proteomic analysis was conducted via liquid chromatography mass spectrometry in data-independent acquisition mode. Cox proportional hazards models were used to assess associations with disease progression, and Spearman's correlation was applied to analyze antibody–protein interactions.

Results. Baseline autoantibody profiling identified two patient subgroups: high expression (SSc_high) and low expression (SSc_low), though their clinical characteristics were similar. Longitudinal analysis revealed that 88.9% of patients with rising autoantibody titers experienced disease progression, whereas 60% of those with decreasing titers showed clinical improvement. Notably, increased CENP-B titers (hazard ratio 5.036) were strongly linked to disease progression. Proteomic analysis identified 112 proteins involved in tissue repair and immune modulation in patients with declining titers and clinical improvement, whereas 46 proteins linked to lipid metabolism and oxidative stress were enriched in those with rising titers and disease progression. SERPINA10 emerged as the strongest risk factor for progression, whereas ENTPD5 was most protective. Antibody–protein correlations that highlight key molecular interactions, including SERPINE1 and muscarinic receptor antibodies, were identified.

Conclusion. Dynamic changes in autoantibody titers, rather than baseline levels, were more strongly associated with SSc trajectory. Proteomic signatures suggest lipid metabolism and oxidative stress as potential drivers, highlighting novel biomarkers and therapeutic targets for personalized SSc management.

INTRODUCTION

Systemic sclerosis (SSc) is a rare, clinically heterogeneous autoimmune disease characterized by inflammation, progressive fibrosis of the skin and internal organs, and microvascular damage. These pathologic features can lead to life-threatening complications affecting the lungs, heart, gastrointestinal tract, and kidneys. The unpredictable nature of the disease presents significant challenges for effective management, highlighting the need for reliable biomarkers to improve patient outcomes.

Previous studies have underscored the critical role of autoantibodies in predicting SSc prognosis. Key examples include anticentromere antibodies (ACA), anti–topoisomerase I antibodies (Scl-70/anti–topo I), and anti–RNA polymerase III antibodies.

Supported by the Chinese National Key Technology R&D Program of the Ministry of Science and Technology (grant 2024YFC2510300), the National Natural Science Foundation of China (grants 82202002, 82471842, 82471840, and 81901664), the Natural Science Foundation of Hunan Province in China (grants 2023JJ41002 and 2020JJ5894), and the Edith Busch Research Award from the World Scleroderma Foundation.

[1]Muyao Guo, PhD, Sijia Liu, PhD, Jing Huang, PhD, Ying Long, MSc, Yu Wei, MBBS, Hui Luo, PhD, Honglin Zhu, PhD: Department of Rheumatology and Immunology, Provincial Clinical Research Center for Rheumatic and Immunologic Diseases, and National Clinical Research Center for Geriatric Disorders, Xiangya Hospital, Central South University, Changsha, China; [2]Quanzhen Li, PhD: Department of Rheumatology and Immunology, Provincial Clinical Research Center for Rheumatic and Immunologic Diseases, and National Clinical Research Center for Geriatric Disorders, Xiangya Hospital, Central South University, Changsha, China, and Genecopoeia, Inc, Rockville, Maryland.

Additional supplementary information cited in this article can be found online in the Supporting Information section (http://acrjournals.onlinelibrary.wiley.com/doi/10.1002/art.43354).

Author disclosures are available at https://onlinelibrary.wiley.com/doi/10.1002/art.43354.

Address correspondence via email to Honglin Zhu, PhD, at honglinzhu@csu.edu.cn.

Submitted for publication March 31, 2025; accepted in revised form July 30, 2025.

Patients with Scl-70 antibodies face a higher risk of severe complications, such as diffuse cutaneous sclerosis and pulmonary fibrosis, whereas those with anti–RNA polymerase III antibodies have a 10-fold increased risk of scleroderma renal crisis.[1] Additionally, anti–protein-arginine *N*-methyltransferase 5 has recently been proposed as a potential biomarker of disease trajectory, whereas others—such as anti–tripartite motif–containing protein 21, anti–interferon-inducible protein 16, anti-gephyrin, anti-gAChR, and anti-SSSCA1—have been linked to pulmonary arterial hypertension, interstitial lung disease (ILD), gastrointestinal dysmotility, cancer risk, and cardiac manifestations.[2] However, up to 11% of patients with SSc test negative for antinuclear antibodies,[3] and as many as 17% lack detectable levels of established SSc-specific antibodies,[4] underscoring the need for additional biomarkers to improve disease classification and prognosis.

Emerging research has identified autoantibodies with potential pathogenic roles, including antiplatelet-derived growth factor receptor antibodies, anti–endothelial cell antibodies, and antifibroblast antibodies. Some autoantibodies also influence the transcriptomic landscape of SSc blood cells. For instance, patients with Scl-70 antibodies exhibit a proinflammatory and fibrotic transcriptional signature characterized by impaired tissue remodeling and elevated carnitine metabolism, whereas ACA-positive patients display a signature associated with immunomodulation, tissue homeostasis, and increased phospholipid metabolism.[5] Single-cell RNA sequencing has revealed distinct gene expression profiles in specific cell clusters across autoantibody-defined SSc subgroups,[6] suggesting the potential of autoantibody profiling as a prognostic biomarker. However, further studies are required to elucidate the mechanistic role of autoantibodies in the pathogenesis of SSc. Exploring the pathogenic roles of autoantibodies may provide valuable insights for identifying new therapeutic targets. Moreover, most studies on autoantibodies in SSc have been cross-sectional, leaving the relationship between autoantibody dynamics and disease progression poorly understood.

In this study, we conducted a comprehensive analysis of autoantibody levels and proteomic profiles in 30 patients newly diagnosed with SSc, who were observed for 6 to 24 months, to assess dynamic changes during treatment and identify biomarkers associated with disease progression. By integrating autoantibody and protein signatures, we aim to advance biomarker-driven strategies for managing the clinical heterogeneity of SSc and to deepen our understanding of its underlying disease mechanisms.

MATERIALS AND METHODS

Patient recruitment. Serum samples were collected at Xiangya Hospital from 30 treatment-naïve patients with SSc at the time of diagnosis (SSc baseline, n = 30), as well as from 38 age- and sex-matched normal controls (NC). In addition, a total of 49 follow-up serum samples were collected from this same cohort at various time points after treatment initiation, including at 6 months (n = 20), 12 months (n = 16), 18 months (n = 5), and 24 months (n = 8) (Supplementary Figure 1). All patients met the 2013 American College of Rheumatology/EULAR classification criteria for SSc, and individuals with malignancies, infections, other autoimmune diseases, or metabolic disorders were excluded.[7]

Disease progression was defined as any of the following criteria:

1. Worsening of dermal fibrosis (≥5-point and 20% increase in the modified Rodnan skin thickness score [MRSS]).[8]
2. Radiologic deterioration of lung fibrosis, based on criteria adapted from the 2022 international guideline for progressive pulmonary fibrosis.[9] Serial high-resolution computed tomography scans were interpreted by experienced thoracic radiologists, and progression was defined by one or more of the following: increased extent or severity of traction bronchiectasis or bronchiolectasis, new ground-glass opacities with associated traction bronchiectasis, new areas of fine reticulation, increased extent or coarseness of reticular abnormalities, new or increased honeycombing, or increased lobar volume loss.
3. An increase in systolic pulmonary artery pressure to >45 mm Hg on echocardiography as a surrogate for pulmonary arterial hypertension.
4. New onset of digital ulcers, renal crisis, or gastrointestinal involvement.[10]

SSc improvement was defined as a ≥5-point and 20% decrease in MRSS over 12 months or a radiologic improvement of ILD.[11]

Demographic and clinical data were collected for all participants (Supplementary Tables 1–3). The study was approved by the ethics committee of Xiangya Hospital, Central South University (Changsha, Hunan, China; ID: 201303293), and written informed consent was obtained from all participants.

Autoantibody profiling. Autoantibody profiling was conducted using the Systemic Autoimmune-Associated Antigen Array (PA001-V3; GeneCopoeia Inc), which detects 120 autoantibodies, including controls. On the day of hybridization, autoantigen slides were equilibrated to room temperature for 30 minutes. A 16-section frame was applied to separate individual arrays, followed by blocking with 50 μl of blocking buffer under gentle agitation for 30 minutes. Serum samples were diluted 1:100 in blocking buffer, an optimized dilution based on preliminary experiments to maximize the signal-to-noise ratio. Then, 50 μl of the diluted serum samples was applied to each array and incubated for 60 minutes with agitation. After incubation, slides were washed three times with 100 μl of washing buffer (phosphate buffered saline [PBS] with 0.05% Tween 20, pH 7.4) for five minutes each under agitation. Cy3-labeled anti-human

IgG (Jackson ImmunoResearch) was applied at a 1:500 dilution, followed by a 60-minute incubation at room temperature. After further washing, the frame was removed, and the slides were briefly immersed in PBS before being spun dry. Fluorescent signals were detected using a GenePix 4000B scanner (Molecular Devices, LLC) with a 532 nm laser (for Cy3). Data processing was based on net signal intensity, calculated as the average fluorescence of each antigen after subtracting local background and negative control signals. Results were normalized to internal Ig controls.[12]

Proteomics analysis. Fasting morning blood samples were collected from NC and patients with SSc. Serum samples were separated by centrifugation at 3,000 revolutions per minute for 10 minutes at 4°C and stored at –80°C until analysis. To enhance the detection of low-abundance proteins, high-abundance proteins such as albumin and Ig were depleted using the Pierce Albumin Depletion Kit (Thermo Fisher Scientific). The depleted serum samples were then denatured with 8*M* urea, alkylated with 50-m*M* iodoacetamide, and digested overnight with trypsin at 37°C (Thermo Fisher Scientific). Peptides were purified using Pierce C18 Spin Columns (Thermo Fisher Scientific), following the manufacturer's protocol. Liquid chromatography mass spectrometry/mass spectrometry was performed in data-independent acquisition mode using a NanoAcquity UHPLC system coupled to an Orbitrap Exploris 240 mass spectrometer (Thermo Fisher Scientific). Briefly, 0.5 μg of peptides were enriched in a trap column at a flow rate of 10 μl/min for 4 minutes and then were separated on an analytical column (2 μm, Acclaim PepMap 100 C18 HPLC, 100 Å, 250 × 0.075 mm [Thermo Fisher Scientific]) at a constant flow rate of 300 nl/min over 150 minutes. Protein expression was quantified using DIA-NN version 1.8.1 (Aptila Biotech GmbH) with the UniProt human protein database (www.uniprot.org/, accessed October 20, 2022) as the reference library and with a precursor false discovery rate threshold of <0.05. Data were normalized using the DEP package in R version 1.16.0 (R Project for Statistical Computing).

Statistical analysis. All statistical analyses were performed using R software. The Shapiro–Wilk test was used to assess data normality. For normally distributed data with homogeneous variances, an unpaired *t*-test was applied, whereas for nonnormally distributed data or those with heterogeneous variances, the Mann–Whitney U test was used. Multiple group comparisons were conducted using the Kruskal–Wallis test, and categorical variables were analyzed using the chi-square test or Fisher exact test. To assess whether autoantibodies and proteins were significant independent predictors of SSc disease progression, the hazard ratio (HR) was calculated using the Cox proportional hazards model, implemented via the survival package. Correlations between autoantibody and protein levels were analyzed using Spearman's rank correlation coefficient. A two-sided *P* value of <0.05 was considered statistically significant.

RESULTS

Identification of high- and low-expression antibody groups in patients with SSc. Using an autoantigen microarray, we profiled 85 autoantibodies in serum samples from 30 treatment-naïve patients with SSc (SSc baseline) and 38 NC after quality control, categorizing them into 10 groups: antinuclear antibodies (eg, Scl-70/anti–topo I, CENP-A, CENP-B), blood factors (Factor B/D/H/I/P, fibrinogen IV), complement proteins (C1q, C3/C3a), cytokines (growth differentiation factor 15 [GDF-15], Transforming growth factor beta-1 proprotein [TGFβ1]), cytoskeletal/extracellular matrix proteins (eg, α-actinin, β-actin, collagen I–VI, vitronectin), inflammatory factors (interferon-α, tumor necrosis factor α), mitochondrial-related antibodies (M2, FARS2), organ-specific antibodies (eg, neuropilin-1, myelin basic protein, Thyroid peroxidase, Tissue transglutaminase), and other antibodies (eg, S100B, amyloid, hemocyanin, aquaporin 4) (Figure 1A). Clustering analysis identified two distinct patient subgroups: a high-expression antibody group (SSc_high) and a low-expression antibody group (SSc_low) (Figure 1A). The anti–Scl-70/anti–topo I antibody was detected in most patients with SSc but was absent in NC. However, comparison between the SSc_high and SSc_low groups revealed no significant differences in demographics (age, sex) or clinical characteristics, including SSc subtype, disease duration, Raynaud phenomenon (RP), ILD, MRSS, or fibrotic laboratory markers (Krebs von den Lungen 6, ferritin) (Figure 1B and C).

Serum antibody level changes correlate with disease progression in patients with SSc. To investigate changes in serum antibody levels during follow-up and their association with disease progression in SSc, we analyzed antibody dynamics in two groups: SSc_high (n = 12) and SSc_low (n = 18), classified based on average antibody density. Antibody changes were categorized into three groups based on a >20% deviation from baseline at the first follow-up: increased, decreased, or unchanged (Supplementary Table 4). Among patients in the SSc_high group, 10 (83.33%) exhibited decreased antibody levels, 1 (8.33%) showed an increase, and 1 remained unchanged. In the SSc_low group, 8 patients (47.05%) had increased antibody levels, 5 (29.41%) showed a decrease, and 4 remained unchanged (Figure 2A and D). These findings suggest that patients with high baseline antibody levels were more likely to experience a decline over time, whereas those with low baseline levels were more prone to an increase.

To further assess the clinical relevance of antibody changes, we classified all patients into three groups based on antibody dynamics—increase (n = 9), decrease (n = 15), or unchanged (n = 5)—and evaluated their disease progression. Among patients

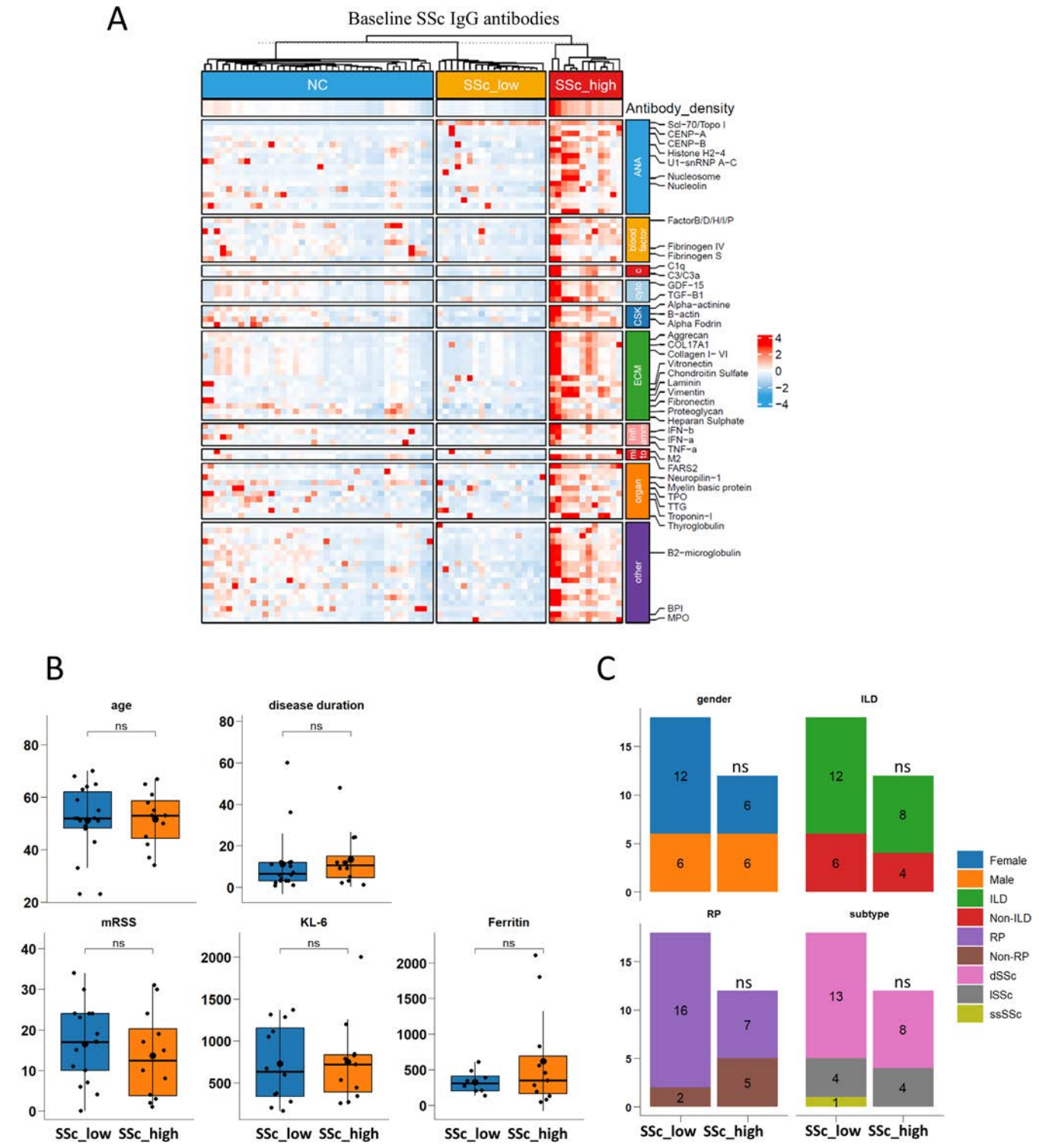

Figure 1. Antibody expression analysis in baseline patients with SSc compared to NC. (A) Heatmap illustrating the distribution of autoantibodies in baseline patients with SSc and NC. (B) Boxplot comparing clinical characteristics between the SSc_high and SSc_low groups. (C) Boxplot comparing the demographics or clinical characteristics between the SSc_high and SSc_low groups. ANA, antinuclear antibody; BPI, bactericidal permeability-increasing protein; CSK, cytoskeletal proteins; dSSc, diffuse cutaneous systemic sclerosis; ECM, extracellular matrix proteins; GAD65, Glutamate decarboxylase 65; GDF-15, growth differentiation factor 15; IFN, interferon; ILD, interstitial lung disease; KL-6, Krebs von den Lungen 6; lSSc, limited cutaneous systemic sclerosis; MPO, myeloperoxidase; mRSS, modified Rodnan skin thickness score; NC, normal controls; ns, not significant; RP, Raynaud's phenomenon; SSc, systemic sclerosis; ssSSc, systemic sclerosis sine scleroderma; TGF-B1, transforming growth factor β1; TNF, tumor necrosis factor; Topo I, topoisomerase I; TPO, Thyroid peroxidase; TTG, Tissue transglutaminase; U1-snRNP, U1 small nuclear ribonucleoprotein.

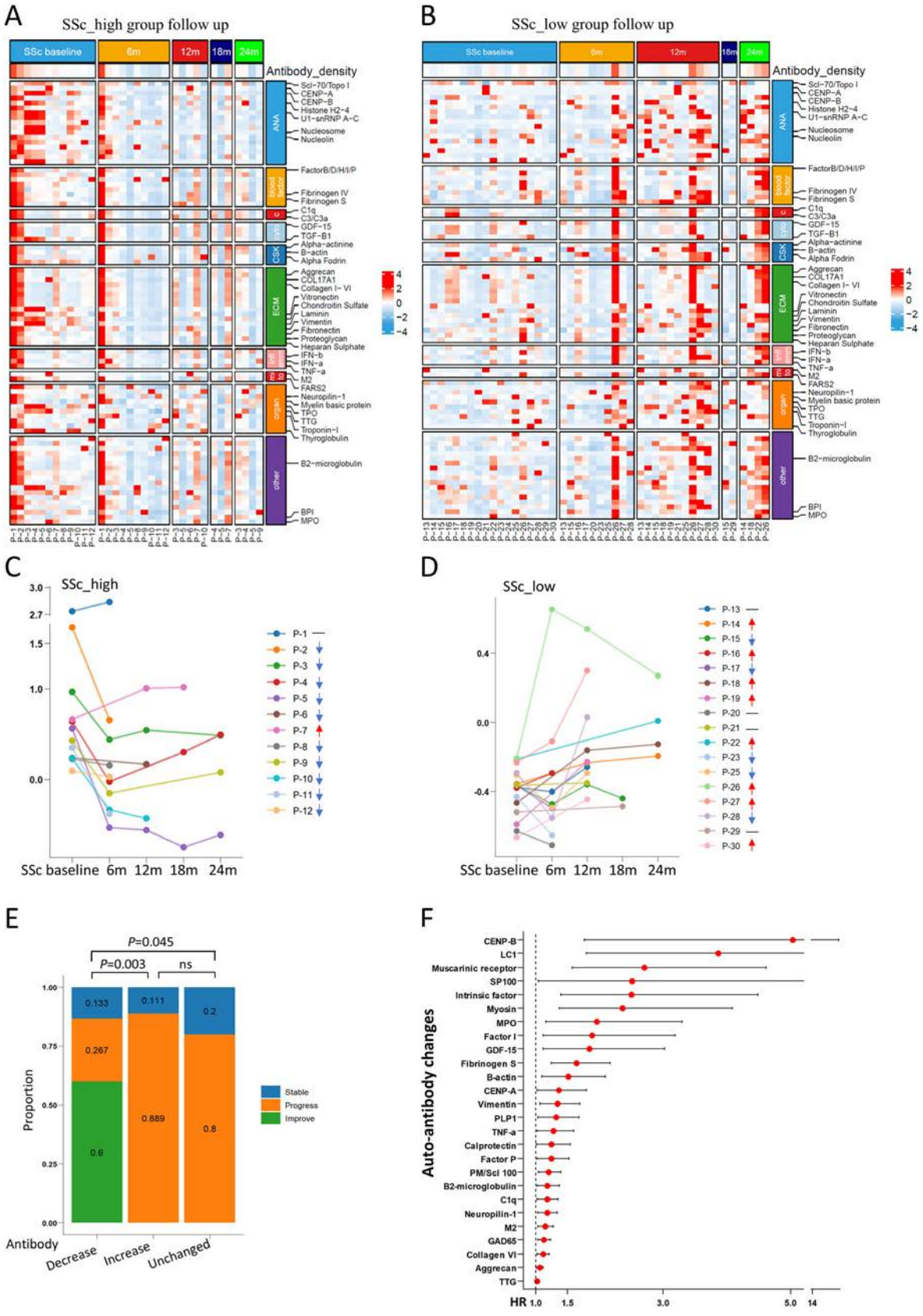

Figure 2. Legend on next page.

in the antibody decrease group, 60% showed clinical improvement, whereas 26.7% experienced disease progression. In contrast, 88.9% of patients in the antibody increase group exhibited disease progression, with no cases of improvement observed in either the increase or unchanged group. The difference in improved patients between the antibody increase and antibody decrease group was statistically significant ($P < 0.05$; Figure 2E, Supplementary Figure 2), indicating that a decline in antibody levels was associated with clinical improvement.

To further explore the role of specific antibody changes in disease progression, we calculated the HR. An increase in 26 antibodies during treatment was significantly associated with disease progression, with CENP-B showing the highest risk (HR 5.036). Other implicated antibodies included LC1, muscarinic receptor, SP100, intrinsic factor, myosin, myeloperoxidase, factor I, GDF-15, fibrinogen S, β-actin, and CENP-A, among others (Figure 2F).

Proteomic changes associated with differential antibody dynamics and disease trajectories. To investigate the influence of antibody titers on disease progression in SSc, we analyzed serum proteomic changes in two patient cohorts: one with significantly decreased antibody titers and clinical improvement and another with significantly increased titers and disease progression. In patients with reduced titers and improved clinical conditions, we identified 112 proteins (54 increased, 58 decreased) that exhibited significant changes, although these proteins remained unchanged in patients with elevated titers and disease progression. Functional analysis revealed that these proteins were primarily involved in leukocyte migration (CD74, intercellular adhesion molecule 1), differentiation (IHH, LGALS1), chemotaxis (phospholipase A_2 group 7, SERPINE1), extracellular matrix organization (VIM, NID2), collagen biosynthesis and metabolism (TGF-β1, IHH), and endothelial cell proliferation (LRG1, platelet-derived growth factor B, SPARC) (Figure 3A and B, Supplementary Table 5–6). Conversely, in patients with increased titers and disease progression, we identified 46 distinct protein changes (16 increased, 30 decreased) that were absent in the improved group; these proteins were predominantly associated with lipid metabolism (ADIPOQ, ANXA2, APOA4, apolipoprotein E), including the regulation of sterol and cholesterol transport, lipid localization, triglyceride metabolism, and cholesterol efflux, as well as with acute inflammatory responses (serum amyloid A1 [SAA1], SAA2, SAA4) and cellular responses to oxygen radicals and superoxide (superoxide dismutase 2). Additionally, seven proteins (one increased, six decreased) common to both groups were linked to glycolytic processes and pyridine/purine nucleotide catabolism (LDHA) (Figure 3A and B, Supplementary Tables 5 and 6).

HR analysis identified SERPINA10, SERPINE1, C1QB, C8G, and MINPP1 as risk factors for disease progression, whereas ENTPD5, HYOU1, LRG1, MMRN2, and CLU were associated with protection against progression (Figure 3C). Additionally, correlation analysis revealed that antibody changes were positively correlated with risk proteins and negatively correlated with protective proteins. Figure 3D highlights the top antibody–protein pairs, with SERPINE1, LDHA, FAH, APOA2, and BID as the proteins most frequently associated with antibody correlations, whereas muscarinic receptor, collagen VI, and aggrecan were the antibodies most frequently linked to protein correlations.

DISCUSSION

In this study, we identified two distinct groups of patients with SSc based on their baseline autoantibody expression levels. However, these baseline levels did not significantly correlate with clinical characteristics, such as the MRSS, ILD, or RP, suggesting that static antibody levels at diagnosis may not accurately reflect disease severity. Instead, our longitudinal analysis demonstrated that dynamic changes in antibody titers were more predictive of disease progression. Patients with rising antibody titers were more likely to experience disease worsening, whereas those with declining titers showed clinical improvement. We hypothesize that rising antibody titers during treatment may reflect ongoing immune activation, insufficient therapeutic response, or impending flare, whereas decreasing titers may signal immune modulation and treatment efficacy. Additionally, antibody kinetics and clinical manifestations may be temporally misaligned. High antibody titers or active immune response at baseline may not always translate to severe fibrotic outcomes, particularly if patients receive timely and effective treatment that mitigates downstream tissue damage.

To gain deeper mechanistic insights, we integrated autoantibody data with proteomic analysis. Patients with decreasing autoantibody titers and clinical improvement exhibited proteomic signatures associated with tissue repair and immune modulation. In contrast, those with increased titers and disease progression showed enrichment in proteins linked to lipid metabolism and oxidative stress. These

Figure 2. Changes in antibody expression during follow-up in patients with SSc. (A) Heatmap depicting changes in autoantibody expression in the SSc_high group. (B) Heatmap showing changes in autoantibody expression in the SSc_low group. (C) Line graph illustrating changes in autoantibody levels in the SSc_high group. (D) Line graph depicting changes in autoantibody levels in the SSc_low group. (E) Bar chart comparing disease progression, improvement, or stability in patients with SSc. (F) Forest plot illustrating the HR of autoantibody level changes on SSc disease progression. ANA, antinuclear antibody; BPI, bactericidal/permeability-increasing protein; CSK, cytoskeletal proteins; ECM, extracellular matrix proteins; GDF-15, growth differentiation factor 15; HR, hazard ratio; IFN, interferon; MPO, myeloperoxidase; ns, not significant; SSc, systemic sclerosis; TGF-B1, transforming growth factor β1; TNF, tumor necrosis factor; Topo I, topoisomerase I; TPO, Thyroid peroxidase; TTG, Tissue transglutaminase; U1-snRNP, U1 small nuclear ribonucleoprotein. Color figure can be viewed in the online issue, which is available at http://onlinelibrary.wiley.com/doi/10.1002/art.43354/abstract.

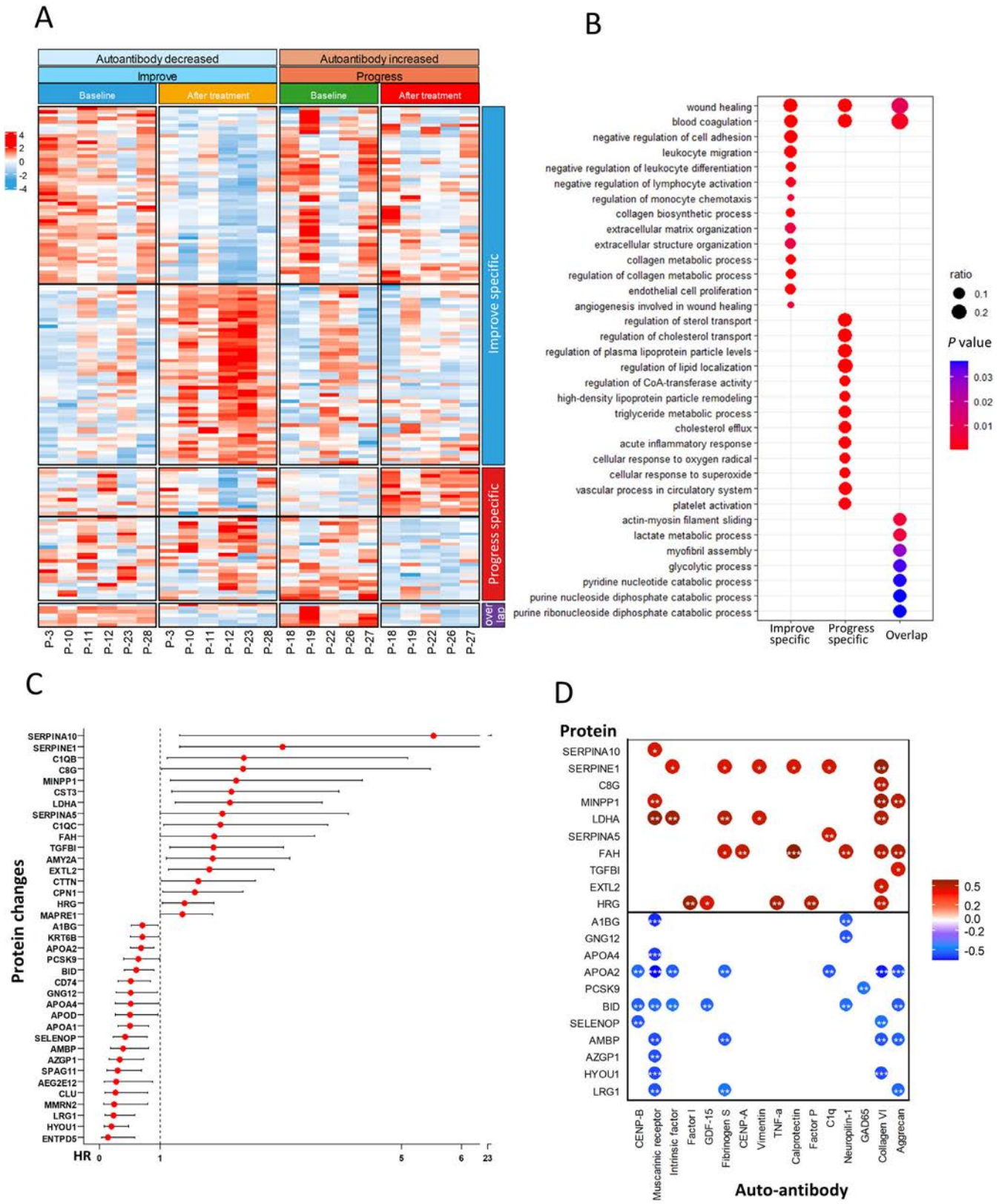

Figure 3. Impact of antibody titer changes on serum proteomic profiles. (A) Heatmap showing changes in serum proteomic profiles in patients with SSc before and after treatment. (B) Bubble plot representing GO pathway enrichment for altered proteins in A. (C) Forest plot showing the HR of altered protein levels on SSc disease progression. (D) Bubble plot illustrating the correlation between changes in protein levels and antibody titer changes. CoA, coenzyme A; GAD65, Glutamate decarboxylase 65; GDF-15, growth differentiation factor 15; GO, Gene Ontology; HR, hazard ratio; HRG, histidine-rich glycoprotein; LDHA, lactate dehydrogenase A; SSc, systemic sclerosis; TGFBI, transforming growth factor β1; TNF-α, tumor necrosis factor α. Color figure can be viewed in the online issue, which is available at http://onlinelibrary.wiley.com/doi/10.1002/art.43354/abstract.

findings suggest that persistent dysregulation of lipid metabolism and oxidative stress may drive disease progression. Targeting these pathways—such as correcting lipid metabolism abnormalities—could offer therapeutic benefits. Additionally, both progression and improvement groups exhibited alterations in glycolysis and nucleotide catabolism, indicating common molecular responses to treatment.

Several antibodies and proteins were significantly associated with disease progression. Among them, plasma serpin family proteins—SERPINE1, SERPINA5, and SERPINA10—were particularly notable. This aligns with prior research demonstrating that elevated SERPINE1 expression in SSc skin is linked to progressive skin fibrosis.[13] Conversely, protective factors such as apolipoproteins (APOA4, APOA2), PCSK9, and oxidative stress-related proteins (SELENOP, HYOU1) were associated with reduced disease severity.

Among the autoantibodies examined, CENP-B and CENP-A demonstrated predictive value for disease progression. This finding is consistent with previous studies showing that the presence of CENP-A and/or CENP-B predicts the extent of skin involvement over time.[14] Similarly, our research highlighted the role of antimuscarinic receptor antibodies in SSc progression, with strong correlations observed between these antibodies and multiple serum proteins. Earlier studies have linked gastrointestinal dysmotility in SSc to circulating autoantibodies against the muscarinic-3 receptor, which inhibit smooth muscle contraction when stimulated by cholinergic agents and block indirect muscle responses triggered by electric field neural stimulation.[15] These results suggest that antimuscarinic receptor antibodies may contribute to SSc-related gastrointestinal dysmotility by disrupting muscarinic neurotransmission.[16]

Anticollagen antibodies reactive to types I, II, III, IV, and V have been well documented in SSc.[17] In our study, we detected antibodies against collagen types I through VI in SSc serum samples and identified changes in anti–collagen VI antibodies as a risk factor for disease progression. Moreover, anti–collagen VI antibodies showed strong correlations with several serum proteins, including SERPINE1, LDHA, and APOA4, among others. However, their precise relationships and potential roles in SSc pathogenesis require further investigation in future studies.

This study has several limitations. First, the relatively small sample size and the decline in patient numbers over time, particularly at the 24-month follow-up, limit the statistical power and the strength of longitudinal conclusions. Additionally, the predominance of Scl-70/anti–topo I–positive patients in this cohort results in a relatively homogeneous autoantibody distribution, which may reduce the generalizability of our findings to the broader SSc population. Larger multicenter studies with more diverse autoantibody profiles are needed to validate these results and improve their applicability. Second, although we observed significant associations between changes in antibody titers, proteomic profiles, and disease progression, the causal relationships remain unclear. Future mechanistic studies are essential to determine how specific antibodies contribute to SSc pathogenesis at the molecular level.

In summary, our findings establish a connection between increasing autoantibody titers, proteomic changes, and the progression of SSc. By combining autoantibody and proteomic data, we have deepened our understanding of SSc pathogenesis, setting the stage for biomarker-driven approaches to manage the disease. Future research should focus on validating these biomarkers in diverse populations, clarifying the roles of the identified proteins, and creating tools for real-time clinical monitoring.

AUTHOR CONTRIBUTIONS

All authors contributed to at least one of the following manuscript preparation roles: conceptualization AND/OR methodology, software, investigation, formal analysis, data curation, visualization, and validation AND drafting or reviewing/editing the final draft. As corresponding author, Dr Zhu confirms that all authors have provided the final approval of the version to be published and takes responsibility for the affirmations regarding article submission (eg, not under consideration by another journal), the integrity of the data presented, and the statements regarding compliance with institutional review board/Declaration of Helsinki requirements.

REFERENCES

1. Penn H, Howie AJ, Kingdon EJ, et al. Scleroderma renal crisis: patient characteristics and long-term outcomes. QJM 2007;100(8):485–494.
2. Liang M, Wang L, Tian X, et al. Identification and validation of anti-protein arginine methyltransferase 5 (PRMT5) antibody as a novel biomarker for systemic sclerosis (SSc). Ann Rheum Dis 2024;83(9):1144–1155.
3. Nihtyanova SI, Denton CP. Autoantibodies as predictive tools in systemic sclerosis. Nat Rev Rheumatol 2010;6(2):112–116.
4. Yang S, Liang M, Chen C, et al. Clinical correlations with disease-associated auto-antibodies in a Chinese cohort with systemic sclerosis. Chin Med J (Engl) 2022;135(15):1878–1880.
5. Rouvière B, Le Dantec C, Bettacchioli E, et al; PRECISESADS Clinical Consortium; PRECISESADS Metabolomic Study Group. Stratification according to autoantibody status in systemic sclerosis reveals distinct molecular signatures. Ann Rheum Dis 2025;84(3):480–490.
6. Clark KEN, Xu S, Attah M, et al. Single-cell analysis reveals key differences between early-stage and late-stage systemic sclerosis skin across autoantibody subgroups. Ann Rheum Dis 2023;82(12):1568–1579.
7. van den Hoogen F, Khanna D, Fransen J, et al. 2013 classification criteria for systemic sclerosis: an American College of Rheumatology/-European League against Rheumatism collaborative initiative. Arthritis Rheum 2013; 65(11):2737–2747.
8. Martyanov V, Kim GJ, Hayes W, et al. Novel lung imaging biomarkers and skin gene expression subsetting in dasatinib treatment of systemic sclerosis-associated interstitial lung disease. PLoS One 2017;12(11):e0187580.
9. Raghu G, Remy-Jardin M, Richeldi L, et al. Idiopathic Pulmonary Fibrosis (an Update) and Progressive Pulmonary Fibrosis in Adults: An Official ATS/ERS/JRS/ALAT Clinical Practice Guideline. Am J Respir Crit Care Med. 2022;205(9):e18-e47.
10. Elhai M, Sritharan N, Boubaya M, et al; EUSTAR collaborators. Stratification in systemic sclerosis according to autoantibody status versus skin involvement: a study of the prospective EUSTAR cohort. Lancet Rheumatol 2022;4(11):e785–e794.

11. Khanna D, Denton CP, Assassi S, et al. A randomised, parallel-group, double-blind, placebo-controlled phase 3 study to Determine the effectiveness of the type I interferon receptor antibody, Anifrolumab, In SYstemic sclerosis: DAISY study design and rationale. Clin Exp Rheumatol 2024;42(8):1635–1644.
12. Li QZ, Zhou J, Wandstrat AE, et al. Protein array autoantibody profiles for insights into systemic lupus erythematosus and incomplete lupus syndromes. Clin Exp Immunol 2007;147(1):60–70.
13. Stifano G, Sornasse T, Rice LM, et al. Skin gene expression is prognostic for the trajectory of skin disease in patients with diffuse cutaneous systemic sclerosis. Arthritis Rheumatol 2018;70(6):912–919.
14. Hudson M, Mahler M, Pope J, et al; Investigators of the Canadian Scleroderma Research Group. Clinical correlates of CENP-A and CENP-B antibodies in a large cohort of patients with systemic sclerosis. J Rheumatol 2012;39(4):787–794.
15. Singh J, Cohen S, Mehendiratta V, et al. Effects of scleroderma antibodies and pooled human immunoglobulin on anal sphincter and colonic smooth muscle function. Gastroenterology 2012;143(5):1308–1318.
16. Kumar S, Singh J, Kedika R, et al. Role of muscarinic-3 receptor antibody in systemic sclerosis: correlation with disease duration and effects of IVIG. Am J Physiol Gastrointest Liver Physiol 2016;310(11):G1052–G1060.
17. Riente L, Marchini B, Dolcher MP, et al. Anti-collagen antibodies in systemic sclerosis and in primary Raynaud's phenomenon. Clin Exp Immunol 1995;102(2):354–359.

Arthritis & Rheumatology
Vol. 78, No. 2, February 2026, pp 403–417
DOI 10.1002/art.43356

American College of Rheumatology
Empowering Rheumatology Professionals

Chitinase 3–Like 1 Promotes Endothelial-to-Mesenchymal Transition in Systemic Sclerosis via Mechanistic Target of Rapamycin Complex 1 Signaling Pathway

Xiuyuan Wang,[1] Xue Han,[1] Jia Yu,[1] Feifei Hu,[1] Chengjie Huang,[2] Cheng Chen,[1] Liuting Huang,[1] Ying Jiang,[1] Xinzhi Xu,[1] Manna Lin,[1] Junxia Huang,[1] Tianbao Ye,[3] and Ji Yang[1]

Objective. Systemic sclerosis (SSc) is a complicated autoimmune connective tissue disorder. Endothelial-to-mesenchymal transition (EndoMT) contributes to vasculopathy and fibrosis in SSc, yet its underlying mechanism remains to be elucidated. Here, we determined the role and mechanism of chitinase 3–like 1 (CHI3L1) in SSc EndoMT.

Methods. Skin sections were immunostained for detecting the EndoMT and the expression pattern of CHI3L1 in patients with SSc. Human umbilical vein endothelial cells (HUVECs) were stimulated with recombinant CHI3L1 and anti-CHI3L1 antibody (CHI3L1 Ab) to explore the effects of CHI3L1 on ECs in vitro. In vivo, the bleomycin (BLM)-induced SSc mice were treated with CHI3L1 Ab to investigate the improvement of vasculopathy and fibrosis. Furthermore, proteomics was conducted to explore the specific mechanism by which CHI3L1 induces EndoMT in ECs.

Results. Immunofluorescence staining of skin sections confirmed EndoMT and the co-localization of CHI3L1 and ECs in patients with SSc. Subsequently, CHI3L1 was demonstrated to facilitate EndoMT in HUVECs. Furthermore, treatment with CHI3L1 Ab in BLM-SSc mice showed alleviation in SSc vasculopathy and fibrosis. Mechanistically, CHI3L1 mediated EndoMT primarily by binding to the CD44 receptor on ECs, then activating the downstream Akt/mechanistic target of rapamycin complex 1 (mTORC1)/S6 kinase signaling pathway, thereby regulating the EndoMT trigger transcription factors Snail and Slug. Finally, administration of rapamycin, an mTORC1 inhibitor, has been shown to inhibit the CHI3L1-mediated EndoMT process.

Conclusion. This research reveals a new function of CHI3L1 in facilitating EndoMT in SSc and highlights CHI3L1 as a promising therapeutic target for SSc.

INTRODUCTION

Systemic sclerosis (SSc) is a complex connective tissue disease marked by microvascular damage, immune dysregulation, and multiorgan fibrosis.[1–3] The excessive and irreversible fibrosis in SSc results in the highest mortality rate among all rheumatic disorders, which is mainly driven by the overproduction of activated myofibroblasts, leading to immoderate collagen-rich extracellular matrix (ECM) deposition.[4–7] Consequently, extensive research has focused on identifying the cellular origins of myofibroblasts due to their critical role in fibrosis. Recent studies have confirmed that vascular endothelial cells (ECs) show remarkable plasticity through endothelial-to-mesenchymal transition (EndoMT), serving as a key source of myofibroblasts.[8–10] EndoMT is a phenotypic conversion in which ECs lose polarity, down-regulate specific markers like CD31 and vascular endothelial cadherin (VE-Cadherin), and gain myofibroblast characteristics including expressing vimentin and α-smooth muscle actin

This study was supported by National Natural Science Foundation of China (grants 82073436 and 82373463), Shanghai Municipal Health Commission Scientific Research Project (grant 2024PT004), Zhongshan Hospital Scientific Research Project (grant ZSLCYJ202323), National Outstanding Young Physician Program, 2024 Shanghai Oriental Talents Program Top Talent Project (grant BJKJ2024048), Shanghai Talent Development Fund (grant R2021-010), Shanghai Academic Leader in Health and Wellness, 2025 National Project on Integration of Chinese and Western Medicine, and Distinguished Professors of Shanghai universities (Oriental Scholar).

[1]Xiuyuan Wang, MD, PhD, Xue Han, BM, Jia Yu, MM, Feifei Hu, MD, PhD, Cheng Chen, BM, Liuting Huang, MM, Ying Jiang, MD, PhD, Xinzhi Xu, MD, PhD, Manna Lin, MM, Junxia Huang, MD, PhD, Ji Yang, MD, PhD: Department of Dermatology, Zhongshan Hospital of Fudan University, Shanghai, China; [2]Chengjie Huang, PhD: School of Basic Medical Sciences, Guangzhou National Laboratory, Guangzhou Medical University, Guangzhou, China; [3]Tianbao Ye, MD, PhD: Xiamen Cardiovascular Hospital of Xiamen University, School of Medicine, Xiamen University, Xiamen, Fujian, China

Drs Wang, Han, and Yu contributed equally to this work.

Additional supplementary information cited in this article can be found online in the Supporting Information section (https://acrjournals.onlinelibrary.wiley.com/doi/10.1002/art.43356).

Author disclosures are available at https://onlinelibrary.wiley.com/doi/10.1002/art.43356.

Address correspondence via email to Ji Yang, MD, PhD, at yang.hua@yeah.net; to Junxia Huang, MD, PhD, at huangjunxia12@163.com; or to Tianbao Ye, MD, PhD, at yetb0220@163.com.

Submitted for publication April 13, 2025; accepted in revised form July 29, 2025.

(α-SMA), together with nuclear translocation of the transcription regulators Snail and Slug, key triggers of EndoMT.[11,12] To date, EndoMT has been recognized as a crucial transdifferentiation process contributing to vascular dysfunction and fibrosis in SSc.[13,14]

Chitinase 3–like 1 (CHI3L1), a member of the glycosyl hydrolase family 18, is a secreted glycoprotein that exhibits characteristics of both cytokines and growth factors, expressed in various cells such as macrophages, neutrophils, and keratinocytes.[15] Numerous studies have demonstrated that CHI3L1 plays a significant role in antigen-induced and oxidative injury responses, inflammation, tissue repair and remodeling, such as in the pathogenesis of rheumatoid arthritis, atopic dermatitis, and liver fibrosis.[16–18] Our recent research found elevated CHI3L1 levels in the skin and serum of patients with SSc, with serum levels linked to fibrosis severity.[19] These results suggest CHI3L1 as a key regulator in pathogenesis of SSc, although its specific role and underlying mechanisms remain unclear.

In this study, we observed that compared with healthy controls (HCs), patients with SSc exhibited significantly increased co-localization of ECs marker CD31 and CHI3L1 in the skin, particularly in those with cutaneous vascular symptoms. Additionally, the serum CHI3L1 concentration was found to be correlated with the vascular injury factor endothelin 1 (ET-1). We further demonstrated that CHI3L1 stimulation drove human umbilical vein ECs (HUVECs) to lose their specific marker CD31 and underwent transdifferentiation into myofibroblasts. This process primarily occurred via the binding of CHI3L1 to CD44, a transmembrane receptor on HUVECs, subsequently activating the downstream Akt/mechanistic target of rapamycin (mTOR) complex 1 (mTORC1)/S6 kinase (S6K) axis. Moreover, by application of humanized antibody against CHI3L1 (CHI3L1 Ab), we further demonstrated that treatment with CHI3L1 Ab ameliorated SSc vasculopathy and fibrosis in bleomycin (BLM)-induced SSc mice.[16] Our research highlights the novel role of CHI3L1 in inducing SSc-related EndoMT and hints CHI3L1 as a promising therapeutic target for improving the clinical outcomes of patients with SSc.

MATERIALS AND METHODS

Methods and materials availability. An extended description of methods and materials is provided in the Supplemental Material.

Patient involvement. Skin biopsies were collected from 10 patients with SSc and 10 healthy subjects for the immunofluorescence staining of skin sections (Supplementary Table S1). Specifically, SSc skin biopsies were obtained from the forearm (n = 5), back (n = 2), thigh (n = 2), and lower leg (n = 1). HC skin biopsies were obtained from the forearm (n = 4), back (n = 2), lower leg (n = 2), thigh (n = 1), and abdomen (n = 1). Serum samples were obtained from 35 patients with SSc (Supplementary Table S2).

Protein–protein interaction network analysis. Correlation of CHI3L1 and EndoMT-related proteins were analyzed using String (https://cn.string-db.org/). Protein–protein interaction (PPI) enrichment analysis was performed using Cytoscape (https://cytoscape.org/).

Cell culture, stimulation, gene delivery, and immunostaining. HUVECs (Promocell, Heidelberg, Germany) were cultured in ECs growth medium maintained at 37°C in a humidified 5% CO_2 atmosphere.

For stimulation, HUVECs were serum starved for 24 hours and then treated with phosphate-buffered saline (PBS), 100 ng/mL recombinant CHI3L1 (rCHI3L1; MedChemExpress [MCE]), 100 ng/mL CHI3L1 Ab, 100 ng/mL human IgG1 kappa Isotype Control (MCE), 100 ng/mL CD44 Ab (MCE), or 50 nM rapamycin (MCE) for an appropriate time.

We used a lentiviral vector containing mTOR short hairpin RNA (shRNA) to inhibit mTOR expression in this study. The lentiviral vectors of mTOR shRNA and control scrambled shRNA were purchased from Hanheng Biotechnology in Shanghai, China. The target sequence for mTOR shRNA was 5'-CCGCTAGTAGGGAGGTTTATT-3.' HUVECs were transduced for 48 hours with appropriate virus units according to the manufacturer's instructions. Subsequently, rCHI3L1 (100 ng/mL) or PBS was added to HUVECs transfected with mTOR shRNA or control shRNA and incubated for 48 hours.

For immunostaining, HUVECs were fixed with 4% paraformaldehyde and permeabilized with 0.03% Triton X-100 for 20 minutes and subsequently blocked with 5% bovine serum albumin (BSA) with 1% donkey serum for 30 minutes. HUVECs were subsequently stained with indicated primary antibodies at 4°C overnight. Afterwards, HUVECs were incubated with labeling fluorescent secondary antibody for 1 hour at room temperature, and nuclear was stained with DAPI (Invitrogen). Fluorescent images were acquired by fluorescent microscopy. Quantification of fluorescence intensity was performed using ImageJ software (version 1.52v).

Real-time quantitative reverse transcription polymerase chain reaction. Total RNA from tissues or cells was extracted using Total RNA Isolation Kit (Vazyme), according to the manufacturer's instructions. Complementary DNA (cDNA) was prepared using HiScript III 1st Strand cDNA Synthesis Kit (Vazyme) following the manufacturer's protocol. Real-time quantitative reverse transcription polymerase chain reaction (qRT-PCR) was conducted using Universal SYBR Green Master Mix (Vazyme). The primers for qRT-PCR were listed in Supplementary Table S3. 18s served as a housekeeping gene.

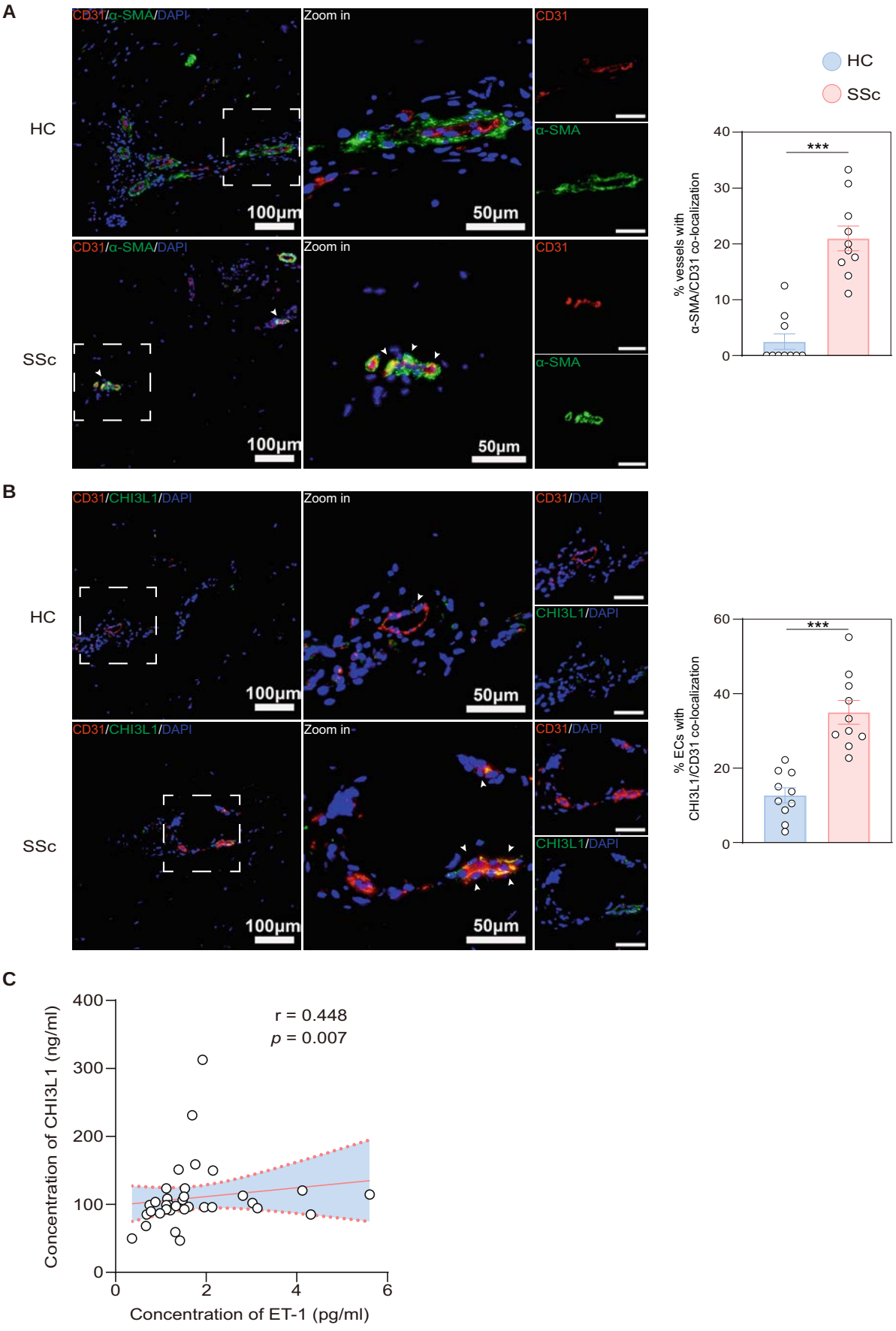

Figure 1. Legend on next page.

Standard comparative C_T method was used for calculating gene expression.

Western blot. Total proteins were extracted from cells or heart tissues using radioimmunoprecipitation assay buffer supplementary with complete protease inhibitor (Roche) and phosphatase inhibitor (Roche). Protein concentration was quantified using Pierce BCA Protein Assay Kit (Thermo Fisher Scientific). Equal amount of protein was added to sodium dodecyl sulfate–polyacrylamide gel electrophoresis (SDS–PAGE) gels. After separation, SDS–PAGE gels proteins were transferred to PVDF membranes and blocked with 5% BSA/Tris-buffered saline. The membranes were incubated with indicated primary antibodies at 4°C overnight (Supplementary Table S4). Membranes were then incubated with horseradish peroxidase–conjugated secondary antibody for 2 hours. The membranes were explored using Tanon instrument and quantified with ImageJ software (1.52 V).

Tube formation assay. Aliquots of matrigel (150 μL; Corning) were added into a 48-well plate and then incubated at 37°C for 30 min. HUVECs were pretreated for 48 hours and then seeded onto the gel at a density of 2×10^4 cells per well. After 12-hour incubation in a humidified incubator (37°C, 5% CO_2), six random fields were selected from each well and photographed. ImageJ software (1.52 V) was used to measure the number of tubules formed.

Transwell assay. An 8-μm transwell system (Corning) was used to conduct invasion assays. HUVECs were plated at 3×10^4 cells per well to the upper chamber with serum-free medium. The bottom well was added with complete medium. Following 24 hours of incubation, cells that did not migrate and were left inside the upper chamber were wiped off. The migratory HUVECs were fixed with 4% paraformaldehyde before being stained with 0.01% Crystal Violet (Sigma) and then counted using microscopy at 6 random fields.

Scratch assay. HUVECs were seeded on six-well plates, cultured to 100% confluency, and serum starved overnight. Scratch wounds were created in confluent monolayers using a sterile p1000 pipette tip. To inhibit cell proliferation, HUVECs were pretreated with 10 μg/mL mitomycin C (Sigma). After the scratch, HUVECs were stimulated for 24 hours. Wound closure was expressed as the percentage of wound reduction relative to the original wound. Wound area was measured using ImageJ software (1.52 V).

Mice, BLM-SSc model, and drug administration. Wild-type C57BL/6 mice (female, 6 weeks) were purchased from JieSiJie Laboratory Animal Ltd (Shanghai, China). Mice were bred under specific pathogen-free conditions. All animal experiments were conducted in strict accordance with the Animal Care and Use Committee of Zhongshan Hospital and Fudan University. All procedures complied with the National Institutes of Health Guidelines for the Care and Use of Laboratory Animals.

To generate BLM-SSc mice, BLM (Nippon Kayaku, Tokyo, Japan) was dissolved in PBS to a concentration of 0.5 mg/mL and injected subcutaneously into the shaved backs of mice at a dose of 100 μL for 21 successive days. Mice receiving PBS injections served as controls for the BLM-SSc group.

To evaluate the effects and safety of blocking CHI3L1, CHI3L1 Ab treatment (0.2 mg/kg) or mouse IgG1 kappa isotype control (eBioscience; 0.2 mg/kg) was subcutaneously injected once a week (days 1, 8, and 15), with daily administration of BLM or PBS for 3 weeks (day 1 to day 21). The mice were euthanized through carbon dioxide inhalation, followed by cervical dislocation.

Immunofluorescence staining of skin tissue. Freshly collected skin tissues were embedded in optimum cutting temperature compound and cut into 7-μm sections. The cryosections were blocked with 10% goat serum albumin and 0.03% Triton X-100 for 1 hour at room temperature after fixation and permeabilization. Then, slides were incubated with indicated primary antibodies overnight at 4°C (Supplementary Table S4). After washing with PBS, the samples were incubated with corresponding fluorescence secondary antibody for 2 hours at room temperature. Finally, the nuclei were stained with DAPI (Invitrogen) for 10 minutes. Slides were viewed using fluorescent microscopy, and fluorescent intensity was analyzed using ImageJ software (1.52 V). Specifically, the ratio of CD31/CHI3L1 co-localized ECs was calculated as the average of five randomly selected vessels exhibiting typical vascular staining in each skin section.

Figure 1. CHI3L1 may contribute to SSc endothelial-to-mesenchymal transition (EndoMT). (A) Representative immunofluorescent micrographs and magnification of skin stained with α-SMA and CD31 (left) and quantification of vessels displaying α-SMA/CD31 co-localization (right) and in HC (n = 10) and patients with SSc (n = 10). In SSc skin, co-localization of CD31 and α-smooth muscle actin exhibits yellow staining, which is prominently observed in transitional EndoMT cells of dermal vessels (arrows). (B) Representative immunofluorescent images of skin stained with CHI3L1 and CD31 (left) and quantification of ECs displaying CHI3L1/CD31 co-localization (right) in HC (n = 10) and patients with SSc (n = 10). (C) Correlations between serum CHI3L1 levels and ET-1 levels of patients with SSc (n = 35). Data are presented as mean ± SEM. (A) and (B), by unpaired Student's *t*-test. (C), by Spearman's rank correlation test. ***$P < 0.001$, compared with corresponding groups. α-SMA, α-smooth muscle actin; CHI3L1, chitinase 3–like 1; EC, endothelial cell; ET-1, endothelian 1; HC, healthy control; ns, no significance; SSc, systemic sclerosis.

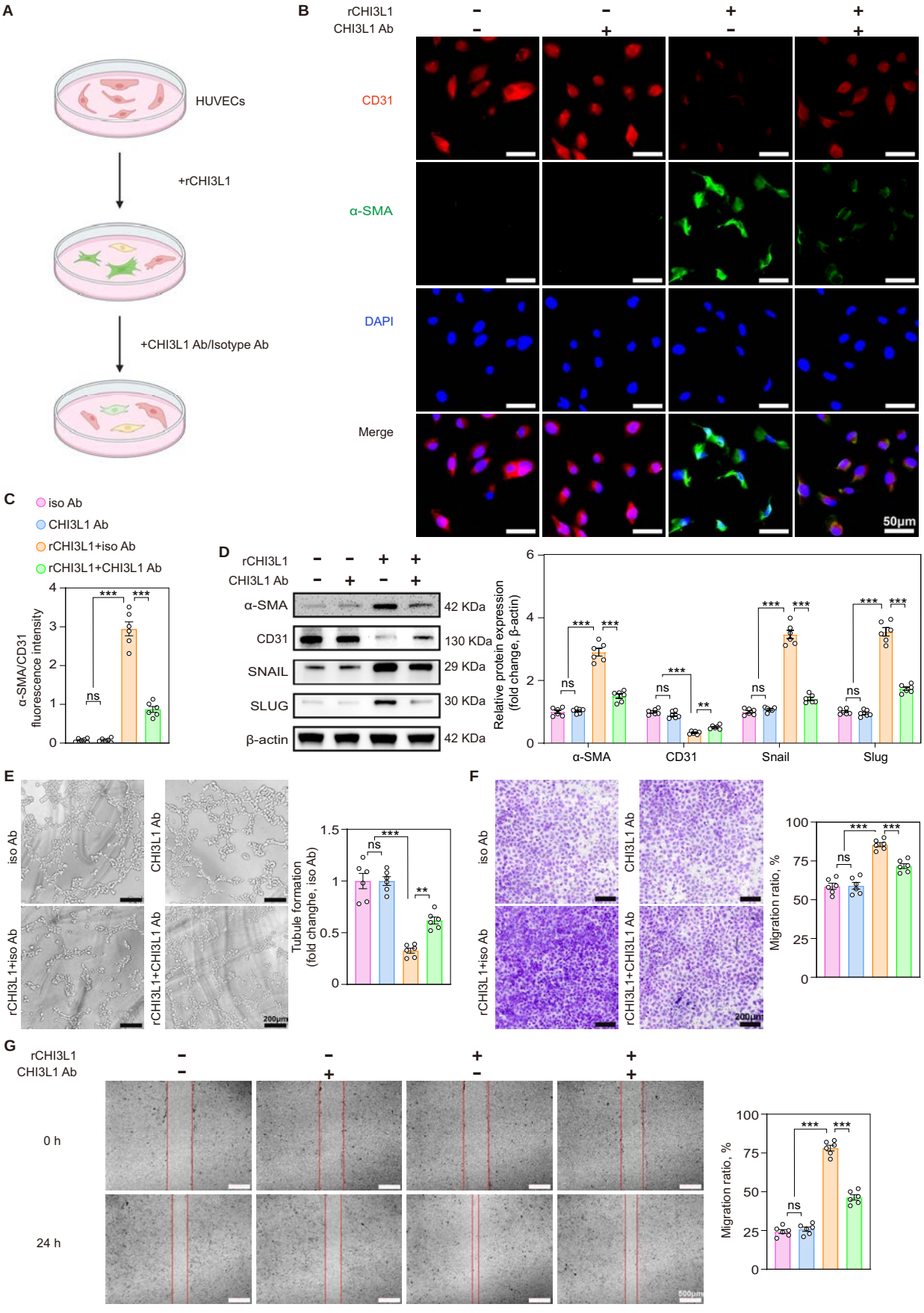

Figure 2. Legend on next page.

Enzyme-linked immunosorbent assay. The serum concentrations of ET-1 and von Willebrand factor (vWF) were measured using specific enzyme-linked immunosorbent assay (ELISA) kits (Cusabio). The assays were conducted following the kit instructions. The absorbance of the plate was measured at 450 nm.

Histology. Formalin-fixed and paraffin-embedded skin and lung tissues were stained with hematoxylin–eosin (HE). Alternatively, the tissues were stained with Masson's trichrome to assess collagen deposition. All sections were analyzed in a blinded manner.

Hydroxyproline assay. The collagen content in the skin and lung tissues of mice was measured using a QuickZyme Total Collagen Assay (QuickZyme), following the manufacturer's guidelines.

Proteomics and analysis. Five thousand HUVECs sorted via fluorescence-activated cell sorting were added into n-dodecyl β-D-maltoside (DDM) lysis buffer (0.1% DDM, 1 mM tris (2 - carboxyethyl) phosphine, and 2 mM chloroacetamide) in low protein-binding tubes and ultrasonicated for 1 hour followed by 1 hour heated at 60°C. Then, the extracted proteins were digested with trypsin (Thermo Fisher Scientific) at a ratio of 1:10 at 37°C overnight, and the reaction was stopped by adding formic acid (FA) to a final concentration of 1%. The extracted peptides were dried immediately and dissolved with 5 μl of 0.1% FA before performing liquid chromatography mass spectrometry/mass spectrometry analysis.

For data independence analysis (DIA), a mixture of peptides derived from each sample was loaded into high-pH, reversed-phase fractionation spin column (Thermo Fisher Scientific), per manufacturer's instruction, to obtain fractions for building a spectra library for DIA. Peptides were quantified equally using Pierce quantitative fluorometric peptide assay according to manufacturer's guidelines before liquid chromatography mass spectrometry measurement. Peptides were identified with Q-ExactivePlus Hybrid Quadrupole-Orbitrap(Thermo Fisher Scientific).

The mass spectrometry raw files were processed with Skyline searched against the UniProt database. The different expression proteins or different modification proteins (fold change > 1.5; $P < 0.05$) were analyzed with GO terms and Kyoto Encyclopedia of Genes and Genomes (KEGG) mapper (https://www.kegg.jp/). Gene Set Enrichment Analysis (GSEA) was performed using GSEA (http://www.gsea-msigdb.org/).

Molecular docking analysis. Rigid protein–protein docking of CHI3L1 and CD44 from human sources was conducted using GRAMM-X (http://gramm.compbio.ku.edu/). Structural information was acquired from the Protein Data Bank (http://www.rcsb.org/). Pymol (version 2.4; Schrödinger, USA) and (Protein Data Bank in Europe Protein Interfaces, Surfaces and Assemblies) PDBePISA (https://www.ebi.ac.uk/pdbe/pisa/) were used for PPI analysis and visualization.

Co-immunoprecipitation assay. HUVECs were treated with human rCHI3L1 (MCE) for 10 minutes. Next, HUVECs were gently rinsed with PBS and lysed using immunoprecipitation lysis buffer (2.5 mM pH 7.4 Tris; 150 mM NaCl, 1 mM EDTA, 1% NP40, 5% glycerol, and protease inhibitor cocktail). Co-immunoprecipitation (Co-IP) was conducted using a Pierce Co-IP kit (Thermo Fisher Scientific) following the manufacturer's instructions. For cell-free in-tube assays, 5 μg human rCHI3L1 (MCE) and 5 μg human recombinant CD44 (rCD44; MCE) were mixed in lysis buffer and shaken at 4°C overnight before performing Co-IP.

Statistical analysis. All quantitative data are shown as the mean ± SEM. The Shapiro-Wilk test was employed to assess data normality. Normally distributed data were analyzed using an unpaired Student's *t*-test for two-group comparisons or analysis of variance for comparisons involving more than two groups. Mann-Whitney tests were applied to data that did not follow a normal distribution. Correlation analysis was performed using Spearman's rank correlation. A *P* value of less than 0.05 was deemed statistically significant. GraphPad Prism version 9.0 (GraphPad Prism Software, Inc) was used for statistical analyses.

Figure 2. CHI3L1 promotes EndoMT in HUVECs. (A) Diagram of the experimental protocol. Four groups were set up: iso Ab, CHI3L1 Ab, rCHI3L1 + iso Ab, and rCHI3L1 + CHI3L1 Ab (rCHI3L1 100 ng/mL; CHI3L1 Ab 100 ng/mL; iso Ab 100 ng/mL). (B) Representative immunofluorescent images of HUVECs stained with α-SMA and CD31 after administration for 48 hours. Scale bar = 50 μm. (C.) Quantification of α-SMA/CD31 fluorescence intensity. n = 6/ea. (D) Representative WB and quantification of α-SMA, CD31, SNAIL, and SLUG in cell lysates of corresponding groups after treatment for 48 hours. n = 6/ea. (E) Representative images and quantification of Matrigel tube formation assay in HUVECs after stimulation for 48 hours. n = 6/ea. Scale bar = 200 μm. (F) Representative images and quantification of transwell assay in the corresponding groups after stimulation for 24 hours. n = 6/ea. Scale bar = 200 μm. (G) Representative images and quantification of scratch assay in the corresponding groups after stimulation for 24 hours. n = 6/ea. Scale bar = 500 μm. Data are presented as mean ± SEM. (C), (D), (E), (F), and (G), by one-way ANOVA. $^{**}P < 0.01$, $^{***}P < 0.001$, compared with corresponding groups. α-SMA, α-smooth muscle actin; ANOVA, analysis of variance; CHI3L1, chitinase 3–like 1; EndoMT, endothelial-to-mesenchymal transition; HUVEC, human umbilical vein endothelial cell; ns, no significance; rCHI3L1, recombinant CHI3L1; WB, Western blot; ea, each. Color figure can be viewed in the online issue, which is available at http://onlinelibrary.wiley.com/doi/10.1002/art.43356/abstract.

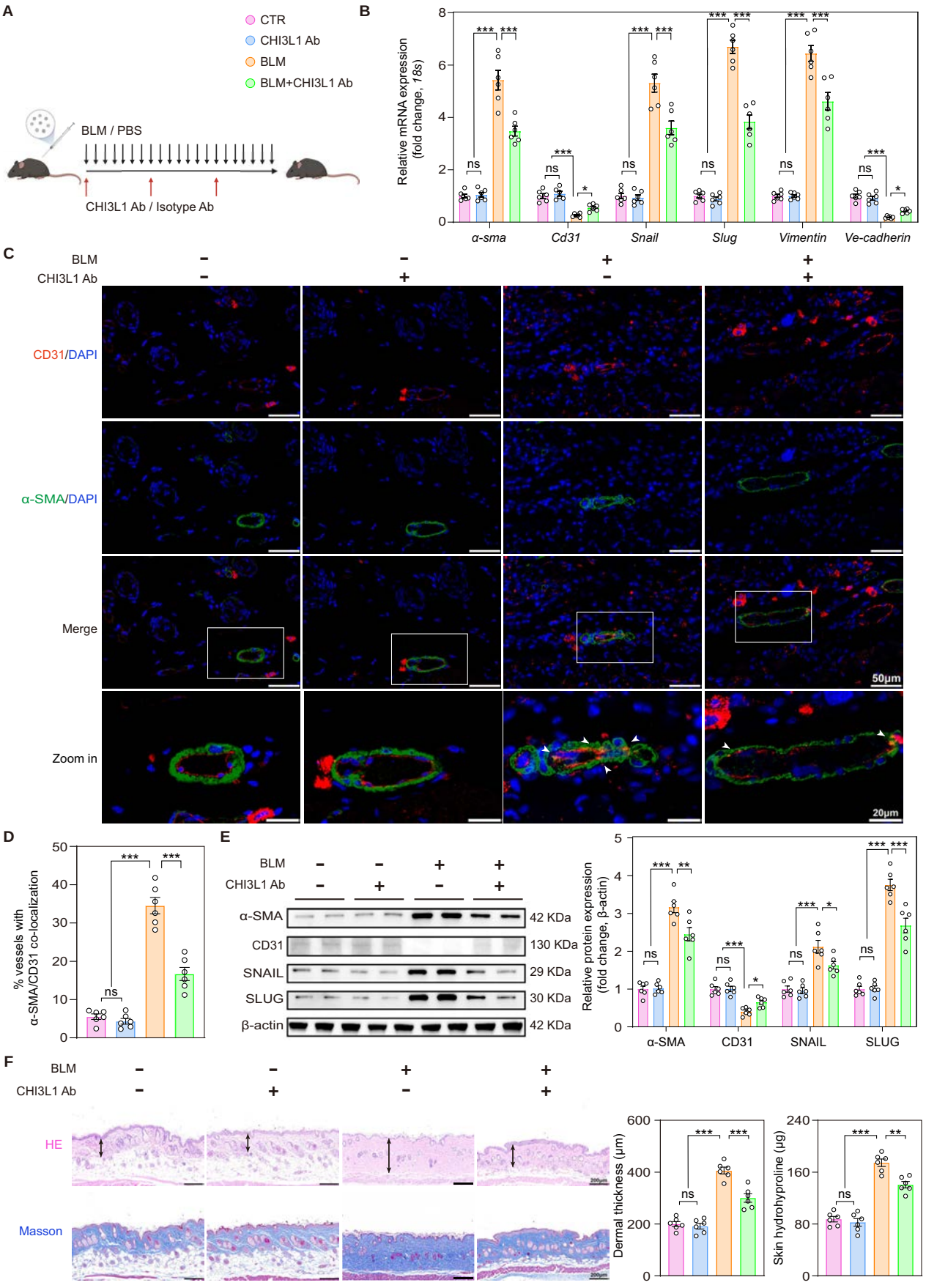

Figure 3. Legend on next page.

Ethics statement. All patients provided written informed consent before enrollment in the study, and the study was approved by the Ethics Committee of Zhongshan Hospital and Fudan University (B2023-414). Animal studies were strictly performed in compliance with Animal Care and Use Committee of Zhongshan Hospital and Fudan University (2023-193).

RESULTS

CHI3L1 may contribute to SSc EndoMT. Recent studies have confirmed that EndoMT contributes to vasculopathy and fibrosis in SSc by promoting ECs dysfunction, myofibroblast differentiation, and ECM depostion.[8,14] Dual immunofluorescence staining for ECs marker CD31 and myofibroblast marker α-SMA in skin sections from HCs and patients with SSc indicated that α-SMA expression was primarily confined to vascular smooth muscle cells surrounding the endothelial layer in the healthy dermis (Figure 1A). Apparent co-localization of α-SMA and CD31 was observed in the dermal vasculature of patients with SSc, indicating ECs in the intermediate stage of EndoMT, which ultimately led to vascular damage and provided additional sources of myofibroblasts (Figure 1A). Additionally, compared with HCs, the percentage of vessels showing co-localization of α-SMA and CD31 was significantly increased in the skin biopsies of patients with SSc (Figure 1A).

Our previous research demonstrated that CHI3L1 is significantly up-regulated in patients with SSc, and PPI network provides the insights suggesting a strong interaction between CHI3L1 and various EndoMT-related proteins (Figure S1).[19] Moreover, we found a strong co-localization of CHI3L1 and CD31 in the skin sections from patients with SSc than in those of HCs (Figure 1B). Indeed, there was a significant increase in CHI3L1 and CD31 co-localized ECs in the dermal vasculature of patients with SSc (Figure 1B). Furthermore, the ratio of CHI3L1/CD31 co-localized ECs was elevated in patients with SSc exhibiting cutaneous vascular symptoms including Raynaud phenomenon (P = 0.178), nail fold bleeding (P = 0.033), pitting scars (P = 0.056), and digital ulcers (P = 0.033; Supplementary Table S5). Additionally, ET-1 plays a pivotal role in vascular dysfunction, fibrosis, and inflammation, hallmark features of SSc, and a significant correlation was observed between serum CHI3L1 and ET-1 levels in patients with SSc (Figure 1C).[20] Patients with Raynaud phenomenon (P = 0.058), nail fold bleeding (P = 0.047), pitting scars (P = 0.107), and digital ulcers (P = 0.241) showed elevated CHI3L1 levels (Supplementary Table S6). These findings suggest that CHI3L1 may exacerbate SSc vasculopathy and fibrosis by interacting with ECs to promote EndoMT.

CHI3L1 promotes EndoMT in HUVECs. To further explore the impact of CHI3L1 on ECs, we treated HUVECs with rCHI3L1 and CHI3L1 Ab to assess whether CHI3L1 could induce HUVECs transition to a myofibroblast-like phenotype (Figure 2A). qRT-PCR analysis showed that administration of rCHI3L1 down-regulated the gene expression levels of the HUVECs markers *CD31* and *VE-cadherin* while up-regulating the expression of myofibroblast markers *vimentin* and *α-SMA*, as well as the key EndoMT-triggering transcription factors *Snail* and *Slug*. However, co-incubation with CHI3L1 Ab reversed these effects (Figure S2). Besides, immunofluorescence staining confirmed that rCHI3L1 stimulation markedly decreased the CD31 expression and promoted their differentiation into myofibroblasts expressing α-SMA (Figures 2B and 2C). The Western blot (WB) results similarly corroborated the findings from the qRT-PCR and immunofluorescence staining, suggesting that CHI3L1 promoted the EndoMT of HUVECs (Figure 2D). Additionally, the tube formation assay demonstrated that CHI3L1 Ab treatment effectively restored the impaired angiogenesis induced by rCHI3L1 (Figure 2E). Furthermore, the transwell and scratch assays showed that rCHI3L1 significantly enhances the migration and invasion capabilities of HUVECs (Figures 2F and 2G). Overall, these in vitro experiments provide strong evidence that CHI3L1 facilitates EndoMT in HUVECs, resulting in the transition to a myofibroblast-like phenotype, increased migratory capacity, and impairment of angiogenesis.

CHI3L1 Ab treatment attenuated vasculopathy and fibrosis in BLM-SSc mice. To further explore the potential effects of CHI3L1 Ab in vivo, we administered CHI3L1 Ab treatment to both the control (CTR) group and BLM-SSc mice, a standard SSc model (Figure 3A).[21] Previous studies have demonstrated EndoMT occurs in BLM-SSc mice skin.[22] qRT-PCR analysis revealed that the administration of CHI3L1 Ab inhibited the up-regulation of EndoMT-related gene expression levels in BLM-SSc mice skin (Figure 3B). Immunofluorescence staining

Figure 3. CHI3L1 Ab treatment attenuated vascular changes in BLM-SSc mice. (A) Diagram of the experimental protocol. BLM-SSc and PBS-treated mice were administrated with CHI3L1 Ab (0.2 mg/kg) or iso Ab (0.2 mg/kg) on days 1, 8, and 15. (B) Relative fold change of indicated mRNA expression level in the corresponding groups. n = 6/ea. (C) Representative immunofluorescent micrographs of skin stained with indicated antibodies in the corresponding groups. (D) Quantification of the dermal vessels displaying CD31/α-SMA co-localization. n = 6/ea. (E) Representative WB and quantification of α-SMA, CD31, SNAIL, and SLUG in skin samples of each group. n = 6/ea. (F) Representative HE and Masson trichrome staining of skin tissue in the corresponding groups (left). Quantification of dermal thickness (middle). Hydroxyproline content of skin samples (right). n = 6/ea. Scale bar = 200 μm. Data are presented as mean ± SEM. (B), (D), and (E) by one-way ANOVA. $^{*}P < 0.05$, $^{**}P < 0.01$, $^{***}P < 0.001$, compared with corresponding groups. α-SMA, α-smooth muscle actin; ANOVA, analysis of variance; BLM, bleomycin; CHI3L1, chitinase 3–like 1; CTR, control; HE, hematoxylin–eosin; mRNA, messenger RNA; ns, no significance; PBS, phosphate-buffered saline; SSc, systemic sclerosis; WB, Western blot; ea, each. Color figure can be viewed in the online issue, which is available at http://onlinelibrary.wiley.com/doi/10.1002/art.43356/abstract.

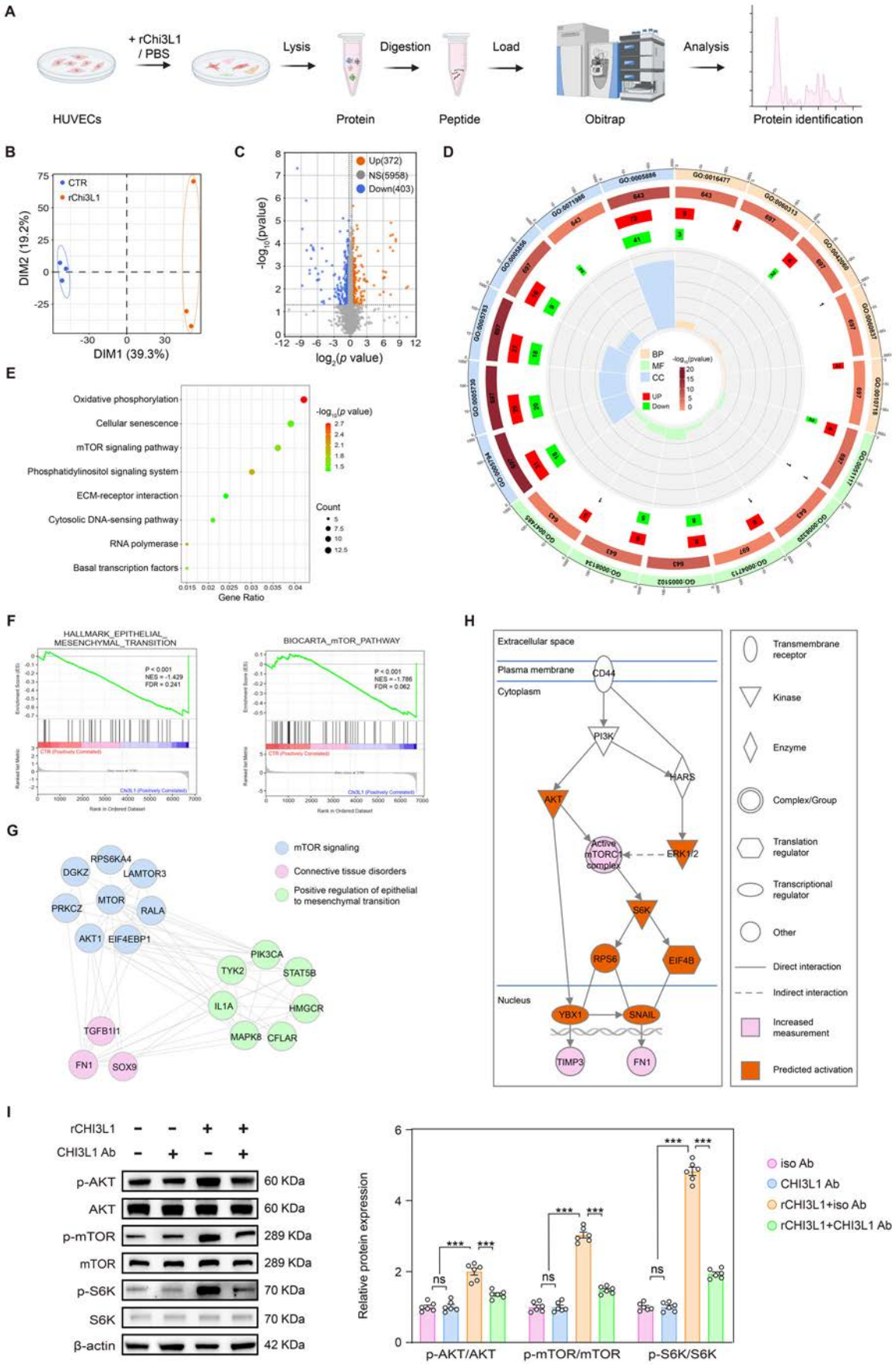

Figure 4. Legend on next page.

was conducted to further evaluate the extent of EndoMT. As observed in patients with SSc, marked co-localization of α-SMA and CD31 was detected in dermal vessels of BLM-SSc mice, suggesting the presence of the EndoMT process (Figure 3C). By contrast, the percentage of vessels showing α-SMA/CD31 co-localization was significantly reduced in the dermis of BLM-SSc mice treated with CHI3L1 Ab, indicating that CHI3L1 Ab treatment effectively alleviates SSc-associated EndoMT (Figures 3C and 3D). WB results also confirmed the findings from qRT-PCR and immunofluorescence staining (Figure 3E). Additionally, ELISA demonstrated that elevated serum concentrations of endothelial injury-related factors (ET-1 and vWF) in BLM-SSc mice were significantly reduced following CHI3L1 Ab administration, further suggesting that CHI3L1 Ab ameliorated vascular injury in SSc (Figure S3).

We then evaluated the extent of fibrosis in different groups of mice. HE indicated that CHI3L1 Ab treatment decreased dermal thickness in BLM-SSc mice (Figure 3F). Meanwhile, Masson's trichrome staining and hydroxyproline content analysis showed reduced collagen levels in BLM-SSc mice skin following CHI3L1 Ab therapy (Figure 3F). Similarly, the administration of CHI3L1 Ab also alleviated the lung fibrosis of BLM-SSc mice (Figure S4). Additionally, no significant differences were observed between the CTR group and the CHI3L1 Ab–treated CTR group in vitro and in vivo, further indicating that CHI3L1 Ab made no effect on cellular and tissue homeostasis. In summary, CHI3L1 induces EndoMT in HUVECs, whereas treatment with CHI3L1 Ab ameliorates vascular alterations and fibrosis in BLM-SSc mice.

CHI3L1 induces EndoMT mainly via activating Akt/mTORC1/S6K pathway. A proteomic analysis was performed to explore the molecular mechanisms of CHI3L1-induced EndoMT by comparing HUVECs with and without CHI3L1 stimulation (Figure 4A).[23] Partial least-squares discrimination analysis identified distinct protein profiles between the CTR and CHI3L1 groups (Figure 4B). About 6,733 proteins were identified, and volcano plot analysis showed that 372 proteins were up-regulated whereas 403 proteins were down-regulated in the CHI3L1-treated group (Figure 4C). GO analysis was conducted to further understand the differentially expressed proteins (DEPs). GO terms illustrated that the DEPs are involved with protein, transcription factor and signal receptor binding, and exert kinase activity, then implicated in biologic processes related to cell migration, ECs differentiation, and EndoMT (Figure 4D, Supplementary Table S7). These results provided further evidence that CHI3L1 could facilitate EndoMT in SSc through the regulation of these DEP expressions.

Next, pathway analysis was performed to investigate the primary pathways by which CHI3L1 promotes EndoMT. KEGG analysis revealed a notable enrichment of the mTOR signaling pathway (Figure 4E). Likewise, GSEA analysis suggested that the mTOR pathway and the EndoMT process were enriched in the CHI3L1-treated group (Figure 4F). PPI network analysis revealed that proteins associated with mTOR signaling pathways were prominent in the cooperation network of DEPs, closely related to EndoMT regulation and connective tissue disorders (Figure 4G). Ingenuity pathway analysis (IPA) further predicted that CHI3L1 may bind to CD44, a cell surface receptor, thereby activating the Akt/mTORC1/S6K pathway, which in turn regulates the EndoMT-related transcription factor Snail1 (Figure 4H).

Subsequently, we examined the alterations in the mTORC1 pathway in both in vitro and in vivo experiments. WB results showed that the phosphorylation levels of Akt, mTOR, and S6K were elevated in CHI3L1-treated HUVECs compared with CTR group, and this up-regulation could be inhibited by CHI3L1 Ab treatment (Figure 4I). In BLM-SSc mice, CHI3L1 Ab treatment inhibited the up-regulation of mTORC1 pathway-related protein phosphorylation levels in the skin (Figure S5). These findings highlight the critical role of the Akt/mTORC1/S6K axis by which CHI3L1 promotes SSc-related EndoMT.

CHI3L1 interact with CD44, thereby initiating mTORC1 signaling pathway. It has been illustrated that CD44 can activate the downstream mTORC1 signaling pathway, and the activation of mTORC1 is associated with the regulation of the EndoMT-related transcription factor Snail.[15,24,25] To confirm the potential interaction between CHI3L1 and CD44 suggested by the IPA results, we performed rigid protein–protein docking analysis of CHI3L1 with CD44. Notably, hydrogen bonds were observed between CHI3L1 and CD44 at specific amino acid residue sites, including LYS 32-CYS 13 and GLU 290-GLY 141, suggesting a stable docking model (Figure 5A, Supplementary Table S8).[26]

Figure 4. CHI3L1 induces EndoMT in HUVECs mainly via activating Akt/mTORC1/S6K pathway. (A) Schematic overview of proteomics. (B) Partial least-squares discrimination analysis (PLS-DA) of proteomic profiling between CHI3L1 and CTR group. (C) Volcano plots of DEPs. (D) GO analysis of DEPs. (E) Signaling pathway classification according to KEGG terms. (F) GSEA analysis via HALLMARK and BIOCARTA database. (G) Cytoscape analysis of PPI network. (H) IPA results of the DEPs. (I) Representative WB images and relative quantitative analysis of indicated proteins in HUVECs with following treatment for 15 minutes. n = 6/ea. Data are presented as mean ± SEM. (I), by one-way ANOVA. ***$P < 0.001$, compared with corresponding groups. ANOVA, analysis of variance; BP, biologic process; CC, cell component; CHI3L1, chitinase 3–like 1; CTR, control; DEP, differentially expressed protein; ECM, extracellular matrix; EndoMT, endothelial-to-mesenchymal transition; FDR, false discovery rate; GO, Gene Ontology; GSEA, Gene Set Enrichment Analysis; HUVEC, human umbilical vein endothelial cell; IPA, ingenuity pathway analysis; KEGG, Kyoto Encyclopedia of Genes and Genomes; MF, molecular function; mTORC1, mechanistic target of rapamycin complex 1; NES, normalized enrichment score; ns, no significance; PBS, phosphate-buffered saline; PPI, protein–protein interaction; rCHI3L1, recombinant CHI3L1; S6K, S6 kinase; WB, Western blot; ea, each. Color figure can be viewed in the online issue, which is available at http://onlinelibrary.wiley.com/doi/10.1002/art.43356/abstract.

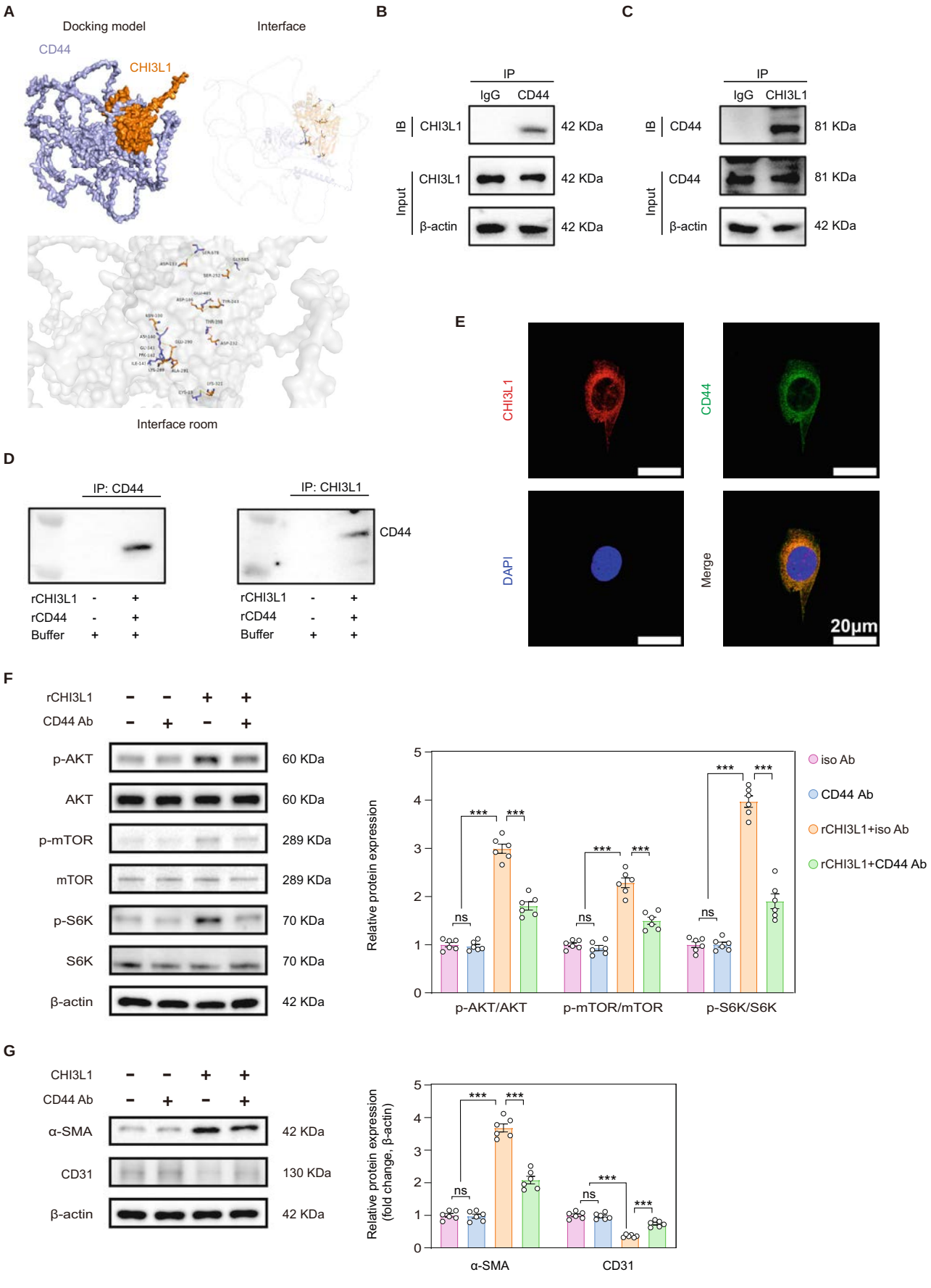

Figure 5. Legend on next page.

Co-IP assays further proved the interaction between CHI3L1 and CD44 in cell lysates from CHI3L1-treated HUVECs (Figures 5B and 5C). The interaction between rCHI3L1 and rCD44 was also validated in a cell-free system (Figure 5D). In addition, immunocytochemistry demonstrated the co-localization of CHI3L1 and CD44 in HUVECs with CHI3L1 administration (Figure 5E). Furthermore, WB results revealed that upon blocking HUVECs with CD44 Ab, the mTORC1 signaling pathway activated by CHI3L1 in HUVECs was significantly attenuated (Figure 5F). Moreover, CHI3L1-induced EndoMT phenotypes, including decreased CD31 expression and increased α-SMA expression, were also markedly abrogated (Figure 5G). To sum up, the data suggest that CHI3L1 can bind to CD44 of HUVECs, which in turn boost the downstream Akt/mTORC1/S6K axis and finally facilitate the EndoMT process.

The mTORC1 inhibitor rapamycin suppresses CHI3L1-mediated EndoMT. Next, we tested whether the effect of CHI3L1 in promoting EndoMT in HUVECs is primarily mediated through the activation of the mTORC1 pathway. Rapamycin is a classic immunosuppressant and specifically acts as an allosteric inhibitor of mTORC1.[27] HUVECs were pretreated with rapamycin or PBS, followed by rCHI3L1 (Figure 6A). Rapamycin treatment significantly reversed CHI3L1-mediated down-regulation of *CD31* and *VE-cadherin* expression, as well as up-regulation of *Vimentin*, *α-SMA*, *Snail*, and *Slug* expression in HUVECs (Figure S6). Immunofluorescence images also demonstrated that administration of rapamycin inhibited the CHI3L1-mediated differentiation of HUVECs into myofibroblast-like phenotype expressing α-SMA (Figures 6B and 6C). Additionally, the WB results corroborated the findings from qRT-PCR and immunofluorescence staining (Figure 6D). Furthermore, rapamycin treatment rescued the impaired angiogenesis ability of HUVECs caused by CHI3L1 (Figure 6E). Meanwhile, rapamycin suppressed the CHI3L1-mediated enhancement in the migratory capacity of HUVECs (Figures 6F and 6G). Analogously, HUVECs transfected with mTOR shRNA showed significantly decreased expression of myofibroblast marker α-SMA and key EndoMT transcription factor Snail upon CHI3L1 stimulation, whereas endothelial marker CD31 expression was markedly increased (Figure S7). In conclusion, these data indicated that the mTORC1 inhibitor rapamycin and mTOR shRNA effectively suppresses CHI3L1-induced EndoMT in HUVECs, suggesting that CHI3L1 promotes EndoMT predominantly through the mTORC1 signaling pathway.

DISCUSSION

In this study, we confirmed that CHI3L1 promotes EndoMT in ECs to exaggerate vasculopathy and fibrosis in SSc. Mechanistically, CHI3L1 interacts with CD44 on ECs, activating the downstream Akt/mTORC1/S6K pathway, thereby regulating the key transcription factors Snail and Slug, triggering EndoMT (Figure S8). Furthermore, CHI3L1 Ab treatment to BLM-SSc mice improved SSc-associated vasculopathy and fibrosis. As far as we know, this study is the first to validate the role of CHI3L1 in enhancing EndoMT in SSc.

Extensive research has expanded the understanding of CHI3L1 in pathophysiologic roles referring to various inflammatory, fibrotic, and tumor-related processes.[28] For instance, CHI3L1 drives atopic dermatitis by promoting M2 macrophage activation and Th2 immunity, contributes to mammalian pulmonary and hepatic fibrosis through enhancing fibroblast differentiation, proliferation, and ECM deposition, and serves as a crucial factor in non–small cell lung cancer metastasis and invasion via inducing epithelial–mesenchymal transition (EMT).[16–18,29,30] Our previous research identified increased CHI3L1 expression in the serum and skin of patients with SSc, with serum CHI3L1 levels correlating with lung function and the modified Rodnan skin score.[19] These findings suggest that CHI3L1 may be closely associated with fibrosis in SSc. In recent research, EndoMT has been identified as an important contributor to vascular dysfunction and fibrosis in SSc by promoting ECs dysfunction, myofibroblast production, and ECM depostion.[14,31] In the current study, we found there was a strong CD31/CHI3L1 co-localization in dermal vascular of patients with SSc, along with a notable elevation in serum CHI3L1 concentration. This trend was more pronounced in patients with SSc with cutaneous vascular symptoms. These findings suggest that CHI3L1 may play an important role in the SSc-related EndoMT process. We then confirmed that CHI3L1 induces EndoMT in HUVECs, enhancing their migratory capacities and impairing angiogenesis. Moreover, treatment with

Figure 5. CHI3L1 may interact with CD44, thereby initiating the mTORC1 signaling pathway. (A) Surface diagram of the docking model and their interfacing residues between CHI3L1 and CD44 protein. (B) and (C) Cellular Co-IP assays of CHI3L1 and CD44. HUVECs were treated with rCHI3L1 (100 ng/mL) for 10 minutes, and then, the lysates were immunoprecipitated with antibody against CD44, (B) immunoblot with CHI3L1 antibody, and (C) vice versa. (D) Co-IP analysis of rCHI3L1 and rCD44 in a cell-free system. (E) Immunofluorescence co-localization of CHI3L1 and CD44 in HUVECs. HUVECs were treated with rCHI3L1 (100 ng/mL) for 10 minutes. (F) Representative WB images and relative quantitative analysis of indicated proteins in HUVECs pretreated with CD44 antibody (100 ng/mL) or iso Ab (100 ng/mL), followed by 15 minutes of treatment with rCHI3L1 or PBS. n = 6/ea. (G) Representative WB images and relative quantitative analysis of indicated proteins in HUVECs after corresponding stimulation for 48 hours. n = 6/ea. Data are presented as mean ± SEM. (F) and (G), by one-way ANOVA. ***$P < 0.001$, compared with corresponding groups. α-SMA, α-smooth muscle actin; ANOVA, analysis of variance; CHI3L1, chitinase 3–like 1; Co-IP, Co-immunoprecipitation; HUVEC, human umbilical vein endothelial cell; mTORC1, mechanistic target of rapamycin complex 1; ns, no significance; PBS, phosphate-buffered saline; rCHI3L1, recombinant CHI3L1; S6K, S6 kinase; WB, Western blot; ea, each. Color figure can be viewed in the online issue, which is available at http://onlinelibrary.wiley.com/doi/10.1002/art.43356/abstract.

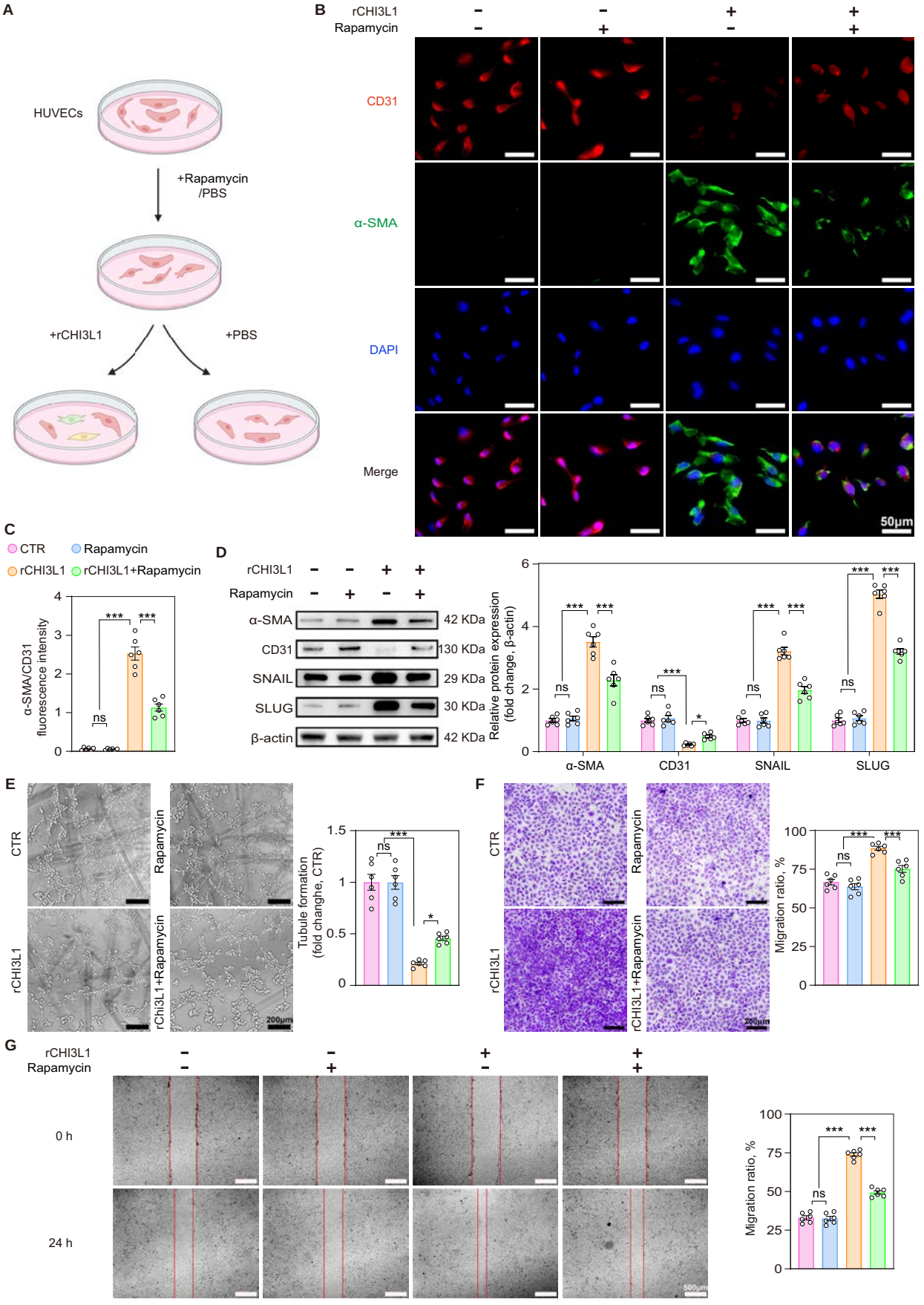

Figure 6. Legend on next page.

CHI3L1 Ab mitigated EndoMT and fibrosis in BLM-SSc mice, suggesting that CHI3L1 may serve as a promising therapeutic target for ameliorating vascular injury and fibrosis in SSc.

We then used proteomics to investigate the specific downstream molecular mechanisms through which CHI3L1 facilitates EndoMT, discovering a significant enrichment of the mTOR pathway in CHI3L1-treated HUVECs. mTOR is a protein kinase that reacts to nutrient availability and growth signals.[32] It forms two distinct protein complexes: the rapamycin-sensitive mTORC1 and the rapamycin-insensitive mTORC2.[33] Currently, our understanding of functions of mTORC2, primarily in metabolism, remains limited. In contrast, numerous studies have established the crucial role of mTORC1 in cell proliferation, growth, and differentiation, and its undue activation has been implicated in SSc.[34] S6K is the main effector molecule of the translational regulation driven by the mTORC1 pathway.[35] The mTORC1/S6K axis is one of the key pathways in the processes of EMT and EndoMT, and it has been shown to regulate the expression and nuclear translocation of the downstream transcription factors Snail1 and Slug.[24,34,36] Based on the results of IPA, we confirmed that CHI3L1 can bind to CD44, a transmembrane receptor known to regulate signaling pathways involved in cell growth, survival, and differentiation. This interaction subsequently activates the Akt/mTORC1/S6K signaling cascade, regulating downstream factors Snail and Slug, which promotes EndoMT. This process leads to vascular dysfunction and serves as a source of myofibroblasts, further increasing collagen synthesis and ECM deposition, ultimately resulting in the exacerbation of fibrosis.

Rapamycin is a classic immunosuppressant that inhibits mTORC1.[37] Previous experiments have shown that rapamycin can effectively alleviate fibrosis in BLM-SSc mice.[38] A randomized, single-blind pilot study involving a series of diffused SSc cases indicated that rapamycin has efficacy comparable to methotrexate.[39,40] Another phase II pilot clinical trial evaluating the safety and efficacy of rapamycin in the treatment of SSc has not yet released its findings (ClinicalTrials.gov ID NCT03365869). Our results confirm that rapamycin can suppress CHI3L1-mediated EndoMT, suggesting that it is a potential therapeutic target for SSc vasculopathy and fibrosis.

Our study also has limitations. CHI3L1 is secreted by various immune and structural cells, and we are still uncertain about the primary source of elevated CHI3L1 in the serum of patients with SSc. Future studies should aim to explore its source and investigate therapeutic interventions targeting CHI3L1 for the treatment of SSc.

In conclusion, our work reveals a novel role of CHI3L1 in enhancing vascular dysfunction and fibrosis in SSc, specifically through promoting ECs to undergo EndoMT, which induces vascular damage and provides a source of myofibroblasts that facilitate fibrosis. Mechanistically, CHI3L1 binds to CD44, subsequently activating the Akt/mTORC1/S6K signaling pathway, which regulates downstream transcription factors Snail and Slug to promote SSc-related EndoMT. More broadly, our research provides a potential therapeutic strategy targeting CHI3L1 for SSc, with significant clinical translational implications.

AUTHOR CONTRIBUTIONS

All authors contributed to at least one of the following manuscript preparation roles: conceptualization AND/OR methodology, software, investigation, formal analysis, data curation, visualization, and validation AND drafting or reviewing/editing the final draft. As corresponding author, Dr Yang confirms that all authors have provided the final approval of the version to be published and takes responsibility for the affirmations regarding article submission (eg, not under consideration by another journal), the integrity of the data presented, and the statements regarding compliance with institutional review board/Declaration of Helsinki requirements.

Data availability statement

Data are available on reasonable request. All quantified data may be available on reasonable request, but the data of patients are not available to the public.

REFERENCES

1. Volkmann ER, Andréasson K, Smith V. Systemic sclerosis. Lancet 2023;401(10373):304–318.
2. Denton CP, Khanna D. Systemic sclerosis. Lancet 2017;390(10103):1685–1699.

Figure 6. The mTORC1 inhibitor rapamycin suppresses CHI3L1-mediated EndoMT. (A) Diagram of the experimental approach. Four groups were set up: PBS, rapamycin, rCHI3L1, and rapamycin + rCHI3L1 (rCHI3L1 100 ng/mL; rapamycin 50 nM). (B) Representative immunofluorescent images of HUVECs stained with CD31 and α-SMA after administration for 48 hours. Scale bar = 50 μm. (C) Quantification of α-SMA/CD31 fluorescence intensity. n = 6/ea. (D) Representative WB and quantification of indicated proteins in cell lysates of corresponding groups after treatment for 48 hours. n = 6/ea. (E) Representative images and relative quantification of matrigel tube formation assay in HUVECs after stimulation for 48 hours. n = 6/ea. Scale bar = 200 μm. (F) Representative images and quantification of transwell assay in the corresponding groups after stimulation for 24 hours. n = 6/ea. Scale bar = 200 μm. (G) Representative images and quantification of scratch assay in the corresponding groups after stimulation for 24 hours. n = 6/ea. Scale bar = 500 μm. Data are presented as mean ± SEM. (C), (D), (E), (F), and (G), by one-way ANOVA. $^{*}P < 0.05$, $^{***}P < 0.001$, compared with corresponding groups. α-SMA, α-smooth muscle actin; ANOVA, analysis of variance; CHI3L1, chitinase 3–like 1; CTR, control; EndoMT, endothelial-to-mesenchymal transition; HUVEC, human umbilical vein endothelial cell; mTORC1, mechanistic target of rapamycin complex 1; ns, no significance; PBS, phosphate-buffered saline; rCHI3L1, recombinant CHI3L1; WB, Western blot; ea, each. Color figure can be viewed in the online issue, which is available at http://onlinelibrary.wiley.com/doi/10.1002/art.43356/abstract.

3. Jerjen R, Nikpour M, Krieg T, et al. Systemic sclerosis in adults. Part I: clinical features and pathogenesis. J Am Acad Dermatol 2022;87(5): 937–954.
4. Bukiri H, Volkmann ER. Current advances in the treatment of systemic sclerosis. Curr Opin Pharmacol 2022;64:102211.
5. Wang X, Liu M, Ye T, et al. A stretchable hardness sensor for the assessment of skin disease in systemic sclerosis. RMD Open 2023; 9(4):e003512.
6. Tabib T, Huang M, Morse N, et al. Myofibroblast transcriptome indicates SFRP2hi fibroblast progenitors in systemic sclerosis skin. Nat Commun 2021;12(1):4384.
7. Deng CC, Hu YF, Zhu DH, et al. Single-cell RNA-seq reveals fibroblast heterogeneity and increased mesenchymal fibroblasts in human fibrotic skin diseases. Nat Commun 2021;12(1):3709.
8. Ma F, Tsou PS, Gharaee-Kermani M, et al. Systems-based identification of the Hippo pathway for promoting fibrotic mesenchymal differentiation in systemic sclerosis. Nat Commun 2024;15(1):210.
9. Zhang S, Li Y, Huang X, et al. Seamless genetic recording of transiently activated mesenchymal gene expression in endothelial cells during cardiac fibrosis. Circulation 2021;144(25):2004–2020.
10. Rius Rigau A, Li YN, Matei AE, et al. Characterization of vascular niche in systemic sclerosis by spatial proteomics. Circ Res 2024;134(7): 875–891.
11. Manetti M, Guiducci S, Matucci-Cerinic M. The origin of the myofibroblast in fibroproliferative vasculopathy: does the endothelial cell steer the pathophysiology of systemic sclerosis? Arthritis Rheum 2011; 63(8):2164–2167.
12. Piera-Velazquez S, Li Z, Jimenez SA. Role of endothelial-mesenchymal transition (EndoMT) in the pathogenesis of fibrotic disorders. Am J Pathol 2011;179(3):1074–1080.
13. Romano E, Rosa I, Fioretto BS, et al. Soluble guanylate cyclase stimulation fosters angiogenesis and blunts myofibroblast-like features of systemic sclerosis endothelial cells. Rheumatology (Oxford) 2023;62 (SI):SI125–SI137.
14. Manetti M, Romano E, Rosa I, et al. Endothelial-to-mesenchymal transition contributes to endothelial dysfunction and dermal fibrosis in systemic sclerosis. Ann Rheum Dis 2017;76(5):924–934.
15. Zhao T, Su Z, Li Y, et al. Chitinase-3 like-protein-1 function and its role in diseases. Signal Transduct Target Ther 2020;5(1):201.
16. Yu JE, Jeon SH, Kim MJ, et al. Anti-chitinase-3-like 1 antibody attenuated atopic dermatitis-like skin inflammation through inhibition of STAT3-dependent CXCL8 expression. Br J Pharmacol 2024; 181(17):3232–3245.
17. Sun X, Nakajima E, Norbrun C, et al. Chitinase 3 like 1 contributes to the development of pulmonary vascular remodeling in pulmonary hypertension. JCI Insight 2022;7(18):e159578.
18. Wang S, Hu M, Qian Y, et al. CHI3L1 in the pathophysiology and diagnosis of liver diseases. Biomed Pharmacother 2020;131:110680.
19. Wang X, Ye T, Huang J, et al. Aberrant chitinase 3-like 1 expression in basal cells contributes to systemic sclerosis fibrosis. Adv Sci (Weinh) 2025;12(6):e2310169.
20. Elisa T, Antonio P, Giuseppe P, et al. Endothelin receptors expressed by immune cells are involved in modulation of inflammation and in fibrosis: relevance to the pathogenesis of systemic sclerosis. J Immunol Res 2015;2015:147616.
21. Kuzumi A, Yoshizaki A, Matsuda KM, et al. Interleukin-31 promotes fibrosis and T helper 2 polarization in systemic sclerosis. Nat Commun 2021;12(1):5947.
22. Zhang W, Chen G, Ren JG, et al. Bleomycin induces endothelial mesenchymal transition through activation of mTOR pathway: a possible mechanism contributing to the sclerotherapy of venous malformations. Br J Pharmacol 2013;170(6):1210–1220.
23. Wang L, Abdulla A, Wang A, et al. Sickle-like inertial microfluidic system for online rare cell separation and tandem label-free quantitative proteomics (orcs-proteomics). Anal Chem 2022;94(15):6026–6035.
24. Daley SR, Coakley KM, Hu DY, et al. Rasgrp1 mutation increases naive T-cell CD44 expression and drives mTOR-dependent accumulation of Helios$^+$ T cells and autoantibodies. eLife 2013;2:e01020.
25. Zheng L, Yang S, Xu R, et al. NQO1 drives glioblastoma cell aggressiveness through EMT induction via the PI3K/Akt/mTOR/Snail pathway. Int J Oncol 2023;63(4):110.
26. Yang Q, Lei X, He J, et al. N4-acetylcytidine drives glycolysis addiction in gastric cancer via NAT10/SEPT9/HIF-1α positive feedback loop. Adv Sci (Weinh) 2023;10(23):e2300898.
27. Lee DJW, Hodzic Kuerec A, Maier AB. Targeting ageing with rapamycin and its derivatives in humans: a systematic review. Lancet Healthy Longev 2024;5(2):e152–e162.
28. Coffman FD. Chitinase 3-like-1 (CHI3L1): a putative disease marker at the interface of proteomics and glycomics. Crit Rev Clin Lab Sci 2008; 45(6):531–562.
29. Morera E, Steinhäuser SS, Budkova Z, et al. YKL-40/CHI3L1 facilitates migration and invasion in HER2 overexpressing breast epithelial progenitor cells and generates a niche for capillary-like network formation. In Vitro Cell Dev Biol Anim 2019;55(10):838–853.
30. Jefri M, Huang YN, Huang WC, et al. YKL-40 regulated epithelial-mesenchymal transition and migration/invasion enhancement in non-small cell lung cancer. BMC Cancer 2015;15(1):590.
31. Shen C, Jiang Y, Li Q, et al. Bone morphogenetic protein-7 inhibits endothelial-to-mesenchymal transition in primary human umbilical vein endothelial cells and mouse model of systemic sclerosis via Akt/mTOR/p70S6K pathway. J Dermatol Sci 2021;103(2):82–92.
32. Szwed A, Kim E, Jacinto E. Regulation and metabolic functions of mTORC1 and mTORC2. Physiol Rev 2021;101(3):1371–1426.
33. Linke M, Fritsch SD, Sukhbaatar N, et al. mTORC1 and mTORC2 as regulators of cell metabolism in immunity. FEBS Lett 2017;591(19): 3089–3103.
34. Jiang Y, Hu F, Li Q, et al. Tanshinone IIA ameliorates the bleomycin-induced endothelial-to-mesenchymal transition via the Akt/mTOR/p70S6K pathway in a murine model of systemic sclerosis. Int Immunopharmacol 2019;77:105968.
35. Dibble CC, Cantley LC. Regulation of mTORC1 by PI3K signaling. Trends Cell Biol 2015;25(9):545–555.
36. Karimi Roshan M, Soltani A, Soleimani A, et al. Role of AKT and mTOR signaling pathways in the induction of epithelial-mesenchymal transition (EMT) process. Biochimie 2019;165:229–234.
37. Li J, Kim SG, Blenis J. Rapamycin: one drug, many effects. Cell Metab 2014;19(3):373–379.
38. Yoshizaki A, Yanaba K, Yoshizaki A, et al. Treatment with rapamycin prevents fibrosis in tight-skin and bleomycin-induced mouse models of systemic sclerosis. Arthritis Rheum 2010;62(8): 2476–2487.
39. Su TI, Khanna D, Furst DE, et al. Rapamycin versus methotrexate in early diffuse systemic sclerosis: results from a randomized, single-blind pilot study. Arthritis Rheum 2009;60(12):3821–3830.
40. Fogel AL, Hill S, Teng JM. Advances in the therapeutic use of mammalian target of rapamycin (mTOR) inhibitors in dermatology. J Am Acad Dermatol 2015;72(5):879–889.

American College of Rheumatology
Empowering Rheumatology Professionals

Arthritis & Rheumatology
Vol. 78, No. 2, February 2026, pp 418–427
DOI 10.1002/art.43370

Skin Biopsies Enhance Prediction of Clinical Trajectory in Diffuse Cutaneous Systemic Sclerosis

Kimberly S. Lakin,[1,2] John Spivack,[1] Jessica K. Gordon,[1,2] Yaxia Zhang,[1,2] Deanna Jannat-Khah,[1,2] Hiranmayi Ravichandran,[3,4] Niroshana Anandasabapathy,[5,6,7] Dana E. Orange,[1,8] and Robert F. Spiera[1,2]

Objective. To evaluate the relationship of skin fibroblast CD34 and α-smooth muscle actin (α-SMA) and immune cell infiltration with disease duration in diffuse cutaneous systemic sclerosis (dcSSc) and identify predictors of improvement.

Methods. Skin biopsies and clinical data were analyzed from patients with dcSSc enrolled in lenabasum (n = 79), belimumab (n = 18), or nilotinib (n = 8) trials. CD34 and α-SMA were scored semiquantitatively. Immune cells (CD20+, CD3+, and CD123+) were counted. Clinical and histologic features were compared between those with early (<18 months) versus later disease (≥18 months). Clinical improvement was defined as >5-point decrease in modified Rodnan skin score (mRSS) at 52 weeks. An Akaike's information criterion–optimal multiple logistic regression model for clinical improvement among 68 mycophenolate mofetil (MMF) users was developed. Fibroblast spatial organization was visualized using imaging mass cytometry (IMC) in a representative sample.

Results. Despite similar baseline mRSS, early disease was associated with lower CD34, higher α-SMA, increased B cells, and greater mRSS improvement compared with later SSc. IMC demonstrated regions of CD34+ fibroblasts in superficial dermis and α-SMA+ fibroblasts in deeper, collagen-dense regions. Among MMF users, high CD34 and α-SMA predicted improvement in early SSc; however, high α-SMA predicted lower odds of improvement in later SSc. The probability of improvement was lowest in early SSc with α-SMA^{low}/CD34^{low} immunophenotype and later SSc with α-SMA^{high}. In later SSc, B cells were higher in α-SMA^{high} versus α-SMA^{low} skin.

Conclusion. Fibroblast immunophenotype varied by baseline disease duration and improved model performance for identifying those with improvement on MMF. Skin biopsies may be useful for refining prognosis and guiding patient management decisions.

INTRODUCTION

Diffuse cutaneous systemic sclerosis (dcSSc) is a rare autoimmune disease characterized by inflammation and fibrosis of the skin and internal organs and carries the highest mortality rate among rheumatic diseases.[1] Although immunosuppressive medications, particularly mycophenolate mofetil (MMF), are used for the treatment of skin involvement,[2–4] the level of evidence for these options is limited, and there is potential for toxicity. In clinical practice, immunosuppressive therapy is given empirically for months before determining its utility. This is a period marked by uncertainty, ongoing symptoms, and potential loss of an optimal

This study was presented as an abstract at the 2024 American College of Rheumatology Annual Meeting (*Arthritis Rheumatol* 2024;76[suppl 9]).

The content is solely the responsibility of the authors and does not necessarily represent the official views of the NIH.

Supported by the National Institute of Arthritis and Musculoskeletal and Skin Diseases (NIAMS), NIH (grant K23-AR-083509 to Dr Lakin). This work was also supported by the National Scleroderma Foundation and the Hospital for Special Surgery Research Institute Kellen Scholars Program (to Dr Lakin). Additional support was provided by the NIAMS, NIH (grants R01-AR-080436 and R01-AR-083208 to Dr Anandasabapathy), and Weill Cornell Medical Center. This study uses data collected in the context of three clinical trials. The Lenabasum Phase III clinical trial was supported by Corbus Pharmaceuticals. The Novartis and belimumab clinical trials were investigator initiated and received research grants from Novartis and GlaxoSmithKline, respectively.

[1]Hospital for Special Surgery, New York City, New York; [2]Weill Cornell Medicine, New York City, New York; [3]Department of Physiology and Biophysics, Institute for Computational Biomedicine, Weill Cornell Medicine, New York City, New York; [4]Caryl and Israel Englander Institute for Precision Medicine, Weill Cornell Medicine, New York City, New York; [5]Department of Dermatology; Department of Microbiology and Immunology, Caryl and Israel Englander Institute for Precision Medicine at Weill Cornell Medicine, New York City, New York; [6]Parker Institute for Cancer Immunotherapy and Sandra and Edward Meyer Cancer Center of Weill Cornell Medicine, New York City, New York; [7]Immunology and Microbial Pathogenesis Program, Weill Cornell Medical College, New York City, New York; [8]Rockefeller University, New York City, New York.

Drs Orange and Spiera are co-last authors and contributed equally to this work.

Additional supplementary information cited in this article can be found online in the Supporting Information section (https://acrjournals.onlinelibrary.wiley.com/doi/10.1002/art.43370).

Author disclosures and graphical abstract are available online at https://onlinelibrary.wiley.com/doi/10.1002/art.43370

Address correspondence via email to Kimberly S. Lakin, MD, MS, at LakinK@hss.edu.

Submitted for publication May 7, 2025; accepted in revised form August 6, 2025.

treatment window for other therapeutic targets and/or clinical trial eligibility.

Estimating individual disease trajectories in dcSSc remains a major unmet need with direct implications for patient care decisions and clinical trial design. Previous observational studies have shown that disease duration and baseline modified Rodnan skin score (mRSS) are associated with disease progression. For example, a large observational study identified high baseline mRSS and absence of tendon friction rubs as predictive of clinical improvement, among 11 candidate predictors, irrespective of disease duration.[5] Additionally, RNA polymerase III positivity has been shown in prior studies to be associated with an earlier and higher mRSS peak compared with those who are RNA polymerase III negative.[6–8] Regarding disease duration, a EULAR Scleroderma Trials and Research study identified disease duration ≤15 months as an independent predictor of dcSSc skin progression, along with low baseline mRSS (≤22 of 51) and joint synovitis.[9] Similarly, an observational study of patients with dcSSc found that those who progressed had shorter disease duration (median 8.1 months vs 12.6 months; $P = 0.001$) and lower baseline mRSS (19 vs 21; $P = 0.03$) compared with nonprogressors.[7] Considering prior findings, these clinical variables have been used to inform timely immunosuppression initiation and patient selection in clinical trials.

Although short disease duration is associated with progressive disease, there is debate regarding the optimal cutoff for clinical trial enrollment. Emerging clinical data suggest that disease duration <18 months may be optimal for clinical trial enrollment because individuals with longer durations of disease may improve spontaneously.[10] However, many dcSSc trials to-date have used three-year[11–13] or five-year[14,15] disease duration thresholds. Reliable predictive tools are needed to refine patient selection for trials and guide individualized treatment decisions.

Dermal fibroblast activation plays a central role in SSc[16] and may provide a window into patient heterogeneity. Our prior work and others' have demonstrated that two inversely related fibroblast markers, α-smooth muscle actin (α-SMA) and CD34, are associated with skin disease severity. α-SMA is a marker of activated myofibroblasts[17] and correlates with worse mRSS and the Combined Response Index in SSc.[18–20] CD34, a stem cell–associated molecule involved in cellular adhesion,[21] is expressed by fibroblasts in healthy skin but is diminished in SSc.[22,23] In normal wound healing, CD34 expression is lost in the early phases of scarring and restored as the scar resolves.[24] However, in keloid scars, which are characterized by persistent fibrosis, CD34 is not reconstituted.[24] These findings suggest that CD34+ fibroblasts represent a resting fibroblast network that is lost in active fibrosis as α-SMA+ myofibroblasts predominate. Although α-SMA and CD34 correlate with disease severity, it has been unclear whether they could distinguish patient trajectories or help identify meaningful subsets within this heterogeneous disease.

Our previous studies using machine learning approaches identified fibroblast activation state, measured by α-SMA and CD34 immunohistochemistry, as a predictor of SSc gene expression subsets.[20,25] We also found that baseline gene expression signatures associated with fibroblast polarization tended to be higher in patients who improved clinically compared with nonimprovers, suggesting that baseline skin histology may provide insight into patient trajectories. However, these analyses were limited to very early dcSSc (median baseline disease duration of 10 months), which left gaps in our understanding of fibroblast heterogeneity in later stages of disease. The small study cohort also limited the assessment of fibroblast immunophenotype as predictive of patient trajectory in the setting of specific treatments. The purpose of this study is to evaluate the relationship among fibroblast activation, immune cell infiltration, and disease duration in dcSSc and to identify predictors of clinical improvement in the setting of MMF therapy.

PATIENTS AND METHODS

Patients. Baseline skin biopsies and clinical data were analyzed from 105 patients enrolled in the lenabasum (n = 79), belimumab (n = 18), or nilotinib (n = 8) clinical trials.[12,13,26] Patients were adults who fulfilled 1980 American College of Rheumatology (ACR) classification criteria for SSc[27] and/or ACR/EULAR 2013 SSc criteria[28] and had dcSSc.[29]

Briefly, the lenabasum study (RESOLVE-1) was a double-blind, randomized, placebo-controlled, international, phase III clinical trial conducted between 2017 and 2020, comparing lenabasum to placebo.[26] A total of 365 patients were included, with disease duration (time since first non-Raynaud phenomenon symptom) up to six years, and stable background immunosuppression was permitted. The belimumab study was a double-blind, randomized, placebo-controlled, single-center trial comparing belimumab with placebo in the setting of background MMF therapy[13] conducted between 2012 and 2015. Twenty patients were included, with disease duration up to three years. The nilotinib study was an open-label, single-center, pilot trial[12] conducted between 2010 and 2014. Ten patients were included who had disease duration up to three years, and background immunosuppression was not permitted. Key inclusion criteria of these three clinical trials may be found in Supplemental Table 1. Patients were included in the present study if skin biopsy tissue as well as clinical data were available for analysis. The study was approved by Hospital for Special Surgery Institutional Review Board (2022-0574). Privacy rights were observed, and informed consent was obtained from all participants.

Clinical data. Clinical data were collected at baseline and 52 weeks, including patient demographics, SSc disease duration, autoantibodies, treatments, mRSS, interstitial lung disease presence, percentage of predicted forced vital capacity (FVC),

Physician and Patient Global Assessment (0–10 visual analog scale), and Health Assessment Questionnaire-Disability Index (HAQ-DI). Disease duration was defined as time between first non-Raynaud phenomenon SSc symptom and baseline skin biopsy date. In this study, "early" disease was defined as <18 months, whereas "later" SSc was defined as ≥18 months. This 18-month threshold has been suggested as optimal for trial enrollment based on observational cohort trajectory analyses.[10] Clinical improvement was defined as >5-point decrease in mRSS at 52 weeks.[5,30,31]

Skin histology. A 3-mm, anterior forearm skin punch biopsy was obtained for skin histology at the baseline visit. Each biopsy was assessed by a single pathologist, blinded to patient characteristics and outcomes. The approach to skin histology scoring and reliability has been previously described[20] and illustrated in Figure 1. Fibroblasts were assessed by CD34 and α-SMA immunohistochemistry and scored semiquantitatively (0–3): 0 to 1 is "low," and 2to 3 is "high." Immune cells (CD20+ B cells, CD3+ T cells, and CD123+ plasmacytoid dendritic cells) were scored as the sum of the cell count within the five most populated high-powered fields (400×), as per previously published methods[32] (Supplemental Table 2A). After scoring was completed, a sensitivity analysis was performed in which the biopsies with the highest cell counts were re-reviewed. There was no difference in the total cell count of the biopsies compared with the summed five most densely populated high-powered fields approach. In other words, biopsies with exceptionally high immune cell counts typically exhibited immune cell clusters that our methods effectively captured.

Imaging mass cytometry. To determine the spatial relationship of fibroblast subpopulations in SSc skin, imaging mass cytometry (IMC; Hyperion) was performed on a representative forearm sample from a patient with early SSc, CD34 and α-SMA positivity, and clinical improvement at 52 weeks. In short, formalin-fixed, paraffin-embedded skin biopsy tissue was dewaxed, rehydrated, and underwent antigen retrieval at pH 9.0, followed by a blocking step using the Thermo Fisher SuperBlock for one hour at room temperature. The skin section was then incubated with a cocktail of metal-conjugated antibodies (CD34, α-SMA, CD31, and Collagen Type I; Supplemental Table 2B) overnight in 4°C. The following day, the tissue section was washed with Tween and Tris-buffered saline to remove excess antibodies and reagents. Cell ID Intercalator-Ir (1:400, Standard BioTools) was used for cellular DNA staining for 30 minutes at room temperature. Finally, the tissue was rinsed, air dried, and set up on the IMC for acquisition following machine calibration.[33,34]

Statistical analysis. Clinical and skin histologic differences between those with early (<18 months) versus later (≥18 months) disease duration at trial enrollment were compared using Fisher's exact, *t*-test, or Wilcoxon rank sum, as appropriate. Among the

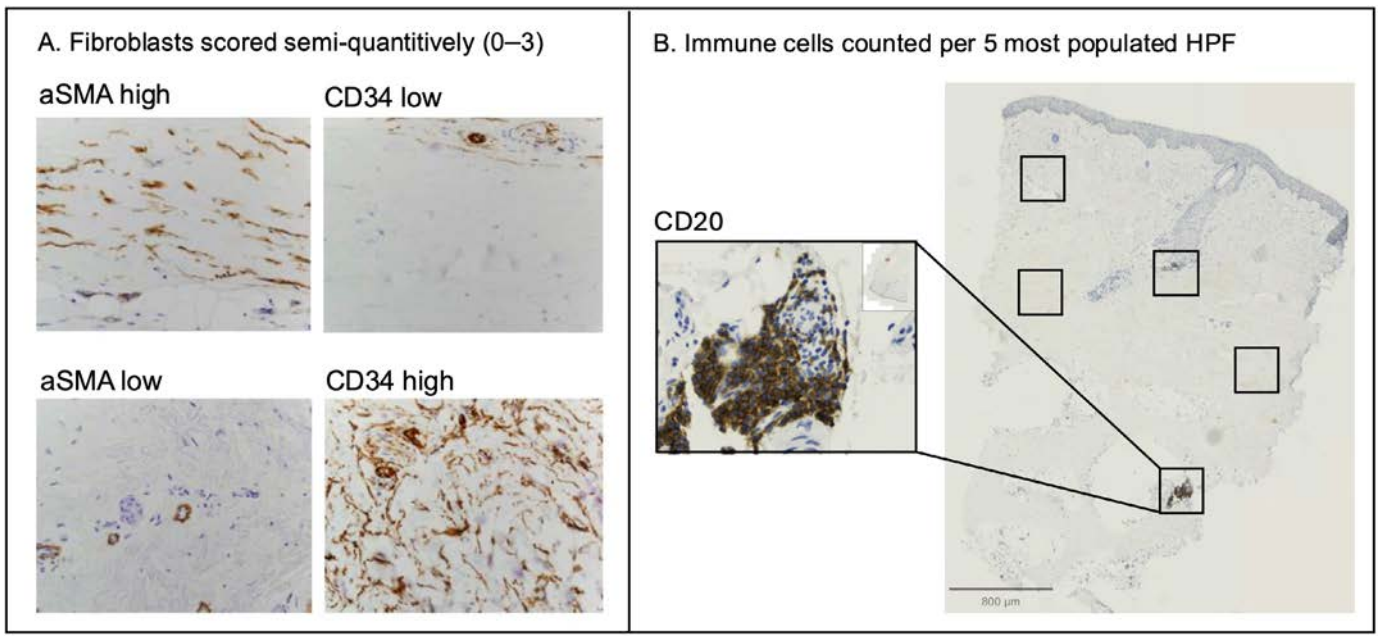

Figure 1. Skin histology assessment. (A) Fibroblasts were assessed by α-SMA and CD34 immunohistochemistry and scored semiquantitatively between 0–3 based upon staining intensity. A low score was defined as a score of 0–1; a high score was defined as a score 2–3. (B) Immune cells (CD20+ B cells, CD3+ T cells, and CD123+ plasmacytoid dendritic cells) were scored as cell count (summed) within the five most populated HPFs (400×). An example of CD20 staining is shown in which most CD20+ cells were clustered within the deep dermis. α-SMA, α-smooth muscle actin; HPF, high-powered field.

68 MMF users, skin histology was compared according to disease duration and α-SMA status using Fisher's exact, *t*-test, or Wilcoxon rank sum, as appropriate.

To identify independent predictors of 52-week clinical improvement with MMF, a multiple logistic regression model was developed using baseline clinical and histologic data from 68 MMF users. Model optimization was performed using the minimum Akaike's information criterion (AIC) to prevent overfitting. Candidate predictors included sex, baseline mRSS, belimumab use, RNA polymerase III status, CD34, α-SMA, CD20, CD3, CD123, and disease duration (<18 or ≥18 months), as well as interactions between predictors and disease duration. The model was also fit using Firth correction.[35] The resulting logistic regression was used to predict the probability of improvement based on the identified independent predictors, with probabilities extrapolated for combinations without available patient results. Statistical analyses were completed using STATA version 16.0 and Python version 3.12 using the statsmodels and SciPy packages.

RESULTS

Among 105 patients with dcSSc, 49 had early SSc and 56 had later SSc (Table 1). The median disease duration for the full cohort was 20 (interquartile range [IQR] 12–36) months

Table 1. Clinical and histologic characteristics among 105 patients with diffuse cutaneous systemic sclerosis according to disease duration*

Characteristics	Early disease (<18 months; n = 49)	Later disease (≥18 months; n = 56)	*P* value
Clinical variables, baseline			
Disease duration, median (IQR), months	10.3 (7.7–13.3)	35.4 (28.1–45.3)	**<0.001**
Male sex, n (%)	11 (22)	16 (29)	0.51
Age, mean (SD), years	52.5 (13.13)	49.8 (14.67)	0.32
Race, n (%)			0.91
White	37 (76)	42 (75)	
Black	4 (8)	3 (5)	
Asian	6 (12)	9 (16)	
Other	2 (4)	2 (4)	
Autoantibodies, n (%)			
Scl-70 positive	9 (18)	27 (48)	**0.002**
RNA polymerase III positive	27 (56)	23 (46)	0.32
Centromere positive	3 (6)	2 (4)	0.66
mRSS, mean (SD)	25 (9.2)	24 (8.8)	0.33
ILD present, n (%)	16 (33)	24 (43)	0.42
FVC baseline, mean (SD)	85 (15.0)	78 (15.9)	**0.02**
HAQ, median (IQR)	1.0 (0.63–1.38)	1.1 (0.50–1.69)	0.36
Patient Global (0–10), median (IQR)	5 (2.27–6)	4 (2.4–5.5)	0.58
Physician Global (0–10), mean (SD)	5.7 (1.66)	5.0 (1.40)	**0.03**
Baseline medication, n (%)			
Mycophenolate mofetil	34 (69)	34 (61)	0.42
Methotrexate	4 (8)	7 (12)	0.54
Steroid (any)	8 (16)	12 (21)	0.62
Additional medications, n (%)			
Belimumab	7 (14)	2 (4)	0.08
Lenabasum	19 (39)	33 (59)	**0.05**
Skin histology, baseline			
α-SMA high fibroblasts, n (%)	24 (49)	17 (30)	0.07
α-SMA score, median (IQR)	1.5 (1–2)	1 (0–2)	**0.02**
CD34 high fibroblasts, n (%)	23 (47)	41 (73)	**0.01**
CD34 score, median (IQR)	1.5 (1–3)	2 (1–3)	0.07
CD20 (B cells), median (IQR)	1 (0–6)	0 (0–2)	**0.05**
CD123 (pDC), median (IQR)	3 (1–7.5)[a]	2 (0–7)	0.12
CD3 (T cells), median (IQR)	70 (45–90)[a]	57.5 (30–95)	0.19
52-week clinical outcomes			
52-week clinical improver, n (%)	33 (70)[b]	34 (61)	0.41
Change in mRSS, median (IQR)	−9 (−15 to −5)[b]	−7 (−10 to −3)	**0.03**

* Bold values indicate statistical significance at an alpha of 0.05.
α-SMA, α-smooth muscle actin; FVC, percentage of predicted forced vital capacity; HAQ, Health Assessment Questionnaire; ILD, interstitial lung disease; IQR, interquartile range; mRSS, modified Rodnan skin score; pDC, plasmacytoid dendritic cell.
[a] n = 48. One patient for both CD123 and CD3 had slides that were unusable due to inadequate staining or incomplete tissue representation.
[b] n = 47. Two patients in the nilotinib study had baseline but not 52-week data. No other variables had missing data. For histology, CD20, CD123, and CD3 are reported as count per five most populated high-powered fields. α-SMA and CD34 are scored semiquantitatively: 0–1 is low, and 2–3 is high.

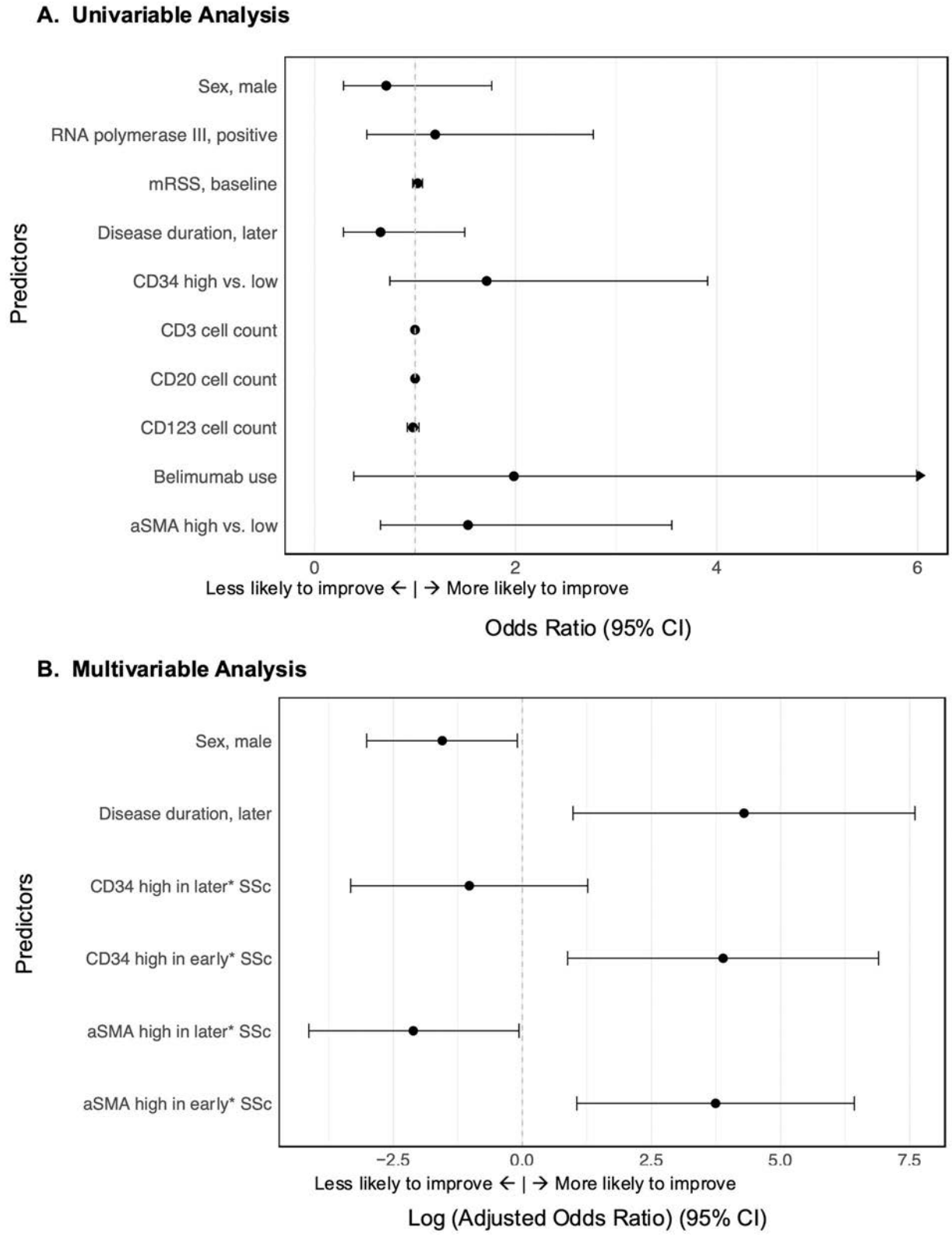

Figure 2. Predictors of 52-week clinical improvement among 68 patients with diffuse cutaneous systemic sclerosis treated with mycophenolate mofetil. (A) presents unadjusted odds ratios, whereas (B) presents the log of adjusted odds ratios from the multivariable model. Early SSc is defined by disease duration (time since first non-Raynaud symptom) <18 months. Later SSc is defined by disease duration ≥18 months. α-SMA, α-smooth muscle actin; CI, confidence interval; mRSS, modified Rodnan skin scale; SSc, systemic sclerosis.

(Supplemental Figure 1) and 10 (IQR 8–13) and 35 (IQR 28–45) months for the early and later groups, respectively. Compared with early SSc, those with later disease at baseline were more likely to have Scl-70 autoantibody positivity (48% vs 18%; $P = 0.002$) and had lower mean percentage of predicted FVC (78 vs 85; $P = 0.02$). Physician global assessment was slightly worse in early SSc (5.7 vs 5; $P = 0.03$), but patient global assessment and HAQ-DI did not differ significantly by disease duration. Baseline mRSS was similar between early and later SSc (25 vs 24, respectively; $P = 0.33$) (Table 1). MMF use was frequent in both groups (69% early SSc, 61% later SSc). Among 68 MMF users, the mean daily dose was 2 (SD 0.81) grams per day. The median MMF treatment duration was 110 (IQR 44–250) days at the time of skin biopsy, among 57 patients with MMF duration data available. Longitudinally, median mRSS improvement was greater in early SSc compared with later SSc in the full cohort and among 68 MMF-treated patients (–9 vs –7, $P = 0.025$; –11 vs –7, $P = 0.038$, respectively). Among MMF users, at the time of skin biopsy, there was no difference in median MMF treatment duration or average dose in improvers compared with nonimprovers (median 115 [IQR 60–227] vs median 106 [IQR 18–301] days, $P = 0.94$; median 2.2 [IQR 0.85] vs median 2.1 [IQR 0.72] grams per day, $P = 0.69$, respectively).

Despite similar baseline mRSS and patient-reported outcomes, histologic differences were observed by disease duration at baseline. Compared with later SSc, the early SSc group had fewer $CD34^{high}$ fibroblasts (47% vs 73%; $P = 0.009$), higher median α-SMA score (1.5 vs 1; $P = 0.018$), and increased CD20+ B cells (1 vs 0; $P = 0.05$; Table 1).

Clinical improvement was observed in 64% (67 of 105) of the overall cohort and 70% (48 of 68) of MMF users. An AIC-optimal multiple logistic regression model was developed to predict clinical improvement among those taking MMF (Figures 2 and 3; Supplemental Table 3). An analysis focused on MMF response was conducted because MMF was the most common medication used in our cohort and due to its prominent role in dcSSc skin treatment in recently published guidelines.[2,4] The strongest predictors in the multivariable model were baseline sex and disease duration, as well as CD34, α-SMA, and their interactions with time. Male sex was associated with lower odds of improvement (unadjusted odds ratio [OR] 0.713, 95% confidence interval [CI] 0.289–1.762; adjusted OR 0.212, 95% CI 0.049–0.909). Although unadjusted analysis suggested later SSc was associated with lower odds of improvement (unadjusted OR 0.656, 95% CI 0.288–1.494), adjusting for fibroblast immunophenotype revealed that later disease duration was associated with increased odds of improvement (adjusted OR 73.137, 95% CI 2.667–2005.441). The effect of fibroblast scores on clinical outcomes varied by disease duration at the time of biopsy. In early SSc, high CD34 and high α-SMA both predicted greater odds of improvement, whereas in later SSc, high α-SMA was associated with lower odds of improvement. Probabilities of clinical improvement based on independent predictors in the model are shown in Figure 3. These results were consistent in sensitivity analyses incorporating baseline mRSS, RNA polymerase III status, MMF treatment duration, belimumab treatment, and immune cell counts (CD20+, CD3+, and CD123+). Given

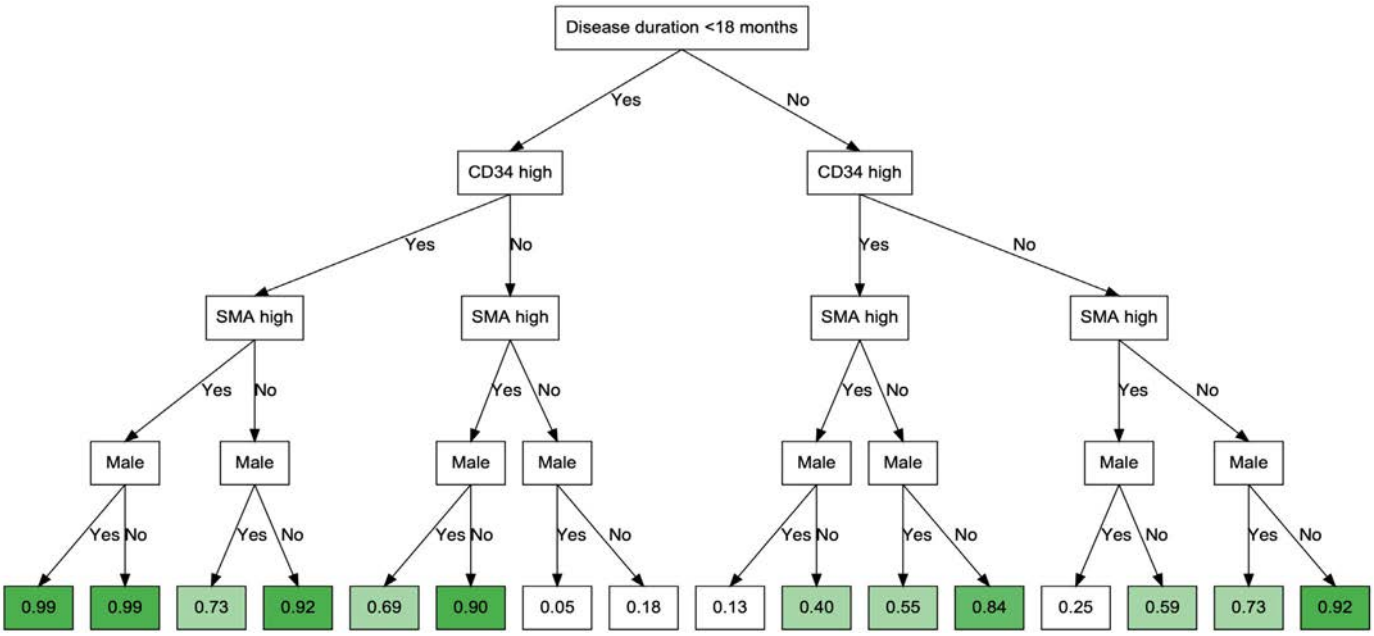

Figure 3. Flowchart summarizing logistic regression-based predictions of 52-week clinical improvement with mycophenolate mofetil in patients with diffuse cutaneous systemic sclerosis based on independent clinical predictors. The terminal nodes display the estimated probability of improvement on mycophenolate mofetil, as predicted by the logistic regression model. SMA, smooth muscle actin.

concerns about potential bias of the maximum likelihood estimates of logistic regression coefficients in small samples, we re-fit the model using the Firth correction. This led to a mild shrinkage of the estimates, but it did not affect the final interpretation (results not shown).

The lowest rate of improvement was observed in early SSc when both CD34 and α-SMA were low (1 of 7; 14%; Table 2). In later SSc, high α-SMA was associated with poorer outcomes, with only 40% to 50% improving regardless of CD34 status. Given that high α-SMA predicts better outcomes in early disease but worse outcomes in later SSc, we further examined the role of sustained α-SMA elevation in late-stage disease. Although immune infiltrates did not differ by α-SMA status in early SSc, in later SSc, B cells were more frequently present in α-SMA^{high} compared with α-SMA^{low} skin (73% vs 22%; $P = 0.008$; Table 2).

The highest rates of improvement were observed in patients with early SSc and both α-SMA^{high}, activated myofibroblasts, and CD34^{high}, relatively healthy fibroblasts. To assess whether this represented a population of transitional fibroblasts co-expressing these markers or two distinct types of fibroblasts coexisting in the same sample, IMC was performed on a representative sample with both α-SMA^{high} and CD34^{high} immunophenotype, early SSc, and clinical improvement. Distinct fibroblast neighborhoods were revealed that associated with varying collagen densities (Figure 4). CD34+ cells localized to more superficial regions of the dermis where collagen bundles were looser, whereas α-SMA+ cells were present in the deeper dermal layer where collagen density was greater.

DISCUSSION

In a cohort of patients enrolled in clinical interventional trials, baseline fibroblast immunophenotype, but not mRSS, varied by disease duration. These findings demonstrate that mRSS alone does not capture key differences in fibroblast immunophenotype between early and later stages of SSc that were shown to influence disease trajectory. Skin fibroblast and immune profiles may offer more precise insights into disease subsets, beyond clinical measures, and may be used to inform patient management decisions.

Skin biopsies are commonly obtained in SSc clinical trials to evaluate treatment effect at the tissue level but obtained less often in the context of clinical care. In prior work, CD34 and α-SMA have been associated with clinical severity, but the strength of these associations has varied between studies. We and others have reported moderate associations with clinical severity and histologic scores (CD34, α-SMA, and collagen), whereas one study that included healthy controls and patients with dcSSc reported strong associations between clinical severity and collagen and myofibroblast scores ($r = 0.83$ and $r = 0.78$, respectively). Importantly, these studies did not stratify samples according to disease duration, which we show to be important in contextualizing a given fibroblast profile.

The prognostic impact of fibroblast profile varies by disease duration at the time of biopsy. In early SSc, high α-SMA and high CD34 confer a high likelihood of improvement on MMF, whereas high α-SMA in later SSc is associated with lower odds of improvement. Taken together, high α-SMA may represent a treatment-receptive phase in early SSc but a treatment-refractory phase in later disease stages. B cells were more common in later SSc

Table 2. Clinical and histologic features by disease duration and α-SMA status among 68 individuals with diffuse cutaneous systemic sclerosis on mycophenolate mofetil*

Features	Early disease (<18 months)			Later disease (≥18 months)		
	α-SMA low (n = 16)	α-SMA high (n = 18)	*P* value	α-SMA low (n = 23)	α-SMA high (n = 11)	*P* value
Clinical improver by α-SMA and CD34 status, n/N (%)						
CD34 low	1/7 (14)	11/13 (85)		1/1 (100)	3/6 (50)	
CD34 high	8/9 (89)	5/5 (100)		17/22 (77)	2/5 (40)	
Clinical						
Baseline mRSS, mean (SD)	24 (8.5)	27 (9.2)	0.36	22 (6.2)	28 (9.5)	**0.037**
Belimumab use, n (%)	2 (12)	5 (28)	0.41	1 (4)	1 (9)	1.00
Lenabasum use, n (%)	8 (50)	6 (33)	0.49	14 (61)	6 (55)	1.00
Steroid (any) use, n (%)	3 (19)	3 (17)	1.00	8 (35)	1 (9)	0.21
mRSS improver, n (%)	9 (56)	16 (89)	**0.05**	18 (78)	5 (45)	0.11
52-week delta mRSS, median (IQR)	−7.5 (−14 to −2.5)	−11 (−17 to −8)	0.21	−7 (−10 to −6)	−4 (−9 to 1)	0.15
Histology						
CD123, median (IQR)	3 (1–8)[a]	3 (1–5)	0.88	2 (0–5)	1 (0–11)	0.97
CD3, median (IQR)	60 (40–80)[a]	67.5 (40–90)	0.37	55 (30–90)	100 (30–180)	0.13
CD20, median (IQR)	1 (0–2.5)	2.5 (1–6)	0.078	0 (0–0)	2 (0–4)	**0.007**
CD20+ cells present, n (%)	9 (56)	14 (78)	0.27	5 (22)	8 (73)	**0.008**
CD34 high, n (%)	9 (56)	5 (28)	0.16	22 (96)	5 (45)	**0.002**

* Clinical improver defined as decrease in mRSS from baseline to 52 weeks >5. Disease duration defined as time since first non-Raynaud phenomenon symptom. Bold values indicate statistical significance at an alpha of 0.05.
α-SMA, α-smooth muscle actin; IQR, interquartile range; mRSS, modified Rodnan skin score.
[a] n = 15.

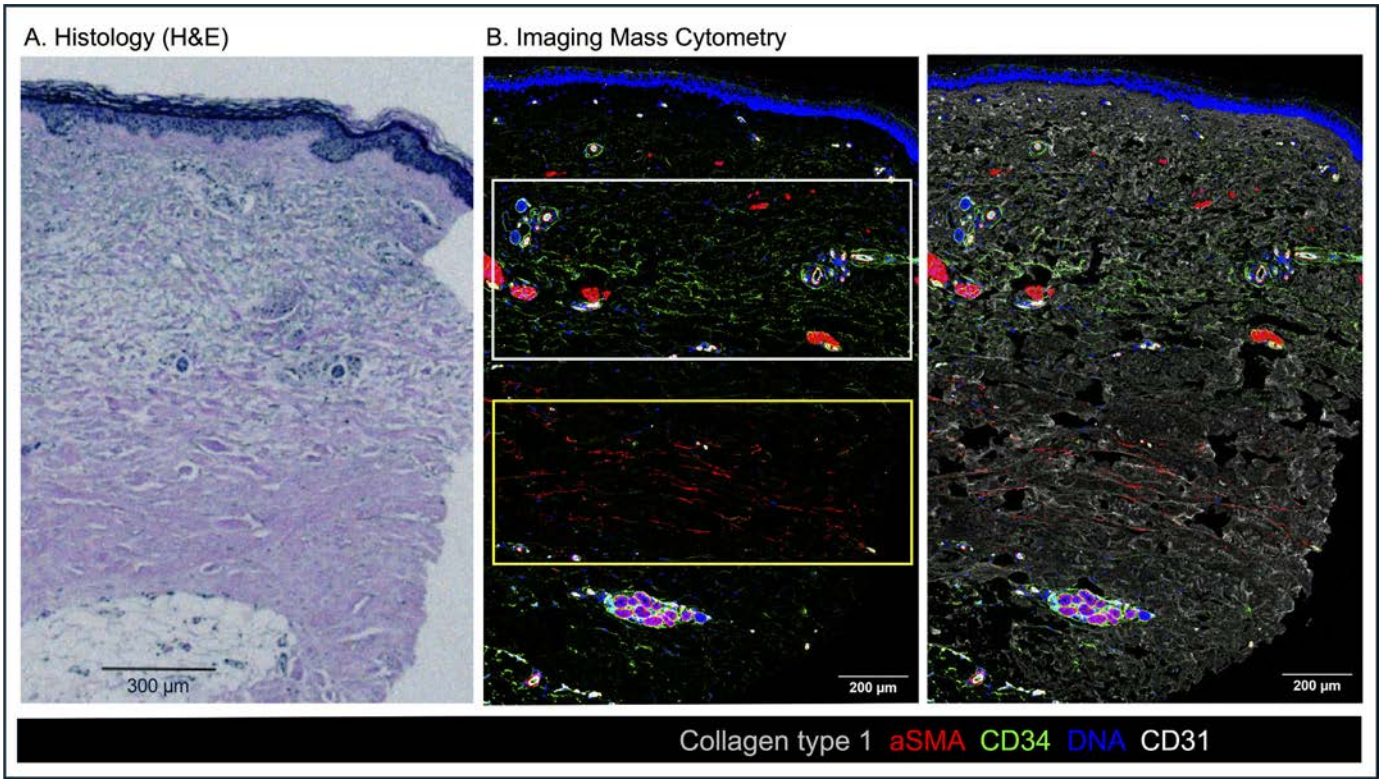

Figure 4. Imaging mass cytometry of diffuse cutaneous systemic sclerosis skin reveals distinct fibroblast microenvironments. In a patient with disease duration of six months who clinically improved at 52 weeks, CD34+ fibroblasts localize to superficial dermal layers (white box) with lower collagen density, whereas α-SMA+ fibroblasts predominate in deeper dermal layers with higher collagen density (yellow box). α-SMA, α-smooth muscle actin; H&E, hematoxylin and eosin.

samples with high (vs low) α-SMA. These patients may benefit from additional therapies, including B cell–targeting agents.

A majority (70%) of MMF users improved, underscoring the use of MMF as treatment for dcSSc as well as the challenges clinical trials face when incorporating MMF as background therapy. As several immunosuppressive therapies have been highlighted as effective in recent SSc skin treatment guidelines,[2,4] conducting clinical trials without background therapy, such as MMF, will become increasingly uncommon due to ethical considerations. In the clinical trial setting, a strong predisposition toward improvement on MMF background therapy could mask meaningful treatment effects of an intervention. Additionally, patients highly likely to improve on MMF alone may not be ideal candidates for add-on therapies that are associated with additional risks. By leveraging fibroblast markers to identify patients who are less likely to respond to MMF, such as those with persistently high α-SMA in later disease, physicians may consider additional treatments earlier, and clinical trials could better target individuals likely to benefit most from novel therapies. However, further investigation is needed to determine if those with disease duration beyond 18 months and high α-SMA would be similarly resistant to therapies beyond MMF, such as B cell–depleting agents. These results underscore the importance of early referral to expert centers for comprehensive patient phenotyping and initiating appropriate therapy, including potential clinical trial referrals.

In contrast to prior studies,[7,9,36] our final model did not identify RNA polymerase III antibody status or baseline mRSS as independent predictors of clinical improvement on MMF. In sensitivity analyses, RNA polymerase III status did not enhance our model performance. The disease duration at which mRSS peaks may differ between RNA polymerase III compared with Scl-70–positive patients and could influence results, given that the later SSc group was enriched with Scl-70–positive patients. Male sex was a significant predictor of worse outcomes in our study, which is consistent with prior reports.[37] Future studies are needed to better elucidate the mechanisms by which sex influences disease trajectory and treatment response. Our study adds to the literature by focusing on MMF users and demonstrates that adjusting for fibroblast immunophenotype influences the association between disease duration and improvement on MMF. Although mRSS improvement on MMF was greater in early SSc, our model incorporating fibroblast markers instead revealed that later disease duration was associated with higher odds of improvement. This suggests that differences in fibroblast phenotype may explain the clinical observation that early-stage patients

appear more likely than later-stage patients to improve with immunosuppression.

We also discovered α-SMA and CD34 fibroblast markers coexisted in a substantial number of patients, which raised the possibility that some patients may harbor double-positive cells in transition. Using IMC, we instead observed regional variations in fibroblast expression within dcSSc skin with fibroblast subtypes localizing to areas within the dermis with differing collagen density visualized by IMC and hematoxylin and eosin. These regional differences are not well assessed using single immunohistochemistry staining and may contribute to varying correlations between histology scores and overall site severity. Where α-SMA localizes in the skin could impact outcomes and vary with disease duration but is not assessed in our current analysis. Future IMC studies are needed that incorporate detailed regional analyses and longitudinal data across different disease stages.

Our study analyzes a relatively large, international cohort of patients with dcSSc with baseline skin biopsies and 52-week clinical, high-quality, trial-level data with minimal missing values. To our knowledge, this is the first study to report baseline histologic predictors of clinical trajectory in SSc. However, we also recognize study limitations. Generalizability is limited to patients who meet the clinical trial inclusion criteria, which excluded those with disease duration beyond six years. Certain fibroblast and disease duration subgroups were underrepresented (eg, $CD34^{low}$ and $\alpha\text{-SMA}^{low}$ in later SSc), which may have impacted model predictions. Additionally, most had been on a stable MMF dose for at least eight weeks before baseline. Measures of compliance, such as MMF levels, were not captured in this analysis and could influence individual trajectories. However, our results are applicable to patients seeking clinical trial enrollment despite MMF use and add to the literature regarding MMF as background therapy in clinical trials.

In conclusion, skin biopsy assessments provide insights related to dcSSc heterogeneity and improve model performance for identifying those likely to improve. The prognostic significance of skin fibroblast profile depends on disease duration, suggesting that skin biopsies have a role, along with disease duration, in identifying periods of time during which patients may be more or less likely to improve with MMF. These results support an expanded role for skin biopsies in refining prognosis and personalizing patient management decisions in clinical practice.

ACKNOWLEDGMENTS

We would like to acknowledge and thank each of the RESOLVE-1 trial investigators as well as the patients and their families. We also thank the research staff of Englander Institute for Precision Medicine Mass Cytometry Core of Weill Cornell Medicine in assisting with the imaging mass cytometry work and the Weill Cornell Center for Translational Pathology, particularly Bing He and Maneeza Bilal, who assisted with this study.

AUTHOR CONTRIBUTIONS

All authors contributed to at least one of the following manuscript preparation roles: conceptualization AND/OR methodology, software, investigation, formal analysis, data curation, visualization, and validation AND drafting or reviewing/editing the final draft. As corresponding author, Dr Lakin confirms that all authors have provided the final approval of the version to be published and takes responsibility for the affirmations regarding article submission (eg, not under consideration by another journal), the integrity of the data presented, and the statements regarding compliance with institutional review board/Declaration of Helsinki requirements.

REFERENCES

1. Volkmann ER, Andréasson K, Smith V. Systemic sclerosis. Lancet 2023;401(10373):304–318.
2. Del Galdo F, Lescoat A, Conaghan PG, et al. EULAR recommendations for the treatment of systemic sclerosis: 2023 update. Ann Rheum Dis 2025;84(1):29–40.
3. White B, Furst DE, Frech TM, et al; RESOLVE-1 investigators. Comparative efficacy of immunosuppressive therapies in the treatment of diffuse cutaneous systemic sclerosis. ACR Open Rheumatol 2025; 7(3):e70004.
4. Denton CP, De Lorenzis E, Roblin E, et al. The 2024 British Society for Rheumatology guideline for management of systemic sclerosis. Rheumatology (Oxford) 2024;63(11):2956–2975.
5. Dobrota R, Maurer B, Graf N, et al; EUSTAR coauthors. Prediction of improvement in skin fibrosis in diffuse cutaneous systemic sclerosis: a EUSTAR analysis. Ann Rheum Dis 2016;75(10):1743–1748.
6. Domsic RT, Medsger TA Jr, Gao S, et al. A data-driven approach finds RNA polymerase III antibody and tendon friction rubs as enrichment tools for early diffuse scleroderma trials. Rheumatology (Oxford) 2023;62(4):1543–1551.
7. Herrick AL, Peytrignet S, Lunt M, et al. Patterns and predictors of skin score change in early diffuse systemic sclerosis from the European Scleroderma Observational Study. Ann Rheum Dis 2018;77(4): 563–570.
8. Domsic RT, Rodriguez-Reyna T, Lucas M, et al. Skin thickness progression rate: a predictor of mortality and early internal organ involvement in diffuse scleroderma. Ann Rheum Dis 2011;70(1):104–109.
9. Maurer B, Graf N, Michel BA, et al; EUSTAR co-authors. Prediction of worsening of skin fibrosis in patients with diffuse cutaneous systemic sclerosis using the EUSTAR database. Ann Rheum Dis 2015;74(6): 1124–1131.
10. Domsic RT, Gao S, Laffoon M, et al. Defining the optimal disease duration of early diffuse systemic sclerosis for clinical trial design. Rheumatology (Oxford) 2021;60(10):4662–4670.
11. Khanna D, Spino C, Johnson S, et al. Abatacept in early diffuse cutaneous systemic sclerosis: results of a phase II investigator-initiated, multicenter, double-blind, randomized, placebo-controlled trial. Arthritis Rheumatol 2020;72(1):125–136.
12. Gordon JK, Martyanov V, Magro C, et al. Nilotinib (Tasigna) in the treatment of early diffuse systemic sclerosis: an open-label, pilot clinical trial. Arthritis Res Ther 2015;17(1):213.
13. Gordon JK, Martyanov V, Franks JM, et al. Belimumab for the treatment of early diffuse systemic sclerosis: results of a randomized, double-blind, placebo-controlled, pilot trial. Arthritis Rheumatol 2018;70(2):308–316.
14. Khanna D, Lin CJF, Furst DE, et al; focuSSced investigators. Tocilizumab in systemic sclerosis: a randomised, double-blind, placebo-controlled, phase 3 trial. Lancet Respir Med 2020;8(10):963–974.

15. Sullivan KM, Goldmuntz EA, Keyes-Elstein L, et al; SCOT Study Investigators. Myeloablative autologous stem-cell transplantation for severe scleroderma. N Engl J Med 2018;378(1):35–47.
16. Gilbane AJ, Denton CP, Holmes AM. Scleroderma pathogenesis: a pivotal role for fibroblasts as effector cells. Arthritis Res Ther 2013; 15(3):215.
17. Hinz B, Phan SH, Thannickal VJ, et al. The myofibroblast: one function, multiple origins. Am J Pathol 2007;170(6):1807–1816.
18. Kissin EY, Merkel PA, Lafyatis R. Myofibroblasts and hyalinized collagen as markers of skin disease in systemic sclerosis. Arthritis Rheum 2006;54(11):3655–3660.
19. Van Praet JT, Smith V, Haspeslagh M, et al. Histopathological cutaneous alterations in systemic sclerosis: a clinicopathological study. Arthritis Res Ther 2011;13(1):R35.
20. Showalter K, Spiera R, Magro C, et al. Machine learning integration of scleroderma histology and gene expression identifies fibroblast polarisation as a hallmark of clinical severity and improvement. Ann Rheum Dis 2021;80(2):228–237.
21. Sidney LE, Branch MJ, Dunphy SE, et al. Concise review: evidence for CD34 as a common marker for diverse progenitors. Stem Cells 2014; 32(6):1380–1389.
22. Aiba S, Tabata N, Ohtani H, et al. CD34+ spindle-shaped cells selectively disappear from the skin lesion of scleroderma. Arch Dermatol 1994;130(5):593–597.
23. Skobieranda K, Helm KF. Decreased expression of the human progenitor cell antigen (CD34) in morphea. Am J Dermatopathol 1995; 17(5):471–475.
24. Ho JD, Chung HJ, Ms Barron A, et al. Extensive CD34-to-CD90 fibroblast transition defines regions of cutaneous reparative, hypertrophic, and keloidal scarring. Am J Dermatopathol 2019;41(1):16–28.
25. Milano A, Pendergrass SA, Sargent JL, et al. Molecular subsets in the gene expression signatures of scleroderma skin. PLoS One 2008; 3(7):e2696.
26. Spiera R, Kuwana M, Khanna D, et al; RESOLVE-1 Study Group. Efficacy and safety of lenabasum, a cannabinoid type 2 receptor agonist, in a phase 3 randomized trial in diffuse cutaneous systemic sclerosis. Arthritis Rheumatol 2023;75(9):1608–1618.
27. Masi AT. Preliminary criteria for the classification of systemic sclerosis (scleroderma). Subcommittee for scleroderma criteria of the American Rheumatism Association Diagnostic and Therapeutic Criteria Committee. Arthritis Rheum 1980;23(5):581–590.
28. van den Hoogen F, Khanna D, Fransen J, et al. 2013 classification criteria for systemic sclerosis: an American College of Rheumatology/-European League against Rheumatism collaborative initiative. Arthritis Rheum 2013;65(11):2737–2747.
29. LeRoy EC, Medsger TA Jr. Criteria for the classification of early systemic sclerosis. J Rheumatol 2001;28(7):1573–1576.
30. Khanna D, Clements PJ, Volkmann ER, et al. Minimal clinically important differences for the modified Rodnan skin score: results from the Scleroderma Lung Studies (SLS-I and SLS-II). Arthritis Res Ther 2019;21(1):23.
31. Khanna D, Furst DE, Hays RD, et al. Minimally important difference in diffuse systemic sclerosis: results from the D-penicillamine study. Ann Rheum Dis 2006;65(10):1325–1329.
32. Ah Kioon MD, Tripodo C, Fernandez D, et al. Plasmacytoid dendritic cells promote systemic sclerosis with a key role for TLR8. Sci Transl Med 2018;10(423):eaam8458.
33. Ijsselsteijn ME, van der Breggen R, Farina Sarasqueta A, et al. A 40-marker panel for high dimensional characterization of cancer immune microenvironments by imaging mass cytometry. Front Immunol 2019;10:2534.
34. Rendeiro AF, Ravichandran H, Bram Y, et al. The spatial landscape of lung pathology during COVID-19 progression. Nature 2021; 593(7860):564–569.
35. Heinze G, Schemper M. A solution to the problem of separation in logistic regression. Stat Med 2002;21(16):2409–2419.
36. Mihai C, Dobrota R, Assassi S, et al. Enrichment strategy for systemic sclerosis clinical trials targeting skin fibrosis: a prospective, multiethnic cohort study. ACR Open Rheumatol 2020;2(8):496–502.
37. Barbacki A, Baron M, Wang M, et al; Australian Scleroderma Interest Group and the Canadian Scleroderma Research Group. Damage trajectories in systemic sclerosis using group-based trajectory modeling. Arthritis Care Res (Hoboken) 2023;75(3):640–647.

Arthritis & Rheumatology
Vol. 78, No. 2, February 2026, pp 428–437
DOI 10.1002/art.43400

American College of Rheumatology
Empowering Rheumatology Professionals

Telomere Length of Peripheral Blood Leukocytes Predicts Disease Severity and Worse Survival in Systemic Sclerosis

Monica M. Yang,[1] Shuo Liu,[2] Michael Wax II ,[3] Seoyeon Lee,[3] Sarah French,[1] Paul J. Wolters,[3] and Francesco Boin[4,5]

Objective. Peripheral blood leukocyte telomere length (PBL-TL) shortening is associated with systemic sclerosis–related interstitial lung disease (SSc-ILD). However, its association with other organ involvement, disease severity, and survival remains unclear. This study aimed to define the relationship of TL with SSc-specific disease manifestations and outcomes.

Methods. PBL-TL was measured by quantitative polymerase chain reaction in 244 patients with SSc and 314 healthy controls. Multivariate modeling was used to assess the association of PBL-TL with disease severity and event-free survival. Longitudinal changes in PBL-TL were measured in a subset of patients. TL was quantified in SSc skin and lung tissues by telomere fluorescence in situ hybridization.

Results. PBL-TL was significantly shorter in patients with SSc than healthy controls. Shortened PBL-TL was associated with presence and severity of ILD and pulmonary hypertension (PH), with the shortest PBL-TL found in subjects with concurrent ILD and PH ($P = 0.04$). PBL-TL was not associated with skin disease or peripheral vascular disease. Shorter PBL-TL was associated with hospitalizations ($P < 0.01$) and worse event-free survival ($P = 0.03$). Patients with early SSc had a faster rate of PBL-TL shortening compared with patients with longer disease duration ($P = 0.04$). TL was shorter in SSc-ILD lung epithelial cells ($P = 0.01$), whereas no difference was found in epithelial cells of SSc skin ($P = 0.82$).

Conclusion. Short PBL-TL is associated with pulmonary disease severity and predicts worse SSc clinical outcomes. This study provides rationale to further investigate the role of telomere dysfunction in SSc pathogenesis and validate TL as a prognostic biomarker in SSc.

INTRODUCTION

Systemic sclerosis (SSc) is a collagen vascular disorder characterized by autoimmunity, vasculopathy, and progressive fibrosis that can affect nearly any organ system.[1] Although SSc is associated with significant morbidity and mortality, its clinical course is highly variable with significant heterogeneity in disease progression, response to therapy, and overall survival. This variability underscores the need to advance our understanding of SSc pathogenesis to aid in biomarker discovery, identifying therapeutic targets and advancing precision medicine in the field.

There is a growing interest in the role of aberrant aging and cellular senescence in SSc pathogenesis. Telomeres are nucleoprotein structures that protect the end of chromosomes and shorten with each cell division.[2] Telomere shortening is a hallmark of aging, and shortened peripheral blood leukocyte telomere length (PBL-TL) has been associated with disease-specific morbidity and mortality.[3,4] Notably, telomere dysfunction is increasingly implicated in the pathogenesis of pulmonary fibrosis, and shortened PBL-TL has been associated with the severity of several forms of interstitial lung disease (ILD), including SSc-related ILD (SSc-ILD).[5–8] Although PBL-TL shortening has been shown

Supported by the Scleroderma Research Foundation, Rheumatology Research Foundation, Arthritis Research Coalition, Nina Ireland Program for Lung Health, NIH (grant R01-HL-139897), and Kao Multispecialty Scleroderma Program at Cedars-Sinai Medical Center.

[1]Division of Rheumatology, Department of Medicine, University of California, San Francisco; [2]Jinqiu Hospital of Liaoning Province, Shenyang, People's Republic of China; [3]Division of Pulmonary, Critical Care, Allergy and Sleep Medicine, Department of Medicine, University of California, San Francisco; [4]Division of Rheumatology, Department of Medicine, Cedar-Sinai Medical Center, Los Angeles, California; [5]Kao Autoimmunity Institute, Cedars-Sinai Medical Center, Los Angeles, California.

Additional supplementary information cited in this article can be found online in the Supporting Information section (https://acrjournals.onlinelibrary.wiley.com/doi/10.1002/art.43400).

Author disclosures are available at https://onlinelibrary.wiley.com/doi/10.1002/art.43400.

Address correspondence via email to Monica M. Yang, MD, at Monica.yang@ucsf.edu; or Francesco Boin, MD, at francesco.boin@cshs.org.

Submitted for publication February 12, 2025; accepted in revised form August 27, 2025.

in patients with SSc-ILD, its association with other SSc organ involvement and with overall SSc mortality is unknown.

The objective of this study was to define the relationship of PBL-TL with SSc-specific disease manifestations, disease severity, and clinical outcomes including mortality. To further the understanding of telomere biology in SSc, we also sought to define PBL-TL attrition rate over time in SSc disease subsets and assess TL in affected tissues such as lung and skin.

MATERIALS AND METHODS

Study population. This is a retrospective longitudinal cohort study using a large observational cohort of 244 patients with SSc prospectively enrolled from the University of California San Francisco (UCSF) Scleroderma Center.[9] All patients met the 2013 American College of Rheumatology/EULAR criteria for SSc. Healthy controls (n = 314) from UCSF were also included in the analysis. This study was approved by the institutional review boards at UCSF, and written informed consent was obtained from all subjects.

Clinical data and endpoints. Demographic and clinical data, including age, sex, self-reported race, smoking status, disease duration, immunosuppression use, cutaneous disease subtype (limited vs diffuse), and presence of autoantibodies, were recorded. Disease duration was defined as time from first non-Raynaud event with early SSc as defined by disease duration of less than 5 years. Primary clinical outcomes of interest included skin disease as measured by modified Rodnan skin score (mRSS), peripheral vascular disease as measured by presence of digital ulcers and Medsger Raynaud phenomenon severity score (RPSS), and pulmonary disease including the presence of ILD on high-resolution computed tomography (HRCT) or pulmonary hypertension (PH) by right heart catheterization using the 2022 European Society of Cardiology/European Respiratory Society guidelines.[10,11] Presence of calcinosis, scleroderma renal crisis, and myocardial involvement, as defined as a Medgser heart severity score of ≥1, was also examined. Data from pulmonary function testing, including forced vital capacity percent predicted (FVC%) and diffusing capacity of carbon monoxide percent predicted (DL_{CO}%), HRCT of the chest, and echocardiogram, including right ventricular systolic pressure, were obtained. ILD severity was defined using baseline FVC% cutoffs, including mild (>75%), moderate (55%–75%), and severe (<55%). Hospitalizations and survival were recorded within five years of baseline with death and lung transplantation considered terminal events.

PBL-TL measurement. DNA was isolated from peripheral blood leukocytes using the Gentra Puregene cell kit (Qiagen, Valencia, California). DNA quality was visualized on agarose gel, and degraded DNA samples were excluded from the analysis. Average PBL-TLs were measured while blinded to the study endpoints using uniplex quantitative polymerase chain reaction (PCR) in triplicate with the acidic ribosomal phosphoprotein 36B4 gene as a reference housekeeping gene, as previously described.[12–14] Average relative TLs were determined by subtracting telomere and reference median cycle threshold values. TLs were calculated by comparison to reference samples.[15] Using these methods, the intra-assay coefficient of variation (CV) was <1%, the interassay CV was <3%, and the intraclass correlation coefficient for triplicate measurements was 0.98 (95% confidence interval 0.97–0.99).

Longitudinal PBL-TL analysis. For a subset of patients with availability of serial DNA samples, PBL-TL was measured at a second timepoint after baseline using the method described above. To limit plate-plate variability, baseline and serial DNA samples were run on the same PCR plate. Using PBL-TL at both timepoints and years between DNA sample collection, a rate of TL change per year was calculated. Association of rate of PBL-TL change with clinical variables was compared using Wilcoxon and Kruskal-Wallis.

TL measurement in tissue with telomere quantitative fluorescence in situ hybridization assay. To examine the TL changes at an organ level, cell-specific TL was measured using telomere quantitative fluorescence in situ hybridization assay (Telo-FISH) in lung and skin tissue.[16] Lung tissue from 20 age-matched and sex-matched subjects, including 15 patients with SSc-ILD and 5 healthy controls, and forearm skin tissue from 12 patients with SSc and 8 healthy controls were used. Lung tissue was obtained immediately after lung transplantation, and skin tissue was obtained from punch biopsy of affected skin from the forearm. Tissues were fixed with 10% formalin overnight and embedded in paraffin and then sectioned to 4-μm thickness. Tissue slides were deparaffinized in xylene and rehydrated in ethanol gradient series. After heat-induced antigen retrieval, tissues were treated with 10 mg/mL RNase solution and incubated with 0.3 μg/mL peptide nucleic acid TelC-Cy3 probe (Panagene, Daejeon, South Korea) in 70% formamide buffer, heated to 78°C for 10 min then overnight at 20°C. Following washing and blocking, tissues were incubated with primary anti-rabbit surfactant protein C antibody, a marker of Type II alveolar (AT2) cells for lung, and anti-rabbit KRT5 antibody, a marker of epithelial cells for skin, followed by secondary antibody. Tissues were mounted with DAPI. Images were acquired using a Zeiss Axio Imager 2 microscope, and telomere signal intensity was quantified in a blinded manner using MetaMorph imaging analysis software (Molecular Devices, Sunnyvale, CA). Pairwise comparisons of TL were made between groups using Kruskal-Wallis test.

Statistical analysis. Patient characteristics were summarized by mean and SD for continuous variables and frequency for categorical variables. Multivariate regression was used to

examine the interaction of PBL-TL with clinical factors, including age, sex, race, smoking, immunosuppression use, disease duration. and autoantibody status. Using a linear model derived from healthy control measurements, an age-adjusted PBL-TL was calculated for each patient with SSc. Association of PBL-TL with clinical variables was compared using Wilcoxon and Kruskal-Wallis and depicted using classical boxplots. For further analysis, patients with SSc were stratified into tertiles based on their age-adjusted PBL-TL with tertile 1 (T1) representing the shortest TL and tertile 3 (T3) representing the longest (Supplementary Table 1). Survival analysis of event-free survival, defined as time to death or lung transplantation, was performed using Kaplan-Meier curve and log-rank test for significance. To account for variations of disease duration at time of PBL-TL measurement, survival analyses were performed with two starting timepoints including 5 years from baseline PBL-TL measurement and 30 years from SSc disease onset, as defined as date of first non-Raynaud symptom. Survival time was censored when a patient was lost to follow-up within the 30-year period.

RESULTS

Cohort characteristics. This study included 244 patients with SSc and 314 healthy controls. Demographic data and clinical characteristics are shown in Table 1 with patients divided into tertiles based on age-adjusted PBL-TL (T1 is the shortest TL, and T3 is the longest TL). The mean age of SSc and control groups were comparable (52.7 ± 12.5 vs 54.7 ± 12.9 years; $P = 0.06$), whereas there were more women and White participants in the control group compared with the SSc group ($P < 0.05$). Of patients with SSc, 161 were limited cutaneous subtype and 83 were diffuse cutaneous subtype, with a mean disease duration of 10.8 ± 8.38 years. The mean mRSS was 6.02 ± 6.87, and the presence of ILD and PH were 57% and 26%, respectively.

Age-adjusted telomere measurements is shortened in patients with SSc. PBL-TL in both cohorts followed a normal distribution and decreased linearly with age (Figure 1A). Patients with SSc had significantly shorter telomeres than healthy controls ($P < 0.01$; Figure 1B). In multivariate modeling, the presence of SSc remained strongly associated with PBL-TL after controlling for age, sex, and race ($P < 0.005$). Among patients with SSc, linear mixed-effects models revealed a strong association of PBL-TL with age ($P < 0.01$), as expected, and weaker association with disease duration ($P = 0.08$). There was no association of PBL-TL with sex, race, body mass index, smoking status, immunosuppression use, or antibody status.

PBL-TL and skin and peripheral vascular disease. Controlling for covariates, PBL-TL was not associated with skin disease or peripheral vascular disease. Specifically, in univariate analysis, PBL-TL was shorter in patients with limited cutaneous SSc compared with patients with diffuse cutaneous SSc ($P = 0.04$; Supplementary Figure 1A); however, SSc cutaneous subtype was not associated with PBL-TL after controlling for age, disease duration, antibody status, and importantly, presence of

Table 1. Demographic and clinical characteristics of study cohorts

Category	Control (n = 314)	SSc T1 (n = 81)	SSc T2 (n = 82)	SSc T3 (n = 81)	All SSc (n = 244)
Age, mean (SD), years	52.7 (12.5)	54.4 (13.3)	54.5 (12.7)	55.1 (12.9)	54.7 (12.9)
Sex, n (%)					
Men	10 (3.2)	10 (12.3)	11 (13.4)	14 (17.3)	35 (14.3)
Women	304 (96.8)	71 (87.7)	71 (86.6)	67 (82.7)	209 (85.7)
Race, n (%)					
White	246 (78.3)	48 (59.3)	50 (61.0)	47 (58.0)	145 (59.4)
Hispanic	19 (6.1)	5 (6.2)	4 (4.9)	9 (11.1)	18 (7.4)
Black	7 (2.2)	11 (13.6)	5 (6.1)	9 (11.1)	25 (10.2)
Asian	42 (13.4)	10 (12.3)	13 (15.9)	9 (11.1)	32 (13.1)
Other	0 (0)	7 (8.6)	10 (12.2)	7 (8.6)	24 (9.8)
SSc subtype, n (%)					
Limited	–	58 (71.6)	54 (65.9)	49 (60.5)	161 (66.0)
Diffuse	–	23 (28.4)	28 (34.1)	32 (39.5)	83 (34.0)
Antibody status, n (%)					
None	–	35 (43.2)	26 (31.7)	22 (27.2)	83 (34.0)
ACA	–	19 (23.5)	19 (23.2)	23 (28.4)	61 (25.0)
Scl-70	–	17 (21.0)	24 (29.3)	22 (27.2)	63 (25.8)
RNAPolIII	–	10 (12.3)	13 (15.9)	14 (17.3)	37 (15.2)
Disease duration, mean (SD), years	–	9.99 (7.89)	10.8 (8.55)	11.7 (8.67)	10.8 (8.38)
mRSS, mean (SD)	–	5.36 (4.96)	6.20 (8.08)	6.51 (7.23)	6.02 (6.87)
ILD present, n (%)	–	50 (61.7)	50 (61.0)	39 (48.1)	139 (57.0)
pHTN present, n (%)	–	26 (32.1)	21 (25.6)	16 (19.8)	63 (25.8)
Severe RP present, n (%)	–	4 (4.9)	5 (6.1)	6 (7.4)	15 (6.1)

* Telomere length divided by tertile with T1 representing the shortest telomere length and T3 representing the longest telomere length. ACA, anticentromere antibody, ILD, interstitial lung disease; mRSS, modified Rodnan skin score; pHTN, pulmonary hypertension; RNAPolIII, RNA polymerase III antibody; RP, Raynaud phenomenon; SSc, systemic sclerosis; T1, tertile 1; T2, tertile 2; T3, tertile 3.

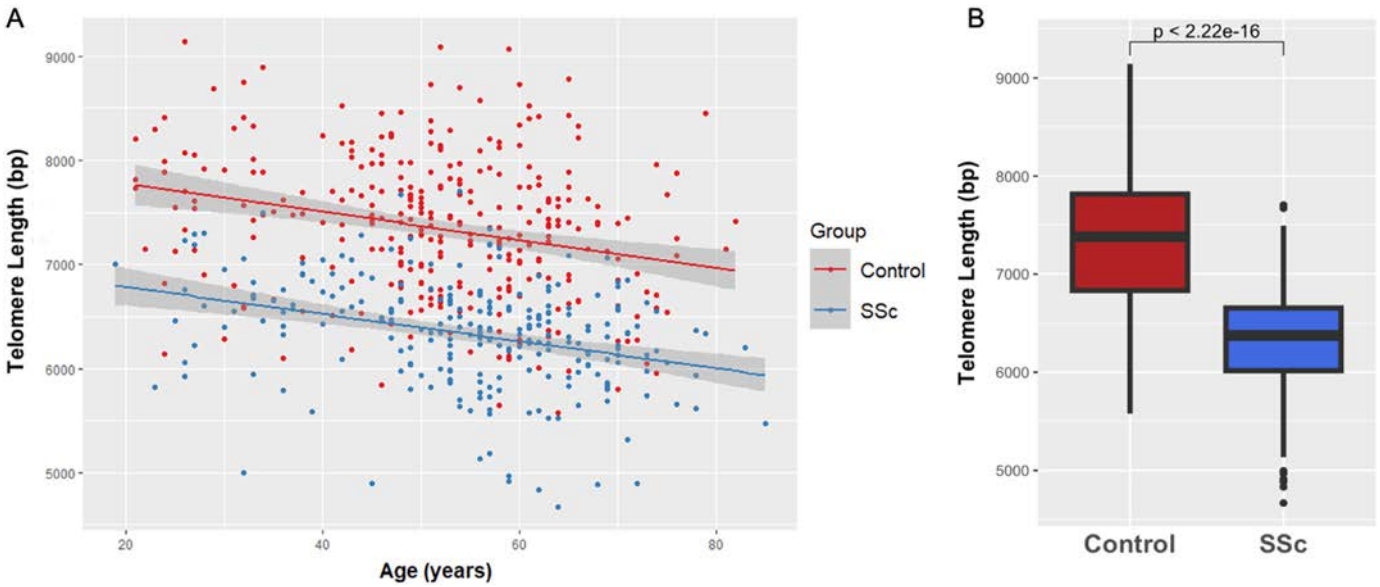

Figure 1. Peripheral blood leukocyte telomere lengths are shortened in patients with SSc compared with controls. (A) Scatterplot of peripheral blood leukocyte telomere length versus age in controls (red) and patients with SSc (blue). Lines represent best fitted lines, and gray shading represents 95% confidence interval. (B) Classical boxplot of peripheral blood leukocyte telomere length by patient cohort demonstrating shorter peripheral blood leukocyte telomere length in patients with SSc. SSc, systemic sclerosis.

pulmonary disease ($P = 0.12$). mRSS was not statistically different between tertiles of PBL-TL ($P = 0.34$; Supplementary Figure 1B). A trend toward shorter PBL-TL was detected in patients without peripheral ulcers ($P = 0.06$), and no significant difference was found among RPSS categories ($P = 0.87$; Supplementary Figure 1C and 1D), overall demonstrating that PBL-TL is not associated with peripheral vascular disease severity. Additionally, no association was found between PBL-TL and secondary clinical outcomes of interest, including the presence of calcinosis, SSc renal crisis, and myocardial involvement ($P > 0.1$).

PBL-TL and pulmonary disease in ILD and PH and associated with pulmonary disease severity and survival. In multivariate modeling, controlling for age, sex, race, smoking, disease duration, and autoantibody status, shortened PBL-TL was significantly associated with the presence of SSc-related pulmonary involvement (odds ratio 3.42 per 1,000-bp shortening; $P = 0.01$; Figure 2A). Within pulmonary disease categories, patients with ILD and PH each had shorter PBL-TL than controls ($P = 0.03$ and $P < 0.01$, respectively), and the shortest PBL-TL was found in subjects with concurrent ILD and PH (Figure 2B). Shortened PBL-TL was also associated with measures of lung disease severity, including lower DL_{CO}% predicted ($P = 0.02$) and usual interstitial pneumonia (UIP) pattern by chest CT compared with nonspecific interstitial pneumonia (NSIP) ($P = 0.007$) but not FVC% predicted ($P = 0.22$; Figure 2C and 2D). Although not significant, there was a trend toward shorter PBL-TL and worsened ILD severity by FVC% ($P = 0.12$; Supplementary Figure 2). PBL-TL shortening was also associated with patients requiring future hospitalization for respiratory or right ventricular failure, thus predicting worse pulmonary outcomes ($P = 0.002$).

PBL-TL was associated with overall survival, with individuals with shorter PBL-TL predicting increased mortality. From baseline PBL-TL measurement, patients with SSc in the first tertile (T1, the shortest TL) had a significantly worse five-year event-free survival compared with patients with longer PBL-TL (T2 and T3; 67% vs 83%; $P = 0.03$; Figure 3A). This association remained when examining 30-year event-free survival from the time of SSc disease onset, with T1 demonstrating a significantly worse survival than T2 and T3 ($P = 0.03$; Figure 3B). The leading underlying cause of death was SSc-associated lung disease (63%), either ILD or PH, followed by cancer (15%) and cardiomyopathy (7%) (Supplementary Table 2).

Telomere shortening in SSc. Serial DNA samples were available for 175 of 244 patients with a mean follow-up time of 1.75 ± 0.7 years between PBL-TL measurements. The average rate of change of PBL-TL in patients with SSc was a loss of 223 ± 595 bp per year, which is greater than the rate of loss reported in healthy individuals of about 30 bp to 60 bp per year.[17–20] There was no association between rate of change with age, sex, race, antibody status, or immunosuppression use. Rate of change of PBL-TL appeared independent of baseline TL length, with each tertile having similar rates of TL shortening ($P = 0.2$; Figure 4A). Patients with early SSc, defined by disease duration of less than five years, had a faster rate of TL shortening compared with patients with SSc with longer disease duration ($P = 0.04$; Figure 4B). In addition, patients with SSc experiencing a terminal event (death or lung transplantation) within five years of

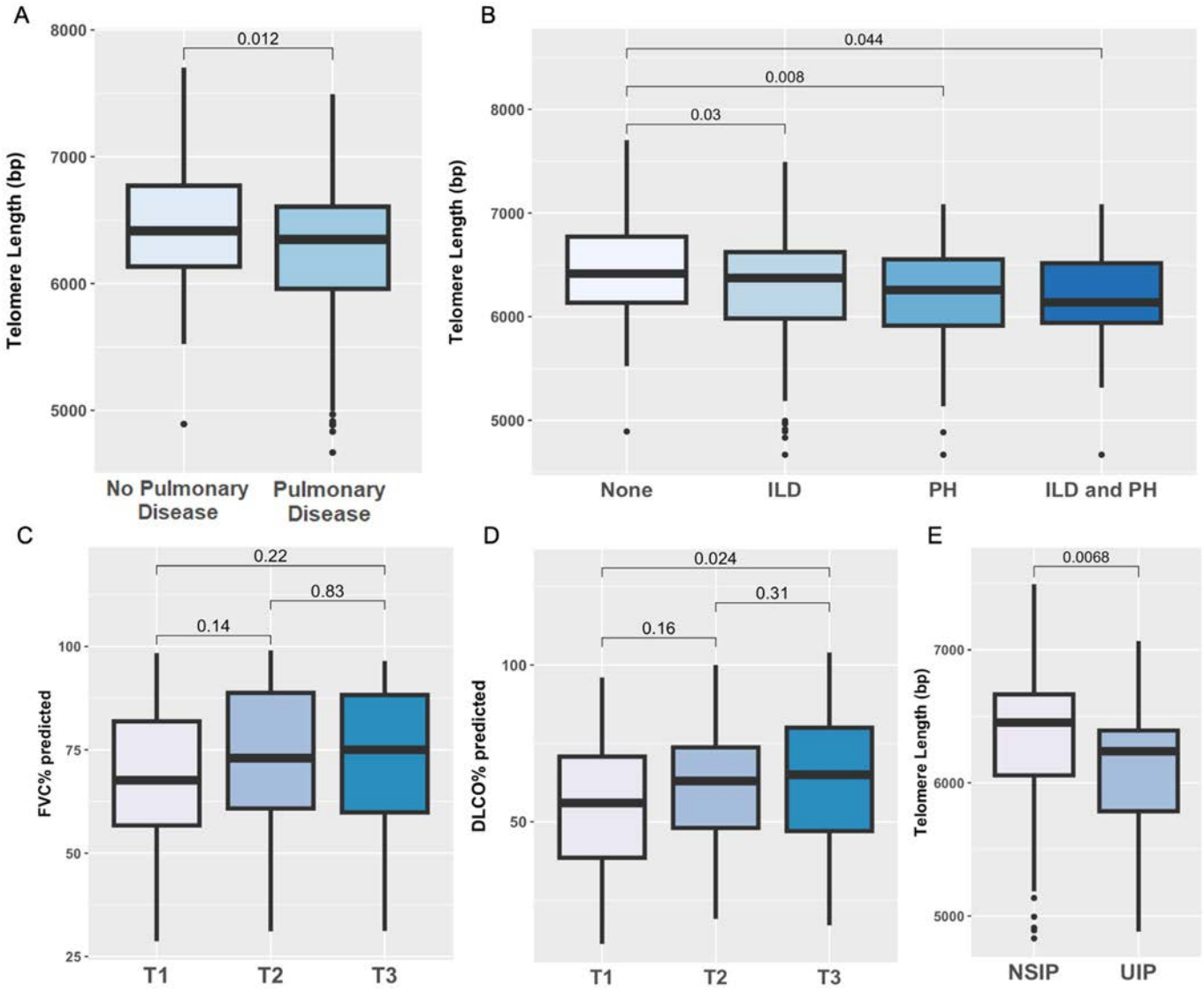

Figure 2. Association of peripheral blood leukocyte telomere length with lung disease presence and severity in patients with systemic sclerosis. (A and B) Comparison of peripheral blood leukocyte telomere length between patients with systemic sclerosis with and without pulmonary disease (n = 155 and n = 89, respectively). Breakdown by disease category demonstrated shortest peripheral blood leukocyte telomere length in patients with ILD and PH (n = 18), compared with patients without pulmonary disease (n = 89), ILD only (n = 116), and PH only (n = 39). (C and D) Comparison of FVC% and DLco% between peripheral blood leukocyte telomere length tertiles. (E) Peripheral blood leukocyte telomere length by radiographic ILD pattern demonstrating shortened peripheral blood leukocyte telomere length associated with UIP pattern compared with NSIP pattern (n = 33 and n = 103, respectively). DLco%, diffusing capacity of carbon monoxide percent predicted; FVC%, peripheral blood leukocyte telomere length; ILD, interstitial lung disease; NSIP, nonspecific interstitial pneumonia; PH, pulmonary hypertension; T1, tertile 1; T2, tertile 2; T3, tertile 3; UIP, usual interstitial pneumonia. Color figure can be viewed in the online issue, which is available at http://onlinelibrary.wiley.com/doi/10.1002/art.43400/abstract.

baseline had a greater rate of PBL-TL shortening than their counterparts (P = 0.05; Figure 4C). Rate of TL shortening was not associated with cutaneous or pulmonary manifestations.

Telomere measurements is shortened in lung but not skin epithelial cells. To explore whether telomere attrition could be detected in SSc target organs, we applied Telo-FISH to measure TL in individual epithelial cells from SSc lung and skin. We found that TL was shorter in AT2 cells of lung tissues obtained from patients with SSc-ILD compared to healthy controls (P = 0.035; Figure 5A). In contrast, no difference was detected between TL measured in SSc skin (KRT5+ epidermal cells) compared with controls (P = 0.78; Figure 5B).

DISCUSSION

This study investigates the association of PBL-TL with SSc disease manifestations severity and outcomes. Shorter PBL-TL

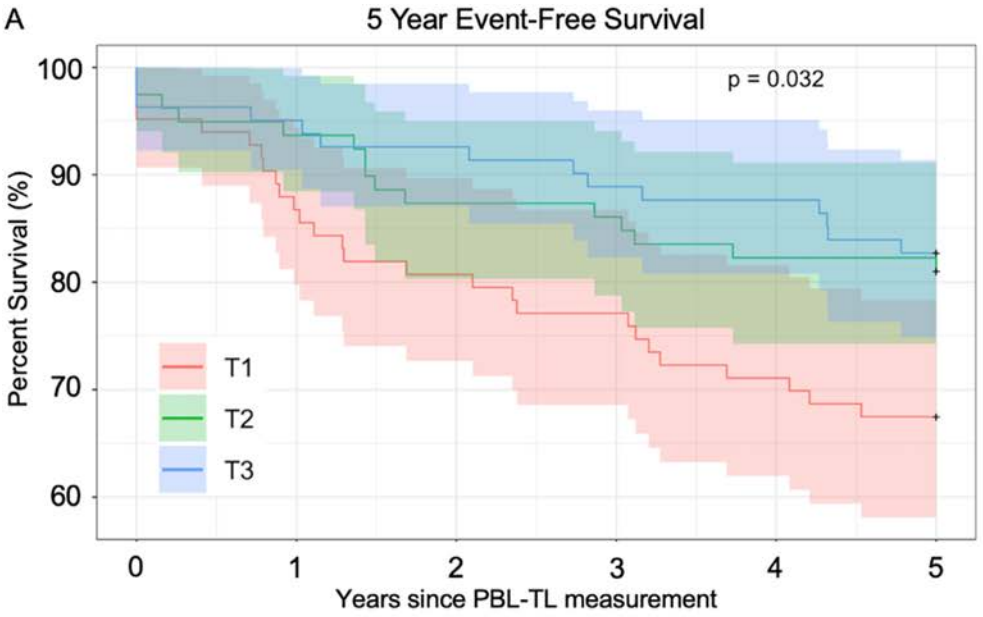

# of Events / # at Risk

T1	11/81	5/70	3/65	5/62	3/57
T2	5/82	5/77	2/72	2/70	1/68
T3	4/81	2/77	3/75	1/72	4/71

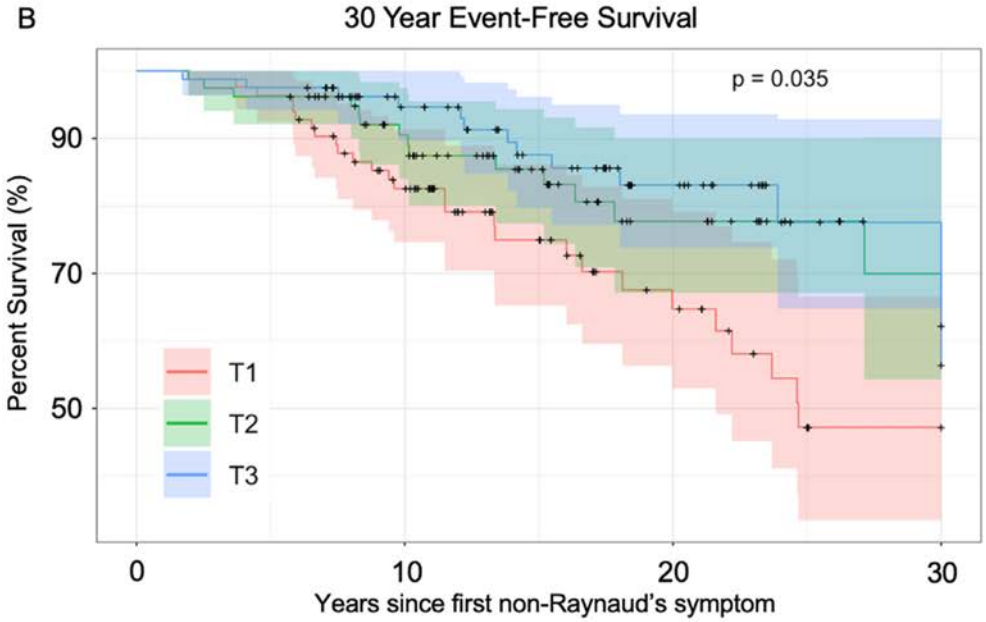

# of Events / # at Risk

T1	14/76	8/32	5/16
T2	7/68	6/32	2/12
T3	4/64	6/34	4/12

Figure 3. PBL-TL is associated with survival outcomes in patients with systemic sclerosis. Kaplan-Meier survival plot depicting survival by PBL-TL tertiles for (A) 5-year event-free survival since time of TL measurement and (B) 30-year event-free survival since onset of first non-Raynaud symptom. PBL-TL, peripheral blood leukocyte telomere length; T1, tertile 1; T2, tertile 2; T3, tertile 3. Color figure can be viewed in the online issue, which is available at http://onlinelibrary.wiley.com/doi/10.1002/art.43400/abstract.

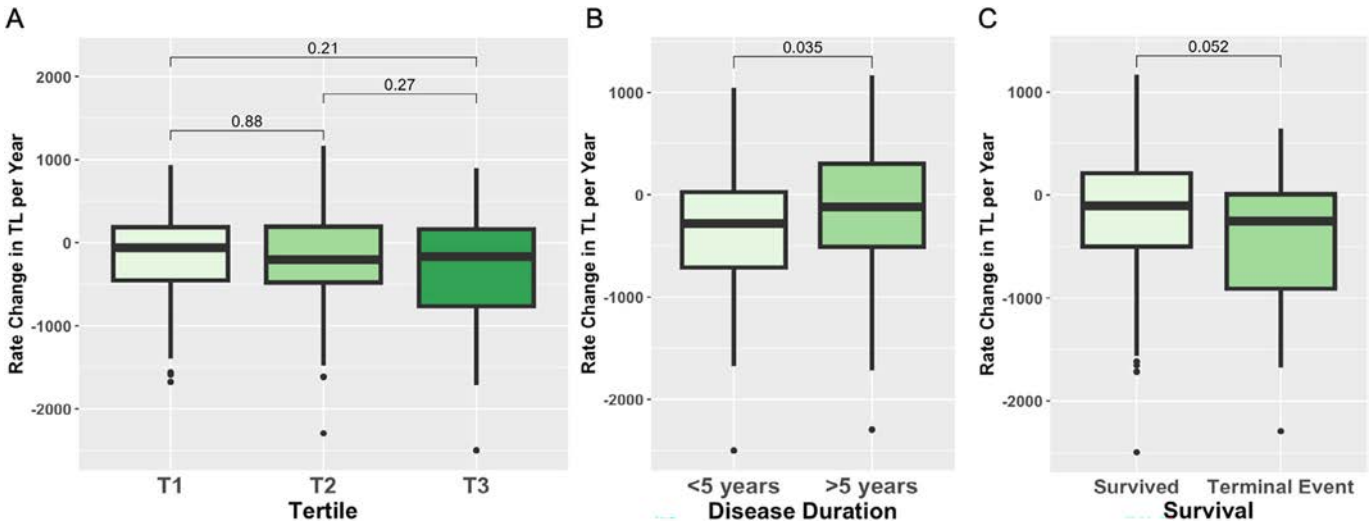

Figure 4. Rate of peripheral blood leukocyte TL shortening is associated with disease duration and survival outcomes. (A) Comparison of TL rate of change per year between peripheral blood leukocyte TL tertiles demonstrating no difference in rate of change by baseline peripheral blood leukocyte TL. (B) Peripheral blood leukocyte TL rate of change by early (<5 years, n = 79) and late (>5 years, n = 165) disease duration. (C) Comparison of peripheral blood leukocyte TL rate of change by five-year event-free survival between those who survived (n = 188) and those with terminal events (n = 56). T1, tertile 1; T2, tertile 2; T3, tertile 3; TL, telomere length. Color figure can be viewed in the online issue, which is available at http://onlinelibrary.wiley.com/doi/10.1002/art.43400/abstract.

was associated with the presence of SSc, pulmonary involvement and severity, and overall worse event-free survival. Patients with SSc with overlapping ILD and PH had the shortest PBL-TL. PBL-TL was not associated with peripheral vascular disease severity or skin involvement, which was concordant with findings that TL was not shortened in skin epithelial cells. A faster rate of TL loss was associated with earlier disease and worse event-free survival. These findings further support the relevant association of aberrant aging with the SSc disease process and, in particular, with SSc lung disease.

Telomere dysfunction has been implicated in several age-related diseases and is associated with all-cause mortality.[3,4] Critically short telomeres lead to DNA instability, activation of the DNA damage response, and accumulation of pathologic senescent cells in affected tissues, contributing to organ dysfunction.[21,22] Fibrotic diseases have been linked to abnormally shortened telomeres, including idiopathic pulmonary fibrosis (IPF), liver cirrhosis, kidney fibrosis, and myelodysplastic syndrome.[6,7,23–26] Both mouse models and human studies have established a causal link between telomere dysfunction and fibrogenesis, implicating its role in disease pathogenesis.[27–30] Increasingly, telomere dysfunction and cell senescence have been studied in rheumatologic diseases. In a large cohort study examining PBL-TL across clinical diagnoses, PBL-TL shortening had the strongest association with increased mortality from rheumatoid arthritis in which senescent T cells are shown to contribute to increased cytokine production, sustaining a proinflammatory microenvironment.[3,31] Given SSc represents a disease of both autoimmunity and progressive fibrosis, there is high relevance in elucidating the role that pathologic aging mechanisms may play in its pathogenesis. This study demonstrates that TL measured in peripheral blood cells of patients with SSc is associated with early disease, increased disease severity, and worse outcomes. This provides further support to the possibility that aging and aberrant telomere function may contribute to the abnormal biologic processes leading to disease onset and may drive a more progressive disease phenotype as well as specific subsets of organ involvement.

Previous studies have shown shortened PBL-TL across several forms of ILD.[5,6,32] This study confirms our previous report about the association between PBL-TL and SSc-ILD[8] and adds to the existing literature by showing that PBL-TL predicts a more severe and progressive lung involvement, including presence of UIP pattern of fibrosis and presence of PH. We found shortened PBL-TL was associated with worse pulmonary outcomes including increased hospitalizations and worse event-free survival, confirming its potential value as a biomarker predicting more severe SSc prognosis. These findings are consistent with the growing evidence that cellular senescence may play a role in not only ILD but also PH. In fact, cultured pulmonary artery smooth muscle cells (PA-SMCs) from patients with PH have demonstrated increased markers of senescence and shorter TL compared with PA-SMCs from controls.[33] These senescent PA-SMCs were shown to stimulate growth and migration of normal PA-SMCs through pathologic signaling, contributing to vascular remodeling. Whether short PA-SMC TL contributes to PH in vivo requires further investigation.

The hypothesis that aberrant aging and telomere dysfunction may play a direct role in the onset and propagation of SSc lung disease compared with other organs is supported by our tissue analysis, showing that TL was shortened in lung AT2 cells. Our

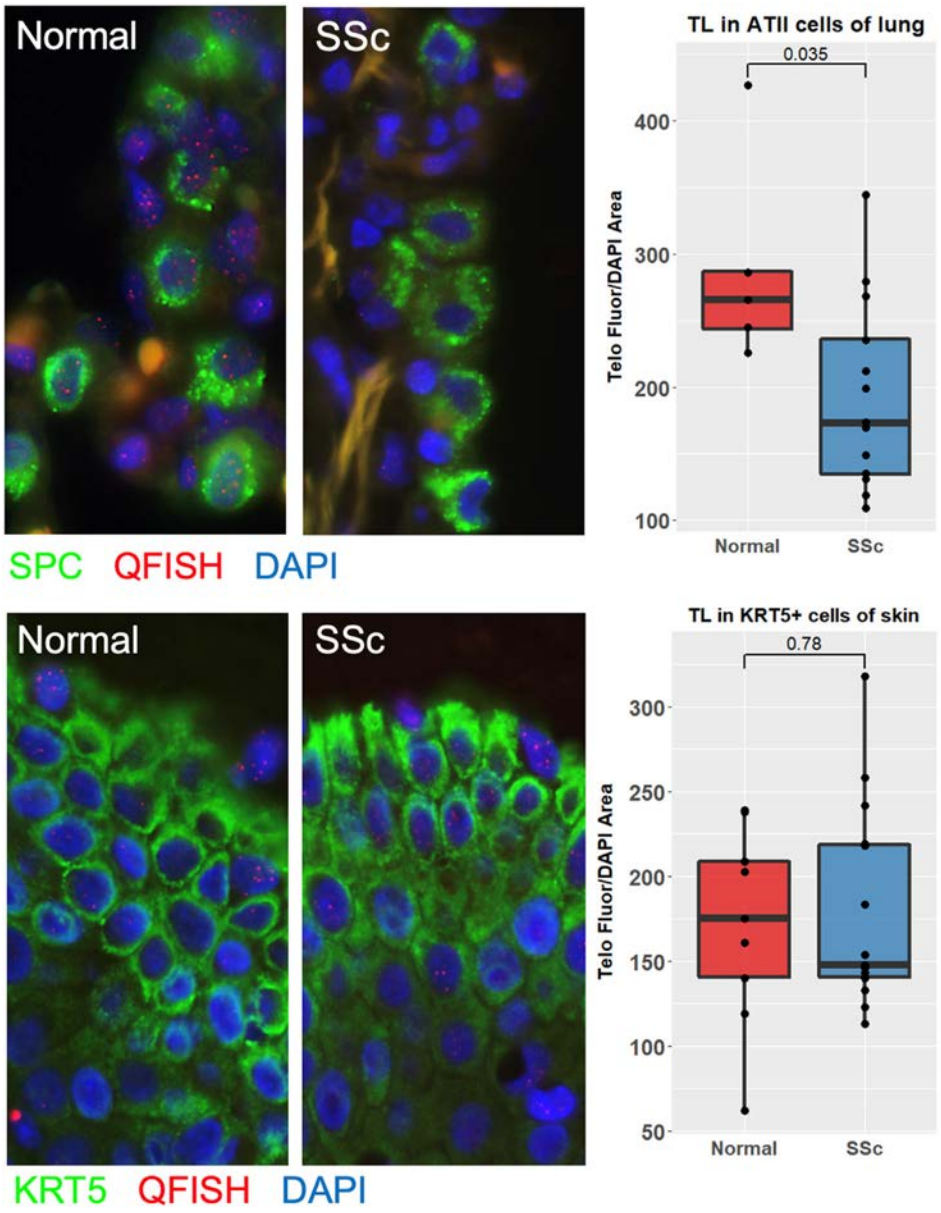

Figure 5. Telomere length is shortened in lung but not skin epithelial cells in patients with SSc. (Top panels) Telomere quantitative fluorescence in situ hybridization assay of (top panels) lung tissue demonstrate shortened TL in ATII cells (SPC+) in SSc-related interstitial lung disease (n = 15) compared with controls (n = 5). (Bottom panels) Affected skin tissue did not demonstrate difference of TL in KRT5+ skin epithelial cells between diffuse SSc (n = 12) compared with controls (n = 8). ATII, Type II alveolar; SPC, surfactant protein C; SSc, systemic sclerosis; TL, telomere length. Color figure can be viewed in the online issue, which is available at http://onlinelibrary.wiley.com/doi/10.1002/art.43400/abstract.

previous work has shown that molecular signatures indicative of aging and cell senescence are increased in lung tissue of SSc-ILD, including pathways related to epithelial–mesenchymal transition, P53, and DNA damage.[34] In contrast, SSc skin epidermal cells did not exhibit telomere shortening, and PBL-TL was not associated with skin disease severity, in keeping with other reports.[35] Together, these findings suggest PBL-TL may be an organ-specific biomarker of SSc lung disease, possibly because telomere dysfunction is a key driver of ILD and pulmonary arterial hypertension or PBL-TL disproportionately reflects telomere attrition of certain cell populations such as AT2 cells or pulmonary vascular endothelial cells. Given senescence signatures have been detected in the skin but telomere shortening has not, it is possible that SSc skin senescence may be driven by nontelomere-related mechanisms and, rather, other potentiators of senescence. Additionally, it is possible that there are niche cell types in the skin, yet to be examined by TL studies, that may be affected by telomere dysfunction. These include pathologic endothelial cells or profibrotic fibroblasts, which have been shown to exhibit the highest enrichment of senescence-related signatures compared with other cell types in affected skin of patients with SSc.[36]

Although PBL-TL is shown to be significantly shortened in SSc, the cause of telomere shortening remains unknown. In other fibrotic diseases such as IPF, genetic mutations in telomere-associated genes have been found to be a cause of telomere dysfunction; however, these mutations have yet to be identified in SSc.[37] A recent study reports that a polymorphic variant of *FAM13A*, an IPF susceptibility gene that regulates the expression of the cellular senescence marker P21 and mitochondrial reactive oxygen species (ROS) production in the airway epithelium, is associated with development of UIP in SSc-ILD.[38,39] Additionally, other disease-associated factors may be driving telomere attrition. We show that PBL-TL shortens more rapidly in patients with SSc compared with what is reported in the general healthy population irrespective of their baseline PBL-TL, especially in subjects with shorter disease duration. This raises the hypothesis that a more vibrant immune activation, usually associated with earlier stages of SSc, may accelerate telomere shortening through replication and increased immune cell turnover. In addition, sustained ROS production and oxidative stress associated with the ongoing inflammatory response and tissue damage could also contribute to telomere attrition in a replication-independent manner.[40,41] Another mechanism to consider that may be driving aberrant telomere shortening in a subset of patients is interference with telomere repair mechanisms by autoantibodies targeting telomerase-associated proteins because these have been detected in our patient cohort.[42]

This study provides robust data supporting the potential use of PBL-TL to stratify patients with SSc at risk for more severe or progressive disease, particularly for lung complications including ILD and PH. The association between age and disease severity has been previously reported because patients who develop SSc later in life have worse prognosis and a more rapid disease course.[43] The data here provided support that measuring PBL-TL could help identify patients who are disproportionately affected by aging mechanisms and at higher risk for more severe disease.[44] Additionally, identifying patients with shortened PBL-TL may have treatment implications. Previous studies have shown that in ILD, shortened PBL-TL is associated with worse outcomes when treated with immunosuppression, including in patients with SSc-ILD.[45,46] This raises the possibility that in later stages of the disease, a subset of patients with SSc may transition from a predominantly inflammatory phenotype, in which rapid telomere attrition occurs, to a more fibrotic phase, in which progressive fibrosis may be further driven by ongoing telomere dysfunction. This "late" disease process becomes less dependent on inflammation and, in the lungs, may develop a pathobiology more similar to IPF. Although further investigation to validate this hypothesis is needed, identification of these patients "at risk" of a progressive fibrotic phenotype using PBL-TL measurements would significantly advance a precision medicine approach in the field of SSc. Overall, given that tools to measure PBL-TL are readily available, PBL-TL represents a potential clinically actionable biomarker that may help further characterize a patient's phenotype and inform about disease trajectory, severity, and prognosis.

A strength of this study has been the ability to measure a biologically relevant biomarker in a large, well-characterized longitudinal cohort of patients with SSc compared with age-matched healthy controls. Additionally, the longitudinal assessment of PBL-TL over time enabled investigation of the rate of PBL-TL attrition in relationship to SSc clinical phenotype. We measured TL in SSc skin and lung tissues to define how telomere dysfunction may impact target organs in SSc. However, our tissue studies were limited to AT2 and KRT5+ epithelial cells. We acknowledge that aberrant telomere function should be investigated in other cell types relevant to the disease pathogenesis. This study was not powered to evaluate the effects of specific medications on changes of PBL-TL nor to assess the impact of shorter PBL-TL on treatment response. We additionally were not able to associate PBL-TL with other serum markers of disease such as sedimentation rate and C-reactive protein.

In conclusion, PBL-TL is shortened in patients with SSc and associated with more severe pulmonary involvement, particularly concurrent ILD and PH. The degree of telomere shortening is also associated with worse clinical outcomes including increased hospitalization due to respiratory failure and worse event-free survival. Collectively, the findings highlight the relevance of telomere dysfunction and aging in SSc and the possible use of PBL-TL as a prognostic marker for disease severity and outcome.

AUTHOR CONTRIBUTIONS

All authors contributed to at least one of the following manuscript preparation roles: conceptualization AND/OR methodology, software, investigation, formal analysis, data curation, visualization, and validation AND drafting or reviewing/editing the final draft. As corresponding author, Drs Yang and Boin confirm that all authors have provided the final approval of the version to be published, and take responsibility for the affirmations regarding article submission (eg, not under consideration by another journal), the integrity of the data presented, and the statements regarding compliance with institutional review board/Declaration of Helsinki requirements.

REFERENCES

1. Volkmann ER, Andréasson K, Smith V. Systemic sclerosis. Lancet 2023;401(10373):304–318.
2. Jones-Weinert C, Mainz L, Karlseder J. Telomere function and regulation from mouse models to human ageing and disease. Nat Rev Mol Cell Biol 2024;26(4):297–313.
3. Schneider CV, Schneider KM, Teumer A, et al. Association of telomere length with risk of disease and mortality. JAMA Intern Med 2022; 182(3):291–300.
4. Cawthon RM, Smith KR, O'Brien E, et al. Association between telomere length in blood and mortality in people aged 60 years or older. Lancet 2003;361(9355):393–395.
5. Adegunsoye A, Newton CA, Oldham JM, et al. Telomere length associates with chronological age and mortality across racially diverse pulmonary fibrosis cohorts. Nat Commun 2023;14(1):1489.

6. Alder JK, Chen JJL, Lancaster L, et al. Short telomeres are a risk factor for idiopathic pulmonary fibrosis. Proc Natl Acad Sci USA 2008; 105(35):13051–13056.
7. Cronkhite JT, Xing C, Raghu G, et al. Telomere shortening in familial and sporadic pulmonary fibrosis. Am J Respir Crit Care Med 2008; 178(7):729–737.
8. Liu S, Chung MP, Ley B, et al. Peripheral blood leucocyte telomere length is associated with progression of interstitial lung disease in systemic sclerosis. Thorax 2021;76(12):1186–1192.
9. van den Hoogen F, Khanna D, Fransen J, et al. 2013 classification criteria for systemic sclerosis: an American college of rheumatology/-European league against rheumatism collaborative initiative. Ann Rheum Dis. 2013;72(11):1747–1755. doi:10.1136/annrheumdis-2013-204424
10. Medsger TA Jr, Bombardieri S, Czirjak L, et al. Assessment of disease severity and prognosis. Clin Exp Rheumatol 2003;21(3 Suppl 29): S42–S46.
11. Humbert M, Kovacs G, Hoeper MM, et al; ESC/ERS Scientific Document Group. 2022 ESC/ERS guidelines for the diagnosis and treatment of pulmonary hypertension. Eur Respir J 2023;61(1):2200879.
12. Cawthon RM. Telomere measurement by quantitative PCR. Nucleic Acids Res 2002;30(10):e47.
13. Faust HE, Golden JA, Rajalingam R, et al. Short lung transplant donor telomere length is associated with decreased CLAD-free survival. Thorax 2017;72(11):1052–1054.
14. Liu S, Wang C, Green G, et al. Peripheral blood leukocyte telomere length is associated with survival of sepsis patients. Eur Respir J 2020;55(1):1901044.
15. Listerman I, Sun J, Gazzaniga FS, et al. The major reverse transcriptase-incompetent splice variant of the human telomerase protein inhibits telomerase activity but protects from apoptosis. Cancer Res 2013;73(9):2817–2828.
16. Ricciardi M, Krampera M, Chilosi M. Quantitative fluorescence in situ hybridization on paraffin embedded tissue. Methods Mol Biol 2013; 976:167–173.
17. Aviv A, Chen W, Gardner JP, et al. Leukocyte telomere dynamics: longitudinal findings among young adults in the Bogalusa Heart Study. Am J Epidemiol 2009;169(3):323–329.
18. Canela A, Vera E, Klatt P, et al. High-throughput telomere length quantification by FISH and its application to human population studies. Proc Natl Acad Sci USA 2007;104(13):5300–5305.
19. Takubo K, Izumiyama-Shimomura N, Honma N, et al. Telomere lengths are characteristic in each human individual. Exp Gerontol 2002;37(4):523–531.
20. Valdes AM, Andrew T, Gardner JP, et al. Obesity, cigarette smoking, and telomere length in women. Lancet 2005;366(9486):662–664.
21. Hemann MT, Strong MA, Hao LY, et al. The shortest telomere, not average telomere length, is critical for cell viability and chromosome stability. Cell 2001;107(1):67–77.
22. He S, Sharpless NE. Senescence in health and disease. Cell 2017; 169(6):1000–1011.
23. Sashida G, Ohyashiki JH, Nakajima A, et al. Telomere dynamics in myelodysplastic syndrome determined by telomere measurement of marrow metaphases. Clin Cancer Res 2003;9(4):1489–1496.
24. Famulski KS, Halloran PF. Molecular events in kidney ageing. Curr Opin Nephrol Hypertens 2005;14(3):243–248.
25. Kitada T, Seki S, Kawakita N, et al. Telomere shortening in chronic liver diseases. Biochem Biophys Res Commun 1995;211(1):33–39.
26. Fazzini F, Lamina C, Raschenberger J, et al; GCKD Investigators. Results from the German Chronic Kidney Disease (GCKD) study support association of relative telomere length with mortality in a large cohort of patients with moderate chronic kidney disease. Kidney Int 2020;98(2):488–497.
27. Alder JK, Barkauskas CE, Limjunyawong N, et al. Telomere dysfunction causes alveolar stem cell failure. Proc Natl Acad Sci USA 2015; 112(16):5099–5104.
28. Naikawadi RP, Disayabutr S, Mallavia B, et al. Telomere dysfunction in alveolar epithelial cells causes lung remodeling and fibrosis. JCI Insight 2016;1(14):e86704.
29. Beier F, Foronda M, Martinez P, et al. Conditional TRF1 knockout in the hematopoietic compartment leads to bone marrow failure and recapitulates clinical features of dyskeratosis congenita. Blood 2012; 120(15):2990–3000.
30. Rudolph KL, Chang S, Millard M, et al. Inhibition of experimental liver cirrhosis in mice by telomerase gene delivery. Science 2000; 287(5456):1253–1258.
31. Weyand CM, Goronzy JJ. Aging of the immune system. Mechanisms and therapeutic targets. Ann Am Thorac Soc 2016;13 Suppl 5(Suppl 5):S422–S428.
32. Ley B, Liu S, Elicker BM, et al. Telomere length in patients with unclassifiable interstitial lung disease: a cohort study. Eur Respir J 2020; 56(2):2000268.
33. Noureddine H, Gary-Bobo G, Alifano M, et al. Pulmonary artery smooth muscle cell senescence is a pathogenic mechanism for pulmonary hypertension in chronic lung disease. Circ Res 2011;109(5): 543–553.
34. Yang MM, Lee S, Neely J, et al. Gene expression meta-analysis reveals aging and cellular senescence signatures in scleroderma-associated interstitial lung disease. Front Immunol 2024;15:1326922.
35. Usategui A, Municio C, Arias-Salgado EG, et al. Evidence of telomere attrition and a potential role for DNA damage in systemic sclerosis. Immun Ageing 2022;19(1):7.
36. Shi B, Tsou PS, Ma F, et al. Senescent cells accumulate in systemic sclerosis skin. J Invest Dermatol 2023;143(4):661–664.e5.
37. Kropski JA, Blackwell TS, Loyd JE. The genetic basis of idiopathic pulmonary fibrosis. Eur Respir J 2015;45(6):1717–1727.
38. Bernstein EJ, Boin F, Elicker B, et al. FAM13A polymorphism is associated with a usual interstitial pneumonia pattern in patients with systemic sclerosis-associated interstitial lung disease. Rheumatology (Oxford) Published online October 17, 2024;keae573. doi: 10.1093/rheumatology/keae573
39. Chen Q, Vasse GF, Nwozor KO, et al. FAM13A regulates cellular senescence marker p21 and mitochondrial reactive oxygen species production in airway epithelial cells. Am J Physiol Lung Cell Mol Physiol 2023;325(4):L460–L466.
40. Jurk D, Wilson C, Passos JF, et al. Chronic inflammation induces telomere dysfunction and accelerates ageing in mice. Nat Commun 2014; 2(1):4172.
41. Jose SS, Bendickova K, Kepak T, et al. Chronic inflammation in immune aging: role of pattern recognition receptor crosstalk with the telomere complex? Front Immunol 2017;8:1078.
42. Adler BL, Boin F, Wolters PJ, et al. Autoantibodies targeting telomere-associated proteins in systemic sclerosis. Ann Rheum Dis 2021;80(7): 912–919.
43. Manno RL, Wigley FM, Gelber AC, et al. Late-age onset systemic sclerosis. J Rheumatol 2011;38(7):1317–1325.
44. Moinzadeh P, Kuhr K, Siegert E, et al; Registry of the German Network for Systemic Scleroderma. Older age onset of systemic sclerosis - accelerated disease progression in all disease subsets. Rheumatology (Oxford) 2020;59(11):3380–3389.
45. Newton CA, Oldham JM, Ley B, et al. Telomere length and genetic variant associations with interstitial lung disease progression and survival. Eur Respir J 2019;53(4):1801641.
46. Zhang D, Adegunsoye A, Oldham JM, et al. Telomere length and immunosuppression in non-idiopathic pulmonary fibrosis interstitial lung disease. Eur Respir J 2023;62(5):2300441.

American College of Rheumatology
Empowering Rheumatology Professionals

Arthritis & Rheumatology
Vol. 78, No. 2, February 2026, pp 438–448
DOI 10.1002/art.43382

Comparative Real-World Effectiveness of Immunomodulatory Therapies for Prevention of Uveitis Relapse in Behçet Disease

Zhenyu Zhong,[1] Jiayi Wang,[1] Lan Xia,[1] Shixiang Jing,[2] Yujie Lai,[1] Tao Cai,[1] and Peizeng Yang[1,2]

Objective. To evaluate comparative effectiveness of cyclosporine, interferon alfa-2a, and adalimumab for the prevention of uveitis relapse in Behçet disease in real-world settings.

Methods. We emulated a target trial involving adult patients with Behçet disease uveitis who initiated cyclosporine, interferon alfa-2a, or adalimumab between April 10, 2008, and August 1, 2024, and were observed up until September 10, 2024. We applied overlap weighting to balance patient characteristics across treatment groups and emulate randomization at baseline. The primary outcome was the annualized relapse rate of uveitis during treatment with study therapy.

Results. The cohort comprised 716 cyclosporine users, 193 interferon alfa-2a users, and 103 adalimumab users. The estimated mean annualized relapse rate of uveitis was 0.95 (95% confidence interval [CI] 0.82–1.10) with cyclosporine, 0.52 (95% CI 0.40–0.69) with interferon alfa-2a, and 0.28 (95% CI 0.19–0.43) with adalimumab. Patients treated with cyclosporine experienced more relapses than those treated with adalimumab (incidence rate ratio [IRR] 3.36 [95% CI 2.23–5.05]; mean difference 0.66 [95% CI 0.48–0.85]; $P < 0.001$) or interferon alfa-2a (IRR 1.81 [95% CI 1.37–2.4]; mean difference 0.42 [95% CI 0.22–0.62]; $P < 0.001$). The relapse rate was higher with interferon alfa-2a than with adalimumab (IRR 1.86 [95% CI 1.16–2.97]; mean difference 0.24 [95% CI 0.05–0.43]; $P = 0.011$).

Conclusion. In Behçet disease, interferon alfa-2a was associated with a reduction in uveitis relapse compared with cyclosporine, whereas adalimumab demonstrated a stronger association with reduced relapse than interferon alfa-2a.

INTRODUCTION

Behçet disease is a multisystem vasculitis that affects both arteries and veins and vessels of any size.[1] This disease has an estimated global prevalence of 10.3 per 100,000 persons, with notable geographic variability.[2] It is often neglected and rare in the US and Northern Europe but is more common in East Asia and the Middle East.[3] This form of vasculitis primarily manifests in the eyes as recurrent relapsing and remitting uveitis in association with retinal vasculitis.[4] Eye involvement often indicates a poor prognosis of the disease and is one of the most common manifestations leading to vision loss and disability.[5,6] This condition has been identified to involve autoimmune and autoinflammatory mechanisms,[7,8] and management aims to prevent relapses and minimize intraocular inflammation.[9,10]

Extensive data have shown that nonglucocorticoid systemic immunomodulatory therapy reduces the risk of relapse and improves disease outcomes.[11,12] EULAR recommendations have emphasized the need for immunomodulatory therapy for any patients with Behçet disease and inflammatory eye disease affecting the posterior segment.[13] However, guidelines vary in the strength of their recommendations for specific immunomodulators,[13,14] which reflects the fact that there are insufficient data on the comparative effectiveness of the currently

Supported by the National Natural Science Foundation Key Program (grant 82230032), National Natural Science Foundation of China (grant 82471059), Chongqing Medical Scientific Research Project: Joint Project of Chongqing Health Commission and Science and Technology Bureau (grant 2025QNKX002), China Postdoctoral Science Foundation (grants BX20230450 and 2024M763900), Chongqing Science and Technology Bureau Mountaineering Project (grants cyyy-xkdfjh-jcyj-202301, cyyy-xkdfjh-lcyj-202303, and cyyy-xkdfjh-cgzh-202302), and Qiande Scientific Talents (grant 2025QDYQ-05).

[1]Ophthalmology Medical Center, Chongqing Key Laboratory for the Prevention and Treatment of Major Blinding Eye Diseases, The First Affiliated Hospital of Chongqing Medical University, Chongqing, China; [2]The First Affiliated Hospital of Zhengzhou University, Henan Province Eye Hospital, Henan International Joint Research Laboratory for Ocular Immunology and Retinal Injury Repair, Zhengzhou, China.

Drs Zhong and Wang contributed equally to this work.

Additional supplementary information cited in this article can be found online in the Supporting Information section (https://acrjournals.onlinelibrary.wiley.com/doi/10.1002/art.43382).

Author disclosures and graphical abstract are available at https://onlinelibrary.wiley.com/doi/10.1002/art.43382.

Address correspondence via email to Peizeng Yang, MD, at peizengycmu@126.com.

Submitted for publication March 26, 2025; accepted in revised form August 27, 2025.

recommended drugs. A recent three-arm randomized trial involving cyclosporine, interferon alfa-2a, and adalimumab suggested adalimumab as a clinical priority for preventing uveitis relapse in severe cases.[15] Nevertheless, this trial involved patients at a high risk for uveitis flares, which limits its relevance to those with milder conditions. Furthermore, results from this trial were inconsistent with earlier data that have shown the superiority of interferon alfa-2a over cyclosporine.[16] Even before this trial, few studies had compared interferon alfa-2a with adalimumab in treating Behçet disease uveitis. Thus, the question remains open as to how interferon alfa-2a ranks in effectiveness among the three drugs. Because the cost of adalimumab is substantially higher than that of interferon alfa-2a or cyclosporine, widely prescribing adalimumab could lead to overtreatment and increase the financial burden on patients as well as health insurance systems. In addition, when considering potential anti-drug antibody development or loss of response to adalimumab,[17] determining whether the other medications can serve as substitutes with acceptable effectiveness remains clinically relevant.

Classic randomized controlled trials usually include highly selected population, which may limit the generalizability of their findings to real-world settings. In contrast, observational studies often include broader, more heterogeneous populations but are more vulnerable to confounding and immortal time bias.[18] Nevertheless, these flaws could be prevented by designing observational analyses to explicitly emulate a rigorous target trial.[18] Within such a framework, we used real-world data to compare the effectiveness of cyclosporine, interferon alfa-2a, and adalimumab in preventing uveitis relapse in Behçet disease.

METHODS

Study design and participants. We designed this observational analysis to emulate a hypothetical pragmatic randomized trial (the target trial) of the comparative effectiveness of cyclosporine, interferon alfa-2a, and adalimumab in patients with Behçet disease uveitis. The key components of the target trial specification and emulation, including eligibility criteria, treatment assignment and strategy, start of follow-up, and outcome measures, are summarized in Supplementary Table 1. This study received approval from the ethics committee of the First Affiliated Hospital of Chongqing Medical University, which also granted a waiver of informed consent.

The inclusion criteria for the target trial required participants to be 18 years or older, have a diagnosis of Behçet disease that was present with compatible uveitis in at least one eye according to the Standardization of Uveitis Nomenclature (SUN) criteria,[19] and have visual acuity of light perception or better in an affected eye. To ensure safety and minimize bias, the target trial would exclude individuals with severe media opacity, other complicated systemic autoimmune diseases, known contraindications to study therapies, or those who had received nonglucocorticoid immunomodulatory therapy within the past two months, long-acting ocular glucocorticoid implants within the past three years, or periocular or intravitreal glucocorticoid injections within the past four weeks. Patients enrolled in the target trial would be randomly assigned to one of the three immunomodulatory therapies and have their ocular conditions and prescriptions recorded during the follow-up.

Data sources and definition. We leveraged the electronic medical records from the Uveitis Center of the First Affiliated Hospital of Chongqing Medical University, Chongqing, China, to emulate the target trial. By 2018, this academic, university-affiliated hospital had established a large medical center specializing in uveitis care, which had received 15,373 uveitis cases from across China that reflected the diverse Chinese patient population.[20] The medical database integrates multiple domains of routine health records, including outpatient encounter data, inpatient care records, and the results of laboratory tests and auxiliary examinations. Routine clinical assessments for each patient visit include slit-lamp microscopy, ophthalmoscopy, and measurements of best-corrected visual acuity (BCVA) and intraocular pressure. Auxiliary examinations, such as fundus photography, optical coherence tomography (OCT), and fundus fluorescein angiography (FFA), are conducted according to clinical needs.

Patients' anterior chamber cell and vitreous haze grades were evaluated using the criteria established by the SUN Working Group, with grades ranging from 0 to 4+, with higher values indicating a worse condition.[21,22] Inflammatory retinal lesions were identified by at least one of the examinations, including ophthalmoscopy, fundus photography, FFA, and OCT. BCVA was assessed using a logarithm of the minimum angle of resolution tumbling E chart. The criteria for macular edema were set at a thickness of 315 μm or greater on Spectralis OCT (Heidelberg Engineering) and 250 μm or greater on Stratus OCT (Carl Zeiss Meditec). Active retinal vascular lesions, also known as the typical retinal vasculitis in Behçet disease, were indicated by clinically visible vascular sheathing with retinal hemorrhages or exudates or by findings of retinal vascular staining, leakage, capillary nonperfusion, or hyperfluorescence of neovascularization on FFA.[23]

Anonymized unique patient identifiers were used to collect information from the medical database. In this study, participants were consecutive individuals who had a record of use of cyclosporine, interferon alfa-2a, or adalimumab between April 10, 2008, and August 1, 2024. The baseline (time zero) was defined as the date of the first filled prescription of study therapy. The final visit was defined as the one that occurred without any further visits in the subsequent six months. Follow-up data were collected until September 10, 2024.

Treatment strategy. The interventions of interest were the initiation and maintained use of cyclosporine, adalimumab, or interferon alpha-2a. Oral cyclosporine could be prescribed at

dose of 2 to 5 mg/kg per day according to the EULAR recommendations.[10] Adalimumab would be administered subcutaneously at 40 mg every two weeks with or without a loading dose. As there is no standard dosing regimen, the dosage of interferon alpha-2a varies widely in real-world settings. To mimic this reality, interferon alpha-2a could be injected subcutaneously at a dose of 3 million IU, with the frequency ranging from once daily to three times a week at the treating clinician's discretion.[11,24,25] Concomitant glucocorticoid treatment was permitted as clinically indicated for patients in each group and adjusted for as post-assignment covariates. The use of other immunomodulatory drugs, such as azathioprine, colchicine, and JAK inhibitors, as well as periocular or intravitreal glucocorticoid injections or implants, was prohibited. Patients would have their data censored if they deviated from the assigned treatment strategy, switched to the other treatment group, commenced any prohibited therapies, and at their final visit (after which no further visits occur within the subsequent six months), whichever occurred first. No deaths were reported in this study.

Outcomes. The primary outcome was the annualized relapse rate of uveitis during treatment with study therapy. A uveitis relapse was defined as a minimum two-step increase in the anterior chamber cell or vitreous haze grade relative to the best state previously recorded, the appearance of new active inflammatory retinal lesions relative to the baseline, or the worsening of previously stable inflammatory retinal lesions relative to the last visit.[15] Secondary outcomes included the time to the first uveitis relapse since baseline and the change in BCVA from baseline at months two, four, and six. We defined a ±30-day window around months two, four, and six and used the available visit closest to the target time. An exploratory outcome was the percentage change from baseline in patients with macular edema in at least one eye at month six.

Covariates. We identified a range of potential confounders from the predetermined electronic medical database, including demographic characteristics, past medical history, main clinical manifestations, and disease severity, based on clinical knowledge, published literature, and previous trial data.[15,26,27] We used a directed acyclic graph (DAG) to guide the final selection of predefined covariates (Supplementary Figure 1 and Supplementary Table 2) that accounted for nonrandom allocation among the groups. The DAG depicts variables as nodes linked by arrows, which illustrates their relationships and facilitates the identification of the minimal set of covariates needed to adjust for confounding.[28] The minimally sufficient adjustment baseline covariates identified by DAG included age, sex, uveitis laterality, daily glucocorticoid dose at baseline, history of treatment with specific immunosuppressants, macular edema in at least one eye, active retinal vascular lesions in at least one eye, and anterior chamber cell and vitreous haze grades in the more severely affected eye. In addition, we prespecified cumulative glucocorticoid dose, ocular surgeries, and visit frequency from baseline to the end of follow-up as post-assignment covariates because they were potential confounders for the effect of immunomodulatory therapies on the primary outcome. The cumulative glucocorticoid dose, representing the burden of concomitant glucocorticoid exposure, was calculated by summing the daily doses from all filled prescriptions throughout the follow-up.

Statistical analysis. Baseline characteristics are summarized as n (%) for categorical data, mean ± SD for normally distributed data, and median (interquartile range [IQR]) for skewed data. To emulate the target trial, we estimated the per-protocol average treatment effect of maintained use of the assigned immunomodulatory therapy. We applied overlap weighting to balance patient characteristics across treatment groups and emulate randomization at baseline. This approach involved assigning a weight to each patient that was proportional to the probability of that patient not being assigned to the actual treatment.[29] Overlap weighting reweights the sample to emphasize the overlap region where treatment groups are most comparable, thus changing the study population.[30] This means that by downweighting individuals with extreme propensity scores (those who are very likely or very unlikely to receive the treatment), covariate balance can be achieved and valid comparisons across treatment groups can be enabled even if the original sample sizes are unevenly distributed across groups.[31] The treatment effect estimate is specific to the overlap population. We estimated treatment assignment probabilities using a multinomial logistic regression with predefined baseline covariates as predictors and then computed the generalized overlap weights for all pairwise comparisons among the three study therapies.[32] For a small number of patients, missing baseline information was imputed with the mean or median of available data, as appropriate. Between-group balance for each covariate was evaluated with the standardized mean difference.

The primary outcome was analyzed by treatment group with the use of a overlap-weighted negative binomial regression model with robust variance estimators, further adjusted for prespecified post-assignment covariates. For this analysis, the total number of uveitis relapses was the response variable, with the natural logarithm of study treatment duration as the offset. In the analysis of total relapses, missing values for variables such as anterior chamber cell and vitreous haze grades at post-baseline visits were imputed with the last observation carried forward (LOCF) method. We used LOCF as the primary analysis because it could yield a lower relapse incidence, thus providing a more conservative estimate of outcomes.

The time to the first relapse was analyzed, and the cumulative probability of uveitis relapse was predicted with an overlap-weighted Cox proportional hazards model that was adjusted for prespecified post-assignment covariates measured from baseline to the time of censoring. Data were censored at the time of the

occurrence of any violations of the treatment strategy or their final visit, whichever came first. No violations of the proportional hazards assumption were identified with Schoenfeld residuals. Longitudinal changes in BCVA were analyzed using an overlap-weighted generalized estimating equation with robust variance estimation and an exchangeable correlation structure to account for the correlation between the eyes of a patient, with adjustment for baseline BCVA values, eye specificity, and prespecified post-assignment covariates. Similarly, taking into account the correlation of repeated measures, we used an overlap-weighted generalized estimating equation with a binomial model and an identity link function to analyze the percentage of macular edema in at least one eye as well as the percentage changes through six months, with adjustment for post-assignment covariates. Assuming that data were missing at random, missing values for BCVA and macular edema status at each analyzed time point were addressed with multiple imputation. Rubin's rules were used to combine effect estimates from 100 imputed datasets.

Regarding the primary outcome, we performed prespecified subgroup analyses according to age (<35 years vs ≥35 years), sex, anterior chamber cell and vitreous haze grades in the more severely affected eye (≤0.5+ vs >0.5+), the presence of macular edema, and active retinal vascular lesions (detected in at least one eye vs not detected) at baseline. Subgroup analyses were conducted by adding each subgroup variable and its corresponding interaction term with treatment assignment to the primary overlap-weighted negative binomial regression model.

We conducted several sensitivity analyses of the primary outcome. First, to dynamically adjust for concomitant glucocorticoid treatment, we incorporated the updated dose at each visit as a time-varying covariate in an overlap-weighted mixed effects model. This model was fitted using a negative binomial regression with a log link, accounting for ocular surgeries, visit frequency, and the variations in glucocorticoid dose by including interactions with visit and participant-level random intercepts. Second, we addressed potential selection bias caused by censoring using inverse probability of censoring weighting. Probabilities of not getting censored were estimated with the logistic regression, which was conditional on all predetermined baseline and post-assignment covariates. We constructed a summarized weight by multiplying overlap weights with inverse probability of censoring weights that was then applied to negative binomial regression to produce effect estimates. Third, assuming missingness at random, the total number of relapses was derived by predicting missing relapse status at each visit using multiple imputation for 100 times instead of using the LOCF method. Fourth, we excluded uveitis relapse events within 30 days after the baseline date to minimize reverse causation. Fifth, we further adjusted for topical glucocorticoid use during follow-up as an additional post-assignment covariate. Sixth, considering that the drug availability for Behçet disease might have shifted over time, we further adjusted for the year of patient enrollment in the regression model. Seventh, to assess the impact of adjustment for post-assignment covariates on the primary outcome, we performed a sensitivity analysis by not adjusting for these covariates within the overlap-weighted negative binomial regression model. Eighth, we additionally account for patients' province of residence, which could serve as a proxy for socioeconomic disparities within our sample,[33] by incorporating this covariate into the overlap weighting model. Finally, the robustness of estimates to unmeasured confounders was assessed with an array-approach analysis.[34] We also calculated the E-value, which is the minimum strength of association that an unmeasured confounder must have with the exposure and outcome to explain away the observed association.[35] All statistical tests were two-sided. Data were analyzed with R software, version 4.4.1 (R Foundation for Statistical Computing).

RESULTS

Of the 2,302 adult patients with Behçet disease identified during the study period, 1,145 fulfilled the eligibility criteria, and 1,012 were included in the primary analysis (Figure 1). The final cohort included 716 cyclosporine users, 193 interferon alfa-2a users, and 103 adalimumab users. The median age of all participants at baseline was 32 years (IQR 26–39), 199 (19.7%) were women, and all were of East Asian ethnicity. The characteristics of the original cohort are detailed in Supplementary Table 3. After applying overlap weighting, all the predefined baseline covariates achieved balance across treatment groups (Table 1), with standardized mean differences less than 0.1 (Supplementary Figures 2–4). For the entire cohort, the per-protocol effect evaluation was based on a median follow-up of 5.4 months (IQR 2.2–10.9).

Among those treated with cyclosporine, the actual median daily dose received was 125 mg (IQR 125 –150). Of 193 interferon alfa-2a users, 184 (95.3%) started with a dose of 3 million IU per day and maintained this regimen for a median of 154 days (IQR 64–202). By the end of follow-up, 22 (11.3%) of these users had adjusted their interferon alfa-2a frequency to every other day, whereas 10 (5.1%) had reduced it to three times a week. During the follow-up, cyclosporine users concomitantly consumed glucocorticoids at a median cumulative dose of 2,620 mg (IQR 1,279–4,958), interferon alfa-2a users at 2,642 mg (IQR 980–4,993), and adalimumab users at 3,380 mg (IQR 1,588–5,745), which was equivalent to a median daily dose of 20.0 mg (IQR 18.9–20.0), 19.3 mg (IQR 16.0–20.0), and 19.2 mg (IQR 16.5–20.0), respectively, averaged over the follow-up period. Topical glucocorticoids were used in 335 (46.8%) patients receiving cyclosporine, 45 (23.3%) receiving interferon alfa-2a, and 33 (32.0%) receiving adalimumab, with each instance lasting no more than 28 days in this cohort.

In the primary analysis, the estimated mean annualized relapse rate of uveitis was 0.95 (95% confidence interval

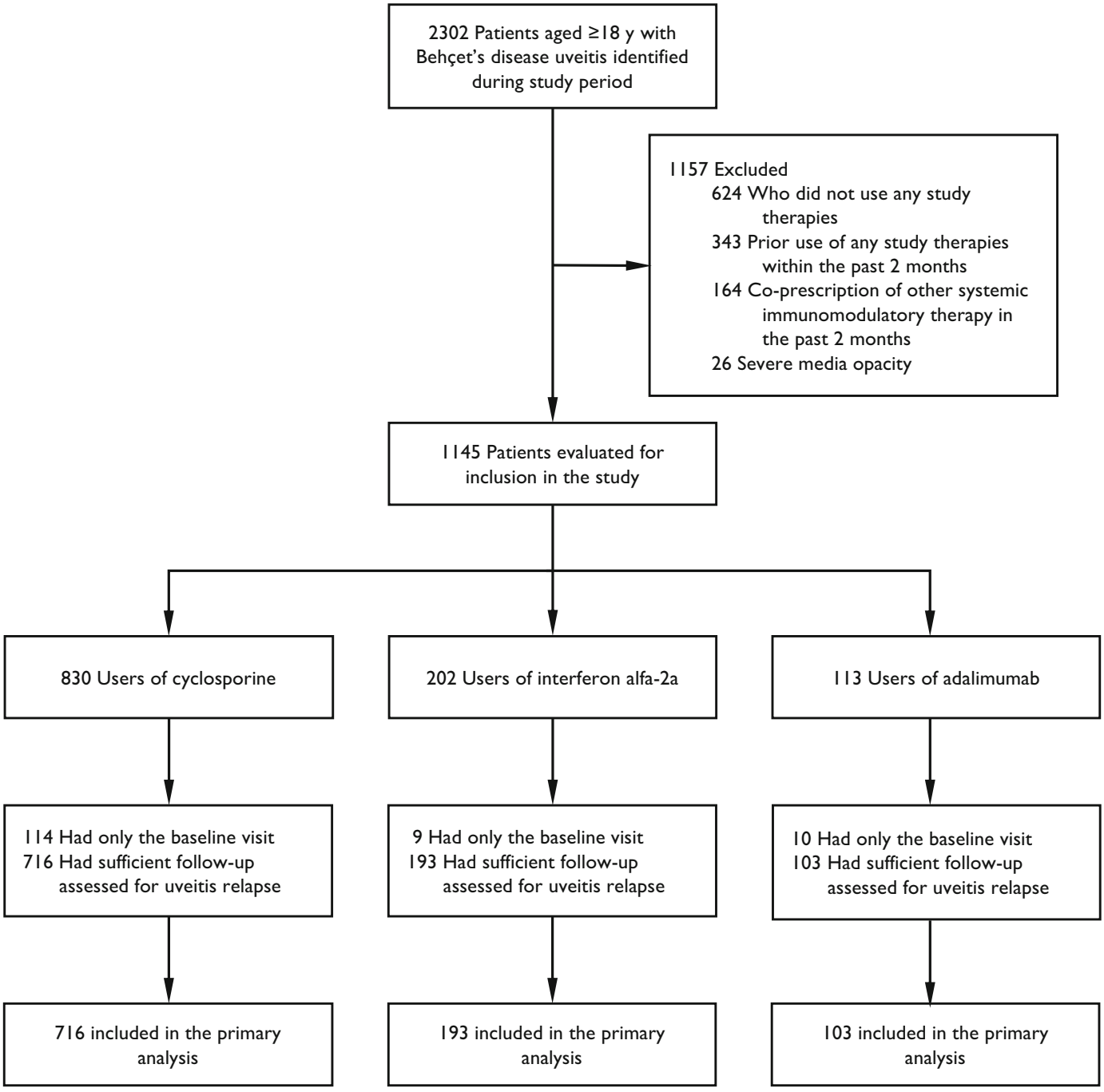

Figure 1. Study flow diagram.

[CI] 0.82–1.10) with cyclosporine, 0.52 (95% CI, 0.40–0.69) with interferon alfa-2a, and 0.28 (95% CI 0.19–0.43) with adalimumab (Table 2). Patients treated with cyclosporine experienced more relapses than those treated with adalimumab (incidence rate ratio [IRR] 3.36 [95% CI 2.23–5.05]; mean difference 0.66 [95% CI 0.48–0.85]; $P < 0.001$) or interferon alfa-2a (IRR 1.81 [95% CI 1.37–2.40]; mean difference 0.42 [95% CI 0.22–0.62]; $P < 0.001$). The relapse rate was higher in the interferon alfa-2a group than in the adalimumab group (IRR 1.86 [95% CI 1.16–2.97]; mean difference 0.24 [95% CI 0.05–0.43]; $P = 0.011$).

The cumulative probability of uveitis relapse in each treatment group is shown in Figure 2. All pairwise differences in the time to the first relapse across treatment groups were directionally concordant with the results of the primary outcome. Treatment with cyclosporine was associated with an earlier relapse of uveitis as compared with adalimumab (adjusted hazard ratio [HR] 2.33

Table 1. Selected baseline characteristics before and after overlap weighting*

Characteristic	Before weighting, n (%)			After weighting, %[a]		
	Cyclosporine (N = 716)	Interferon alfa-2a (N = 193)	Adalimumab (N = 103)	Cyclosporine	Interferon alfa-2a	Adalimumab
Age, median (IQR), year	32 (26–39)	33 (28–41)	33 (26–42)	33 (27–41)	33 (28–41)	33 (26–42)
Female	137 (19.1)	37 (19.2)	25 (24.3)	22.0	21.7	22.3
Bilateral uveitis	565 (78.9)	158 (81.9)	82 (79.6)	80.3	80.3	79.4
GC dose, mean (SD), mg/day	21.3 (3.1)	20.0 (2.0)	20.4 (2.4)	20.3 (2.5)	20.2 (1.7)	20.4 (2.4)
History of treatment						
Colchicine	23 (3.2)	24 (12.4)	5 (4.9)	5.9	5.3	5.9
Cyclophosphamide	21 (2.9)	14 (7.3)	4 (3.9)	4.4	4.2	4.0
Chlorambucil	8 (1.1)	10 (5.2)	3 (2.9)	2.8	3.3	3.6
Mycophenolate mofetil	3 (0.4)	7 (3.6)	2 (1.9)	1.6	1.9	1.3
Anterior chamber cell[b]						
0	512 (71.5)	147 (76.2)	76 (73.8)	74.9	73.9	77.4
0.5	26 (3.6)	11 (5.7)	3 (2.9)	3.6	3.7	3.6
1	80 (11.2)	16 (8.3)	7 (6.8)	8.5	8.5	7.7
2	52 (7.3)	12 (6.2)	7 (6.8)	6.7	8.1	6.0
3	26 (3.6)	5 (2.6)	5 (4.9)	3.8	3.5	3.3
4	20 (2.8)	2 (1.0)	5 (4.9)	2.5	2.3	2.0
Vitreous haze[b,c]						
0	319 (46.2)	109 (57.7)	41 (41.0)	46.3	46.9	47.1
1	190 (27.5)	41 (21.7)	37 (37.0)	32.9	32.7	33.5
2	75 (10.9)	13 (6.9)	13 (13.0)	10.7	10.0	10.0
3	74 (10.7)	13 (6.9)	4 (4.0)	5.1	4.8	4.3
4	33 (4.8)	13 (6.9)	5 (5.0)	5.1	5.7	5.0
Macular edema[d]	100 (14.8)	37 (19.4)	26 (25.2)	20.6	21.8	21.7
Active retinal vascular lesions[e]	511 (74.6)	145 (75.9)	73 (70.9)	70.5	71.1	69.8

* GC, glucocorticoid.
[a] Numbers of patients are not given because, after weighting, a single individual no longer represents a single data entity.
[b] Grades represented the more severely affected eye. Values range from 0 to 4+, with higher values indicating poorer condition.
[c] Data were not available for 25 patients in the cyclosporine group, 4 patients in the interferon alfa-2a group, and 3 patients in the adalimumab group.
[d] Macular edema was detected in at least one eye. Data were not available for 40 patients in the cyclosporine group and 2 patients in the interferon alfa-2a group.
[e] Active retinal vascular lesions were detected in at least one eye. Data were not available for 31 patients in the cyclosporine group and 2 patients in the interferon alfa-2a group.

[95% CI, 1.37–3.96]) or interferon alfa-2a (adjusted HR 1.57 [95% CI 1.15–2.14]). Patients receiving interferon alfa-2a had a marginally shorter time to relapse than those receiving adalimumab (adjusted HR,1.48 [95% CI 0.85–2.57]). Patients in all three groups showed significant improvements in BCVA at months two, four, and six compared with their baseline levels, with no notable differences in the extent of improvement among the three groups (Supplementary Figure 5). No significant differences in percentage changes of macular edema were observed across the treatment groups (Supplementary Figure 6). Under the condition that covariate balances within subgroups were not verified, the subgroup analyses roughly produced point estimates consistent in direction with those of the primary analysis (Figure 3). All sensitivity analyses yielded similar estimates to those from the

Table 2. Primary outcome*

Outcome[a]	Cyclosporine (N = 716)	Interferon alfa-2a (N = 193)	Adalimumab (N = 103)
Annualized relapse rate (95% CI)	0.95 (0.82–1.10)	0.52 (0.40–0.69)	0.28 (0.19–0.43)
Between-group difference (95% CI)			
vs interferon alfa-2a	0.42 (0.22–0.62)	–	−0.24 (−0.43 to −0.05)
vs adalimumab	0.66 (0.48–0.85)	0.24 (0.05–0.43)	–
IRR (95% CI)			
vs interferon alfa-2a	1.81 (1.37–2.40)	–	0.54 (0.34–0.86)
vs adalimumab	3.36 (2.23–5.05)	1.86 (1.16–2.97)	–

* CI, confidence ratio; IRR, incidence rate ratio.
[a] Values were determined with the use of an overlap-weighted negative binomial regression model with further adjustment for prespecified post-assignment covariates. Data are expressed as means or rate ratios with 95% CI.

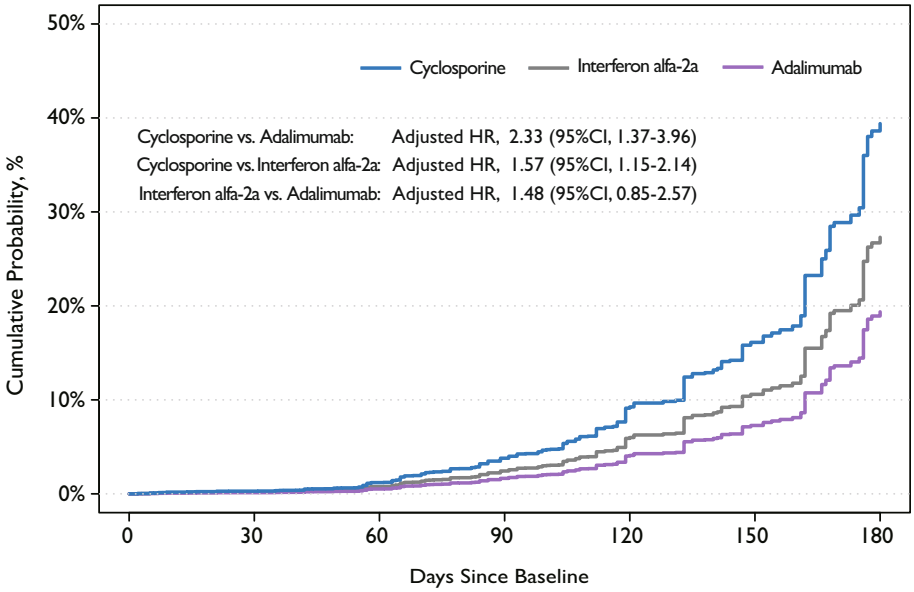

Figure 2. Cumulative probability of uveitis relapse. Predicted probabilities and adjusted HRs were estimated using an overlap-weighted Cox proportional hazards model with further adjustment for post-assignment covariates. Numbers of individuals at risk are not given because, after weighting, a single individual no longer represents a single data entity. CI, confidence interval; HR, hazard ratio.

primary analysis (Supplementary Table 4–12). To completely attenuate the primary outcome differences (Supplementary Figure 7–9), particularly the smallest one between interferon alfa-2a and adalimumab, we estimated that an unmeasured confounder should be very strongly associated with the primary outcome (ie, IRR <0.4 or >2.5, with a prevalence difference of at least 10%) or highly imbalanced across treatment groups (ie, a prevalence difference >40%, with an IRR of <0.6 or >1.7). When comparing cyclosporine with adalimumab and interferon alfa-2a, and comparing interferon alfa-2a with adalimumab, the corresponding E-values for the observed IRR were 6.18, 3.02, and 3.12, and those for the lower bound of the confidence interval were 3.89, 2.08, and 1.59, respectively.

DISCUSSION

In this target trial emulation study involving patients with Behçet disease, we observed that treatment with adalimumab was associated with fewer attacks of uveitis relapse compared with both cyclosporine and interferon alfa-2a, whereas interferon alfa-2a was associated with a lower relapse rate than cyclosporine. This study was adequately powered to quantify the comparative effectiveness of the three immunomodulatory therapies, with a particular ability to discern a more nuanced difference between interferon alfa-2a and adalimumab that had not been conclusively determined.[15] Our results were derived from a diverse population of real-world patients with varying ages, sex, degrees of inflammation in the anterior and posterior segments, and complications including macular edema. Despite the exploratory nature of the subgroup analyses and their relatively wider confidence intervals, the results from each subgroup appeared directionally consistent with those from the primary analysis. Our main conclusions might apply to a broader population compared with the findings from previous trial settings.[15]

Our study reinforces previous findings demonstrating the effectiveness superiority of adalimumab.[15,36,37] Most of these previous studies were performed in patients with severe Behçet disease or those refractory to conventional treatments. In contrast, our study encompasses a less selectively recruited consecutive population, including a higher proportion of patients with milder disease, as evidenced by mean annualized relapse rates below 1.0 across all three groups. These rates are apparently lower than those observed in the previous trial involving severely affected patients.[15] A previous six-month trial involving 74 patients showed that infliximab (another anti–tumor necrosis factor drug used off-label) did not show noticeable differences compared with interferon alfa-2a in managing ocular symptoms in Behçet disease.[38] Nonetheless, we provide more precise estimates favoring adalimumab over interferon alfa-2a in terms of uveitis relapse rate. Our study also corroborates results from a pilot trial, showing interferon alfa-2a to be more effective than cyclosporine.[16] The cyclosporine dosage used in our cohort, although within the EULAR recommended range,[10] was lower than in previous studies.[15,16] Nevertheless, we observed a low absolute number of uveitis relapse and visual improvements among cyclosporine users, which suggest that some of the less severe patients might not actually require high doses for treatment in real-world practice.

Our effectiveness data support the use of adalimumab as a clinical priority for preventing uveitis relapse in Behçet disease,

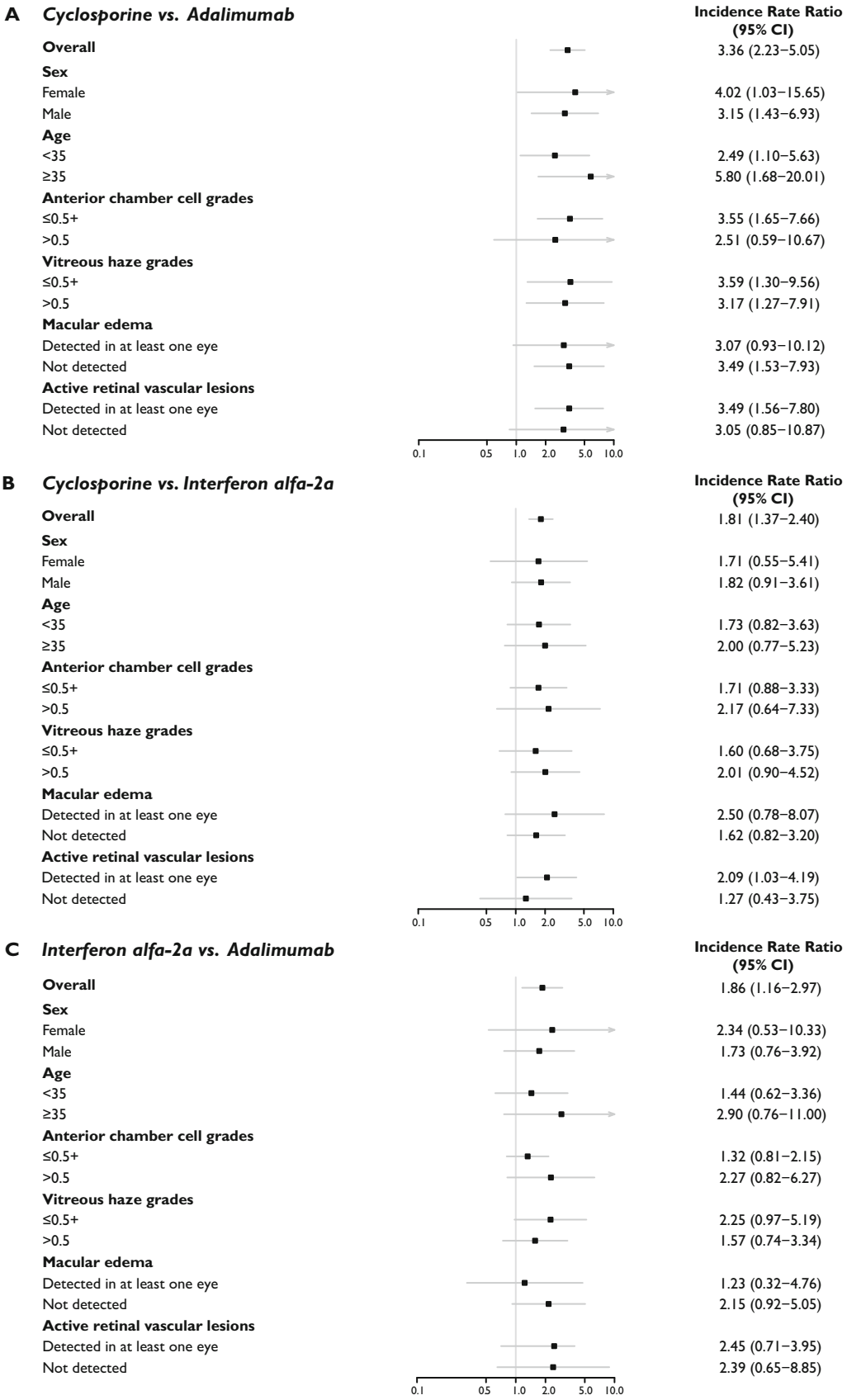

Figure 3. Subgroup analyses. Forest plots show the comparative effects of (A) cyclosporine versus adalimumab, (B) cyclosporine versus interferon alfa-2a, and (C) interferon alfa-2a versus adalimumab across subgroups. CI, confidence interval.

with such a benefit extending beyond severe or refractory cases.[15] These results are in line with recommendations that include adalimumab among the first-line immunomodulatory drugs for Behçet disease uveitis.[39] Nevertheless, in this study, the degree to which vision improved among adalimumab users was similar to that of interferon alfa-2a and cyclosporine users. These results can guide patient counseling regarding alternative treatments to adalimumab, particularly for those with milder conditions or infrequent relapses. Further research and validation are also needed to determine whether and when adalimumab treatment can indeed translate into additional benefits in visual outcomes and disease remission. Meanwhile, it may be because of a small proportion of patients with macular edema at baseline and low statistical power that no differences were found with respect to improvements in macular edema across treatment groups. Therefore, future powered studies would be warranted to assess treatment differences in macular edema. In addition, the safety profiles from the previous clinical trial suggested that the incidence of adverse events was lower with adalimumab than that with cyclosporine or interferon alfa-2a when each combined with glucocorticoids.[15] Because of the lack of data, our study has not yet made a comparison of adverse events. Clinicians still need to balance drug safety and effectiveness when making medication decisions.

Strengths of this study include the use of real-world data, which provided a more realistic reflection of drug performance in usual care rather than in a monitored trial setting. Our broad patient population from daily practice enhances study power and representativeness, overcoming recruitment challenges typical in traditional trials for this rare disease. We explicitly emulated a target trial with the active comparator new-user design by excluding prevalent users, ensuring that eligibility and treatment assignment were synchronized with time zero, thus minimizing immortal time bias.[40,41] We applied various analytic approaches to address potential confounding and scrutinize the success of emulation in multiple sensitivity analyses. Compared with previous trials,[15,16] interpretation of our findings is more straightforward because we estimated independent effects of each immunomodulatory drug, accounting for varying background glucocorticoid treatments. These previous trials only provided indirect inferences of drug effectiveness through standardized glucocorticoid regimens and intention-to-treat analysis on combination therapies.

This study also has some limitations. First, as with many observational analyses, the target trial emulation may carry the potential risk of residual confounding.[41] We used overlap weighting to address uneven sample sizes and baseline imbalance across treatment groups in the original cohort. We have controlled for a range of major covariates through weighting and adjustment. Regardless, the sensitivity analyses suggest that the effect estimates are unlikely to be entirely attenuated by minor unmeasured confounders. We also recognize that overadjustment, particularly for those post-baseline variables that may be impacted by treatment, risks blocking part of the treatment effect. Nevertheless, a sensitivity analysis without adjusting for post-treatment variables gave reassuring results, which were consistent with those from the primary model. Second, our per-protocol analysis had a median follow-up of 5.4 months, with a quarter of patients observed for more than 10.9 months. This reflects the limited duration of drug retention among real-world patients under the predefined treatment strategies, necessitating data censoring for those who deviated from the treatment plan. However, among those who strictly followed the treatment strategies during the follow-up, our study was already powered to observe notable differences across the treatment groups. Third, similar to previous analyses using annualized relapse rates as the endpoint,[42] we did not conduct an observational analog of the intention-to-treat effect. This endpoint is closely relevant to the duration of maintained use of the study therapy, whereas the intention-to-treat effect is determined by the initiation of the study therapy, not its maintained use. We believe that the per-protocol analysis would provide a more accurate estimate of treatment-specific annualized relapse rates because data were censored during the analysis when the specific treatment strategy was no longer maintained. Fourth, because the subgroup analyses were exploratory, they should be interpreted with caution, particularly because the lack of subgroup covariate balancing may result in biased causal effect estimates.[43]

In conclusion, among adult patients with Behçet disease, interferon alfa-2a was associated with a reduction in uveitis relapse compared with cyclosporine, whereas adalimumab demonstrated a stronger association with reduced relapse than interferon alfa-2a. Visual improvements were noted with all three treatments, although none was found to be associated with better improvement compared with the others. These findings provide real-world insights into the comparative effectiveness of the three commonly used drugs for Behçet disease and could guide the choice of immunomodulatory therapy.

AUTHOR CONTRIBUTIONS

All authors contributed to at least one of the following manuscript preparation roles: conceptualization AND/OR methodology, software, investigation, formal analysis, data curation, visualization, and validation AND drafting or reviewing/editing the final draft. As corresponding author, Dr Yang confirms that all authors have provided the final approval of the version to be published, and takes responsibility for the affirmations regarding article submission (eg, not under consideration by another journal), the integrity of the data presented, and the statements regarding compliance with institutional review board/Declaration of Helsinki requirements.

REFERENCES

1. Saadoun D, Bodaghi B, Cacoub P. Behçet's Syndrome. N Engl J Med 2024;390(7):640–651.

2. Maldini C, Druce K, Basu N, et al. Exploring the variability in Behçet's disease prevalence: a meta-analytical approach. Rheumatology (Oxford) 2018;57(1):185–195.
3. Emmi G, Bettiol A, Hatemi G, et al. Behçet's syndrome. Lancet 2024; 403(10431):1093–1108.
4. Zhong Z, Su G, Yang P. Risk factors, clinical features and treatment of Behçet's disease uveitis. Prog Retin Eye Res 2023;97:101216.
5. Yazici H, Seyahi E, Hatemi G, et al. Behçet syndrome: a contemporary view. Nat Rev Rheumatol 2018;14(2):107–119.
6. Yang P, Fang W, Meng Q, et al. Clinical features of Chinese patients with Behçet's disease. Ophthalmology 2008;115(2): 312–318.e4.
7. Zhong Z, Su G, Kijlstra A, Yang P. Activation of the interleukin-23/interleukin-17 signalling pathway in autoinflammatory and autoimmune uveitis. Prog Retin Eye Res 2021;80:100866.
8. Yazici Y, Hatemi G, Bodaghi B, et al. Behçet syndrome. Nat Rev Dis Primers 2021;7(1):67.
9. Ozguler Y, Leccese P, Christensen R, et al. Management of major organ involvement of Behçet's syndrome: a systematic review for update of the EULAR recommendations. Rheumatology (Oxford) 2018;57(12):2200–2212.
10. Hatemi G, Silman A, Bang D, et al; EULAR Expert Committee. EULAR recommendations for the management of Behçet disease. Ann Rheum Dis 2008;67(12):1656–1662.
11. Yang P, Huang G, Du L, et al. Long-term efficacy and safety of interferon alpha-2a in the treatment of Chinese patients with Behçet's uveitis not responding to conventional therapy. Ocul Immunol Inflamm 2019;27(1):7–14.
12. Ramdoss J, Singh P, Ahmed AS, et al Clinical profile and management with immunosuppressants and biologics in Behcet's uveitis: a cohort of 25 patients from a tertiary eye care center in South India. Indian J Ophthalmol 2023;71(5):1972–1976.
13. Hatemi G, Christensen R, Bang D, et al 2018 update of the EULAR recommendations for the management of Behçet's syndrome. Ann Rheum Dis 2018;77(6):808–818.
14. Dick AD, Rosenbaum JT, Al-Dhibi HA, et al; Fundamentals of Care for Uveitis International Consensus Group. Guidance on noncorticosteroid systemic immunomodulatory therapy in noninfectious uveitis: Fundamentals Of Care for UveitiS (FOCUS) Initiative. Ophthalmology 2018;125(5):757–773.
15. Zhong Z, Deng D, Gao Y, et al. Combinations of immunomodulatory agents for prevention of uveitis relapse in patients with severe Behçet's disease already on corticosteroid therapy: a randomised, open-label, head-to-head trial. Lancet Rheumatol 2024;6(11):e780–e790.
16. Qian Y, Qu Y, Gao F, et al. Comparison of the safety and efficacy of interferon alpha-2a and cyclosporine-a when combined with glucocorticoid in the treatment of refractory Behçet's uveitis: a randomized controlled prospective study. Front Pharmacol 2021;12: 699903.
17. Bellur S, McHarg M, Kongwattananon W, et al. Antidrug antibodies to tumor necrosis factor α inhibitors in patients with noninfectious uveitis. JAMA Ophthalmol 2023;141(2):150–156.
18. Danaei G, García Rodríguez LA, Cantero OF, et al. Electronic medical records can be used to emulate target trials of sustained treatment strategies. J Clin Epidemiol 2018;96:12–22.
19. Jabs DA, Dick AD, Dunn JP, et al; Standardization of Uveitis Nomenclature (SUN) Working Group. Classification criteria for Behçet disease uveitis. Am J Ophthalmol 2021;228:80–88.
20. Yang P, Zhong Z, Du L, et al. Prevalence and clinical features of systemic diseases in Chinese patients with uveitis. Br J Ophthalmol 2021;105(1):75–82.
21. Jabs DA, Nussenblatt RB, Rosenbaum JT; Standardization of Uveitis Nomenclature (SUN) Working Group. Standardization of uveitis nomenclature for reporting clinical data. Results of the First International Workshop. Am J Ophthalmol 2005;140(3): 509–516.
22. Nussenblatt RB, Palestine AG, Chan CC, et al. Standardization of vitreal inflammatory activity in intermediate and posterior uveitis. Ophthalmology 1985;92(4):467–471.
23. El-Asrar AM, Herbort CP, Tabbara KF. A clinical approach to the diagnosis of retinal vasculitis. Int Ophthalmol 2010;30(2):149–173.
24. De Simone L, Invernizzi A, Aldigeri R, et al. Effectiveness of infliximab and interferon alpha-2a for the treatment of Behçet's uveitis: customizing therapy according to the clinical features. Ocul Immunol Inflamm 2022;30(2):506–514.
25. Lee JH, Lee CS, Lee SC. Interferon alpha-2a treatment for refractory Behcet uveitis in Korean patients. BMC Ophthalmol 2018;18(1):52.
26. Jaffe GJ, Dick AD, Brézin AP, et al. Adalimumab in patients with active noninfectious uveitis. N Engl J Med 2016;375(10): 932–943.
27. Nguyen QD, Merrill PT, Jaffe GJ, et al. Adalimumab for prevention of uveitic flare in patients with inactive non-infectious uveitis controlled by corticosteroids (VISUAL II): a multicentre, double-masked, randomised, placebo-controlled phase 3 trial. Lancet 2016;388(10050): 1183–1192.
28. Knüppel S, Stang A. DAG program: identifying minimal sufficient adjustment sets. Epidemiology 2010;21(1):159.
29. Li F, Morgan KL, Zaslavsky AM. Balancing covariates via propensity score weighting. J Am Stat Assoc 2018;113(521):390–400.
30. Li F, Thomas LE, Li F. Addressing extreme propensity scores via the overlap weights. Am J Epidemiol 2019;188(1):250–257.
31. Thomas LE, Li F, Pencina MJ. Overlap weighting: a propensity score method that mimics attributes of a randomized clinical trial. JAMA 2020;323(23):2417–2418.
32. Li F, Li F. Propensity score weighting for causal inference with multiple treatments. Ann Appl Stat 2019;13(4):2389–2415.
33. Jia Y, Hu M, Fu H, Yip W. Provincial variations in catastrophic health expenditure and medical impoverishment in China: a nationwide population-based study. Lancet Reg Health West Pac 2022;31: 100633.
34. Schneeweiss S. Sensitivity analysis and external adjustment for unmeasured confounders in epidemiologic database studies of therapeutics. Pharmacoepidemiol Drug Saf 2006;15(5): 291–303.
35. VanderWeele TJ, Ding P. Sensitivity analysis in observational research: introducing the E-value. Ann Intern Med 2017;167(4): 268–274.
36. Zhou X, Shi X, Ren Y, et al. Anti-tumour necrosis factor-alpha agent therapy, compared with conventional therapy, reduces the relapse of uveitis in patients with Behçet's disease: a systematic review of controlled trials. Front Pharmacol 2022;13:912906.
37. Talarico R, Italiano N, Emmi G, et al. Efficacy and safety of infliximab or adalimumab in severe mucocutaneous Behçet's syndrome refractory to traditional immunosuppressants: a 6-month, multicentre, randomised controlled, prospective, parallel group, single-blind trial. Ann Rheum Dis Published online December 20, 2024. doi:10.1136/ard-2024–226113
38. Moots RJ, Fortune F, Jackson R, et al. Infliximab vs interferon-α in the treatment of Behçet's syndrome: clinical data from the BIO-BEHÇET'S randomized controlled trial. Rheumatology (Oxford) 2025; 64(5):2882–2891.
39. Levy-Clarke G, Jabs DA, Read RW, et al. Expert panel recommendations for the use of anti-tumor necrosis factor biologic agents in

patients with ocular inflammatory disorders. Ophthalmology 2014; 121(3):785–96.e3.

40. Dickerman BA, García-Albéniz X, Logan RW, et al. Avoidable flaws in observational analyses: an application to statins and cancer. Nat Med 2019;25(10):1601–1606.

41. Hubbard RA, Gatsonis CA, Hogan JW, et al. "Target trial emulation" for observational studies - potential and pitfalls. N Engl J Med 2024; 391(21):1975–1977.

42. Kalincik T, Sharmin S, Roos I, et al; MSBase Study Group Collaborators; MSBase Study Group Authors; MSBase Study Group. Comparative effectiveness of autologous hematopoietic stem cell transplant vs fingolimod, natalizumab, and ocrelizumab in highly active relapsing-remitting multiple sclerosis. JAMA Neurol 2023;80(7): 702–713.

43. Yang S, Lorenzi E, Papadogeorgou G, et al. Propensity score weighting for causal subgroup analysis. Stat Med 2021;40(19): 4294–4309.

Arthritis & Rheumatology
Vol. 78, No. 2, February 2026, pp 449–462
DOI 10.1002/art.43367

American College of Rheumatology
Empowering Rheumatology Professionals

Spermidine Reproduces the Anti-Inflammatory Effects of Intermittent Fasting and Prevents Urate and Calcium Pyrophosphate Crystal-Induced Inflammation

Chinh Nghia Pham,[1,2] Florence Castelli,[3] Flora Finet,[1] Charles Leroy,[1] Céline Chollet,[3] Twinu W. Chirayath,[1] Subhalaxmi Moitra,[1] Mylène Zarka,[1] Agnès Ostertag,[1] François Brial,[1] Christèle Combes,[4] Augustin Latourte,[5] Thomas Bardin,[1] François Fenaille,[3] Pascal Richette,[5] and Hang Korng Ea[5]

Objective. Gout caused by the formation of monosodium urate (MSU) crystals and calcium pyrophosphate (CPP) deposition disease are two major types of microcrystalline pathologies in adults. They are responsible for recurrent flares that rely on interleukin (IL) 1β via activation of the NLRP3 inflammasome. Intermittent fasting (IF) is a nonpharmacologic intervention that improves age-related diseases and reduces inflammation.

Methods. In an air pouch model, crystal-induced inflammation was compared between mice fed ad libitum and mice under IF. Systemic (liver and serum) and local (air pouch cavity) modifications were evaluated by metabolomics analysis. The anti-inflammatory potential of metabolites was tested in vitro and in vivo.

Results. We observe that two nonconsecutive days of fasting during one week significantly prevents the inflammation provoked by MSU and CPP crystal injection into the air pouch cavity in a mouse model. This short-term fasting is associated with increased serum abundances of numerous anti-inflammatory metabolites, including β-hydroxybutyrate and spermidine (SPD), a polyamine able to reproduce biologic effects of IF. Conversely, crystal stimulation in mice fed ad libitum decreases the local production of these metabolites in the air pouch membrane. Supplementation of SPD reproduces the anti-inflammatory effect of IF and prevents crystal-induced inflammation through inhibition of NF-κB and NLRP3 inflammasome. Finally, down-regulation of SPD/spermine acetyltransferase 1, which encodes the enzyme that degrades SPD, reduces IL-1β production induced by crystal stimulation.

Conclusion. In summary, we have identified several metabolites that recapitulate the anti-inflammatory effects of IF and could be used as IF mimetics to prevent microcrystal inflammation.

INTRODUCTION

Gout and calcium pyrophosphate (CPP) crystal deposition disease are the two main types of microcrystalline diseases. Gout is caused by the deposition of monosodium urate (MSU) crystals after chronic elevation of serum urate level. In 2020, >55.8 million people experienced gout worldwide, which represents an increase of 22.5% within 30 years.[1] The prevalence of CPP deposition (CPPD) disease is also high, ranging from 7% to 10% in people aged >60 years.[2]

Both gout and CPPD disease are responsible for severe recurrent inflammatory painful flares.[3,4] Low-dose colchicine, nonsteroidal anti-inflammatory drugs, and corticosteroids are recommended as the first-line treatment of gout flares, whereas

Supported by the French Society of Rheumatology (Société Française de Rhumatologie) and ArtViggo.

[1]Chinh Nghia Pham, MD, PhD, Flora Finet, MD, Charles Leroy, MS, Twinu W. Chirayath, PhD, Subhalaxmi Moitra, MS, Mylène Zarka, PhD, Agnès Ostertag, PhD, François Brial, PhD, Thomas Bardin, MD, PhD: Université Paris Cité, Inserm U1132, BIOSCAR, Hôpital Lariboisière, Paris, France; [2]Chinh Nghia Pham, MD, PhD: Internal Medicine Department, Haiphong University of Medicine and Pharmacy, Haiphong, Vietnam; [3]Florence Castelli, PhD, Céline Chollet, MS, François Fenaille, PhD: Université Paris-Saclay, French Alternative Energies and Atomic Energy Commission, National Research Institute for Agriculture, Food and Environment, Département Médicaments et Technologies pour La Santé, MetaboHUB, Gif-sur-Yvette, France; [4]Christèle Combes, PhD: Interuniversity Research Center Engineering Materials, Toulouse Integrated Preparatory School, Université Toulouse 3 Paul Sabatier, CNRS, Université de Toulouse, École Nationale Supérieure des Ingénieurs en Arts Chimiques et Technologiques, Toulouse, France; [5]Augustin Latourte, MD, PhD, Pascal Richette, MD, PhD, Hang Korng Ea, MD, PhD: Université Paris Cité, Inserm U1132, BIOSCAR, Hôpital Lariboisière and Department of Rheumatology, AP-HP, Hôpital Lariboisière, Centre Viggo Petersen, DMU Locomotion, Paris, France.

Additional supplementary information cited in this article can be found online in the Supporting Information section (http://onlinelibrary.wiley.com/doi/10.1002/art.43367).

Author disclosures and graphical abstract are available at https://onlinelibrary.wiley.com/doi/10.1002/art.43367.

Address correspondence via email to Hang Korng Ea, MD, PhD, at hang-korng.ea@aphp.fr or korngea@yahoo.fr.

Submitted for publication March 9, 2025; accepted in revised form August 13, 2025.

interleukin (IL) 1β blockers are proposed to patients who do not respond to or are intolerant to these treatments.[4,5] Although these four treatment options are effective, approximately 50% of patients still have pain after 24 to 72 hours of treatment, and these drugs can cause side effects.[6–8] There is therefore a need to identify novel, effective, and well-tolerated anti-inflammatory therapies. Gout and CPPD flares are driven by multiple inflammatory mediators, including IL-1β, IL-6, tumor necrosis factor (TNF) superfamily 14 and prostaglandins.[9–11] IL-1β production is a two-step process and relies on NLRP3 inflammasome activation.[12] The first signal depends on the activation of transcription factors including NF-κB, activator protein 1, and C-JUN[12–14] and promotes production of pro–IL-1β. The second signal triggers activation of NLRP3 inflammasome leading to the formation of active caspase-1, which induces cleavage of pro–IL-1β to mature IL-1β.[12]

Caloric restriction (CR) without malnutrition and intermittent fasting (IF) are nonpharmacologic interventions that improve health and increase longevity in almost all organisms, including nonhuman primates.[15–18] CR and IF induce neuroendocrine and metabolic adaptations combining transcriptome, epigenome, proteome, and metabolome changes, which improve energy balance by reducing anabolic processes while promoting catabolism, biogenesis of mitochondria and lysosome, recycling of damaged organelles and proteins, and reducing inflammation.[17,19] CR and IF reduce inflammation through multiple molecular mechanisms including promotion of autophagy and inhibition of NF-κB activity, NLRP3 inflammasome activation, and IL-1β production.[15,19] Interestingly, a pilot study reports that CR to 1,600 kcal/day for 4 months is associated with flare reduction in 13 patients with gout.[20] Although this observation is limited by the small number of patients, together with the abovementioned molecular mechanisms it supports the hypothesis that CR may reduce crystal inflammation. However, long-term adherence to CR or IF is difficult, and most participants are unable to adapt to the CR diet for long periods of time. To overcome this issue, supplementation with CR or IF mimetics, which would reproduce and mimic the beneficial biologic effects of CR/IF, is considered an attractive therapeutic option.

Spermidine (SPD), a natural polyamine, appears to be one of the most promising CR mimetics.[21–23] The synthesis of polyamine, which includes putrescine, spermine, and SPD, relies on metabolism of arginine, ornithine, and methionine.[21,22,24,25] SPD is generated from its precursor putrescine or by degradation from spermine. Putrescine formation is connected to arginine. Arginase 1 metabolizes arginine to ornithine, which leads to putrescine formation via ornithine decarboxylase 1 (ODC1). SPD synthase promotes the formation of SPD from putrescine using decarboxylated S-adenosylmethionine, which is formed from the methionine pathway. SPD production is increased during fasting in several organisms including yeast, flies, mice, and humans.[21] SPD supplementation mimics the effects of IF, improving age-associated metabolic disorders and reducing inflammation by inhibiting NF-κB, TNF, and IL-1β and promoting autophagy and M2 macrophage polarization.[21,22,26–28] Furthermore, inhibition of SPD production abolishes the lifespan-extending, cardioprotective and antiarthritic effects of IF.[21] These results further suggest that CR, IF, and CR mimetics such as SPD may reduce crystal-induced inflammation.

Here, we explore this hypothesis and find that two nonconsecutive days of fasting during one week are sufficient to significantly prevent the inflammation induced by MSU and CPP crystals. This IF is associated with increased production of β-hydroxybutyrate (BHB) and SPD. SPD supplementation mimics the anti-inflammatory effect of IF and prevents crystal-induced inflammation in vivo and in vitro through inhibition of NF-κB and NLRP3 inflammasome.

MATERIALS AND METHODS

Ethics statement, IF, SPD supplementation, and mouse air pouch model. This study was approved by the French national ethical committee *Le comité d'éthique en expérimentation animale Lariboisière/Villemin n°9* (APAFIS#38700_2022081715327484_V5). Mouse studies were conducted in accordance with European Union directives (2010/63/UE) and French ethical laws guidelines (act no. R214; 87-137; *Ministère de l'Agriculture*) and followed the ARRIVE guidelines (Animal Research: Reporting of In vivo Experiments; http://www.nc3rs.org.uk). See the Supplementary Materials for the complete methods.

Male 8-week-old wild-type C57Bl/6J mice were provided by the Janvier Laboratory. Mice were assigned to two groups: mice fed ad libitum, designated as normal diet (ND), and mice fasted for two nonconsecutive days per week (no food for 24 hours, water provided ad libitum), designated as IF. An air pouch was created by dorsal subcutaneous injections of 3 mL of sterile air on days –6 and –3. On day 0, at the end of the second fasted day, crystals (MSU 1 mg/mL or CPP 1 mg/mL) or phosphate-buffered saline (PBS; 1 mL) were injected into the air pouch (Figure 1A). Inflammation was studied 6 hours after crystal or PBS stimulation, assessing the concentration of inflammatory mediators in air pouch lavages by enzyme-linked immunosorbent assay (IL-1β, Invitrogen; CXCL-1, R&D System) and cell infiltration by manual counting (absolute number). Air pouch membranes, serum, and liver were collected and nitrogen frozen for metabolomics (the three compartments) and transcriptomics (liver) studies. Half of the air pouch membranes were fixed with paraformaldehyde 4% for the histology study.

For the SPD supplementation experiment, a group of mice drank water containing high-purity SPD (6 mM; Merck, #0266) during 21 days before crystal stimulation. The day before crystals injection, SPD (100 mg/kg) was injected into the air pouch. The control group of mice drank normal water and received 1 mL of

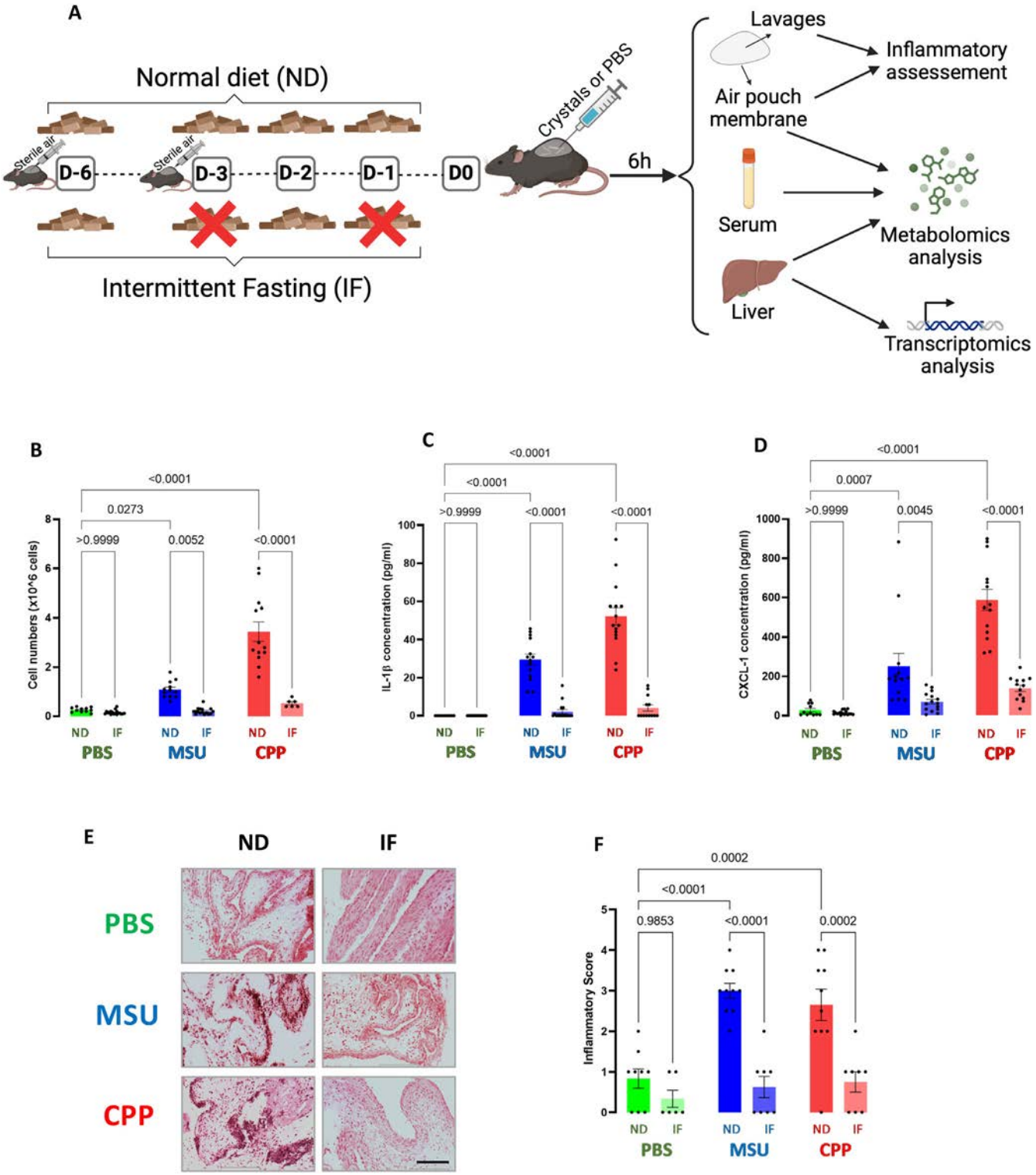

Figure 1. IF in vivo reduces crystal-induced inflammation. (A) Experimental protocol cartoon: an air pouch was created in the back area of 8-week-old male C57BL6 wild-type mice by injection of sterile air 6 days before the experiment. In the intervention group, mice were fasted two nonconsecutive days during one week whereas the control group were fed ad libitum, designated as ND. Biologic samples were collected 6 hours after stimulation for different analysis. (B–D) Inflammation induced by crystal was compared between ND and IF mice assessing (B) in air pouch washing liquid cell infiltration, (C) IL-1β, and (D) CXCL-1 concentrations. Inflammatory cell infiltration in the air pouch membrane (assessed by hematoxylin and eosin staining) was (E) visualized and (F) scored. Scale bar in (E) = 100 μm. Values are mean ± SEM with two-way analysis of variance with the Sidak multiple comparison test; there were n = 7 to 13 mice per group, and each dot represented one mouse. CPP, calcium pyrophosphate; IF, intermittent fasting; IL-Iβ, interleukin-1β; MSU, monosodium urate; ND, normal diet; PBS, phosphate-buffered saline.

PBS into the pouch the day before crystal injection. Crystal stimulation and tissue collection were performed as described in the fasting experiment. In a second experiment, SPD supplementation was only administrated by intrapouch injection the day before crystal stimulation. To investigate the role of SPD during IF, we treated IF mice with an ODC1 inhibitor, α-difluoromethylornithine (DFMO), which was added in drinking water at 0.5% (weight/volume) (Medchem, #HY-B0744) for 21 days before injection of MSU crystals into air pouch.

Metabolomics analysis. The statistical analysis was performed with the metaboanalyst.ca web-based platform. Raw data were normalized with log10 transformation and autoscaled. Fold change (FC) analysis was performed by applying a *t*-test (FC cutoff = 1.2, statistic significant threshold with $P < 0.05$). The synchronized 3D plots for principal component analysis (PCA) were made with the help of the web-based platform. Hierarchical clustering heatmaps were also performed with the Euclidean-Ward method by applying a one-way analysis of variance test. See the Supplementary Materials for the complete metabolomics description.

We analyzed metabolome change on the iPath3.0 website (https://pathways.embl.de/ipath3.cgi). The mapping change was operated by selecting metabolites and FC with $P < 0.05$. The opacity of the nodes depends on the magnitude of the FC. Pathways associated with significantly modified metabolites are colored: red indicates up-regulated metabolites and pathways and blue down-regulated ones.

Transcriptomics analysis on THP-1 cells. RNA from primed THP-1 stimulated by PBS, MSU, or CPP crystals was extracted with the Qiagen RNeasy Plus Mini kit (Qiagen, #74136). All RNAs had RNA integrity numbers > 8.0 (2100 Bioanalyzer, Agilent). RNA transcriptome was performed by Integragen. Reads were aligned to the human genome (Gencode v39) using STAR, and gene-level raw counts were generated (including protein-coding genes and antisense and long intergenic noncoding RNAs). The extracted count matrix was normalized for library size and coding length of genes to compute fragments per kb of transcript per million mapped reads (FPKM) expression levels. Only genes with FPKM ≥ 0.1 in at least one sample were considered for statistical modeling.

Unsupervised analysis. Raw counts were imported into R using the Bioconductor edgeR package. Normalization was performed using trimmed mean of M-values (TMM), and log2 counts per million (CPMs) were calculated. These values were used for exploratory analysis such as PCA and clustering.

Differential expression analysis was performed using the Bioconductor limma package and the variance modeling at the observational-level transformation using raw read counts of genes with FPKM ≥ 0.1. A *Q* value threshold < 0.05 (for comparison of CPP vs PBS) or *P* value threshold < 0.05 (for comparison of MSU vs PBS) and a minimum FC of 2 were used to define differentially expressed genes (Supplementary Data S3).

Pathway enrichment analysis. The pathway enrichment analysis was performed on the shinyGO 0.80 platform (http://bioinformatics.sdstate.edu/go/). A database of HALLMARKS was selected.

Gene expression correlation analysis. The Spearman rank correlation coefficient was applied to perform pairwise correlation of SPD/spermine N-acetyltransferase 1 (*SAT1*) with other genes by using the bigomics.ch platform. The list of *SAT1*-correlated genes was shown, and we also used this list to explore pathway enrichment analysis by shinyGO 0.80.

Liver transcriptome analysis. *RNA isolation.* Total liver RNA was isolated using the RNeasy kit (Qiagen) by Alithea Genomics SA. The RNA quantity and quality of the RNA was determined using a NanoDrop spectrophotometer (Thermo Fisher Scientific) and the concentration normalized to 100 ng/uL.

Library preparation and sequencing. The generation of bulk RNA barcoding and sequencing (BRB-seq) libraries was performed using the MERCURIUS BRB-seq library preparation kit for Illumina following the manufacturer's manual (Alithea Genomics, #10813).[29] The library was sequenced on an Illumina Novaseq 6000.

Alignment and quantification. In this study, we applied STARsolo v2.7.9a to align and quantify the raw barcodes RNA sequencing reads against the GRCh38.104 (human) genome.[29] We used the parameters "–soloUMIdedup NoDedup 1MM_Directional" and "–quantMode GeneCounts."[30] We generated raw and unique molecular identifier–deduplicated count matrixes, opting for nondeduplicated counts for subsequent analyses.

Unsupervised analysis. The raw data with ensemble gene IDs and their raw counts were processed in iDEP2.01 (http://bioinformatics.sdstate.edu/idep/), an R language-based platform. For exploratory purposes (eg, clustering and visualization), raw counts were imported into R using the Bioconductor edgeR package, and normalized log2 CPMs were computed using the TMM method. Genes with a minimum CPM of 0.5 in at least one sample were retained. Differential expression analysis was performed using the Bioconductor DEseq2 package. An adjusted *P* value threshold of < 0.05 and a minimum log2 FC of 1 were used to define differentially expressed genes.

Gene set enrichment analysis. Gene set enrichment analysis (GSEA) was performed using the preranked fast and easy GSEA method on iDEP v2.01, with the Kyoto Encyclopedia of Genes and Genomes (KEGG) database as reference. Genes were ranked by log2 FC. A false discovery rate cutoff of 0.05 was applied to identify significant pathways. Results were visualized using the hierarchical tree view showing up-regulated (red) and down-regulated (blue) pathways.

RESULTS

IF reduces crystal-induced inflammation. To investigate whether IF prevents crystal-induced inflammation, we used the air pouch model and compared the inflammatory response between mice fed ad libitum, hereafter referred to as ND, and mice fasted for two nonconsecutive days per week (no food for 24 hours, water provided ad libitum), referred to as IF (Figure 1A). During the fasting day, mice lost approximately 8% to 14% of their weight, which was restored on the next refeeding day (Supplementary Figure S1A). Compared with the injection of PBS, injection of MSU or CPP crystals into the air pouch cavity provoked inflammation in ND mice, characterized by increased infiltration of inflammatory cells and higher production of inflammatory cytokines (IL-1β and CXCL-1) in air pouch lavages (Figure 1B–D) and higher inflammatory score of air pouch membranes (Figure 1E and F).

This crystal-induced inflammation was substantially diminished by IF with reduction of number of inflammatory cells and concentration of inflammatory cytokines (IL-1β and CXCL-1) in air pouch lavages and decrease of inflammation score (Figure 1B–F). Next, we explored whether IF could reduce the inflammation in a curative aspect. To test this hypothesis, we first provoked inflammation by crystal injection and then compared the inflammatory response between mice fed ad libitum and mice fasted overnight for 15 hours (Supplementary Figure S1B). We observed that 15-hour fasted mice developed lower inflammation than mice fed ad libitum with decreased cell numbers in air pouch lavages and inflammatory score of air pouch membranes (Supplementary Figure S1C, E, and F). However, this short 15-hour fasting period was not sufficient to modulate IL-1β production (Supplementary Figure S1D). Altogether, these results suggest that IF has anti-inflammatory properties that allow regulation of crystal-induced inflammation.

IF modulates liver metabolomics and transcriptomics profiles. To assess systemic metabolic changes associated with IF, we performed metabolomics and transcriptomics analysis of the liver, an organ that plays a central role in metabolism (Figure 2A–G). All biologic samples were collected at the end of the second fasting day and 6 hours after crystal or PBS injection into the air pouch cavity (Figure 1A). We observed that two nonconsecutive days of fasting highly modified liver metabolisms. The PCA of metabolites and transcript expressions revealed two distinct profiles between IF and ND mice (Supplementary Figure S2A and B). In contrast, crystal stimulation had little impact on liver metabolite and transcriptome profiles in both IF and ND mice (Supplementary Figure S2A–F). Thus, local air pouch crystal inflammation had little effect on liver metabolism, which was highly modulated by IF (Supplementary Figure S2A and B). IF changed the liver abundance of 163 metabolites including an increase of 73 and a reduction of 90 (Figure 2A and B; Supplementary Data S1). Similarly, IF altered the expression of 2,394 genes including up-regulation of 1,263 and down-regulation of 1,131 (Figure 2E and F; Supplementary Data S2). A list of all metabolites detected by ultra high-performance liquid chromatography high-resolution mass spectrometry and transcripts is in Supplementary Data S1 to S3.

Using interactive pathway explorer v3 software (iPATH3; https://pathways.embl.de/ipath3.cgi), we observed that IF modulated four major metabolism pathways including metabolisms of carbohydrates, fatty acids, and amino acids and the tricarboxylic acid (TCA) cycle (Figure 2C). During IF, the abundance of metabolites involved in carbohydrate metabolism was reduced whereas that involved in the three other pathways enriched. Interestingly, IF increased the liver abundance of well-known anti-inflammatory metabolites such as ketone body BHB, corticosterone, and unsaturated fatty acids (oleic acid, eicosapentaenoic acid) (Supplementary Data S1).[31–33] In contrast, the liver abundance of SPD, which had also anti-inflammatory properties, was decreased during IF. KEGG pathway enrichment analysis showed that IF enriched carbohydrate, fatty acid, and amino acid pathways (Figure 2D). Similarly, the GSEA of liver transcriptome confirmed the same enrichment pathways, specifically fatty acid degradation and elongation, biosynthesis of unsaturated fatty acid, amino acid metabolisms, and biosynthesis such as alanine, aspartate, glutamate, and arginine (Figure 2E–G). These results suggest that during IF, a state of nutrient deprivation, particularly of glucose, the liver favors the catabolism of fatty acids, amino acids, and the TCA cycle to ensure energy production and cellular homeostasis. These metabolism changes may promote the production of metabolites with anti-inflammatory properties to reduce inflammation, which is a condition of high energy expenditure.[16,31,34,35]

IF modulates concentration of SPD in serum and air pouch membrane. We next analyzed metabolic changes in systemic (serum) and local (air pouch membrane) compartments during crystal-induced inflammation in ND and IF mice. As observed in the liver, PCA of sera showed two distinct profiles between ND and IF mice whereas the metabolite profiles of PBS and crystal stimulation overlapped no matter the dietary regimen (Figure 3A). Serum abundances of 111 metabolites were modified during IF including an increase of 69 and a decrease of 42 (Figure 3B). Importantly, we observed that fasting also increased the serum abundance of anti-inflammatory metabolites. Some of them were previously identified in liver and others were not, such as acetyl carnitine and SPD.[22,36,37] Enrichment pathway analysis showed that IF increased serum metabolites involved in amino acid metabolism including the proline and arginine pathway (Figure 3C). Arginine is the precursor of the polyamine pathway and leads to the production of putrescine and SPD (Figure S3A).

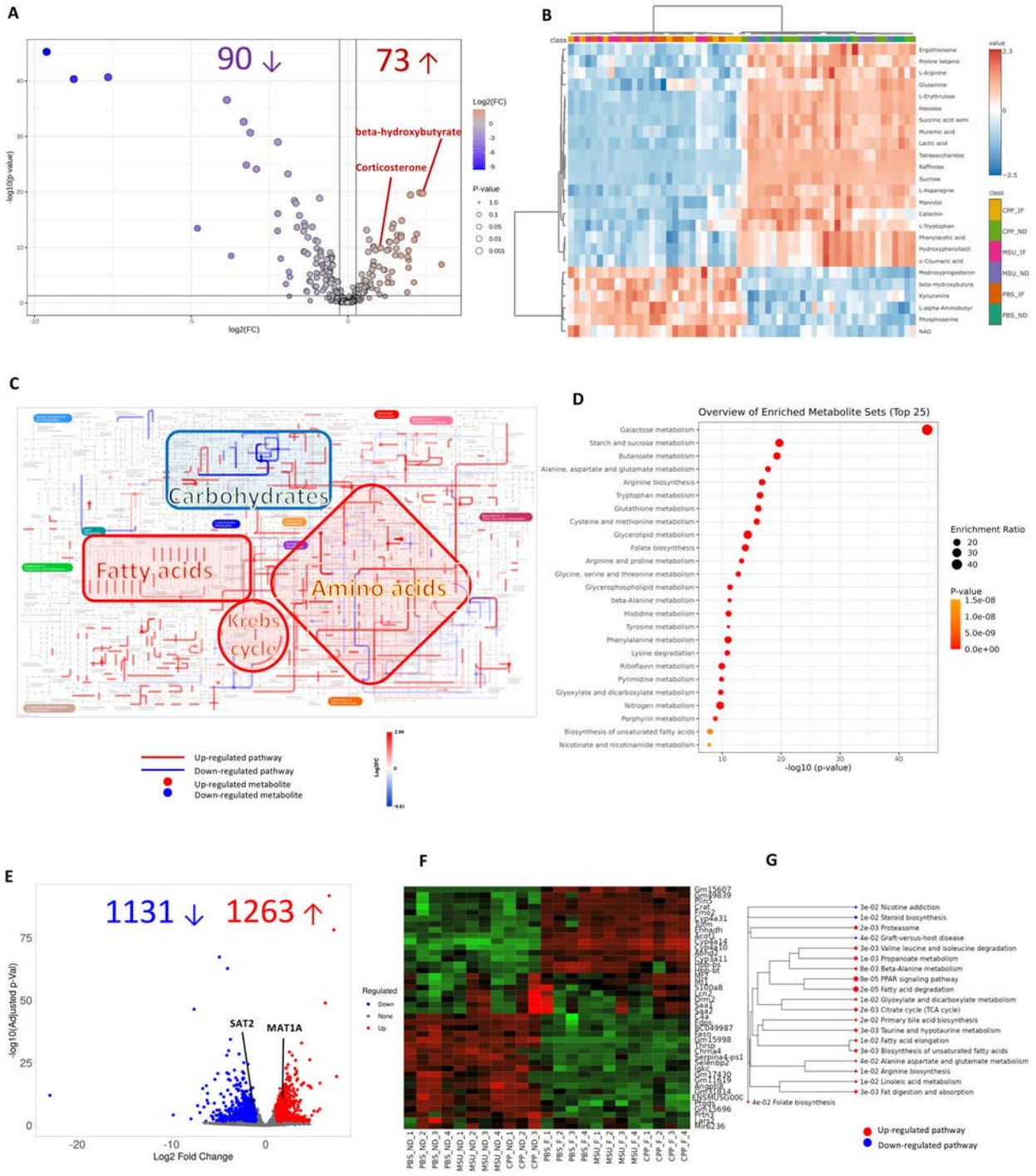

Figure 2. IF changes four main pathways of liver metabolisms. (A) Volcano plot showing the metabolite modification compared between IF (n = 12) and ND (n = 11) (FC cutoff = 1.2, adjusted $P < 0.05$). Up-regulated metabolites are shown on the right in orange, and down-regulated metabolites are in blue on the left. (B) Clustering heatmap of the metabolite modifications in liver of all groups. (C) Mapping of metabolome modification highlighted four main pathway groups (carbohydrate metabolism, fatty acid metabolism, TCA cycle, and amino acid metabolism). Up-regulation was shown in red and down-regulation in blue. (D) Kyoto Encyclopedia of Genes and Genomes pathway enrichment analysis with top 25 enriched metabolite set compared between IF and ND. (E) Transcriptomic modification was shown in a volcano plot (log2 FC cutoff = 1, adjusted $P < 0.05$; n = 23 mice for IF and ND). Significant overexpression genes are shown on the right in red, and underexpressed genes are in blue on the left. (F) A heat map shows in detail the most regulated genes in all the samples (up-regulation in red and down-regulation in green). (G) Gene set enrichment analysis compared between IF and ND. Up-regulated pathways are in red, and down-regulated ones are in blue. CPP, calcium pyrophosphate; FC, fold change; IF, intermittent fasting; MSU, monosodium urate; NAD, nicotinamide adenine dinucleotide; ND, normal diet; PBS, phosphate-buffered saline; TCA, tricarboxylic acid. Color figure can be viewed in the online issue, which is available at http://onlinelibrary.wiley.com/doi/10.1002/art.43367/abstract.

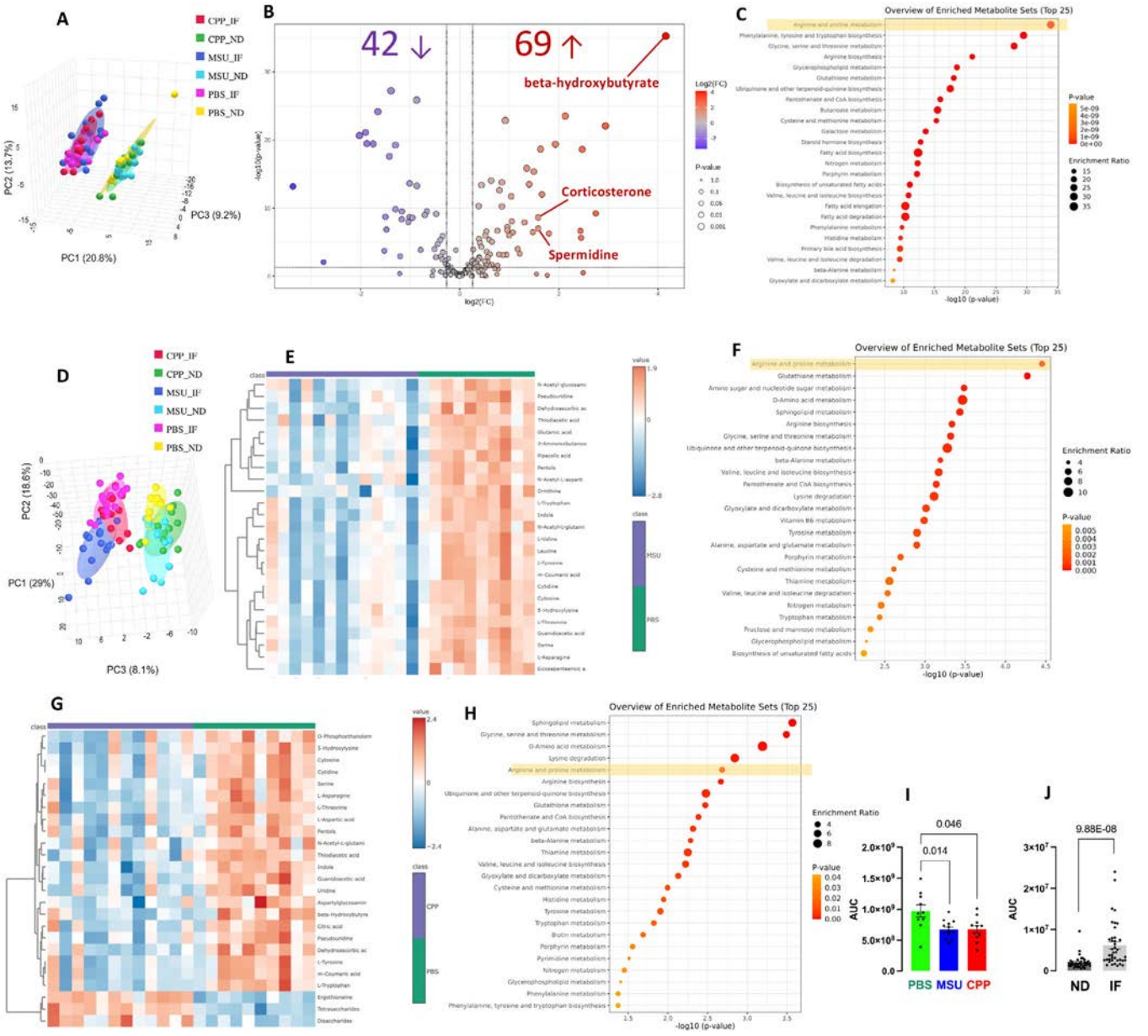

Figure 3. Spermidine abundance was increased in the serum after IF but reduced in the membrane after crystal stimulation (A) Principal component analysis of all six groups (IF and ND) stimulated by PBS, MSU, and CPP (in the serum). (B) Volcano plot shows up-regulated (in red) and down-regulated (in purple) metabolites compared between IF and ND groups ($P < 0.05$; FC cutoff = 1.2, and n = 40 IF and 35 ND). (C) Kyoto Encyclopedia of Genes and Genomes pathway enrichment analysis (top 25 pathways) compared between IF and ND groups between ND (n = 35) and IF (n = 40) (in serum). (D) Principal component analysis of all six groups (IF n = 43 and ND n = 35) stimulated by PBS, MSU, and CPP (in the membrane). (E and G) Clustering heatmap shows expression changes of metabolites in (E) pairs of MSU (n = 13) versus PBS (n = 10) and (G) CPP (n = 12) versus PBS (n = 10) groups (in ND membrane). (F and H) Kyoto Encyclopedia of Genes and Genomes pathway enrichment analysis (top 25 pathways) compared between MSU or CPP versus PBS groups (ND membrane). (I) Comparisons of spermidine abundances in air pouch membranes between groups stimulated with PBS (n = 10) versus MSU (n = 13) or CPP (n = 11) crystals, values are mean ± SEM with one-way analysis of variance with the Sidak multiple comparison test. (J) Comparison of serum spermidine abundances between the IF (n = 43) and ND (n = 35) groups, values are mean ± SEM with two-tailed unpaired *t*-test. adj, adjusted; AUC, area under the curve; CoA, coenzyme A; CPP, calcium pyrophosphate; FC, fold change; IF, intermittent fasting; MSU, monosodium urate; ND, normal diet; PBS, phosphate-buffered saline. Color figure can be viewed in the online issue, which is available at http://onlinelibrary.wiley.com/doi/10.1002/art.43367/abstract.

In contrast to the serum, the production of metabolites in the air pouch membrane was modulated by both crystal inflammation and IF (Figure 3D). PCA analysis showed that the effect of fasting was superior to crystal stimulation. Compared with PBS stimulation, MSU and CPP crystal stimulation decreased the abundance of 102 and 51 metabolites, respectively, in ND mice (Figure 3E and G; Supplementary Figure S3C and D). Interestingly, MSU and CPP crystal stimulation reduced the abundance

of anti-inflammatory metabolites identified in liver and serum (Figure 3E, G, and Figure S3B; Supplementary Data S1). Notably, the proline and arginine pathway was also enriched in the air pouch membrane after crystal stimulation (Figure 3F and H). Overall, we observed that crystal stimulation locally decreased the production of anti-inflammatory metabolites, whereas fasting enhances their production in liver and their abundance in blood stream (serum). These anti-inflammatory metabolites may contribute to the anti-inflammatory effect of IF.

SPD supplementation reduces microcrystal-induced inflammation. BHB and SPD are two metabolites with anti-inflammatory properties.[22,31,36] Their abundance increased during IF but reduced during crystal-induced inflammation, suggesting that they might contribute to the anti-inflammatory effect of IF (Figure S3B). The efficacy of BHB to reduce MSU crystal inflammation is known whereas that of SPD remains unexplored.[31,36,38] Crystal stimulation or IF modulated the abundance of metabolites related to the polyamine pathway in liver, serum, and the air pouch membrane (Figure 3I, J, Figure S3B). To test whether SPD reduced crystal inflammation, we first performed in vitro experiments using human THP-1 cell line and mouse bone marrow–derived macrophages (Figure 4A). SPD supplementation dose-dependently decreased THP-1 production of IL-1β and TNF induced by MSU and CPP crystal stimulation (Figure 4B and C). Similarly, SPD reduced the production of inflammatory cytokines (IL-1β and CXCL-1) by bone marrow–derived macrophages stimulated by crystals (Figure 4H and I). SPD also reduced crystal-induced cell death, as suggested by the diminution of lactate dehydrogenase release in cell culture supernatants (Figure 4D). Finally, we observed that SPD inhibited IL-1β production through modulation of the two steps of IL-1β activation by reducing NF-κB activation (Figure 4E) and ASC speck formation (Figure 4F and G). These results suggest that SPD has a broad anti-inflammatory effect, acting on inflammasome NLRP3-dependent and -independent cytokines.

We next confirmed the anti-inflammatory effect of SPD in vivo (Figure 5A). Supplementation of high-purity SPD in drinking water (6 mM, 21 days) and in the air pouch (1 injection of 100 mg/kg) prevented the inflammation induced by crystal injection, as shown by a significant reduction in cell number and inflammatory cytokine (IL-1β and CXCL-1) concentration in air pouch lavage and a decrease of inflammatory score of air pouch membranes (Figure 5B–G). Interestingly, this inflammation decrease was associated with an increased ratio of M2/M1 macrophages in the air pouch membrane, which was also observed during IF (Supplementary Figure 4A–D). These results suggested that IF and SPD supplementation favored M2 macrophage polarization. Next, we investigated the effect of intrapouch supplementation alone. We observed that one injection of SPD (100 mg/kg) into the air pouch was not sufficient to prevent MSU crystal-induced inflammation but did lower the concentration of CXCL-1 in air pouch lavages (Supplementary Figure 5A–E).

Inhibition of *SAT1* reduces crystal inflammation. Our results suggest that SPD contributes to the prevention of crystal inflammation during IF. We then performed transcriptomic analysis on THP-1 cells to investigate whether crystal stimulation modulates the expression of genes involved in the polyamine pathway in monocytes and macrophages, which are central cells involved in crystal detection and crystal-induced inflammation (Figure 6A). We observed that MSU and CPP crystals induced a roughly similar gene expression by PMA-primed THP-1 cells compared with PBS stimulation. Expression of 74 genes was modified by MSU crystal stimulation compared with PBS stimulation, including increased expression of 65 genes and reduced expression of 9 genes (Figure 6B). Interestingly, HALLMARKS pathway enrichment analysis indicated that MSU and CPP crystals mainly enriched the same pathways, especially TNF signaling via the NF-κB pathway (Figure 6C).

Next we focused our analysis on the expression of genes involved in the polyamine pathway and found that expression of the *SAT1* gene was up-regulated after MSU and CPP crystal stimulation (Figures 3I and 6D). Interestingly, *SAT1* gene expression correlated with that of numerous genes (Figure 6E) that were associated with TNF signaling via the NF-κB pathway (Figure 6F). These results suggest that increased expression of *SAT1* induced by crystals may contribute to crystal inflammation. To address this hypothesis, we down-regulated *SAT1* expression using small interfering RNA (siRNA). *SAT1* siRNA reduced *SAT1* expression by 60% compared with control siRNA (Figure 6G) and also reduced IL-1β production induced by MSU and CPP crystals (Figure 6H).

Collectively, our study reveals that IF prevents crystal-induced inflammation through modulation of systemic and local metabolism pathways leading to the production of anti-inflammatory metabolites such as BHB, corticosterone, and SPD. SPD supplementation acts as IF mimetics and prevents crystal-induced inflammation through inhibition of NF-κB and NLRP3 inflammasome. Similarly, down-regulation of *SAT1* expression diminishes crystal inflammation (Figure 6H).

DISCUSSION

IF together with CR, alternate-day fasting, and time-restricted feeding are nutrition strategies that improve age-related and inflammatory diseases including serum transfer arthritis (K/BxN mouse model).[15,16,21,39–41] Here, we provided evidence that a short-time IF in mice prevented crystal-induced inflammation through modulation of local and systemic cell metabolisms including enrichment of amino acids and fatty acid pathways and promotion of M2 macrophage polarization. IF decreased the in vivo production of IL-1β and CXCL-1 provoked by crystal

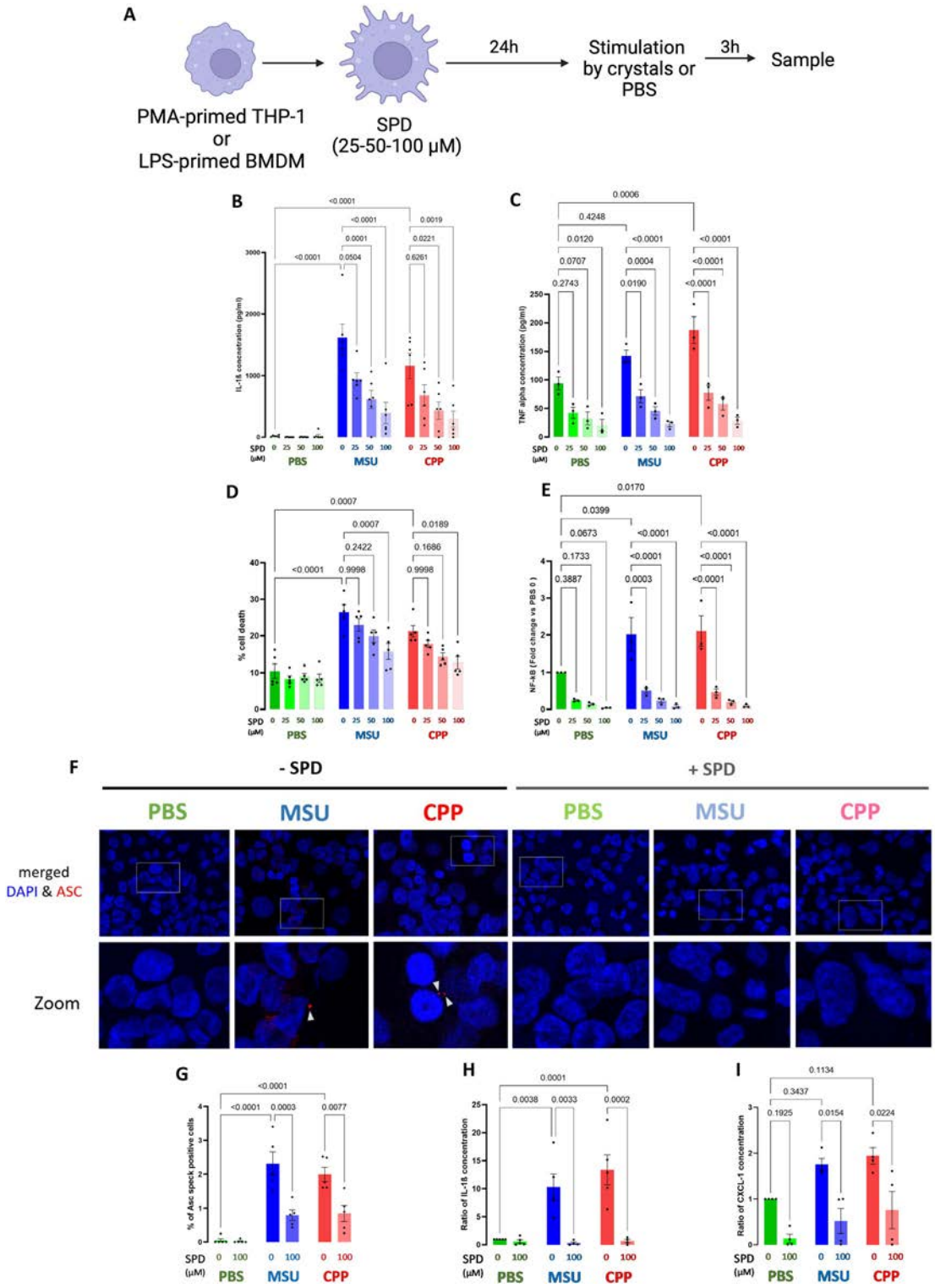

Figure 4. SPD supplementation reduces crystal-induced inflammation in vitro. (A) Illustration of in vitro protocols assessing SPD supplementation in PMA-primed THP-1 and LPS-primed BMDM cells. (B) IL-1β and (C) TNF production quantified by enzyme-linked immunosorbent assay. (D) Lactate dehydrogenase release in culture supernatants. (E) NF-κB activity was assessed by measuring luciferase activity. (F and G) ASC specks formation was assessed by confocal microscopy. An arrow head indicated (F) ASC speck formation (red dots); (G) quantification of ASC speck. (H) IL-1β and (I) CXCL-1 production by BMDMs simulated by PBS or crystals in the presence or not of SPD. Values are mean ± SEM, two-way analysis of variance with the Sidak multiple comparison test; n = 3 to 6 independent experiments. BMDM, bone marrow–derived macrophage; CPP, calcium pyrophosphate; IL-1β, interleukin-1β; LPS, lipopolysaccharide; MSU, monosodium urate; PBS, phosphate-buffered saline; PMA, phorbol myristate acetate; SPD, spermidine; TNF, tumor necrosis factor. Color figure can be viewed in the online issue, which is available at http://onlinelibrary.wiley.com/doi/10.1002/art.43367/abstract.

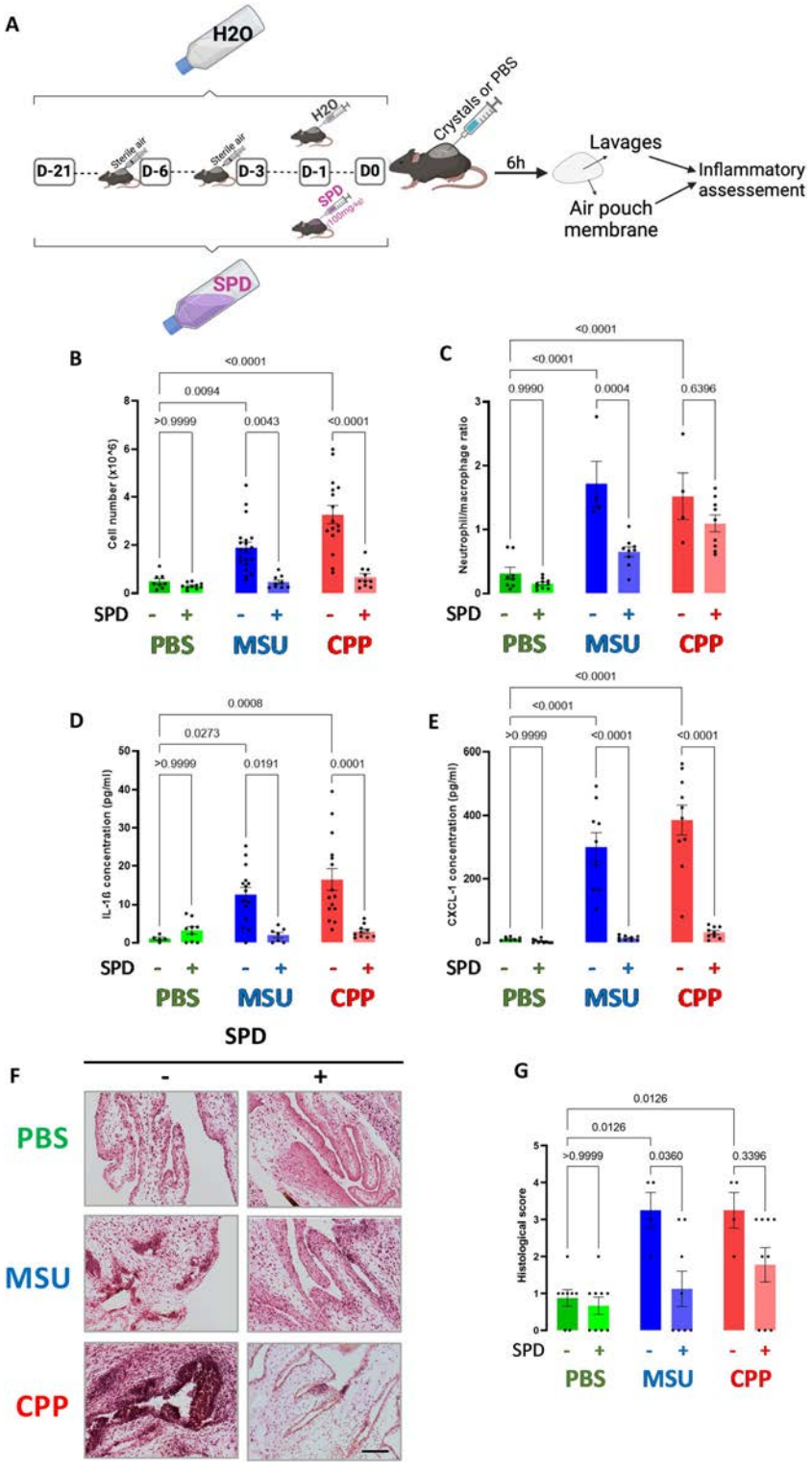

Figure 5. SPD supplementation prevents crystal-induced inflammation in vivo. (A) Mice drank either water or water containing SPD (6 mM) for 21 days. One day before inflammation provoked by crystal stimulation, SPD (10 mg/kg) or water was injected into the air pouch. Inflammation was assessed after 6 hours of stimulation. (B–G) Level of crystal-induced inflammation between mice with/without SPD supplementation assessing (B) in-cell infiltration, (C) ratio of neutrophils/macrophages, (D) production of IL-1β, (E) CXCL-1 in air pouch washing liquids, and (F and G) inflammatory score of air pouch membrane assessed by hematoxylin & eosin staining. Scale bar = 100 μm. Values are mean ± SEM, two-way analysis of variance with the Sidak multiple comparison test; n = 4 to 15 mice per group. CPP, calcium pyrophosphate; IL-1β, interleukin-1β; MSU, monosodium urate; PBS, phosphate-buffered saline; SPD, spermidine. Color figure can be viewed in the online issue, which is available at http://onlinelibrary.wiley.com/doi/10.1002/art.43367/abstract.

stimulation, confirming that IF had broad anti-inflammatory effects affecting the inflammasome NLRP3-dependent and -independent cytokines as previously reported in other inflammatory models and in humans.[39–41] For example, the transcript levels of *IL-1β*, *TNF*, *NLRP3*, and *IL-18* were lower in unstimulated monocytes isolated from 19 volunteers after 24-hour fasting than in monocytes isolated from same volunteers 3 hours after refeeding. Upon lipopolysaccharide (LPS) and ATP stimulation, the production of IL-1β and TNF was lower in peripheral blood mononuclear cells (PBMCs) and monocytes isolated after the fasting period than in cells isolated after refeeding time.[40] In another study involving 20 healthy volunteers, 36 hours of fasting highly modulated plasma metabolomes and plasma inflammatory potential. Plasma drawn 36 hours after fasting had a lower capacity to stimulate the production of reactive oxygen species and TNF and the activity of cyclooxygenase and nitric oxide synthase than plasma collected 2 hours after refeeding. Fasted plasma had a lower ability to induce macrophage M1 polarization than fed plasma while favoring macrophage M2 polarization.[42] Several factors contributed to the anti-inflammatory effect of IF such as the diminution of the NF-κB activity in PBMCs and monocytes, decrease of plasma oxidative stress potential, and enhanced production of anti-inflammatory metabolites such as ketone bodies, SPD, 1-methylnicotinamide, palmitoylethanolamide, and oleoylethanolamide.[40,42]

Here, we also observed that IF enhanced local or systemic (liver and serum) abundance of metabolites with anti-inflammatory properties such as ketone body BHB, corticosterone, and SPD. Ketones bodies derived from fatty acid oxidation that occurred in the liver during a fasting period and were used as a major alternative source of energy by numerous tissues, especially the brain. Ketone body concentration increased within 8 to 12 hours after the onset of fasting in humans and within 4 to 8 hours in rodents.[40,43] BHB inhibited NLRP3 inflammasome activation and IL-1β production by mouse or human macrophages, human neutrophils, and PBMCs stimulated by MSU crystals, silica particles, or other inflammasome activators.[31,36,44] BHB-reduced NLRP3 inflammasome and IL-1β production through the inhibition of NF-κB and class I histone deacetylase (HDAC). In this study, we did not assess whether the increased level of BHB contributed to the reduction of crystal inflammation by IF.

We uncovered the capacity of SPD to reproduce the anti-inflammatory effect of IF and to reduce MSU and CPP crystal inflammation, adding two new inflammatory diseases to the list of diseases improved by SPD. Endogenous SPD biosynthesis was essential for the anti-inflammatory effect of IF in a different mouse model of joint inflammation, namely K/BxN serum transfer arthritis. In this model, both genetic deletion and pharmacologic inhibition of ODC1, the enzyme responsible for the rate-limiting step of polyamine synthesis, suppressed the anti-inflammatory effect of IF.[21] Here, we observed that ODC inhibition by DFMO did not reverse the effect of IF (Supplementary Figure 6A–C). However, we had tested only one dose of DFMO (0.5%), which was two times lower than the dose used in the K/BxN model.[21] In addition, we did not know whether this dose of DFMO effectively inhibited SPD production. Further studies are necessary to address whether suppression of crystal inflammation by IF relied on SPD synthesis.

We observed enrichment of the arginine/proline pathway during IF in liver, air pouch membrane, and serum. The same observation was recently reported showing that the polyamine pathway was stimulated during IF in several mouse tissues (kidney, muscle, intestine, pancreas, and heart) and several human cell lines and PBMCs.[21,42] Collectively, these results suggested that IF enhanced endogenous biosynthesis of SPD. Interestingly, we observed that the abundance of SPD and putrescine was decreased in liver during IF as also reported by Hofer et al.[21] This decrease in the liver might reflect an active export of SPD into the blood stream to ensure its systemic effect. This hypothesis is supported by (1) the decreased expression of *SAT2* in the liver during IF, which might promote SPD pool; (2) the up-regulation of methionine adenosyltransferase 2A, which also promotes SPD formation; and (3) the fact that the liver expressed several polyamine transporter genes including *ATP13A2*, *ATP13A3*, *SLC3A2*, and *SLC18B1*.[45–47]

SPD reduces inflammation through several mechanisms. SPD is a major activator of autophagy and most SPD biology effects, especially geroprotection, cardioprotection, and suppression of inflammation, depend on autophagy activation.[21,22,24,48] SPD activates autophagy through hypusination of eukaryotic initiation factor 5A (eIF5A) and induction of the lysosome biogenesis and mitogenesis transcription factor EB (TFEB).[21,48] Hypusination is a posttranslational modification of a specific lysine residue in eIF5A and strictly depends on SPD. Hypusination of eIF5A leads to its activation, which promotes the expression of autophagy-related genes and TFEB. SPD also activates autophagy through regulation of acetylation status of cytoplasmic and nuclear proteins. SPD inhibits acetyltransferases while stimulating deacetylases, which favors autophagy activation. For example, SPD inhibits acetyltransferase E1A binding protein P300 while stimulating sirtuins and histone deacetylases (eg, HDAC).[21,24,40]

In addition, polyamine catabolism necessitates consumption of acetyl coenzyme A (CoA), which depletes acetyl-CoA pools and favors protein deacetylation and autophagy activation. Here, our data suggested that reduction of crystal inflammation by SPD involved at least three different mechanisms. First, it might be because of modulation of protein acetylation. This hypothesis was based on (1) induction of *SAT1* expression in primed THP-1 monocytes stimulated by MSU and CPP crystals and (2) down-regulation of *SAT1* expression, which reduced IL-1β production provoked by crystal stimulation. Second, we observed that SPD inhibited crystal-induced NF-κB activity and NLRP3 inflammasome-induced ASC speck formation as previously

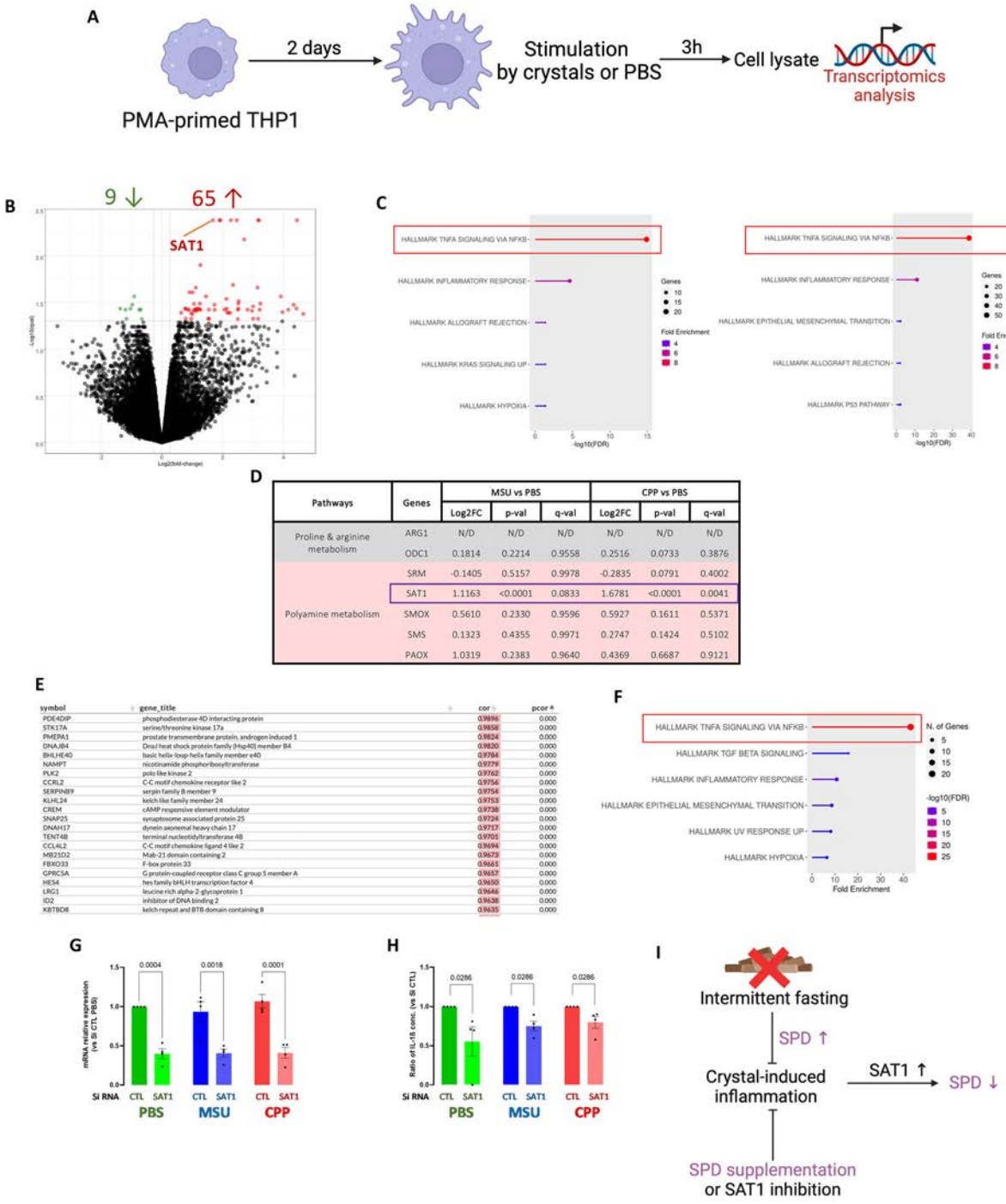

Pathways	Genes	MSU vs PBS			CPP vs PBS		
		Log2FC	p-val	q-val	Log2FC	p-val	q-val
Proline & arginine metabolism	ARG1	N/D	N/D	N/D	N/D	N/D	N/D
	ODC1	0.1814	0.2214	0.9558	0.2516	0.0733	0.3876
Polyamine metabolism	SRM	-0.1405	0.5157	0.9978	-0.2835	0.0791	0.4002
	SAT1	1.1163	<0.0001	0.0833	1.6781	<0.0001	0.0041
	SMOX	0.5610	0.2330	0.9596	0.5927	0.1611	0.5371
	SMS	0.1323	0.4355	0.9971	0.2747	0.1424	0.5102
	PAOX	1.0319	0.2383	0.9640	0.4369	0.6687	0.9121

symbol	gene_title	cor	pcor
PDE4DIP	phosphodiesterase 4D interacting protein	0.9896	0.000
STK17A	serine/threonine kinase 17a	0.9858	0.000
PMEPA1	prostate transmembrane protein, androgen induced 1	0.9824	0.000
DNAJB4	DnaJ heat shock protein family (Hsp40) member B4	0.9820	0.000
BHLHE40	basic helix-loop-helix family member e40	0.9784	0.000
NAMPT	nicotinamide phosphoribosyltransferase	0.9779	0.000
PLK2	polo like kinase 2	0.9762	0.000
CCRL2	C-C motif chemokine receptor like 2	0.9756	0.000
SERPINB9	serpin family B member 9	0.9754	0.000
KLHL24	kelch like family member 24	0.9753	0.000
CREM	cAMP responsive element modulator	0.9738	0.000
SNAP25	synaptosome associated protein 25	0.9724	0.000
DNAH17	dynein axonemal heavy chain 17	0.9717	0.000
TENT4B	terminal nucleotidyltransferase 4B	0.9701	0.000
CCL4L2	C-C motif chemokine ligand 4 like 2	0.9694	0.000
MB21D2	Mab-21 domain containing 2	0.9673	0.000
FBXO33	F-box protein 33	0.9661	0.000
GPRC5A	G protein-coupled receptor class C group 5 member A	0.9657	0.000
HES4	hes family bHLH transcription factor 4	0.9650	0.000
LRG1	leucine rich alpha-2-glycoprotein 1	0.9646	0.000
ID2	inhibitor of DNA binding 2	0.9638	0.000
KBTBD8	kelch repeat and BTB domain containing 8	0.9635	0.000

Figure 6. Down-regulation of *SAT1* expression reduces crystal-induced inflammation. (A) Illustration of in vitro experiment for transcriptomics analysis in THP-1 cells stimulated by crystals. (B) Volcano plot shows up-regulated (in red) and down-regulated (in green) expression of genes by PMA-primed THP-1 stimulated with MSU crystals or PBS ($P < 0.05$, FC cutoff = 1.2, n = 3 independent experiments). (C) HALLMARKS pathway enrichment analysis compared between MSU/CPP and PBS stimulations. (D) Effect of MSU and CPP crystals on enzyme-coding genes involved in proline, arginine, and polyamine metabolism pathways. (E) Top of correlated genes with *SAT1*. (F) HALLMARKS enrichment pathways associated with *SAT1*-correlated genes. (G) *SAT1* gene expression after SiRNA treatment was assessed by quantitative reverse transcription polymerase chain reaction. (H) IL-1β quantification by enzyme-linked immunosorbent assay. (I) Summary of results. Values are mean ± SEM, two-way analysis of variance with the (H) Sidak multiple comparison test and (I) Mann-Whitney test; n = 4 independent experiments. ARG1, arginase 1; CPP, calcium pyrophosphate; CTL, control; FC, fold change; FDR, false discovery rate; mRNA, messenger RNA; MSU, monosodium urate; N/D, not detectable; ODC1, ornithine decarboxylase 1; PAOX, polyamine oxidase; PBS, phosphate-buffered saline; PMA, phorbol myristate acetate; *SAT1*, spermidine/spermine N-acetyltransferase 1; SiRNA, small interfering RNA; SMOX, spermine oxidase; SMS, spermine synthase; SRM, spermidine synthase; TGF, transforming growth factor; TNFA, tumor necrosis factor α. Color figure can be viewed in the online issue, which is available at http://onlinelibrary.wiley.com/doi/10.1002/art.43367/abstract.

reported in RAW 264.7 macrophages stimulated by LPS.[49] And third, SPD promoted M2 macrophage differentiation.

SPD and polyamine production is an evolutionary conserved pathway. SPD abundance depends on diet, intestinal microbiota production, intestinal uptake, cell metabolisms, and urinary excretion. SPD production seems to be decreasing with age because of a reduction of activity of enzymes involved in polyamine synthesis. This aging decline of SPD may contribute to age-related degenerative and cardiovascular diseases and age-related-inflammation and inflammatory diseases including CPP. Consequently, avoiding SPD reduction may influence and prevent or delay their development. This can be achieved through IF, consumption of SPD-rich foods (durian fruit, wheat germ, fermented milk and soy such as mature cheeses and natto, mushrooms, and nuts), and stimulation of intestinal microbiota production through food supplements containing the SPD precursor arginine and probiotics.[22,24] Several ongoing clinical trials assess the effect of SPD supplementation on neuronal and cardiovascular functions (NCT05128331) and on inflammation (NCT05017428).

This work has limitations. First, we did not fully characterize how IF prevented crystal-induced inflammation although we conducted a large analysis that permitted comprehensive characterization of metabolomics modulation by IF on different compartments including liver, serum, and an inflamed compartment (air pouch membrane). This analysis identified that IF changed the abundance of multiple pro- and anti-inflammatory metabolites. Second, this analysis did not give the exact concentration of metabolites but solely their relative abundance changes. Third, we did not assess whether SPD supplementation reproduced metabolites modifications induced by IF, especially whether SPD supplementation permitted obtaining same abundance of SPD observed during IF. Fourth, our study did not investigate whether oral SPD supplementation alone was able to prevent crystal inflammation. However, we observed that local SPD supplementation by one intrapouch injection with a high concentration of SPD had only a mild effect and was not sufficient to prevent crystal inflammation. Fifth, we did not assess the contribution of other metabolites in the anti-inflammatory effect of IF. This latter effect may be secondary to a combination of both increased production of anti-inflammatory metabolites and decreased production of proinflammatory metabolites, along with modulation of autophagy, macrophage phenotypes, and other immune cells. Lastly, mechanistic studies are necessary to characterize how the combination of oral and intrapouch SPD supplementation reduces inflammation.

Collectively, IF inhibited crystal inflammation and induced the production of numerous anti-inflammatory metabolites. SPD supplementation contributed to the anti-inflammatory effect of IF and prevented crystal-induced inflammation. These IF mimetics might be used as alternative therapeutic interventions to dampen crystal inflammation.

ACKNOWLEDGMENTS

Figures 1A, 3I, 4A, 5A, 6A, and 6I were created with BioRender.com and released under a Creative Commons Attribution-NonCommercial-NoDerivatives 4.0 International license (https://creativecommons.org/licenses/by-nc-nd/4.0/deed.en).

AUTHOR CONTRIBUTIONS

All authors contributed to at least one of the following manuscript preparation roles: conceptualization AND/OR methodology, software, investigation, formal analysis, data curation, visualization, and validation AND drafting or reviewing/editing the final draft. As corresponding author, Dr Ea confirms that all authors have provided the final approval of the version to be published and takes responsibility for the affirmations regarding article submission (eg, not under consideration by another journal), the integrity of the data presented, and the statements regarding compliance with institutional review board/Declaration of Helsinki requirements.

REFERENCES

1. Cross M, Ong KL, Culbreth GT, et al; GBD 2021 Gout Collaborators. Global, regional, and national burden of gout, 1990-2020, and projections to 2050: a systematic analysis of the Global Burden of Disease Study 2021. Lancet Rheumatol 2024;6(8):e507–e517.
2. Richette P, Bardin T, Doherty M. An update on the epidemiology of calcium pyrophosphate dihydrate crystal deposition disease. Rheumatology (Oxford) 2009;48(7):711–715.
3. Pascart T, Filippou G, Lioté F, et al. Calcium pyrophosphate deposition disease. Lancet Rheumatol 2024;6(11):e791–e804.
4. Richette P, Doherty M, Pascual E, et al. 2018 updated European League Against Rheumatism evidence-based recommendations for the diagnosis of gout. Ann Rheum Dis 2020;79(1):31–38.
5. FitzGerald JD, Dalbeth N, Mikuls T, et al. 2020 American College of Rheumatology guideline for the management of gout. Arthritis Rheumatol 2020;72(6):879–895.
6. Ahern MJ, Reid C, Gordon TP, et al. Does colchicine work? The results of the first controlled study in acute gout. Aust N Z J Med 1987;17(3):301–304.
7. Janssens HJEM, Janssen M, van de Lisdonk EH, et al. Use of oral prednisolone or naproxen for the treatment of gout arthritis: a double-blind, randomised equivalence trial. Lancet 2008;371(9627):1854–1860.
8. Janssen CA, Oude Voshaar MAH, Vonkeman HE, et al. Anakinra for the treatment of acute gout flares: a randomized, double-blind, placebo-controlled, active-comparator, non-inferiority trial. Rheumatology (Oxford) 2019;58(8):1344–1352.
9. Martinon F, Pétrilli V, Mayor A, et al. Gout-associated uric acid crystals activate the NALP3 inflammasome. Nature 2006;440(7081):237–241.
10. Ea HK, Kischkel B, Chirayath TW, et al. Systemic inflammatory cytokine profiles in patients with gout during flare, intercritical and treat-to-target phases: TNFSF14 as new biomarker. Ann Rheum Dis 2024;83(7):945–956.
11. Chirayath TW, Ollivier M, Kayatekin M, et al. Activation of osmosensitive LRRC8 anion channels in macrophages is important for micro-crystallin joint inflammation. Nat Commun 2024;15(1):8179.
12. Martinon F, Pétrilli V, Mayor A, et al. Gout-associated uric acid crystals activate the NALP3 inflammasome. Nature 2006;440(7081):237–241.
13. Renaudin F, Orliaguet L, Castelli F, et al. Gout and pseudo-gout-related crystals promote GLUT1-mediated glycolysis that

governs NLRP3 and interleukin-1β activation on macrophages. Ann Rheum Dis 2020;79(11):1506–1514.
14. Cobo I, Cheng A, Murillo-Saich J, et al. Monosodium urate crystals regulate a unique JNK-dependent macrophage metabolic and inflammatory response. Cell Rep 2022;38(10):110489.
15. Spadaro O, Youm Y, Shchukina I, et al. Caloric restriction in humans reveals immunometabolic regulators of health span. Science 2022; 375(6581):671–677.
16. Longo VD, Mattson MP. Fasting: molecular mechanisms and clinical applications. Cell Metab 2014;19(2):181–192.
17. Madeo F, Carmona-Gutierrez D, Hofer SJ, et al. Caloric restriction mimetics against age-associated disease: targets, mechanisms, and therapeutic potential. Cell Metab 2019;29(3):592–610.
18. Mattison JA, Colman RJ, Beasley TM, et al. Caloric restriction improves health and survival of rhesus monkeys. Nat Commun 2017;8(1):14063.
19. Green CL, Lamming DW, Fontana L. Molecular mechanisms of dietary restriction promoting health and longevity. Nat Rev Mol Cell Biol 2022;23(1):56–73.
20. Dessein PH, Shipton EA, Stanwix AE, et al. Beneficial effects of weight loss associated with moderate calorie/carbohydrate restriction, and increased proportional intake of protein and unsaturated fat on serum urate and lipoprotein levels in gout: a pilot study. Ann Rheum Dis 2000;59(7):539–543.
21. Hofer SJ, Daskalaki I, Bergmann M, et al. Spermidine is essential for fasting-mediated autophagy and longevity. Nat Cell Biol 2024;26(9): 1571–1584.
22. Madeo F, Eisenberg T, Pietrocola F, et al. Spermidine in health and disease. Science 2018;359(6374):eaan2788.
23. Morselli E, Galluzzi L, Kepp O, et al. Autophagy mediates pharmacological lifespan extension by spermidine and resveratrol. Aging (Albany NY) 2009;1(12):961–970.
24. Hofer SJ, Simon AK, Bergmann M, et al. Mechanisms of spermidine-induced autophagy and geroprotection. Nat Aging 2022;2(12): 1112–1129.
25. Chamoto K, Zhang B, Tajima M, et al. Spermidine - an old molecule with a new age-defying immune function. Trends Cell Biol 2024; 34(5):363–370.
26. Yang Q, Zheng C, Cao J, et al. Spermidine alleviates experimental autoimmune encephalomyelitis through inducing inhibitory macrophages. Cell Death Differ 2016;23(11):1850–1861.
27. Schroeder S, Hofer SJ, Zimmermann A, et al. Dietary spermidine improves cognitive function. Cell Rep 2021;35(2):108985.
28. Zeng J, Ye Z, Shi S, et al. Targeted inhibition of eIF5Ahpu suppresses tumor growth and polarization of M2-like tumor-associated macrophages in oral cancer. Cell Death Dis 2023;14(8):579.
29. Alpern D, Gardeux V, Russeil J, et al. BRB-seq: ultra-affordable high-throughput transcriptomics enabled by bulk RNA barcoding and sequencing. Genome Biol 2019;20(1):71.
30. Kaminow B, Yunusov D, Dobin A. STARsolo: accurate, fast and versatile mapping/quantification of single-cell and single-nucleus RNA-seq data. bioRxiv Preprint posted online May 5, 2021. doi: 10.1101/2021.05.05.442755
31. Youm YH, Nguyen KY, Grant RW, et al. The ketone metabolite β-hydroxybutyrate blocks NLRP3 inflammasome-mediated inflammatory disease. Nat Med 2015;21(3):263–269.
32. Nakamura Y, Walker BR, Ikuta T. Systematic review and meta-analysis reveals acutely elevated plasma cortisol following fasting but not less severe calorie restriction. Stress 2016;19(2):151–157.
33. Coniglio S, Shumskaya M, Vassiliou E. Unsaturated fatty acids and their immunomodulatory properties. Biology (Basel) 2023;12(2):279.
34. Borkum JM. The tricarboxylic acid cycle as a central regulator of the rate of aging: implications for metabolic interventions. Adv Biol (Weinh) 2023;7(7):e2300095.
35. Namgaladze D, Brüne B. Macrophage fatty acid oxidation and its roles in macrophage polarization and fatty acid-induced inflammation. Biochim Biophys Acta 2016;1861(11):1796–1807.
36. Goldberg EL, Asher JL, Molony RD, et al. β-hydroxybutyrate deactivates neutrophil NLRP3 inflammasome to relieve gout flares. Cell Rep 2017;18(9):2077–2087.
37. Lin K, Zheng W, Guo M, et al. The intestinal microbial metabolite acetyl l-carnitine improves gut inflammation and immune homeostasis via CADM2. Biochim Biophys Acta Mol Basis Dis 2024;1870(4):167089.
38. Hooftman A, Angiari S, Hester S, et al. The immunomodulatory metabolite itaconate modifies NLRP3 and inhibits inflammasome activation. Cell Metab 2020;32(3):468–478.e7.
39. Pereira M, Liang J, Edwards-Hicks J, et al. Arachidonic acid inhibition of the NLRP3 inflammasome is a mechanism to explain the anti-inflammatory effects of fasting. Cell Rep 2024;43(2): 113700.
40. Traba J, Kwarteng-Siaw M, Okoli TC, et al. Fasting and refeeding differentially regulate NLRP3 inflammasome activation in human subjects. J Clin Invest 2015;125(12):4592–4600.
41. Traba J, Geiger SS, Kwarteng-Siaw M, et al. Prolonged fasting suppresses mitochondrial NLRP3 inflammasome assembly and activation via SIRT3-mediated activation of superoxide dismutase 2. J Biol Chem 2017;292(29):12153–12164.
42. Rhodes CH, Zhu C, Agus J, et al. Human fasting modulates macrophage function and upregulates multiple bioactive metabolites that extend lifespan in *Caenorhabditis elegans*: a pilot clinical study. Am J Clin Nutr 2023;117(2):286–297.
43. de Cabo R, Mattson MP. Effects of intermittent fasting on health, aging, and disease. N Engl J Med 2019;381(26):2541–2551.
44. Cleophas MCP, Crişan TO, Lemmers H, et al. Suppression of monosodium urate crystal-induced cytokine production by butyrate is mediated by the inhibition of class I histone deacetylases. Ann Rheum Dis 2016;75(3):593–600.
45. Sim SI, von Bülow S, Hummer G, et al. Structural basis of polyamine transport by human ATP13A2 (PARK9). Mol Cell 2021;81(22):4635–4649.e8.
46. Eom J, Choi J, Suh SS, et al. SLC3A2 and SLC7A2 mediate the exogenous putrescine-induced adipocyte differentiation. Mol Cells 2022; 45(12):963–975.
47. Hiasa M, Miyaji T, Haruna Y, et al. Identification of a mammalian vesicular polyamine transporter. Sci Rep 2014;4(1):6836.
48. Eisenberg T, Abdellatif M, Schroeder S, et al. Cardioprotection and lifespan extension by the natural polyamine spermidine. Nat Med 2016;22(12):1428–1438.
49. Jeong JW, Cha HJ, Han MH, et al. Spermidine protects against oxidative stress in inflammation models using macrophages and zebrafish. Biomol Ther (Seoul) 2018;26(2):146–156.

Arthritis & Rheumatology
Vol. 78, No. 2, February 2026, pp 463–474
DOI 10.1002/art.43349

American College of Rheumatology
Empowering Rheumatology Professionals

Serum Cytokine Profiling Differentiates Underlying Diseases in Cytokine Storm Syndrome

Shuya Kaneko,[1] Maho Hatano,[1] Asami Shimbo,[1] Futaba Miyaoka,[1] Hitoshi Irabu,[1] Yuko Akutsu,[1] Yuko Hayashi,[2] Mao Mizuta,[3] Yasuo Nakagishi,[3] Keiji Akamine,[4] Naomi Iwata,[5] Kenji Furuno,[6] Takayuki Tanaka,[7] Kazuyuki Ueno,[8] Shuhei Fujita,[8] Koji Yokoyama,[9] Toshinori Minato,[10] Kazushi Izawa,[11] Takahiro Yasumi,[12] Tadashi Matsubayashi,[13] Tadashi Hosoya,[14] Hiroki Nishikawa,[15] Junya Fujimura,[16] Ryoko Asano,[17] Yuko Sugita,[18] Kenichi Watanabe,[19] Anna Kobayashi,[20] Takuya Endo,[21] Katsuhide Eguchi,[22] Ryuta Nishikomori,[23] Ryuhei Yasuoka,[24] Takaki Asano,[25] Miyako Kanno,[26] Kazuya Hamada,[27] Yuji Fujita,[28] Daisuke Hayashi,[29] Shojiro Watanabe,[30] Takeshi Shiba,[31] Shinsuke Yasuda,[14] Masaaki Mori,[32] Hirokazu Kanegane,[33] Masatoshi Takagi,[1] and Masaki Shimizu[2]

Objective. Cytokine storm syndrome (CSS), commonly associated with hemophagocytic lymphohistiocytosis (HLH), is a fatal hyperinflammatory syndrome. Differentiating the underlying diseases responsible for CSS is essential for timely therapeutic decisions. This study explored the clinical usefulness of serum cytokine profiling in distinguishing underlying diseases in patients with CSS.

Methods. Serum samples were collected from 143 adult and pediatric patients with CSS and 22 healthy controls. The cohort included patients with various diagnoses of primary and secondary HLH and Kawasaki disease (KD)-like hyperinflammatory syndromes. Serum levels of 48 cytokines were analyzed in 97 patients using a bead-based multiplex immunoassay (Luminex assay). Serum levels of interferon alpha (IFN-α), interleukin-18 (IL-18), IL-6, CXCL9, and soluble tumor necrosis factor receptor II (sTNF-RII) were measured in 165 participants using enzyme-linked immunosorbent assay (ELISA).

Results. Luminex assay categorized patients with CSS into five clusters based on serum cytokine patterns. ELISA revealed distinct cytokine patterns, wherein patients with histiocytic necrotizing lymphadenitis-associated HLH and systemic lupus erythematosus-associated macrophage activation syndrome (MAS) showed elevated IFN-α; systemic juvenile idiopathic arthritis–associated and adult-onset Still's disease–associated MAS, X-linked inhibitor of apoptosis protein deficiency with HLH, and NLRC4-associated autoinflammatory disorder exhibited higher IL-18 levels. Additionally, KD shock syndrome had higher IL-6 levels than the other groups. CXCL9 was significantly elevated in patients with virus-associated HLH, familial HLH, malignant lymphoma-associated HLH, and KD-MAS. Multisystem inflammatory syndrome in children and toxic shock syndrome also showed moderate elevations of CXCL9 and IL-6 levels.

Conclusion. Serum cytokine profiling effectively differentiates CSS subtypes, facilitating better diagnosis and personalized treatment strategies based on specific disease backgrounds.

Supported by grants from Medical and Biological Laboratories Co, Ltd.
[1]Shuya Kaneko, MD, PhD, Maho Hatano, MD, Asami Shimbo, MD, Futaba Miyaoka, MD, Hitoshi Irabu, MD, PhD, Yuko Akutsu, MD, Masatoshi Takagi, MD, PhD: Department of Pediatrics and Developmental Biology, Graduate School of Medical and Dental Sciences, Institute of Science Tokyo, Tokyo, Japan; [2]Yuko Hayashi, MD, PhD, Masaki Shimizu, MD, PhD: Department of Pediatrics, Perinatal and Maternal Medicine, Graduate School of Medical and Dental Sciences, Institute of Science Tokyo, Tokyo, Japan; [3]Mao Mizuta, MD, PhD, Yasuo Nakagishi, MD: Department of Pediatric Rheumatology, Hyogo Prefectural Kobe Children's Hospital, Kobe, Japan; [4]Keiji Akamine, MD: Department of Nephrology and Rheumatology, Tokyo Metropolitan Children's Medical Center, Fuchu, Japan; [5]Naomi Iwata, MD: Department of Immunology and Infectious Diseases, Aichi Children's Health and Medical Center, Obu, Japan; [6]Kenji Furuno, MD (current address: Department of Pediatrics, Japanese Red Cross Fukuoka Hospital, Fukuoka, Japan): Department of General Pediatrics and Interdisciplinary Medicine, Fukuoka Children's Hospital, Fukuoka, Japan; [7]Takayuki Tanaka, MD, PhD: Department of Pediatrics, Japanese Red Cross Otsu Hospital, Otsu, Japan; [8]Kazuyuki Ueno, MD, PhD, Shuhei Fujita, MD, PhD: Department of Pediatrics, Toyama Prefectural Central Hospital, Toyama, Japan; [9]Koji Yokoyama, MD, PhD: Department of Pediatrics, Japanese Red Cross Wakayama Medical Center, Wakayama, Japan; [10]Toshinori Minato, MD, PhD: Department of Pediatrics, Toyooka Hospital, Toyooka, Japan; [11]Kazushi Izawa, MD, PhD; Department of Pediatrics, Kyoto University Graduate School of Medicine, Kyoto, Japan; [12]Takahiro Yasumi, MD, PhD: Department of Pediatrics, Kyoto University Graduate School of Medicine, and Japan Environment and Children's Study Kyoto Regional Center, Kyoto University Graduate School of Medicine, Kyoto, Japan; [13]Tadashi Matsubayashi, MD, PhD: Department of Pediatrics, Seirei Hamamatsu General Hospital, Hamamatsu, Japan; [14]Tadashi Hosoya, MD, PhD, Shinsuke Yasuda, MD, PhD: Department of Rheumatology, Graduate School of Medical and Dental

INTRODUCTION

Cytokine storm syndrome (CSS) is a severe inflammatory condition caused by excessive cytokine production. It represents one of the most crucial inflammatory events for patients and clinicians. Although its definition is vague and does not refer to a single disease, CSS is frequently associated with hemophagocytic lymphohistiocytosis (HLH) and macrophage activation syndrome (MAS), which complicates HLH in rheumatic diseases.[1] Various factors contribute to CSS development, including genetic backgrounds that predispose individuals to inflammatory conditions, including autoinflammatory diseases, immunodeficiencies, malignant diseases, and infections.[1,2] These diseases cause uncontrolled activation and proliferation of immune cells, resulting in severe inflammation. Different aforementioned causes trigger CSS, and the term has come to be used as an umbrella concept encompassing these conditions.[3] Treatment plans must differ based on the underlying diagnosis despite the similarity in clinical and laboratory findings. Treatment with immunosuppressive or cytotoxic agents, such as etoposide or alemtuzumab, and rapid donor search are required to treat patients with primary HLH—a subset of monogenic inborn errors of immunity (IEIs) characterized by impaired cytotoxic lymphocyte function. Current standard treatments include glucocorticoids combined with etoposide and, in selected cases, emapalumab, an anti–interferon (IFN)-γ monoclonal antibody,[4,5] whereas glucocorticoids, cyclosporine, or cytokine-targeted therapies are appropriate for treating patients with secondary HLH or MAS.[1,2,6] Furthermore, CSS may be the initial manifestation of undiagnosed autoimmune or autoinflammatory diseases. Early identification of CSS etiologies is crucial for patient survival. Nevertheless, differentiating among these causes at an early stage is difficult, thus emphasizing the need for techniques to make an early diagnosis.

Historically, excessive production of inflammatory cytokines, including IFN-γ and tumor necrosis factor alpha (TNF-α), and their high serum levels have been closely associated with the pathogenesis of CSS.[2,7–12] Moreover, several studies have emphasized significant interleukin-18 (IL-18) hypercytokinemia in patients with MAS, which frequently complicates systemic juvenile idiopathic arthritis (sJIA) in children and adult-onset Still's disease (AOSD) in adults.[13–16] 16 In addition, patients with IEIs, such as X-linked inhibitor of apoptosis (XIAP) deficiency and NLRC4-associated autoinflammatory disorder (NLRC4-AID), frequently present with HLH and exhibit abnormally high serum IL-18 levels.[17,18] Severe cases of COVID-19 were associated with excessive IL-6 production during the COVID-19 pandemic, and treatment with IL-6 inhibitors has been confirmed to be effective.[19,20] Similarly, IL-6 inhibitors have demonstrated efficacy in controlling the cytokine release syndrome (CRS) after chimeric antigen receptor–T cell therapy for hematologic malignancies, suggesting that IL-6 may contribute to CRS pathology.[21] Moreover, congenital disorders characterized by excessive type I IFN signaling, termed "interferonopathies," have been reported in the past few decades. These conditions exhibit MAS-like symptoms, including fever, cytopenia, hepatosplenomegaly, and hyperferritinemia, and are gaining attention as a novel CSS subgroup.[22–25] IFN-α has also been reported as a central mediator in the pathogenesis of systemic lupus erythematosus (SLE) and other rheumatic diseases that may be complicated with HLH and MAS.[26]

Recent evidence supports the clinical efficacy of direct cytokine blockade in primary HLH. A pivotal trial demonstrated that emapalumab, an anti–IFN-γ monoclonal antibody, effectively controlled hyperinflammation in pediatric patients with primary HLH.[5] A comprehensive review by Cron et al further emphasizes the central role of cytokine dysregulation in CSS and the potential of cytokine-targeted therapies, including IL-1, IL-6, and IFN-γ blockade, as part of precision medicine strategies.[1]

Given the clinical urgency of early diagnosis, recent studies have highlighted the utility of comprehensive cytokine profiling to distinguish among the underlying etiologies of CSSs. For example, Kessel et al systematically identified serum biomarkers,

Sciences, Institute of Science Tokyo, Tokyo, Japan; [15]Hiroki Nishikawa, MD: Department of Pediatrics, Nara Prefecture General Medical Center, Nara, Japan; [16]Junya Fujimura, MD, PhD: Department of Pediatrics, Kakogawa Central City Hospital, Kakogawa, Japan; [17]Ryoko Asano, MD: First Department of Internal Medicine, University of Toyama, Toyama, Japan; [18]Yuko Sugita, MD: Department of Pediatrics, School of Medicine, Osaka Medical and Pharmaceutical University, Takatsuki, Japan; [19]Kenichi Watanabe, MD, PhD: Department of Pediatrics, Japanese Red Cross Nagaoka Hospital, Nagaoka, Japan; [20]Anna Kobayashi, MD: Department of Pediatrics, University of Yamanashi, Yamanashi, Japan; [21]Takuya Endo, MD: Department of Pediatrics, Saitama Medical University, Kawagoe, Japan; [22]Katsuhide Eguchi, MD: Department of Pediatrics, Graduate School of Medical Sciences, Kyushu University, Fukuoka, Japan; [23]Ryuta Nishikomori, MD, PhD: Department of Pediatrics and Child Health, Kurume University School of Medicine, Kurume, Japan; [24]Ryuhei Yasuoka, MD, PhD: Department of Pediatrics, Hamamatsu University School of Medicine, Hamamatsu, Japan; [25]Takaki Asano, MD, PhD: Department of Pediatrics, Hiroshima University Graduate School of Biomedical and Health Sciences and Department of Genetics and Cell Biology, Research Institute for Radiation Biology and Medicine, Hiroshima University, Hiroshima, Japan; [26]Miyako Kanno, MD, PhD: Department of Pediatrics, Yamagata University School of Medicine, Yamagata, Japan; [27]Kazuya Hamada, MD: Department of Child Health and Welfare (Pediatrics), Graduate School of Medicine, University of the Ryukyus, Nakagami-gun, Japan; [28]Yuji Fujita, MD: Department of Pediatrics, Dokkyo Medical University, Shimotsuga-gun, Japan; [29]Daisuke Hayashi, MD: Department of Pediatrics, Tsuchiura Kyodo General Hospital, Tsuchiura, Japan; [30]Shojiro Watanabe, MD, PhD: Department of Pediatrics, Ehime University Graduate School of Medicine, Toon, Japan; [31]Takeshi Shiba, MD, PhD: Department of Pediatrics, Tenri Hospital, Tenri, Japan; [32]Masaaki Mori, MD, PhD: Joint Research Department of Lifelong Immunotherapy, Institute of Science Tokyo, Tokyo, Japan, and Division of Rheumatology and Allergology, Department of Internal Medicine, St. Marianna University School of Medicine, Kawasaki, Japan; [33]Hirokazu Kanegane, MD, PhD: Department of Child Health and Development, Graduate School of Medical and Dental Sciences, Institute of Science Tokyo, Tokyo, Japan.

Additional supplementary information cited in this article can be found online in the Supporting Information section (https://acrjournals.onlinelibrary.wiley.com/doi/10.1002/art.43349).

Author disclosures and a graphical abstract are available online at https://onlinelibrary.wiley.com/doi/10.1002/art.43349.

Address correspondence via email to Masaki Shimizu, MD, PhD, at mshimizu.ped@tmd.ac.jp.

Submitted for publication April 1, 2025; accepted in revised form July 22, 2025.

including S100A12 and IL-18, that could distinguish sJIA-MAS from primary or secondary HLH using multiplex immunoassays and validated them across independent cohorts.[27] Carol et al further demonstrated, through a real-time hyperferritinemia screening system, that markedly elevated IL-18 and IL-18/CXCL9 ratios were characteristic of MAS and differentiated them from other inflammatory causes including sepsis and immune dysregulation.[28] Gallo et al developed a multiplex cytokine panel that successfully differentiated hyperinflammatory syndromes such as HLH, multisystem inflammatory syndrome in children (MIS-C), and sepsis in pediatric intensive care unit settings.[29] These findings underscore the potential of targeted cytokine profiling not only as a diagnostic adjunct but also as a tool to stratify hyperinflammatory syndromes by etiology and severity in real time.

We hypothesized that combining cytokine measurements would enable classifying CSS into specific groups and identifying their underlying diseases at earlier stages. In this study, we analyzed a wide range of biomarkers in the serum of patients with CSS using a 48-multiplex bead-based immunoassay, including major CSS-related cytokines such as IFN-γ, TNF, IL-18, IL-6, and IFN-α, and investigated whether cytokine measurements could help in classifying patients with CSS with diverse underlying conditions. Moreover, to confirm the validity of that classification, we analyzed those key cytokines related to CSS by enzyme-linked immunosorbent assay (ELISA) in a larger cohort of adult and pediatric patients with CSS. On the basis of those results, we propose an algorithm for a rapid and accurate classification of the underlying conditions.

MATERIALS AND METHODS

Patients and samples. We enrolled 15 adult and 128 pediatric patients with CSS and 22 healthy controls (HCs). Patients with the following conditions were included in this study: IEI-associated CSS, including familial HLH (FHL), NLRC4-AID, Griscelli syndrome type 2 (GS2), and XIAP deficiency-complicated HLH (XIAP-HLH); mevalonate kinase deficiency-complicated MAS (MKD-MAS); secondary CSS, including virus-associated hemophagocytic syndrome (VAHS), such as Epstein–Barr virus (EBV)-related HLH, malignant lymphoma-associated HLH (LAHS), histiocytic necrotizing lymphadenitis complicating HLH (HNL-HLH), sJIA-MAS, AOSD-MAS, SLE (SLE-MAS), vacuoles, E1 enzyme, X-linked, autoinflammatory, somatic syndrome (VEXAS) syndrome (VEXAS-MAS), and Kawasaki disease (KD; KD-MAS); and CSS with KD-like hyperinflammatory syndromes, such as MIS-C, a systemic inflammatory syndrome reported in children during the COVID-19 pandemic, toxic shock syndrome (TSS), and KD shock syndrome (KDSS). Diagnoses of FHL, GS2, XIAP-HLH, NLRC4-AID, MKD-MAS, VAHS, LAHS, and VEXAS-MAS were made by clinicians based on the 2004 HLH criteria.[4] AOSD-MAS, sJIA-MAS, and KD-MAS were diagnosed based on the 2016 American College of Rheumatology (ACR)/EULAR sJIA-MAS criteria.[30] SLE-MAS and HNL-HLH were diagnosed based on the 2009 and 2021 preliminary diagnostic criteria for SLE-MAS,[31,32] and KDSS, MIS-C, and TSS were diagnosed based on their respective diagnostic criteria.[33–35] Serum was isolated from blood samples, aliquoted, and stored at −80°C until use. Serum samples were analyzed before initiating therapeutic agents, including glucocorticoids. This study was approved by the institutional review board of the Institute of Science Tokyo, and all specimens were used after obtaining informed consent from the patients. The committee's reference numbers are M2020-062 and G2019-004.

Luminex assay: a bead-based multiplex immunoassay. Serum levels of cutaneous T cell–attracting chemokine, eotaxin, basic fibroblast growth factor, granulocyte colony-stimulating factor, granulocyte-macrophage colony-stimulating factor, growth-related oncogene 1α, hepatocyte growth factor, IFN-α2, IFN-γ, IL-1α, IL-1β, IL-1RA, IL-2, IL-2Rα, IL-3, IL-4, IL-5, IL-6, IL-7, IL-8, IL-9, IL-10, IL-12 (p40), IL-12 (p70), IL-13, IL-15–18, IFN-γ–induced protein 10 kDa, leukemia inhibitory factor, monocyte chemoattractant protein–1 (MCP-1), MCP-3, macrophage colony-stimulating factor, macrophage migration inhibitory factor, mitogen-inducible gene, macrophage inflammatory protein–1α (MIP-1α), MIP-1β, β-nerve growth factor, platelet-derived growth factor–BB, RANTES, stem cell factor, stem cell growth factor–β, stromal cell-derived factor–1α, TNF, lymphotoxin-α, TNF-related apoptosis-inducing ligand, and vascular endothelial growth factor–A (VEGF-A) were measured in 88 patients with CSS and 9 HCs using Bio-Plex Pro Human Cytokine Panel 48-plex (Bio-Rad Laboratories, Cat. #12007283) according to the manufacturer's instructions. According to the manufacturer's instructions, the panel shows <10% analyte cross-reactivity, intra-assay precision ≤15% coefficient of variation (CV), inter-assay precision ≤25% CV, and spike-and-recovery accuracy of 70% to 130%. Data analyses were conducted using the Bio-Plex Manager Software version 6.1 (Bio-Rad Laboratories).

ELISA. Serum levels of IFN-α, IL-18, CXCL9, IL-6, and soluble TNF receptor II (sTNF-RII) were measured in all 165 participants with commercial ELISA kits (IFN-α: PBL Assay Science; IL-6, CXCL9, and sTNF-RII: R&D Systems, Inc; and IL-18: MBL) according to the manufacturer's instructions.

Analytical rationale. CXCL9 is induced exclusively by IFN-γ,[36,37] whereas sTNF-RII reflects TNF bioactivity[38,39]; these assays therefore serve as surrogates for IFN-γ and TNF activity, respectively.

Precision assessment. All samples were analyzed in duplicate, and the mean was used for downstream analyses. To assess intra-assay variability, triplicate repeats were performed on a subset of 77 sera with sufficient volume; CVs were <20% for every cytokine (Supplementary Table S1).

Exploratory measurement of IL-18 binding protein. IL-18 binding protein (IL-18BP) was quantified by ELISA (R&D Systems) in a subset of 77 patients for whom sufficient residual serum was available; triplicate measurements yielded CVs <20% (Supplementary Table S2). To further evaluate IL-18 pathway activity, we also measured serum IL-18BP and calculated the IL-18/IL-18BP ratio in this subset.

Statistical analysis. Statistical analysis was conducted using GraphPad Prism 10 (GraphPad) and R software for macOS version 4.3.3 (R Foundation). For principal component analysis (PCA), we used the "FactoMineR" package, and visualizations were created using "ggplot2." For hierarchical clustering and heatmap generation, the "pheatmap" package was used, and data transformation was performed using "reshape2." Excel files were imported using "readxl." Fisher's exact test, unpaired *t*-test with a two-tailed *P* value, and the Mann–Whitney U test were conducted to compare variables within two groups. Comparisons among several groups were conducted using the Kruskal–Wallis rank test. One-way analysis of variance with Dunn's multiple comparison test was performed to compare several groups. For group comparisons, disease categories with fewer than three patients were excluded from formal statistical testing. Clustering analysis was conducted by hierarchical clustering. $P < 0.05$ indicated statistical significance. The optimal cut-off values for receiver operating characteristic (ROC) curve analysis were identified using Youden's index, a method that maximizes sensitivity and specificity (sensitivity + specificity – 1).

Data availability. The datasets generated during and/or analyzed during the current study are not publicly available but are available from the corresponding author on reasonable request.

RESULTS

Clinical characteristics of patients with CSS. Table 1 shows the clinical characteristics of patients in each group. We enrolled 15 adults and 128 pediatric patients, with an age range from 20 days to 82 years. One of each case of MKD-MAS, GS2, and VEXAS-MAS was included, whereas other patient groups involved at least three patients. Among the 13 patients registered as having VAHS, 11 were caused by EBV, 1 by human parvovirus B19, and 1 by adenovirus. Of the six FHL cases, three cases were each type 2 and type 3. Remarkably, two patients with FHL type 2 were diagnosed at age 22 years. The TSS group consisted of nine patients, including three caused by *Staphylococcus* infection and six caused by *Yersinia pseudotuberculosis* infection.

Patients with CSS and HCs are categorized into six groups based on the levels of 48 cytokines. We measured the levels of 48 cytokines and chemokines in the serum of 88 patients with CSS and 9 HCs using the Luminex assay to evaluate the use of multiple cytokine levels in classifying patients with CSS (Supplementary Table S3). Based on hierarchical clustering analysis, patients with CSS and HCs were broadly categorized into several groups (Figure 1). Specifically, one group included most patients with sJIA-MAS, AOSD-MAS, XIAP-HLH, and NLRC4-AID (clusters in rows 1–16 and 75–81); another group involved most patients with KDSS (rows 27–30); another cluster (rows 37–61) contained most patients with MIS-C, TSS, and KD-MAS; and a final cluster (rows 63–71) consisted of several patients with SLE-MAS and HNL-HLH. Nevertheless, specific clusters were not established by patients with VAHS, LAHS, or FHL. PCA of these 97 cases revealed some grouping, with an obscure differentiation (Supplementary Figure S1). Hence, patients with CSS having 15 different clinical diagnoses could be categorized into several patterns based on comprehensive serum cytokine profiles.

Differences among assays in the measurement results of five CSS representative cytokines. Mysteriously, no marked increases in IFN-α2 levels were detected in patients with SLE or HNL, in whom IFN-α is generally important in disease pathogenesis, compared with those in other CSS groups (Figure 1). Considering that cytokine levels differ depending on the measurement method, we also quantified the levels of CXCL9, sTNF-RII, IL-6, IL-18, and IFN-α by ELISA in the same serum samples of 97 patients analyzed using the Luminex assay and then compared those results. Serum IFN-α levels measured using an ELISA kit that detects all subtypes exhibited a significant increase in patients with HNL-HLH and those with SLE-MAS; however, there was no significant increase in IFN-α2 levels measured using the Luminex assay in patients with HNL-HLH and those with SLE-MAS (Figure 2A). Significant correlations were confirmed between the Luminex assay and ELISA measurements for the other cytokines, but there was little correlation between IFN-α and IFN-α2 levels (Figure 2B, 2C). In the Luminex assay kit we used in the present study, only IFN-α2 could be quantified of the 13 IFN-α subtypes. Analyzing only a single subtype may not be sufficient to evaluate the upregulation of the IFN-α pathway in patients with CSS, and quantifying IFN-α in all subtypes may be required as in the ELISA kit we used. Therefore, the results of the Luminex assay for IFN-α2 were confirmed inaccurate as representative values for IFN-α signaling in patients with CSS.

Patterns of elevation in serum levels of five representative cytokines differ among groups of patients with CSS. Due to the aforementioned result, we analyzed several key cytokines that are believed crucial for CSS pathogenesis in a larger cohort of patients to more accurately and easily determine the classification patterns. We quantified IFN-α, IL-6, IL-18, CXCL9, and sTNF-RII levels in the serum of 143 patients with CSS and 22 HCs using ELISA (Figure 3A,

Table 1. Clinical features of patients with CSS*

	HNL-HLH	SLE-MAS	AOSD-MAS	sJIA-MAS	XIAP-HLH	NLRC4-AID	MKD-MAS	KDSS	VEXAS-MAS	FHL	GS2	VAHS	LAHS	KD-MAS	MIS-C	TSS
Number of patients, n	3	10	6	27	6	3	1	9	1	6	1	13	4	9	35	9
Male	1 (33.3)	1 (10.0)	1 (16.7)	13 (48.1)	1 (16.7)	1 (33.3)	0 (0.0)	5 (55.6)	1 (100.0)	5 (83.3)	0 (0.0)	5 (38.5)	1 (25.0)	5 (55.6)	19 (54.3)	3 (33.3)
Age, y	13 (10–14)	12.5 (10–29)	44.5 (20–82)	7 (0.33–14)	6 (0.08–19)	0.06 (0.04–4)	0.06	2 (0.17–7)	69	0.08 (0.08–22)	11	4 (1.33–22)	13 (11–15)	7 (0.83–14)	8 (0.75–15)	9 (1.16–15)
WBC, 10^3/μL	1.0 (0.93–1.8)	2.4 (1.8–8.0)	12.7 (5.1–21.1)	8.9 (2.3–52.9)	4.8 (3.2–8.7)	22.9 (19.3–23.8)	10.8	19.5 (6.7–57.4)	1.4	3.6 (1.1–4.7)	2.4	2.1 (0.5–14.2)	2.6 (0.6–3.2)	5.8 (2.1–11.4)	9.9 (3.3–20.3)	10.9 (5.2–22.2)
Hemoglobin, g/dL	13.8 (11.7–13.9)	11.8 (8.9–12.9)	11.6 (8–13.9)	11.5 (7.4–14.1)	11.2 (9.5–13.0)	10.0 (9.4–10.3)	12.1	9.9 (6.8–13)	9.9	7.9 (5.7–11.0)	10.8	11.4 (7.1–14.2)	10.6 (9.7–11.6)	11.1 (9.8–13.7)	12.2 (6.7–14.8)	13.4 (9.4–15.0)
Platelets, 10^4/μL	12.5 (12.3–13.0)	12.4 (7.1–26.8)	10.9 (8.4–36.9)	16.8 (7.1–32.7)	12.0 (5.2–55.1)	39.8 (12.1–41.2)	11.8	22.3 (7.1–44.8)	10.6	6.9 (1.8–12.3)	2.0	6.6 (2.3–24.4)	13.6 (5.8–35.1)	8.4 (5.1–20.5)	13.6 (2.8–69.9)	23.2 (6.9–32.1)
CRP, mg/dL	0.43 (0.12–0.50)	0.2 (0.03–7.99)	10.4 (0.69–19.9)	2.8 (0.03–20.1)	1.2 (0.14–18.7)	8.4 (5.2–9.0)	1.2	18.7 (4.4–34.0)	0.3	0.9 (0.3–21.0)	6.29	2.1 (0.3–31.2)	2.7 (2.2–3.9)	3.8 (0.47–15.6)	2.0 (9.9–23.3)	11.8 (0.3–22.2)
AST, IU/L	59 (26–320)	76 (22–363)	106 (63–1,082)	136 (36–1,591)	56 (28–214)	24 (16–37)	559	58 (17–498)	97	151 (46–698)	150	170 (43–888)	106 (26–241)	133 (38–2,218)	40 (12–269)	38 (16–159)
LDH, IU/L	728 (710–889)	675 (334–1,578)	439 (811–2,822)	872 (412–4,395)	655 (268–1,241)	341 (311–627)	557	301 (192–1,157)	810	487 (329–1,337)	382	1,168 (457–8,013)	657 (489–1,394)	731 (220–1,452)	306 (117–675)	278 (199–470)
Triglycerides, mg/dL	161 (106–194)	173 (144–520)	165 (98–214)	173 (86–811)	198 (88–405)	509 (120–2,319)	277	97 (62–128)	233	223 (118–342)	271	202 (103-414)	135 (106–579)	156 (42–408)	121 (46–478)	147 (69–179)
Fibrinogen, mg/dL	336 (252–384)	322 (140–460)	271 (172–644)	258 (73–597)	183 (145–445)	260 (115–406)	223	518 (219–765)	112	199 (109–266)	197	194 (88–267)	253 (218–374)	295 (84–699)	489 (286–766)	539 (238–705)
FDP-DD, ng/mL	2.7 (1.6–2.9)	3.5 (1.5–88.5)	10.9 (9.4–12.4)	6.2 (0.6–217.6)	29.6 (0.9–97.5)	21.9 (2.6–39.6)	1.1	3.8 (0.7–34.5)	43.5	10.4 (1.2–14.0)	14.2	22.1 (1.6–88.7)	5.1 (1.2–30.9)	7.5 (2.9–54.6)	3.6 (1.1–51.4)	3.4 (0.8–7.1)
sIL-2R, IU/mL	1,015 (909–1,120)	1,543 (852–2,683)	3,158 (2,090–3,379)	2,214 (933–5,660)	1,688 (756–3,601)	2,108 (1,355–2,861)	4,188	7,099 (2,852–11,345)	1,923	13,618 (4,958–22,699)	8,821	9,886 (1,157–22,975)	1,740 (1,300–2,440)	4,385 (2,052–7,418)	2,423 (800–9,877)	4,750 (2,639–5,467)
Ferritin, ng/mL	794 (378–7,794)	1,519 (599–8,074)	21,614 (801–202,254)	5,140 (963–173,921)	3,468 (337–16,315)	1,025 (80–4,317)	1,591	641 (128–3,497)	5,148	2,151 (239–12,485)	1,282	3,898 (467–39,387)	1,572 (275–7,425)	1,429 (688–6,472)	555 (62–29,058)	251 (76–1,107)
HScore, points (0–337)	159 (122–185)	153 (90–204)	198 (141–235)	198 (135–289)	168 (95–221)	158 (87–235)	106	114 (87–141)	250	225 (106–309)	204	225 (106–309)	179 (106–309)	146 (106–254)	112 (68–170)	79 (49–142)

* Data are n (%) or median (range) unless specified. AOSD, adult-onset Still's disease; AST, aspartate aminotransferase; CRP, C-reactive protein; CSS, cytokine storm syndrome; FDP-DD, fibrin/fibrinogen degradation products-D dimer; FHL, familial HLH; GS2, Griscelli syndrome type 2; HLH, hemophagocytic lymphohistiocytosis; HNL, histiocytic necrotizing lymphadenitis; KD, Kawasaki disease; KDSS, KD shock syndrome; LAHS, lymphoma-associated HLH; LDH, lactate dehydrogenase; MAS, macrophage activation syndrome; MIS-C, multisystem inflammatory syndrome in children; MKD, mevalonate kinase deficiency; NLRC4-AID, NLRC4-associated autoinflammatory disorder; sIL-2R, soluble interleukin receptor type 2; sJIA, systemic juvenile idiopathic arthritis; SLE, systemic lupus erythematosus; TSS, toxic shock syndrome; VAHS, virus-associated hemophagocytic syndrome; VEXAS, vacuoles, E1 enzyme, X-linked, autoinflammatory, somatic syndrome; WBC, white blood cell counts; XIAP, X-linked inhibitor of apoptosis protein.

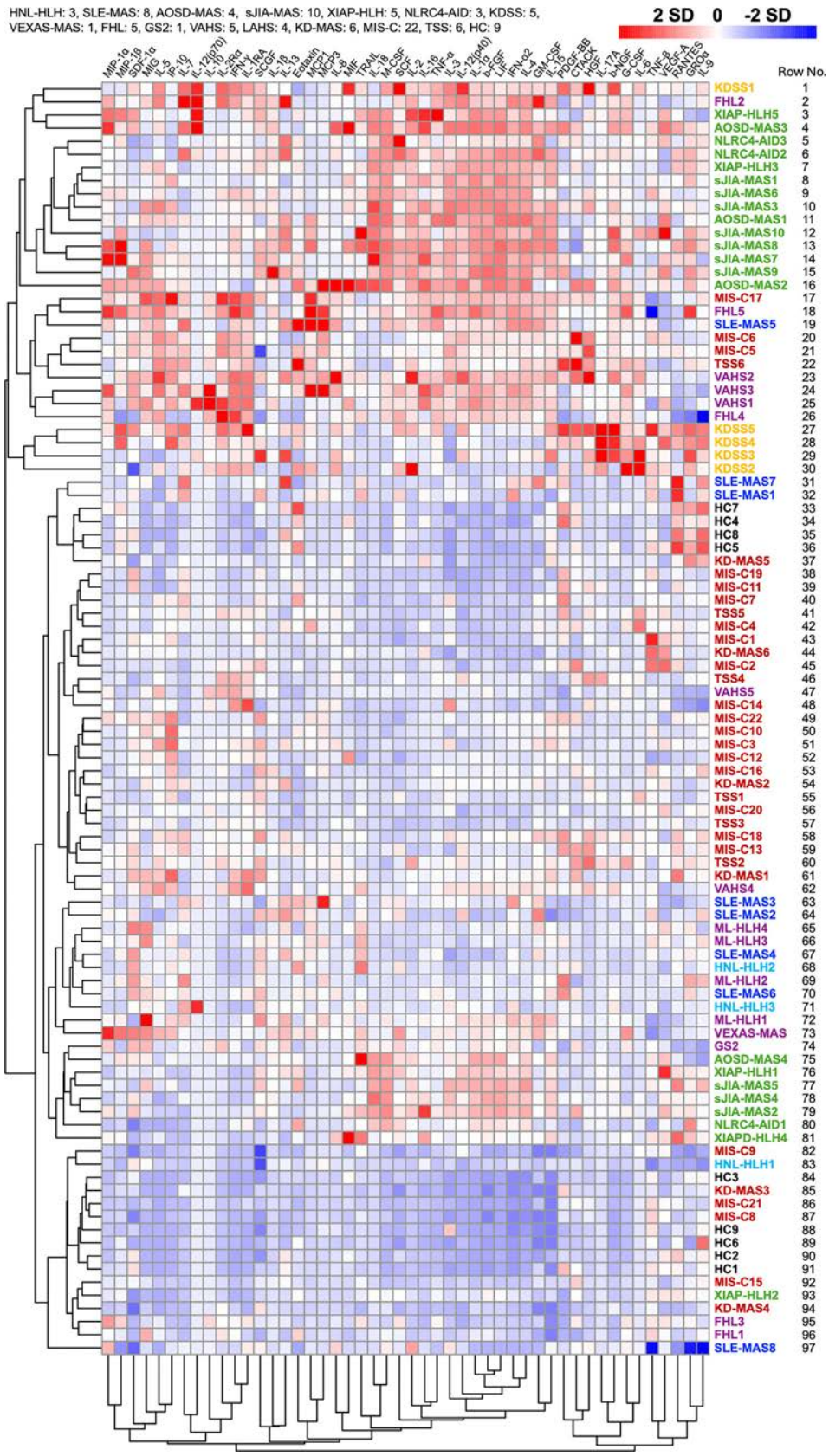

Figure 1. Legend on next page.

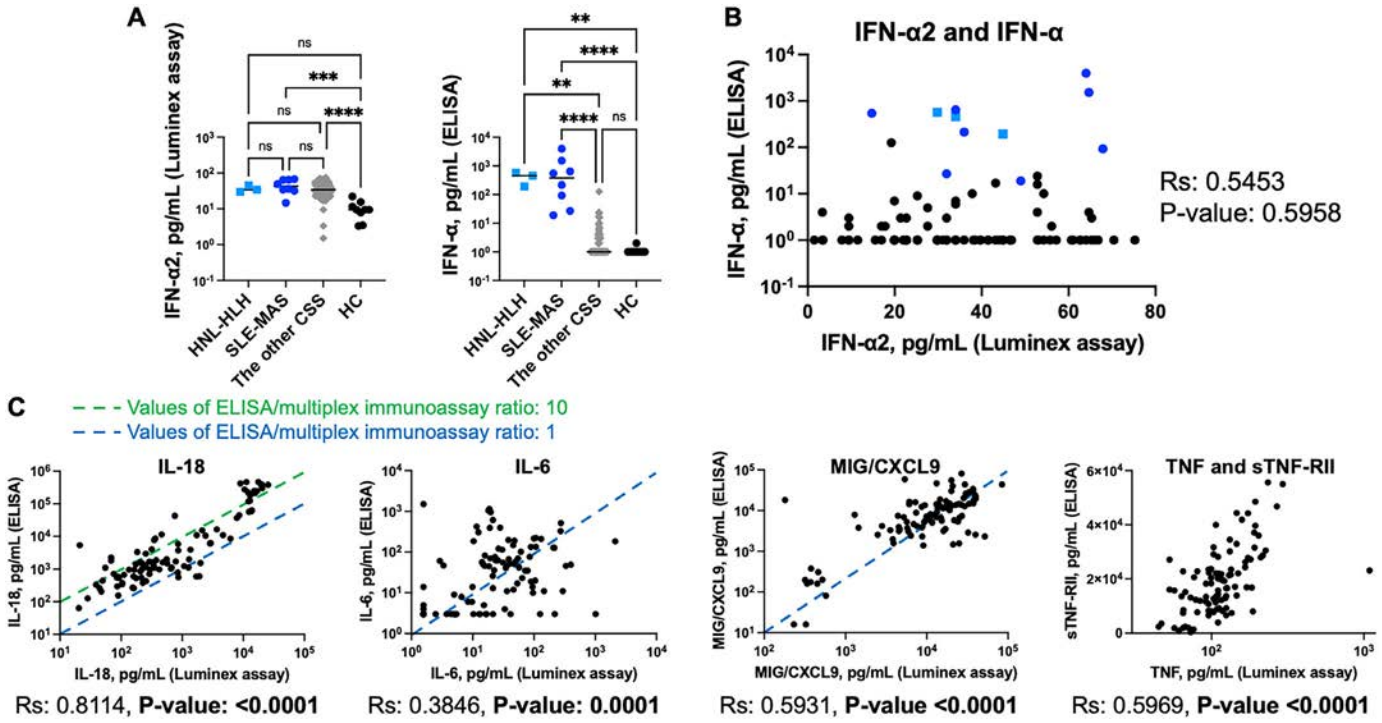

Figure 2. Differences and correlations of serum cytokine levels quantified by ELISA and Luminex assay. (A) Comparison of serum IFN-α2 levels determined by the Luminex assay and serum IFN-α levels determined by ELISA. (B, C) Correlations of serum cytokine and chemokine levels. The X-axis shows cytokine levels in serum quantified by the Luminex assay, and the Y-axis shows cytokine levels in serum quantified by ELISA. The green dotted line indicates that the value of the ELISA/Luminex assay ratio is 10, and the blue line indicates that the ratio is 1. Statistically significant differences among each patient group are shown as $^{*}P < 0.05$, $^{**}P < 0.01$, $^{***}P < 0.001$, and $^{****}P < 0.0001$. CSS, cytokine storm syndrome; ELISA, enzyme-linked immunosorbent assay; HC, healthy control; HNL-HLH, histiocytic necrotizing lymphadenitis complicating hemophagocytic lymphohistiocytosis; IFN-α, interferon alpha; IL, interleukin; MIG, monokine induced by IFN-γ; SLE-MAS, systemic lupus erythematosus–macrophage activation syndrome; sTNF-RII, soluble tumor necrosis factor receptor II; TNF, tumor necrosis factor.

Supplementary Table S4). Patients with HNL-HLH and those with SLE-MAS showed significantly higher serum IFN-α levels than other groups of patients with CSS. Patients with AOSD-MAS and those with sJIA-MAS exhibited significantly higher IL-18 levels than other groups of patients with CSS. Furthermore, serum IL-18 levels in patients with XIAP-HLH and NLRC4-AID increased compared with those in the other groups, although this may be due to the small sample size, with no statistically significant difference. Serum IL-18BP levels showed minimal variation across CSS groups, with no significant differences except in sJIA-MAS and VAHS. The IL-18/IL-18BP ratio was notably higher in sJIA-MAS and AOSD-MAS, consistent with the results of IL-18 levels (Supplementary Figure S2 and Supplementary Table S2). Patients with KDSS showed significantly increased serum IL-6 levels compared with other patients with CSS. Serum CXCL9 levels were markedly elevated in several patients with CSS compared with HCs, with particularly high levels in patients with FHL, VAHS, LAHS, and KD-MAS. Moreover, sTNF-RII levels increased in patients with CSS compared with HCs, but with no distinctive differences among CSS subgroups (Figure 3A).

Classification of patients with CSS into five groups based on dominant cytokines. PCA conducted using the

Figure 1. Hierarchical cluster analysis with serum levels of 48 cytokines and chemokines in patients with CSS. Serum biomarker profiles of 97 patients with CSS. Data comprising 48 analytes are presented as a heat map after unsupervised hierarchical clustering of biomarker expression profiles according to correlation distance. Colors indicate column Z score. AOSD, Adult onset Still's disease; FHL, familial hemophagocytic lymphohistiocytosis; GS2, Griscelli syndrome type 2; HC, healthy controls; HLH, hemophagocytic lymphohistiocytosis; HNL, histiocytic necrotizing lymphadenitis; KDSS, Kawasaki disease shock syndrome; LAHS, lymphoma associated HLH; MAS, macrophage activation syndrome; MIS-C, multisystem inflammatory syndrome in children; MKD, Mevalonate kinase deficiency; NLRC4-AID, NLR-family CARD domain-containing protein 4 associated autoinflammatory disorder; SLE, systemic lupus erythematosus; TSS, toxic shock syndrome; VAHS, virus-associated hemophagocytic syndrome; XIAP, X-linked inhibitor of apoptosis.

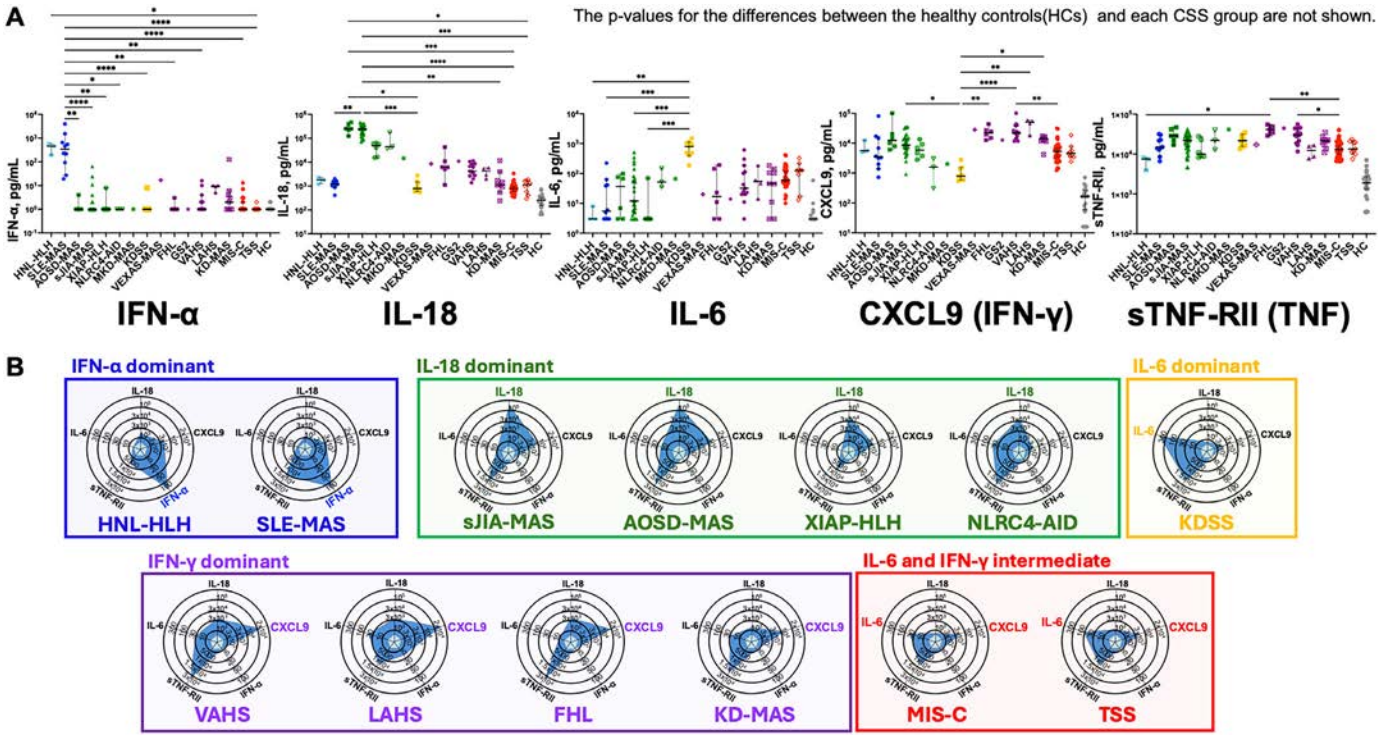

Figure 3. Comparison of serum cytokine levels in patients with CSS. (A) Serum cytokine levels of patients with CSS. Bars represent median levels and interquartile ranges. Statistically significant differences among each patient group are shown as $^{*}P < 0.05$, $^{**}P < 0.01$, $^{***}P < 0.001$, and $^{****}P < 0.0001$. All units of cytokines are pg/mL. (B) Serum cytokine profiles in each patient group. The blue hexagons show median levels of serum cytokines in patients with each background disease, and the white hexagons show those in HCs. All units of cytokines are pg/mL. GS2, Griscelli syndrome type 2; HNL, histiocytic necrotizing lymphadenitis; KDSS, Kawasaki disease shock syndrome; LAHS, lymphoma associated HLH; MKD, Mevalonate kinase deficiency; NLRC4-AID, NLR-family CARD domain-containing protein 4 associated autoinflammatory disorder; TSS, toxic shock syndrome; VAHS, virus-associated hemophagocytic syndrome; XIAP, X-linked inhibitor of apoptosis.

aforementioned five cytokines enabled clearer group classification than the 48-cytokine analysis conducted using the Luminex assay. PCA revealed the following groups: HNL-HLH and SLE-MAS (IFN-α–dominant group); AOSD-MAS, sJIA-MAS, XIAP-HLH, and NLRC4-AID (IL-18–dominant group); KDSS (IL-6–dominant group); VAHS, LAHS, FHL, and KD-MAS (IFN-γ–dominant group); MIS-C and TSS (IL-6– and IFN-γ–intermediate group); and HCs (Supplementary Figure S3). Visual representation of these cytokine median values with radar charts enabled a clear differentiation of CSS-related underlying conditions (Figure 3B). Interestingly, the PCA using a limited panel of five cytokines (IL-18, CXCL9, IFN-α, IL-6, and sTNF-RII) demonstrated even tighter separation between CSS patients and HCs than that achieved with the full 48-cytokine dataset (Supplementary Figure S1 and S3). This suggests that a small focused cytokine set may be sufficient for practical disease stratification.

An analysis of variable contributions to principle component 1 (Supplementary Figure S4) of the 48-cytokine analysis by the Luminex assay revealed that several top-contributing cytokines were not strongly associated with canonical CSS pathways (eg, CXCL9, IL-18, IL-6). This may indicate that inclusion of less relevant cytokines introduced additional variance, thereby obscuring group differentiation. In contrast, PCA based on a restricted set of five cytokines more clearly delineated CSS from controls (Supplementary Figure S3), supporting the utility of a focused panel for practical CSS stratification.

Stepwise algorithm for the differential diagnosis of CSS. A stepwise ROC curve analysis was confirmed effective for differential diagnosis (Figure 4). Patients with SLE-MAS and HNL-HLH showed a significant increase in serum IFN-α levels compared with other groups, with a cutoff of 18.0 pg/mL, area under the ROC curve (AUC) of 0.9964, sensitivity of 1.00, and specificity of 0.9764. Moreover, among the remaining groups, significant increases in serum IL-18 levels were observed in AOSD-MAS, sJIA-MAS, XIAP-HLH, and NLRC4-AID groups compared with that in the other groups, with a cutoff of 13,420 pg/mL, AUC of 0.9989, sensitivity of 1.00, and specificity of 0.9882. In addition, the abnormal increase in serum IL-6 levels was detected only in the KDSS group among the remaining groups and was useful for distinguishing the KDSS group from the other groups, with a cutoff of 185.5 pg/mL, AUC of 0.9770, sensitivity of 1.00, and specificity of 0.8816. Finally, serum CXCL9 levels were significantly higher in patients with FHL, VAHS, LAHS, and KD-MAS than in patients with MIS-C and TSS, with a cutoff of 10,337 pg/mL, AUC of 0.9212, sensitivity of 0.9688, and

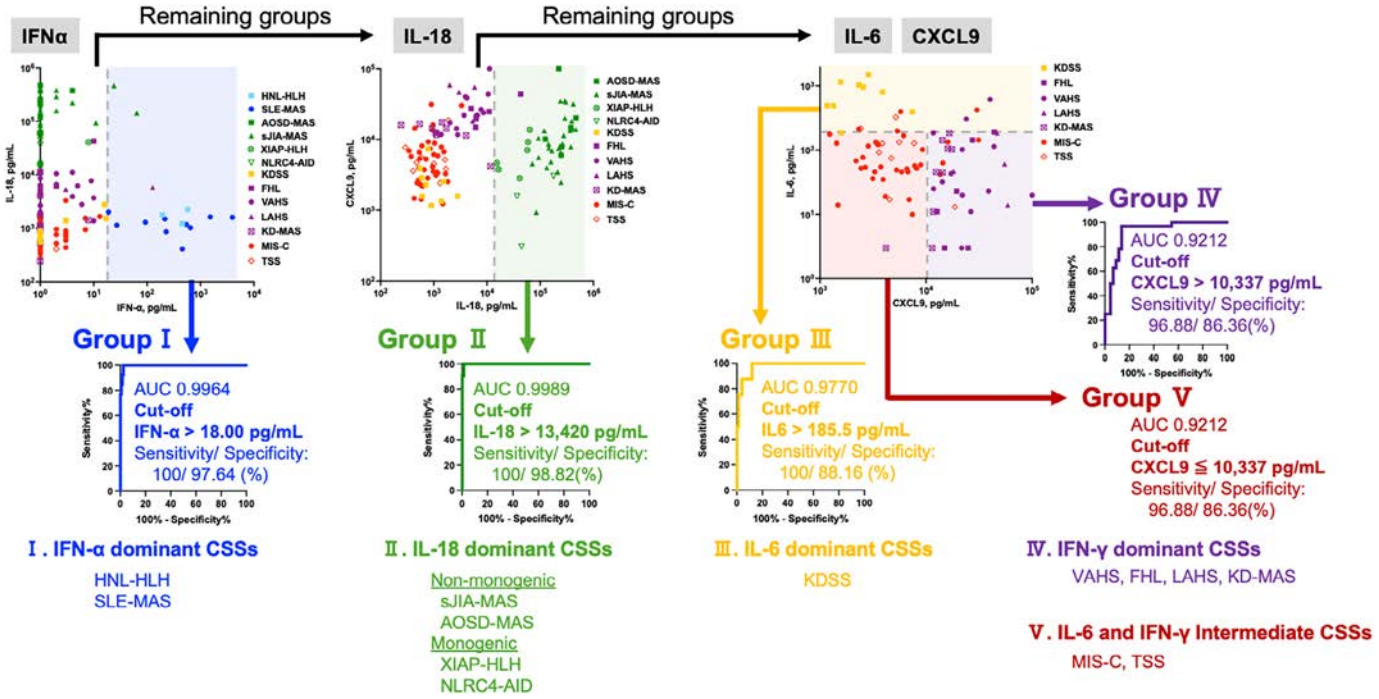

Figure 4. Stepwise ROC curve analysis and classification algorithm for patients with CSS. For the 165 cases, the high group was defined as "IFN-α–dominant CSS" with a cutoff of 18.0 pg/mL for IFN-α, and for the remaining groups with an IFN-α level ≤18.0 pg/mL, the high group was defined as "IL-18–dominant CSS" with a cutoff of 13,420 pg/mL for IL-18. For the remaining groups with an IL-18 level ≤13,420 pg/mL, the group with an IL-6 level >185.5 pg/mL was defined as "IL-6–dominant CSS," and the remaining groups were defined as "IFN-γ–dominant CSS" with a CXCL9 level of 10,337 pg/mL as the cutoff. The group with levels <10,337 pg/mL was classified as "IL-6– and IFN-γ–intermediate CSS." HNL, histiocytic necrotizing lymphadenitis; KDSS, Kawasaki disease shock syndrome; LAHS, lymphoma associated HLH; NLRC4-AID, NLR-family CARD domain-containing protein 4 associated autoinflammatory disorder; TSS, toxic shock syndrome; VAHS, virus-associated hemophagocytic syndrome; XIAP, X-linked inhibitor of apoptosis.

specificity of 0.8636. Patients with MKD-MAS, VEXAS-MAS, and GS2 were represented by single cases and were excluded from statistical comparisons.

We defined these groups as "IFN-α–dominant CSS," "IL-18–dominant CSS," "IL-6–dominant CSS," "IFN-γ–dominant CSS," and "IL-6– and IFN-γ–intermediate CSS," respectively.

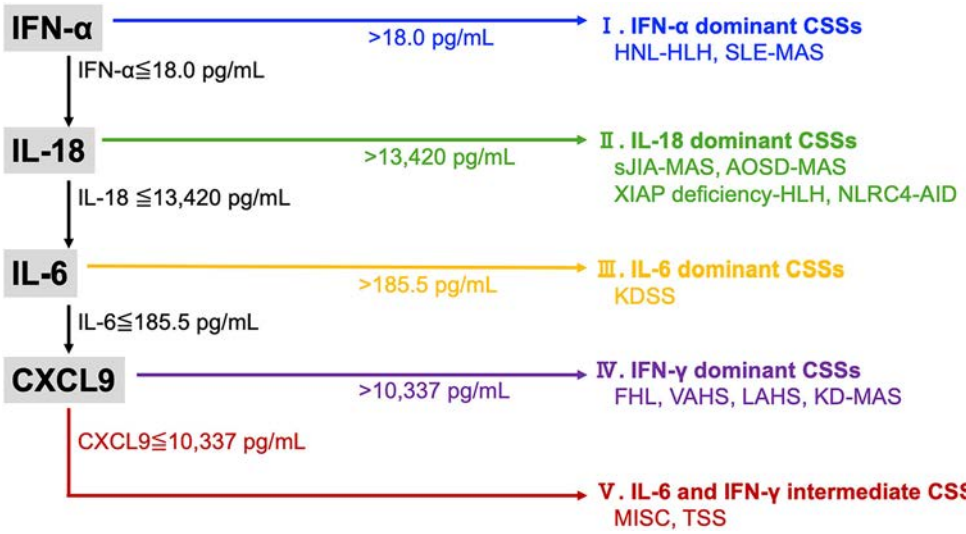

Figure 5. Classification algorithm for CSS using multiple serum cytokine levels. A stepwise classification algorithm for the background diseases of CSS using five cytokines. CSS, cytokine storm syndrome; IFN, interferon; IL, interleukin.

We summarized these data and proposed a classification algorithm for CSS using multiple serum cytokine levels (Figure 5).

DISCUSSION

This study demonstrated that clinically similar patients with CSS with various background diseases can be categorized into several groups through a comprehensive analysis of serum cytokines despite their extremely similar clinical characteristics. We also proposed an algorithm that classifies CSS with high accuracy by evaluating several important CSS cytokines and chemokines in combination. Assuming the background disease early on will significantly contribute toward making decisions regarding subsequent examinations and treatments.

Inflammatory cytokines, such as IFN-γ and TNF, have long been recognized to be deeply involved in the pathology of CSS, and we detected a high increase in CXCL9 levels, which reflects IFN-γ production,[36,37] and sTNF-RII levels, which reflects TNF production,[38,39] in most patients in this study. Conversely, a marked increase in IFN-α levels was uniquely observed in the CSS group in patients with abnormal autoimmune diseases such as HNL-HLH and SLE-MAS. This finding suggests the overactivation of plasmacytoid dendritic cells and some monocytes, which are the primary sources of IFN-α production.[40,41] We also detected a highly distinctive increase in IL-18 levels in "IL-18–dominant CSS," including in patients with AOSD-MAS, sJIA-MAS, XIAP-HLH, and NLRC4-AID. Patients with these diseases are known to show extremely elevated serum IL-18 levels, and we again confirmed that these levels are distinctively elevated compared with those in other CSS groups, which is useful in diagnosis and classification. In these diseases, excessive production of IL-18 may be caused by hyperactivation of the inflammasome and the innate immune system; hence, future therapies targeting the inflammasome are also anticipated.[42,43] Moreover, the patient with MKD-MAS demonstrated a highly elevated serum IL-18 level, although milder than those in patients with NLRC4-AID and XIAP-HLH. The pathogenesis of MKD is closely related to the activation of the inflammasome, and it is also an IEI that sometimes complicates MAS.[44] There have been no studies on the serum cytokines of patients with MKD-MAS, and our results must be confirmed with a larger cohort study.

Furthermore, a marked increase in serum IL-6 levels was observed in the "IL-6–dominant CSS" group, including KDSS, compared with that in the other CSS groups, and this was a pattern resembling the extreme type that directly exacerbated the inflammatory pathology of KD. In addition, an excessive inflammatory pathology centered on IL-6 may be important in KDSS. Moreover, a particularly prominent increase in CXCL9 levels was detected in the "IFN-γ–dominant CSS" group, such as in patients with FHL, VAHS, LAHS, and KD-MAS, compared with that in the other CSS groups. The primary pathology and cause of these diseases is generally the runaway of excessive cellular immunity, centering on cytotoxic T cells, and our results are consistent with previous reports.[5–9] Furthermore, toxins produced by pathogens such as *Staphylococcus*, and *Y. pseudotuberculosis* act as superantigens, causing excessive activation of T cells in "IL-6– and IFN-γ–intermediate CSS," such as in patients with TSS. Although MIS-C shares clinical features with toxin-mediated syndromes such as TSS, current evidence suggests that it is primarily driven by postinfectious immune dysregulation and may involve superantigen-like responses rather than classical bacterial toxins.[45–48] Therefore, this result comprehensively presented an intermediate pattern involving therapy for the increase in IL-6 levels associated with infection and the elevation in IFN-γ levels due to T cell activation.

There has been some research on developing biomarkers for pediatric patients with primary and secondary HLH in the past decade. For instance, Kessel et al conducted a comprehensive analysis of serum cytokines and chemokines using the Luminex assay and reported IL-18, CXCL9, and S100A12 as useful markers for distinguishing primary HLH, including FHL, and sJIA-MAS.[27] More recently, Carol et al used a proximity extension assay (PEA) to evaluate serum protein levels and reported IL-18, ANGPT1, and VEGF receptor 2 as promising biomarkers for early identification of hyperferritinemic conditions, including MAS and sepsis-related HLH.[28] These studies, although valuable, focused primarily on pediatric populations and a relatively limited disease spectrum, mainly involving sJIA-MAS and infection-associated CSS. In a broader clinical context, Gallo et al reported the real-world implementation of a rapid multiplex cytokine panel in pediatric practice. Their large-scale analysis demonstrated that cytokine profiles reflected the disease severity and enabled differentiation between FHL or CRS and bacterial sepsis using specific ratios, such as [IFN-γ + IL-10]/[IL-6 + IL-8]. However, their in-house panel did not include key cytokines, such as IL-18 or CXCL9, which are essential for evaluating IL-18–dominant or IFN-γ–dominant CSS subtypes.[29]

Our study included both pediatric and adult patients and encompassed a broader spectrum of CSS etiologies—including rare conditions such as HNL-HLH, SLE-MAS, KD-MAS, and IEI-associated CSS (eg, XIAP-HLH and NLRC4-AID), as well as adult-onset CSS like AOSD-MAS. Furthermore, we assessed a wider array of cytokines, including IL-18, CXCL9, IFN-α, and sTNF-RII, allowing more nuanced classification of CSS phenotypes. The stepwise classification algorithm according to the combination of multiple cytokine levels developed from our results provides a more accurate and rapid method for determining the underlying conditions of CSS compared with that using individual biomarkers. Although the stepwise cytokine-based approach presented here offers a potential framework for CSS classification, its clinical utility remains to be validated in larger multicenter and prospective cohorts. Future studies will be necessary to assess its generalizability across age groups and clinical settings.

We also confirmed the differences in values between the two representative cytokine quantification methods, ELISA and the

Luminex assay (Figure 2C). In particular, for IL-18, the levels determined by ELISA were approximately 4.7 times higher than those determined by the Luminex assay on median (Figure 2C). Carol et al[28] also confirmed the correlation and differences between the Luminex assay and PEA and indicated that there are unique limitations for each measurement method, such as the "hook effect" in PEA. Therefore, to apply serum cytokine profiling to clinical practice in the future, it is necessary to establish a universally standard cytokine measurement method.

In addition to its analytical performance, the five-cytokine panel offers notable logistical advantages. These cytokines can be quantified by standard ELISA, which provides a broader dynamic range, requires less specialized equipment, and is considerably more accessible and cost-effective than the Luminex assay. These features make the five-cytokine panel a promising candidate for translation into routine clinical use.

Our study has several limitations. First, we included patients with CSS with diverse underlying diseases; however, the sample size is small, and certain conditions that can cause CSS, such as metabolic diseases (eg, HLH associated with lysinuric protein intolerance), were not included, although it may be impossible to enroll all patients with CSS. Furthermore, prospective validation of the predefined thresholds in independent, disease-matched cohorts remains essential before clinical implementation. Second, there were limitations in terms of ethnic diversity because most of the analyzed patients were Japanese. Third, the retrospective design and limited sample size for several subgroups preclude the immediate clinical application of the proposed classification algorithm. Prospective validation in larger and more diverse cohorts is needed to confirm its utility in practice. Although data from rare disorders such as GS2, MKD-MAS and VEXAS-MAS were included in the analyses, these cases were not used to define dominant cytokine-based groups owing to the small sample size. Their cytokine profiles are shown for descriptive purposes only and should be interpreted with caution.

In conclusion, patients with CSS can be categorized into several groups according to their underlying diseases. Serum cytokine profiling was confirmed as an effective method for their differentiation.

ACKNOWLEDGMENTS

We would like to thank Maruzen-Yushodo Co, Ltd (kw.maruzen.co.jp/kousei-honyaku/) for English language editing and Editage (www.editage.com) for assistance with the graphical abstract.

AUTHOR CONTRIBUTIONS

All authors contributed to at least one of the following manuscript preparation roles: conceptualization AND/OR methodology, software, investigation, formal analysis, data curation, visualization, and validation AND drafting or reviewing/editing the final draft. As corresponding author, Dr Shimizu confirms that all authors have provided the final approval of the version to be published and takes responsibility for the affirmations regarding article submission (eg, not under consideration by another journal), the integrity of the data presented, and the statements regarding compliance with institutional review board/Declaration of Helsinki requirements.

ROLE OF THE STUDY SPONSOR

Medical and Biological Laboratories Co, Ltd had no role in the study design or in the collection, analysis, or interpretation of the data, the writing of the manuscript, or the decision to submit the manuscript for publication. Publication of this article was not contingent upon approval by Medical and Biological Laboratories Co, Ltd.

REFERENCES

1. Cron RQ, Goyal G, Chatham WW. Cytokine storm syndrome. Annu Rev Med 2023;74(1):321–337.
2. Fajgenbaum DC, June CH. Cytokine storm. N Engl J Med 2020; 383(23):2255–2273.
3. Henderson LA, Canna SW, Schulert GS, et al. On the alert for cytokine storm: immunopathology in COVID-19. Arthritis Rheumatol 2020; 72(7):1059–1063.
4. Henter JI, Horne A, Aricó M, et al. HLH-2004: diagnostic and therapeutic guidelines for hemophagocytic lymphohistiocytosis. Pediatr Blood Cancer 2007;48(2):124–131.
5. Locatelli F, Jordan MB, Allen C, et al. Emapalumab in children with primary hemophagocytic lymphohistiocytosis. N Engl J Med 2020; 382(19):1811–1822.
6. Shakoory B, Geerlinks A, Wilejto M, et al; HLH/MAS task force. The 2022 EULAR/ACR points to consider at the early stages of diagnosis and management of suspected haemophagocytic lymphohistiocytosis/macrophage activation syndrome (HLH/MAS). Arthritis Rheumatol 2023;75(10):1714–1732.
7. Sieni E, Cetica V, Mastrodicasa E, et al. Familial hemophagocytic lymphohistiocytosis: a model for understanding the human machinery of cellular cytotoxicity. Cell Mol Life Sci 2012;69(1):29–40.
8. Henter JI, Elinder G, Söder O, et al. Hypercytokinemia in familial hemophagocytic lymphohistiocytosis. Blood 1991;78(11):2918–2922.
9. Jordan MB, Hildeman D, Kappler J, et al. An animal model of hemophagocytic lymphohistiocytosis (HLH): CD8+ T cells and interferon gamma are essential for the disorder. Blood 2004;104(3):735–743.
10. Clark MA, Plank LD, Connolly AB, et al. Effect of a chimeric antibody to tumor necrosis factor-alpha on cytokine and physiologic responses in patients with severe sepsis--a randomized, clinical trial. Crit Care Med 1998;26(10):1650–1659.
11. Créput C, Galicier L, Buyse S, et al. Understanding organ dysfunction in hemophagocytic lymphohistiocytosis. Intensive Care Med 2008; 34(7):1177–1187.
12. Makay B, Yilmaz S, Türkyilmaz Z, et al. Etanercept for therapy-resistant macrophage activation syndrome. Pediatr Blood Cancer 2008;50(2):419–421.
13. Shimizu M, Nakagishi Y, Inoue N, et al. Interleukin-18 for predicting the development of macrophage activation syndrome in systemic juvenile idiopathic arthritis. Clin Immunol 2015;160(2):277–281.
14. Krei JM, Møller HJ, Larsen JB. The role of interleukin-18 in the diagnosis and monitoring of hemophagocytic lymphohistiocytosis/macrophage activation syndrome - a systematic review. Clin Exp Immunol 2021; 203(2):174–182.
15. Inoue N, Shimizu M, Tsunoda S, et al. Cytokine profile in adult-onset Still's disease: comparison with systemic juvenile idiopathic arthritis. Clin Immunol 2016;169:8–13.

16. Tang Y, Xu Q, Luo H, et al. Excessive IL-10 and IL-18 trigger hemophagocytic lymphohistiocytosis-like hyperinflammation and enhanced myelopoiesis. J Allergy Clin Immunol 2022;150(5):1154–1167.
17. Canna SW, de Jesus AA, Gouni S, et al. An activating NLRC4 inflammasome mutation causes autoinflammation with recurrent macrophage activation syndrome. Nat Genet 2014;46(10):1140–1146.
18. Wada T, Kanegane H, Ohta K, et al. Sustained elevation of serum interleukin-18 and its association with hemophagocytic lymphohistiocytosis in XIAP deficiency. Cytokine 2014;65(1):74–78.
19. Angriman F, Ferreyro BL, Burry L, et al. Interleukin-6 receptor blockade in patients with COVID-19: placing clinical trials into context. Lancet Respir Med 2021;9(6):655–664.
20. Rubin EJ, Longo DL, Baden LR. Interleukin-6 receptor inhibition in Covid-19—cooling the inflammatory soup. N Engl J Med 2021; 384(16):1564–1565.
21. Grupp SA, Kalos M, Barrett D, et al. Chimeric antigen receptor-modified T cells for acute lymphoid leukemia. N Engl J Med 2013; 368(16):1509–1518.
22. de Jesus AA, Hou Y, Brooks S, et al. Distinct interferon signatures and cytokine patterns define additional systemic autoinflammatory diseases. J Clin Invest 2020;130(4):1669–1682.
23. de Jesus AA, Canna SW, Liu Y, et al. Molecular mechanisms in genetically defined autoinflammatory diseases: disorders of amplified danger signaling. Annu Rev Immunol 2015;33(1):823–874.
24. Rice G, Patrick T, Parmar R, et al. Clinical and molecular phenotype of Aicardi-Goutieres syndrome. Am J Hum Genet 2007;81(4):713–725.
25. Tüngler V, König N, Günther C, et al. Response to: 'JAK inhibition in STING-associated interferonopathy' by Crow et al. Ann Rheum Dis 2016;75(12):e76.
26. Muskardin TLW, Niewold TB. Type I interferon in rheumatic diseases. Nat Rev Rheumatol 2018;14(4):214–228.
27. Kessel C, Fall N, Grom A, et al. Definition and validation of serum biomarkers for optimal differentiation of hyperferritinaemic cytokine storm conditions in children: a retrospective cohort study. Lancet Rheumatol 2021;3(8):e563–e573.
28. Carol HA, Mayer AS, Zhang MS, et al. Hyperferritinemia screening to aid identification and differentiation of patients with hyperinflammatory disorders. J Clin Immunol 2024;45(1):4.
29. Gallo PM, Kim J, McNerney KO, et al. Serum cytokine panels in pediatric clinical practice. J Allergy Clin Immunol 2025;155(2):594–604.e5.
30. Ravelli A, Minoia F, Davì S, et al; Paediatric Rheumatology International Trials Organisation; Childhood Arthritis and Rheumatology Research Alliance; Pediatric Rheumatology Collaborative Study Group; Histiocyte Society. 2016 classification criteria for macrophage activation syndrome complicating systemic juvenile idiopathic arthritis: a European league against rheumatism/American College of Rheumatology/Paediatric Rheumatology International Trials Organisation collaborative initiative. Arthritis Rheumatol 2016;68(3): 566–576.
31. Parodi A, Davì S, Pringe AB, et al; Lupus Working Group of the Paediatric Rheumatology European Society. Macrophage activation syndrome in juvenile systemic lupus erythematosus: a multinational multicenter study of thirty-eight patients. Arthritis Rheum 2009; 60(11):3388–3399.
32. Gerstein M, Borgia RE, Dominguez D, et al. Predicting macrophage activation syndrome in childhood-onset systemic lupus erythematosus patients at diagnosis. J Rheumatol 2021;48(9):1450–1457.
33. Kanegaye JT, Wilder MS, Molkara D, et al. Recognition of a Kawasaki disease shock syndrome. Pediatrics 2009;123(5):e783–e789.
34. COVID-19–Associated Multisystem Inflammatory Syndrome in Children — United States, March–July 2020. MMWR Morb Mortal Wkly Rep. 2020;69(32):1074–1080. https://www.cdc.gov/mmwr/volumes/69/wr/mm6932e2.htm
35. Centers for Disease Control and Prevention. Case definitions for infectious conditions under public health surveillance. MMWR Recomm Rep 1997;46(RR-10):1–55.
36. Berthoud TK, Dunachie SJ, Todryk S, et al. MIG (CXCL9) is a more sensitive measure than IFN-gamma of vaccine induced T-cell responses in volunteers receiving investigated malaria vaccines. J Immunol Methods 2009;340(1):33–41.
37. Groom JR, Luster AD. CXCR3 ligands: redundant, collaborative and antagonistic functions. Immunol Cell Biol 2011;89(2):207–215.
38. Aukrust P, Liabakk NB, Müller F, et al. Serum levels of tumor necrosis factor-alpha (TNF alpha) and soluble TNF receptors in human immunodeficiency virus type 1 infection--correlations to clinical, immunologic, and virologic parameters. J Infect Dis 1994;169(2):420–424.
39. Zangerle R, Gallati H, Sarcletti M, et al. Tumor necrosis factor alpha and soluble tumor necrosis factor receptors in individuals with human immunodeficiency virus infection. Immunol Lett 1994;41(2-3): 229–234.
40. Farkas L, Beiske K, Lund-Johansen F, et al. Plasmacytoid dendritic cells (natural interferon- alpha/beta-producing cells) accumulate in cutaneous lupus erythematosus lesions. Am J Pathol 2001;159(1): 237–243.
41. Cervantes-Barragan L, Lewis KL, Firner S, et al. Plasmacytoid dendritic cells control T-cell response to chronic viral infection. Proc Natl Acad Sci USA 2012;109(8):3012–3017.
42. Li Y, Huang H, Liu B, et al. Inflammasomes as therapeutic targets in human diseases. Signal Transduct Target Ther 2021;6(1):247.
43. Coll RC, Schroder K. Inflammasome components as new therapeutic targets in inflammatory disease. Nat Rev Immunol 2025;25(1):22–41.
44. Ter Haar NM, Jeyaratnam J, Lachmann HJ, et al; Paediatric Rheumatology International Trials Organisation and Eurofever Project. The phenotype and genotype of mevalonate kinase deficiency: a series of 114 cases from the Eurofever registry. Arthritis Rheumatol 2016; 68(11):2795–2805.
45. Moreews M, Le Gouge K, Khaldi-Plassart S, et al. Polyclonal expansion of TCR Vbeta 21.3^{+} CD4^{+} and CD8^{+} T cells is a hallmark of multisystem inflammatory syndrome in children. Sci Immunol 2021;6(59): eabh1516.
46. Porritt RA, Paschold L, Rivas MN, et al. HLA class I-associated expansion of TRBV11-2 T cells in multisystem inflammatory syndrome in children. J Clin Invest 2021;131(10):e146614.
47. Cheng MH, Zhang S, Porritt RA, et al. Superantigenic character of an insert unique to SARS-CoV-2 spike supported by skewed TCR repertoire in patients with hyperinflammation. Proc Natl Acad Sci USA 2020;117(41):25254–25262.
48. Kaneko S, Noguchi Y, Hatano M, et al. Clinical usefulness of T-cell receptor Vβ repertoire analysis for differentiating multisystem inflammatory syndrome in Japanese children from toxic shock syndrome and Kawasaki disease. Pediatr Infect Dis J 2024;43(4):e125–e127.

Arthritis & Rheumatology
Vol. 78, No. 2, February 2026, pp 475–482
DOI 10.1002/art.43384

American College of Rheumatology
Empowering Rheumatology Professionals

Comparative Efficacy and Safety of Anakinra and Canakinumab in Patients With VEXAS Syndrome: An International Multicenter Study

Tali Eviatar,[1,2] Dafne Capelusnik,[1,2,3] Corrado Campochiaro,[4] Valentin Lacombe,[5,6] Vincent Jachiet,[7] Michael Zisapel,[1,2] Iftach Sagy,[8,9] Oshrat E. Tayer-Shifman,[2,10] David Ozeri,[11] Shaye Kivity,[2,10] Alessandro Tomelleri,[4] Benjamin Terrier,[12] Hagit Peleg,[13,14] Thibault Comont,[15] Karim Sacre,[16] Pascal Woaye-Hune,[17] Laurent Arnaud,[18] Estibaliz Lazaro,[19] Vincent Grobost,[20] Francois Lifermann,[21] Maxime Samson,[22,23] Samuel Ardois,[24] Alice Garnier,[25] Alexandre Maria,[26] Alain Cantagrel,[27] Aurore Meyer,[28] Jean-David Bouaziz,[29] Mael Heiblig,[30] Lorenzo Dagna,[4] Elisa Diral,[4] Olivier Kosmider,[31] Ori Elkayam,[1,2] Jérôme Hadjadj,[7] Sophie Georgin-Lavialle,[32] Olivier Fain,[7] and Arsene Mekinian[7]

Objective. The aim of this study was to compare differences in clinical response, drug survival, and adverse event rates between anakinra and canakinumab in VEXAS (vacuoles, E1 enzyme, X-linked, autoinflammatory, somatic) syndrome.

Methods. This multicenter international study includes patients with VEXAS from France, Israel, and Italy treated with interleukin-1 inhibition. Global response (GR) was defined as the absence of inflammatory symptoms and ≥50% decrease in steroid dose and C-reactive protein. Multiple regression analysis was performed to identify associated variables. Drug survival was analyzed using Kaplan-Meier plots and log-rank test, with Cox regression models for associated factors.

Results. We included 47 male patients with VEXAS; 44 received anakinra and 9 received canakinumab, with 6 patients using both at different time points. GR at 1 month was 34% for anakinra and 100% for canakinumab ($P < 0.001$) and 22% and 78% at 3 months, respectively ($P = 0.001$). Treatment with canakinumab was associated with a higher odds ratio (OR) of achieving GR at 3 months (OR 28.8, 95% confidence interval 3.0–273.9; $P = 0.004$) in a multivariable analysis. Median drug survival was 54 (interquartile range [IQR] 30–56) months for canakinumab at 300 mg/month compared with 7 (IQR 4–8) months for canakinumab 150 mg/month and 1 (IQR 1–2.5) months for anakinra ($P = 0.01$). Injection-site reactions were only recorded for the anakinra group (47 vs 0%; $P = 0.006$), whereas infections were more frequent in the anakinra group (31% and 11%; $P = 0.3$).

Conclusion. Canakinumab demonstrated superior clinical response and drug survival with fewer adverse events compared with anakinra. Monthly canakinumab 300 mg may be considered as an effective steroid-sparing therapeutic option for patients with VEXAS.

INTRODUCTION

VEXAS (vacuoles, E1 enzyme, X-linked, autoinflammatory, somatic) syndrome is an acquired hemato-autoinflammatory disease affecting mostly male, adult patients. It is characterized by macrocytosis, anemia, myelodysplastic syndrome (MDS), and episodes of inflammation with neutrophilic rashes, chondritis, inflammatory eye disease, pulmonary

[1]Rheumatology Department, Tel Aviv Medical Center, Tel Aviv, Israel; [2]Faculty of Medical and Health Sciences, Tel Aviv University, Tel Aviv, Israel; [3]Care and Public Health Research Institute, Maastricht University, Maastricht, the Netherlands; [4]Unit of Immunology, Rheumatology, Allergy and Rare Diseases, San Raffaele Scientific Institute, Milan, Italy; [5]Médecine Interne et Polyvalente, Centre Hospitalier du Haut-Anjou, Château-Gontier, France; [6]Médecine Interne et Immunologie Clinique, Centre Hospitalier Universitaire d'Angers, Angers, France; [7]Sorbonne Université, Service de Médecine Interne, Hôpital Saint-Antoine, CEREMAIAA, AP-HP, Paris, France; [8]Soroka Medical Center, Rheumatic Disease Unit, Be'er Sheva, Israel; [9]Clinical Research Center, Soroka Medical Center, Be'er Sheva, Israel; [10]Meir Medical Center, Rheumatology Unit, Kfar Saba, Israel; [11]Sheba Medical Center, Rheumatology Unit, Tel HaShomer, Israel; [12]Médecine Interne, Hôpital Cochin, AP-HP, Université Paris Cité, Paris, France; [13]Rheumatology Unit, Hadassah University Medical Center, Jerusalem, Israel; [14]Internal Medicine Department, Hadassah University Medical Center, Jerusalem, Israel; [15]Service de Médecine Interne, Institut Universitaire Du Cancer De Toulouse Oncopole, Centre Hospitalier Universitaire de Toulouse, Université Paul Sabatier, Toulouse, France; [16]Department of Internal Medicine, Bichat-Claude Bernard Hospital, Paris, France; [17]Service de Médecine Interne, Centre Hospitalier Départemental Vendée, La Roche-sur-Yon, France; [18]Department of Rheumatology, National Reference Center for Rare Diseases, Hôpitaux Universitaires de Strasbourg, INSERM UMR-S 1109, Strasbourg, France; [19]Internal

inflammation, and venous thromboembolism, among other manifestations.[1,2]

The etiology of VEXAS syndrome is attributed to the amount of the active cytoplasmic UBA1b isoform of *UBA1*. Somatic mutations in the *UBA1* gene are translated to a decrease in the amount of activity of UBA1b, and with the canonical mutations, also a shift toward elevated amounts of the catalytically flawed UBA1c. This contributes to an inflammatory milieu driven primarily by myelocytes of the *UBA1* mutated clone.[3,4]

The cytokine profile of patients with VEXAS syndrome suggests inflammasome activation and is characterized by elevation of interleukin (IL) 1β, IL-18, and tumor necrosis factor-α through the NFκB pathway. These findings have raised the possibility of targeting these cytokines in the effort to control inflammatory disease activity.[5]

Although IL-1 inhibition (IL-1i) is a cornerstone in the treatment of many autoinflammatory diseases, both monogenic and acquired (such as Still disease, Schnitzler syndrome, Sweet syndrome, and gout),[6] current data suggest that their use in VEXAS may be limited by severe adverse events, primarily serious skin reactions. The first report of anakinra, an IL-1 receptor antagonist, in patients with VEXAS by Beck et al[2] described severe skin reactions in patients with VEXAS, including ulceration and abscess formation, in up to 75% of patients.[7] Subsequent reports have confirmed similar severe skin reactions with anakinra in this population.[8] Although injection-site reactions are a well-recognized effect of anakinra, occurring in up to 81% of patients with rheumatoid arthritis in clinical trials, these reactions are typically mild,[9,10] dose-dependent, and attributed to mast-cell degranulation.[9] The mechanism driving the unusually severe skin reactions to anakinra in VEXAS remains unclear but may be linked to the disease itself and increased skin reactivity to stimuli, similar to pathergy. Atypical and exacerbated skin reactions have been reported in patients with VEXAS after exposure to other injected medications (tocilizumab, azacitidine, messenger RNA vaccine, or influenza vaccine) or skin triggers.[11–13]

In terms of efficacy, the French VEXAS registry reported that only 9% of 33 treatment episodes with IL-1i, 30 of them with anakinra and 3 with canakinumab, achieved a clinical response at 3 months.[14] A recent multicenter retrospective study from the UK reported on 13 patients receiving anakinra, 8 of them still receiving it in 3 months, having an 88% clinical response rate. At 6 months, four patients continued to receive anakinra, with three having a clinical response. Discontinuation of anakinra was mostly because of severe injection-site reactions.[15] Data regarding canakinumab use are scarce, with only a few reported cases in the literature. From the UK cohort, two patients switched from anakinra to canakinumab, both discontinuing it before 6 months; one died because of *Legionella* infection.[15] One case describes a patient successfully treated with canakinumab for 5 years after experiencing intolerable skin reactions to anakinra and failing tocilizumab and other immunosuppressants.[16] Additionally, a case series involving 12 Dutch patients included 7 treated with anakinra: 2 had a good response, 4 experienced severe skin reactions, and 3 were treated with canakinumab after anakinra failure, showing variable responses.[17] The objective of this study was to compare the clinical response and drug survival between two IL-1 inhibitors, anakinra and canakinumab, and to evaluate the adverse events reported for each drug for the treatment of VEXAS syndrome.

PATIENTS AND METHODS

Study population. For this retrospective study, data gathered from November 2020 and September 2024 from two national multicenter registries were used: the French FRENVEX registry, described previously,[14] and the Israeli VEXAS registry. In addition, data from one Italian center were included.

The French FRENVEX registry is a national multicenter study group network inviting internists, rheumatologists, and hematologists to share anonymous VEXAS patient data, and 31 of 318 patients from this registry were included in this study. The Israeli VEXAS registry is a national multicenter registry inviting rheumatologists, geneticists, hematologists, immunologists, and other specialties to participate in sharing anonymous patient data. Ten Israeli patients from the registry made up of 28 patients were included in this analysis.[18] Six Italian patients were added by author CC and colleagues, some of them previously reported in the literature.[19]

Medicine, Centre Hospitalier Universitaire de Bordeaux, Bordeaux, France; [20]Médecine Interne, Centre Hospitalier Universitaire Clermont-Ferrand Estaing, Clermont-Ferrand, France; [21]Service de Médecine Interne, Centre Hospitalier Dax, Dax, France; [22]Service de Médecine Interne et Immunologie Clinique, Centre de Référence Constitutif des Maladies Auto-immunes et Auto-inflammatoires Rares de l'adulte, Centre Hospitalier Universitaire Dijon-Bourgogne, Dijon, France; [23]Université de Bourgogne Franche-Comté, INSERM, EFS BFC, UMR1098, RIGHT Interactions Greffon-Hôte-Tumeur/Ingénierie Cellulaire et Génique, Besançon, France; [24]Médecine Interne, Centre Hospitalier Universitaire Rennes, Rennes, France; [25]Hematology Department, Nantes University Hospital, Nantes, France; [26]Department of Internal Medicine - Multiorgan Diseases, Saint Eloi Hospital, Montpellier University Hospital, University Montpellier, Montpellier, France; [27]Service de Rhumatologie, Hôpital Pierre-Paul Riquet, Centre Hospitalier Universitaire de Toulouse, Toulouse, France; [28]Service d'Immunologie Clinique et Médecine Interne, Hôpitaux Universitaires de Strasbourg, Strasbourg, France; [29]Dermatology, Hôpital Saint-Louis, Paris, France; [30]Hématologie, Hôpital Lyon Sud, Hospices Civils de Lyon, Pierre-Bénite, France; [31]Université Paris Cité, Institut Cochin, INSERM U1016, CNRS UMR8104 AP-HP, Laboratory of Hematology, Hôpital Cochin, Paris, France; [32]Médecine Interne, CEREMAIA, Sorbonne Université, Hospital Tenon, Paris, France.

Additional supplementary information cited in this article can be found online in the Supporting Information section (https://acrjournals.onlinelibrary.wiley.com/doi/10.1002/art.43384).

Author disclosures and graphical abstract are available at https://onlinelibrary.wiley.com/doi/10.1002/art.43384.

Address correspondence via email to Tali Eviatar, MD, at talieviatar@gmail.com or talie@tlvmc.gov.il.

Submitted for publication May 13, 2025; accepted in revised form August 12, 2025.

All patients were genetically diagnosed with a *UBA1* mutation, confirmed at their local or national genetic laboratory and medical center. For this analysis, only patients who received IL-1i with either anakinra or canakinumab were included. They may have received other synthetic or biologic treatments before or after IL-1i. Demographic and clinical data, including clinical VEXAS symptoms; presence of MDS and monoclonal gammopathy of unknown significance (MGUS); co-occurrence of MDS mutations other than *UBA1*, analyzed by next-generation sequencing (eg, *TET2*, *DNMT3A*, *IDH1*, *IDH2*, *ASXL1*, *EZH2*, *SF3B1*, *SRSF2*, *U2AF1*, *JAK2*, *KIT*, *TP53*, *NRAS*, and *KRAS*); and medication use and dose (prednisone; immunosuppressives, such as methotrexate, cyclophosphamide, cyclosporine, colchicine, and mycophenolate; biologics; and targeted synthetic medications) were collected from medical files.

IL-1i treatments. Specific data related to IL-1i, such as the VEXAS indication for IL-1i, treatment response (clinical response, C-reactive protein [CRP] levels, prednisone or equivalent daily dose, blood count, and transfusion dependence), reasons for discontinuation, and adverse events (including injection-site reactions, systemic allergic or other responses, cardiovascular events, malignancies, thromboembolic events, cytopenias, and infections) were also included.

Complete response (CR) at each time point was defined as the absence of inflammatory symptoms (clinical remission) together with a prednisone daily dose of <10 mg or equivalent and a CRP level ≤10 mg/L. A partial response (PR) was defined as a lack of clinical inflammatory symptoms, a reduction of ≤50% in CRP and daily prednisone doses compared with the pre-initiation of IL-1i levels. Our primary outcome, global response (GR) was defined as the sum of CR and PR. Treatment failure was defined as a persistent inflammatory clinical or laboratory syndrome, an inability to decrease steroid doses, or an adverse event requiring cessation of the treatment. If data such as CRP levels or the prednisone doses used to define CR or PR were missing, a response value from a later time point was imputed backward, meaning, for example, that response data from 6 months were considered the same as at 3 months. Actual CRP levels and prednisone doses were not imputed. The safety assessment included the rate of adverse events as reported by physicians, and adverse events of special interest included injection-site reactions, allergic and systemic reactions, malignancies, cardiovascular and venous thromboembolic events, and infections.

Statistical analysis. Descriptive analysis was performed, and continuous variables were expressed as mean with SD, whereas categorical variables were reported as frequency with percentage. To compare the characteristics of patients treated with canakinumab and anakinra, categorical variables were analyzed using the chi-square test or Fisher exact test, whereas continuous variables were compared using the Student's *t*-test or Mann-Whitney test, as appropriate.

The rates of CR, PR, no response, and treatment withdrawal were described at each time point (1, 3, 6, and 12 months) according to the specific drug. Univariable analyses were conducted to identify variables associated with GR at 3 months (this was chosen because of the high discontinuation rate in the anakinra arm in the later timepoints). Variables that showed an association ($P \leq 0.15$) or a confounding effect or were considered relevant by the investigator were included in a multivariate logistic regression analysis to identify variables independently associated with GR at 3 months. Kaplan-Meier plots were constructed to analyze drug survival, and survival curves for different drugs and doses were compared using the log-rank test. Cox proportional regression analysis was performed to identify variables associated with drug discontinuation. All analyses were performed using Stata SE (version 17; StataCorp).

Ethics approval. This study involves human participants and was approved by the Ethical Review Committee for publications of the Cochin University Hospital (AAA-2021- 08040) and the Tel Aviv Medical Center (TLV-0389-23). The boards waived informed consents.

Data availability statement. Data, including study protocol, statistical analysis plan, and individual participant data that underlie the results reported in this article, after de-identification, may be available upon reasonable request from the corresponding author (talieviatar@gmail.com), Jérôme Hadjadj (jerome.hadjadj@aphp.fr), or Arsene Mekinian (arsene.mekinian@aphp.fr).

RESULTS

The analysis included a total of 47 patients with VEXAS. All of them were male, with a mean ± SD age of 72 ± 9 years at the time of IL-1i initiation. Of these, 44 participants received anakinra and 9 received canakinumab (Supplementary Table S1), with 6 patients using both drugs at different time points.

As shown in Supplementary Table S2, the patient characteristics were similar between the two treatment groups. The most common *UBA1* mutation was Met41Val (34%), followed by Met41Thr (23%), Met41Leu (19%), and splice site mutations (11%). A concurrent diagnosis of MDS was made in 36% of patients, and 17% had an MGUS. At the time of IL-1i initiation, clinical inflammatory manifestations were also similar between groups. Over the course of the disease the most frequently reported symptoms included cutaneous manifestations (neutrophilic and vasculitic rashes) in 94%, pulmonary manifestations in 54%, ocular involvement in 43%, and venous thromboembolisms in 39%.

Most patients were receiving concomitant prednisone at IL-1i initiation, with comparable doses between groups (84%, 34.0

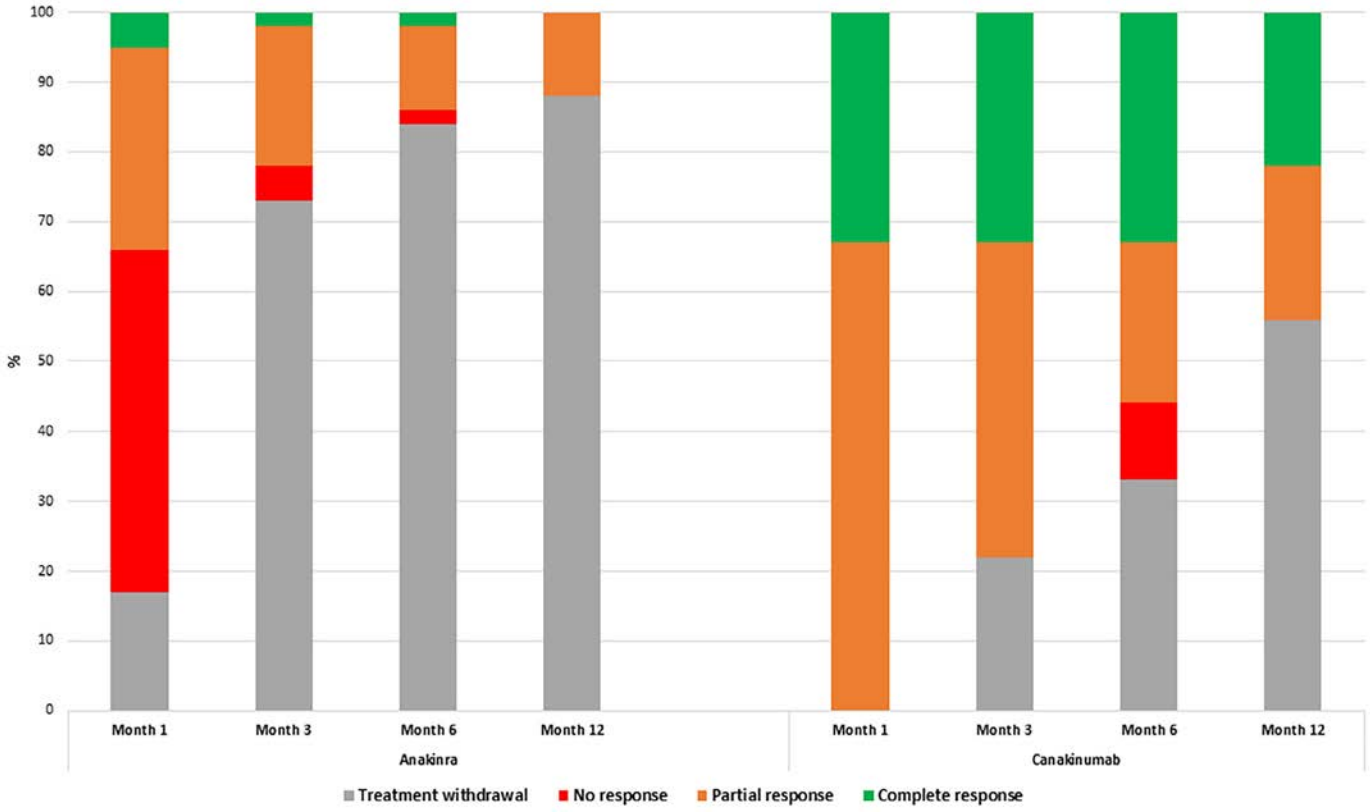

Figure 1. Response rates of anakinra and canakinumab-treated patients with VEXAS (vacuoles, E1 enzyme, X-linked, autoinflammatory, somatic) syndrome at 1, 3, 6, and 12 months from treatment initiation.

± 22.0 mg/day and 89%, 31.1 ± 25.1 mg/day, for the anakinra and canakinumab groups, respectively). CRP levels at IL-1i initiation were not statistically different between groups, although they were slightly higher in the anakinra group (96.5 ± 85.3 mg/L and 74.3 ± 76.7 mg/L).

All patients treated with anakinra received a 100 mg/day dose, and two patients increased the dosage to 200 mg/day. In the canakinumab group, four patients were treated with 300 mg every month, and five received 150 mg every month, with two of them increasing the dosage to 300 mg every month.

Table 1. Clinical response to anakinra and canakinumab treatment in patients with VEXAS (vacuoles, E1 enzyme, X-linked, autoinflammatory, somatic) syndrome

	Month 1		Month 3		Month 6		Month 12	
	Anakinra (n = 41)*	Canakinumab (n = 9)	Anakinra (n = 41)*,[a]	Canakinumab (n = 9)	Anakinra (n = 41)*	Canakinumab (n = 9)	Anakinra (n = 41)*	Canakinumab (n = 9)
Clinical response, n (%)[b]								
Complete	2 (5)	3 (33)	1 (2)	3 (33)	1 (2)	3 (33)	0 (0)	2 (22)
Partial	12 (29)	6 (67)	8 (20)	4 (45)	5 (12)	2 (23)	5 (12)	2 (22)
No response	20 (49)	0 (0)	2 (5)	0 (0)	1 (2)	1 (11)	0 (0)	0 (0)
Treatment withdrawal	7 (17)	0 (0)	30 (73)	2 (22)	34 (84)	3 (33)	36 (88)	5 (56)
Prednisone daily dose, n/N (%)								
No prednisone	3/26 (11)	0/5 (0)	1/6 (17)	1/5 (20)	2/7 (29)	0/4 (0)	0/4 (0)	0/3 (0)
≤5 mg/d	0/26 (0)	1/5 (20)	1/6 (17)	1/5 (20)	1/7 (14)	1/4 (25)	1/4 (25)	0/3 (0)
≤10 mg/d	5/26 (19)	1/5 (20)	1/6 (17)	3/5 (60)	2/7 (29)	2/4 (50)	2/4 (50)	2 (67)
>10 mg/d	18/26 (69)	3/5 (60)	3/6 (50)	0/5 (0)	2/7 (29)	1/4 (25)	1/4 (25)	1 (33)
CRP, n/N (%)								
≤10 mg/L	10/24 (42)	4/5 (80)	3/5 (60)	2/3 (67)	3/7 (43)	3/4 (75)	1/2 (50)	3/3 (100)
>10 mg/L	14/24 (58)	1/5 (20)	2/5 (40)	1/3 (33)	4/7 (57)	1/4 (25)	1/2 (50)	0/3 (0)

* CRP, C-reactive protein.
[a] Outcome data were missing and could not be imputed for three patients.
[b] When prednisone dose or CRP levels were missing at a specific timepoint, clinical response was imputed from the next timepoint (if these were available then). Actual prednisone doses and CRP levels were not imputed.

Comparative efficacy of anakinra and canakinumab. Efficacy was measured by the rates of GR and of overall drug survival. Rates of GR in anakinra and canakinumab groups were 34% (n = 14/41) and 100% (n = 9/9) at 1 month ($P < 0.001$) and 22% (n = 9/41) and 78% (n = 7/9) at 3 months ($P = 0.001$). At 6 and 12 months, the numbers of patients remaining on IL-1i therapy without withdrawal were small (6/41 [15%] vs 5/9 [56%], $P = 0.007$ at 6 months and 5/41 (12%) vs 4/9 (44%), $P = 0.023$ at 12 months for anakinra and canakinumab, respectively) (Figure 1; Table 1; Supplementary Figure S1).

In the univariate analysis, being treated with canakinumab (odds ratio [OR] 12.06; 95% confidence interval [CI] 2.1–68.5) and canakinumab dose 300 mg/4 weeks (OR 18.75; 95% CI 1.91–184.1) were associated with a higher OR of achieving GR at 3 months. (Table 2). In the regression analysis after age adjustment, being treated with canakinumab was the only variable independently associated with a higher odds of achieving GR (OR 28.78; 95% CI 3.0–273.9; $P = 0.004$). No additional associations were identified.

In the survival analysis, patients treated with canakinumab had significantly longer drug survival than those treated with anakinra, with a median of 15 (interquartile range [IQR] 7–54) months vs 1 (IQR 1–2.5) months, respectively ($P = 0.006$) (Supplementary Table S2 and Figure 2A). When stratifying by canakinumab dose, patients receiving canakinumab 300 mg/4 weeks had the longest survival, with a median of 54 (IQR 30–56) months, compared with 7 (IQR 4–8) months in the canakinumab 150 mg/4 weeks group and 1 (IQR 1–2.5) months in the anakinra group ($P = 0.01$) (Figure 2B).

In a Cox regression analysis for drug discontinuation, using canakinumab 300 mg as the reference, anakinra had a hazard ratio (HR) for treatment withdrawal of 6.27 (95% CI 1.48–26.54; $P = 0.013$). Canakinumab 150 mg had an HR of 4.58 (95% CI 0.74–28.2; $P = 0.101$).

At the end of the study, 9% of anakinra-treated patients continued the medication, compared with 33% of canakinumab-treated patients ($P = 0.055$). The reasons for discontinuation were not significantly different between the groups: inefficacy/flare in 36% and 50%; adverse event in 41% and 33%; and a combination of both inefficacy and an adverse event in 18% and 17% in the anakinra and canakinumab groups, respectively ($P = 0.849$) (Table 3). In patients for whom the only declared reason for discontinuation was inefficacy/flare, adverse events were reported in 10, all of them treated with anakinra: 2 had an injection-site reaction, one major, and the other a minor reaction together with an infection, and 9 patients had other adverse events (5 infections, 2 allergic reactions, 1 with neutropenia, and 1 death).

Regarding steroid-sparing effects (data were missing for 18 [41%] of the anakinra group and 5 [56%] of the canakinumab group), after 3 months all canakinumab-treated patients and 50% of anakinra-treated patients were receiving <10 mg/day of prednisone (Table 1). Lastly, for markers of inflammation, CRP levels were <10 mg/L in 42% and 80% of anakinra- and canakinumab-treated patients, respectively, who remained on treatment after 1 month, 60% and 67% after 3 months, 43% and 75% after 6 months, and 50% and 100% after 12 months, respectively (Table 1).

Table 2. Univariate analysis of factors associated with clinical global response at 3 months*

Variable	Odds ratio (95% confidence interval)	*P* value
Age	1.04 (0.97–1.13)	0.287
UBA1 mutation		
Met41Val	1.59 (0.45–5.57)	0.468
Met41Thr	1.25 (0.30–5.17)	0.761
Met41Leu	0.86 (0.19–3.92)	0.842
Other mutations	2.62 (0.67–10.35)	0.168
MDS	2.07 (0.59–7.24)	0.253
MGUS	0.28 (0.03–2.54)	0.256
CRP at IL-1i initiation	1.00 (0.99–1.01)	0.991
Hemoglobin	1.04 (0.81–1.35)	0.739
Clinical manifestations		
Constitutional	0.75 (0.11–5.02)	0.767
Skin	0.20 (0.03–1.24)	0.084
Arthralgia	0.46 (0.13–1.59)	0.219
Arthritis	0.66 (0.17–2.60)	0.560
Lymphadenopathy	0.54 (0.12–2.36)	0.412
Pulmonary	0.30 (0.07–1.28)	0.105
Chondritis	0.83 (0.23–3.00)	0.772
Ocular	0.70 (0.18–2.73)	0.607
Myalgia	3.00 (0.58–15.53)	0.190
Gastrointestinal	0.60 (0.06–8.29)	0.670
Renal	1.29 (0.19–8.61)	0.796
Nervous system	2.00 (0.25–15.73)	0.510
Cardiac	1.93 (0.11–33.12)	0.649
Venous thromboembolism	0.38 (0.10–1.49)	0.166
Thrombocytopenia	0.46 (0.11–2.00)	0.296
Prednisone dose	0.99 (0.96–1.02)	0.546
Adverse events to IL-1i		
Any injection-site reaction	0.40 (0.11–1.50)	0.175
Infection	2.33 (0.59–9.22)	0.227
Indication for IL-1i		
Relapse	1.58 (0.46–5.41)	0.464
Refractory disease	0.32 (0.08–1.23)	0.097
Steroid dependance	0.37 (0.08–1.77)	0.213
IL-1i medication		
Anakinra	Reference	
Canakinumab	12.06 (2.12–68.5)	**0.005**
IL-1i dose		
Anakinra 100 mg	Reference	
Anakinra 200 mg	3.75 (0.21–66.76)	0.368
Canakinumab 150 mg	9.66 (0.60–93.59)	0.118
Canakinumab 300 mg	18.75 (1.91–184.10)	**0.012**

* *P* values < 0.05 are significant and indicated with bold font. CRP, C-reactive protein; IL-1i, interleukin-1 inhibition; MDS, myelodysplastic syndrome; Met41Leu, *UBA1* mutation replacing methionine 41 with leucine; Met41Thr, *UBA1* mutation replacing methionine 41 with threonine; Met41Val, *UBA1* mutation replacing methionine 41 with valine; MGUS, monoclonal gammopathy of unknown significance.

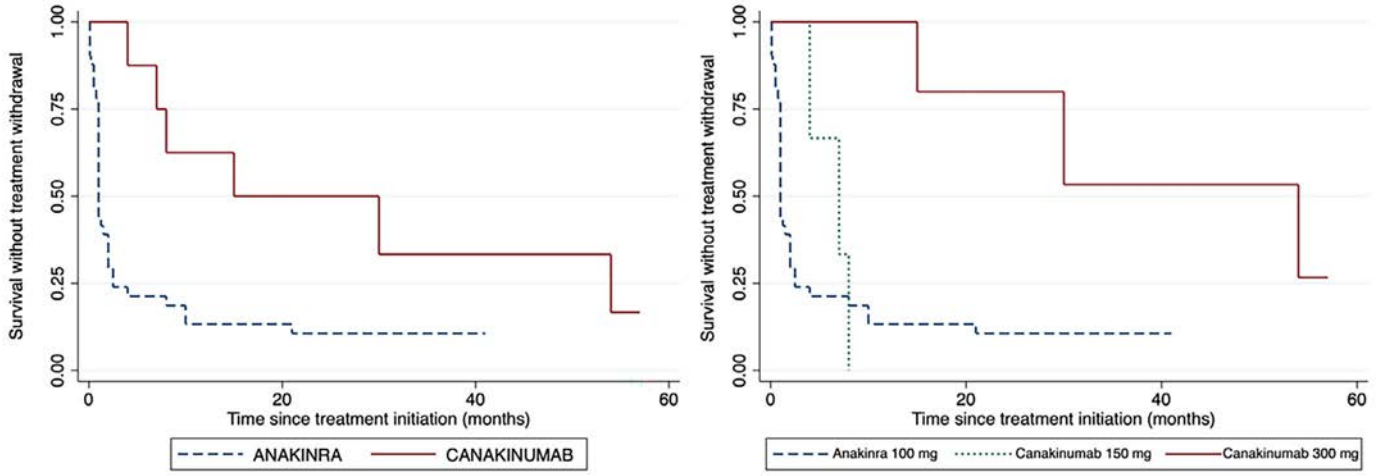

Figure 2. (Left) Kaplan-Meier curves of interleukin-1 inhibition therapy survival in patients with VEXAS (vacuoles, E1 enzyme, X-linked, autoinflammatory, somatic) syndrome receiving anakinra and canakinumab (P = 0.006). (Right) Kaplan-Meier curves of interleukin-1 inhibition therapy survival in patients with VEXAS (vacuoles, E1 enzyme, X-linked, autoinflammatory, somatic) syndrome receiving anakinra 100 mg/day, canakinumab 150 mg every 4 weeks, and canakinumab 300 mg every 4 weeks (P = 0.01). Color figure can be viewed in the online issue, which is available at http://onlinelibrary.wiley.com/doi/10.1002/art.43384/abstract.

Comparative safety of anakinra and canakinumab. Adverse events were reported in 31 patients (69%) receiving anakinra and 3 patients (30%) receiving canakinumab (P = 0.028) (Table 4). Regarding adverse events of special interest, the incidence of injection-site reactions and major injection-site reactions was recorded only in the anakinra group (47% and 0%, P = 0.006, and 32% and 0%, P = 0.048, respectively) (Table 4).

The rate of infections was higher in the anakinra group (31% and 11%, respectively), with pneumonia and cellulitis being the most common. Additionally, two patients developed *Clostridium difficile*–associated disease, one had a Salmonella infection, one had COVID-19, and one of the patients with a urinary tract infection progressed to septic shock. Neutropenia, significant enough to temporarily stop the medication, was reported at similar rates in both groups. No venous thromboembolic events were reported while receiving IL-1i, and one cardiovascular event was reported in the anakinra group. Four patients died while receiving IL-1i; one after 7 months of treatment with monthly canakinumab 150 mg, which his treating physician considered to be the most effective treatment for him (he previously received cyclosporine, infliximab, anakinra, and tocilizumab), because of a suspected myocardial infarction and/or a fatal arrhythmia. Three patients died while being treated with anakinra: one after 2 months of anakinra treatment while hospitalized, one of VEXAS evolution after 2 months of treatment, and one of an unspecified infection after 21 months of therapy.

Table 3. Reasons for discontinuation of interleukin-1 inhibitor therapy

	Anakinra (n = 44), n (%)	Canakinumab (n = 9), n (%)	*P* value
Stopped treatment	39 (91)	6 (67)	0.055
Inefficacy/flare	14 (36)	3 (50)	0.849
Adverse event	16 (41)	2 (33)	
Inefficacy/flare and adverse event	7 (18)	1 (17)	

DISCUSSION

In this multicenter, international, retrospective study of patients with VEXAS treated with IL-1i, we found that canakinumab exhibited better efficacy compared with anakinra, as reflected by a higher clinical response and longer drug survival.

Table 4. Adverse events of interest in patients receiving anakinra and canakinumab*

Adverse event	Anakinra (n = 44), n (%)	Canakinumab (n = 9), n (%)	*P* value
Any adverse event	31 (70)	3 (33)	**0.028**
Infection	11 (31)	1 (11)	0.3
Pneumonia	6 (14)	1 (11)	–
Cellulitis	3 (7)	0 (0)	–
UTI	1 (2)	0 (0)	–
CDAD	2 (5)	0 (0)	–
Other	3 (7)	0 (0)	–
Cardiovascular events	1 (2)	0 (0)	0.648
Injection-site reaction	21 (47)	0 (0)	**0.006**
Minor injection-site reaction	8 (18)	0 (0)	0.165
Major injection-site reaction	14 (32)	0 (0)	**0.048**
Minor systemic reaction	4 (9)	0 (0)	0.347
Allergic reaction	1 (2)	0 (0)	0.648
Neutropenia	5 (11)	1 (11)	0.983
GI bleeding	1 (2)	0 (0)	0.634
Death	3 (7)	1 (11)	0.657

* P values < 0.05 are significant and indicated with bold font. CDAD, *Clostridium difficile*–associated disease; GI, gastrointestinal; UTI, urinary tract infection.

Additionally, canakinumab exhibited a superior safety profile, with no injection-site reactions and numerically fewer infections compared with anakinra.

The results of this study are different than those of the French VEXAS registry published earlier, which combined IL-1i together, in which only three patients treated with canakinumab were included, finding only 9% GR in 3 months.[14] Nevertheless, our results are somewhat aligned with those of the UK study that reported an 88% response in 3 months for IL-1i.[15] The response of patients with VEXAS to an IL-1i medication may be expected, considering the cytokine profile characteristic of this monogenic acquired autoinflammatory disease.[5] Still, in clinical practice, most patients with VEXAS remain dependent on steroids, albeit at reduced doses, when treated with biologic or targeted synthetic therapies, as well as azacitidine as steroid-sparing agents.[2,20] Current practice to date, based on expert opinion, recommends using IL-6 receptor inhibitors or JAK inhibitors (JAKis; usually ruxolitinib) in patients without MDS or with low-risk MDS, and azacitidine or allogeneic hematopoietic stem cell transplantation for patients with intermediate or high-risk MDS or transfusion dependence.[21]

The theoretical advantage of IL-1i, including canakinumab, in autoinflammatory syndromes is its superiority in terms of time to clinical response, which can be observed within hours to days. Second, adverse events and specifically infections seem to be less common than in IL6 inhibition (IL-6i) and JAKi, which is an important aspect in VEXAS morbidity and mortality.[15,22,23]

According to the French VEXAS study by Hadjadj et al, the GR to IL-6i and JAKi after 3 months was reported to be 32% and 24%, respectively.[14] In the UK study, responses were better with 62% and 56% GR at 3 months, respectively.[15] Although direct comparisons cannot be made because these are separate studies and some data were missing in our cohort, along with small patient numbers, the GR for canakinumab (78%) observed in our study was notably high. In terms of survival, JAKi has shown a better survival rate than other biologics, with 75% of patients continuing to receive the medication after 12 months.[14] This rate is similar to the general survival rate for canakinumab, whereas canakinumab at 300 mg exhibited an even better survival rate, with 75% of patients still receiving the medication after 30 months.

Some limitations should be raised. First, this was a retrospective registry study, which means that some data are missing. Because of this, we had to impute some responses to the medication based on reported outcomes at the next time point. Given the relatively small number of patients, we chose to retain these cases rather than exclude them, to preserve the informational value and allow for meaningful comparisons across time points. This should be considered when drawing conclusions from the study. Another limitation of this analysis is the lack of full independence between treatment groups, as six patients received both anakinra and canakinumab sequentially. Although treatment groups were defined by treatment episodes, this overlap may introduce some degree of correlation that could not be fully addressed because of the small number of patients in the canakinumab group. Additionally, there is a significant selection bias; the groups were not randomized, and patients were treated according to local practices. For instance, canakinumab was used after anakinra in all patients, indicating that the treatment design was sequential and not comparative for most. Furthermore, the canakinumab group was small with only nine patients. This led to unstable estimates. Additionally, four patients received canakinumab for less than a year, resulting in significantly fewer patient-years in the canakinumab arm, which affects the total number of events. Lastly, response rates, as defined in this study, are similar to those in other studies dealing with treatment options for patients with VEXAS.[14,15] They include the decline of CRP, which may be somewhat artificially lowered by IL-1i, although less so than by IL-6i.[24] Thus, the results should be interpreted with caution, and comparisons should be repeated in a prospective randomized controlled study with a larger population of participants.

This is the largest study to date to examine IL-1i in VEXAS and, specifically, canakinumab treatment. This was a multicenter, international study with a representative group of patients with VEXAS. We assessed efficacy longitudinally and safety, including infections, injection-site reactions, and cytopenias, which may be the most common and disturbing adverse events in patients with VEXAS.

In conclusion, although VEXAS was first described >4 years ago, the optimal treatment approach remains uncertain. In this retrospective international study, the drug survival rate for canakinumab was greater than that for anakinra, with a median survival among patients receiving the 300 mg/month dose of four and a half years and for the 150 mg/month dose and the anakinra group was approximately 7 and 1 months, respectively. Adverse events may significantly limit the survival of anakinra use in patients with VEXAS. When considering financial factors, IL-1i for patients with VEXAS may be used sequentially, with canakinumab regarded as a rescue therapy for patients who do not tolerate anakinra. Specifically, canakinumab at 300 mg/month may be considered an additional steroid-sparing therapeutic option for patients with VEXAS alongside ruxolitinib, tocilizumab, and azacitidine.

ACKNOWLEDGMENTS

During the preparation of this work, the authors used Grammarly to improve language and readability. After using this tool, the authors reviewed and edited the content as needed and take full responsibility for the content of the publication.

AUTHOR CONTRIBUTIONS

All authors contributed to at least one of the following manuscript preparation roles: conceptualization AND/OR methodology, software, investigation, formal analysis, data curation, visualization, and validation AND drafting or reviewing/editing the final draft. As corresponding author, Dr Eviatar confirms that all authors have provided the final

approval of the version to be published and takes responsibility for the affirmations regarding article submission (eg, not under consideration by another journal), the integrity of the data presented, and the statements regarding compliance with institutional review board/Declaration of Helsinki requirements.

REFERENCES

1. Grayson PC, Patel BA, Young NS. VEXAS syndrome. Blood 2021; 137(26):3591–3594.
2. Beck DB, Ferrada MA, Sikora KA, et al. Somatic mutations in *UBA1* and severe adult-onset autoinflammatory disease. N Engl J Med 2020;383(27):2628–2638.
3. Ferrada MA, Savic S, Cardona DO, et al. Translation of cytoplasmic UBA1 contributes to VEXAS syndrome pathogenesis. Blood 2022; 140(13):1496–1506.
4. Collins JC, Magaziner SJ, English M, et al. Shared and distinct mechanisms of UBA1 inactivation across different diseases. EMBO J 2024; 43(10):1919–1946.
5. Kosmider O, Possémé C, Templé M, et al. VEXAS syndrome is characterized by inflammasome activation and monocyte dysregulation. Nat Commun 2024;15(1):910.
6. Jesus AA, Goldbach-Mansky R. IL-1 blockade in autoinflammatory syndromes. Annu Rev Med 2014;65(1):223–244.
7. Tan IJ, Ferrada MA, Ahmad S, et al. Skin manifestations of VEXAS syndrome and associated genotypes. JAMA Dermatol 2024;160(8): 822–829.
8. Staels F, Betrains A, Woei-A-Jin FJSH, et al. Case report: VEXAS syndrome: from mild symptoms to life-threatening macrophage activation syndrome. Front Immunol 2021;12:678927.
9. Kaiser C, Knight A, Nordström D, et al. Injection-site reactions upon Kineret (anakinra) administration: experiences and explanations. Rheumatol Int 2012;32(2):295–299.
10. Ramírez J, Cañete JD. Anakinra for the treatment of rheumatoid arthritis: a safety evaluation. Expert Opin Drug Saf 2018;17(7):727–732.
11. Estes J, Malus M, Wilson L, et al. A case of VEXAS: vacuoles, E1 enzyme, X-linked, autoinflammatory, somatic syndrome with coexisting DNA (cytosine-5)-methyltransferase 3A mutation complicated by localized skin reaction to tocilizumab and azacitidine. Cureus 2023; 15(6):e39906.
12. Ciprian G. Adverse reaction to COVID-19 mRNA vaccination in a patient with VEXAS syndrome. Cureus 2022;14(3):e23456.
13. Miyagi Y, Kobayashi H, Umebayashi Y, et al. A Japanese case of VEXAS syndrome after COVID-19 vaccination: comparison with previously reported cases. Mod Rheumatol Case Rep 2025;9(1):218–223.
14. Hadjadj J, Nguyen Y, Mouloudj D, et al; FRENVEX. Efficacy and safety of targeted therapies in VEXAS syndrome: retrospective study from the FRENVEX. Ann Rheum Dis 2024;83(10):1358–1367.
15. Al-Hakim A, Trikha R, Phyu Htut EE, et al. Treatment outcomes in patients with VEXAS syndrome: a retrospective cohort study. Lancet Rheumatol 2025;7(7):e472–e484.
16. Collantes-Rodríguez C, Jiménez-Gallo D, de la Varga- Martínez R, et al. Vexas syndrome successfully treated with canakinumab. J Dtsch Dermatol Ges 2023;21(1):69–70.
17. van der Made CI, Potjewijd J, Hoogstins A, et al. Adult-onset autoinflammation caused by somatic mutations in UBA1: a Dutch case series of patients with VEXAS. J Allergy Clin Immunol 2022;149(1): 432–439.e4.
18. Eviatar T, Zisapel M, Feinstein Goren N, et al. POS1198 epidemiology of VEXAS syndrome in Israel – a high prevalence of UBA1 p.M41V pathogenic variant in Israeli VEXAS patients. Ann Rheum Dis 2024; 83:548–549.
19. Campochiaro C, Tomelleri A, Cavalli G, et al. Successful use of cyclosporin A and interleukin-1 blocker combination in VEXAS syndrome: a single-center case series. Arthritis Rheumatol 2022;74(7):1302–1303.
20. Georgin-Lavialle S, Terrier B, Guedon AF, et al. Further characterization of clinical and laboratory features in VEXAS syndrome: large-scale analysis of a multicentre case series of 116 French patients. Br J Dermatol 2022;186(3):564–574.
21. Khitri MY, Hadjadj J, Mekinian A, et al. VEXAS syndrome: an update. Joint Bone Spine 2024;91(4):105700.
22. Fautrel B, Mitrovic S, De Matteis A, et al. EULAR/PReS recommendations for the diagnosis and management of Still's disease, comprising systemic juvenile idiopathic arthritis and adult-onset Still's disease. Ann Rheum Dis 2024;83(12):1614–1627.
23. Gutierrez-Rodrigues F, Kusne Y, Fernandez J, et al. Spectrum of clonal hematopoiesis in VEXAS syndrome. Blood 2023;142(3): 244–259.
24. Ridker PM. From C-reactive protein to interleukin-6 to interleukin-1: moving upstream to identify novel targets for atheroprotection. Circ Res 2016;118(1):145–156.

Arthritis & Rheumatology
Vol. 78, No. 2, February 2026, pp 483–488
DOI 10.1002/art.43315

American College of Rheumatology
Empowering Rheumatology Professionals

BRIEF REPORT

Autoantibody Response Toward Chromatin in Patients With Juvenile Idiopathic Arthritis

Viola Pitkänen,[1] Terhi Remes-Pakarinen,[2] Paula Vähäsalo,[3] Milja Möttönen,[4] Minna-Maija Grönlund,[4] Miika Arvonen,[2] Mikael Knip,[5] Riitta Veijola,[3] Jorma Toppari,[4] Jorma Ilonen,[6] Johanna Lempainen,[4] Anna-Mari Schroderus,[1] Liisa Kröger,[2] and Tuure Kinnunen[7]

Objective. Patients with juvenile idiopathic arthritis (JIA) frequently exhibit antinuclear antibodies (ANAs), but the specific antigen target recognized by them and the presence of additional autoantibody specificities in patients with JIA remains elusive.

Methods. Plasma samples from 110 untreated patients with active JIA, as well as from 14 children with unspecified arthritis and 151 age- and sex-matched healthy children, were analyzed with multiple modern clinical-grade autoantibody assays, including automated indirect immunofluorescence to screen for ANAs with HEp-2 cells, and specific immune assays to detect reactivity to individual autoantigens. In addition, a HuProt proteome microarray was used to screen for novel autoantibody targets in plasma samples from five patients with ANA-positive JIA and four ANA-negative healthy controls.

Results. Homogeneous nuclear ANA staining, indicating reactivity toward chromatin, was detected in most (61.8%) patients with JIA but rarely in healthy controls (2.6%; $P < 0.0001$). No antibody reactivity to specific nuclear antigens or other autoantigens associated with connective tissue diseases was detected. However, 20% of patients with JIA harbored antibodies against double-stranded DNA (dsDNA)–nucleosome complexes (compared with 2.6% of controls, $P < 0.0001$). Finally, the proteome microarray revealed core histone H2A variant H2AFY, part of the nucleosome, to be the most widely recognized human protein by autoantibodies of patients with JIA.

Conclusion. Autoantibody reactivity in JIA primarily targets chromatin, but the epitopes targeted are likely either posttranslationally modified or multimolecule epitopes, such as dsDNA–nucleosome complexes, rather than epitopes on individual native proteins or purified dsDNA.

INTRODUCTION

Juvenile idiopathic arthritis (JIA) is the most common chronic rheumatic disease in children. It is a heterogeneous condition, likely of autoimmune origin, and is currently classified into seven different subtypes according to the International League of Associations for Rheumatology (ILAR) criteria. These subtypes are oligoarthritis, rheumatoid factor–negative polyarthritis (Poly RF–), rheumatoid factor–positive polyarthritis (Poly RF+), systemic JIA, enthesitis-related arthritis, psoriatic arthritis, and undifferentiated arthritis.[1]

Approximately 30% to 60% of all patients with JIA test positive for antinuclear antibodies (ANAs).[2–5] ANA positivity is linked to specific JIA phenotypes and disease outcomes, such as early disease onset, female sex, oligoarthritis, and a higher risk of uveitis.[2–5] Based on this, ANA positivity has recently

Supported by The Foundation for Pediatric Research, Päivikki and Sakari Sohlberg Foundation, and ISLAB Laboratory Centre.

[1]Viola Pitkänen, MSc, Anna-Mari Schroderus, PhD: University of Eastern Finland, Kuopio, Finland; [2]Terhi Remes-Pakarinen, MD, PhD, Miika Arvonen, MD, PhD, Liisa Kröger, MD, PhD: Kuopio University Hospital, Kuopio; [3]Paula Vähäsalo, MD, PhD, Riitta Veijola, MD, PhD: Oulu University Hospital and University of Oulu, Oulu, Finland; [4]Milja Möttönen, MD, PhD, Minna-Maija Grönlund, MD, PhD, Jorma Toppari, MD, PhD, Johanna Lempainen, MD, PhD: University of Turku and Turku University Hospital, Turku, Finland; [5]Mikael Knip, MD, PhD: Tampere University Hospital, Tampere, and University of Helsinki, Helsinki, Finland; [6]Jorma Ilonen, MD, PhD: University of Turku, Turku, Finland; [7]Tuure Kinnunen, MD, PhD: University of Eastern Finland and ISLAB Laboratory Centre, Kuopio, Finland.

Additional supplementary information cited in this article can be found online in the Supporting Information section (http://onlinelibrary.wiley.com/doi/10.1002/art.43315).

Author disclosures are available at https://onlinelibrary.wiley.com/doi/10.1002/art.43315.

Address correspondence via email to Tuure Kinnunen, MD, PhD, at tuure.kinnunen@uef.fi.

Submitted for publication April 23, 2025; accepted in revised form July 1, 2025.

been proposed as a classification criteria for redefined JIA subgroups.[1]

ANA testing is currently poorly standardized, with significant variability in methods and cutoff values across different countries and laboratories, and specific nuclear staining patterns detected have rarely been reported in published studies.[2] Moreover, the exact autoantibody targets in JIA remain elusive. Reactivity to extractable nuclear antigens (ENAs), common autoantibody targets in other systemic rheumatic diseases, such as systemic lupus erythematosus (SLE), Sjögren disease, or systemic sclerosis, is rarely observed in patients with JIA.[5,6] However, the most common ANA staining pattern detected in patients with JIA appears to be homogeneous nuclear staining,[5] suggesting autoantibody reactivity against chromatin or its individual components: nucleosomes that further consist of double-stranded DNA (dsDNA) wrapped around histone proteins. In line with this, some earlier studies have reported increased reactivity to these structures in patients with JIA.[5,7,8]

In this study, we set out to explore the autoantibody reactivity in patients with JIA using a modern, highly standardizable automated immunofluorescence test system for ANA detection, several clinical-level antibody detection methods using well-defined autoantigens, and finally, a human protein microarray for unbiased discovery of autoantibody reactivity against the entire human proteome.

MATERIALS AND METHODS

Study participants. The study cohort included 110 pediatric patients, who met the ILAR criteria for JIA,[1] 151 healthy age- and sex-matched control children, and 14 children with the diagnosis of unspecified arthritis, that is, a single arthritis episode of unknown etiology not fulfilling the ILAR criteria for JIA (Supplementary Table 1). Patients with JIA were enrolled by pediatric rheumatologists at the Kuopio, Turku, and Oulu University Hospitals at the time of diagnosis or during clinical relapse after medication discontinuation. All patients with JIA either were treatment naive or had not used immunomodulatory medications for two months before the sampling. Healthy control children participated in the Finnish Type 1 Diabetes Prediction and Prevention follow-up study (http://dipp.utu.fi). Written informed consent was obtained from all study participants and/or their legal guardians, as mandated by the Declaration of Helsinki, and the study was approved by the ethics committees of the participating University Hospitals of Kuopio, Oulu, and Turku.

Samples. Peripheral blood samples from patients with JIA, healthy controls, and children with the diagnosis of unspecified arthritis were collected between May 2020 and October 2023 into lithium heparin blood collection tubes. The samples were centrifuged at 1,000 × *g* for 10 minutes, and plasma samples were collected and stored at –80 °C until analysis.

ANA detection by indirect immunofluorescence test. ANA measurements were performed using a fully automated indirect immunofluorescence test (IIFT) system. HEp-2 cell slides were stained using an IF Sprinter, and images were recorded with the Europattern Microscope Live automated microscope (both from Euroimmun AG). Plasma dilutions starting from 1:80 were used, and the immunofluorescence patterns were coded according to International Consensus on ANA Patterns (https://anapatterns.org/) recommendations. All samples were evaluated by a single laboratory physician with the aid of the Europattern Classifier software (Euroimmun AG).

Autoantibody assays. The anti–citrullinated protein/peptide (CCP) antibody and Phadia EliA connective tissue disease (CTD) screen assays (Thermo Fisher Scientific) were performed according to the manufacturer's instructions on a Phadia 250 instrument (Thermo Fisher Scientific). The individual antigens tested after a positive CTD screen were dsDNA, Sm, SSA/Ro52 and Ro60, SS-B/La, centromere B, Scl-70, Mi-2, RNA-Pol III, PM/Scl, Jo-1, PCNA, Ribosomal-P protein, U1-RNP (RNP-70, A, C), and fibrillarin. The Microblot-Array (MBA) ANA plus assay (TestLine Clinical Diagnostics), which detects 44 distinct autoantibodies using an immunoblot array in a microtiter format, was performed according to the manufacturer's instructions. Anti-dsDNA enzyme-linked immunosorbent assay (ELISA) (IgG), anti-dsDNA-NcX ELISA (IgG), anti-histone ELISA (IgG), and anti-nucleosomes ELISA (IgG) (all from Euroimmun AG) were performed according to the manufacturer's instructions.

HuProt proteome microarray. Five plasma samples from patients with ANA-positive JIA and four plasma samples from ANA-negative healthy control children were sent to Cambridge Protein Arrays Ltd for autoantibody profiling using the HuProt version 4.0 Human Proteome Microarray. For further details, please see Supplementary Methods.

Statistical analyses. GraphPad Prism software (version 10.4.1) was used for statistical analysis. Mann–Whitney U test, Kruskal-Wallis test with Dunn's posttest, Fisher's exact test, and McNemar test were used as indicated. A P value <0.05 was considered statistically significant.

RESULTS

Our study cohort included 110 children with JIA, sampled during active disease, either at diagnosis or during a disease relapse after medication discontinuation. As control groups, we had 14 children diagnosed with unspecified arthritis (disease controls) and 151 age- and sex-matched healthy control children. The majority of patients with JIA were diagnosed with Poly RF– (n = 38), oligoarthritis (n = 56), or enthesitis-related arthritis (n = 9), with the remaining patients diagnosed with Poly RF+

(n = 3), psoriatic arthritis (n = 2), or other juvenile arthritis (n = 2). The demographic and clinical characteristics of the study groups are detailed in Supplementary Table 1.

We first screened the plasma samples for ANAs using a highly standardized, fully automated IIFT method. ANA positivity at a titer of ≥1:160 was observed in 86 out of 110 (78.2%) patients with JIA, compared with 57 out of 151 (37.7%) healthy children and six out of 14 (42.9%) children with unspecified arthritis (Figure 1A). Several patients with JIA displayed ANA positivity at higher titers (≥1:640), which was not detected in the healthy children (Figure 1A). In addition to ANA titer, the staining pattern of ANA reactivity was determined. The majority of ANA-positive samples exhibited either a speckled or homogeneous nuclear staining pattern (Figure 1B). The speckled nuclear staining pattern, indicating autoantibody reactivity to nuclear proteins not part of the chromatin, was most commonly observed in healthy children. In contrast, the homogeneous nuclear staining pattern, indicating reactivity to chromatin, was dominant in patients with JIA

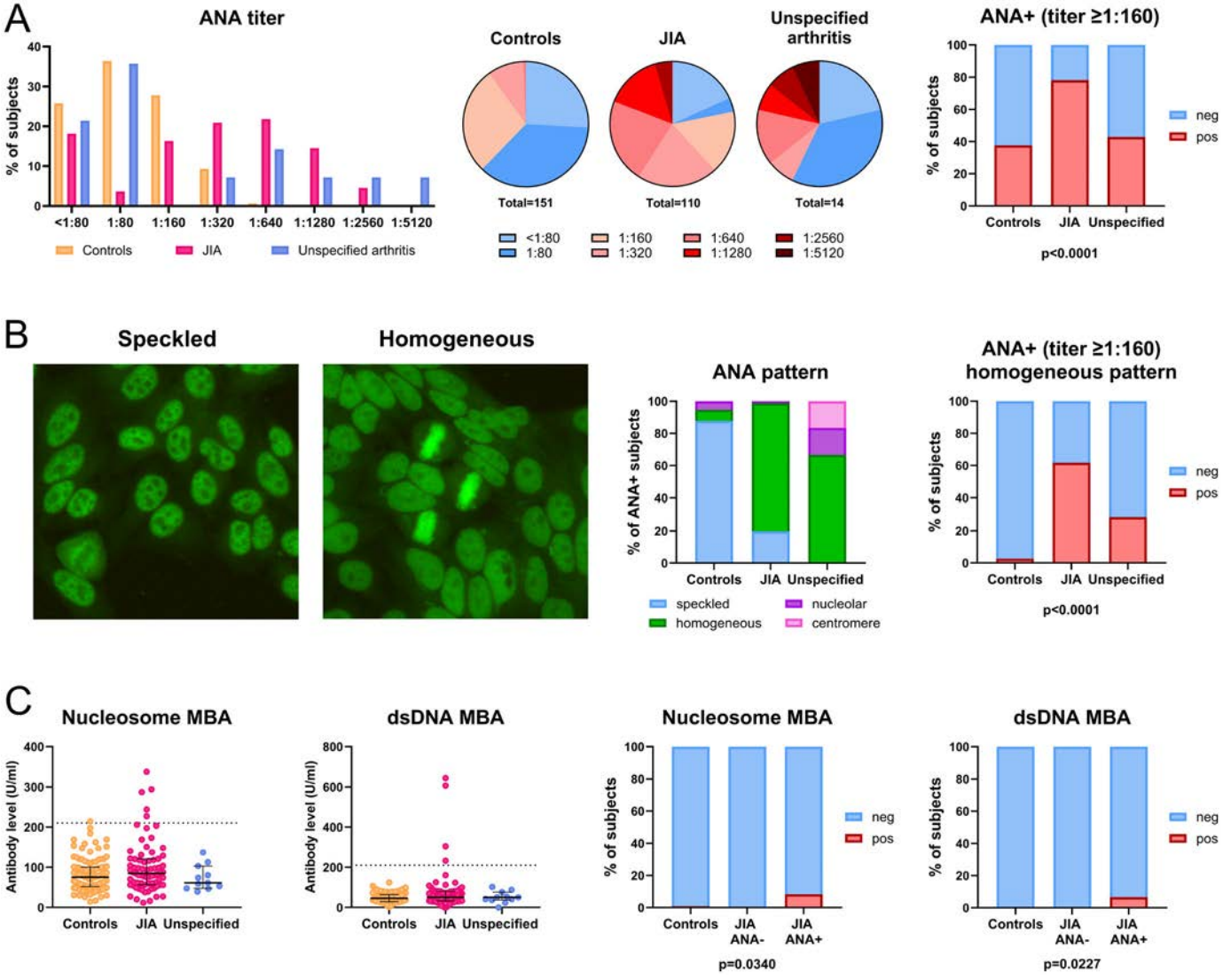

Figure 1. Homogeneous nuclear ANA staining in patients with JIA suggests autoantibody reactivity toward chromatin. (A) Frequency (left panel) and distribution (middle panel) of different ANA titers observed in the study groups using an IIFT. Frequency of ANA-positive subjects (ANA ≥1:160) in the different study groups (right panel). (B) Representative speckled and homogeneous nuclear ANA staining patterns in HEp-2 cells using IIFT (left panel). Distribution of nuclear ANA staining patterns in ANA-positive (ANA ≥1:160) subjects in the different study groups (middle panel). Frequency of ANA-positive subjects (ANA ≥1:160) with a homogeneous nuclear staining pattern in the different study groups (right panel). (C) Reactivity toward nucleosomes and dsDNA in the MBA presented as concentration (U/mL) of antibodies (left panels), with the error bars depicting concentration median and interquartile range. The frequency of subjects testing positive for nucleosomes or dsDNA at a cutoff value of 210 U/mL (dotted line) in the controls, and patients with ANA-negative (ANA <1:160) and ANA-positive (ANA ≥1:160) JIA (right panels). Fisher's exact test was used for statistical analysis. ANA, antinuclear antibody; dsDNA, double-stranded DNA; IIFT, indirect immunofluorescence test; JIA, juvenile idiopathic arthritis; MBA, Microblot-Array.

(Figure 1B). In fact, a homogeneous nuclear ANA staining result at a titer of ≥1:160 distinguished patients with JIA (68 out of 110; 61.8%) from healthy children (4 out of 151; 2.6%) more effectively than overall ANA positivity at the same titer ($P < 0.001$; McNemar test), with children with unspecified arthritis again falling in between (4 out of 14; 28.6%) (Figure 1B). Because our sampling period (2020–2023) spanned the COVID-19 pandemic, we also assessed the ANA results longitudinally. Interestingly, whereas the frequency of ANA positivity remained stable in patients with JIA, it increased in healthy controls from late 2021 onward (Supplementary Figure 1). This was driven by an increase in low-titer (1:160 or 1:320) ANA positivity with a speckled nuclear staining pattern. Consequently, no temporal shifts were observed when using ANA positivity at a titer of ≥1:160 with a homogeneous nuclear staining pattern as the criteria for positivity (Supplementary Figure 1).

Consistent with previous studies,[2–5] ANA positivity at a titer of ≥1:160, particularly with a homogeneous nuclear staining pattern, was associated with female sex, risk of uveitis, and younger age at disease onset in patients with JIA (Supplementary Figure 2). Moreover, higher erythrocyte sedimentation rate and C-reactive protein values were detected in patients with ANA-positive JIA at sampling, but no association with HLA-B27 positivity, number of active joints, Juvenile Arthritis Disease Activity Score 10, or cytomegalovirus seropositivity was detected (Supplementary Figure 2).

To further explore autoantibody reactivity in patients with JIA, we first screened the plasma samples for CCP antibodies, which are diagnostic of rheumatoid arthritis, and for 16 specific ENAs commonly observed in systemic autoimmune rheumatic diseases. CCPs were detected only in the three patients with JIA diagnosed with Poly RF+, as expected, and low levels of ENAs were detected only in a few isolated patients, with dsDNA antibodies being the most common finding (detected in four patients with JIA; Supplementary Table 2). We then performed a broader autoantibody screening using an immunoblot array (MBA), which allows probing autoantibody reactivity against 44 distinct autoantigens associated with different autoimmune diseases. Again, a few isolated patients with JIA displayed autoantibody reactivity against nucleosomes (5 out of 73; 6.8%) and dsDNA (4 out of 73, 5.5%) and even more rarely to the other 42 autoantigens tested (Figure 1C; Supplementary Table 3). Notably, all patients with JIA displaying reactivity against dsDNA or nucleosomes also showed ANA positivity in IIFT (Figure 1C).

Given the predominant homogeneous nuclear ANA staining pattern and the rare specific autoantibody reactivities to dsDNA or nucleosomes detected in patients with JIA, we further explored autoantibody reactivity to components of chromatin. Chromatin consists of linker dsDNA and repeating units of nucleosomes, that is, dsDNA coiled around an octamer of core histone proteins (Figure 2A). Therefore, the plasma samples were assayed with clinical-grade ELISAs detecting autoantibodies against purified dsDNA, histone, and nucleosomes, but no differences were observed between the study cohorts (Supplementary Figure 3). We also tested the samples with a dsDNA-NcX ELISA kit, which uses dsDNA complexed with nucleosomes, a more natural antigen structure compared with purified dsDNA or nucleosomes, and has shown better performance compared with dsDNA ELISAs in diagnosing SLE.[9] Surprisingly, samples from patients with JIA showed increased reactivity in this ELISA, with 22 out of 110 (20.0%) samples from patients with JIA positive using the manufacturer's cutoff compared with four out of 151 (2.6%) healthy children and none of 14 (0%) children with unspecified arthritis (Figure 2B). The dsDNA-NcX reactivity also strongly correlated with ANA positivity, with 21 out of 86 (24.4%) patients with ANA-positive JIA showing a positive response compared with only one out of 24 (4.2%) ANA-negative patients (Figure 2B).

Finally, to perform an unbiased screening for autoantibody targets, we used the HuProt human proteome microarray, which consists of more than 21,000 unique human proteins and isoform variants. For this exploratory study, we selected five samples from female patients with early-onset JIA exhibiting high-titer homogeneous nuclear ANA staining and compared them with four samples from age- and sex-matched, ANA-negative healthy controls. Interestingly, H2AFY (core histone macro-H2A) was identified as the most abundantly recognized autoantibody target in patients with JIA (Figure 2C). H2AFY is a variant of the H2A subunit of the nucleosome and subsequently part of the chromatin, making it a logical autoantigen hit given the homogeneous nuclear ANA staining pattern observed in the studied patients with JIA. Overall, between 50 and 103 individual proteins were identified as highly antibody-binding targets (Z score of >3) for each of the five JIA patient samples studied. Filtering these to proteins recognized with a Z score of >3 by at least three out of five patients with JIA but by none of the four healthy controls identified six additional proteins (in addition to H2AFY) as putative autoantibody targets: MAGI1 (membrane-associated guanylate kinase WW and PDZ domain–containing 1), KEAP1 (Kelch-like ECH-associated protein 1), CCNB2 (cyclin B2), MYOD1 (myogenic differentiation antigen 1), HSPA13 (heat shock protein 70 family A member 13), and NEDD9 (neural precursor cell expressed developmentally down-regulated protein 9) (Figure 2C).

DISCUSSION

In this study, we first confirmed using a highly standardized ANA IIFT method that the majority of children with JIA are positive for ANAs, with most displaying a homogeneous nuclear staining pattern. This pattern suggests the presence of autoantibodies targeting chromatin, which are rarely detected in healthy children. Using several clinical-grade autoantibody assays, we verified that this reactivity is not primarily due to autoantibodies against common nuclear antigens detected in other CTDs[5,6] or to individual components of chromatin, such as purified dsDNA, histone

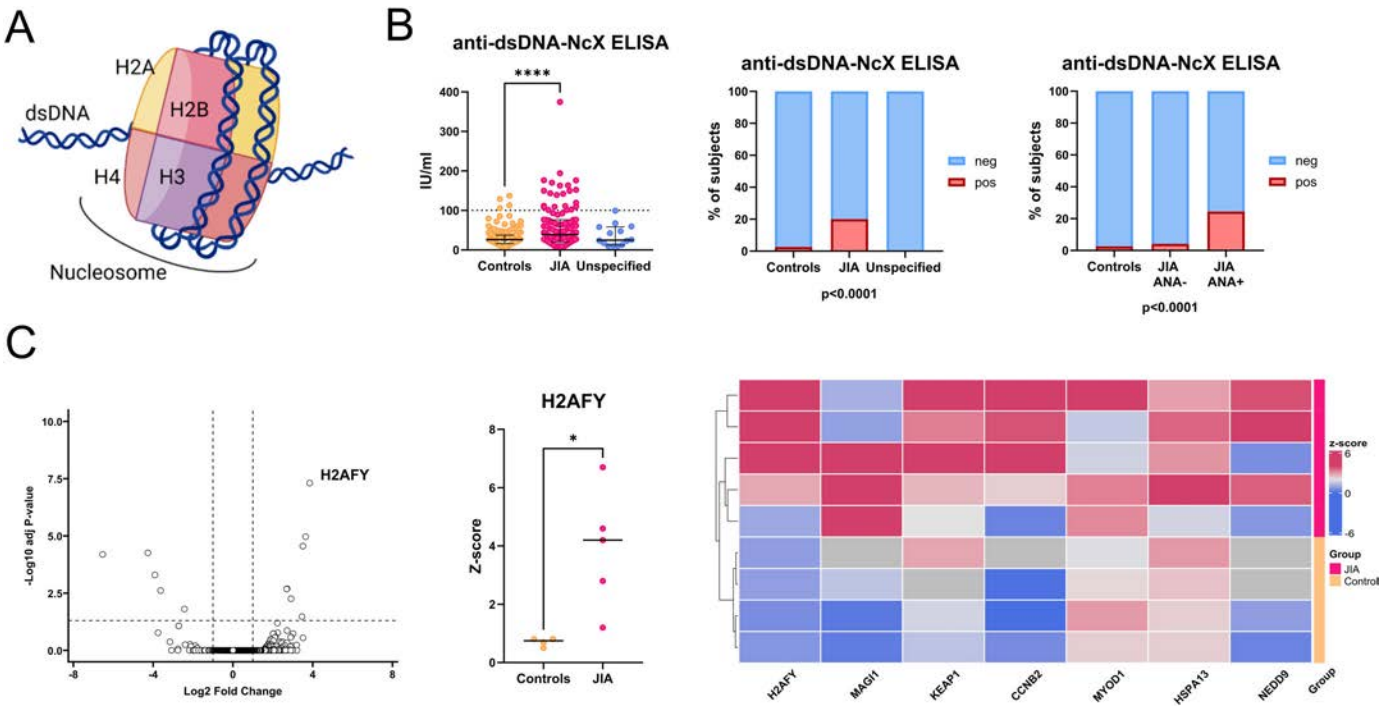

Figure 2. Patients with JIA show increased reactivity toward dsDNA-NcX. (A) A schematic representation of the basic structure of chromatin, which consists of linker dsDNA and repeating units of nucleosomes, that is, dsDNA coiled around an octamer consisting of two pairs of core histone proteins H2A, H2B, H3, and H4. Image created with BioRender.com. (B) Results from anti-dsDNA-NcX ELISA presented as concentration of antibodies (left panel), with the error bars depicting concentration median and interquartile range. Frequency of subjects testing positive at a cutoff value of 100 IU/mL (dotted line) in the different study groups (middle panel), and with patients with JIA separated into ANA-negative (<1:160) and ANA-positive (≥1:160) subgroups (right panel). Statistical testing was performed using Kruskal-Wallis test with Dunn's posttest (left panel) or Fisher's exact test (middle and right panels). (C) Differentially detected autoantibody targets in patients with JIA compared with controls depicted as a volcano plot of the HuProt microarray data (left panel). Z scores of H2AFY reactivity in healthy controls and patients with JIA (middle panel). Mann–Whitney U test was used for statistical testing. Heatmap visualization of reactivities (Z scores) of autoantibody targets recognized with a Z score of >3 by at least three out of five patients with JIA but by none of the four healthy controls. *P < 0.05, ****P < 0.0001. CCNB2, cyclin B2; dsDNA, double-stranded DNA; dsDNA-NcX, double-stranded DNA–nucleosome complexes; ELISA, enzyme-linked immunosorbent assay; H2A, histone H2A; H2AFY, histone 2A variant; H2B, histone H2B; H3, histone H3; H4, histone H4; HSPA13, heat shock protein family A member 13; KEAP1, Kelch-like ECH-associated protein 1; MAGI1, membrane associated guanylate kinase WW and PDZ domain containing 1; MYOD1, myogenic differentiation antigen 1; NEDD9, neural precursor cell expressed developmentally down-regulated protein 9.

proteins, or nucleosomes because reactivity to these was detected in only a small fraction of the patients in this study. In contrast, however, 20% of patients with JIA showed reactivity to dsDNA-NcX, which consists of dsDNA–nucleosome complexes. This structure likely represents a more natural antigen compared with purified dsDNA or nucleosomes because in vivo dsDNA is bound to nucleosomes within apoptotic cell fragments presented to the immune system.[9] Interestingly, a previous study assaying autoantibody reactivity to a different artificial histone-dsDNA construct reported highly similar results, with reactivity seen in 24% of patients with JIA but in none of the controls.[7] Collectively, these findings suggest that a major autoantibody target in JIA is a conformational epitope formed by a dsDNA–nucleosome complex rather than epitopes on dsDNA or individual histone proteins.

It is important to note the discrepancy between the level of reactivity to dsDNA-NcX (20%) and antichromatin reactivity observed in the IIFT assay (>60% at the titer of ≥160). This suggests that dsDNA-NcX may not contain all the conformational structures present in chromatin of intact HEp-2 cells used in the IIFT assay. Alternatively, chromatin proteins in HEp-2 cells may have undergone posttranslational modifications not present in the purified antigens used in laboratory assays. For example, some studies have suggested that citrullinated or carbamylated histone structures could be targets of autoantibodies in JIA.[10,11]

Besides autoantibodies against chromatin, there may be other autoantibody targets in JIA not detectable with HEp-2 IIFT. To investigate this, we conducted a human protein microarray screening for antibody reactivity to more than 21,000 distinct human proteins and isoform variants, the broadest autoantibody screening performed in JIA, to our knowledge. Interestingly, the most broadly recognized protein was H2AFY, a histone protein forming part of the nucleosome, reinforcing the central role of chromatin as the major autoantibody target in JIA. Previous studies exploring autoantibody reactivity in JIA using more limited protein microarrays or peptide libraries[12–15] have yielded highly variable results. A limitation of some of these previous studies is

that only linear, but not conformational, epitopes can be identified when using peptide fragments instead of whole proteins as targets. Moreover, the few potential protein targets, in addition to H2AFY, identified in our study were not part of the more restricted libraries screened in the previous studies, so their potential as autoantibody targets would need to be confirmed in future studies. An important limitation even of our large-scale proteome study using whole proteins is that conformational epitopes not part of individual proteins, such as the dsDNA-NcX structure, or posttranslationally modified protein epitopes would not be detected. However, overall, both our current and the previous screening studies suggest that no single natural protein target is likely recognized by the autoantibodies of a majority of the patients with JIA.

In this study, we noted that from late 2021 onward, healthy control children showed a rising incidence of low-titer ANA positivity with a speckled nuclear pattern. This phenomenon temporally coincides with the drastic increase in SARS-CoV-2 infections in children after relaxation of COVID-19 restrictions in Finland.[16] Several small studies have suggested that SARS-CoV-2 infections can lead to an increase in low-titer autoantibodies, including ANAs,[17] aligning with our findings. Importantly, however, the proportion of ANA-positive samples with a homogeneous nuclear pattern remained unchanged over time in both patients with JIA and controls, indicating that the chromatin-targeted autoantibody reactivity predominant in patients with JIA was stable and unaffected by the pandemic.

In conclusion, our comprehensive assessment of autoantibody reactivity in patients with JIA suggests that (1) chromatin is the main target of autoantibody reactivity in JIA and (2) the epitopes targeted are likely conformational structures formed by different molecules, such as the dsDNA-nucleosome complexes, and/or posttranslationally modified epitopes of chromatin proteins. The detection of a typical homogeneous nuclear staining pattern with a highly standardized ANA IIFT assay remains the best diagnostic modality to detect JIA-associated autoantibodies. However, our current data suggest that the dsDNA-NcX assay, or further modifications of it, could be used as a supporting method for a highly specific detection of JIA-associated anti–chromatin autoantibody reactivity.

ACKNOWLEDGMENTS

We thank the skillful technical assistance of Hanna Eskelinen (University of Eastern Finland), Anne Suominen (University of Turku), Birgitta Grekula (University of Oulu), Virpi Glumoff (University of Oulu), Nelli Rönkä (University of Oulu), Tiia Honkanen (University of Oulu), Leila Venäläinen (ISLAB Laboratory Centre), and Elsa Kokkonen (ISLAB Laboratory Centre). We thank Tuomas Selander (Kuopio University Hospital) for help with statistical analysis. Open access publishing facilitated by Ita-Suomen yliopisto, as part of the Wiley - FinELib agreement.

AUTHOR CONTRIBUTIONS

All authors contributed to at least one of the following manuscript preparation roles: conceptualization AND/OR methodology, software, investigation, formal analysis, data curation, visualization, and validation AND drafting or reviewing/editing the final draft. As corresponding author, Dr Kinnunen confirms that all authors have provided the final approval of the version to be published and takes responsibility for the affirmations regarding article submission (eg, not under consideration by another journal), the integrity of the data presented, and the statements regarding compliance with institutional review board/Declaration of Helsinki requirements.

REFERENCES

1. Nigrovic PA, Colbert RA, Holers VM, et al. Biological classification of childhood arthritis: roadmap to a molecular nomenclature. Nat Rev Rheumatol 2021;17(5):257–269.
2. Storwick JA, Brett AC, Buhler K, et al. Prevalence and titres of antinuclear antibodies in juvenile idiopathic arthritis: a systematic review and meta-analysis. Autoimmun Rev 2022;21(6):103086.
3. Saurenmann RK, Levin AV, Feldman BM, et al. Prevalence, risk factors, and outcome of uveitis in juvenile idiopathic arthritis: a long-term followup study. Arthritis Rheum 2007;56(2):647–657.
4. Glerup M, Herlin T, Twilt M. Remission rate is not dependent on the presence of antinuclear antibodies in juvenile idiopathic arthritis. Clin Rheumatol 2017;36(3):671–676.
5. Nordal EB, Songstad NT, Berntson L, et al. Biomarkers of chronic uveitis in juvenile idiopathic arthritis: predictive value of antihistone antibodies and antinuclear antibodies. J Rheumatol 2009;36(8):1737–1743.
6. Schulz C, Fuehner S, Schlüter B, et al. Prevalence of autoantibodies in patients with juvenile idiopathic arthritis: results from the German inception cohort ICON-JIA. Pediatr Rheumatol Online J 2022;20(1):8.
7. Ingegnoli F, Del Papa N, Comina DP, et al. Autoantibodies to chromatin: prevalence and clinical significance in juvenile rheumatoid arthritis. Clin Exp Rheumatol 2004;22(4):499–501.
8. Leak AM, Woo P. Juvenile chronic arthritis, chronic iridocyclitis, and reactivity to histones. Ann Rheum Dis 1991;50(9):653–657.
9. Biesen R, Dähnrich C, Rosemann A, et al. Anti-dsDNA-NcX ELISA: dsDNA-loaded nucleosomes improve diagnosis and monitoring of disease activity in systemic lupus erythematosus. Arthritis Res Ther 2011;13(1):R26.
10. Parackova Z, Zentsova I, Malcova H, et al. Increased histone citrullination in juvenile idiopathic arthritis. Front Med (Lausanne) 2022;9:971121.
11. Muller PCEH, Anink J, Shi J, et al. Anticarbamylated protein (anti-CarP) antibodies are present in sera of juvenile idiopathic arthritis (JIA) patients. Ann Rheum Dis 2013;72(12):2053–2055.
12. Stoll ML, Li Q-Z, Zhou J, et al. Elevated IgG autoantibody production in oligoarticular juvenile idiopathic arthritis may predict a refractory course. Clin Exp Rheumatol 2011;29(4):736–742.
13. Gibson DS, Qiu J, Mendoza EA, et al. Circulating and synovial antibody profiling of juvenile arthritis patients by nucleic acid programmable protein arrays. Arthritis Res Ther 2012;14(2):R77.
14. Arve-Butler S, Mossberg A, Kahn F, et al. Identification of novel autoantigens as potential biomarkers in juvenile idiopathic arthritis associated uveitis. Front Pediatr 2023;10:1091308.
15. Araujo GR, Fujimura PT, Vaz ER, et al. A novel reactive epitope-based antigen targeted by serum autoantibodies in oligoarticular and polyarticular juvenile idiopathic arthritis and development of an electrochemical biosensor. Immunobiology 2016;221(5):634–640.
16. Kuitunen I, Artama M, Haapanen M, et al. Respiratory virus circulation in children after relaxation of COVID-19 restrictions in fall 2021-a nationwide register study in Finland. J Med Virol 2022;94(9):4528–4532.
17. Galipeau Y, Cooper C, Langlois M-A. Autoantibodies in COVID-19: implications for disease severity and clinical outcomes. Front Immunol 2025;15:1509289.

Arthritis & Rheumatology
Vol. 78, No. 2, February 2026, pp 489

DOI 10.1002/art.43340

Clinical Images: Methotrexate-induced melanonychia

The patient, a 62-year-old woman diagnosed with rheumatoid arthritis and erosive osteoarthritis, has been treated with methotrexate (MTX) for three years. She was in clinical remission but presented with nail changes and discoloration of the nails three years after MTX initiation. A physical examination revealed the presence of dystrophic nails, characterized by nail plates with black discoloration and an increased transverse curvature involving all fingernails with cuticle and lunula disappearance (top and middle). Laboratory tests showed normal renal and hepatic function and a C-reactive protein level of 0.07 mg/dL. She was positive for rheumatoid factor (211 IU/mL) and anticyclic citrullinated peptide antibody (30 U/mL). Test results for antinuclear antibody, antineutrophil cytoplasmic antibodies, antiphospholipid antibodies, several tumor markers, adrenal hormone, and thyroid hormone were negative or normal. T-SPOT.TB test, β-D-glucan, and blood cultures were negative. A biopsy of her nail excluded dermatological diseases, including psoriasis; fungal infection; and malignant diseases. She was diagnosed with MTX-induced melanonychia. MTX was withdrawn, and she was switched to sulfasalazine. One year after MTX withdrawal, her nails returned to almost normal (bottom). Melanonychia has been known to be associated with dermatological diseases, nutritional disorders, and endocrine abnormalities and could also be induced by certain drugs, including bleomycin sulfate, cyclophosphamide, doxorubicin, MTX, hydroxychloroquine, and infliximab.[1] This case should remind readers to consider not only dermatological diseases, nutritional disorders, and endocrine abnormalities but also drug-induced conditions, including from MTX, as underlying causes of melanonychia in patients with rheumatic disease.

Author disclosures are available at https://onlinelibrary.wiley.com/doi/10.1002/art.43340.

1. Jefferson J, Rich P. Melanonychia. Dermatol Res Pract 2012;2012: 952186.

Yoshinori Taniguchi, MD
yoshii.tan@gmail.com
Department of Rheumatology, Bay Side Misato Medical Center
Kochi, Japan
and Department of Endocrinology, Metabolism, Nephrology and Rheumatology, Kochi Medical
School Hospital
Nankoku, Japan

Hirotaka Yamamoto, MD
Department of Endocrinology, Metabolism, Nephrology and Rheumatology, Kochi Medical
School Hospital
Nankoku, Japan
and Department of Internal Medicine, Kochi Prefectural Hata-Kenmin Hospital
Sukumo, Japan

Arthritis & Rheumatology
Vol. 78, No. 2, February 2026, pp 490

DOI 10.1002/art.43353

Clinical Images: Syphilis as the great imitator; Behçet disease mimic

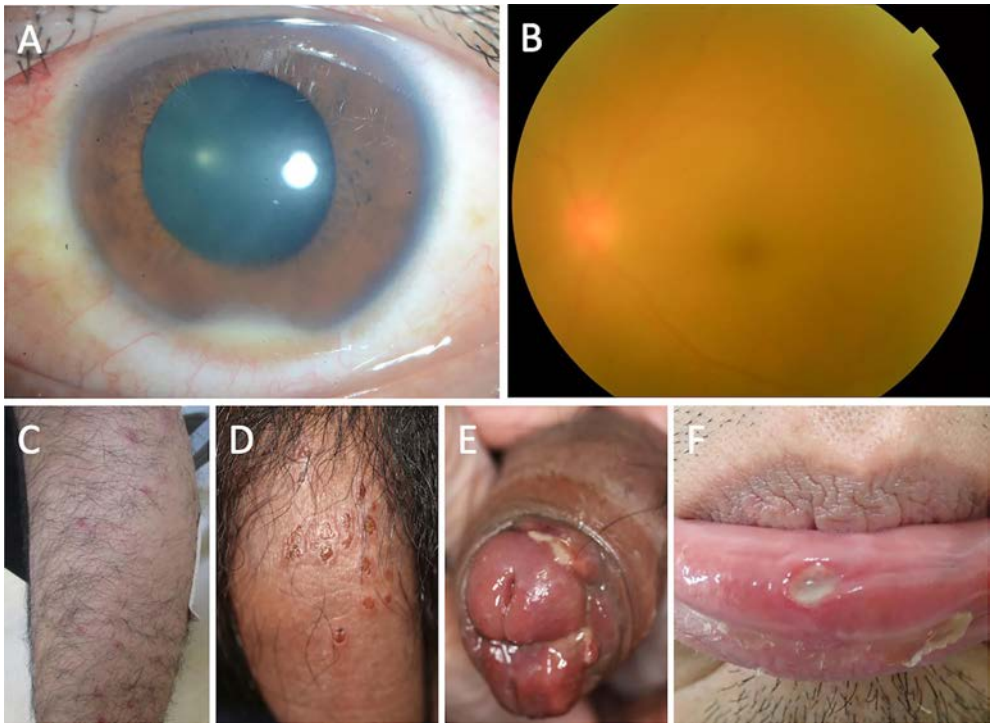

A 40-year-old man presented to the ophthalmology department with a one-day history of blurred vision in the left eye. For approximately three weeks, he suffered with penile swelling, painless erythema, and erosions on his penis and scrotum. The left eye best-corrected visual acuity decreased to 20/63. Slit-lamp examination revealed inflammatory cells in the anterior chamber with (A) hypopyon and (B) vitreous in his left eye. (C) Upon physical examination, reddish-brown papules on the trunk and legs were observed. The patient also had ulcerative lesions on the (D) penile skin and (E) glans penis. (F) He later developed ulceration of the lips. This patient presented uveitis with hypopyon, along with mucocutaneous manifestations including skin lesions and genital and oral aphthous ulcers. These clinical features were suggestive of Behçet disease.[1] However, the test results for rapid plasma reagin, treponema pallidum hemagglutination, and a cerebrospinal fluid fluorescent treponemal antibody absorption were positive. This led the diagnosis to uveitis and other systemic symptoms due to secondary syphilis. After treatment with intravenous aqueous penicillin G, the systemic and ocular symptoms were cured. Vision was restored. Uveitis, consequent to Behçet disease, sarcoidosis, and Vogt–Koyanagi–Harada disease, is often diagnosed based on characteristic ocular inflammation in conjunction with various systemic manifestations. However, syphilis, known as "the great imitator," is often characterized by a wide spectrum of systemic presentations; syphilitic uveitis also exhibits diverse patterns of uveitis.[2] This report reminds clinicians that syphilis can be a great imitator of Behçet disease.

Author disclosures are available at https://onlinelibrary.wiley.com/doi/10.1002/art.43353.

1. Emmi G, Bettiol A, Hatemi G, Prisco D. Behcet's syndrome. Lancet 2024;403:1093–1108.
2. Peeling RW, Mabey D, Chen XS, Garcia PJ. Syphilis. Lancet 2023;402:336–346.

Ken Fukuda, MD, PhD
k.fukuda@kochi-u.ac.jp
Kenji Yamashiro, MD, PhD
Department of Ophthalmology and Visual Science, Kochi Medical School, Kochi University
Nankoku City, Kochi, Japan

Arthritis & Rheumatology
Vol. 78, No. 2, February 2026, pp 491–492

American College of Rheumatology
Empowering Rheumatology Professionals

DOI 10.1002/art.43351

Clinical Images: Paradoxical hepatic encephalopathy in lupus nephritis: a diagnostic challenge

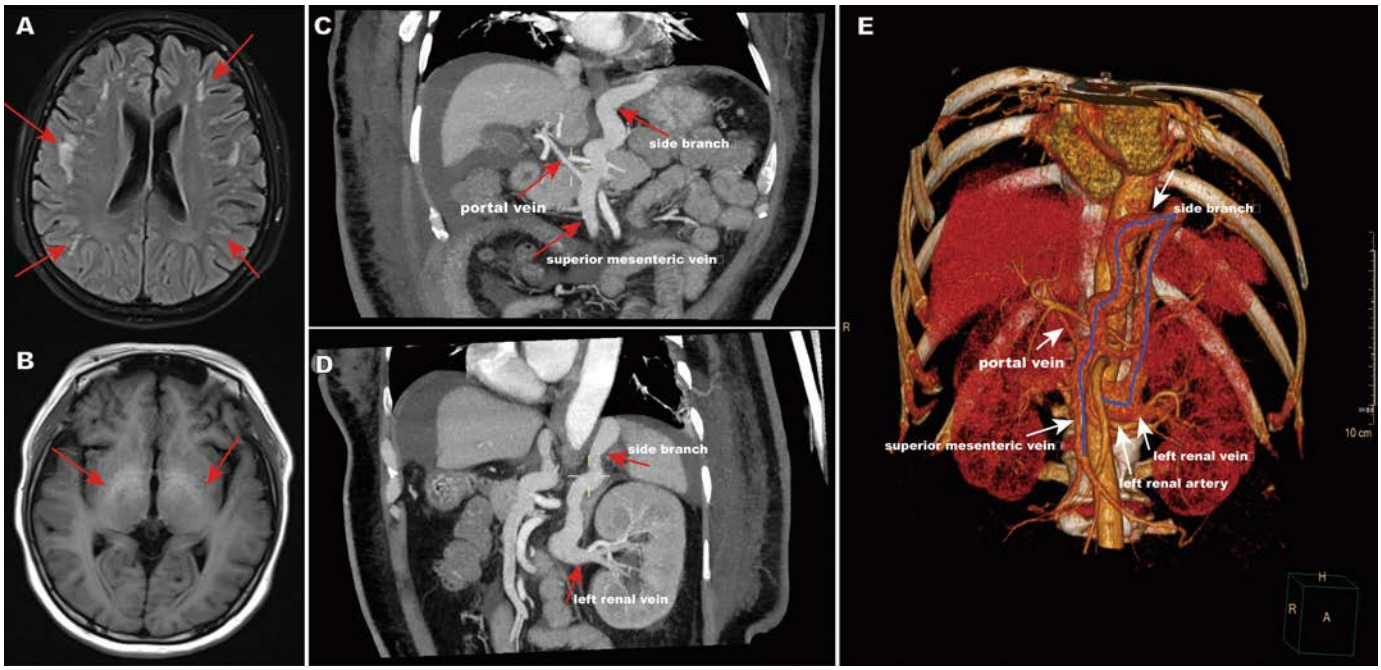

The patient, a 60-year-old woman with class V lupus nephritis, presented with acute encephalopathy and urinary retention shortly after the initiation of methylprednisolone. The initial brain magnetic resonance image (MRI) demonstrated nonspecific subcortical white matter hyperintensities on T2 fluid-attenuated inversion recovery (A). Infectious etiologies were excluded by cerebrospinal fluid analysis, and neuropsychiatric lupus was initially suspected. Despite prompt initiation of intravenous pulse steroids, the patient developed recurrent episodes of encephalopathy accompanied by asterixis. On hospital day 10, repeat brain MRI revealed symmetrical hyperintensity of the bilateral globus pallidus on T1-weighted imaging (B), prompting a workup for metabolic derangements. A markedly elevated serum ammonia level (238 μmol/L) was detected, leading to a contrast-enhanced abdominal computed tomography scan that identified a congenital portosystemic shunt (CEPS); the superior mesenteric vein drained via a prominent collateral channel into the left renal vein, with hypoplastic portal vasculature (C–E). An initiation of ammonia-lowering therapy (including lactulose, rifaximin, L-ornithine L-aspartate, and branched-chain amino acids), along with a gradual tapering of steroids, resulted in a complete resolution of her neurologic symptoms. She was subsequently managed in consultation with hepatology and interventional radiology, with plans for long-term monitoring of hepatic and neurocognitive function. This case underscores the importance of considering metabolic encephalopathies in patients with autoimmune diseases presenting with altered mental status, especially when treatment for neuropsychiatric lupus proves ineffective. The sequential evolution of radiologic findings—from nonspecific white matter changes to classic basal ganglia involvement—demonstrates the diagnostic utility of repeated neuroimaging in such complex cases. Although CEPS are exceedingly rare, particularly in adults and in the context of lupus nephritis,[1] their timely diagnosis is crucial, as they represent a reversible cause of chronic hyperammonemic encephalopathy. Close multidisciplinary follow-up is necessary to monitor for potential complications and to optimize long-term outcomes.[2,3]

Author disclosures are available at https://onlinelibrary.wiley.com/doi/10.1002/art.43351.

1. Shastri A, De A, Ashraf MU, et al. Congenital intrahepatic portosystemic shunt presenting with recurrent hepatic encephalopathy in adulthood. J Clin Exp Hepatol 2025;15(6):102630.
2. Legge AC, Hanly JG. Recent advances in the diagnosis and management of neuropsychiatric lupus. Nat Rev Rheumatol 2024;20(11):712–728.
3. Karino K, Kono M, Takeyama S, et al. Inhibitor of NF-κB kinase subunit ε contributes to neuropsychiatric manifestations in lupus-prone mice through microglial activation. Arthritis Rheumatol 2023;75(3):411–423.

Xu-jie Zhou, MD, PhD
zhouxujie@bjmu.edu.cn
Renal Division, Peking University First Hospital, Kidney Genetics Center, Peking University Institute of Nephrology, Key Laboratory of Renal Disease, National Health Commission, Key Laboratory of Chronic Kidney Disease Prevention and Treatment (Peking University), Ministry of Education; and State Key Laboratory of Vascular Homeostasis and Remodeling, Peking University, Beijing, People's Republic of China
Rui Wang, MD, PhD
Department of Radiology, Peking University First Hospital, Beijing, People's Republic of China
Li-juan He, MD
Rong Xu, MD
xrailzz@sina.com
Renal Division, Peking University First Hospital, Kidney Genetics Center, Peking University Institute of Nephrology, Key Laboratory of Renal Disease, National Health Commission, Key Laboratory of Chronic Kidney Disease Prevention and Treatment (Peking University), Ministry of Education; and State Key Laboratory of Vascular Homeostasis and Remodeling, Peking University, Beijing, People's Republic of China

Arthritis & Rheumatology
Vol. 78, No. 2, February 2026, pp 493–494

DOI 10.1002/art.43355

Clinical Images: Sarcoidosis revealed by recurrent dactylitis

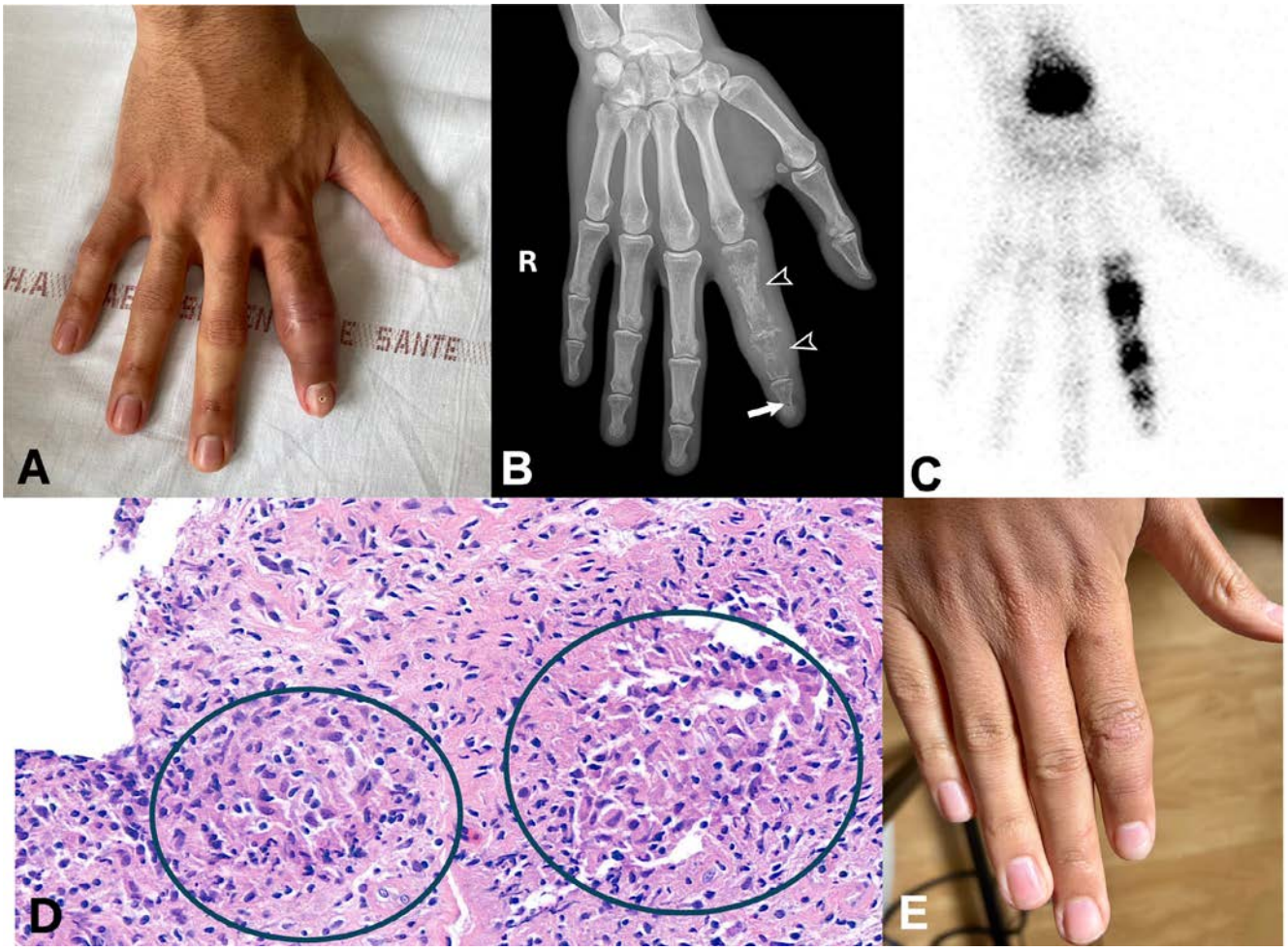

(A) A 21-year-old man presented with chronic and recurrent dactylitis of the index finger. (B) The conventional radiography showed osteolytic changes in the three phalanges of the right index finger, with a characteristic honeycomb (or lattice) appearance in P1 and P2 (black arrowheads) and a cystoid lesion in P3 (white arrow) associated with thickening of the surrounding soft tissues. Of note, there is no joint space narrowing in the metacarpophalangeal and interphalangeal joints. (C) Technetium-99 scintigraphy identified multiple areas of increased uptake. (D) Histopathological analysis of biopsies obtained by a hand surgeon showed chronic aseptic osteitis and noncaseating granulomas (green circles) within the synovium, consistent with a diagnosis of sarcoidosis. Interferon-γ release assay for *Mycobacterium tuberculosis* was negative, as was culture for mycobacteria and *M tuberculosis* polymerase chain reaction. Additional findings supporting the diagnosis of systemic sarcoidosis included hypermetabolic mediastinal and hilar lymphadenopathies on positron emission tomography–computed tomography with pulmonary micronodules, elevated angiotensin-converting enzyme, hypergammaglobulinemia, and lymphopenia. Bone involvement may be present in 1% to 15% of patients with sarcoidosis and is often asymptomatic.[1] The spine is the most commonly affected site, followed by the pelvis.[2,3] The classic lesions in the small bones of the hands and feet like in this case are known as Perthes and Jüngling disease.[2] (E) The patient was treated with a tapering course of glucocorticoids and methotrexate, and there was improvement in the dactylitis.

Drs Subervie and Willaume contributed equally to this work.

Author disclosures are available at https://onlinelibrary.wiley.com/doi/10.1002/art.43355.

1. Kucharz EJ. Osseous manifestations of sarcoidosis. Reumatologia 2020;58:93–100.
2. Hassine IB, Rein C, Comarmond C, et al. Osseous sarcoidosis: a multicenter retrospective case-control study of 48 patients. Joint Bone Spine 2019;86:789–93.
3. Zhou Y, Lower EE, Li H, et al. Clinical characteristics of patients with bone sarcoidosis. Semin Arthritis Rheum 2017;47(1):143–148.

Thomas Subervie, MD
thomas.subervie@chru-strasbourg.fr
Thibault Willaume, MD
Amin Maazouzi, MD
Jacques-Eric Gottenberg, MD, PhD
Jean Sibilia, MD, PhD
Noëlle Weingertner, MD
Strasbourg University Hospital
Strasbourg, France

Eden Sebbag, MD
National Center for Rare Autoimmune Systemic Diseases Est Sud-Ouest, Strasbourg University Hospital
Strasbourg, France
Marc Scherlinger, MD, PhD
National Center for Rare Autoimmune Systemic Diseases Est Sud-Ouest, Strasbourg University Hospital and UMR_S INSERM 1109, Immunorhumatologie Moléculaire
Strasbourg, France

Arthritis & Rheumatology
Vol. 78, No. 2, February 2026, pp 495–496

American College of Rheumatology
Empowering Rheumatology Professionals

DOI 10.1002/art.43357

Clinical Images: When ankylosing spondylitis encounters spinal trauma

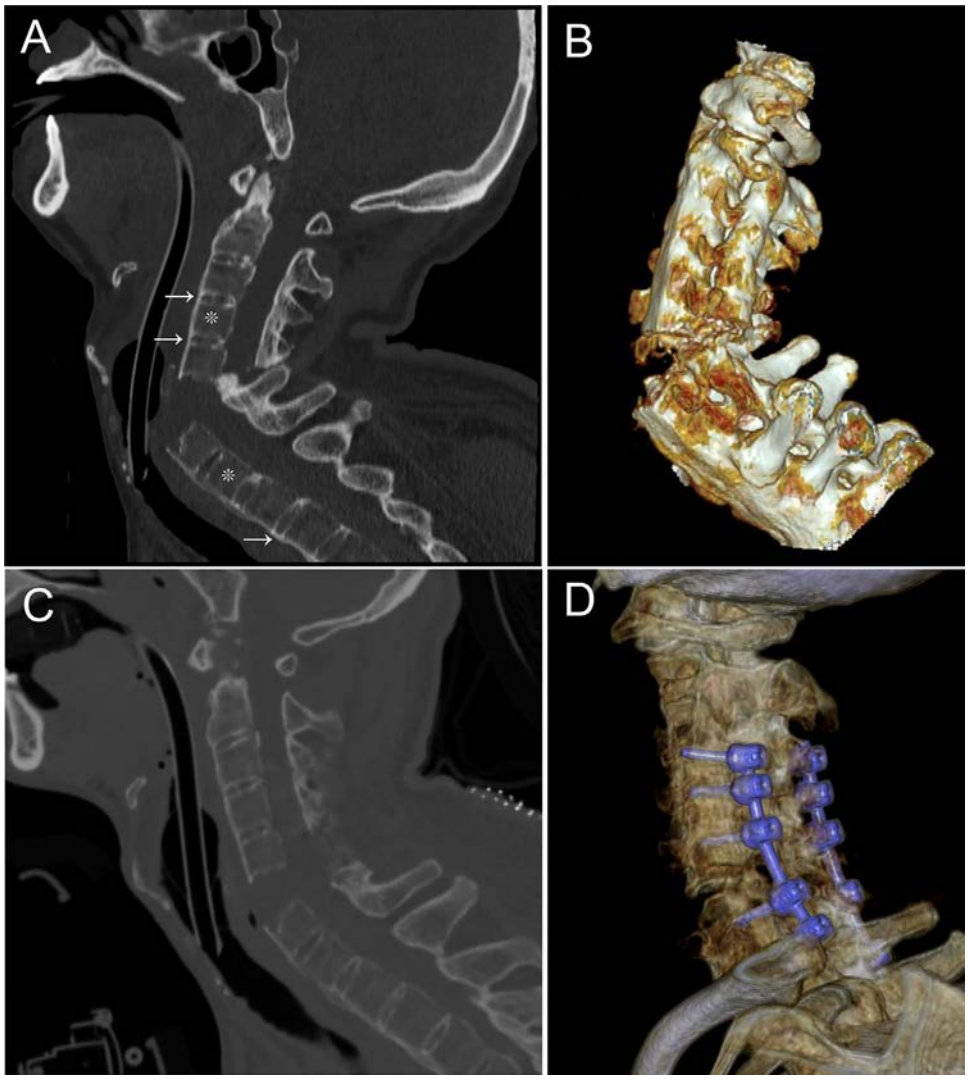

The patient, a 51-year-old woman with a history of ankylosing spondylitis (AS), presented with quadriplegia after a neck flexion-distraction injury during a motor vehicle accident. Over the past 10 years, she has received irregular treatment for AS. The neurologic assessment revealed hallmark signs of acute compression in the lower cervical spinal cord. Given the vasodilation associated with neurogenic shock, vasopressors were applied to restore adequate perfusion, and catheterization was implemented to treat acute urinary retention. Sagittal cervical computed tomography revealed severe displacement and unstable comminuted fracture in fused vertebral bodies, also known as chalk-stick fractures, at the C5 to C6 level (arrows; A). The corresponding spinal cord was significantly compressed and deformed. Three-dimensional reconstruction confirmed a serious dislocated transverse fracture at the segment (B). Surgical decompression and cervical internal fixation were performed (C, D). After the surgery, the patient's upper-limb function improved, but she died of pneumonia 6 weeks later.

AS is a chronic inflammatory rheumatic immune disease that mainly affects the axial bone. Patients with AS often suffer from osteoporosis, and thus, even low-energy injuries can lead to severe spinal fractures.[1] Because of long-term inflammation and repair response, the angle of the anterior edge of the vertebral body becomes round, blunt, and straight, gradually presenting with a squaring of vertebral bodies. Calcification of the lateral and anterior longitudinal ligaments of the vertebral body leads to the formation of bone bridges in the

paravertebral and anterior vertebral edges, resulting in the appearance of the spine as fused bone columns, known as the bamboo spine, which significantly decline the flexibility and ability to absorb the impact of the spine.[2] Chalk-stick fracture is a serious spinal fusion fracture that occurs in patients with AS, characterized by a complete horizontal fracture at the intervertebral disc–vertebral junction and surrounding spinal structures.[3] The complications of chalk-stick fracture include epidural hematoma, cauda equina syndrome, erosive arachnoiditis, and spinal cord injury. The consequences of spinal cord injury in chalk-stick fracture are often catastrophic. Management of a stable chalk-stick fracture may be conservative; otherwise, surgical intervention is required. The operation principle is to relieve spinal nerve compression, rebuild spinal stability, and restore sagittal balance of spinal force lines.[4]

Supported by the funding of Anhui Provincial Health Research Project (AHWJ2023BAa20205) and Anhui Excellent Scientific Research and Innovation Team (2022AH010073).

Author disclosures are available at https://onlinelibrary.wiley.com/doi/10.1002/art.43357.

1. Taurog JD, Chhabra A, Colbert RA. Ankylosing spondylitis and axial spondyloarthritis. N Engl J Med 2016;374(26):2563–2574.
2. Timsans J, Tiihonen R, Kauppi M. A chalk-stick fracture in an 81-year-old man with ankylosing spondylitis. CMAJ 2025;197(4):E97.
3. Ramos GB, Martins RR, de Souza JCC, et al. Spinal cord injury, vertebral artery dissection, and cerebellar strokes after chiropractic manipulation. Neurology 2022;99(22):995–996.
4. Kang KH, Seok SY, Cho JH. Concurrently occurring spinal cord cross-section and aortic injury after a chalk-stick fracture and dislocation in patient with ankylosing spondylitis: clinical image. World Neurosurg 2024;184:149–151.

Chenhui Zhao, PhD
Xiaochun Jiang, MD
jiangxiaochun@wnmc.edu.cn
The First Affiliated Hospital of Wannan Medical College
Wuhu, China

Arthritis & Rheumatology
Vol. 78, No. 2, February 2026, pp 497–507

American College of Rheumatology
Empowering Rheumatology Professionals

LETTER

DOI 10.1002/art.43306

2024 ACR lupus nephritis guideline: comment on the article by Sammaritano et al

To the Editor:

We read with great interest the recently published "2024 American College of Rheumatology (ACR) Guideline for the Screening, Treatment, and Management of Lupus Nephritis."[1] The emphasis on early initiation of therapy and combination regimens represents a meaningful shift, aligned with the principle that in lupus nephritis (LN), "time is nephron." This approach underscores the urgency of achieving rapid disease control to preserve renal function.

Nevertheless, we would like to highlight two areas of concern that may have unintended consequences, particularly in settings with limited resources or adherence challenges. First, the guideline includes calcineurin inhibitors (CNIs) as part of the recommended triple therapy but does not distinguish between agents with notably different pharmacological properties. Tacrolimus, cyclosporine, and voclosporin differ in potency, side effect profiles, monitoring needs, and ease of use. The lack of specification could lead regulatory and reimbursement authorities to interpret these drugs as interchangeable. In cost-driven health care systems, this could restrict access to the most suitable CNI for each patient. Although head-to-head trials comparing these CNIs in LN are not available, consistent evidence shows that voclosporin combined with mycophenolate mofetil (MMF) is superior to MMF alone.[2] Similarly, transplant data indicate that tacrolimus outperforms cyclosporine in improving graft survival and preventing acute rejection.[3–5] These differences are clinically relevant and merit clearer guidance.

Second, we are concerned about the practical implications of an increased pill burden. Adding 4 to 6 six tablets daily to standard immunosuppressive therapy may result in patients taking up to 10 pills per day, excluding glucocorticoids and supportive treatments. This complexity can negatively impact adherence, a well-recognized challenge in LN care. Poor adherence is associated with worse outcomes and higher relapse rates, particularly in younger patients or those facing socioeconomic barriers.

Although we support the intent to improve remission rates through combination strategies, it is essential to consider real-world feasibility. Guidelines must address not only efficacy but also patient-centered implementation, especially in diverse global health care settings.

We commend ACR for advancing the standard of care in LN and appreciate the rigorous work behind these recommendations. We hope our comments contribute to ongoing discussions aimed at optimizing both access and adherence while maintaining high standards of care for all patients living with LN.

Dr Bonfa's work was supported by GSK (grant NCT05879419), São Paulo Research Foundation (FAPESP grant 2022/12925-8), and National Council for Scientific and Technological Development (CNPq grant 305242/2019-9).

GSK had no role in the study design or in the collection, analysis, or interpretation of the data, the writing of the manuscript, or the decision to submit the manuscript for publication. Publication of this article was not contingent upon approval by GSK.

Author disclosures are available online at https://onlinelibrary.wiley.com/doi/10.1002/art.43306

Luciana Seguro, MD, PhD
Eloisa Bonfa
eloisa.bonfa@hc.fm.usp.br
Rheumatology Division, Hospital das Clinicas da Faculdade de Medicina da Universidade de Sao Paulo
Sao Paulo, Brazil

1. Sammaritano LR, Askanase A, Bermas BL, et al. 2024 American College of Rheumatology (ACR) Guideline for the Screening, Treatment, and Management of Lupus Nephritis. Arthritis Rheumatol 2025; 77(9):1115–1135.
2. Rovin BH, Teng YKO, Ginzler EM, et al. Efficacy and safety of voclosporin versus placebo for lupus nephritis (AURORA 1): a double-blind, randomised, multicentre, placebo-controlled, phase 3 trial. Lancet 2021;397(10289):2070–2080.
3. Webster AC, Woodroffe RC, Taylor RS, et al. Tacrolimus versus ciclosporin as primary immunosuppression for kidney transplant recipients: meta-analysis and meta-regression of randomised trial data. BMJ 2005;331(7520):810.
4. McAlister VC, Haddad E, Renouf E, et al. Cyclosporin versus tacrolimus as primary immunosuppressant after liver transplantation: a meta-analysis. Am J Transplant 2006;6(7):1578–1585.
5. Ye F, Ying-Bin X, Yu-Guo W, et al. Tacrolimus versus cyclosporine microemulsion for heart transplant recipients: a meta-analysis. J Heart Lung Transplant 2009;28(1):58–66.

DOI 10.1002/art.43343

Reply

To the Editor:

We appreciate the thoughtful feedback offered in Drs Seguro and Bonfa's letter regarding the recommendation for the use of calcineurin inhibitor (CNI) therapy and the important issue of patient pill burden in the setting of triple therapy in our recent American College of Rheumatology lupus nephritis management guideline.[1] These two issues are indeed related, given both accessibility

concerns and the number of capsules required for voclosporin therapy. Their comments emphasize the critical issue of real-world feasibility and the challenge in optimizing efficacy and patient-centered implementation, especially in diverse health care settings.

Although we briefly acknowledged these concerns in the guideline text, we could not fully address their complexity—including variations in CNI side effects—due to space limitations. These issues were discussed extensively by the Voting Panel. Voclosporin is likely better tolerated in terms of side effects and does not require therapeutic drug monitoring, which is an advantage in many settings. However, the absence of drug-level monitoring may make adherence more difficult to assess, and six capsules daily (plus other medications) may prove challenging for many patients. Panel members reported difficulty with accessing voclosporin due to expense or lack of insurance coverage; as a result, they often used tacrolimus for triple therapy.

Randomized controlled trials for triple therapy with CNIs exist for both voclosporin and tacrolimus,[2,3] but the lack of comparative effectiveness and safety studies made it necessary to be more general in our recommendation. Access to voclosporin in the United States and globally is variable, and a patient-centered guideline should acknowledge such factors and include therapies that are available and implementable in real-world contexts. Additionally, our guideline addresses both adult and pediatric patients, and voclosporin is not approved for use in pediatric patients.

We recognize the impact of pill burden on medication adherence. Voclosporin in particular may contribute to this well-recognized challenge. This guideline includes alternative therapies with lower pill burden: intravenous or subcutaneous belimumab with either mycophenolate or low-dose cyclophosphamide. Our Patient Panel was very clear about the importance of offering choices when discussing medication options and emphasized that shared decision-making—at its best—is a dynamic, ongoing process influenced by patient values, individual disease course, stage of life, medication tolerance (including pill burden), efficacy, and side effects.

In conclusion, we thank Drs Seguro and Bonfa for their important comments highlighting the complex challenges of lupus nephritis treatment. Future studies should further inform optimal therapy, especially as emerging treatments become available. We share their commitment to guiding individualized care that maximizes efficacy, tolerability, and accessibility for all people living with lupus nephritis.

American College of Rheumatology (ACR) Lupus Nephritis Guideline Core Team members, on behalf of the 2024 ACR Lupus Nephritis Guideline Team:

Lisa R. Sammaritano, MD
sammaritanol@hss.edu
Hospital for Special Surgery
New York, NY
Anca Askanase, MD, MPH
Columbia University Medical Center
New York, NY
Bonnie L. Bermas, MD
University of Texas Southwestern Medical Center
Dallas, TX
Maria Dall'Era, MD
University of California
San Francisco, CA
Ali Duarte-Garcia, MD, MSc
Mayo Clinic
Rochester, MN
Linda T. Hiraki, MD, FRCPC, ScD
The Hospital for Sick Children
Toronto, Ontario, Canada
Brad H. Rovin, MD
The Ohio State University College of Medicine
Columbus, OH
Mary Beth F. Son, MD
Boston Children's Hospital
Boston, MA
Amy S. Turner
American College of Rheumatology
Atlanta, GA
Reem A. Mustafa, MD, PhD, MPH
University of Kansas Medical Center
Kansas City, KS

1. Sammaritano LR, Askanase A, Bermas BL, et al. 2024 American College of Rheumatology (ACR) guideline for the screening, treatment, and management of lupus nephritis. Arthritis Rheumatol 2025;77(9):1115–1135.
2. Rovin BH, Teng YKO, Ginzler EM, et al. Efficacy and safety of voclosporin versus placebo for lupus nephritis (AURORA 1): a double-blind, randomised, multicentre, placebo-controlled, phase 3 trial. Lancet 2021;397(10289):2070–2080.
3. Liu Z, Zhang H, Liu Z, et al. Multitarget therapy for induction treatment of lupus nephritis: a randomized trial. Ann Intern Med 2015;162(1):18–26.

DOI 10.1002/art.43308

Limitations in targeting Modic type 1 changes with systemic TNF inhibition: comment on the article by Gjefsen et al

To the Editor:

We read with great interest the recent randomized controlled trial by Gjefsen et al evaluating infliximab in patients with chronic low-back pain (CLBP) and Modic type 1 changes (MC1).[1] Although the study represents a rigorous effort to address an

unmet need in CLBP management, we wish to highlight critical implications and future directions.

The BackToBasic trial demonstrated no superiority of infliximab over placebo in reducing pain-related disability (95% confidence interval –2.1 to 4.6, $P = 0.45$) or secondary outcomes at five months.[1] These findings contrast with earlier hypotheses that tumor necrosis factor (TNF) inhibition might alleviate inflammation-driven pain in MC1, as seen in axial spondyloarthritis.[2] Notably, the trial's methodologic strengths—multicenter design, triple blinding, and standardized magnetic resonance imaging (MRI) protocols—enhance its validity. However, several considerations warrant discussion:

1. Heterogeneity of MC1: a critical unaddressed confounder

The study's patient selection criteria raise concerns about pathologic heterogeneity. MC1 represents a dynamic spectrum of inflammatory and degenerative processes, often transitioning to MC2 (fatty changes) within 12 to 24 months. The median symptom duration in this cohort was 36 months, suggesting many participants had chronic, potentially "burned-out" MC1 lesions. Histopathologic studies indicate that MC1 in early stages (less than six months) exhibits pronounced inflammatory infiltrates (elevated TNF-α levels, interleukin-1β), whereas chronic MC1 shows fibrosis and diminished cytokine activity.[2] By including patients with prolonged symptoms, the trial may have diluted the treatment effect in a subgroup with active inflammation. Post hoc stratification by symptom duration or MRI-based quantification of edema extent could have clarified this. Furthermore, MC1 was diagnosed qualitatively by two radiologists. Quantitative MRI techniques are increasingly used to objectively grade Modic changes. The trial did not stratify participants by MRI features such as edema volume or endplate disruption or biomarkers such as serum TNF levels or interleukin profiles. This heterogeneity may obscure subgroup-specific treatment effects. Notably, a post hoc analysis of the nine-month data hints at a delayed divergence in Oswestry Disability Index (ODI) scores (–4.2 points favoring infliximab, albeit nonsignificant), suggesting prolonged anti-inflammatory effects in certain phenotypes. Future trials should incorporate advanced imaging and biomarker profiling to identify responders.

2. Pharmacological considerations: dose, timing, and target engagement

Multiple sclerosis is a complex chronic disease of the central nervous system; the infliximab regimen mirrors protocols for rheumatoid arthritis but may be suboptimal for spinal pathology.[3] Unlike synovial joints, the avascular intervertebral disc and vertebral endplate represent a pharmacologically privileged site.[4] Cerebrospinal fluid levels of infliximab after intravenous administration are <1% of serum concentrations, suggesting limited penetration to the MC1 microenvironment, and this may be the primary reason for the lack of difference from placebo in efficacy. A subcutaneous TNF inhibitor with better tissue penetration or intradiscal delivery methods might yield different results.

3. Outcome measures and placebo response

The placebo group exhibited a clinically notable ODI improvement (–6.4 points), consistent with high placebo responses in CLBP trials. Although the authors minimized cointerventions, the lack of objective outcome measures (quantitative sensory testing or functional MRI) limits mechanistic insights. Composite endpoints integrating pain, disability, and markers of inflammation may better capture treatment effects.

This trial is a pivotal step toward personalized CLBP management. Although infliximab did not meet its primary endpoint, the findings underscore the complexity of MC1-associated pain and the need for deeper phenotyping. We commend the authors for their contribution and advocate for continued exploration of immunomodulatory strategies in this challenging population.

Author disclosures are available online at https://onlinelibrary.wiley.com/doi/10.1002/art.43308.

This work was funded by Multidisciplinary Interdisciplinary Team Project for Traditional Chinese Medicine Technology Innovation at Liaoning University of Traditional Chinese Medicine (2025-Dxkjc-23-03), China Postdoctoral Science Foundation (GZC20231025) and Liaoning Provincial Natural Science Foundation Doctoral Research Initiation Program (2025-BS-0711).

Qu Zheng, PhD
Bao-qiang Dong, PhD
Xingxing Lin, PhD
18004012223@163.com
Liaoning University of Traditional Chinese Medicine
Shenyang, China
Yiyan Han, PhD
hyy-zjtn@lnutcm.edu.cn
Liaoning University of Traditional Chinese Medicine
Shenyang, China
Key Laboratory of Acupuncture and Moxibustion
Health and Rehabilitation in Liaoning Province
Liaoning University of Traditional Chinese Medicine
Shenyang, China

1. Gjefsen E, Bråten LC, Ponzi E, et al. Efficacy of a tumor necrosis factor inhibitor in chronic low-back pain with Modic type 1 changes: a randomized controlled trial. Arthritis Rheumatol 2025;77(5):615–623.
2. Lassmann H. Multiple sclerosis pathology. Cold Spring Harb Perspect Med 2018;8(3):a028936.
3. Lorenzut S, Negro ID, Pauletto G, et al. Exploring the pathophysiology, diagnosis, and treatment options of multiple sclerosis. J Integr Neurosci 2025;24(1):25081.
4. Gullbrand SE, Peterson J, Mastropolo R, et al. Drug-induced changes to the vertebral endplate vasculature affect transport into the intervertebral disc in vivo. J Orthop Res 2014;32(12):1694–1700.

DOI 10.1002/art.43309

Reply

To the Editor:

We appreciate the thoughtful comments from Zheng and colleagues regarding the BackToBasic study.[1] In designing the trial, we prioritized feasibility for clinical practice and outcomes that are meaningful to the patient population.

First, we acknowledge the concerns regarding pathologic heterogeneity in this population, particularly with Modic type 1 changes (MC1), which encompass a range of inflammatory and degenerative processes. In the study protocol, we preplanned to analyze whether symptom duration or extent of MC edema modified the treatment effect, and as reported in the main article from the trial (Supplementary Table 5 in ref 1), symptom duration did not modify the treatment effect.[1] Further, edema extent at baseline did not modify the treatment effect at five or nine months' follow-up. This was reported in a separate article published May 13, 2025, in which edema was evaluated both qualitatively and quantitatively using edema-sensitive short tau inversion series.[2]

Zheng et al noted the interesting trend at nine months, where the difference in Oswestry Disability Index (ODI) scores between infliximab and placebo groups increased to 4.2 points. The primary endpoint at five months was chosen based on the recommendations for assessment of treatment effect for patients with spondylarthritis,[3] but, as commented, the divergency at nine months should be explored. We have accordingly collected long-term data that will be analyzed to elucidate this trend. In addition, we have collected biobank samples for post hoc investigations that may help identify potential biomarkers. Notably, the primary endpoint analysis showed equal numbers of good responders (a 10-point change in ODI) in both infliximab and placebo groups.

On pharmacological considerations, the infliximab dosing regimen in our study followed standard protocols for spondylarthritis, using 5-mg/kg doses at specified intervals rather than the lower dose of 3 mg/kg, which is commonly used for rheumatoid arthritis.[4,5] Hence, patients were given doses considered optimal for treating inflammatory processes in the spine. It is reasonable to believe that these doses would also impact inflammatory processes in MC. Although subcutaneous delivery might provide enhanced tissue penetration, this formulation was not available in Norway at the time. Throughout the study, we measured trough serum infliximab levels, with analyses showing no difference in outcomes even after excluding those with subtherapeutic levels.[1]

As for outcome measures, we employed the recommended metrics for clinical trials of chronic low back pain.[6] Patient-reported outcome measures were used to capture various dimensions such as function and quality of life, prioritized for our trial's relevance to patients' experiences. Although objective measures such as functional magnetic resonance imaging or quantitative sensory testing hold promise, their practical application remains limited.[7–9]

Precision medicine for nonspecific low back pain poses challenges in identifying patient subphenotypes. We value the potential of MC for subgroup stratification and agree that advanced imaging and biomarker profiling could enhance our understanding of treatment responses. However, ensuring that these methods are also feasible within routine clinical settings is crucial for conducting future research.

Elisabeth Gjefsen, MD
e.gjefsen@gmail.com
John A. Zwart, MD, PhD
Department of Research and Innovation, Division of Clinical Neuroscience, Oslo University Hospital and Institute of Clinical Medicine, University of Oslo Oslo, Norway
Lars C. Bråten, MD, PhD
Department of Research and Innovation, Division of Clinical Neuroscience, Oslo University Hospital, Oslo, Norway
Ansgar Espeland, MD, PhD
Department of Radiology, Haukeland University Hospital and Department of Clinical Medicine, University of Bergen Bergen, Norway
Guro L. Goll, MD, PhD
Center for Treatment of Rheumatic and Musculoskeletal Diseases, Diakonhjemmet Hospital and Institute of Health and Society, University of Oslo Oslo, Norway
Kjersti Storheim, PhD
Department of Research and Innovation, Division of Clinical Neuroscience, Oslo University Hospital and Department of Rehabilitation Science and Health Technology, Faculty of Health Sciences, Oslo Metropolitan University, Oslo, Norway

1. Gjefsen E, Bråten LC, Ponzi E, et al. Efficacy of a tumor necrosis factor inhibitor in chronic low-back pain with Modic type 1 changes: a randomized controlled trial. Arthritis Rheumatol 2025;77(5):615–623.
2. Dagestad MH, Vetti N, Haugli Bråten LC, et al. Modic change edema in chronic low back pain treated with infliximab or placebo: the BackToBasic trial. Spine 2025;50(16):1091–1101.
3. Ramiro S, Nikiphorou E, Sepriano A, et al. ASAS-EULAR recommendations for the management of axial spondyloarthritis: 2022 update. Ann Rheum Dis 2023;82(1):19–34.
4. Brandt J, Haibel H, Reddig J, et al. Successful short term treatment of severe undifferentiated spondyloarthropathy with the anti-tumor necrosis factor-alpha monoclonal antibody infliximab. J Rheumatol 2002;29(1):118–122.
5. Brandt J, Haibel H, Cornely D, et al. Successful treatment of active ankylosing spondylitis with the anti-tumor necrosis factor α monoclonal antibody infliximab. Arthritis Rheum 2000;43(6):1346–1352.

6. Chiarotto A, Boers M, Deyo RA, et al. Core outcome measurement instruments for clinical trials in nonspecific low back pain. Pain 2018; 159(3):481–495.
7. Goodman L-R, Dass R, Daniel E, et al. Quantitative sensory testing and exercise-induced hypoalgesia protocols in low back pain: a scoping review. J Pain 2025;28:104725.
8. Schliessbach J, Siegenthaler A, Bütikofer L, et al. Predicting drug efficacy in chronic low back pain by quantitative sensory tests. Eur J Pain 2018;22(5):973–988.
9. Davis KD, Flor H, Greely HT, et al. Brain imaging tests for chronic pain: medical, legal and ethical issues and recommendations. Nat Rev Neurol 2017;13(10):624–638.

DOI 10.1002/art.43317

Insights on axial spondyloarthritis in multicenter cohorts of undiagnosed back pain patients: comment on the article by Maksymowych et al

To the Editor:

We read the study "Features of Axial Spondyloarthritis in Two Multicenter Cohorts of Patients with Psoriasis, Uveitis, and Colitis Presenting with Undiagnosed Back Pain" by Maksymowych et al[1] with great interest. This multicenter study provides valuable insights into the diagnostic challenges of axial spondyloarthritis (axSpA) in these patient populations through its comprehensive evaluation of clinical and imaging features. However, several important clinical questions emerge from these findings.

First, although the study highlights the importance of magnetic resonance imaging (MRI), the divergent MRI protocols between Screening for axSpA in Psoriasis (PsO), Iritis, and Colitis 1 (SASPIC-1 [on-demand]) and 2 (SASPIC-2 [routine]) introduce confounding variables. The 25% lower axSpA diagnosis rate in HLA-B27–negative PsO/inflammatory bowel disease (IBD) patients in SASPIC-2 may reflect not only MRI's diagnostic value but also differences in clinical judgment across cohorts. Future research should employ standardized MRI protocols to isolate the impact of systematic imaging from variability in rheumatologist decision-making.

Second, the study's reliance on HLA-B27 and traditional clinical features may overlook emerging biomarkers. Recent studies have shown that serum vascular endothelial growth factor levels are associated with axSpA disease activity and may be a promising biomarker for axSpA.[2] Integrating such biomarkers with MRI data might enhance diagnostic precision, especially in PsO and IBD subgroups in which HLA-B27 prevalence is low (30%–50%).

Third, the study's focus on tertiary care centers may limit generalizability to community settings in which access to rheumatologists and MRI is constrained. The authors' recommendation for rheumatologist referral and MRI in all high-risk patients is pragmatic but may face implementation barriers in resource-limited regions. Future studies could explore simplified screening algorithms or telemedicine approaches to bridge this gap.

In conclusion, this study provides valuable insights into the features and diagnosis of axSpA in patients with PsO, acute anterior uveitis, and IBD. However, future research should focus on standardized imaging protocols, identification of novel biomarkers to improve the diagnosis, and management of axSpA in these patient groups.

Author disclosures are available at https://onlinelibrary.wiley.com/doi/10.1002/art.43317.

Qing Long, MM
Department of Traditional Chinese Medicine,
The Affiliated Hospital, Southwest Medical University
Luzhou, Sichuan Province, China
Yan Li, MM
619319374@qq.com
Department of Dermatology,
The Affiliated Traditional Chinese Medicine Hospital, Southwest Medical University
Luzhou, Sichuan Province, China

1. Maksymowych WP, Carmona R, Weber U, et al. Features of axial spondyloarthritis in two multicenter cohorts of patients with psoriasis, uveitis, and colitis presenting with undiagnosed back pain. Arthritis Rheumatol 2025;77(1):47–58.
2. Gulec Yazir M, Durak Ediboglu E, Alp G, et al. AB0773 serum VEGF level may be have a role in the evaluation of treatment response and disease activity during TNFi therapy in patients with AxSpA. Ann Rheum Dis 2022;81(suppl 1):1512–1513.

DOI 10.1002/art.43314

Reply

To the Editor:

We greatly appreciate the valuable comments from Long and Li on our two prospective Screening for Axial Spondyloarthritis (axSpA) in Psoriasis (PsO), Iritis, and Colitis (SASPIC-1 and -2) cohorts evaluating the frequency and diagnostic ascertainment of axSpA in patients presenting with undiagnosed back pain and PsO, iritis, or colitis.[1] Their comments pointed out several aspects of the study that require clarification and, also, essential topics for future research.

First, magnetic resonance imaging (MRI) of the sacroiliac joints (SIJs) was done in SASPIC-1 on an as-required basis, typical of routine care, and mostly in cases that were negative for radiographic sacroiliitis (76.7%). In SASPIC-2, all cases had MRI of the SIJ. MRI of the SIJ was conducted according to the same standardized protocol in both cohorts.[2] This difference in study design was aimed at understanding the impact of on-demand versus required MRI evaluation on diagnostic ascertainment. We observed a substantial impact on proportions of cases diagnosed with axSpA, primarily in HLA-B27–negative cases, in which

diagnoses of axSpA were made in 41.2%, 31.8%, and 39.7% of patients with PsO, acute anterior uveitis (AAU), and inflammatory bowel disease (IBD), respectively, in SASPIC-1, and in 15.9%, 43.8%, and 14.7% of patients with PsO, AAU, and IBD, respectively, in SASPIC-2. Moreover, rheumatologist level of confidence in ruling in and ruling out the diagnosis increased primarily after MRI evaluation. We doubt that these differences reflect differences in clinical judgement between the two cohorts because seven of eight study sites in SASPIC-2 were among the 10 sites who participated in SASPIC-1. It was, therefore, a major conclusion of our study that conducting MRI in all patients with PsO, AAU, or IBD, presenting with undiagnosed back pain enhances diagnostic accuracy.

Second, we agree that there is an unmet need for diagnostic biomarkers in axSpA, especially in patients with PsO or IBD in which the prevalence of HLA-B27 is lower than in other subtypes of axSpA. Although several serological biomarkers have been evaluated in axSpA, none have been considered to have sufficient diagnostic capacity for application in clinical practice beyond C-reactive protein.[3] There are data supporting a potential role for vascular endothelial growth factor in monitoring disease activity, but we are unaware of data supporting a role in diagnosis.

Third, of the 10 sites who participated in SASPIC-1 and eight sites in SASPIC-2, one-half were community based, and one-half were tertiary referral centers, which suggests our findings are generalizable. We appreciate the implementation barriers to rheumatologist referral and MRI evaluation in resource-limited regions, but our study demonstrates that reliance on clinical assessment and radiography alone may lead to an inaccurate diagnosis with consequences for appropriate treatment. In particular, our data suggest that the addition of MRI might reduce costs related to false positive diagnoses and inappropriate prescribing of advanced therapies.

Walter P. Maksymowych, MB ChB, FRCPC
walter.maksymowych@ualberta.ca
Robert G. Lambert, MB BCh, FRCPC
University of Alberta
Edmonton, Alberta, Canada
Jonathan Chan, MD, FRCPC
University of British Columbia
Vancouver, British Columbia, Canada

1. Maksymowych WP, Carmona R, Weber U, et al. Features of axial spondyloarthritis in two multicenter cohorts of patients with psoriasis, uveitis, and colitis presenting with undiagnosed back pain. Arthritis Rheumatol 2025;77(1):47–58.
2. Lambert RGW, Bakker PAC, van der Heijde D, et al. Defining active sacroiliitis on MRI for classification of axial spondyloarthritis: update by the ASAS MRI working group. Ann Rheum Dis 2016;75(11):1958–1963.
3. Brown MA, Li Z, Cao KL. Biomarker development for axial spondyloarthritis. Nature Rev Rheumatol 2020;16(8):448–463.

DOI 10.1002/art.43305

Absence of functional autoantibodies in systemic sclerosis: is now the right time to broaden reactome analysis? Comment on the article by van Oostveen et al

To the Editor:

We read with interest the rigorous publication by van Oostveen et al, which aimed to replicate data evaluating the presence and role of autoantibodies targeting the angiotensin II receptor type 1 (AT_1) and endothelin 1 type A receptor (ET_AR) in systemic sclerosis (SSc).[1]

Functional autoantibodies (FAs) in SSc may have a pathogenic role by activating G protein–coupled receptors.[2] Van Oostveen et al found no evidence of AT_1 or ET_AR activation in endothelial cells (ECs) or cell lines overexpressing these receptors when stimulated with purified IgG from patients with SSc positive for anti-AT_1 or anti-ET_AR. The authors built a new protein-capture assay independent of receptor activation that did not provide evidence for the presence of anti-AT_1 in patients with SSc. Although FAs above the cutoff levels of solid-phase enzyme-linked immunosorbent assay (ELISA) were detected, this study did not find evidence supporting the presence of FAs capable of functioning as receptor agonists in SSc.[1] Of note, van Oostveen et al used total IgG and not monoclonal FAs or specifically purified FAs. Because one study showed lung and skin inflammation in a murine model of monoclonal anti-AT_1 (mAT_1)-passive transfer, testing the agonist effect of human mAT_1 would have had a nice added value.[3]

SSc IgG did not seem to activate ECs using a selected readout. Nevertheless, as discussed by the authors, the number of patients whose IgG levels were tested was low (n = 5–10), and a targeted readout might not fully capture EC modifications.[1] Recently, we explored the omics profile expression of ECs in the presence of purified SSc IgG. EC molecular profiles were impacted by SSc IgG in an antinuclear autoantibody (ANA) serotype-dependent manner, as previously shown in fibroblasts.[4,5] IgG from anti–topoisomerase 1 antibody (ATA) positive patients induced distinct EC proteomic profiles, which were validated in an external cohort. In both cohorts, anti-AT_1 and anti-ET_AR measured by ELISA neither explained nor influenced the obtained EC profiles.[4] The van Oostveen et al hypothesis that FA might react with nuclear antigens is supported by a previous study showing correlation between FA and ATA, suggesting that FA positivity observed in various cohorts could, in fact, reflect partly ATA presence.[1,4]

ANAs are traditionally considered simple biomarkers but not direct actors. In *Science*, Jaycox et al recently suggested that autoantibodies influence a wide range of conditions beyond autoimmune diseases. The whole IgG repertoire could have protective as well as pathologic roles in disease, underpinning an ambivalent role of the reactome.[6,7] Although most studies on SSc

autoantibodies have focused on one specificity at a time (implying that a single epitope-directed response is dominant), it might be worthwhile to broaden the scope toward more exploratory, systemwide analyses. Examining a large number of variables without any a priori assumptions, as current high-throughput "-omics" methods make possible, could still reveal important insights into the effects of IgG from both patients and healthy individuals. We formulate that these data combined with today's computational resources may eventually help clarify the broader role of the reactome.

Author disclosures are available at https://onlinelibrary.wiley.com/doi/10.1002/art.43305.

Aurélien Chepy, MD
David Launay, MD, PhD
Univ. Lille, Inserm, CHU Lille, U1286 - INFINITE - Institute for Translational Research in Inflammation, F-59000 Lille, France
CHU Lille, Département de Médecine Interne et Immunologie Clinique
Centre de Référence des Maladies Auto-Immunes et Auto-Inflammatoires Rares du Nord, Nord-Ouest, Méditerranée et Guadeloupe (CeRAINOM)
Lille, France
Sylvain Dubucquoi, MD, PhD
Univ. Lille, Inserm, CHU Lille, U1286 - INFINITE - Institute for Translational Research in Inflammation, F-59000 Lille, France
CHU Lille, Institut d'Immunologie
Lille, France
Vincent Sobanski, MD, PhD
vincent.sobanski@univ-lille.fr
Univ. Lille, Inserm, CHU Lille, U1286 - INFINITE - Institute for Translational Research in Inflammation, F-59000 Lille, France
CHU Lille, Département de Médecine Interne et Immunologie Clinique
Centre de Référence des Maladies Auto-Immunes et Auto-Inflammatoires Rares du Nord, Nord-Ouest, Méditerranée et Guadeloupe (CeRAINOM)
Lille, France
Institut Universitaire de France (IUF)
Paris, France

1. van Oostveen WM, Hoekstra EM, Levarht EWN, et al. Absence of functional autoantibodies targeting angiotensin II receptor type 1 and endothelin-1 type A receptor in circulation and purified IgG from patients with systemic sclerosis. Arthritis Rheumatol 2025;77(7):901–913.
2. Riemekasten G, Philippe A, Näther M, et al. Involvement of functional autoantibodies against vascular receptors in systemic sclerosis. Ann Rheum Dis 2011;70(3):530–536.
3. Yue X, Yin J, Wang X, et al. Induced antibodies directed to the angiotensin receptor type 1 provoke skin and lung inflammation, dermal fibrosis and act species overarching. Ann Rheum Dis 2022;81(9):1281–1289.
4. Chepy A, Vivier S, Bray F, et al. Immunoglobulins G from patients with systemic sclerosis modify the molecular signatures of endothelial cells. RMD Open 2025;11(1):e004290.
5. Chepy A, Vivier S, Bray F, et al. Effects of Immunoglobulins G from systemic sclerosis patients in normal dermal fibroblasts: a multi-omics study. Front Immunol 2022;13:904631.
6. Jaycox JR, Dai Y, Ring AM. Decoding the autoantibody reactome. Science 2024;383(6684):705–707.
7. Chepy A, Collet A, Launay D, et al. Autoantibodies in systemic sclerosis: from disease bystanders to pathogenic players. J Transl Autoimmun 2025;10:100272.

DOI 10.1002/art.43348

Reply

To the Editor:

We thank Chepy et al[1] and Akbarzadeh et al[2] for their interest in our recent publication, "Absence of functional autoantibodies targeting angiotensin II receptor type 1 and endothelin 1 type A receptor in circulation and purified IgG from patients with systemic sclerosis",[3] and appreciate the opportunity to respond to their comments.

In our study, we investigated whether total IgG from patients with systemic sclerosis (SSc) (n = 5–18) could induce signaling and cell activation through angiotensin II receptor type 1 (AT_1) and endothelin 1 type A receptor (ET_AR) using various cellular readouts, including endothelial cells (ECs) with endogenous receptor expression and Chinese hamster ovary (CHO) cells overexpressing AT_1 or ET_AR. Because neither approach detected functional AT_1- or ET_AR-activating autoantibodies in purified IgG from patients with SSc (SSc-IgG), we developed a novel protein capture assay to detect circulating anti-AT_1 antibodies in isolated SSc-IgG (n = 28). Using this approach, we found no evidence of specific AT_1-binding IgG. These findings align with observations from Chepy et al, who did not find a correlation between anti-AT_1 or anti-ET_AR seropositivity and changes in EC proteome on incubation with SSc-IgG.[4] Interestingly, Chepy et al described an association between antinuclear antibody (ANA) positivity and distinct EC proteomic signatures.

We agree with Akbarzadeh et al that the functional effects observed using SSc-IgG may relate to experimental design and assay conditions. According to their comments, both the CHO cell lines and ECs used may not accurately detect antibody–receptor interactions. However, we are convinced that robust antibody-mediated effects should be reproducible across laboratories and model systems. We specifically selected CHO cells overexpressing AT_1 or ET_AR to replicate the cellular background of the original studies first reporting these autoantibodies.[5] Our data confirmed that these overexpressing CHO cell lines exhibited normal receptor signaling on stimulation with their natural agonists, and this signaling could be blocked by receptor-specific antagonists, indicating proper receptor function and downstream signaling. As noted by Akbarzadeh et al, varying functional readouts may lead to different interpretations. Therefore, we also

applied two additional assays to analyze SSc-IgG reactivity to AT_1 and ET_AR. We observed no differences in results between primary human dermal microvascular ECs and immortalized human umbilical vein ECs. Notably, the reported protein captur eassay employed solubilized membrane proteins from nontransfected cells as a negative control, an essential step in confirming assay specificity, which is not always included in the development of an anti-AT_1 enzyme-linked immunosorbent assay (ELISA).[5]

Chepy et al also referred to a murine monoclonal antibody (mAb) reported to recognize human AT_1, which might help validate AT_1 signaling or binding.[6] Unfortunately, we did not have access to this mAb for inclusion in our experimental models. This mAb was generated by immunizing mice with membrane extracts from CHO cells overexpressing AT_1, followed by screening hybridoma supernatant against the same membrane preparations in ELISA. Because the target recognized by the mAb was not molecularly defined, nonspecific binding to unrelated components cannot be excluded. Thus, although interesting, these results should be interpreted cautiously, especially because confirmatory data using validated models and molecularly defined readouts, such as testing on transfected versus parental cells, were not available.

The authors noted that patient-specific factors, such as genetic variations in AT_1, immune activation status, or individual IgG reactivity, might influence outcomes of SSc-IgG binding to ET_AR or AT_1. We agree and emphasize that a deeper understanding of autoantibody roles in SSc is likely better achieved by focusing on ANAs and/or the B cells producing them. ANAs—particularly against anti–topoisomerase I (ATA) and anticentromere protein B—are disease specific and strongly associated with distinct clinical phenotypes, and their presence and levels correlate with disease development.[7] The recent success of CD19 chimeric antigen receptor T cell therapy in SSc, in which treatment led to decreased ATA levels, supports this concept.[8–10]

In conclusion, we emphasize the importance of reproducibility to confirm antibody-mediated effects in validated, molecularly defined assays. Given conflicting reports on AT_1- and ET_AR-targeting autoantibodies in SSc, focusing on ANAs and/or ANA-producing B cells may provide key insights into autoreactive B cell responses in SSc.

Author disclosures are available at https://onlinelibrary.wiley.com/doi/10.1002/art.43348.

Wieke M. van Oostveen, MSc
w.m.van_oostveen@lumc.nl
Eva M. Hoekstra, MD, PhD
E. W. Nivine Levarht, BSc
René E.M. Toes, PhD
Jeska K. de Vries-Bouwstra, MD, PhD
Cynthia M. Fehres, PhD
c.m.fehres@lumc.nl
Leiden University Medical Center
Leiden, The Netherlands

Ilana B. Kotliar
The Rockefeller University
and Tri-Institutional PhD Program in Chemical Biology
New York, New York
Thomas P. Sakmar, MD
The Rockefeller University
New York, New York
Laura H. Heitman, PhD
Leiden University
and Oncode Institute
Leiden, The Netherlands

1. Chepy A, Collet A, Launay D, Dubucquoi S, Sobanski V. Autoantibodies in systemic sclerosis: From disease bystanders to pathogenic players. J Transl Autoimmun 2025;10:100272. https://doi.org/10.1016/j.jtauto.2025.100272.
2. Akbarzadeh R, Hackel A, Humrich JY, Riemekasten G, Kusche-Vihrog K. Antibodies targeting G protein-coupled receptors in systemic sclerosis. Comment on the article by van Oostveen WM et al. Arthritis Rheumatol. Portico 2026;78(1):268–269.
3. van Oostveen WM, Hoekstra EM, Levarht EWN, et al. Absence of functional autoantibodies targeting angiotensin II receptor type 1 and endothelin-1 type A receptor in circulation and purified IgG from patients with systemic clerosis. Arthritis Rheumatol 2025;77(7):901–913.
4. Chepy A, Vivier S, Bray F, et al. Immunoglobulins G from patients with systemic sclerosis modify the molecular signatures of endothelial cells. RMD Open 2025;11(1):e004290.
5. Riemekasten G, Philippe A, Näther M, et al. Involvement of functional autoantibodies against vascular receptors in systemic sclerosis. Ann Rheum Dis 2011;70(3):530–536.
6. Yue X, Yin J, Wang X, et al. Induced antibodies directed to the angiotensin receptor type 1 provoke skin and lung inflammation, dermal fibrosis and act species overarching. Ann Rheum Dis 2022;81(9):1281–1289.
7. van Leeuwen NM, Boonstra M, Bakker JA, et al. Anticentromere antibody levels and isotypes and the development of systemic sclerosis. Arthritis Rheumatol 2021;73(12):2338–2347.
8. Auth J, Müller F, Völkl S, et al. CD19-targeting CAR T-cell therapy in patients with diffuse systemic sclerosis: a case series. Lancet Rheumatol 2025;7(2):e83–e93.
9. Müller F, Taubmann J, Bucci L, et al. CD19 CAR T-cell therapy in autoimmune disease — a case series with follow-up. N Eng J Med 2024;390(8):687–700.
10. Wang X, Zhang Y, Jin Y, et al. An iPSC-derived CD19/BCMA CAR-NK therapy in a patient with systemic sclerosis. Cell 2025;188(16):4225–4238.e12.

DOI 10.1002/art.43344

TIPIC syndrome induced by G-CSF: comment on the article by Namineni et al

To the Editor:

Recently, Namineni et al reported a patient with transient perivascular inflammation of the carotid artery (TIPIC) syndrome.[1] TIPIC syndrome is a rare disease of unknown etiology characterized by transient local inflammation around the carotid artery.

The syndrome typically presents with unilateral neck pain and swelling that spontaneously improves within two weeks. TIPIC syndrome was introduced by Lecler et al in 2017, who proposed four major diagnostic criteria.[2]

I, respectfully, express my concerns about whether the patient should be diagnosed with TIPIC syndrome. According to the criteria, the diagnosis of TIPIC syndrome should only be confirmed after ruling out another vascular diagnosis.[2] The patient presented by Namineni et al had underlying pancreatic cancer and had been treated with adjuvant chemotherapy just two weeks before developing TIPIC syndrome. The patient may have received granulocyte colony-stimulating factors (G-CSF) in addition to chemotherapy. Rarely, G-CSF can induce large-vessel vasculitis.[3] Namely, this condition might have been caused by G-CSF–induced aortitis.

G-CSF–induced aortitis is recognized as a rare adverse effect of G-CSF.[3] Among the classes of G-CSF, filgrastim or its long-acting agent pegfilgrastim is the most commonly reported inducing drug. In various malignancies, G-CSF–induced aortitis typically develops several days after administration of G-CSF, and the affected vessels include the aortic arch, thoracic aorta, and subclavian and carotid arteries. Notably, in previously reported cases, one-fifth involved vascular inflammation limited to the carotid artery, and in some patients, the condition resolved without glucocorticoid treatment.[3,4] These patients might be misdiagnosed as having Takayasu arteritis, giant cell arteritis, or TIPIC syndrome if G-CSF is not identified as a causative agent.

In conclusion, TIPIC syndrome that develops after G-CSF administration may represent a mild form of G-CSF–induced aortitis. When TIPIC syndrome is suspected, it is important to thoroughly evaluate the underlying diseases and medications, because drug-induced causes may be involved.

Author disclosures are available at https://onlinelibrary.wiley.com/doi/10.1002/art.43344.

Takao Nagashima, MD, PhD
naga4ma@jichi.ac.jp
Division of Rheumatology, Department of Medicine, Jichi Medical University Saitama Medical Center
Saitama, Japan

1. Namineni N, Mahalingam S, Danve A. Clinical images: transient perivascular inflammation of the carotid artery syndrome. Arthritis Rheumatol 2025;77(7):942–943.
2. Lecler A, Obadia M, Savatovsky J, et al. TIPIC syndrome: beyond the myth of carotidynia, a new distinct unclassified entity. AJNR Am J Neuroradiol 2017;38(7):1391–1398.
3. Taimen K, Heino S, Kohonen I, et al. Granulocyte colony-stimulating factor- and chemotherapy-induced large-vessel vasculitis: six patient cases and a systematic literature review. Rheumatol Adv Pract 2020;4(1):rkaa004.
4. Nagashima T, Yabe H, Sekiguchi Y. G-CSF-induced aortitis mimicking TIPIC syndrome. Intern Med Published online May 8, 2025.

DOI 10.1002/art.43321

Diagnostic value of flame sign for acute gluteus medius calcific tendinitis

To the Editor:

Hip pain is a common clinical complaint and usually located anteriorly, laterally, or posteriorly. Its etiologies are multiple, and diagnosis is challenging. The most common cause of lateral hip pain is greater trochanteric pain syndrome, which includes gluteus medius tendinopathy or tear, bursitis, and iliotibial band friction.[1] Gluteus medius calcific tendinitis is one of the etiologies of acute lateral hip pain, and its diagnosis is clearly dependent on the imaging examinations.[2] We observed the corresponding clinico-radio-pathologic correlations and firstly proposed the "flame sign" of magnetic resonance imaging (MRI), which is of diagnostic value for acute gluteus medius calcific tendinitis. The imaging flame sign conforms to the pathologic stages more accurately than the dose "torch fire sign" published by us before.[3]

Calcific tendinitis is a self-limiting basic calcium phosphate deposition (BCPD) disease. It can involve any tendon, among which shoulder rotator cuff (especially supraspinatus tendon) is most common, and gluteal tendons (especially gluteus medius) are secondly common.[4] Gluteus medius calcific tendinitis has a high prevalence in women compared to men (2:1). Its clinical symptoms are coincident with the pathologic stages of BCPD, which can be divided into crystal formative, resting, and resorptive phases.[5] The acute pain typically occurs during the resorptive phase in which the calcium deposit is phagocytosed by macrophages and multinucleated cells, giving the calcification an ill-defined, blurred, and fragmented appearance on x-ray (Figure 1A). Typically, it forms a hyposignal central resting zone of oval calcifications, mixed-signal transitional resorptive zone of crystal breakdown, and hypersignal-surrounding edematous zone of pennate gluteus medius on MRI, which wholly appears like a flame (Figure 1B).

The flame sign can confirm the diagnosis of acute gluteus medius calcific tendinitis and differentiate from its mimickers such as gout, pseudogout, infection, or tumors. Gout is the monosodium urate crystal deposit within and around the joint. Its typical radiologic findings include well-defined, punched-out bone erosions with overhanging edges and tophi calcifications. Periarticular gouty tophi may appear very similar to BCPD, especially on MRI, in which both will show a significant soft tissue's inflammatory edema. On x-ray, the calcifications of BCPD are relatively more clearly defined than those in gouty tophi, which are fainter and cloudlike.[6] Pseudogout, a calcium pyrophosphate deposition disease, always affects the older population (aged >60 years) and primarily shows intraarticular linear chondrocalcinosis on x-ray comparing with periarticular nodular apatite calcifications in

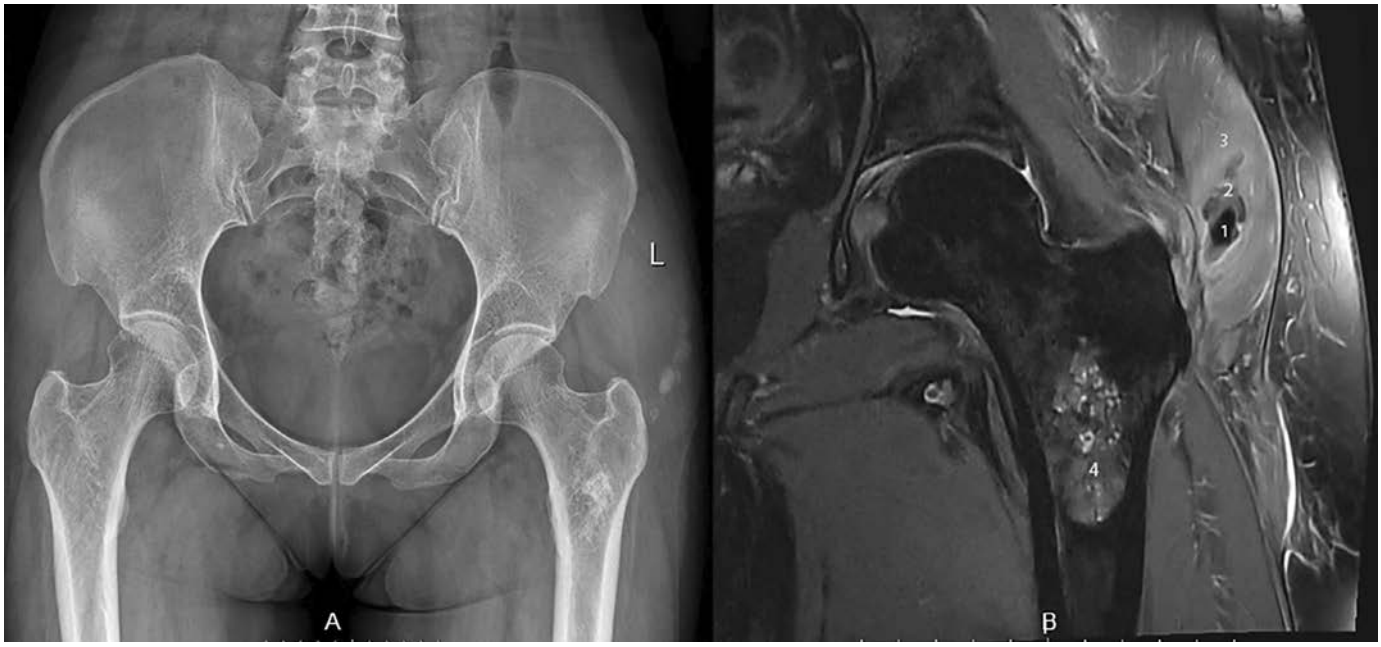

Figure 1. Images of acute gluteus medius calcific tendinitis. (A) Pelvic posteroanterior plain radiograph for a 51-year-old woman with a 2-week history of acute atraumatic left lateral hip pain showed some ill-defined, blurred, and fragmented calcifications along gluteal insertion to the left greater trochanter. (B) Hip coronal proton density fat-saturated magnetic resonance image showed a (1) hyposignal central resting zone of oval calcifications, (2) mixed-signal transitional resorptive zone of crystal breakdown, and (3) hypersignal-surrounding edematous zone of pennate gluteus medius, which wholly appeared like a flame. (4) Note an enchondroma in the proximal femur rather than intraosseous calcification migration.

BCPD.[7] Intramuscular pyogenic infection can show septation or abscess formation with ill-defined inflammatory edema on MRI. Hyperphosphatemic familial tumoral calcinosis tends to be larger and lobulated on x-ray, with a distribution along the extensor surfaces of large joints.[8] The intraosseous calcification migration or cortical erosion adjacent to the periarticular calcifications in BCPD may cause marked bone marrow edema on MRI, which may mimic an aggressive bone-forming neoplasm like osteosarcoma.

We have had the ethics approval and consent of the Shanxi Provincial People's Hospital Ethics Committee (202501231). We have had the written consent for publication from the patient. All data, models, or code generated or used during the study are available from the corresponding author by request.

Author disclosures are available at https://onlinelibrary.wiley.com/doi/10.1002/art.43321.

De-an Qin, MD
qindean.student@sina.comqda.509121@sxmu.edu.cn
Qi-jun An, MD
Department of Orthopedics
Shanxi Provincial People's Hospital
Taiyuan, China
Jie Yuan, MD
Department of Medical Imaging Center
Shanxi Provincial People's Hospital
Taiyuan, China

1. Chamberlain R. Hip pain in adults: evaluation and differential diagnosis. Am Fam Physician 2021;103(2):81–89.
2. Mandl P, D'Agostino MA, Navarro-Compán V, et al. 2023 EULAR recommendations on imaging in diagnosis and management of crystal-induced arthropathies in clinical practice. Ann Rheum Dis 2024;83(6):752–759.
3. An QJ, Qin DA. "Torch fire sign" for acute calcific tendinitis of gluteus medius on MRI. Int J Surg 2022;102:106666.
4. Dalla-Torre R, Le Goff B, Darrieutort-Laffite C. Periarticular calcifications: clinical features and treatment options. Gout Urate Cryst Depos Dis 2024; 2(3):266–274.
5. Kong M, Walters H, Teh J. Updates in deposition arthritis other than gout. Semin Musculoskelet Radiol 2025;29(2):275–292.
6. Reijnierse M, Schwabl C, Klauser A. Imaging of crystal disorders: calcium pyrophosphate dihydrate crystal deposition disease, calcium hydroxyapatite crystal deposition disease and gout pathophysiology, imaging, and diagnosis. Radiol Clin North Am 2022;60(4):641–656.
7. Pascart T, Filippou G, Lioté F, et al. Calcium pyrophosphate deposition disease. Lancet Rheumatol 2024;6:e791–e804.
8. Kaszycki M, Villalpando B, Hickson L, et al. Hyperphosphatemic familial tumoral calcinosis. South Med J 2024;117(12):705–708.

DOI 10.1002/art.43330

Pharmacological weight loss in gout prevention: emphasizing dynamic risk assessment and community strategies: comment on the article by Wei et al

To the Editor:

With rising obesity rates worldwide, the burden of gout, a common comorbidity, has also grown. Although obesity is a recognized modifiable risk factor, evidence on the effects of pharmacologically induced weight loss on gout incidence and recurrence

remains limited. Defining the role of weight loss in gout prevention is crucial for improving intervention strategies and reducing disease burden.

We appreciate the work of Wei et al[1] in examining the link between obesity intervention and gout risk. Using The Health Improvement Network database, the authors applied a cloning, censoring, and weighting method to classify patients based on one-year weight change after starting orlistat. They analyzed the five-year risk of incident and recurrent gout in individuals with and without prior gout. Greater weight loss (≥10%) was associated with a significantly reduced risk, showing a dose-response pattern. This study offers valuable real-world evidence supporting the role of pharmacologically assisted weight loss in both primary and secondary gout prevention, although some aspects merit further refinement.

First, we recognize the authors' subgroup analysis based on baseline serum urate levels. However, given current dietary shifts and the rising prevalence of hyperuricemia,[2] the binary classification of ≤404 μmol/L and >404 μmol/L may not fully capture risk heterogeneity, limiting clinical relevance. Second, the study did not clearly exclude pregnant women, whose weight changes are largely physiologic and may introduce bias.[3] Lastly, weight change was treated as a static exposure without updates during follow-up. As weight fluctuation is common, static classification may cause misclassification and impact causal inference.

To address these limitations, future studies should refine baseline serum urate stratification (eg, <300, 300-400, 400-500, >500 μmol/L) to better capture risk heterogeneity. Pregnant women should be clearly identified or excluded, with sensitivity analyses conducted if needed to reduce bias from physiologic weight changes. Weight change should be treated as a time-updated exposure using models like time-updated Cox or joint longitudinal-survival analysis to better reflect dynamic effects. Importantly, weight management and gout monitoring should be integrated into community health care. Training community health workers to monitor weight and initiate early interventions could support real-time risk tracking and promote early, community-based prevention strategies.

Author disclosures are available at https://onlinelibrary.wiley.com/doi/10.1002/art.43330.

Xueneng Yang, MM
Department of Traumatology
The Second Affiliated Hospital of Kunming Medical University
Kunming, Yunnan, China
Ruijuan Li, MM
280295772@qq.com
Department of Burn
The Second Affiliated Hospital of Kunming Medical University
Kunming, Yunnan, China

1. Wei J, Wang Y, Dalbeth N, et al. Weight loss after receiving anti-obesity medications and gout among individuals with overweight and obese: a population-based cohort study. Arthritis Rheumatol 2025;77(3):335–345.
2. Weinstein S, Maor E, Bleier J, et al. Non-interventional weight changes are associated with alterations in serum uric acid levels. J Clin Med 2024;13(8):13.
3. Shin D, Lee KW, Song WO. Dietary patterns during pregnancy are associated with gestational weight gain. Matern Child Health J 2016; 20(12):2527–2538.